DISSERTATION

MECHANISTIC INVESTIGATIONS AND LIGAND DEVELOPMENT FOR RHODIUM CATALYZED [2+2+2] AND ZINC CATALYZED [4+2] CYCLOADDITIONS

Submitted by

Derek M. Dalton

Department of Chemistry

In partial fulfillment of the requirements

For the Degree of Doctor of Philosophy

Colorado State University

Fort Collins, Colorado

Summer 2013

Doctoral Committee:

Advisor: Tomislav Rovis

John L. Wood
Alan J. Kennan
Anthony K. Rappé
Christopher D. Snow

ABSTRACT

MECHANISTIC INVESTIGATIONS AND LIGAND DEVELOPMENT FOR RHODIUM CATALYZED [2+2+2] AND ZINC CATALYZED [4+2] CYCLOADDITIONS

Described herein are mechanistic studies and ligand development for Rh(I) catalyzed [2+2+2] cycloaddition reactions of alkene tethered isocyanates and exogenous alkynes. A mechanistic hypothesis has been proposed and supported through experiment. Novel perfluoroaryl Taddol phosphoramidite ligands were developed based on the mechanistic hypothesis. Improvements in product and enantioselectivity were found using the perfluoroaryl Taddol phosphoramidite ligand, CKphos. This catalyst system was studied by NMR, X-ray and DFT calculations. Rh(I)–C_6F_5 and Co(-1)–C_6F_5 interactions were found in the course of studying the CKphos catalysts. The Rh•CKphos catalyst system was used in the synthesis of the tricyclic core structure of the cylindricine and lepadiformine alkaloids. Finally a Zn(II) catalyzed [4+2] cycloaddition of 1-azabutadienes and nitro olefins was discovered and developed as an efficient and selective means to synthesize tetrahydropyridines.

ACKNOWLEDGEMENTS

A heartfelt thank you to Tom for welcoming me into his research group. My experience at CSU has been wonderfully rich, challenging and rewarding. Tom, thank you for giving me the freedom to explore my ideas, many of which led to dead ends while a few did bear fruit. Your willingness to be honest and correct my mistakes has helped me develop as a scientist. My development is by no means complete but on a trajectory that I feel good about. Finally, thank you, Tom, for taking an interest in my growth and well-being as a person and not simply a scientist.

Thank you to the current and former Rovis group members. It is overwhelming to think of the memories we shared in my time at CSU. So many people helped me that it is perhaps unfair to single out a few, but I must. Kevin Oberg, Dan DiRocco and Philip Wheeler - it was a pleasure to go through this experience with you three. Each of you pushed me intellectually and for that I am grateful. Kevin, it really has been excellent collaborating with you. Your strengths complement my weaknesses; the full paper on Rh(I) [2+2+2] cycloadditions became my gold standard for quality publication thanks to your contributions. B311 it has been a pleasure working with you (former and current members). I expect good things to continue to come from each person who works in this lab.

Tony Rappé thank you for modeling the Rh(I)•phosphoramidite complexes. We have a better understanding of our catalysts thanks to your efforts. Chris Rithner thank you for helping me with ^{19}F-NMR decoupling experiments. I'd also like to thank Oren Anderson, Susie Miller and Brian Newell for teaching me the ways of X-ray crystallography.

My parents, sisters and friends have provided me with more support than I could possibly have asked for and their support continues. I'd also like to thank Ona Fisher for helping me rekindle my curiosity of the world we live in when I struggled to see it on my own. As genuinely as I can write with words, I thank each person who selflessly touched my life while I was in Ft. Collins. Thank you.

TABLE OF CONTENTS

CHAPTER 1

Rh(I)-Catalyzed [2+2+2] Cycloadditions for N-Heterocycle Synthesis

1.1 Introduction

1.1.1 Metal Catalyzed Cycloadditions

Due to the prevalence of enantioenriched nitrogen containing heterocycles in current medicinal and biologically active agents, we focused on establishing new chemical tools to synthesize nitrogen containing heterocycles efficiently and selectively. Transition metal catalyzed cycloadditions are capable of efficiently making complex molecules with high degrees of selectivity.[1] In 1948 Reppe and Schweckendiek[2] found transition metals catalyzed the cycloaddition of alkynes to form substituted benzenes. Since this discovery, transition metals have been found to facilitate numerous cycloadditions, including use of π-components that contain nitrogen. Importantly, [2+2+2] cycloadditions may be used to form substituted benzenes and N-heterocycles, such as pyridines, pyridones, indolizidinones and quinolizidinones.[3-22]

1.1.2 Anatomy of a Cycloaddition reaction

A typical transition metal catalyzed [2+2+2] cycloaddition reaction involves cyclization of three π-components to form a cyclic product composed of the π-components in a single reaction. [2+2+2] cycloadditions begin with coordination of two of the three π-components to the transition metal (Scheme 1.1). After coordination, an oxidative cyclization occurs to form a five-membered metallacycle **AI**, resulting in the oxidation of the metal center and reduction of the π-components. Coordination of a third π-component to the metal leads to migratory insertion forming seven-membered metallacycle **AII**. Reductive elimination of metallacycle **AII** provides cyclic product and regenerates the metal catalyst.

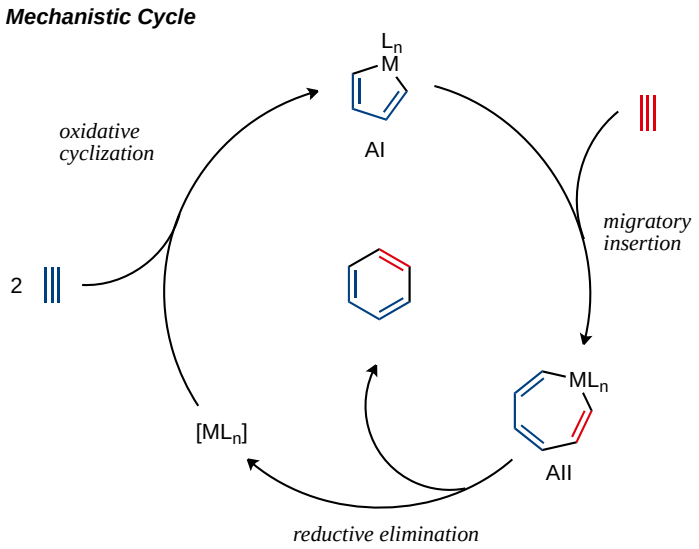

Scheme 1.1 Mechanistic cycle for metal catalyzed [2+2+2] cycloadditions.

1.1.3 π-Components Involved in [2+2+2] Cycloadditions

Alkynes are ubiquitous in metal catalyzed cycloadditions. There are many reasons for this. Many alkynes are commercially available or readily synthesized by a variety of methods so they are abundant and bond strongly to transition metals. Alkene and alkyne metal bonding is described by the Dewar-Chatt model.[76] The Dewar-Chatt model describes donation of C=C π-electrons to an empty metal d_σ orbital. This binding delocalizes electrons over three centers (C, C, M). By analogy with CO binding, donation of alkene π-electrons to metal d_σ orbitals is referred to as a σ bond (Figure 1.1). The σ-bond is accompanied by back donation of metal d_π-electrons to empty alkene π* orbitals at the LUMO level. This type of bonding is referred to conventionally as a π-bond. π-backbonding is necessary for tight binding of alkenes and alkynes to metals as σ-donation alone is often insufficient. As a result, d^0 metals, such as Ti(IV), do not form strong bonds with alkenes.

Alkynes, as opposed to alkenes, have a second set of orthogonal *p*-orbitals that are capable of interacting with metals.[76] A necessary requirement for this type of binding to occur is empty metal d orbitals properly positioned to accept electron density. When coordination of the orthogonal π-system occurs, the alkyne is acting as a 4 electron donor. Not all metals are capable of accepting 4 electrons from an alkyne. For example, with d^6 metals 4 electron binding is rare because of electron repulsion between filled metal d_π orbitals and the second alkyne π-system. Due to increased electronegativity, alkynes are

better π-acceptors than alkenes. This encourages metal backdonation and as a result M–C bond distances are shorter and the bond stronger. Alkene and alkyne metal binding often lengthens the C=C bond. The M–C σ-bond decreases electron density in the C=C through delocalization onto the metal. Delocalization slightly changes the bond order resulting in a weakened and thus lengthened C=C bond. π-backdonation into empty π* orbitals has a more pronounced effect on lengthening the C=C and changing bond order. Cases exist with strongly π-basic metals where back donation is strong enough to approach the extreme of a metallacyclopropane.

Although less common than alkynes, allenes and alkenes are also used in [2+2+2] cycloadditions.[23,24] Typically they replace one of the three alkynes, and in some cases two or three allenes/alkenes are used. Nitriles, isocyanates and imines are the most common nitrogen containing π-components found in [2+2+2] cycloadditions.[7] N-containing π-components are slightly more challenging to successfully incorporate into [2+2+2] cycloadditions in part this is due to the additional binding mode available to N-π-components. Nitriles, isocyanates and imines may bind metals through two electron donation from the nitrogen lone pair, functioning as L-type ligands on the metal or by coordination through the π-system as discussed previously.[25]

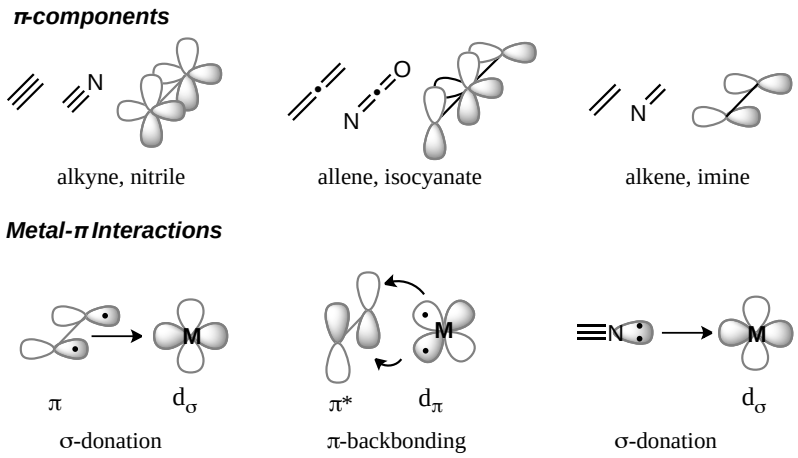

Figure 1.1 Molecular orbital diagrams of π-components involved in metal catalyzed cycloadditions and binding modes.

1.1.4 Regioselectivity in Intermolecular [2+2+2] Cycloadditions

Certainly the first barrier to successful development of an efficient cycloaddition is activation of requisite π-components. The second barrier to successful reaction development is to control selectivity. For a reaction to be efficient and consequently useful, the reaction outcome must be predictable; this is especially an issue in transition metal catalyzed fully intermolecular [2+2+2] cycloadditions.[26] Multiple regioisomeric products are formed dependent on the choice of metal and ligands (Scheme 1.2).[27] Several metallacycles may result from oxidative cyclization of two, identical alkynes as depicted in Scheme 1.2. Steric and electronic nature of the alkyne and the metal•ligand environment are used to control regioselectivity of oxidative cyclization, enabling selective formation of metallacycles, such as **AIII**, **AIV** or **AV**.

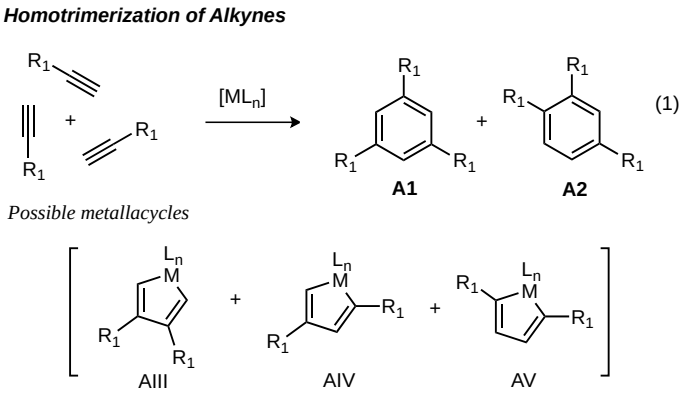

Scheme 1.2 Homotrimerization of alkynes by metal catalyzed [2+2+2] cycloaddition.

Oxidative cyclization of two different unsymmetrical alkynes creates not three but 9 possible metallacycles. With electronically differentiated π-components and proper choice of metal•ligand catalyst the chemo- and regioselectivity can be controlled in the 2-component intermolecular [2+2+2] cycloaddition (Table 1.1).[23,28-33] A challenge and opportunity for fully intermolecular [2+2+2] cycloadditions is to predict and control oxidative cyclization and migratory insertion so that a single arene forms, containing each of the π-components with broad tolerance of functional groups.

Table 1.1 Possible metallacycles formed in 3-component [2+2+2] cycloadditions.

Heterotrimerization of Alkynes

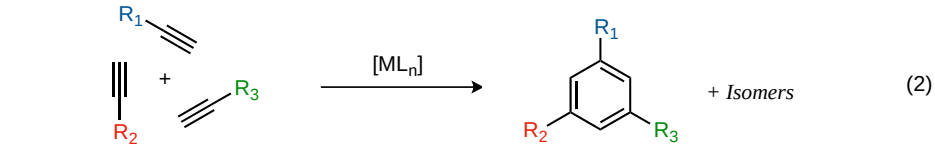

Possible Metallacycles

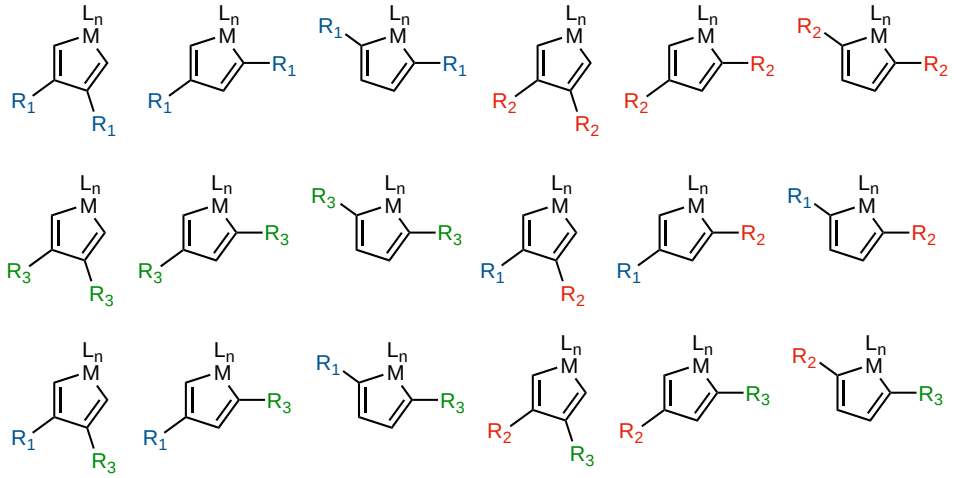

Proper choice of the metal•ligand catalyst with the desired substrates in mind can make possible selective oxidative cyclizations. 3-component cycloadditions represent a significant challenge for control of chemo- and regio selectivity besides the challenge of incorporating each component. In a 3-component cycloaddition the number of possible metallacycles increases to 24 (Table 1.1), and the number of possible products accessible is 37 (Table 1.2). However, control of the three-component fully intermolecular cycloaddition has been found using proper metal/ligand catalysts with select substrates[34] and for the most part, tethering strategies have been used to control selectivity.

Table 1.2 Three-component, fully intermolecular [2+2+2] cycloaddition potential products.

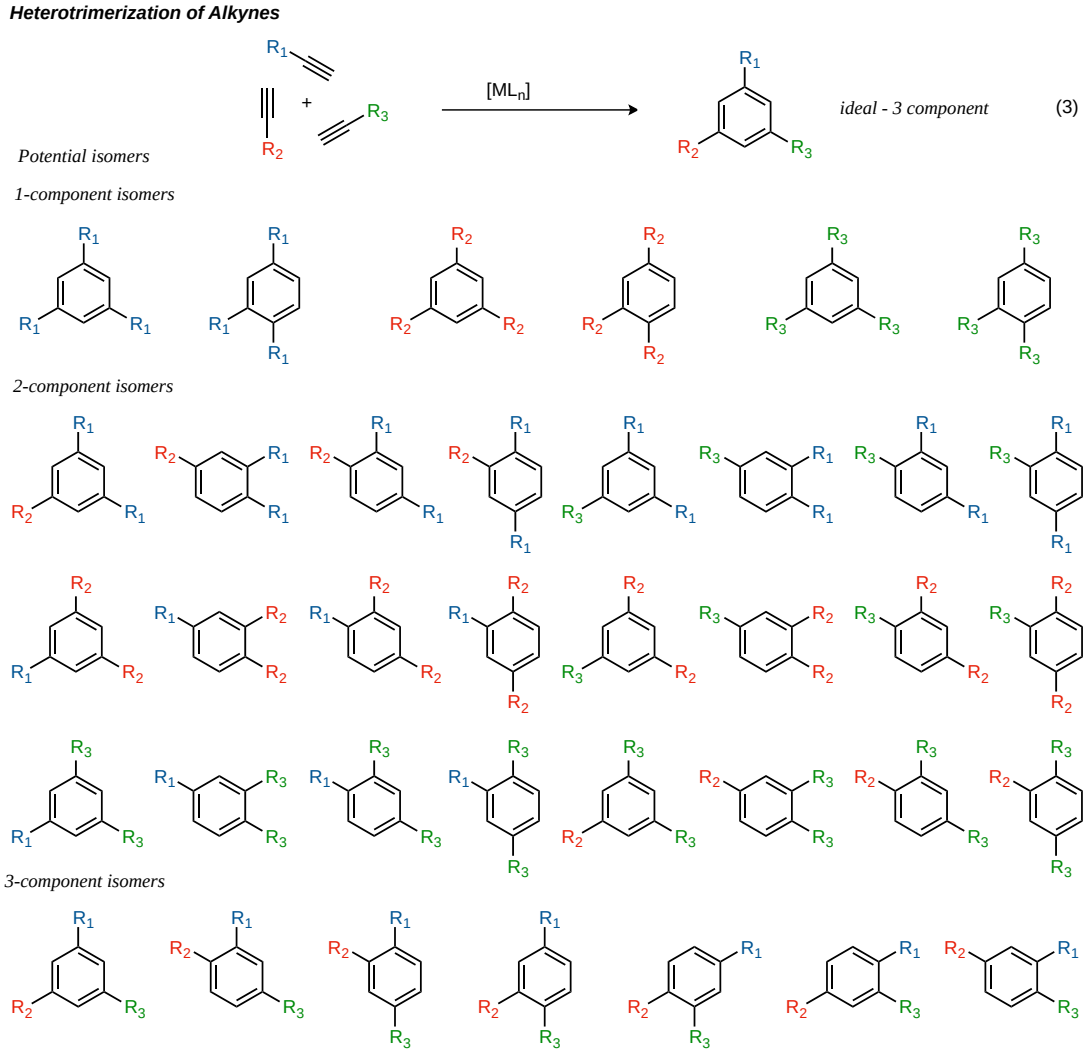

1.1.5 Tethering Strategies Used to Address Selectivity Issues

Tethering π-components to each other is an effective means to control selectivity and promote reactivity in cycloadditions (Scheme 1.3).[3,7,12,14,20,35] This strategy is effective for a wide-range of tether lengths, including simple straight-chain alkane as well as functionalized tethers. Tethers as small as two methylene units and up to at least 14 are effective (eqs 4, 5, 6). Tethers may include heteroatoms (N, O, S), aromatic/non-aromatic rings and geminal substituents–commonly esters, methyls.[36-39] Tethers may be between two or three π-components in fully intramolecular cycloadditions (eqs 7, 8).[40,41] Alkynes, allenes, alkenes, nitriles, isocyanates, and imines have been included as reactive components in tethered cycloadditions.[42] In many cases, less reactive π-components (alkenes, isocyanates, imines) are tethered to

strongly coordinating groups (alkynes) to promote their incorporation by decreasing the entropic activation energy of the coordination event (eq 6).[43-45]

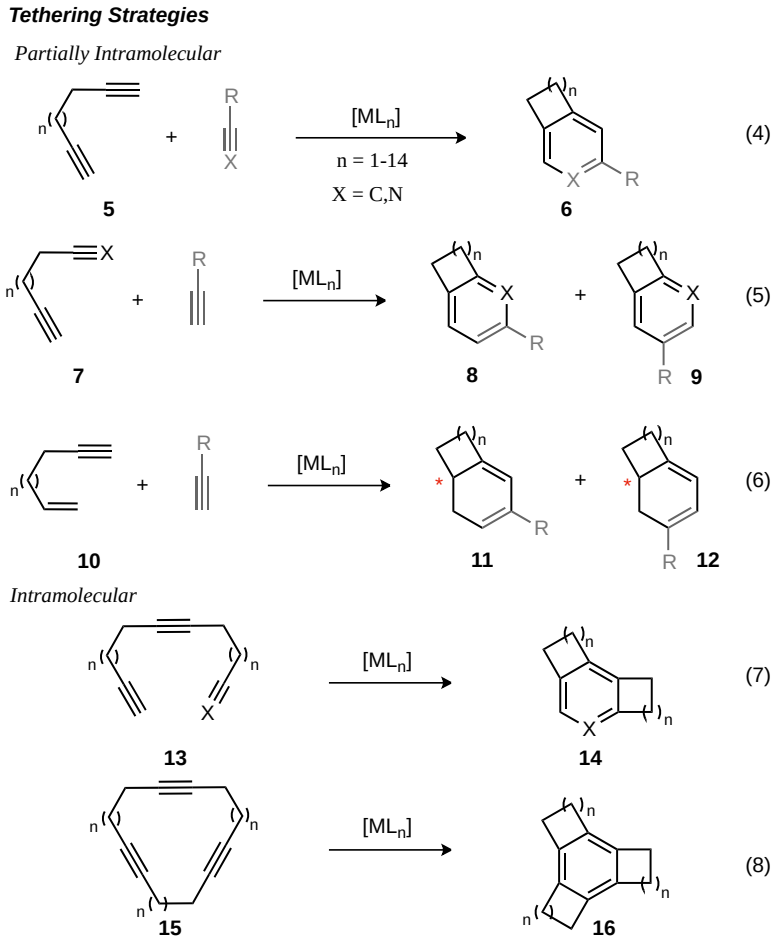

Scheme 1.3 Tethering strategy to solve regioselectivity and reactivity issues in [2+2+2] cycloadditions.

1.1.6 Metal Catalyzed Cycloadditions with Alkynes and Isocyanates

In 1977, Yamazaki reported the first metal catalyzed cycloaddition involving isocyanates and alkynes (Scheme 1.4).[46] In the early 1980's, Hoberg reported similar metal catalyzed [2+2+2] cycloaddition involving isocyanates and alkynes and in fully intermolecular fashion.[47,48] Since then numerous cycloadditions with isocyanates have been developed, establishing isocyanates as competent π-components for cycloadditions reactions. Many metal catalysts are capable of enacting [2+2+2] cycloadditions reactions with isocyanates,[7] including Co,[49,50] Ru, [51] Ni,[33,52-54] Rh,[55] Ir,[56]. The π-component partners may be alkynes, isocyanates, allenes and alkenes and are commonly tethered.

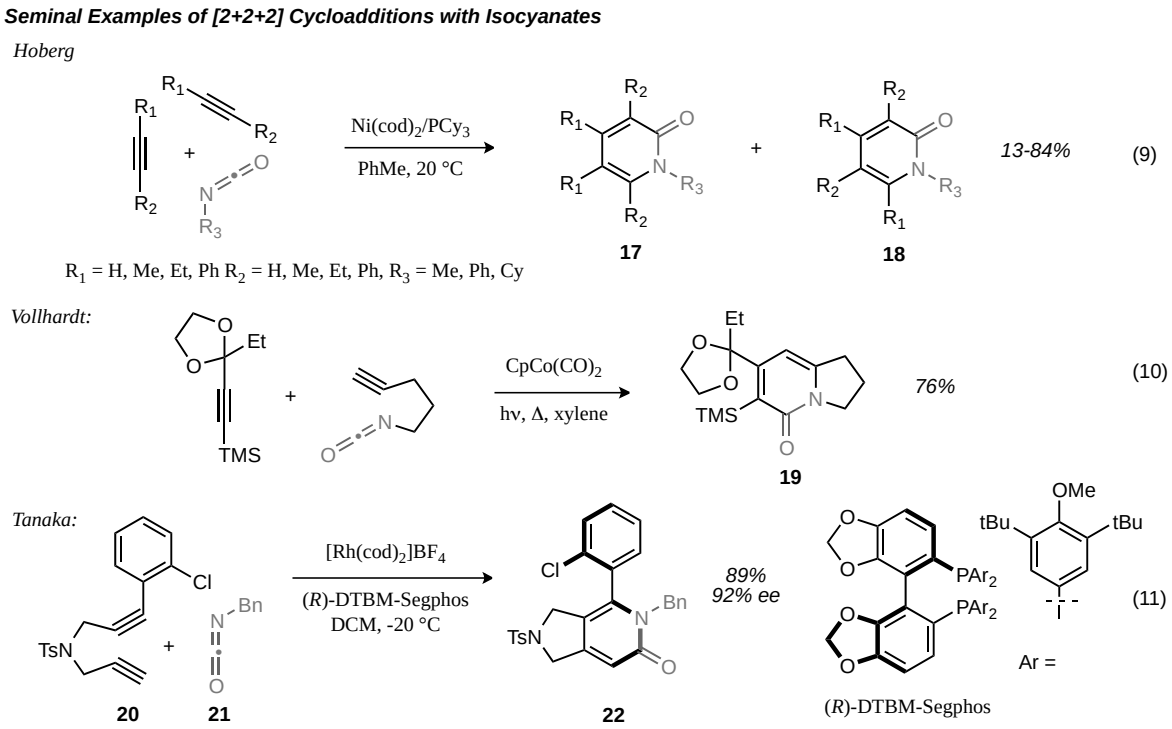

Scheme 1.4 Metal catalyzed [2+2+2] cycloadditions with alkynes and isocyanates.

1.2 Rh(I)-Catalyzed [2+2+2] Cycloadditions to Form N-Heterocycles

1.2.1 Development of Rh(I)-Catalyzed Cycloadditions of Alkene Tethered Isocyanates and Exogenous Alkynes

In 2006, Yu and Rovis reported the Rh(I) catalyzed [2+2+2] cycloaddition of alkenyl isocyanates and exogenous internal, symmetrical alkynes.[57] $[Rh(C_2H_4)_2Cl]_2$ was found to be the most effective precatalyst at 5 mol% of the dimer, and electron-rich phosphines the most effective ligand at 10 mol% loading. With internal alkyl alkyne the expected lactam, bicyclic indolizinone forms in good yields (Table 1.3). Internal aryl alkynes form a vinylogous amide product that is the result of an unusual, unexpected CO migration. The structure of the CO migration product was confirmed by X-ray analysis and many internal symmetrical aryl/alkenyl alkynes facilitate this migration. In general, electron-rich alkynes form indolizinones in higher yields than electron deficient alkynes with this first generation catalyst system.

Table 1.3 Rh(I) catalyzed [2+2+2] cycloaddition of alkenyl isocyanates and internal alkynes.

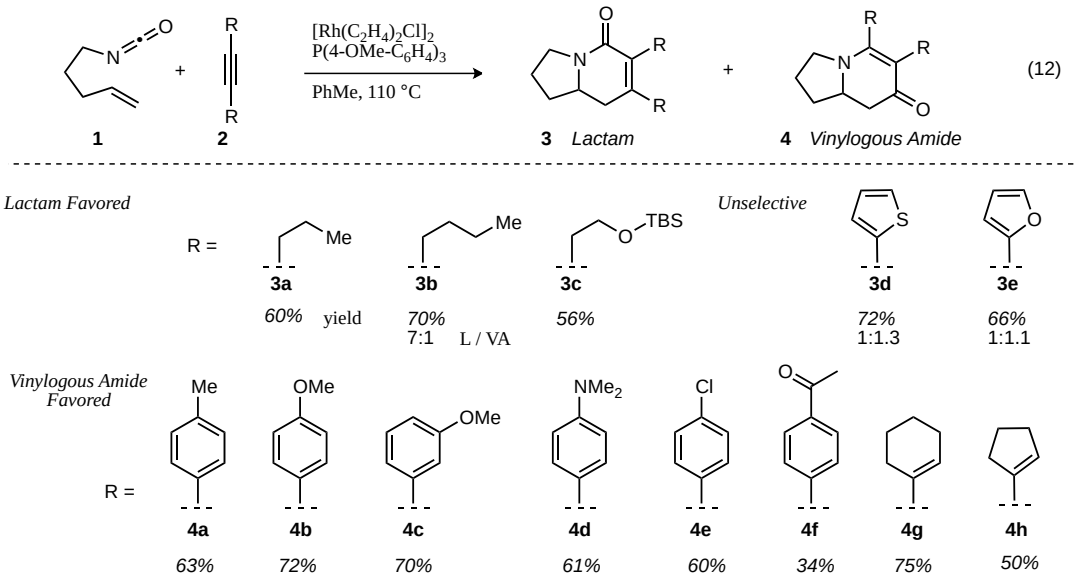

1.2.2 Proposed Mechanistic Cycle

The proposed mechanistic cycle that accounts for formation of lactam, vinylogous amide, 2- and 4-pyridones is shown in Scheme 1.5. Coordination of alkyne and isocyanate occurs with π-components orthogonal to the square plane. Both lactam and vinylogous amide indolizinones are proposed to originate from a single coordination complex that precedes irreversible oxidative cyclization. For lactam **3**, oxidative cyclization results in C–C bond formation to generate 5-membered rhodacycle **AVIIa**. 1,2-Migratory insertion of the tethered alkene provides seven-membered rhodacycle **AVIIIa** and reductive elimination gives lactam product. For vinylogous amide **4**, oxidative cyclization results in C–N bond formation to make rhodacycle **AVIIb**. Due to a prohibitively strained geometry during the coordination event, 1,2-migratory insertion of the alkene does not occur. We propose that a CO migration takes place via four-membered intermediate **AVIIIb**, to form five membered rhodacycle **AIXb**. In rhodacycle **AIXb**, the tethered alkene is properly positioned for migratory insertion to occur and generate seven-membered rhodacycle **AXb**. Reductive elimination provides vinylogous amide **4**. 2- and 4-pyridones are formed as by products and result from competitive coordination and migratory insertion of a second alkyne equivalent prior to tethered alkene migratory insertion. Further details will be provided in chapter 2 of this thesis.

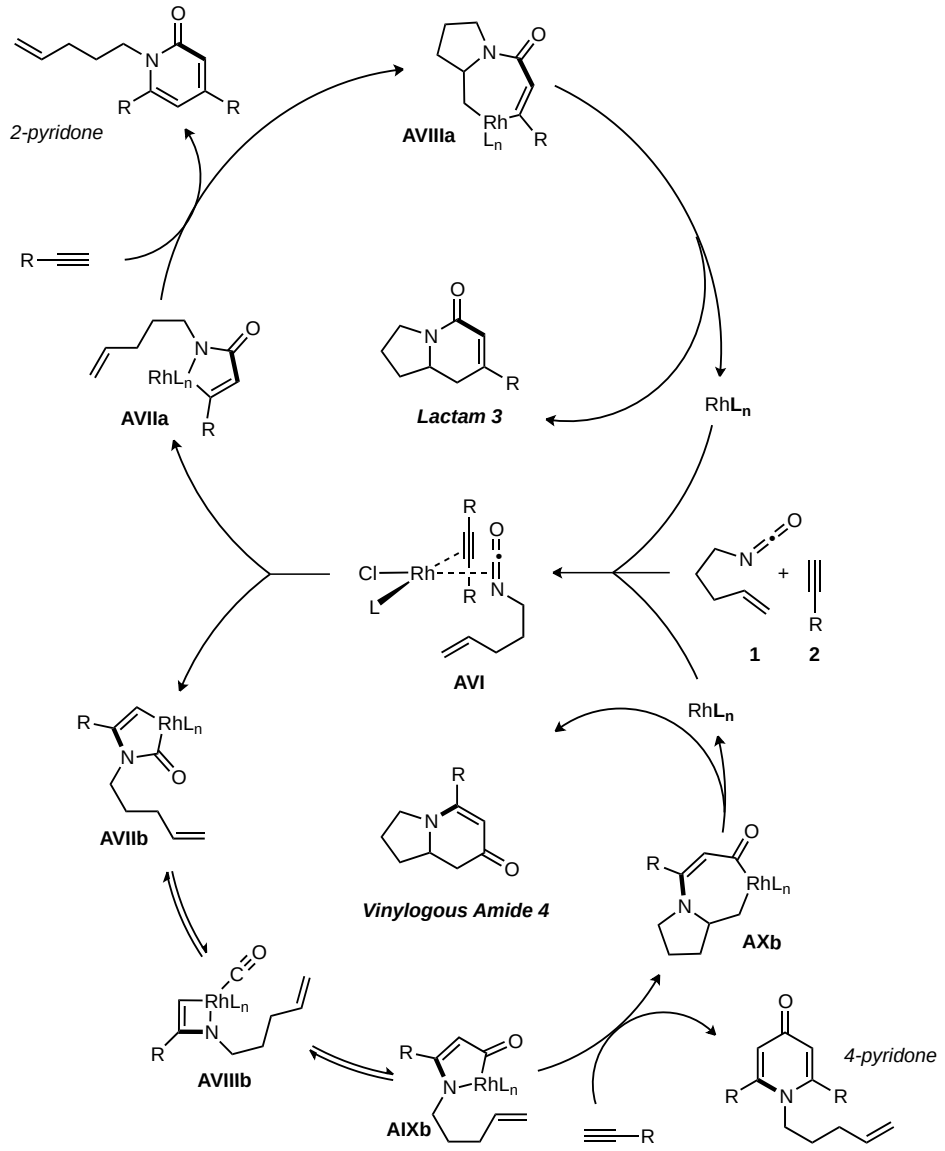

Scheme 1.5 Proposed mechanistic cycle for lactam, vinylogous amide and pyridone products.

1.2.3 Asymmetric Rh(I)-Catalyzed [2+2+2] Cycloadditions of Alkenyl Isocyanates and Alkynes

The enantioselective rhodium catalyzed [2+2+2] cycloaddition of alkenyl isocyanates and terminal alkynes was developed in 2006 (eq 13).[58] Using the first generation catalyst system (RhCl•Phosphine) terminal alkyne dimerization was rapid, making terminal alkynes unusable substrates. Robert Yu explored other phosphorous ligands and found that phosphoramidites suppressed alkyne dimerization. Fortuitously he found Binol- and Taddol-based phosphoramidites rendered the cycloaddition asymmetric (Table 1.4). Excellent enantioselectivities are possible with Taddol-based phosphoramidites, using $[Rh(C_2H_4)_2Cl]_2$ as

precatalyst. Modification of the amine portion of Taddol phosphoramidites affects both product- and enantioselectivity (for further details see chapter 2).

Table 1.4 Ligand screen for asymmetric [2+2+2] Rh-catalyzed cycloaddition.

Ligand Screen

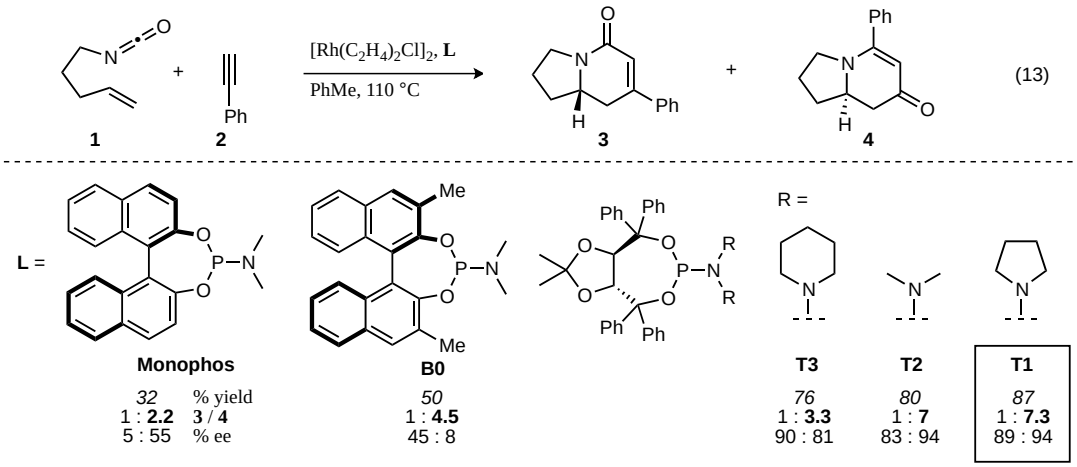

	Monophos	B0	T3	T2	T1
	32	*50*	*76*	*80*	*87*
% yield	1 : **2.2**	1 : **4.5**	1 : **3.3**	1 : **7**	1 : **7.3**
3 / **4**	5 : 55	45 : 8	90 : 81	83 : 94	89 : 94
% ee					

The scope of the asymmetric [2+2+2] cycloaddition with terminal alkynes is quite large. Within the aryl alkynes studied, there is a correlation between the electron-donating ability of the aryl substituents and product selectivity, which will be discussed in greater detail in the next chapter. Electron-rich aryl acetylenes tend to favor vinylogous amide **4** while electron-deficient aryl acetylenes shift preference to lactam **3** (Table 1.5). Small and electron deficient alkyl alkynes favor lactam while large alkyl substituents provide no selectivity. A wide range of substrate based product selectivities is observed, but some selectivities are high (>20:1). Enantioselectivities with Taddol based phosphoramidites ranges from very good (**3g**, 80%) to excellent (**3l**, 95%). The broad substrate tolerance and good to excellent selectivities make this an attractive route to the synthesis of indolizidinone natural products.

Table 1.5 Substrate scope of [2+2+2] cycloaddition with terminal alkynes.

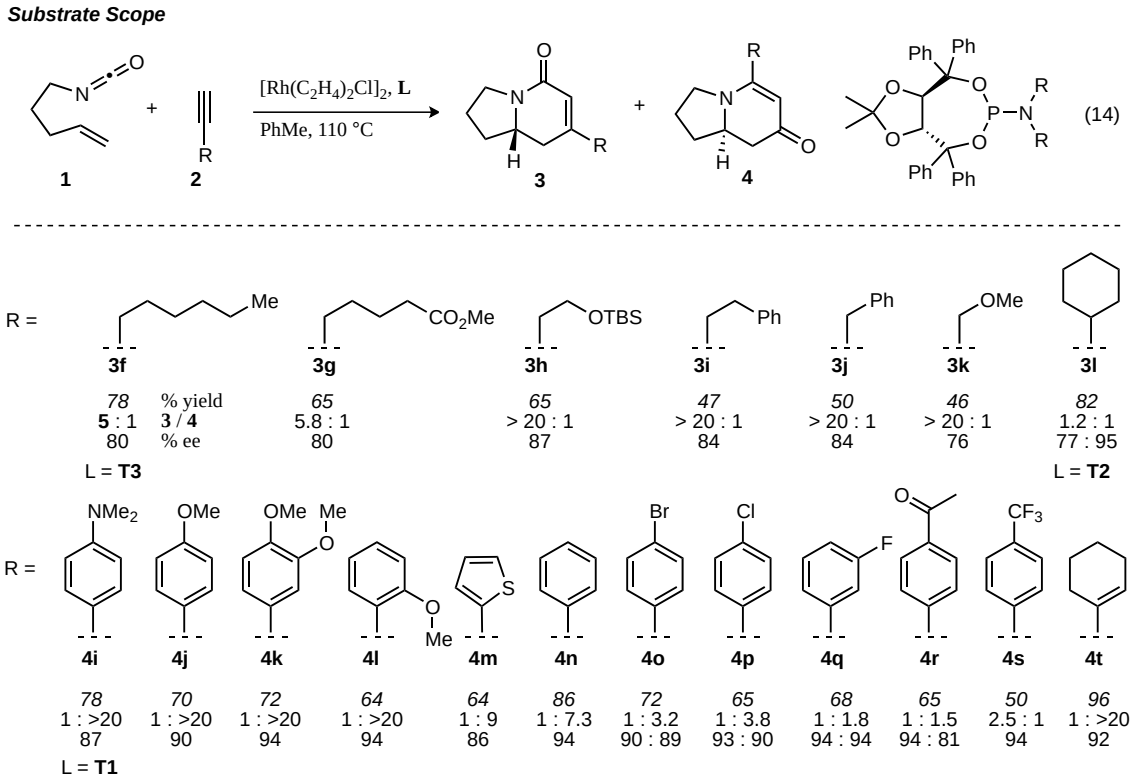

1.2.4 Asymmetric Synthesis of Bicyclic Amidines with Alkenyl Carbodiimides

In 2008, Yu and Rovis discovered that carbodiimides reversed the product selectivity preference seen with terminal aryl acetylenes from favoring lactam (with isocyanates) to vinylogous amide (with carbodiimides).[59] The aryl substituent of the alkene tethered carbodiimide was found to have an effect of product selectivity with electron-deficient N-aryl substituents providing a greater bias for bicyclic amidine **24** over vinylogous amidine **25** (Table 1.6). o-Anisidine carbodiimide **23b** was found to have the best blend of yield (68%), product-(3.8:1) and enantioselectivity (98%) and was chosen for the exploration of alkyne tolerance. Electron-deficient aryl and alkyl acetylenes overwhelmingly favor amidine **24** while only electron-rich alkynes show a preference for vinylogous amidine **25**. This trend in product selectivity parallels what is seen with isocyanates; specifically electron-rich alkynes provide more of the CO migration product, vinylogous amide **4**. Enantioselectivities with m-Xylyl Taddol phosphoramidite **T4** are universally excellent in the transformation of carbodiimides to bicyclic amidines.

Table 1.6 Substrate scope of [2+2+2] cycloaddition with carbodiimides and terminal alkynes.

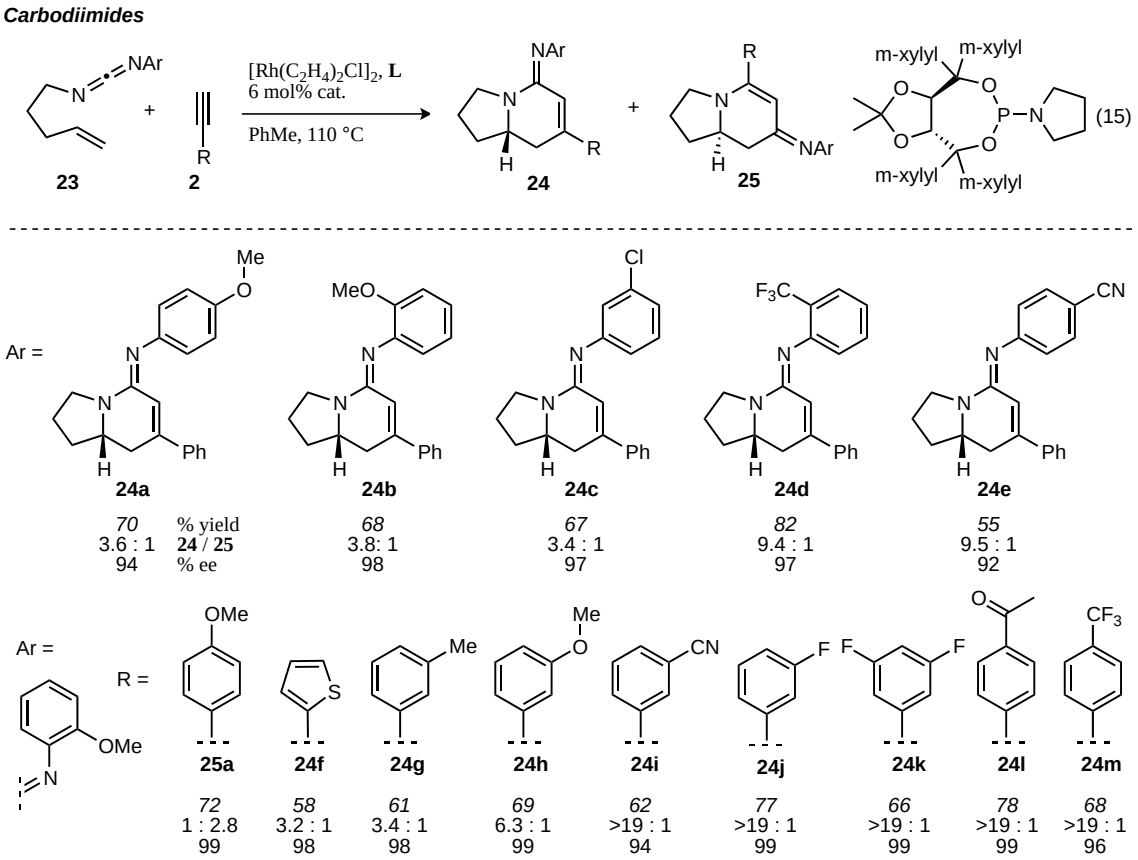

1.2.5 Enantioselective Synthesis of Tetrasubstituted Stereocenters by [2+2+2] Cycloaddition

In 2008, Lee and Rovis developed Rh(I) catalyzed [2+2+2] cycloadditions of 1,1-disubstituted alkenyl isocyanates and alkynes to form tetrasubstituted stereocenters enantioselectively.[60] Numerous indolizidine and quinolizidine natural products contain tetrasubstituted carbon stereocenters making this an important synthetic contribution. Taddol-based phosphoramidites provide high-levels of enantioinduction when paired with $[Rh(C_2H_4)_2Cl]_2$ as the precatalyst (Table 1.7). Alkyl acetylenes provide lactam products in moderate to good product selectivities and excellent enantioselectivities. p-OMe-phenyl acetylene enables excellent product and enantioselectivity for vinylogous amide **4**, simplifying analysis. Modification of the alkene substituents with p-OMe-phenyl acetylene revealed the cycloaddition tolerates a variety of alkenyl substituents, including sterically hindered functionalities.

Table 1.7 Substrate scope with 1,1-disubstituted alkenyl isocyanates and alkynes.

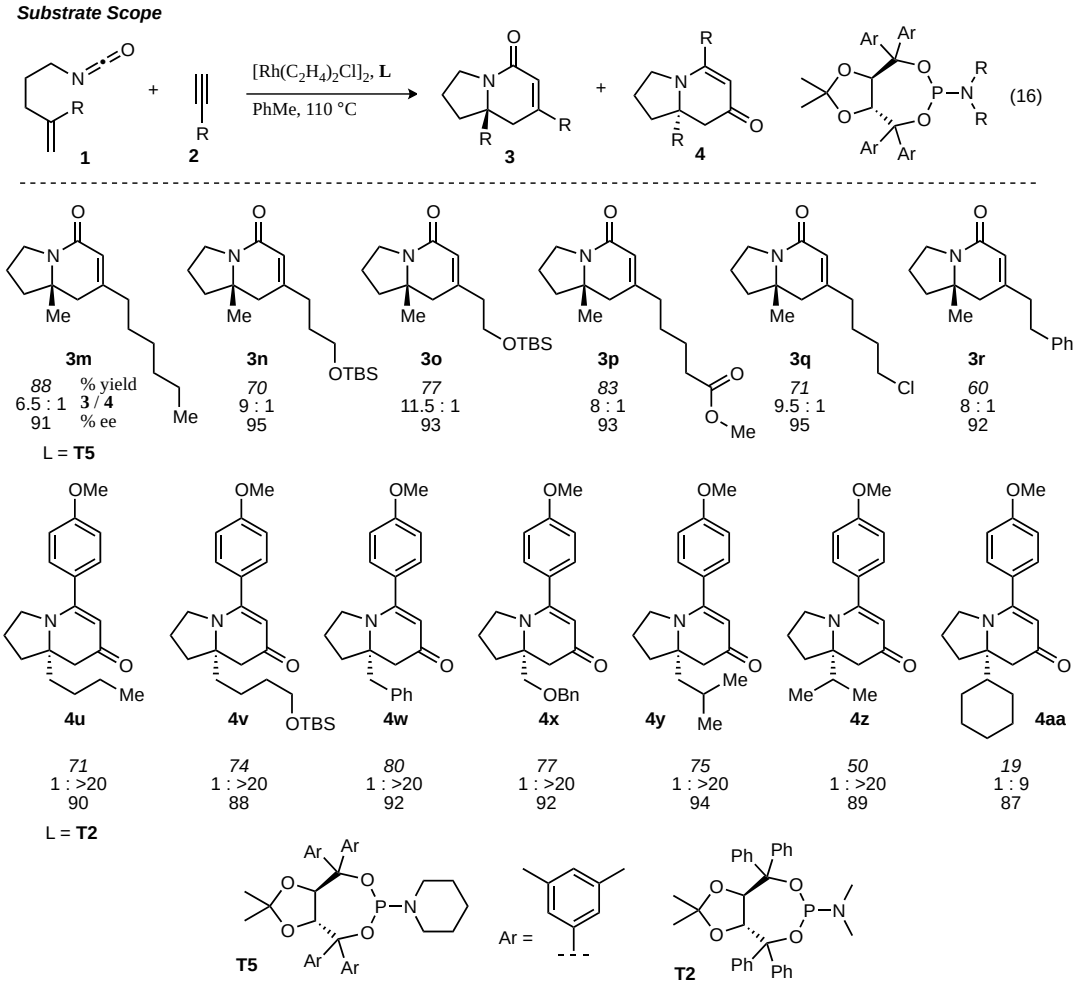

1.2.6 Regioselective Insertion of Unsymmetrical Internal Alkynes

In 2009, Friedman and Rovis reported the regioselective insertion of unsymmetrical internal alkynes in the Rh(I) catalyzed [2+2+2] cycloaddition with alkenyl isocyanates. Both steric and electronic natural were found to affect the regioselectivity of 1,2-insertion (Table 1.8). Large and electron-rich alkyne substituents insert distal to the metal in metallacycle formation while small electron-deficient substituents tend to insert proximal. Substrate scope is broad; product and enantioselectivities are moderate with Binol-based phosphoramidite (Guiphos). Enantioselectivities and reactivity is enhanced when 1,1-disubstituted dienyl isocyanates are used.[61]

Table 1.8 Substrate scope with alkenyl isocyanates and internal unsymmetrical alkynes.

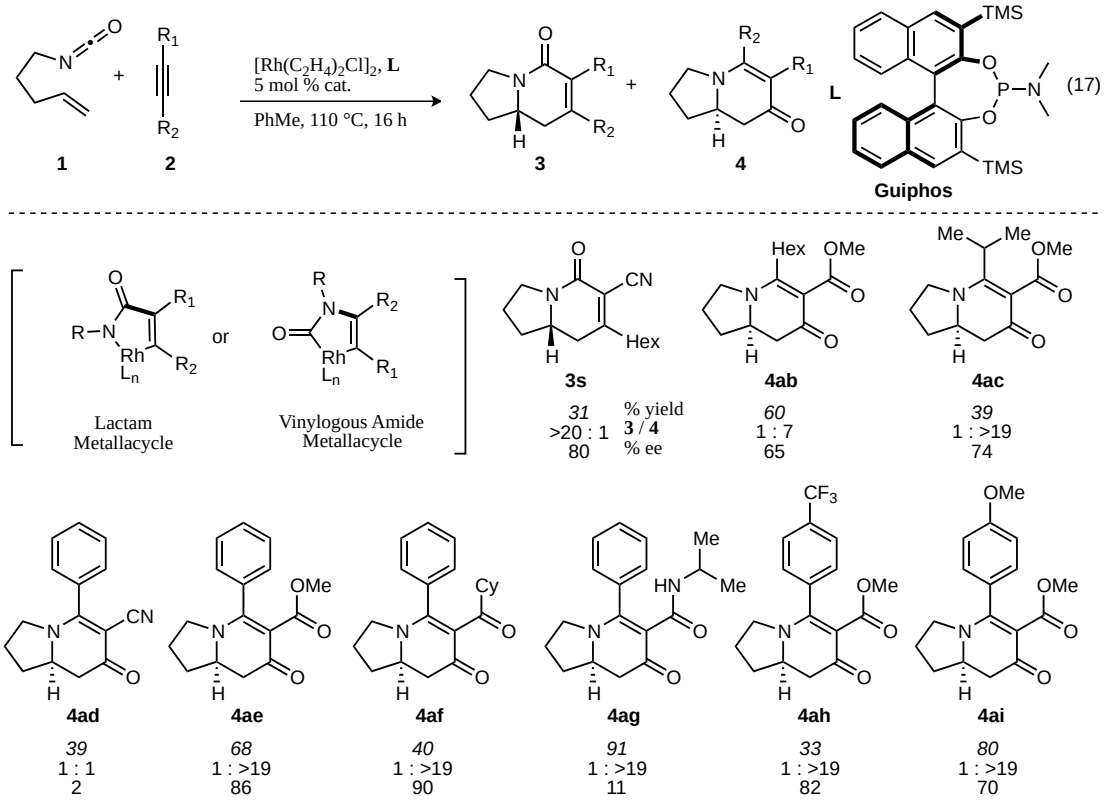

1.2.7 Intermolecular Cycloadditions Form 2- and 4-Pyridones

In 2009, Oberg, Lee and Rovis reported the regio- and chemoselective fully intermolecular [2+2+2] cycloaddition of isocyanates and alkynes (Table 1.9).[32] The optimal catalyst was found to be *t*-Butyl Biaryl Phosphoramidite **B1** in a screen of five catalysts. A variety of acetylenes are tolerated in the cycloaddition with benzyl isocyanate. Electron-deficient aryls (*m*-F-Aryl **26b**, 46%) provide slightly lower yields than electron-releasing substituents (*p*-OMe-Aryl **26c**, 88%) in the formation of 2-pyridones. Alkenyl substrates provide high yields (cyclohexenyl **26g**, 92%). Alkyl acetylene participate but yields are generally lower (19-38%). Variation of the isocyanate revealed the cycloaddition tolerates alkyl, aryl and sterically large isocyanates. The formation of 4-pyridones increased when aryl isocyanates were used; electron-deficient, *p*-CF_3-aryl isocyanate gave the highest ratio of 4-pyridone (34 : 30, **26** : **27**). This suggests that oxidative cyclization is possible with even electron deficient isocyanates.

Table 1.9 Investigation of cycloaddition to form 2- and 4-pyridones.

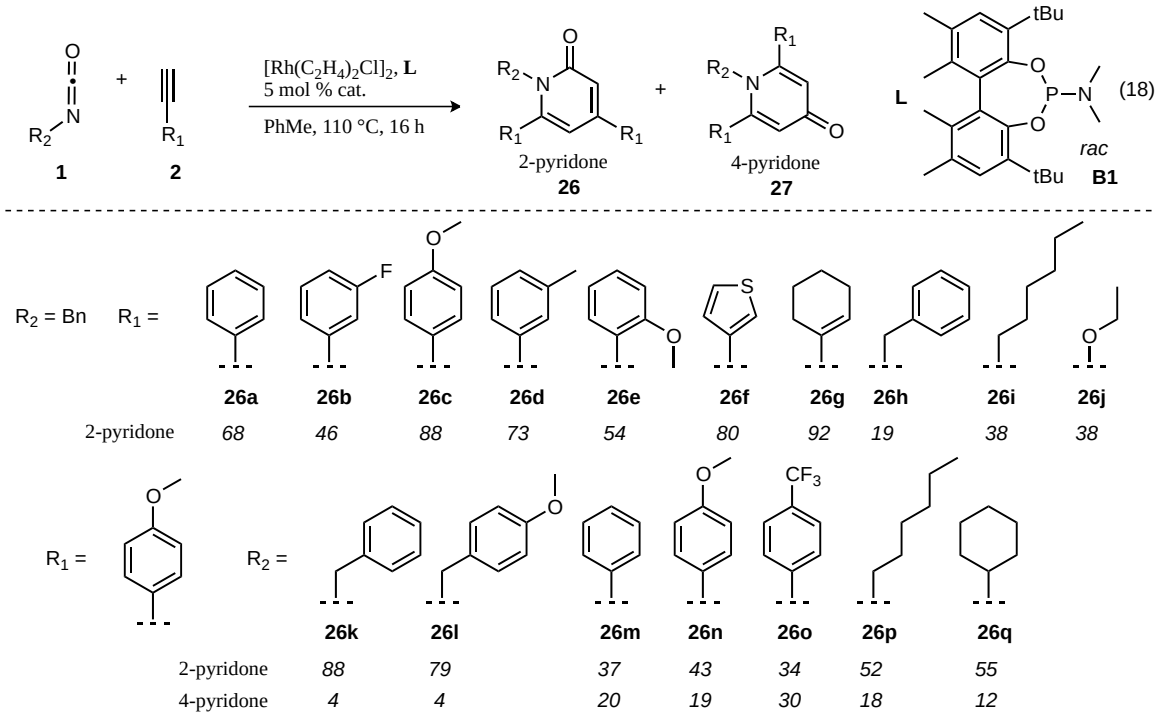

1.2.8 Rh(I)-Catalyzed Cycloadditions with Dienyl Isocyanates and Alkynes

In 2009 Yu, Keller-Friedman and Rovis reported the highly asymmetric, Rh(I) catalyzed [4+2+2] cycloaddition of dienyl isocyanates and alkynes (Table 1.10).[62] Initial results found that two cycloadducts were accessible with $Rh(C_2H_4)_2Cl$•phosphoramidite catalysts and their formation was dependent on the E/Z geometry of the diene. The major product in all cases is the 5,8-azocine **28**; this product is favored with >19:1 E diene geometry. A mixture of 1.4:1 E/Z geometry provides a mixture of the 5,8-azocine and the 5,6-lactam products. The optimal catalyst is *m*-xylyl Taddol phosphoramidite **T5**, which provides the azocine product in good yields and exquisite enantioselectivity. The reaction tolerates a variety of alkyl and electron-deficient aryl acetylenes. Good yields are seen with all alkyl acetylenes investigated while *p*-Br-phenyl acetylene **28g** provides modest yield. Notably the protected phthalimide **28e** is the only N-protecting group found to be tolerated by the reaction conditions at the time of publication.

Table 1.10 Ligand screen and substrate scope for Rh(I) catalyzed [4+2+2] cycloaddition.

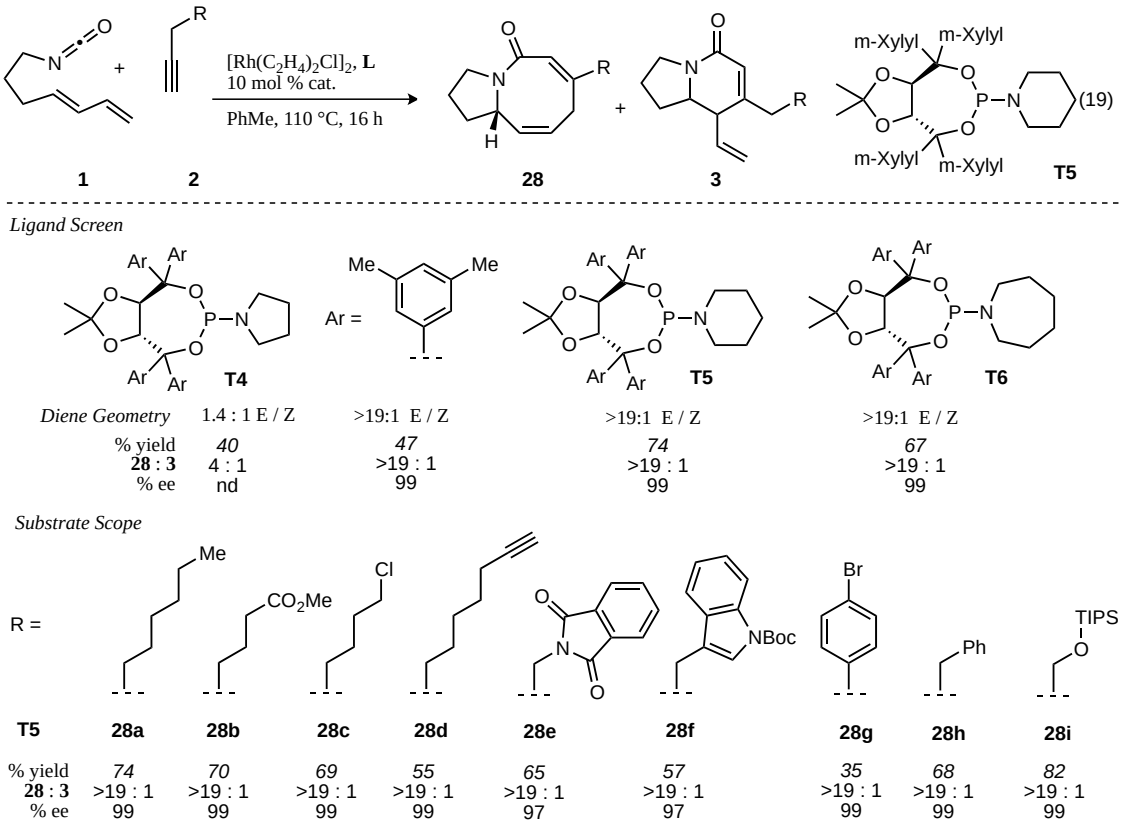

A competition experiment between dienyl isocyanates **1ai** and **1aii** with 1-octyne (ratio of **1ai**:**1aii**:1-octyne is 1:1:1) provides a 2:1 ratio of azocine products **28ai** and **28aii**, suggesting the mechanism may involve oxidative cyclization of the diene and isocyanate followed by migratory insertion of the alkyne and reductive elimination (Scheme 1.6). We propose this pathway because the ratio of products formed in 2:1. This indicates substitution at the 3 position of the diene affects the product determining step in the catalytic cycle, which would presumably be oxidative addition of the isocyanate and diene rather than alkyne. Oxidative cyclization of alkyne and isocyanate would not involve the diene. Therefore substitution at the dienyl 3 position would have no effect on cyclization and product distribution would be expected to be 1:1, assuming oxidative cyclization is irreversible.

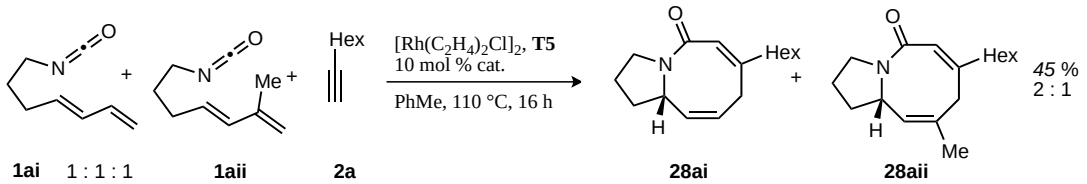

Scheme 1.6 Competition experiment between dienyl isocyanates.

1.2.9 Ligand Effects on Product Selectivity

In 2009, Yu, Lee, Malik and Rovis found biaryl-based phosphoramidites affected product selectivity with alkyl alkynes.[63] Until this discovery, there was an alkyne substrate bias in the determination of product selectivity, where alkyl alkynes favored the lactam product and aryl/alkenyl alkynes provided vinylogous amide. A screen of biaryl-based phosphoramidites found these ligands override the substrate bias of product selectivity (Table 1.11). *t*-Bu-biaryl phosphoramidite **B1** provides modest product selectivity (1:6.2) for vinylogous amide **4** with 1-octyne while maintaining excellent enantioselectivity (91%).

Table 1.11 Ligand screen for vinylogous amide formation with biaryl phosphoramidites.

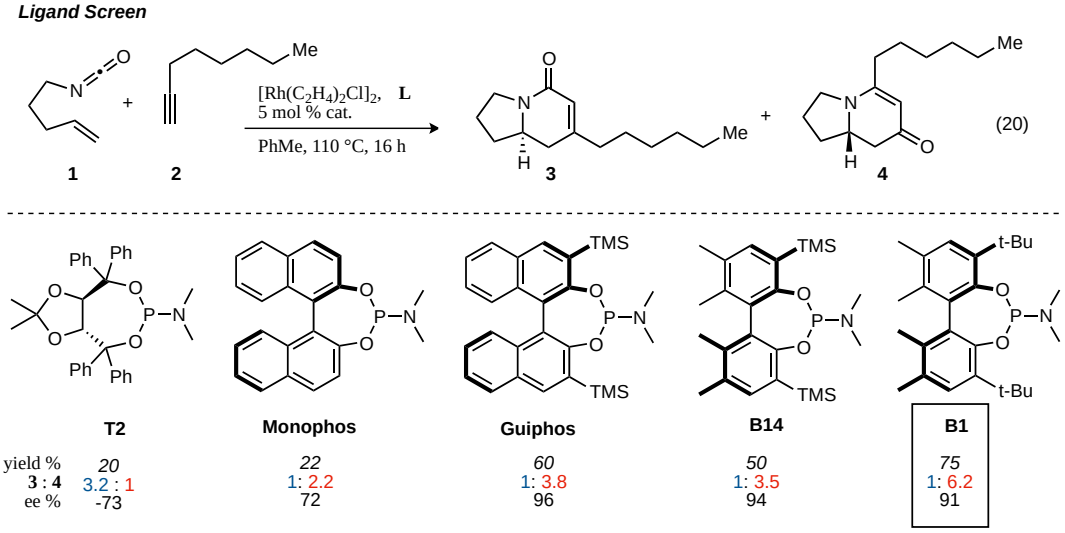

The substrate scope of the transformation is quite large (Table 1.12). A variety of functional groups are tolerated including: chlorides, esters, silyl alcohols, pendant alkynes, Weinreb amides, and aryls. Modest product selectivities (1.6:1 to 1: >20) for the vinylogous amide product were found with a variety of functionalized terminal alkyl-alkynes. Large alkyl alkynes (**4av**) give enhanced product selectivity and small, electron-deficient alkynes (**4ar**) provide poor selectivity. Enantioselectivities for long chain alkyl alkynes are all excellent. Silyl propargyl alcohol **4ar** and di- and trisubstituted alkyl alkynes (**4av, 4aw**) give slightly lower enantioselectivities.

Table 1.12 Substrate scope of [2+2+2] with terminal alkyl alkynes.

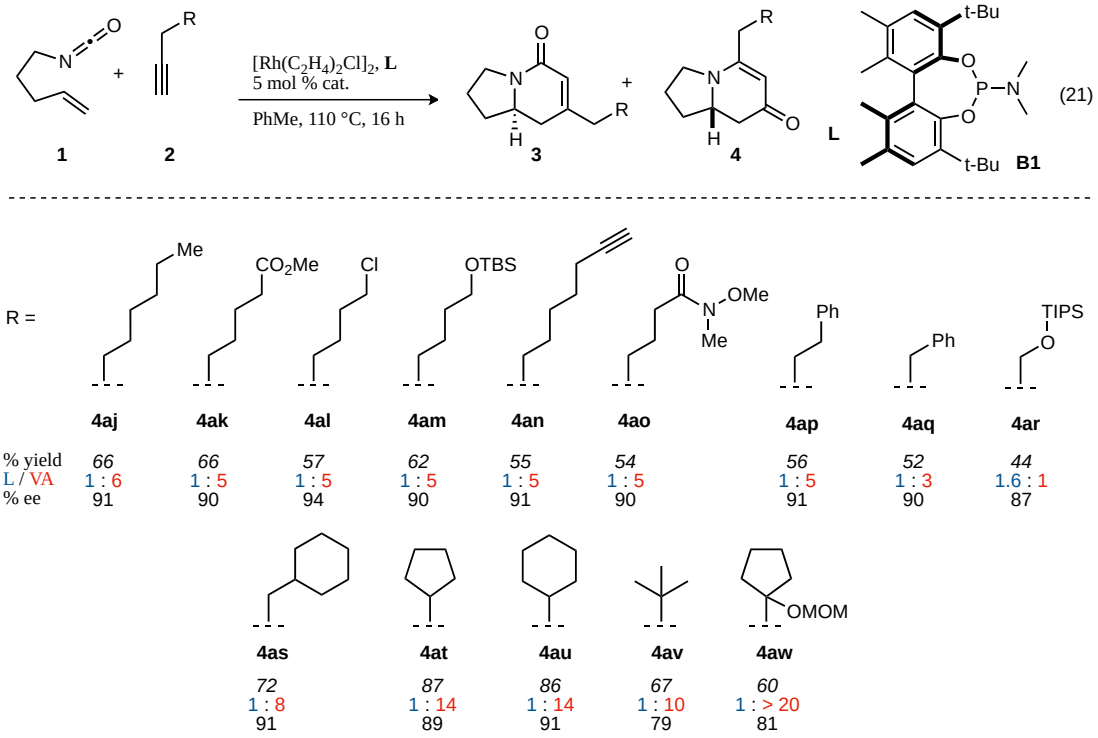

1.2.10 Additive Affects Enantioinduction with Biaryl Phosphoramidites and Tolanes

In 2009, Oinen and Rovis reported on the ability of weakly coordinating ligands to affect enantioinduction in the $Rh(C_2H_4)_2Cl$•Guiphos catalyzed [2+2+2] cycloaddition of alkenyl isocyanates and tolanes (diarylacetylenes, Table 1.13).[64] They found that pyridines with electron-withdrawing substituents at the meta position (**A2**, **A4**) increased enantioselectivity with a number of tolanes. Pyridine (**A1**) coordinates too strongly to rhodium, halting catalysis. They proposed coordination of the pyridine ligand to Rh(III) during 1,2-migratory insertion increased rhodium facial discrimination and increased enantioinduction. Finally, the addition of an additive slowed reactivity and in some cases resulted in lower yields for the reaction.

Table 1.13 Additive effects on enantioselectivity with tolanes.

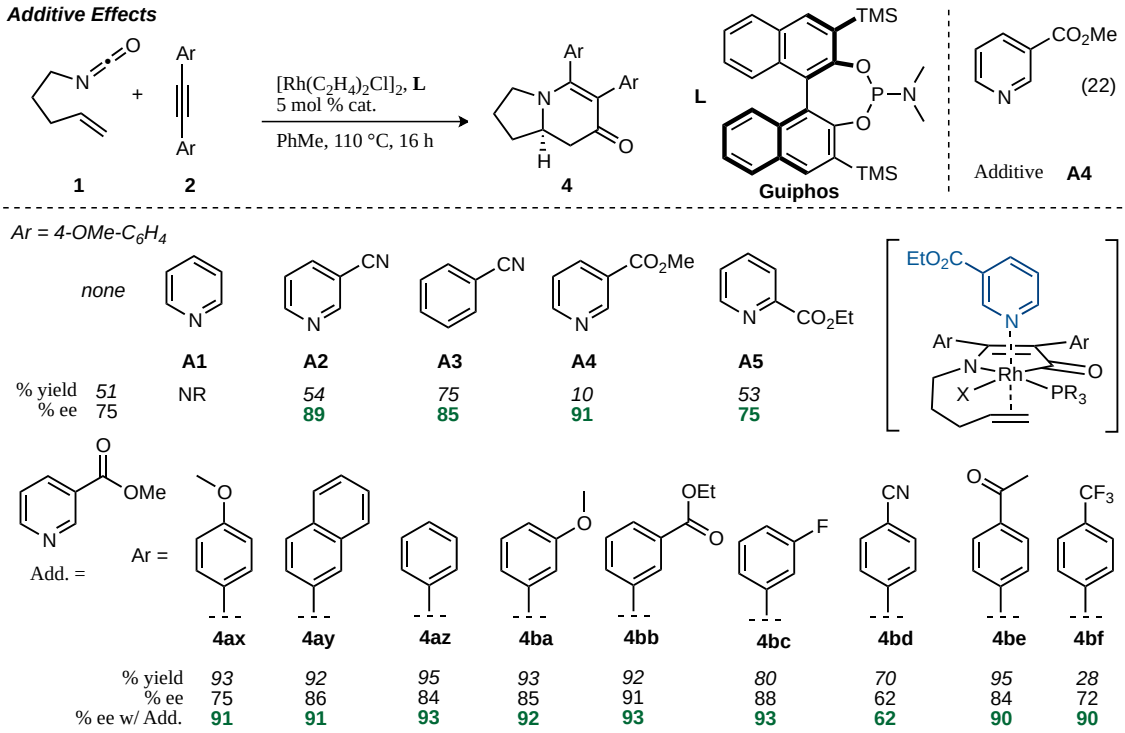

1.2.11 Application of [2+2+2] to Natural Product Synthesis

Yu and Rovis showcase the ability of Rh(I) catalyzed [2+2+2] cycloadditions to efficiently and selectively synthesize biologically active indolizidine and quinolizidine natural products through the asymmetric syntheses of (+)-lasubine II and indolizidine alkaloid (–)-209D. Indolizidine and quinolizidine alkaloids are incredibly abundant natural products.[65-74] A few selected indolizidine and quinolizidine containing natural products are shown in Figure 1.2.

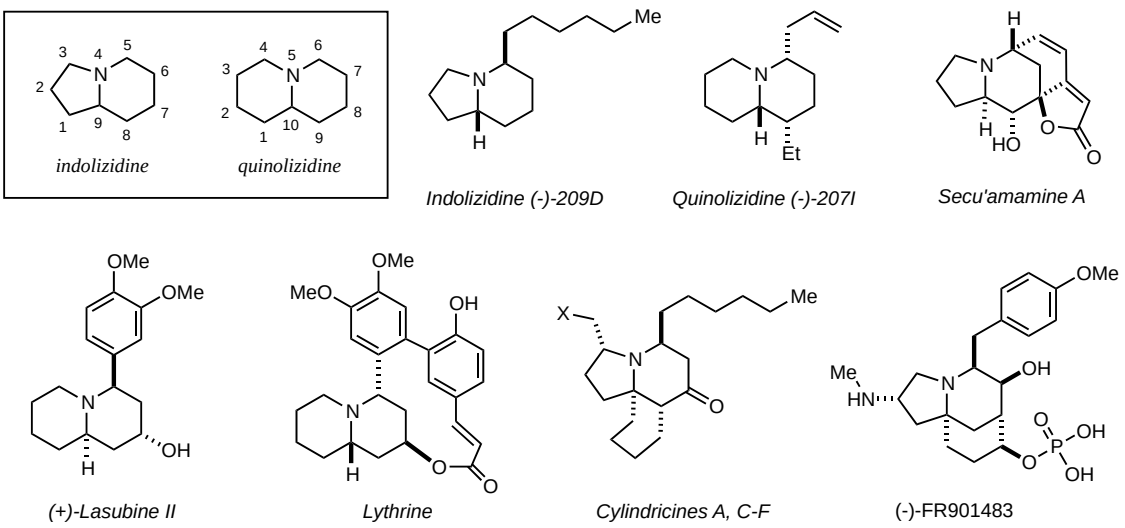

Figure 1.2 Indolizidine and quinolizidine containing natural products.

(+)-lasubine II and (–)-indolizidine 209D were synthesized using enantioselective RhCl•Phosphoramidite catalyzed [2+2+2] cycloadditions as the key step in the respective syntheses. Both cycloadditions proceed with moderate to good yields and product selectivities, and enantioselectivities in both cases are excellent. The total synthesis of (+)-lasubine II was completed with a Rh(I)-catalyzed cycloaddition of hexenyl isocyanate and 3,4-dimethoxy phenyl acetylene to yield exclusively vinylogous amide quinolizinone **4k** in 45% yield and 98% ee (Scheme 1.7). Palladium on carbon catalyzed hydrogenation of quinolizinone **4k** in methanol reduces both the alkene and ketone of the vinylogous amide to provide amino alcohol **29** in good yield as a single diastereomer.[58] Treatment of amino alcohol **29** with triphenylphosphine, *p*-NO_2-benzoic acid and diethylazodicarboxylate (DEAD) forms the p-NO_2-aryl ester with an inversion of alcohol stereochemistry. This ester is saponified by potassium carbonate and aqueous methanol to make the corresponding alcohol. The Mitsunobu protocol completes the synthesis, forming (+)-lasubine II in four steps and 18% overall yield.

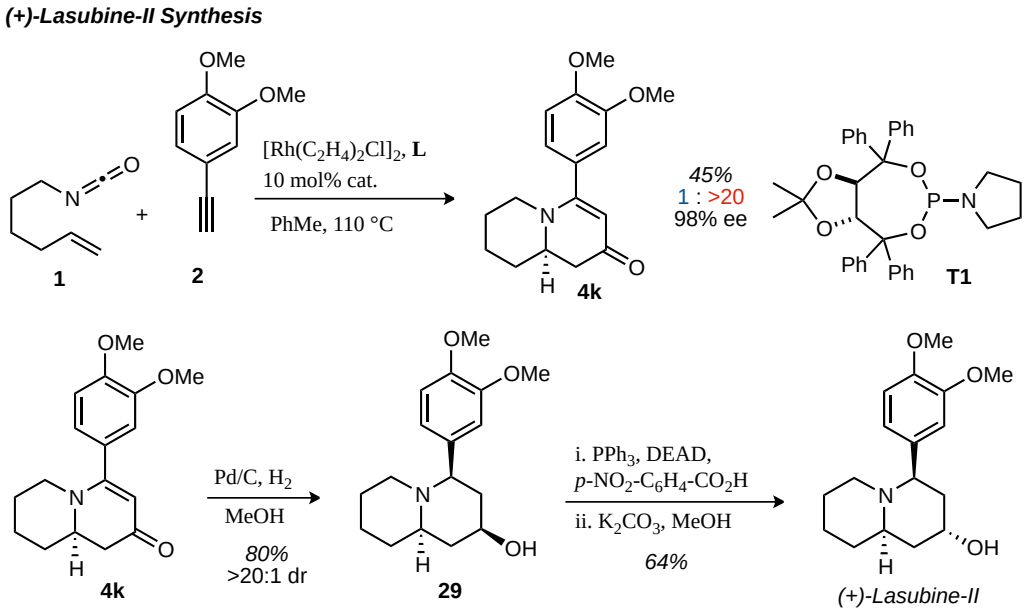

Scheme 1.7 Total synthesis of Lasubine-II.

(–)-indolizidine 209D was synthesized by Rh(I)-catalyzed cycloaddition of pentenyl isocyanate and 1-octyne (Scheme 1.8). Cycloaddition provided indolizinone **4k** in 66% yield, 1:6 product selectivity (**3**:**4**) and 91% ee for the vinylogous amide. Palladium/carbon catalyzed hydrogenation of indolizidinone **4aj** in methanol yields amino-alcohol **30** as a single diastereomer in good yield.[63] Resultant alcohol **30** is treated with thiocarbonyldiimidazole and 4-dimethylaminopyridine (DMAP) neat at 50 ˚C to form the imidazole thioester, which is treated with azobisisobutyronitrile (AIBN) as a radical initiator and tributyl tin hydride to effect a radical Barton-McCombie deoxygenation. The Barton-McCombie deoxygenation protocol furnishes indolizidine alkaloid (–)-209D in 5 linear steps and 24% overall yield.

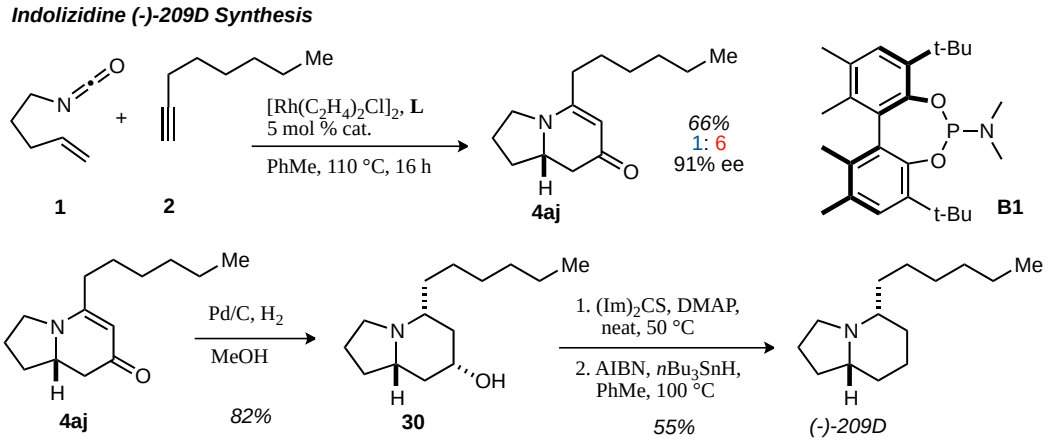

Scheme 1.8 Total synthesis of indolizidine (–)-209D.

1.2.12 Rh(I)-Catalyzed [4+2] Cycloaddition of α,β-unsaturated Imines and Isocyanates

In 2011 Oberg and Rovis reported a highly asymmetric $Rh(C_2H_4)_2Cl$•phosphoramidite catalyzed [4+2] cycloaddition of α,β-unsaturated imines and isocyanates to form pyrimidinones (Table 1.14, eq 23). [75] No reaction occurs in either the absence of catalyst or in the presence of phosphoramidite alone. Furthermore, neither $Ni(cod)_2$ with tetramethylethylenediamine (TMEDA) or $Rh(PPh_3)_3Cl$ (Wilkinson's catalyst) provide appreciable amounts of product. Of the Rh(I)•phosphoramidites investigated $Rh(C_2H_4)_2Cl$•**B1** was found to be the optimal catalyst providing pyrimidinones in good yields and excellent enantioselectivities. Moderate yields (49-65%) and excellent enantioselectivity (89-91%) is seen when the N-substituent of the imine is an electron-rich, electron-deficient or neutral aryl. Alkyl substituents are also well tolerated with increases in ee seen for benzyl, phenethyl and *p*-MeO-benzyl (93-94%); however, cyclohexyl **31d** provides a decrease in enantioselectivity (75%). Alkyl isocyanates provide higher yields and enantioselectivities than phenyl acetylene. Aryl, electron-rich aryl, sterically hindered aryl, electron-deficient aryl, furyl, alkenyl and alkyl substitution are tolerated at the pyrimidinone 4-position (R_2). Slight decreases in yield and ee are seen with straight chain and substituted alkyl substituents. Electron-deficient *p*-NO_2-aryl **32n** shows a small decrease in yield. This represents a highly efficient and selective method to pyrimidinones that complements the traditional Biginelli approach.

Table 1.14 Rh(I)-catalyzed [4+2] cycloaddition substrate scope.

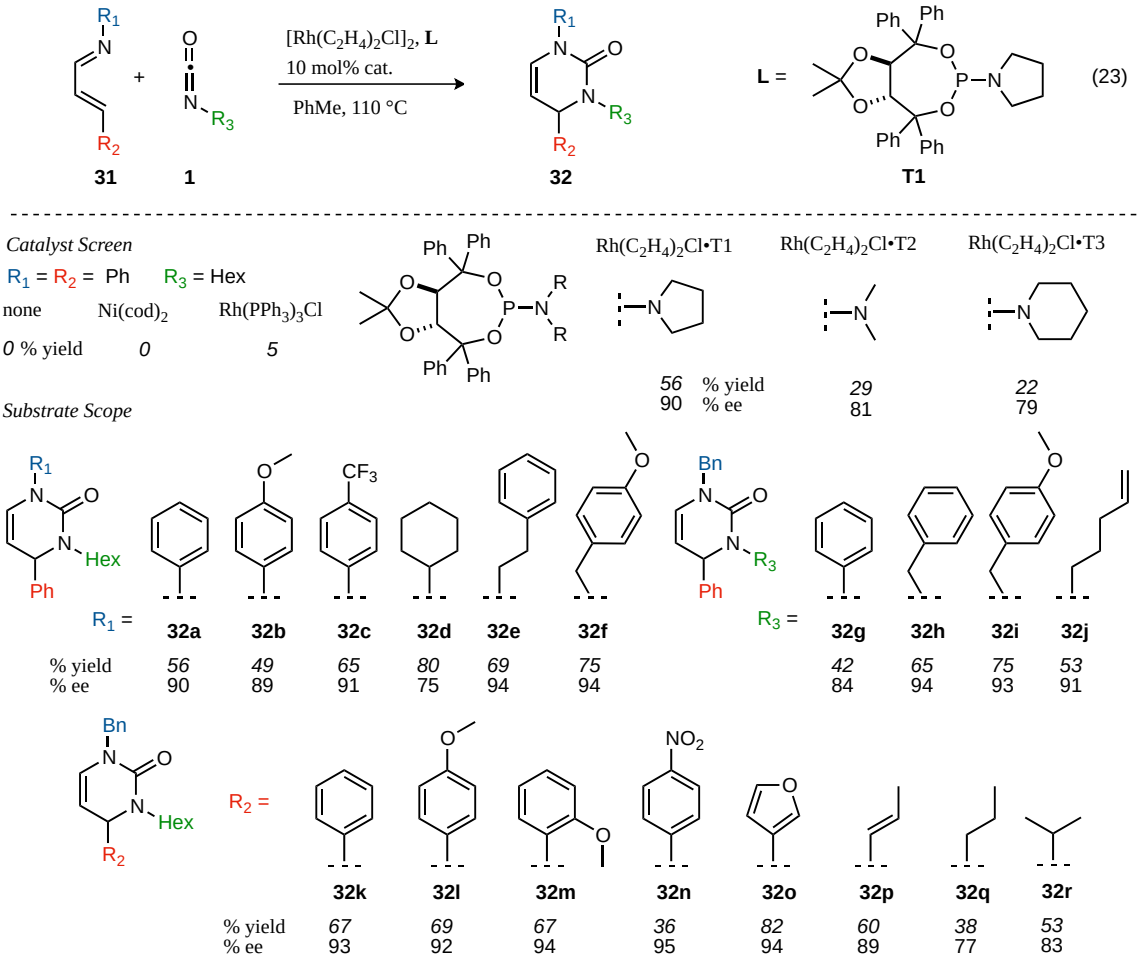

The rhodium catalyzed [4+2] reaction is proposed to occur via imine-isocyanate oxidative cyclization, followed by an η^1-η^3-η^1 shift and reductive elimination to form the pyrimidinone products (eq 24). Product selectivity is proposed to be determined during oxidative cyclization and enantioselectivity is controlled by the phosphoramidite ligand on Rh during the η^1-η^3-η^1 shift.

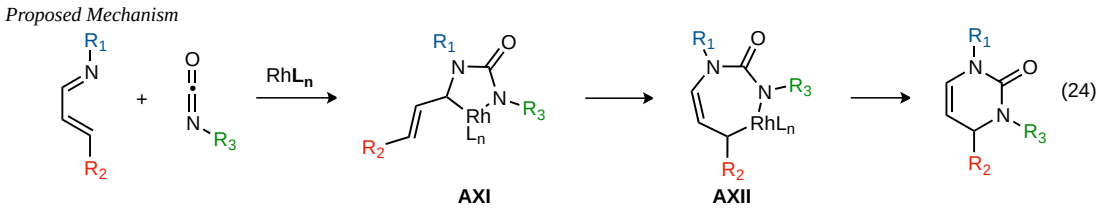

1.3 Conclusion

In summary, this chapter serves as an introduction to the possibilities and challenges of metal catalyzed cycloadditions to form nitrogen containing heterocycles. A history of metal catalyzed asymmetric N-heterocycle synthesis in the Rovis group has been provided. This history set the stage for further exploration of Rh(I)-catalyzed [2+2+2] cycloadditions in the context of complex natural products with highly reactive alkynes.

1.4 References

(1) Wender, P. A.; Bi, F. C.; Gamber, G. G.; Gosselin, F.; Hubbard, R. D.; Scanio, M. J. C.; Sun, R.; Williams, T. J.; Zhang, L. *Pure Appl. Chem.* **2002**, *74*, 25–32.

(2) Reppe, V. W.; Shweckendiek, W. J. *Justus Liebigs Annalen Der Chemie* **1948**, *560*, 104–116.

(3) Vollhardt, K. P. C. *Acc. Chem. Res.* **1977**, *10*, 1–8.

(4) Vollhardt, K. P. C. *Angew. Chem. Int. Ed.* **1984**, *23*, 539–556.

(5) Lautens, M.; Klute, W.; Tam, W. *Chem. Rev.* **1996**, *96*, 49–92.

(6) Saito, S.; Yamamoto, Y. *Chem. Rev.* **2000**, *100*, 2901–2915.

(7) Varela, J. A. J.; Saá, C. C. *Chem. Rev.* **2003**, *103*, 3787–3801.

(8) Nakamura, I.; Yamamoto, Y. *Chem. Rev.* **2004**, *104*, 2127–2198.

(9) Gandon, V.; Aubert, C.; Malacria, M. *Curr. Org. Chem.* **2005**, *9*, 1699–1712.

(10) Kotha, S.; Brahmachary, E.; Lahiri, K. *Eur. J. Org. Chem.* **2005**, *2005*, 4741–4767.

(11) Louie, J. *Curr. Org. Chem.* **2005**, *9*, 605–623.

(12) Chopade, P. R.; Louie, J. *Adv. Synth. Catal.* **2006**, *348*, 2307–2327.

(13) D'Souza, D. M.; Müller, T. J. J. *Chem. Soc. Rev.* **2007**, *36*, 1095–1108.

(14) Heller, B.; Hapke, M. *Chem. Soc. Rev.* **2007**, *36*, 1085–1094.

(15) Shibata, T. T.; Tsuchikama, K. K. *Org. Biomol. Chem.* **2008**, *6*, 1317–1323.

(16) Garcia-Rubin, S.; Varela, J. A.; Castedo, L.; Saa, C. *Chem.-Eur. J.* **2008**, *14*, 9772–9778.

(17) Galan, B. R.; Rovis, T. *Angew. Chem. Int. Ed.* **2009**, NA–NA.

(18) Perreault, S.; Rovis, T. *Chem. Soc. Rev.* **2009**, *38*, 3149–3159.

(19) Friedman, R. K.; Oberg, K. M.; Dalton, D. M.; Rovis, T. *Pure Appl. Chem.* **2009**, *82*, 1353–1364.

(20) Domínguez, G. G.; Pérez-Castells, J. J. *Chem. Soc. Rev.* **2011**, *40*, 3430–3444.

(21) Broere, D.; Ruijter, E. *Synthesis* **2012**, *44*, 2639–2672.

(22) Shibata, Y.; Tanaka, K. *Synthesis* **2012**, *44*, 323–350.

(23) Macomber, D. W.; Verma, A. G.; Rogers, R. D. *Organometallics* **1988**, *7*, 1241–1253.

(24) Aubert, C.; Llerena, D.; Malacria, M. *Tetrahedron Lett.* **1994**, *35*, 2341–2344.

(25) Hoberg, H.; Korff, J. *J. Organomet. Chem.* **1978**, *150*, C20–C22.

(26) Wu, C.-Y.; Lin, Y.-C.; Chou, P.-T.; Wang, Y.; Liu, Y.-H. *Chem. Commun.* **2011**, *40*, 3748.

(27) Komine, Y.; Miyauchi, Y.; Kobayashi, M.; Tanaka, K. *Synlett* **2010**, *2010*, 3092–3098.

(28) Ikeda, S.-I.; Kondo, H.; Arii, T.; Odashima, K. *Chem. Commun.* **2002**, 2422–2423.

(29) Ura, Y.; Sato, Y.; Shiotsuki, M.; Kondo, T.; Mitsudo, T.-A. *J. Mol. Catal. A-Chem.* **2004**, *209*, 35–39.

(30) Duong, H. A.; Louie, J. *J. Organomet. Chem.* **2006**, *62*, 7552–7559.

(31) Hilt, G.; Paul, A.; Harms, K. *J. Org. Chem.* **2008**, *73*, 5187–5190.

(32) Oberg, K. M.; Lee, E. E.; Rovis, T. *Tetrahedron* **2009**, *65*, 6–6.

(33) Miura, T.; Morimoto, M.; Murakami, M. *J. Am. Chem. Soc.* **2010**, *132*, 15836–15838.

(34) Ogoshi, S.; Nishimura, A.; Ohashi, M. *Org. Lett.* **2010**, *12*, 3450–3452.

(35) Maryanoff, B. E.; Zhang, H. C. *ARKIVOC* **2007**, *12*, 7–35.

(36) Tanaka, K.; Takeishi, K.; Noguchi, K. *J. Am. Chem. Soc.* **2006**, *128*, 4586–4587.

(37) Tanaka, K.; Suda, T.; Noguchi, K.; Hirano, M. *J. Org. Chem.* **2007**, *72*, 2243–2246.

(38) Komine, Y.; Kamisawa, A.; Tanaka, K. *Org. Lett.* **2009**, *11*, 2361–2364.

(39) Kobayashi, M.; Suda, T.; Noguchi, K.; Tanaka, K. *Angew. Chem. Int. Ed.* **2011**, *50*, 1664–1667.

(40) Aalbersberg, W.; Vollhardt, K. P. C. *Tetrahedron Lett.* **1979**, 1939–1942.

(41) Shibata, T.; Uchiyama, T.; Yoshinami, Y.; Takayasu, S.; Tsuchikama, K.; Endo, K. *Chem. Commun.* **2012**, *48*, 1311.

(42) Garcia, P.; Evanno, Y.; George, P.; Sevrin, M.; Ricci, G.; Malacria, M.; Aubert, C.; Gandon, V. *Eur. J. Org. Chem.* **2012**, *18*, 4337–4344.

(43) Yamamoto, Y.; Kinpara, K.; Ogawa, R.; Nishiyama, H.; Itoh, K. *Eur. J. Org. Chem.* **2006**, *12*, 5618–5631.

(44) Shibata, T.; Otomo, M.; Tahara, Y.-K.; Endo, K. *Chem. Commun.* **2008**, *6*, 4296.

(45) Obora, Y.; Satoh, Y.; Ishii, Y. *J. Org. Chem.* **2010**, *75*, 6046–6049.

(46) Hona, P.; Yamazaki, H. *Tetrahedron Lett.* **1977**, *15*, 1333–1336.

(47) Hoberg, H.; Schaefer, D. *J. Organomet. Chem.* **1982**, *238*, 383–387.

(48) Hoberg, H.; Oster, B. W. *Synthesis* **1982**, 4, 324–325.

(49) Earl, R. A.; Vollhardt, K. P. C. *J. Am. Chem. Soc.* **1983**, *105*, 6991–6993.

(50) Boñaga, L. V. R.; Zhang, H.-C.; Gauthier, D. A.; Reddy, I.; Maryanoff, B. E. *Org. Lett.* **2003**, *5*, 4537–4540.

(51) Yamamoto, Y.; Takagishi, H.; Itoh, K. *Org. Lett.* **2001**, *3*, 2117–2119.

(52) Tsuda, T.; Tobisawa, A. *Macromolecules* **1994**, *27*, 5943–5947.

(53) Tsuda, T.; Tobisawa, A. *Macromolecules* **1995**, *28*, 1360–1363.

(54) D'Souza, B. R.; Louie, J. *Org. Lett.* **2009**, *11*, 4168–4171.

(55) Tanaka, K.; Wada, A.; Noguchi, K. *Org. Lett.* **2005**, *7*, 4737–4739.

(56) Onodera, G.; Suto, M.; Takeuchi, R. *J. Org. Chem.* **2012**, *77*, 908–920.

(57) Yu, R. T.; Rovis, T. *J. Am. Chem. Soc.* **2006**, *128*, 2782–2783.

(58) Yu, R. T.; Rovis, T. *J. Am. Chem. Soc.* **2006**, *128*, 12370–12371.

(59) Yu, R. T.; Rovis, T. *J. Am. Chem. Soc.* **2008**, *130*, 3262–3263.

(60) Lee, E. E.; Rovis, T. *Org. Lett.* **2008**, *10*, 1231–1234.

(61) Friedman, R. K.; Rovis, T. *J. Am. Chem. Soc.* **2009**, *131*, 10775–10782.

(62) Yu, R. T.; Friedman, R. K.; Rovis, T. *J. Am. Chem. Soc.* **2009**, *131*, 13250–13251.

(63) Yu, R. T.; Lee, E. E.; Malik, G.; Rovis, T. *Angew. Chem. Int. Ed.* **2009**, *48*, 2379–2382.

(64) Oinen, M. E.; Yu, R. T.; Rovis, T. *Org. Lett.* **2009**, *11*, 4934–4937.

(65) Michael, J. P. *Nat. Prod. Rep.* **2001**, *18*, 520–542.

(66) Michael, J. *Nat. Prod. Rep.* **2004**, *21*, 625–649.

(67) Daly, J. W.; Spande, T. F.; Garraffo, H. M. *J. Nat. Prod.* **2005**, *68*, 1556–1575.

(68) Michael, J. *Nat. Prod. Rep.* **2005**, *22*, 603–626.

(69) Michael, J. P. *Beilstein J. Org. Chem.* **2007**, *3*, 27.

(70) Michael, J. *Nat. Prod. Rep.* **2007**, *24*, 191–222.

(71) Michael, J. P. *Nat. Prod. Rep.* **2008**, *25*, 139–165.

(72) Samoylenko, V.; Ashfaq, M. K.; Jacob, M. R.; Tekwani, B. L.; Khan, S. I.; Manly, S. P.; Joshi, V. C.; Walker, L. A.; Muhammad, I. *J. Nat. Prod.* **2009**, *72*, 92–98.

(73) Samoylenko, V.; Ashfaq, M. K.; Jacob, M. R.; Tekwani, B. L.; Khan, S. I.; Manly, S. P.; Joshi, V. C.; Walker, L. A.; Muhammad, I. *J. Nat. Prod.* **2009**, 8.

(74) Pivavarchyk, M.; Smith, A. M.; Zhang, Z.; Zhou, D.; Wang, X.; Toyooka, N.; Tsuneki, H.; Sasaoka, T.; McIntosh, J. M.; Crooks, P. A.; Dwoskin, L. P. *Eur. J. Pharmacol.* **2011**, *658*, 132–139.

(75) Oberg, K. M.; Rovis, T. *J. Am. Chem. Soc.* **2011**, *133*, 4785–4787.

(76) Crabtree, R. H. *The Organometallic Chemistry of the Transition Metals*, 3rd Edition; John Wiley & Sons, New York, 2001.

CHAPTER 2

Rh(I)-Catalyzed [2+2+2] Cycloadditions of Alkenyl Isocyanates and Strained Cyclic Alkynes

2.1 Introduction

2.1.1 Rh(I)-Catalyzed [2+2+2] Cycloadditions

Asymmetric rhodium(I) catalyzed [2+2+2] cycloadditions of alkenyl isocyanates and alkynes are established, efficient methods used to access indolizidine and quinolizidine natural products, as demonstrated by Rovis and coworkers.[1,2] Thus, it was the goal of this project to explore the limits of the methodology by using unexplored, highly reactive, functionalized cycloalkynes to synthesize complex natural products. In 2008, diarylacetylenes[3,4] and arylpropiolates[5] served as the most reactive π-components tested in the methodology; the most complicated natural products synthesized then were quinolizidine (+)-lasubine II and indolizidine alkaloid (–)-209D. Our ambitious aim was to use strained cyclic alkynes to access the complex, biologically active natural products, acosmine and dasycarpumine (Figure 2.1).[6]

2.1.2 Acosmine and Dasycarpumine

Brewed into bitter tea from stems and roots of *acosmium panamense* or *acosmium dasycarpum*, tall trees found from Venezuela to Mexico, acosmine and dasycarpumine have been used as traditional medicines to treat a myriad of maladies including: inflammation, skin diseases, neurological and cardiovascular disorders, malaria, and syphilis (Figure 2.1).[6] Recently, acosmine was found to be effective in treatment of diabetes in rats, serving to increase insulin secretion.[7] Diaza-adamantane compounds have demonstrated affinity for muscarinic acetocholine receptors and exhibit diuretic properties.[6] These uncommon diaza-adamantane alkaloids have received attention recently by the scientific community for their pharmacological properties.

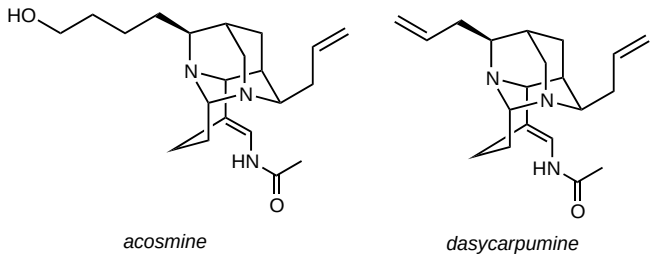

Figure 2.1 Acosmine and Dasycarpumine Natural Products.

In addition to their biological significance, acosmine and dasycarpumine are desirable synthetic targets because they possess a unique molecular architecture. Acosmine has two nitrogens embedded in an adamantane skeleton, six stereocenters (five are contiguous), and four fused rings. This architecture poses unique synthetic challenges that provide an opportunity to develop new reactivity. Furthermore, the application of the rhodium(I) catalyzed [2+2+2] cycloaddition to the synthesis of acosmine will push the limits of this methodology by coupling a functionalized, highly reactive cyclooctyne **2** with hexenyl isocyanate **1** to form tricyclic 6,6,8-quinolizinone **4** (Scheme 2.1, eq. 1). Tricyclic quinolizinone **4** contains all but one carbon of the carbon skeleton of acosmine. Several challenges presented by this route include the reactivity of the cyclic alkyne, tolerance of a highly functionalized alkyne, control of alkyne insertion regioselectivity as well as product and enantioselectivity. In short, this would be a challenging application of the methodology. To date there are no reported syntheses of either of these natural products so an efficient, asymmetric synthesis would be a beneficial contribution to the scientific community.

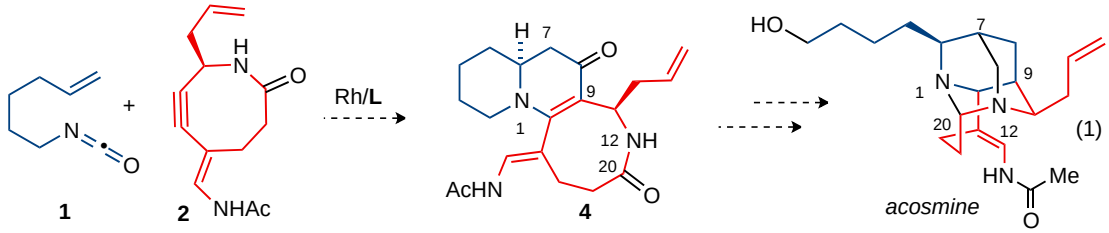

Scheme 2.1 Proposed [2+2+2] cycloaddition in the synthesis of acosmine.

2.1.3 Cyclooctyne Use in Cycloadditions

Cyclooctyne (**2b**) is a readily accessible and highly reactive synthon for organic synthesis. Although first synthesized by Blomquist and Liu in 1953,[8] cyclooctyne did not receive great consideration from the synthetic community until 1978 when Brandsma and Verkruijsse published an improved, large scale

synthesis of it from 1-bromocyclooctene **6** (Scheme 2.2).[9] Cyclooctyne's enhanced reactivity is due to strained, cyclic geometry. Bond angles of 158.5˚ have been reported for cyclooctyne; 21.5˚ less than the ideal bonding angle of 180˚ for C_{sp} hybridized carbons. This strained geometry has calculated total strain energy (E_{st}) of 18.5 kcal/mol.[10]

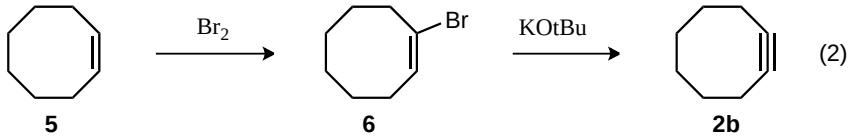

Scheme 2.2 Improved cyclooctyne synthesis.

Since the publication of an improved synthesis in 1978, cyclooctyne's simple preparation and enhanced reactivity have made it an appealing partner in cycloaddition reactions, including [2+2+2] cyclotrimerizations (Scheme 2.3, eq 3), [4+2] Diels-Alder (eq 4) and [3+2] Huisgen cycloadditions (eq 5). Tochterman and coworkers demonstrated cyclooctyne's enhanced reactivity through its participation in [4+2] cycloadditions with both electron deficient and electron rich dienes (eq 4).[11] Recently Bertozzi and coworkers exploited the reactivity of the difluorocyclooctyne dipolarophile (**2c**) in a copper-free azide-alkyne cycloaddition for use as an in-vivo sensor in biological systems (eq 5).[12] Despite its accessibility, cyclooctyne's participation in [2+2+2] reactions other than cyclotrimerization reactions remains unreported (eq 3). Likely, this is due to cyclooctyne's propensity to out-compete other cycloaddition partners in the presence of transition metals, leading to cyclotrimerization. Our aim was to develop a means to suppress cyclotrimerization allowing other π-components, such as isocyanates and alkenes, to participate in the [2+2+2] cycloaddition with cyclooctyne.

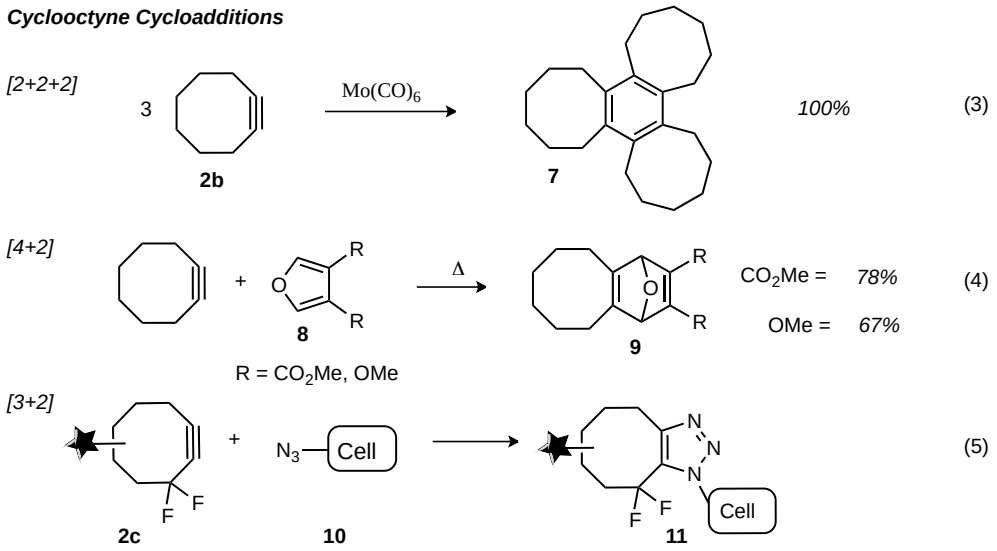

Scheme 2.3 Cycloadditions with cyclooctyne.

2.1.4 Isocyanate Synthesis

Alkenyl isocyanates are readily synthesized from the corresponding carboxylic acid by formation of an acyl azide (caution: do not heat) and subsequent Curtius rearrangement (Scheme 2.4). The two step process is operationally simple and yields reproducible. For example, reaction of hexenoic acid **12** with diphenylphosphoryl azide and triethylamine forms acyl azide **13**, which will slowly undergo the Curtius rearrangement to extrude N_2 (g) and form the isocyanate. The Curtius rearrangement is slow enough with alkyl acyl azides that the acyl azide can be purified by column chromatography. Once isolated, the acyl azide is allowed to sit neat for 12 h with very slight heating for the rearrangement to complete. A benefit of this method is the easy access it provides to many isocyanates, since carboxylic acids are common functional groups.

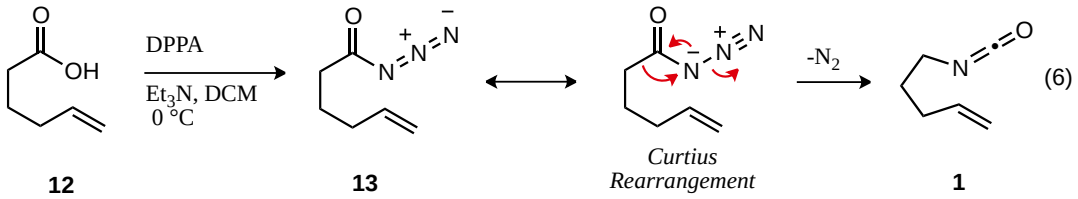

Scheme 2.4 Isocyanate synthesis.

2.2 Results

2.2.1 Developing [2+2+2] Cycloadditions with Cyclooctyne

A simple model system was devised to probe the feasibility of our strategy to synthesize diaza-adamantane alkaloids by [2+2+2] cycloaddition. Coupling pentenyl isocyanate (**1**) with cyclooctyne (**2b**) in the presence of a catalytic amount of Rh(I)•phosphoramidite complex found cyclooctyne was exclusively cyclotrimerized, and in context, the most reactive alkyne we had tried. Reaction of cyclooctyne in the presence of rhodium catalyst alone resulted exclusively in trimer **7** in 68% yield (Scheme 2.5).

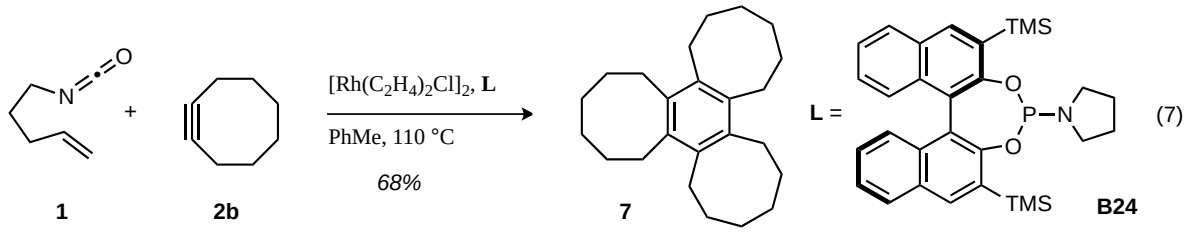

Scheme 2.5 Rh(I) catalyzed cyclotrimerization of cyclooctyne.

We were able to overcome cyclotrimerization by slow addition of a solution of cyclooctyne and isocyanate to the Rh(I) catalyst as shown in Table 2.1. Slow addition of cyclooctyne over 8 h provided both lactam **3** and vinylogous amide **4** in 35% yield (entry 3); extending time of addition to 16 h increased yield to 49%. We decreased time of addition to a more user-friendly 4 h and screened a number of concentrations. Ultimately, we found that a concentration of 0.02 M coupled with 4 h slow addition of reagents to a solution of Rh(I) catalyst was optimal, providing the desired cycloadducts in 71% yield. Once the reactivity of cyclooctyne was no longer a debilitating issue, we sought to control product and enantioselectivity by screening chiral phosphoramidite ligands.

Table 2.1 Rh(I) catalyzed [2+2+2] cycloaddition of cyclic alkynes and alkenyl isocyanates. (a) Reaction conditions: **1**, **2b**, $[Rh(C_2H_4)_2Cl]_2$ 2.5 mol %, **T5** 5 mol % in PhMe at 110 °C for 16 h. (b) Combined isolated yield.

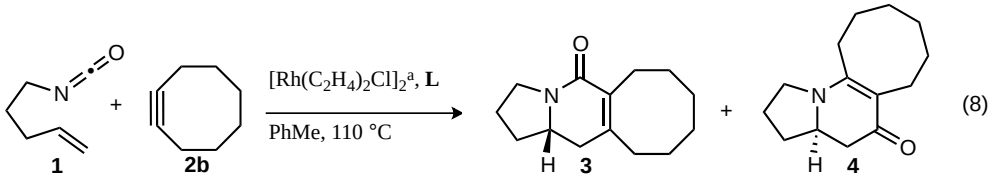

entry	[M]	slow addition (h)	yield[b] (%)
1	0.05	0	0
2	0.05	2	0
3	0.05	8	35
4	0.05	16	49
5	0.03	4	49
6	***0.02***	***4***	***71***
7	0.01	4	56

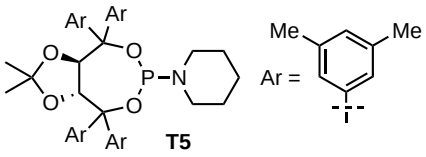

2.2.2 Ligand Effects on Product and Enantioselectivity

We found that phosphoramidite ligands influence product- and enantioselectivity in Rh(I) catalyzed [2+2+2] cycloadditions of alkenyl isocyanates with cyclic alkynes but not to the same extent as is seen with less reactive alkynes (Table 2.2). Cyclooctyne does not behave like a typical alkyl alkyne with regard to product selectivity. Ligands that typically influence product selectivity strongly with alkyl or aryl alkynes have a little to no effect with cyclooctyne. For this reason, an exhaustive ligand screen was conducted with every available phosphoramidite ligand accessible within the department.

Most of the Taddol-based phosphoramidites investigated provide moderate to good yields and poor product selectivities (Table 2.2). Exceptions to this include alkynyl amine ligands **T9** and **T10,** which provide vinylogous amide exclusively. Yields with **T9** and **T10** are poor and although enantioselectivities are useful, they were not pursued. In general, enantioselectivities with Taddol based phosphoramidites are excellent. m-Xylyl Taddol **T15** and morpholine substituted **T7** provide enantioselectivities greater than 97% *ee* and good yields. Unfortunately, poor product selectivity is seen with both (1.5:1 and 1:1, Lactam

(L): vinylogous amide (VA)). While encouraged by the moderate to good yields and excellent enantioselectivities, lack of product selectivity moved us to investigate other ligand scaffolds.

Table 2.2 Taddol phosphoramidite ligand screen.

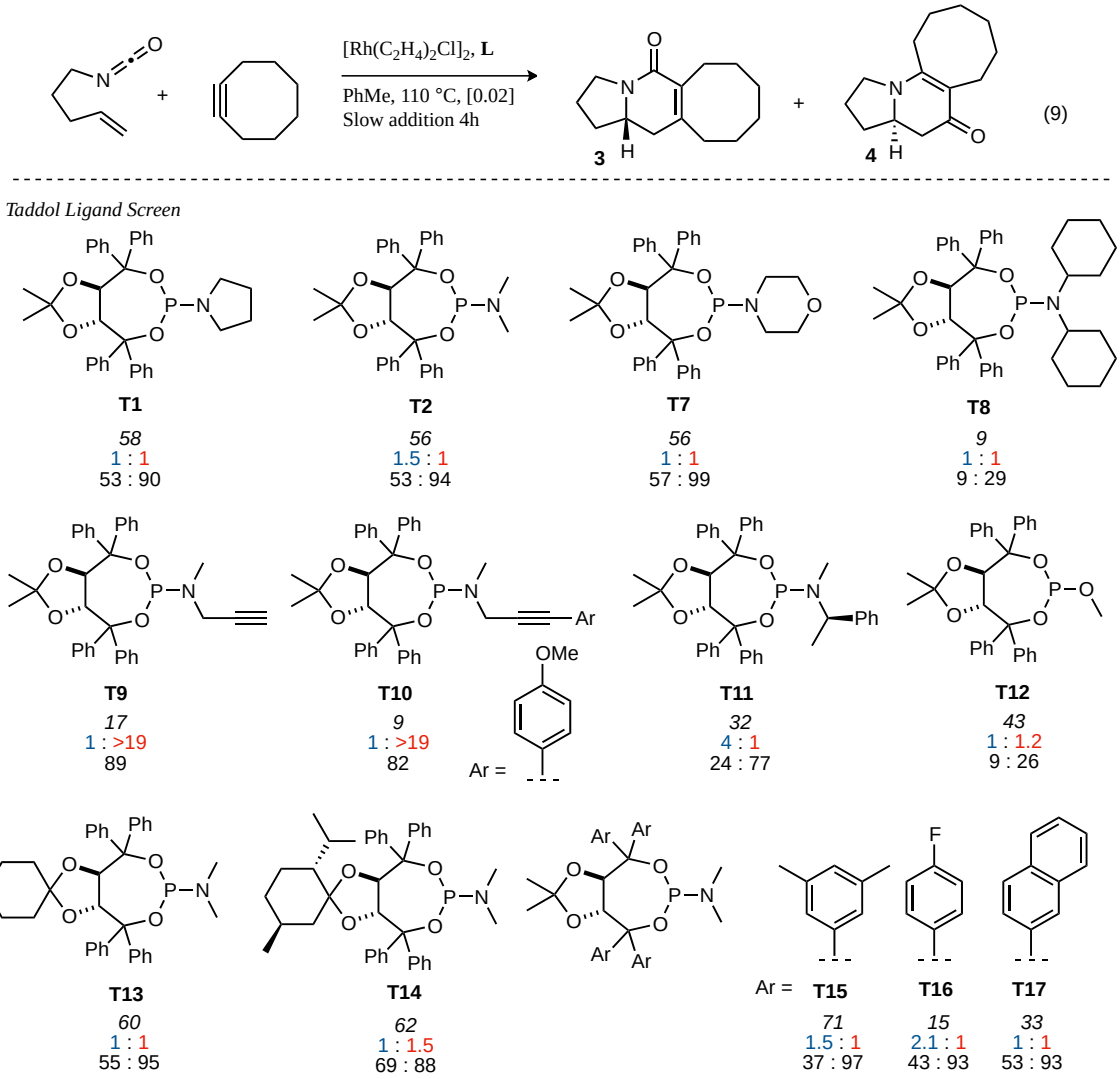

Binol-based phosphoramidites provide moderate yields in the [2+2+2] cycloaddition with cyclooctyne and in general tend to modestly favor the vinylogous amide product (Table 2.3). Diester Binol **B6** and thiophenyl binol **B8** are exceptions in that both provide 2:1 selectivity for the lactam product. Enantioselectivities with the Binol ligands studies are lower than that seen with the Taddol phosphoramidites. Notably, TMS-substituted Binol **B2** (Guiphos) provides a useful blend of moderate

yield (60%), product selectivity in favor of vinylogous amide (1:2 L:VA) and enantioselectivity (*ee*) (81%).

Table 2.3 Binol-based phosphoramidite ligand screen.

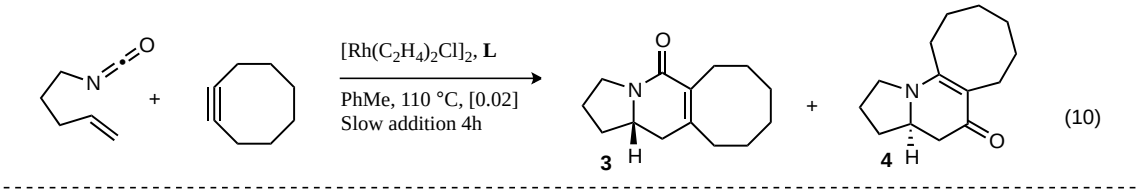

Binol Ligand Screen

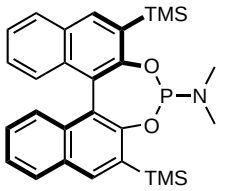

B2

60
1 : 2.5
63 : 81

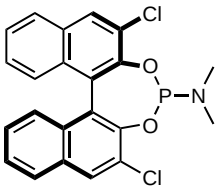

B3

47
1 : 2.5
31 : 7

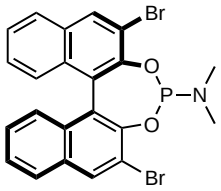

B4

47
1 : 3.4
33 : 8

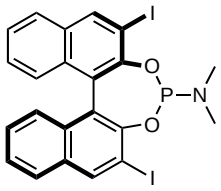

B5

37
1 : 2
24 : 15

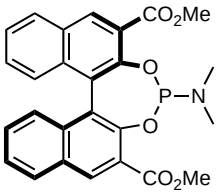

B6

41
2 : 1
39 : 57

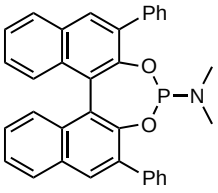

B7

75
1 : 4

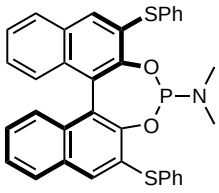

B8

32
2 : 1
50 : 27

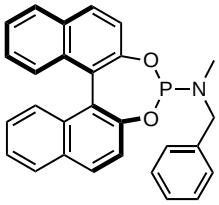

B9

45
1 : >19
13 : 25

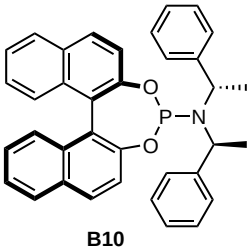

B10

21
1 : 4
53 : 37

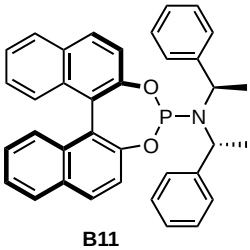

B11

52
1 : 5
46 : 43

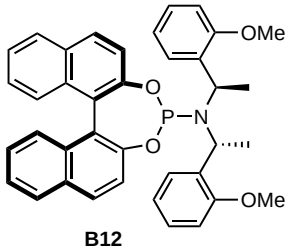

B12

19
1 : 1
73 : 33

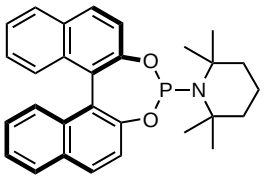

B13

9
1 : 1
91 : 4

Finally we investigated a number of biaryl phosphoramidites to find a scaffold that affected product selectivity in favor of vinylogous amide. Of the scaffolds studied, naphthyl derived phosphoramidite **B17** (Vanol) and spirobiindane-derived **B19** (Siphos) were found to provide good product selectivity for vinylogous amide (1:6.8 and 1:7, L:VA) with good yields. Unfortunately *ee*'s with these ligands are poor.

Phenanthrenyl-derived phosphoramidite **B18** (Vapol) provides increased *ee* but product selectivity decreases slightly. 3,3'-disubstituted biaryl ligands **B14** and **B1** give disappointingly low product and enantioselectivity in light of the high enantioselectivities and moderate product selectivities seen with terminal alkyl alkynes. Achiral methylene linked aryl phosphoramidites with chiral amines show poor reactivity and enantioselectivity. t-Bubiaryl **B22** provides excellent product selectivity for the lactam product however yield and enantioselectivity are low.

Table 2.4 Biaryl-based phosphoramidite ligand screen.

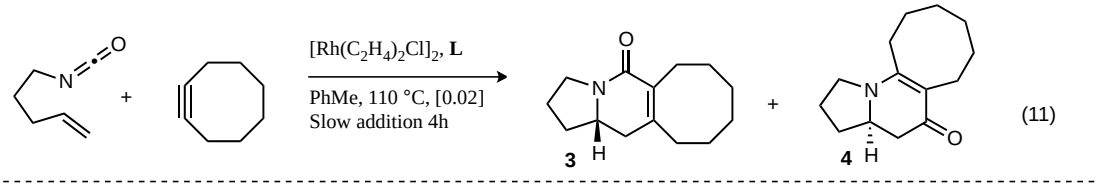

Biaryl Ligand Screen

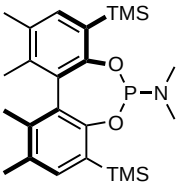

B14

63
1 : 2
45 : 60

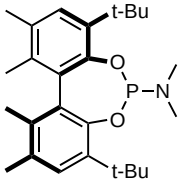

B1

28
1 : 2
76 : 31

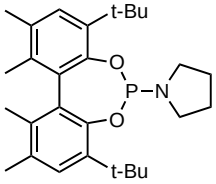

B15

32
1 : 1

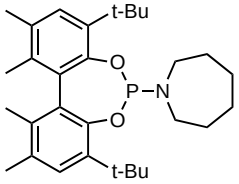

B16

28
1 : 1

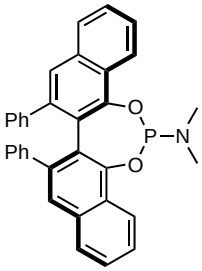

B17

67
1 : 6.8
24 : 31

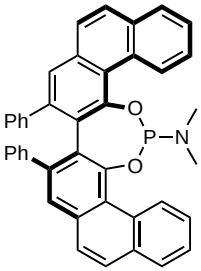

B18

67
1 : 4.2
3 : 51

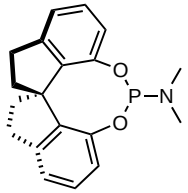

B19

69
1 : 7
27 : 22

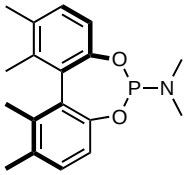

B20

62
1 : 2
25

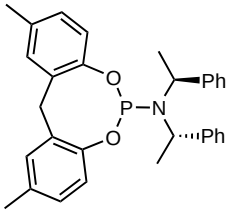

B21

32
2 : 1
7 : 29

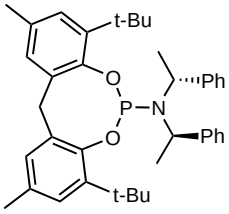

B22

13
>19 : 1
3

In summary, several promising ligand scaffolds were identified as a result of the ligand screen (Tables 2.2, 2.3, 2.4). VANOL-based phosphoramidites (**B17**) and commercially available SIPHOS (**B19**) both favor vinylogous amide with moderate ratios. Product selectivity changes are attributed to structural differences in the scaffold backbone affecting the ligand steric environment as opposed to a difference in ligand electronics. Unfortunately, these ligands do not satisfactorily render the reaction asymmetric as *ee* for vinylogous amide products remain low. Substitution at the 3,3'-positions of the BINOL-based (**B2**) and biaryl (**B14**) phosphoramidites is crucial for high vinylogous amide enantioselectivity and could be explored with the Vanol and Siphos backbones. Overall, Guiphos provides the best blend of modest product selectivity in favor of vinylogous amide with moderate enantioselectivity (81%) and yield. Taddols **T7** and **T15** give the best vinylogous amide enantioselectivity (99%, 97%) in good yields but poor product selectivities. We hypothesized that we may be able to favor the CO migration pathway while maintaining excellent enantioselectivity by modification of the Taddol phosphoramidite (aryl, amine and acetonide).

2.2.3 Ligand Development

The ligand screen indicated that Taddol phosphoramidites give excellent *ee* for vinylogous amide, but poor product selectivity. We sought to increase the product selectivity by modifying the electronics of the Taddol aryls. Aryl, amine, and acetal groups can be easily manipulated thanks to the modular nature of the Taddol phosphoramidite synthesis (Scheme 2.6).[13,14] Fischer esterification and acetonide protection of enantiopure tartaric acid affords diester **14**. A Grignard reaction installs the desired aryl groups resulting in diol **15,** which is subsequently treated with phosphorus trichloride and the desired amine to form Taddol phosphoramidite **T3**.

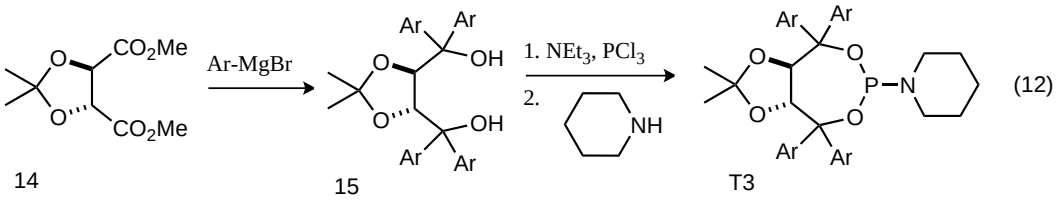

Scheme 2.6 Synthesis of Taddol Phosphoramidites

Two electron-rich and one electron-deficient aryl Taddol phosphoramidites were made (Table 2.5). Both the electron withdrawing *p*-CF_3 ligand **T19** (1:1.7) and the electron rich *p*-OMe-phenyl **T22** (1:1.3) favor the vinylogous amide **4** while the 3,4,5-trimethoxyphenyl **T27** favors the lactam **3** by 2:1. Enantioselectivities range from good to excellent with *p*-OMe **T22** providing 97% *ee* with a modest 34% yield. With cyclooctyne aryl electronics of the Taddol phosphoramidites have minimal effect on product selectivity.

Table 2.5 Effects of aryl electronics in Taddol Phosphoramidites on product and selectivity.

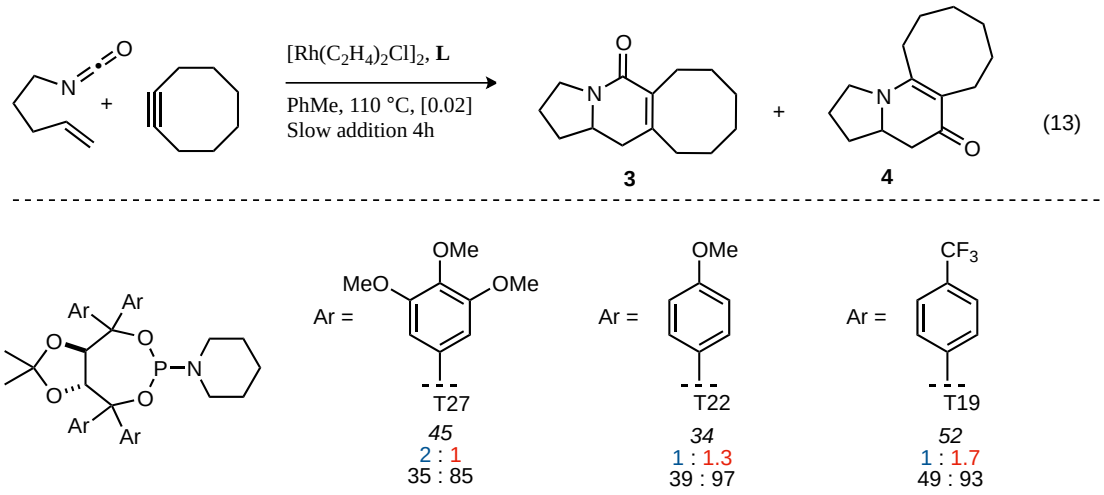

2.2.4 Synthesis of Strained Cyclic Alkynes

As we sought to use the developed methodology with functionalized cyclooctynes to synthesize acosmine and dasycarpumine (Scheme 2.1), we investigated tolerance of the Rh(I) catalysis with other strained cyclic alkynes. Substituted cyclooctynes, such as **19**, are readily synthesized from either the cyclic ketone or alkene precursor (Scheme 2.7). Beginning with cyclooctanone **16**, deprotonation and methylation of the resultant enolate arrives at α-methyl ketone **17** in excellent yield (eq. 14). Formation of the kinetic enolate of **17** using lithium diisopropylamide (LDA) and subsequent trapping with N-phenyltriflimide forms vinyl triflate **18**, which is eliminated with LDA to give 3-methylcyclooctyne (**19)** in good yield. Cyclononyne **22** is synthesized from cyclooctanone **16** by dibromocarbene addition to the ketone, subsequent reduction to the vinyl bromide **21,** and finally a Fritsch-Buttenberg-Wiechell

rearrangement to alkyne **22** (eq. 15).[15] Cyclodecyne is synthesized from cyclodecanone **23** by forming the vinyl triflate **24**, which is eliminated in good yield to provide alkyne **25** (eq. 16).

Alkyne Substrate Synthesis

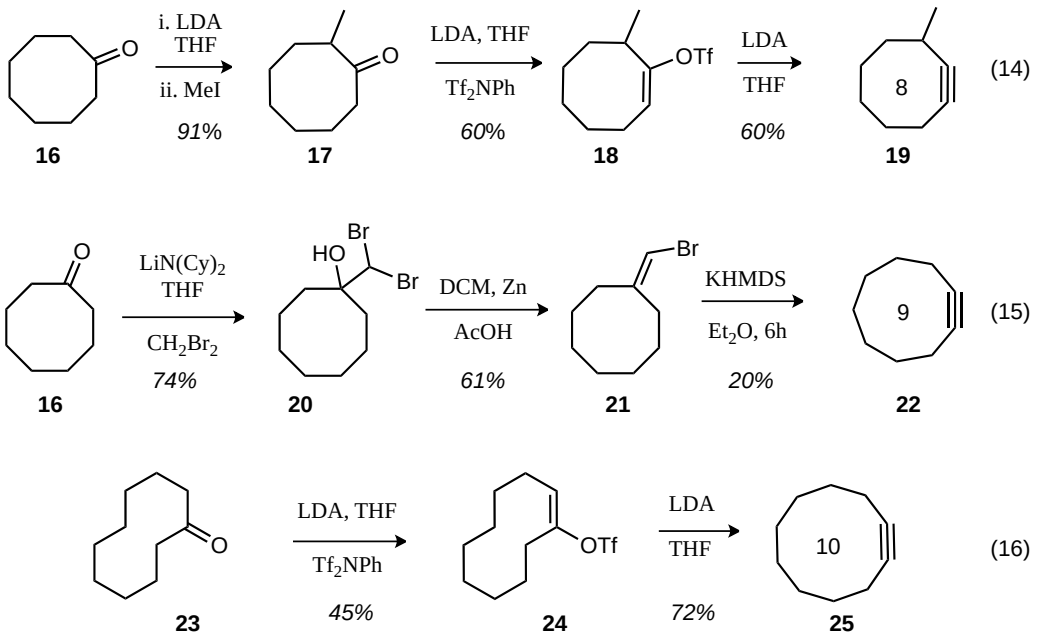

Scheme 2.7 Synthesis of strained cyclic alkynes

2.2.5 Substrate Scope of Strained Cyclic Alkyne Cycloadditions

Several cyclic alkynes are tolerated by the Rh(I) catalyzed cycloaddition developed for cyclooctyne. Multiple polycyclic indolizidinone and quinolizidinone scaffolds are accessible in moderate to excellent yields (43-96%). Yields increase with larger ring sizes while enantioselectivity decreases. At best, the method provides moderate control of enantioselectivity (81%). Product selectivity also varies widely (1:2 to 1:14) depending on the size of the cyclic alkyne.

Yield increase with larger ring sizes is attributed to steric interactions between the cyclic alkyne and Rh(I) catalyst that reduce both pyridone formation and cyclotrimerization. However, large cyclic alkynes suffer from a decrease in alkene facial discrimination in the 1,2-migratory insertion event, resulting in poor enantioselectivity (**4c, 4g, 4i,** 5%, 3%, 9% *ee*) for reasons that are not clear at this time (see chapter 3 for an enantioselectivity model). Unsymmetrical internal alkyne, 3-methylcyclooctyne **19**, enhances product selectivity (**4d** 1:6, **4h** 1:14, **3:4**) with comparable yields to those found with cyclooctyne. These

results parallel what was reported by Friedman and Rovis.[5] We suspect that the increase in product selectivity is due to enhanced steric interactions between the α-methyl of **19** and the phosphoramidite during oxidative cyclization favoring vinylogous amide as discussed in Chapter 3. Enantioselectivity for the two **4d** diastereomers is poor for one diastereomer and exquisite with the other, suggesting a match-mismatch scenario between catalyst and substrate.

Table 2.6 Strained cyclic alkyne substrate scope.

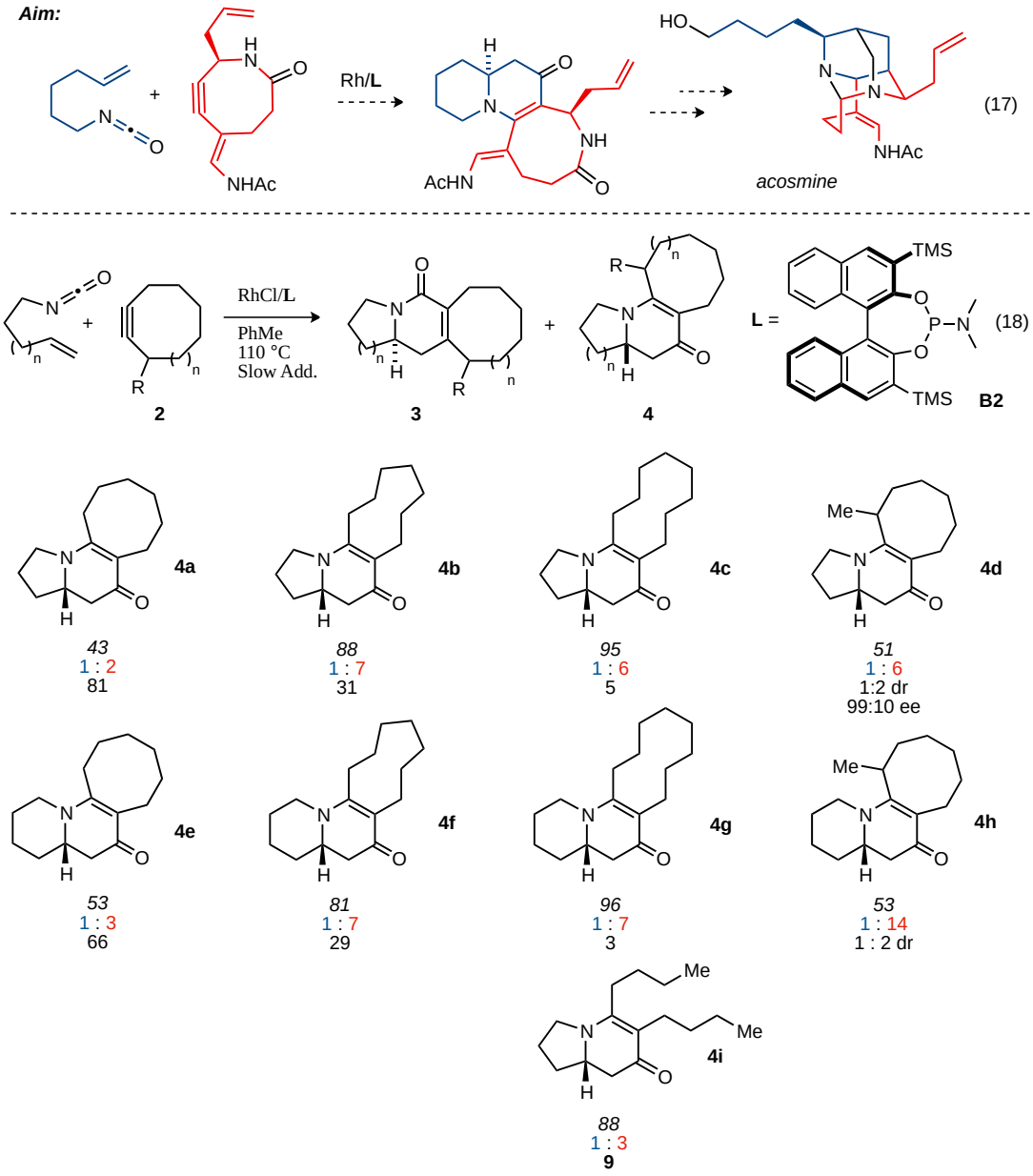

2.2.6 Effect of Ring Strain on Reactivity in the [2+2+2] Cycloaddition.

Cyclooctyne's calculated total strain energy of 18.5 kcal/mol is slightly higher than that determined for cyclononyne and cyclodecyne, which have calculated total strain energies of 16.37 and 9.90 kcal/mol respectively.[16] Cyclononyne and cyclodecyne behave similarly to cyclooctyne in the Rh(I) catalyzed cycloaddition, although slightly less reactive with fewer byproducts seen.

Cyclooctyne's reactivity is markedly greater than other alkynes investigated; apart from other strained cyclic alkynes, dimethylacetylenedicarboxylate (DMAD) is the closest equivalent. DMAD also has a similar propensity to cyclotrimerize with Rh(I) catalysts.[17] Regarding product selectivity, cyclooctyne behaves similar to cyclohexylacetylene and electron-deficient aryl acetylenes with Taddol phosphoramidites and poor product selectivities are found. In comparison to other alkyl alkynes, such as 1-octyne or 5-decyne, where product selectivity favors lactam **3** 5:1 and 7:1 (**3**:**4**) with Taddol **T3**, essentially no product selectivity (1.5:1) is seen with cyclooctyne and **T3**. Presumably this is due to cyclooctyne's strain energy being sufficient to override the ligand's control of oxidative cyclization (Chapter 3). Furthermore, Biaryl-based phosphoramidites do not sway product selectivity to the same degree with cyclooctyne as they do for 1-octyne. **B1** provides vinylogous amide **4** (from 1-octyne, Chapter 3) in 1:6.2 product selectivity, whereas product selectivity with cyclooctyne is only 1:2.

2.3 Conclusion

We developed an efficient method for rhodium(I) catalyzed [2+2+2] cycloaddition of alkenyl isocyanates and strained, cyclic alkynes. This is the first report of strained cyclic alkynes participating in metal catalyzed [2+2+2] cycloadditions without cyclotrimerization. Control of product- and enantioselectivity at the same time is challenging but may be addressed through future catalyst design. Acosmine and dasycarpumine's total syntheses were not pursued beyond this model system. A better mechanistic understanding of the cycloaddition was needed to address selectivity issues before this method was applied to a proper total synthesis.

2.4 References

(1) Friedman, R. K.; Oberg, K. M.; Dalton, D. M.; Rovis, T. *Pure Appl. Chem.* **2009**, *82*, 1353–1364.

(2) Perreault, S.; Rovis, T. *Chem. Soc. Rev.* **2009**, *38*, 3149–3159.

(3) Yu, R. T.; Rovis, T. *J. Am. Chem. Soc.* **2006**, *128*, 2782–2783.

(4) Oinen, M. E.; Yu, R. T.; Rovis, T. *Org. Lett.* **2009**, *11*, 4934–4937.

(5) Friedman, R. K.; Rovis, T. *J. Am. Chem. Soc.* **2009**, *131*, 10775–10782.

(6) Trevisan, T.; Silva, E.; Dall'Oglio, E.; da Silva, L. *Tetrahedron Lett.* **2008**, *49*, 6289-6292.

(7) Andrade-Cetto, A.; Wiedenfeld, H. *J. Ethnopharmacol.* **2004**, *90*, 217-220.

(8) Blomquist, A.; Liu, L. *J. Am. Chem. Soc.* **1953**, *75*, 2153–2154.

(9) Heber, D.; Rosner, P.; Tochtermann, W. *Eur. J. Org. Chem.* **2005**, 4231–4247.

(10) Traetteberg, M; Luttke, W.; Machinek, R.; Krebs, A.; Hohlt, H. *J. Mol. Struct.* **1985**, *128*, 217–232.

(11) Tochtermann, W.; Rijsner, P. *Tetrahedron Lett.* **1980**, *21*, 4905–4908.

(12) Baskin, J. M.; Prescher, J. A.; Laughlin, S. T.; Agard, N. J.; Chang, P. V.; Miller, I. A.; Lo, A.; Codelli, J. A.; Bertozzi, C. R. *Proc. Natl. Acad. Sci. U.S.A.* **2007**, *104*, 16793–16797.

(13) Seebach, D.; Pichota, A.; Beck, A.; Pinkerton, A.; Litz, T.; Karjalainen, J.; Gramlich, V. *Org. Lett.* **1999**, *1*, 55–58.

(14) Seebach, D.; Beck, A.; Heckel, A. *Angew. Chem. Int. Ed.* **2001**, *40*, 92–138.

(15) Knorr, R. *Chem. Rev.* **2004**, *104*, 3795–3849.

(16) Allinger, N. L.; Meyer, A. Y. *Tetrahedron* **1975**, *31*, 1807–1811.

(17) Collins, S.; Rovis, T. *Rhodium Catalyzed [2+2+2] Cycloadditions Using an Isocyanate Tethered Alkene with Symmetrical Internal Alkynes*; Undergraduate Honors Thesis, Colorado State University, Department of Chemistry, Fort Collins, **2009**.

CHAPTER 3

Mechanistic Investigations of Rh(I)-Catalyzed [2+2+2] Cycloadditions

3.1 Introduction

3.1.1 Project Aim

The development of chemical tools that rapidly, efficiently and selectively synthesize biologically active molecules is of utmost importance to the discovery of potential drug candidates for pharmaceuticals. Transition metal-catalysis is one of the most powerful chemical synthetic tools. Not only are metal catalysts robust with high catalyst turnover numbers seen, but they can quickly and efficiently make complex molecules from simple starting materials with high levels of selectivity. The metal ligand environment controls the type and degree of selectivity, and a wide array of ligand scaffolds have been developed to transfer stereochemical information to the desired products. For a given methodology to be adopted by the synthetic community, the outcome of a given reaction must be highly predictable, reproducible and controllable. To this end we have proposed a working mechanistic model that explains our hypotheses of what controls regio-, product- and enantioselectivity in the Rh(I)-catalyzed [2+2+2] cycloadditions of alkenyl isocyanates and exogenous alkynes. These cycloadditions access indolizinone and quinolizinone natural product motifs in a single step with high degrees of selectivity.

3.1.2 Initial Ligand Screen

Early attempts to incorporate terminal alkynes in the Rh(I) catalyzed [2+2+2] cycloaddition used conditions effective for internal alkynes.[1] Yu and Rovis found that the ligand tris(*para*-methoxyphenyl)phosphine (**L1**) provides less than 20% of **3** and **4** in a 1:1 ratio (Table 3.1); the low yield is due to the known dimerization of terminal alkynes to form enynes **6** and **7** (Scheme 3.1).[2-4]

Alkyne Dimerization

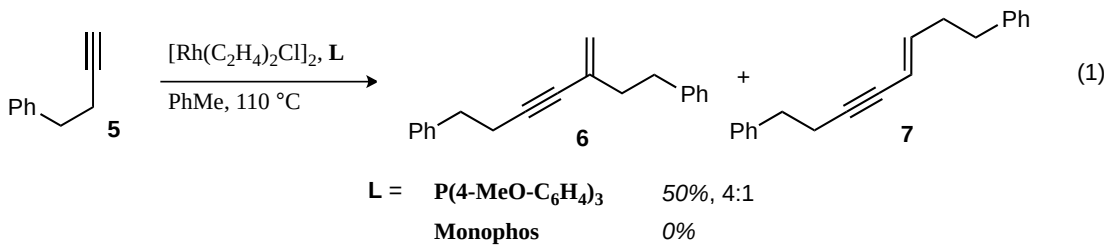

L =		
	P(4-MeO-C_6H_4)$_3$	*50%*, 4:1
	Monophos	*0%*

Scheme 3.1 Rh(I) catalyzed dimerization of alkynes.

BINAP gives no desired product while dppb affords only trace amounts of **3a**, suggesting that a monodentate ligand is required (Table 3.1). Monophos affords a 32% yield and induces a modest 55% ee. Phosphoramidites do not promote dimerization of terminal alkynes and consequently provide higher yields. Binol-based phosphoramidite **B0** provides a slightly higher yield of vinylogous amide but poor enantioselectivity, while phosphite **B3** shows lower yields than monophos and **B0**. Finally, Taddol-based phosphoramidite **T2** increases yield (80%), product selectivity toward vinylogous amide (1:7.0), and enantioselectivity (94%). After modifying the amine, **T1** was found to be the optimal ligand for this transformation.

Table 3.1 Initial Ligand Screen.

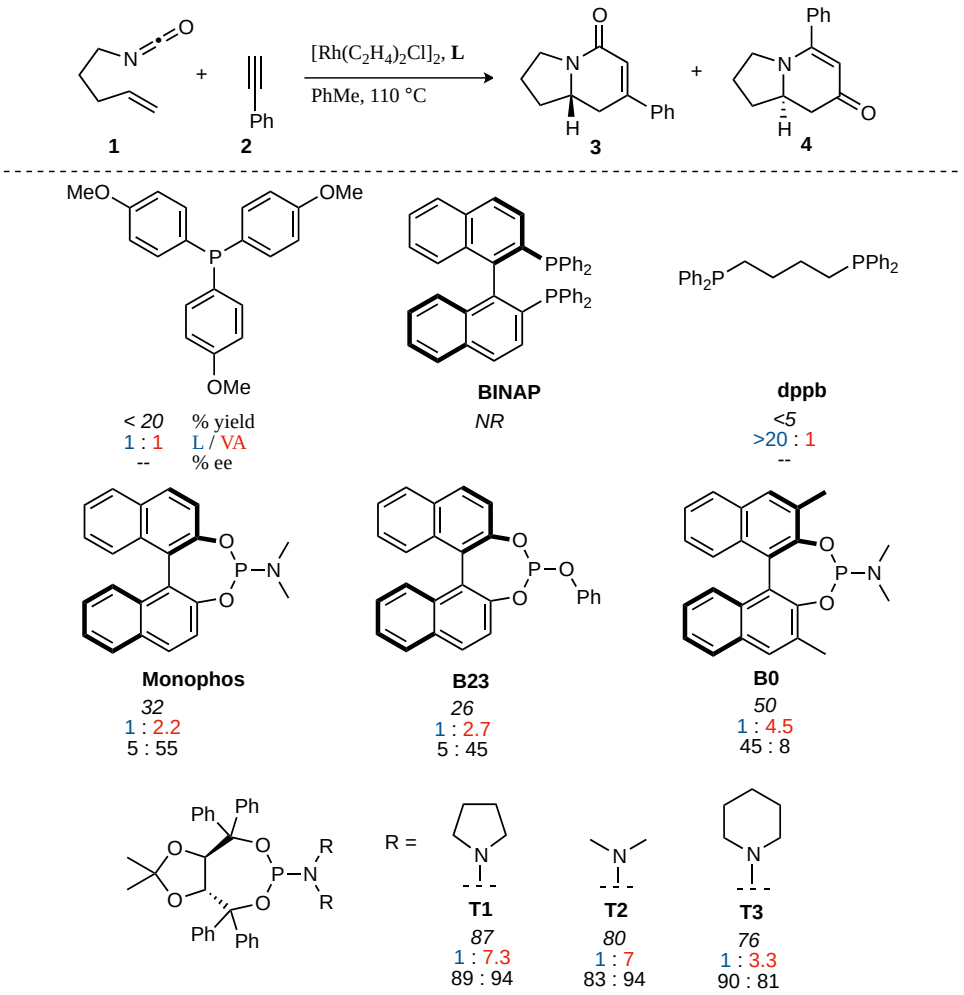

3.1.3 Terminal Alkyne Scope and Product Selectivity

Yu and Rovis investigated the scope of this reaction with terminal aryl alkynes (Table 3.2) and found electron-rich aryl alkynes provide exclusively vinylogous amide **4** in good yield and high enantioselectivity. As the alkyne is made more electron-deficient, increasing amounts of lactam **3** are seen. The substrate scope with terminal aryl acetylenes clearly shows that substrate electronics (with terminal aryl alkynes) can be used to tune product selectivity.

Table 3.2 Terminal aryl alkynes used for Hammett plot

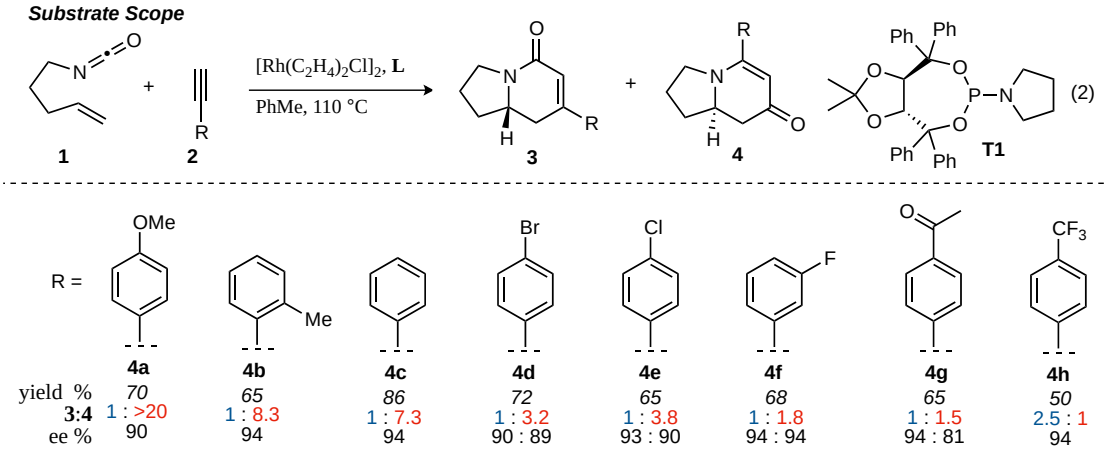

A plot of electron-rich and deficient aryl alkynes versus Hammett $\sigma_{m/p}$ values indicates a clear linear free energy relationship with an R^2 value of 0.93 (Figure 3.1).[5] In general, the electronics of the aryl alkyne bias product selectivity such that electron-rich favor vinylogous amide **4** while strongly electron-deficient generate lactam **3**. This suggests that the lactam product is favored when an aryl substituent is able to stabilize a partial positive charge in the transition state of the product determining step (oxidative cyclization).

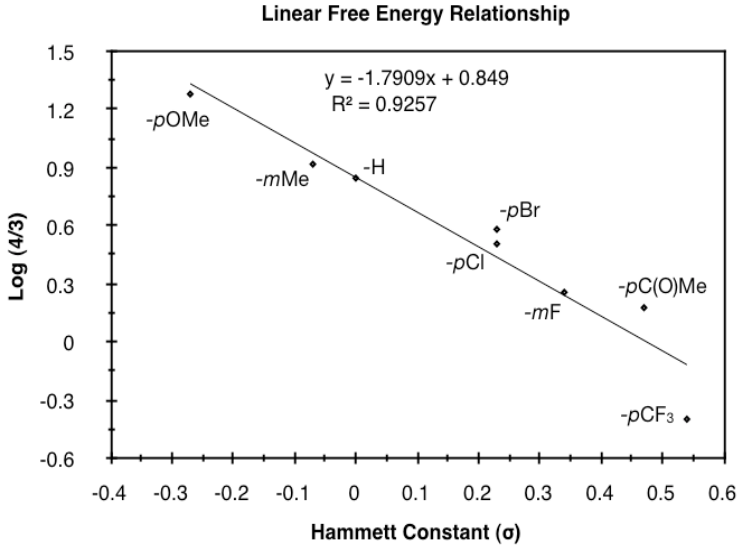

Figure 3.1 Linear free energy relationship of aryl acetylenes

An examination of the data gathered by Rovis and coworkers since the inception of the project reveals trends in product selectivity based on the characteristics of the acetylene substrate (Table 3.3).[6]

Small and electron-deficient alkyl alkynes, such as propargyl ether or benzyl substituents, heavily favor lactam **3** (>19:1, **3**:**4**) with Taddol phosphoramidites. Longer-chain alkyl alkynes show modest product selectivity (~5:1, **3**:**4**) for lactam while sterically bulky (cyclohexyl, or t-Bu) substituents provide no selectivity, which is in itself a shift toward vinylogous amide. Electron-releasing substituents (alkenyl or aryl) heavily favor the vinylogous amide product (1: >19, **3**:**4**). However, if electron-deficient aryl substituents are present, product selectivity shifts in favor of lactam by up to 2.5:1.

Table 3.3 Substrate based product selectivity trends.

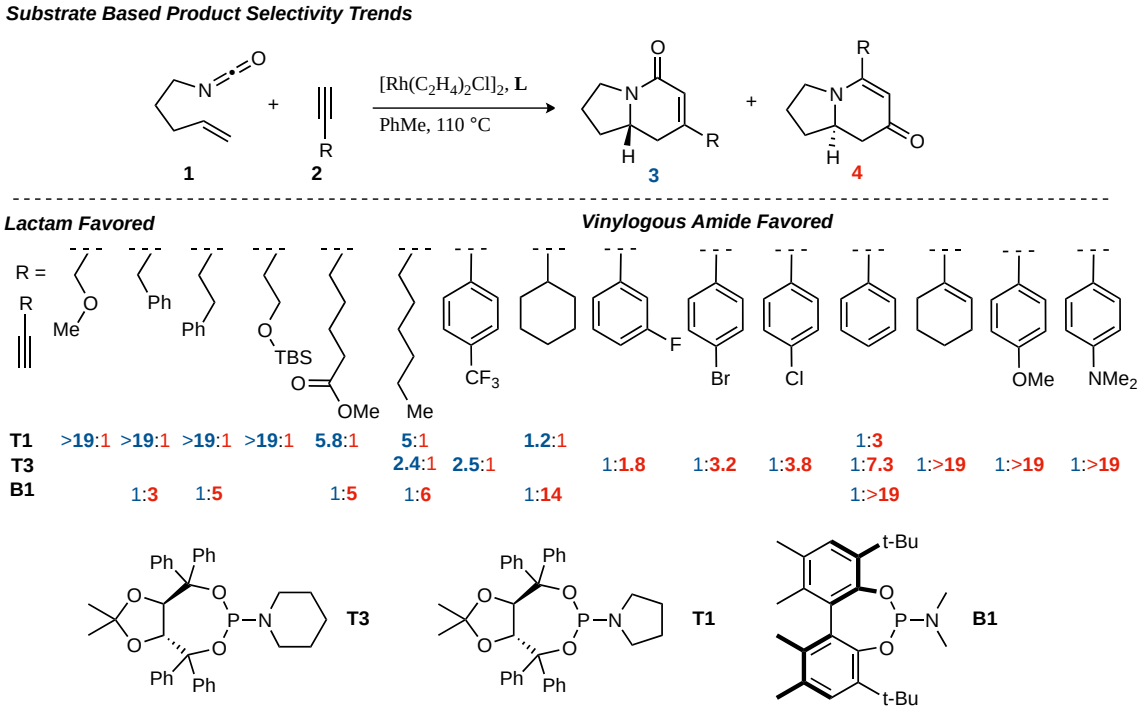

Product selectivity can be affected by the choice of ligand as well. Yu and Rovis found that biaryl-based phosphoramidite **B1** increases product selectivity for the vinylogous amide product to modest levels with alkyl alkynes.[7] At the time of publication it was not clear what factors were affecting shifts in product selectivity and a systematic study was undertaken to find the origins of these effects.

3.2 Results

3.2.1 Phosphoramidite Ligand Structure Activity Relationship (SAR)

An examination of the structure and electronics of the phosphoramidite revealed that the reaction is sensitive to both (Table 3.4). In general, Taddol-based phosphoramidites (**T5**, **T3**) give more lactam

product with aliphatic alkynes, while Binol and biaryl phosphoramidites (**B1**, **B0**) favor vinylogous amide. Interestingly when the amine of Taddol ligands is changed from pyrrolidine **T1** to piperidine **T3**, product selectivity shifts in favor of lactam **3** from 1:7.3 to 1:3.3 (Table 3.4) with phenyl acetylene and 2.4:1 to 5:1 (Table 3.4) with 1-octyne, and this trend can be extended to all Taddol ligands investigated so far. We suspect that it is the size of the amine that is affecting product selectivity, as the basicity of pyrrolidine (11.27 pKa) and piperidine (11.22 pKa) are very similar.[8] Furthermore, very large amines, such as dicyclohexyl amine, completely favor the lactam product, albeit in low yield. Interestingly, the size of the amine has less effect on product selectivity with Binol/biaryl phosphoramidites. These results show that the steric environment created by the phosphoramidite plays a major role in determining product selectivity.

Table 3.4a Ligand structure activity relationship (SAR) with 1-octyne.

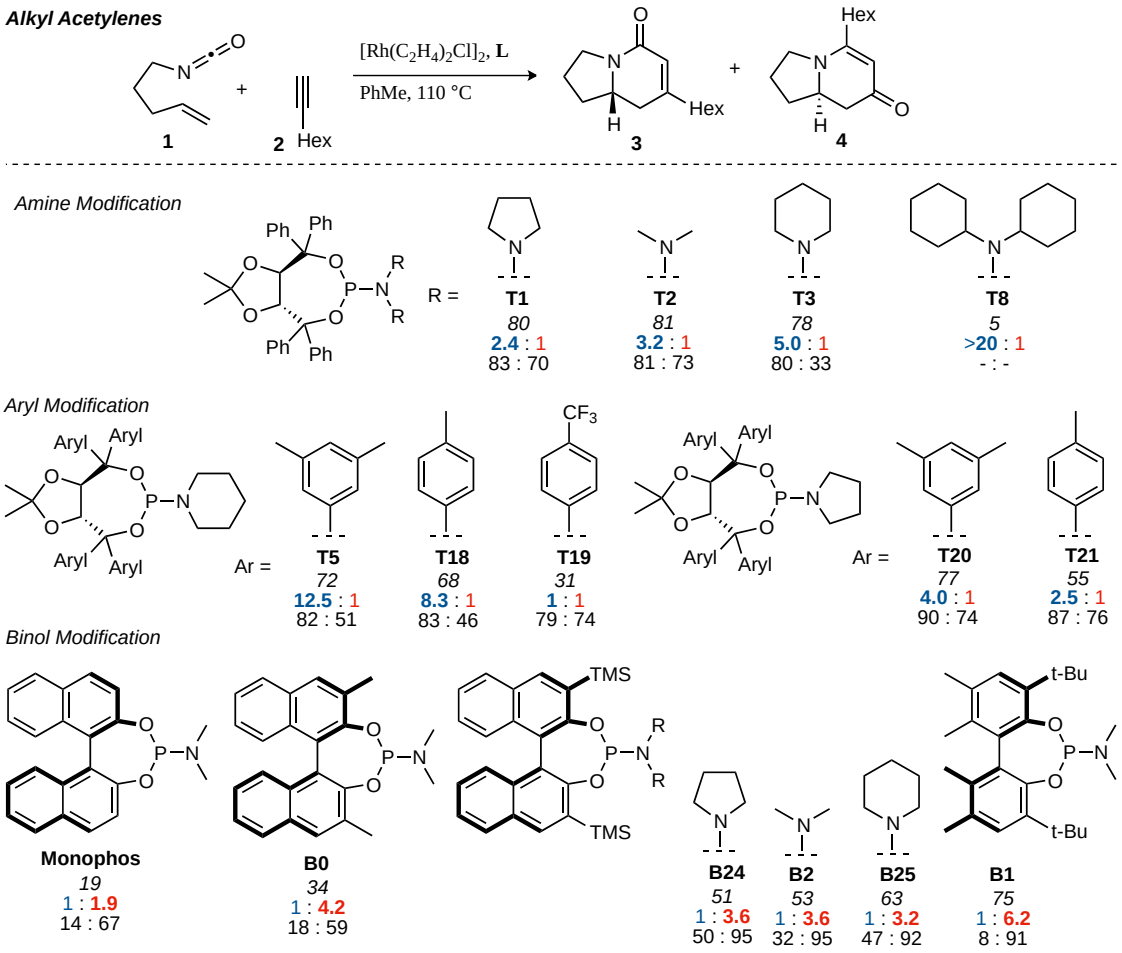

Table 3.4b Ligand structure activity relationship (SAR) with phenyl acetylene.

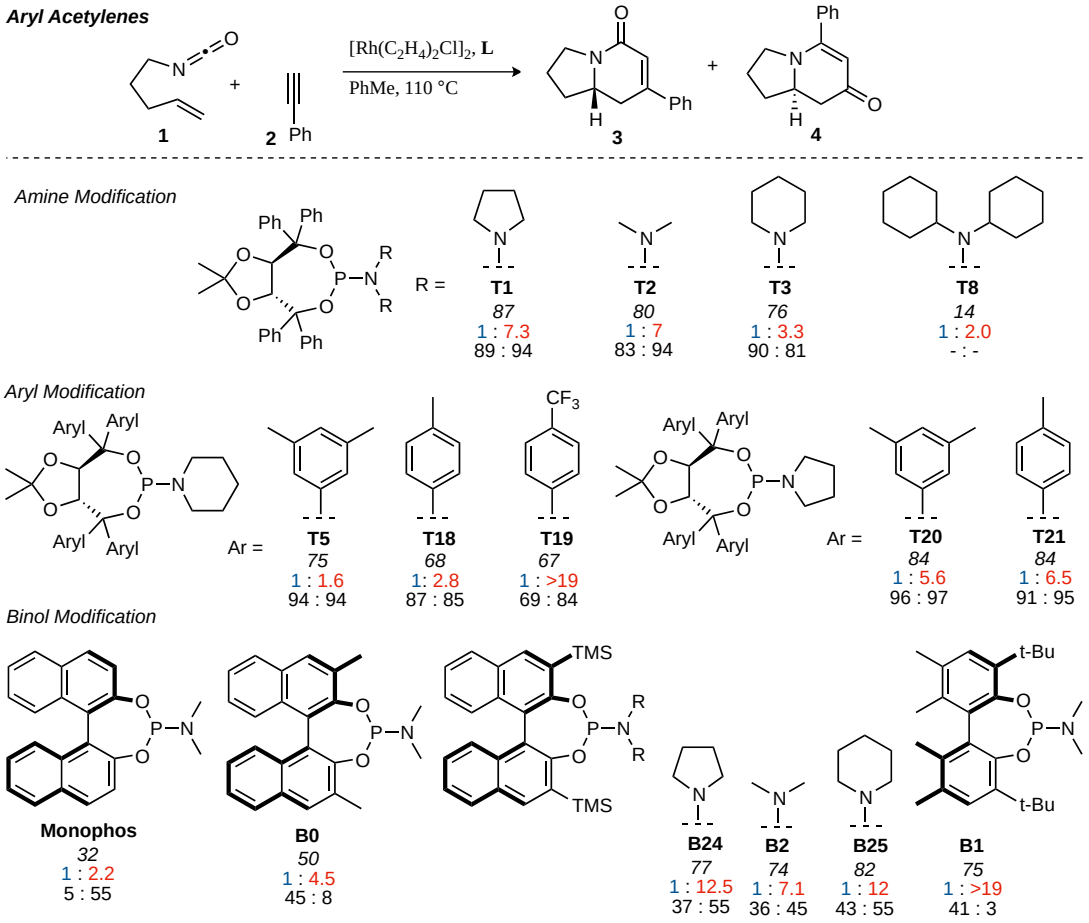

To investigate the effect of ligand electronics, we synthesized a ligand (**T19**) that differs from **T18** only in the aryl substituents: *p*-MeC_6H_4 vs *p*-$CF_3C_6H_4$. This more electron-deficient ligand increases product selectivity for vinylogous amide with both aryl (1: >20 from 1:2.8) and alkyl alkynes (1:1 from 8.3:1), demonstrating that ligand electronics can enhance product selectivity. Also, electron-rich *m*-xylyl Taddol **T5** gives a relative increase in the amount of lactam product formed with aryl (1:1.6, Table 3.4b) and alkyl acetylenes (12.5:1, Table 3.4a).

Taddol ligands provide the highest enantioselectivities for aryl alkynes (81-97%) with **T20** and **T1** being optimal, while Binol and biaryl ligands give higher enantioselectivity for alkyl alkynes (59-95%) with **B2** and **B2** being highest. Substitution at the 3,3'-positions of the Binol/biaryl proves to be essential to improving the enantioselectivity with alkyl acetylenes. Biaryl **B1** provides the highest product ratio (1:6.2) and excellent enantioselectivity (91%) for vinylogous amide with alkyl acetylenes.

3.2.2 Proposed Mechanism

The proposed mechanism for formation of lactam **3** and vinylogous amide **4** via the Rh(I) catalyzed [2+2+2] cycloaddition is illustrated in Scheme 3.2. From a single coordination complex **I** both lactam and vinylogous amide products are formed; this depends on the direction of oxidative cyclization. The lactam product is formed from oxidative cyclization resulting in C-C bond formation to generate 5-membered rhodacycle **IIa**.[9-13] Migratory insertion of the pendant alkene into **IIa** produces 7-membered rhodacycle **IIIa**; subsequent reductive elimination provides lactam **3**. Vinylogous amide **4** occurs from oxidative cyclization leading to C-N bond formation, which results in 5-membered rhodacycle **IIb**. Coordination of the pendant alkene to rhodium in **IIb** is inhibited by a strained, bridged geometry of the tether during coordination. As a consequence, migratory insertion of the alkene into rhodacycle **IIb** does not occur, and we propose a reversible CO extrusion-insertion[14-16] takes place to access 5-membered rhodacycle **IVb**, which allows alkene coordination and insertion to generate 7-membered rhodacycle **Vb**. Reductive elimination of **Vb** provides vinylogous amide **4** and regenerates active catalyst. Formation of 2-pyridone can be explained from exogenous alkyne migratory insertion into either rhodacycles **IIa** or **IIb** before insertion of the tethered alkene.[17] 4-pyridone can be formed from alkyne interception of rhodacycle **IVb**.

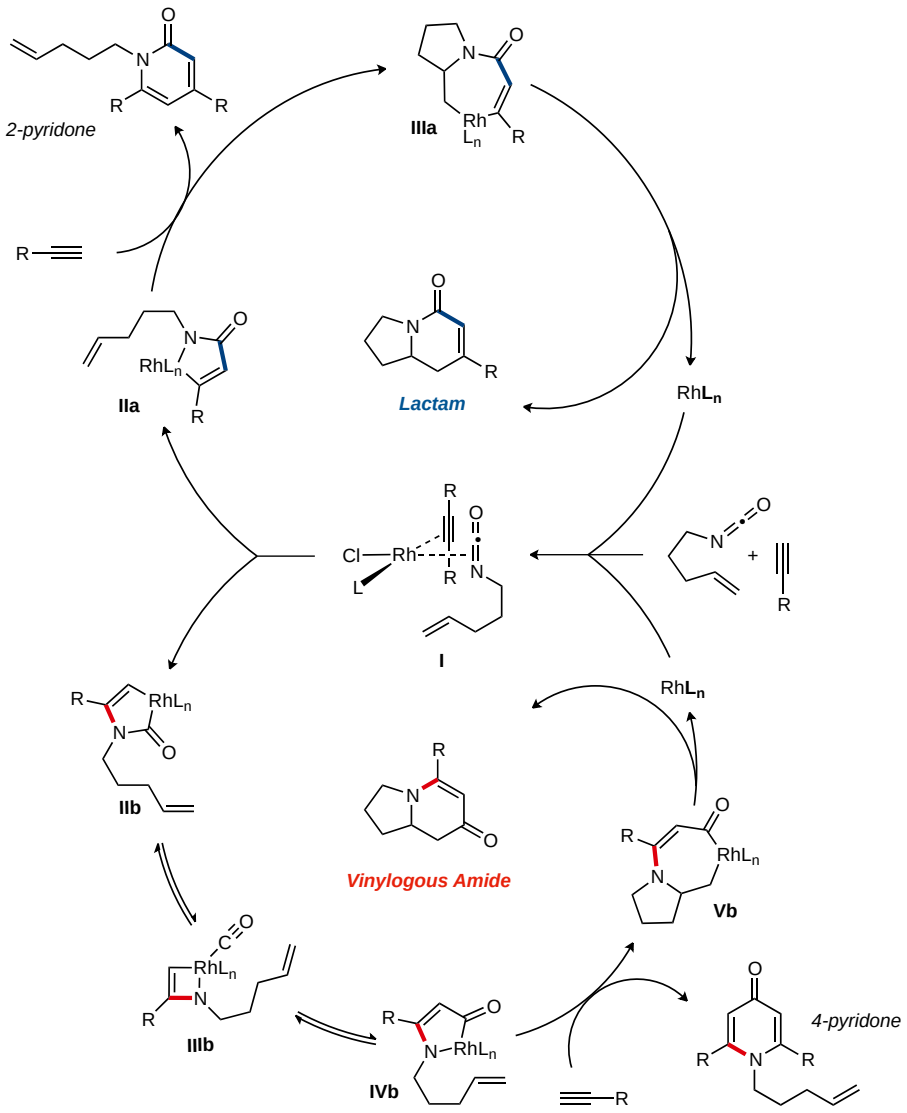

Scheme 3.2 Proposed mechanistic cycle

3.2.3 Alternative Mechanism

An alternative catalytic cycle can be proposed to account for lactam and vinylogous amide formation, in which the alkene of the alkenyl isocyanate coordinates to the rhodium (**Ic**) in lieu of an alkyne and undergoes oxidative cyclization to form **IIc** (Scheme 3.3). Such oxidative cyclization would lead to C–N bond formation, and set the stereochemistry for both lactam **3** and vinylogous amide **4**. 1,2-Migratory alkyne insertion would give **IIIa** and subsequent reductive elimination would generate lactam **3**. Alternatively, CO migration via **IIIc** could take place prior to alkyne insertion making bicycle **IVc**, which would then undergo alkyne insertion (**Vb**) and reductive elimination to form vinylogous amide **4**.

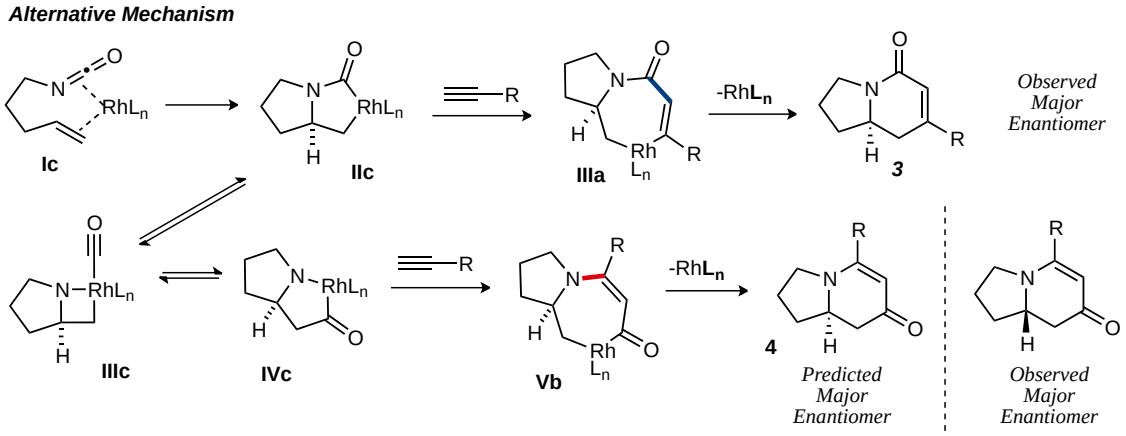

Scheme 3.3 Alternative proposed catalytic cycle

Several observations suggest that this alternative mechanism is not the operative catalytic cycle. First, two competition experiments were conducted between mono (**1a**) and 1,1-disubstituted (**1b**) alkenyl isocyanates (eqs 3, 4) in the presence of either aryl (**2a**) or alkyl (**2b**) acetylenes (Scheme 3.4). These yield a 1:1 ratio of vinylogous amide or lactam products respectively. We would predict that isocyanate **1a** should react at a different rate than **1b** due to slower complexation rates for trisubstituted olefins, leading to an unequal product mixture.[18] Because olefin substitution has no effect on the ratio of products obtained, we propose that the olefin is not involved in the turnover-limiting step.

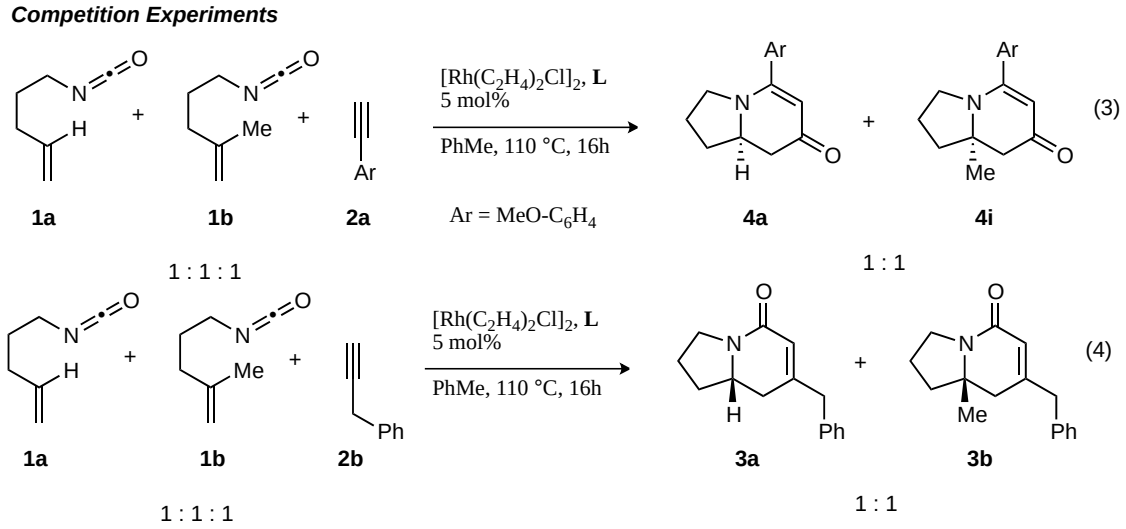

Scheme 3.4 Alkene migratory insertion competition experiments

Further evidence that the alkene is the last π-component to be incorporated is found in concentration studies and pyridone formation. Higher reaction concentrations (0.12 M vs 0.04 M) or bulky alkene

substituents increase pyridone formation. Higher concentrations favor intermolecular interception of metallacycle **IIa/b** by a second equivalent of alkyne over intramolecular migratory insertion of the tethered alkene. Furthermore, bulky substituents inhibit migratory insertion of the alkene favoring intermolecular insertion of a second alkyne to form pyridone (Scheme 3.5). These results suggest that the alkyne and isocyanate are the first components to oxidatively cyclize. This is further supported by the observation that 1,7-octadiyne **1y** and 1,8-nonadiyne **1z** furnish vinylogous amides **4y** and **4z** showing an apparent kinetic preference for *intermolecular* coordination and activation of the isocyanate in spite of the entropically favored *intramolecular* coordination of the second terminal alkyne (Chapter 1, Table 1.12). Finally, vinylogous amide and lactam products obtained with the same Taddol phosphoramidite are opposite major enantiomers (Scheme 3.3). This suggests that both products are not formed from rhodacycle **IIc** as stereoinduction would occur prior to CO migration.

A mechanism where the alkyne and alkene oxidatively cyclize to make a rhodacyclopentene followed by isocyanate insertion can be proposed, but this is unlikely because there is no plausible pathway to form vinylogous amide **4** or 4-pyridone.[19-21] Considering these observations, we propose that the alkene is the last π-component to be incorporated and the operative catalytic cycle is likely that shown in Scheme 3.2.

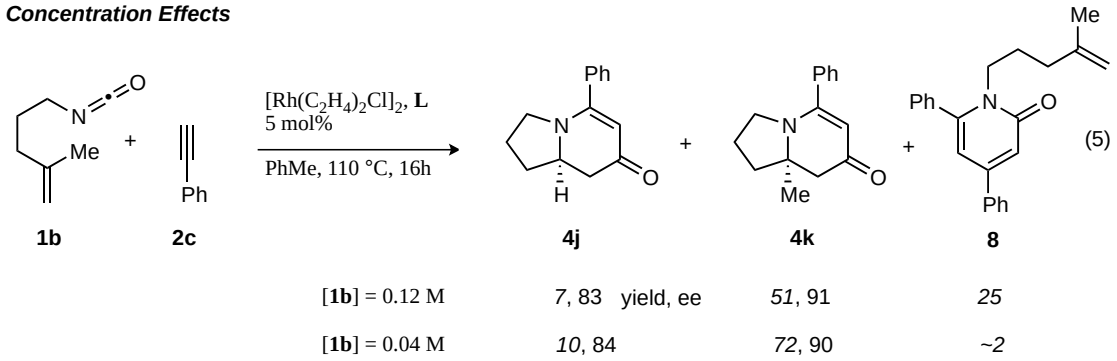

Scheme 3.5 Pyridone formation dependent on concentration

3.2.4 X-ray Analysis of Rh(cod)Cl•Phosphoramidites

Remarkable alkyne regioselectivity is observed in the Rh(I) catalyzed cycloaddition, where the vinyl hydrogen is α to the carbonyl in all terminal alkyne products. As part of our ongoing efforts to explain the regio- and product selectivity of the reaction, single crystal X-ray analyses of Rh(I)

(cod)Cl•phosphoramidite complexes were undertaken.[22-27] Rh(cod)Cl•**T5** is depicted in Figure 3.2. Rhodium is in the square planar geometry and the phosphoramidite is coordinated via phosphorus as an L-type ligand. Chloride is also bound to rhodium, participating as an X-type ligand. Cyclooctadiene is also ligated to rhodium via the two alkenes with both acting predominately as L-ligands. Rh(cod)Cl•**B2** has similar coordination geometry to that seen with the Taddol-based phosphoramidites (Figure 3.3). The only notable exception is the steric environment provided by the ligand around rhodium. As will be discussed later, the different environments have a similar affect on substrate coordination and oxidative cyclization.

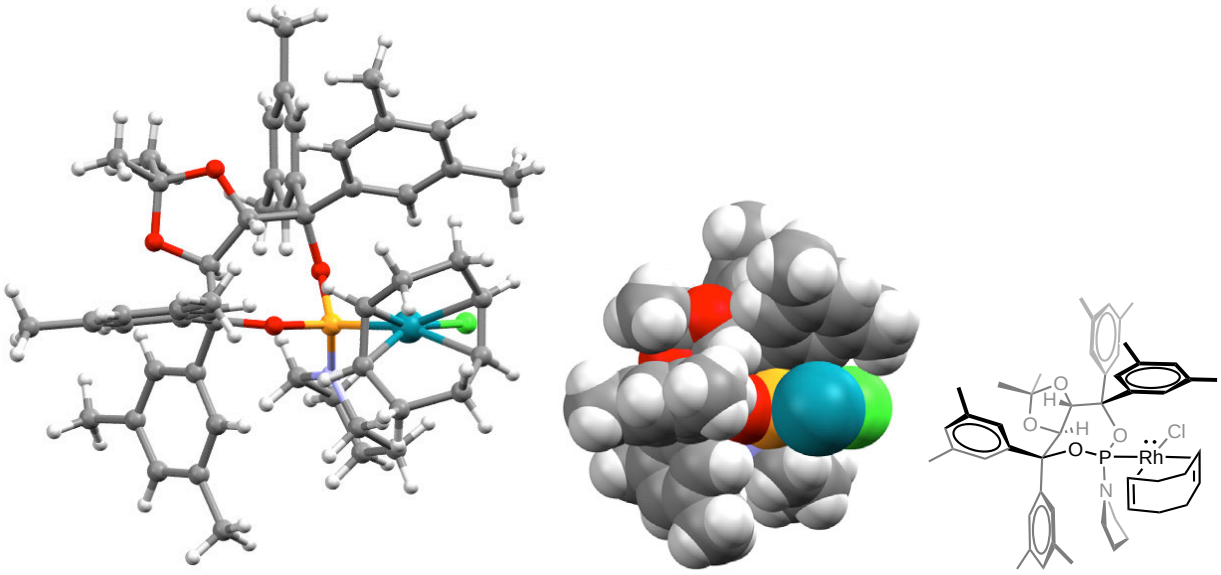

Figure 3.2 Ball and Stick representation of Rh(cod)Cl•**T5** X-ray structure. C = grey, H = white, N = light blue, O = red, P = orange, Cl = green, Rh = teal. Cod ligand has been removed from spacefilling model for clarity.

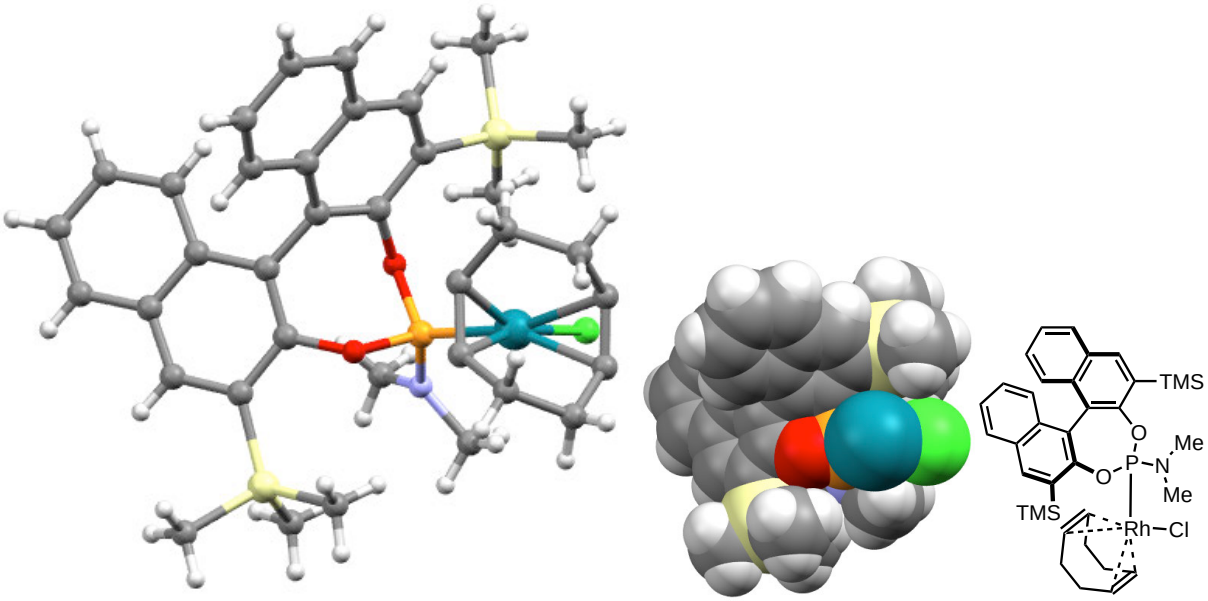

Figure 3.3 Ball and Stick representation of Rh(cod)Cl•**B2** X-ray structure. C = grey, H = white, N = light blue, O = red, P = orange, Cl = green, Rh = teal, Si = yellow. Cod ligand has been removed from spacefilling model for clarity.

Examination of the X-ray data shows a correlation between Rh–P bond distance and product selectivity. Longer Rh–P bond distances correlate with increased formation of lactam **3** while shorter Rh–P bond distances show a preference toward vinylogous amide **4** (Table 3.5). For example, *m*-Xylyl Taddol phosphoramidite **T5** has a Rh–P bond distance of 2.270 Å and provides a 12.5:1 product selectivity for the lactam product in the cycloaddition with 1-octyne while biaryl phosphoramidite **B1** has a 2.245 Å Rh–P and gives product selectivity of 1:6.2. The correlation is not perfect. Binol-based phosphoramidite **B2** (Guiphos) has the shortest Rh–P but does not give the highest level of product selectivity, suggesting that other factors beyond Rh–P affect product selectivity. This is not surprising given the reaction is known to be sensitive to the electronics of the alkyne component, indicating a stereoelectronic component is also involved. A graph of Rh–P bond distance and product selectivity shows a strong correlation with an R^2 value of 0.95 (Figure 3.4).

Table 3.5 X-ray analysis shows trends between product selectivity and Rh–P bond length.

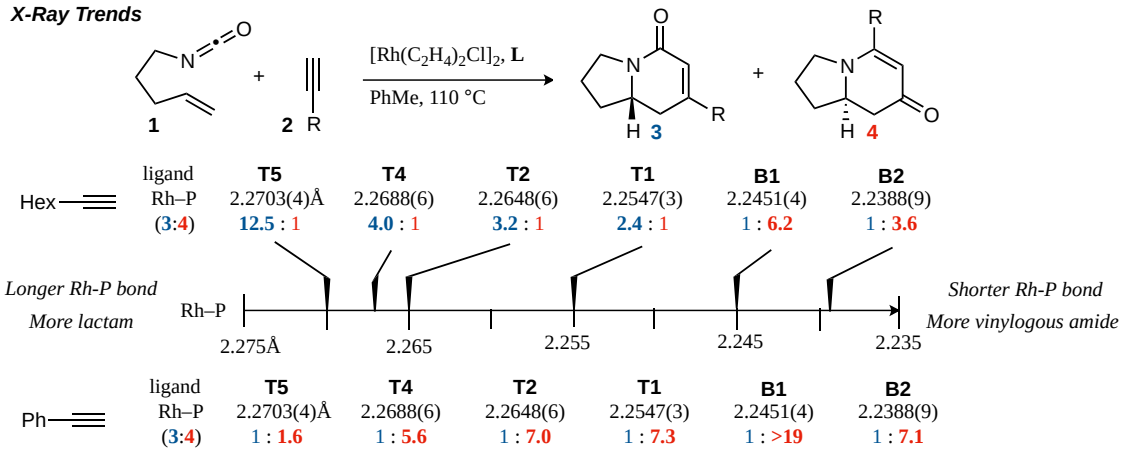

Ligand	Rh–P	Rh–Cl	*Trans to P* Rh–C=C*	C=C	*Trans to Cl* Rh–C=C*	C=C
T5	2.2703(4)Å	2.3654(4)	2.132	1.409(2)	1.994	1.413(3)
T4	2.2688(6)	2.3765(6)	2.131	1.377(4)	1.992	1.395(4)
T2	2.2648(6)	2.3777(6)	2.140	1.376(4)	1.997	1.417(3)
T1	2.2547(3)	2.3842(3)	2.152	1.3781(18)	1.995	1.4131(16)
B1	2.2451(4)	2.3485(4)	2.162	1.369(3)	2.013	1.409(2)
B2	2.2388(9)	2.3455(8)	2.151	1.365(5)	2.003	1.396(5)

* Bond length from Rh to centroid of alkene

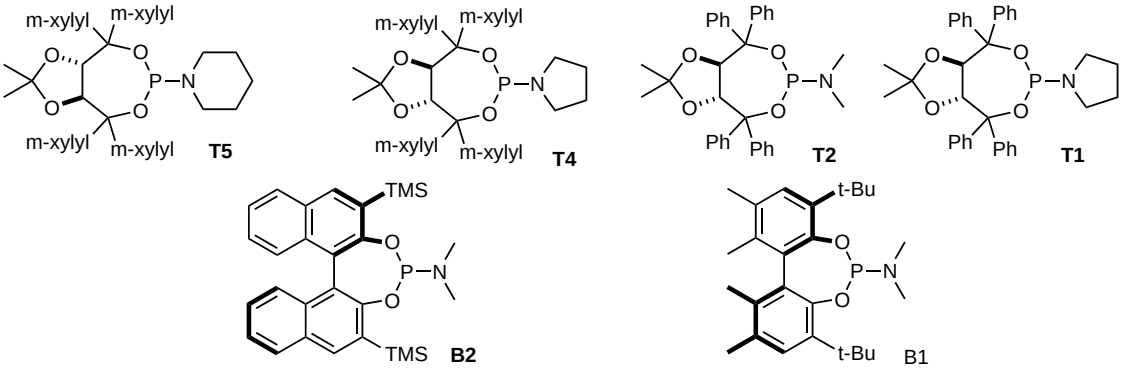

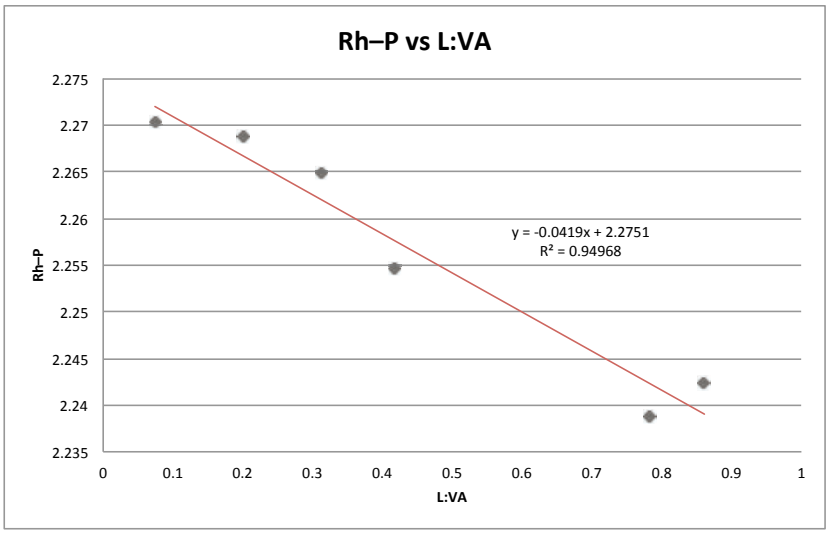

Figure 3.4 Graph of product selectivity as a function of Rh–P bond distance.

The C=C trans to phosphorus for *m*-Xylyl Taddol phosphoramidite **T5** is 1.409 Å and indicates that rhodium is relatively π-basic in this complex and is backdonating electron density to the alkene giving it metallacyclopropane character. On the other hand, the C=C trans to phosphorus for biaryl phosphoramidite **B1** is 1.369 Å suggesting that rhodium is relatively π-acidic and is accepting electron density from the alkene, which explains the bond distance closer to that of the free alkene. For reference the C=C bond length of $[Rh(cod)Cl]_2$ is 1.424 Å and the average unligated C=C bond distance is 1.337 Å, representing the relative extremes possible in Rh–alkene coordination.[28] While no significant changes are seen in the C=C trans to Cl with ligand modification, the Rh–Cl bond distance increases within the Taddol phosphoramidite series.

3.2.5 Phosphoramidite Ligands Hinder One Face of Rh(I) Square plane

Examination of the X-ray crystal structures revealed that the steric environment created by monodentate, C_2-symmetric phosphoramidite ligands sterically hinder one face of the square planar rhodium(I) complex. This may explain the exceptional regioselectivity seen in the cycloaddition. One of the *m*-Xylyl groups sits above the rhodium square plane in the structure of Rh(cod)Cl•**T5**, with the opposite side of the complex much more exposed (Figure 3.2). The naphthyl and trimethylsilyl hinders this face in the Rh(cod)Cl•**B2** complex (Figure 3.3). These effects are evident in each of the other Rh•phosphoramidite crystal structures (Figure 3.5).

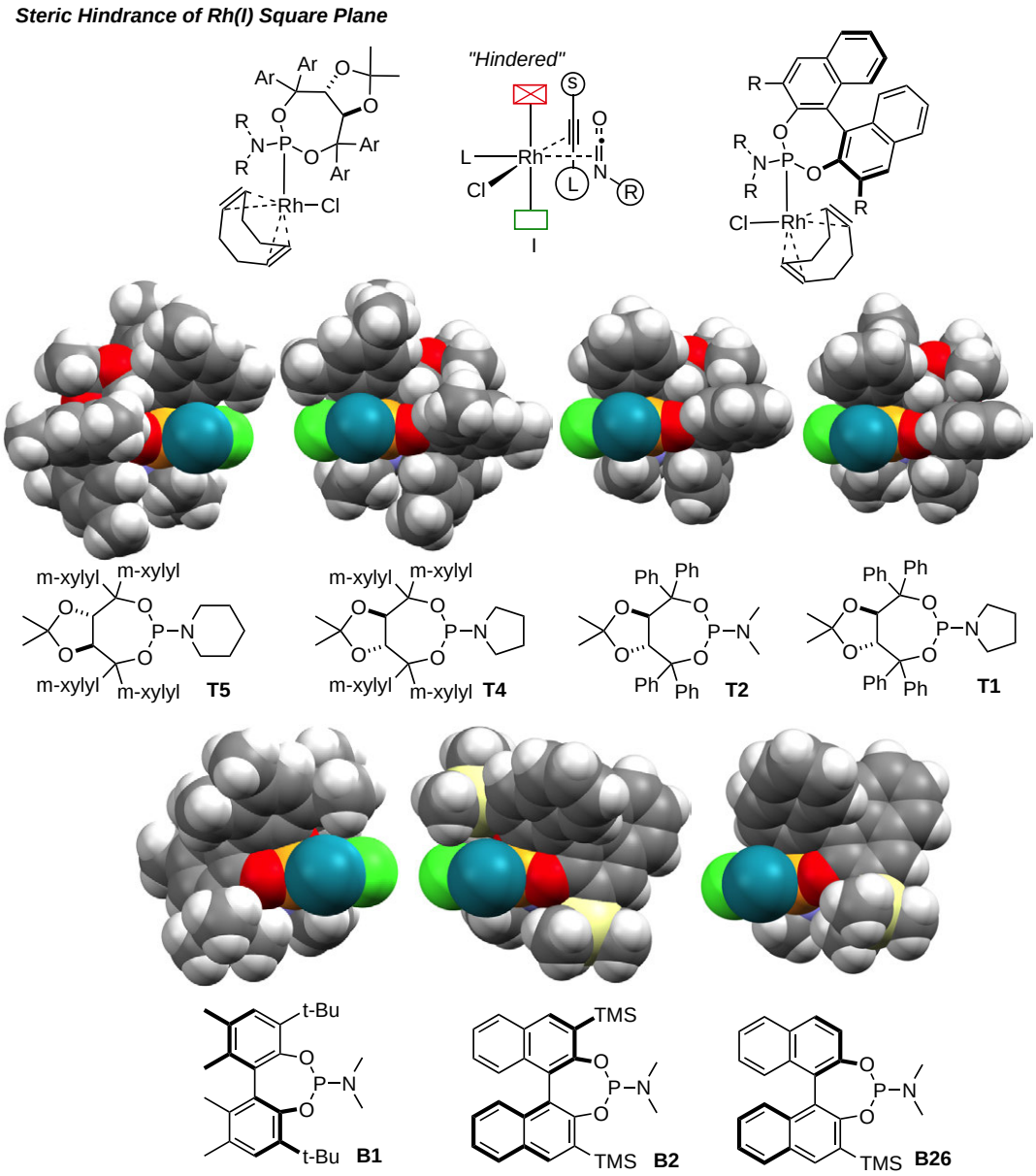

Figure 3.5 X-ray structures show phosphoramidite steric hindrance of Rh(I) square plane. C = grey, H = white, N = light blue, O = red, P = orange, Cl = green, Rh = teal, Si = yellow. Cod ligand has been removed from spacefilling model for clarity.

We propose that steric hindrance organizes coordination of the alkyne and isocyanate such that the sterically smaller substituents are in the same hemisphere of the square plane as shown in **I** (Table 3.6). We suggest that the alkynes displace ethylene prior to association of isocyanate, and as the phosphoramidite has a greater *trans* influence than chloride, we predict that the isocyanate coordinates *trans* to the phosphoramidite. From this coordination complex, oxidative cyclization accounts for the

single regioisomer of the lactam and vinylogous amide observed. Regioselectivity of the alkyne is controlled predominately by the sterics of the phosphoramidite ligand orienting coordination of both alkyne and isocyanate based on steric interaction with the ligand based on substituent size.

3.2.6 Steric Control of Oxidative Cyclization

The alkyne and isocyanate coordinate to rhodium perpendicular rather than parallel[29] to the square plane. We base this on Wakatsuki and Yamazaki's calculations of cobaltacyclopentadienes[30] and ground state X-ray crystal analysis of other d^8 metal complexes.[31-33] They suggest that an orthogonal coordination of π-components is operative because steric repulsion between π-components is minimized and better back donative stabilization is possible when orthogonal. Wakatsuki-Yamazaki's regioselectivity model is based on observations and calculations of cobaltacyclopentadiene formation (Scheme 3.6). The major product results from a head to tail orientation of the large alkyne substituents to form cobaltacyclopentadienes **Id** and **IId**. We do not observe either lactam or vinylogous amide products derived from such an orientation. Wakatsuki and Yamazaki claim the minor product **IId** is kinetically favored over **Id** due to steric interactions between large alkyne substituents as shown in **TSIII** (Scheme 3.6). When the alkynes are not head to tail, they suggest that the large substituents prefer to be α to the metal.

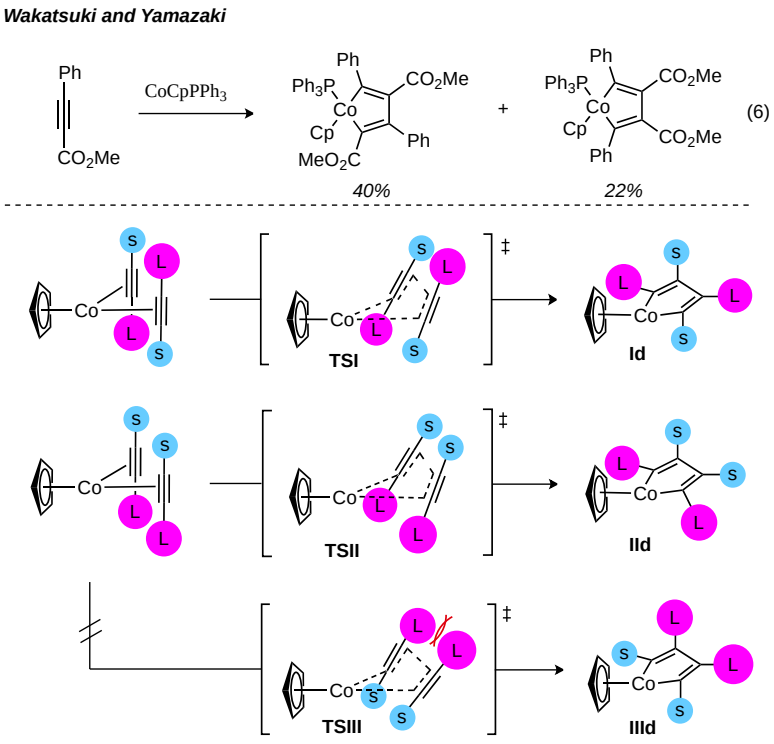

Scheme 3.6 Steric effects on oxidative cyclization.

This model accounts for the regioselectivity of oxidative cyclization of π-components seen in rhodacycle **IIa**, which generates lactam (Scheme 3.2). Using this argument, one would predict that larger alkyne substituents would favor lactam; however, more vinylogous amide is seen (cyclohexyl, Table 3.3). Finally, this model does not account for vinylogous amide formation, since the larger groups are β to the metal in rhodacycle **IIb** (Scheme 3.2). As product selectivity could not be completely explained by substrate steric control alone, we sought another model to rationalize selectivity based on stereoelectronic effects.

3.2.7 Stereoelectronic Effects on Oxidative Cyclization

Stockis and Hoffman discuss the effects polarized π-components have on regioselectivity of oxidative cyclization when devoid of steric contributions.[34] Based on calculations and correlation with experimental data, they propose a stereoelectronic model to explain regioselectivity in oxidative cyclization and metallacycle formation. They hypothesize that polarized π-components oxidatively

cyclize so that the greatest LUMO coefficient is β to the metal in the resultant metallacycle. This is due to enhanced π* mixing with filled d_{xy} orbitals in the oxidative cyclization transition state (Scheme 3.7).

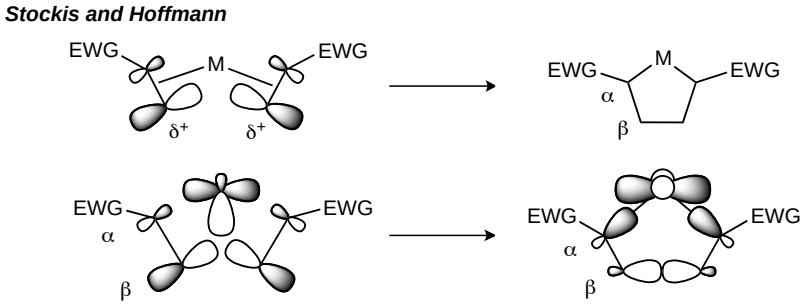

Scheme 3.7 Stereoelectronic effects on oxidative cyclization

In Rh(I) catalyzed [2+2+2] cycloadditions, we observe a propensity for lactam formation when the sterics of the phosphoramidite and alkyne substrate decrease and the alkyne is electron-deficient. Lactam formation is controlled by the isocyanate's large LUMO coefficient strongly interacting with rhodium d_{xy} during oxidative cyclization so that the carbonyl of the isocyanate is β to rhodium in the resultant metallacycle **IIa** (Scheme 3.2). However, this does not explain isocyanate regioselectivity for vinylogous amide formation in which the largest LUMO coefficients of at least one of the π-components is α to the metal in the resultant metallacycle; this is contrary to the predictions of the Stockis-Hoffman model.

3.2.8 Model for Oxidative Cyclization and Product Selectivity

As neither the Wakatsuki-Yamazaki steric nor the Stockis-Hoffman stereoelectronic models adequately explain the product selectivity seen in the cycloaddition, we developed a hybrid model to account for product selectivity based on steric and stereoelectronic contributions to coordination and oxidative cyclization (Scheme 3.8). Single regioisomeric products are explained by alkyne and isocyanate coordination dictated by phosphoramidite sterics, placing the small substituent of each π-component in a *cis* orientation. The two π-components are coordinated orthogonal to the square plane (**Ia**, **Ib**), as proposed by Wakatsuki-Yamazaki and corroborated by crystal structures.[35,36] To generate rhodacycle **IIa** en route to lactam from the orthogonal coordination seen in **Ia**, the CO of the isocyanate and the terminal C–H of the alkyne must bend away from the Rh center and toward each other passing through **TSIV**

forming the C–C bond. Similarly, the N–R^2 group of the isocyanate and the C–R^1 bond of the terminal alkyne bend away from the Rh center, forming the C–N bond via **TSV**, en route to rhodacycle **IIb** in the vinylogous amide pathway.

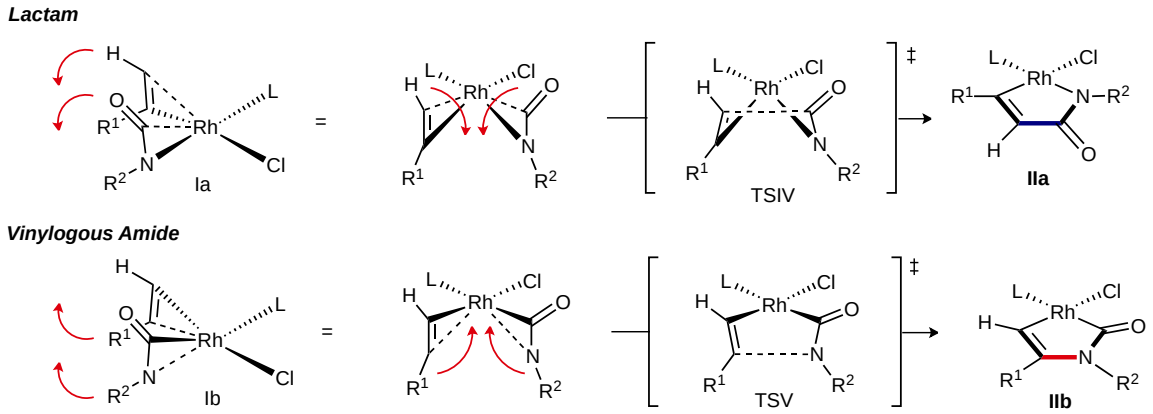

Scheme 3.8 Coordination and direction of oxidative cyclization.

For product selectivity, the LUMO of the isocyanate favors formation of lactam, but is overridden by sterics of the substrate and ligand. Smaller alkynes (1-octyne, Table 3.3) generate lactam and oxidative cycloaddition is controlled by isocyanate electronics. Larger alkynes (cyclohexylacetylene) produce more vinylogous amide due to ligand-alkyne steric interactions in transition state **TSIVa**, favoring **TSVa** in which less steric interaction is suspected **(**Scheme 3.9). Alkyne electronics modify product selectivity. Electron-deficient aryl alkynes override steric control to favor lactam, as the alkyne and isocyanate LUMOs are β to the metal in **TSIVb**. Electron-rich aryl alkynes generate vinylogous amide due to unfavorable steric interactions between the alkyne and ligand (**TSIV**), and this selectivity is reinforced by the alkyne LUMO because it will be β to the metal in **TSVa**.

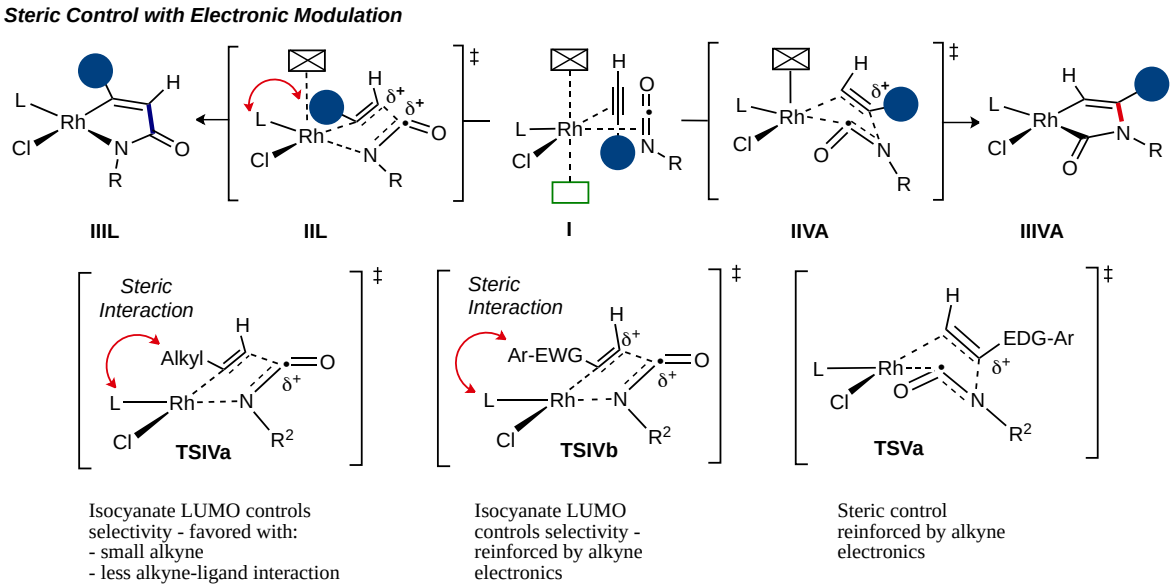

Scheme 3.9 Proposed model for product selectivity based on oxidative cyclization.

These unfavorable alkyne-phosphoramidite interactions are exacerbated by changes in the Rh–P bond length, where a shorter bond favors vinylogous amide and a longer bond favors lactam (Figure 3.4). Electron-deficient phosphoramidites have shorter Rh–P bond lengths, which accentuate the ligand/alkyne steric interaction in transition state (**TSIVa/b**) and funnel reagents down the vinylogous amide pathway. On the other hand, electron-rich phosphoramidites have longer Rh–P bonds, which alleviate the steric interactions between the alkyne and ligand to generate more lactam. Finally, we have seen that in the Taddol ligand series large amines favor lactam product and we don't have a good explanation for this.

3.2.9 Models for Migratory Insertion and Enantioselectivity

A proposed model to rationalize observed enantioselectivity is shown in Scheme 3.10. In metallacycle **IIa** leading to lactam, we postulate that there are two factors controlling enantioinduction: facial selectivity of the alkene dictated by the geometry of the tether and facial selectivity at the rhodium center as influenced by the phosphoramidite ligand. Each of the Rh(cod)Cl•phosphoramidite crystal structures show that the ligand hinders one face on the rhodium square plane and suggest this facial, steric hindrance is present in Rh(III) intermediates.

For migratory insertion to occur the alkene must be *syn*-coplanar with the Rh–N bond, and as a result, only four alkene coordination scenarios are proposed. In the first two scenarios, **IIa^1** and **IIa^2**, the alkene

has to coordinate to the hindered rhodium face and are, thus, disfavored. **IIa^1** requires the alkene tether to be in an undesirable twist-boat conformation. As shown in model **IIa^2** the tether can adopt a chair conformation; 1,2-migratory insertion as shown in **IIa^2** leads to the minor enantiomer observed (Minor 3). With models **IIa^3** and **IIa^4**, we have shown the alkene coordinating to the less hindered face of rhodium, opposite the face obstructed by the phosphoramidite ligand. As discussed with model **IIa^1**, alkene coordination in model **IIa^3** is disfavored due to a strained, twist-boat tether conformation. The tether as shown in metallacycle **IIa^4** adopts a favorable chair conformation and migratory insertion as depicted in this model would provide the major, observed lactam enantiomer (Major **3)**.

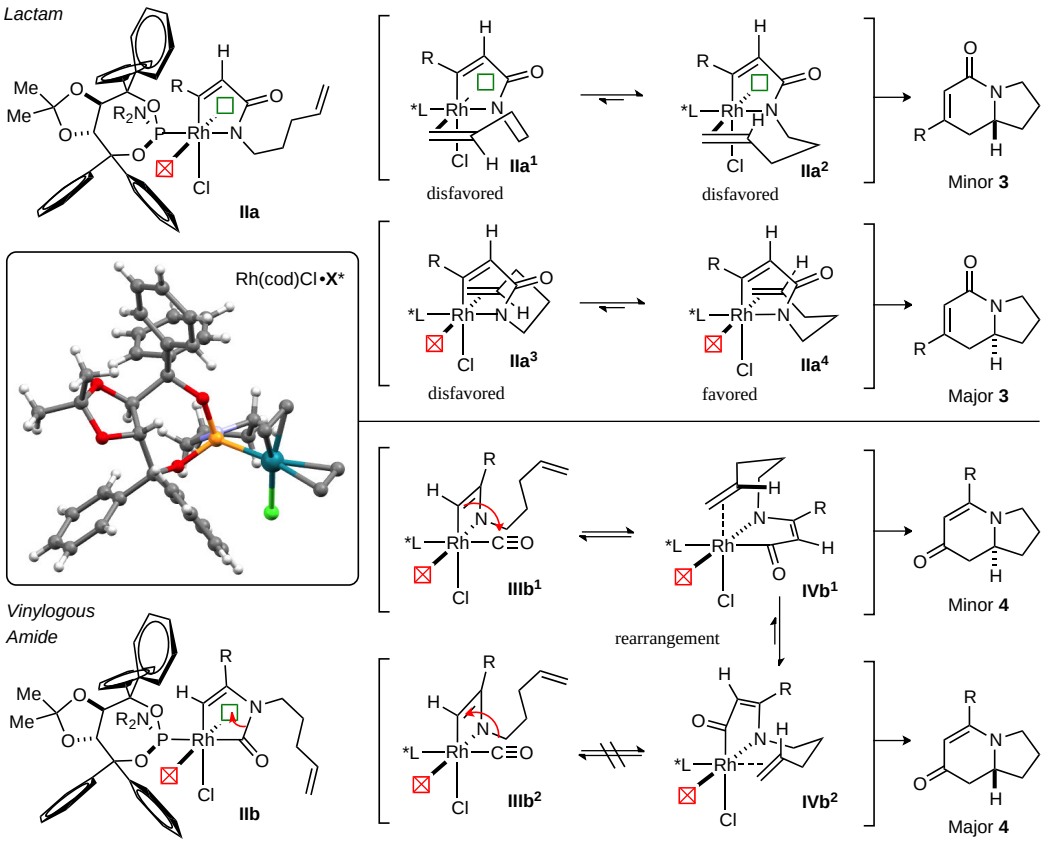

Scheme 3.10 Model for enantioselectivity

Rationalizing enantioselectivity for vinylogous amide is more difficult because enantioinduction occurs after several ligand rearrangements on rhodium(III) species. CO migration from **IIb** presumably occurs from amide bond cleavage and amine migration to the unhindered open coordination site, resulting in metallacycle **IIIb^{1,2}**. We presume that the alkenyl carbon migrates to the CO ligand as seen in **IIIb^1**

leading to metallacycle **IVb[1]**. However, coordination of the alkene and migratory insertion of this metallacycle leads to the minor enantiomer observed for vinylogous amide. The major enantiomer could be formed by CO migration onto the alkenyl carbon (**IIIb[2]**), but such a migration is unprecedented.[14-16] Rapid rearrangement of **IVb[1]** to **IVb[2]** and subsequent alkene insertion would provide the major observed enantiomer. This rearrangement is potentially influenced by steric interactions between the alkenyl tether and ligand disfavoring **IVb[1]**. As these models are for an unobservable rhodium(III) species, we can only speculate as to the actual ligand rearrangements.

3.3 Conclusion

Mechanistic studies were undertaken to understand the Rh(I) catalyzed cycloaddition of alkenyl isocyanates and alkynes. We found that these cycloadditions occur by irreversible oxidative cyclization of the isocyanate and alkyne. Coordination of the π-components is organized by the phosphoramidite steric environment which leads to single regioisomeric products. Oxidative cyclization from a single coordination complex can be used to account for both lactam and vinylogous amide products. Product selectivity is determined by the direction of oxidative cyclization and is sensitive to both steric and electronic factors. Finally, enantioinduction is controlled by steric hindrance of one face of the rhodium square plane. The proposed model is useful for predicting the outcome of a given cycloaddition based on the desired alkyne and ligand involved.

3.4 References

(1) Yu, R. T.; Rovis, T. *J. Am. Chem. Soc.* **2006**, *128*, 12370–12371.

(2) Albano, P.; Aresta, M. *J. Organomet. Chem.* **1980**, *190*, 243–246.

(3) Schäfer, H.-A.; Marcy, R.; Rüping, T.; Singer, H. *J. Organomet. Chem.* **1982**, *240*, 17–25.

(4) Ohshita, J.; Furumori, K.; Matsuguchi, A.; Ishikawa, M. *J. Org. Chem.* **1990**, *55*, 3277–3280.

(5) Hansch, C.; Leo, A.; Taft, R. *Chem. Rev.* **1991**, *91*, 165–195.

(6) Dalton, D. M.; Oberg, K. M.; Yu, R. T.; Lee, E. E.; Perreault, S.; Oinen, M. E.; Pease, M. L.; Malik, G.; Rovis, T. *J. Am. Chem. Soc.* **2009**, *131*, 15717–15728.

(7) Yu, R. T.; Lee, E. E.; Malik, G.; Rovis, T. *Angew. Chem. Int. Ed.* **2009**, *48*, 2379–2382.

(8) Hall, H. K. *J. Am. Chem. Soc.* **1957**, *79*, 5441–5444.

(9) Hoberg, H. *J. Organomet. Chem.* **1988**, *358*, 507–517.

(10) Duong, H. A.; Louie, J. *J. Organomet. Chem.* **2005**, *690*, 5098–5104.

(11) Yamamoto, Y.; Kinpara, K.; Saigoku, F.; Takagishi, H.; Okuda, S.; Nishiyama, H.; Itoh, K. *J. Am. Chem. Soc.* **2005**, *127*, 605–613.

(12) Kondo, T.; Nomura, M.; Ura, Y.; Wada, K.; Mitsudo, T.-A. *Tetrahedron Lett.* **2006**, *47*, 7107–7111.

(13) Miura, T.; Morimoto, M.; Murakami, M. *J. Am. Chem. Soc.* **2010**, *132*, 15836–15838.

(14) Cavallo, L.; Sola, M. *J. Am. Chem. Soc.* **2001**, *123*, 12294–12302.

(15) Gonsalvi, L.; Adams, H.; Sunley, G.; Ditzel, E.; Haynes, A. *J. Am. Chem. Soc.* **2002**, *124*, 13597–13612.

(16) Gonsalvi, L.; Gaunt, J.; Adams, H.; Castro, A.; Sunley, G.; Haynes, A. *Organometallics* **2003**, *22*, 1047–1054.

Oberg, K. M.; Lee, E. E.; Rovis, T. *Tetrahedron* **2009**, *65*, 5056–5061.

(18) Tolman, C. *J. Am. Chem. Soc.* **1974**, *96*, 2780–2789.

(19) Schmid, R.; Kirchner, K. *J. Org. Chem.* **2003**, *68*, 8339–8344.

(20) Dazinger, G.; Schmidt, R.; Kirchner, K. *New J. Chem.* **2004**, *28*, 153–155.

(21) Dazinger, G.; Torres-Rodrigues, M.; Kirchner, K.; Calhorda, M. J.; Costa, P. J. *J. Organomet. Chem.* **2006**, *691*, 4434–4445.

(22) Bartels, B.; García Yebra, C.; Rominger, F.; Helmchen, G. *Eur. J. Inorg. Chem.* **2002**, *2002*, 2569–2586.

(23) Leitner, A.; Shekhar, S.; Pouy, M. J.; Hartwig, J. F. *J. Am. Chem. Soc.* **2005**, *127*, 15506–15514.

(24) Faller, J. W.; Milheiro, S. C.; Parr, J. *J. Organomet. Chem.* **2006**, *691*, 4945–4955.

(25) Giacomina, F.; Meetsma, A.; Panella, L.; Lefort, L.; De Vries, A. H. M.; De Vries, J. G. *Angew. Chem. Int. Ed.* **2007**, *46*, 1497–1500.

(26) Mikhel, I. S.; Rüegger, H.; Butti, P.; Camponovo, F.; Huber, D.; Mezzetti, A. *Organometallics* **2008**, *27*, 2937–2948.

(27) Filipuzzi, S.; Maennel, E.; Pregosin, P. S.; Albinati, A.; Rizzato, S.; Veiros, L. F. *Organometallics* **2008**, *27*, 4580–4588.

(28) De Ridder, D. J. A.; Imhoff, P. *Acta Crystallogr. E* **1994**, *50*, 1569–1572.

(29) Imabayashi, T.; Fujiwara, Y.; Nakao, Y.; Sato, H.; Sakaki, S. *Organometallics* **2005**, *24*, 2129–2140.

(30) Wakatsuki, Y.; Nomura, O.; Kitaura, K.; Morokuma, K.; Yamazaki, H. *J. Am. Chem. Soc.* **1983**, *105*, 1907–1912.

(31) Davies, G. R.; Hewertson, W.; Mais, R. H. B.; Owston, P. G.; Patel, C. G. *J. Chem. Soc., A.* **1970**, 1873–1877.

(32) Beauchamp, A. L.; Rochon, F. D.; Theophanides, T. *Can. J. Chem.* **1973**, *51*, 126-131.

(33) de Vaal, P.; Dedieu, A. *J. Organomet. Chem.* **1994**, *478*, 121–129.

(34) Stockis, A.; Hoffmann, R. *J. Am. Chem. Soc.* **1980**, *102*, 2952–2962.

(35) Barlow, J. H.; Clark, G. R.; Curl, M. G.; Howden, M. E.; Kemmitt, R. D. W.; Russell, D. R. *J. Organomet. Chem.* **1978**, *144*, C47–C51.

(36) Barlow, J. H.; Curl, M. G.; Russell, D. R.; Clark, G. R. *J. Organomet. Chem.* **1982**, *235*, 231–241.

CHAPTER 4

Ligand Development for Rh(I)-Catalyzed [2+2+2] Cycloadditions of Alkyl Alkynes

4.1 Introduction

4.1.1 5-Alkyl Substituted Indolizidines

Indolizidines and quinolizidines are abundant natural product structural motifs with unique biological properties (Figure 4.1).[1-12] As of 2005, more than 800 alkaloids have been isolated from amphibian skin and characterized into 20 classes of compounds. Of those twenty classes, the indolizidine motif is found in more than 300 alkaloids and more than 200 indolizidines contain an alkyl substituent at the 5 position. The abundance and known biological activity of indolizidines make these scaffolds important synthetic targets. Classic syntheses of these scaffolds include S_n2 cyclization of amines, lactamization, and ring closing metathesis. Modern syntheses of this class of alkaloids have increased efficiency but are typically racemic[13] or have lengthy starting material syntheses.[14] Since 2006, we have developed rapid, efficient and asymmetric syntheses of indolizidinone and quinolizidinone products.

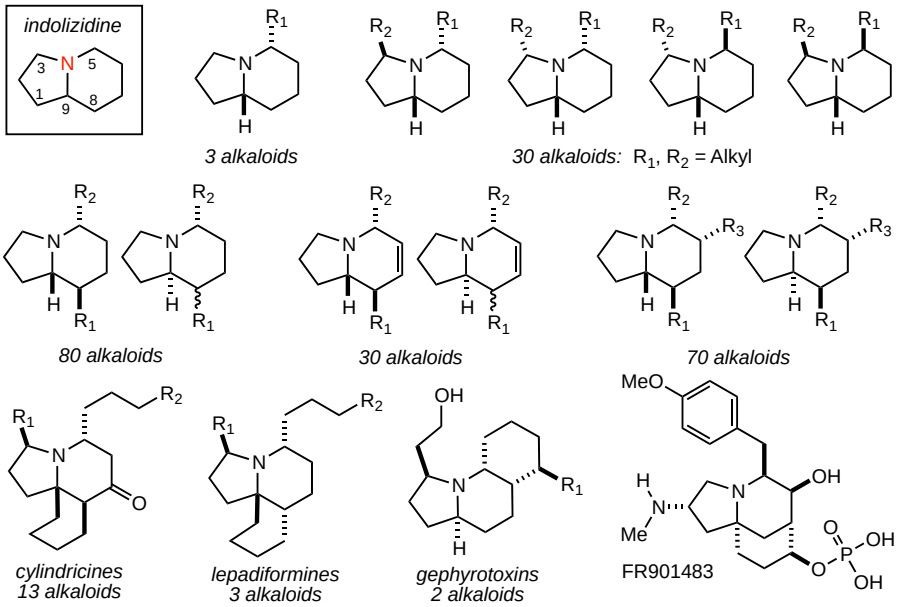

Figure 4.1 Selected 5-alkyl substituted indolizidines.

4.1.2 Substrate-based Control of Product Selectivity

A significant challenge in the development of this methodology has been the control of product selectivity between lactam **3** and vinylogous amide **4** (Scheme 4.1). Product selectivity is typically dictated by the steric and electronic nature of the alkyne. Alkyl alkynes favor lactam **3** and aryl/alkenyl alkynes provide vinylogous amide **4**. Yu and Rovis found that carbodiimide π-components alter product selectivity with aryl acetylenes to modestly favor amidine products, which, after hydrolysis, provide the lactam product.[15] This provides a useful method to access lactam products with aryl acetylenes. However, a similar substrate based solution to favor vinylogous amide products with alkyl alkynes has not been found.

Yu and Rovis reported in 2009 that *t*-Bu-biaryl phosphoramidite **B1** could be used to alter product selectivity with alkyl alkynes in favor of vinylogous amide.[16] At that time, it was not clear what factors were affecting product selectivity and nor how to further increase selectivity. Nevertheless Yu's finding was an important contribution because alkyl substituted vinylogous amide products are efficiently used to synthesize 5-alkyl substituted indolizidines as demonstrated by the 4 step asymmetric synthesis of indolizidine 209-d, and using a ligand to change product selectivity is an elegant solution. Working within our proposed mechanistic hypothesis, we sought to tame substrate control of product selectivity through ligand design and development.

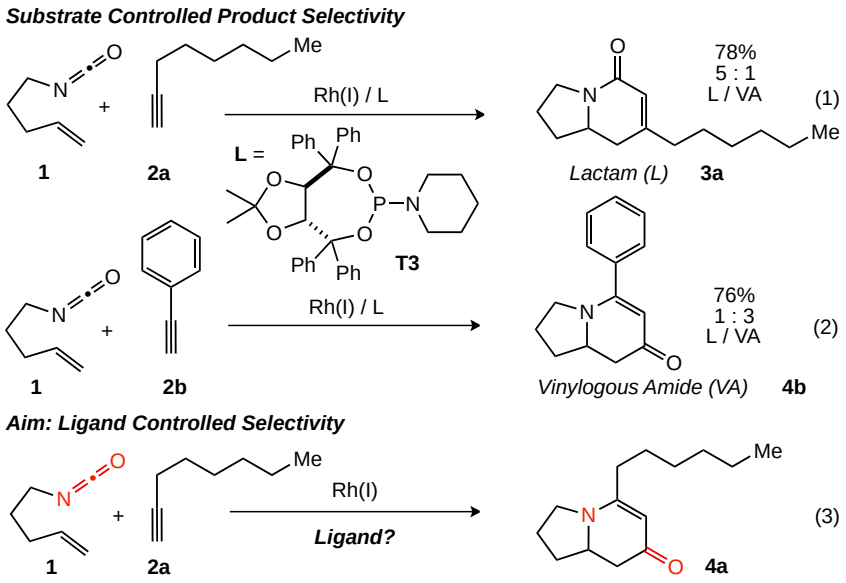

Scheme 4.1 Depiction of substrate controlled product selectivity

4.2 Results

4.2.1 Ligand Development Used to Override Substrate Control of Product Selectivity

Since the steric and electronic nature of the alkyne influences CO migration, we hypothesised that steric and electronic manipulation of the ligand could be used to control product selectivity; our aim was to override substrate-based control of product selectivity (Scheme 4.1) through ligand development.

Yu and Rovis reported that Taddol phosphoramidites favor lactam **3** with alkyl alkynes with modest to good product selectivities (Chapter 1). Yu found that *p*-tolyl Taddol **T18** and *m*-xylyl Taddol **T5** increase selectivity for lactam **3** better than phenyl-Taddol **T3** in the reaction of pentenyl isocyanate and 1-octyne (Table 4.1). Curious if the increase in product selectivity was due to a steric or electronic effect, we synthesized electron-rich, *p*-MeO-phenyl Taddol **T22**, believing it to be sterically similar to **T18** and that it would allow us to make a direct comparison between sterics and electronics. *p*-MeO **T22** increases product selectivity for lactam over both *p*-tolyl **T18** and *m*-xylyl **T5**. Although yield with **T22** is low (22%) and ee is good (75%), this result indicated that aryl electronics could be used to change product selectivity.

If electronic manipulation of the aryl was affecting product selectivity more than sterics, perhaps sterically similar p-CF_3-aryl Taddol **T23** would alter product selectivity in favor of vinylogous amide **4**.

This is the case and 1:2.3 (L:VA) selectivity is seen. This was the first example of a Taddol-based phosphoramidite favoring vinylogous amide with an alkyl alkyne. Encouraged by this result, 3,5-bis-CF_3-Taddol **T24** was made and found that it provides 1:8.1 product selectivity. A comparison of this result with sterically identical m-Xylyl **T5,** which gives a 12.5:1 selectivity for lactam, suggests that the electronics of the aryl affects product selectivity as opposed to the sterics of the 3,5-disubstituted aryl. Thus we incorporated the most electron deficient aryl that we had access to, C_6F_5, onto the Taddol framework. C_6F_5-Taddol **T25** (CKphos) heavily favors vinylogous amide **4** with product selectivity greater than 1:19 and excellent yield (86%) and enantioselectivity (96%) with 1-octyne.

Table 4.1 Ligand development for the Rh(I) catalyzed [2+2+2].

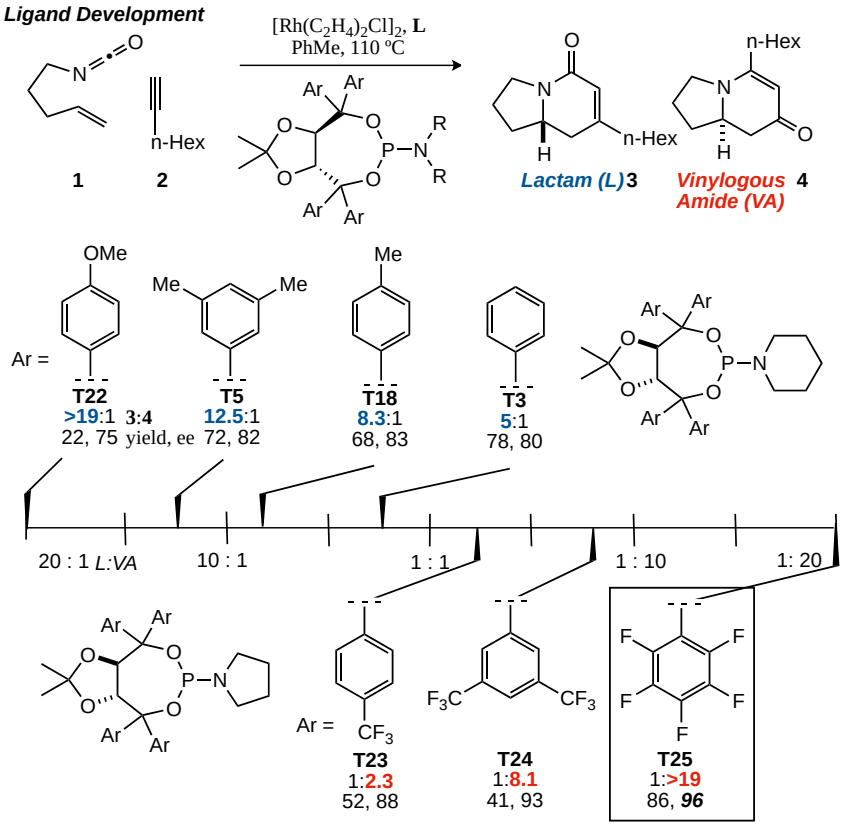

4.2.2 Substrate Scope with Perfluoroaryl Taddol Phosphoramidites

A wide range of alkyl substituted terminal alkynes may not be converted into the corresponding vinylogous amide with excellent product selectivities using the perfluorinated Taddol ligand (**T25,** CKphos), as shown in Table 4.2. With long straight chain alkyl alkynes excellent product and enantioselectivities are found. A variety of functional groups are tolerated including alkyl chlorides, pendant alkynes, silyl ethers, protected nitrogens (phthalimide), aromatic substrates. Substrates that previously favor lactam formation (with ligand **T3**) such as small and/or electron-deficient alkyl alkynes (propargyl **2e**, phthalimide **2f** or benzyl **2i**), are now synthesized as vinylogous amide **4** with CKphos in good product selectivity (1:7 or 1:>19, L:VA) and excellent enantioselectivity (97-99%). Sterically bulky alkyl alkynes (cyclohexyl **4g** and *t*-Butyl **4h**) are well tolerated with improvement in product selectivity and enantioselectivity seen. Phenyl and electron-deficient aryl alkynes are problematic substrates. For example phenyl-Taddol **T3** provides poor product selectivities for these substrates. *t*-Bu-biaryl **B1**

improves the product selectivity issue however it is unable to achieve high levels of enantioselectivity. C_6F_5-**T25** (CKphos) provides excellent product and enantioselectivity for electron-deficient aryl alkynes, which previously favored lactam.

Table 4.2 Substrate scope of terminal alkynes. Enantiomeric excess shown is of the major product. b) Results previously reported[16]; 2 equiv of 2 used. c) Methoxypropargyl acetylene used.

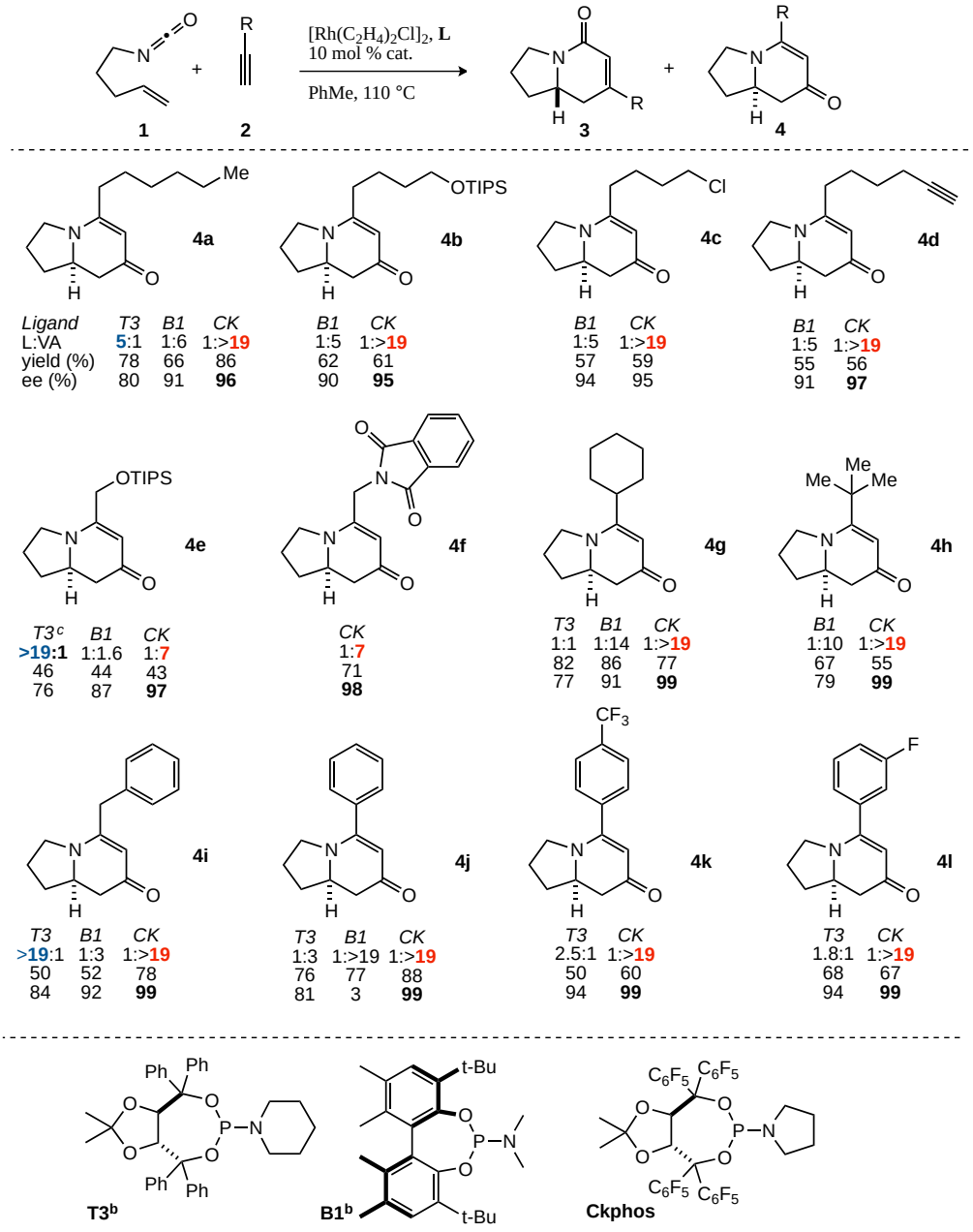

4.2.3 Ligand Screen with Cyclooctyne

Control of product selectivity remained a significant challenge in the [2+2+2] cycloaddition with strained cyclic alkynes. We decided to briefly reinvestigate these substrates with the newly developed electron-deficient phosphoramidites (Chapter 2). For screening purposes, hexenyl isocyanate was chosen. We found that *p*-CF_3-Taddol phosphoramidites with pyrrolidyl (**T23**) or piperidyl (**T19**) amine provide no selectivity between lactam and vinylogous amide in the cycloaddition of hexenyl isocyanate and cyclooctyne (Table 4.3). Pyrrolidyl *p*-CF_3-**T23** gave 60% ee, which is comparable to the ee seen with Guiphos **B2** (66%). Unfortunately, neither of the bis-CF_3 Taddol phosphoramidites (**T26** or **T24**) provide good product selectivity (1:1.2, **T26**, 1:5.2, **T24**). C_6F_5 Taddol **T25** provides excellent product selectivity (1:15) favoring vinylogous amide. Unfortunately, very low enantioinduction is observed (7%) for reasons that are not clear. There appears to be an inverse relationship between product selectivity and enantioselectivity with internal, symmetrical alkyl alkynes.

Table 4.3 Ligand effects with cyclooctyne.

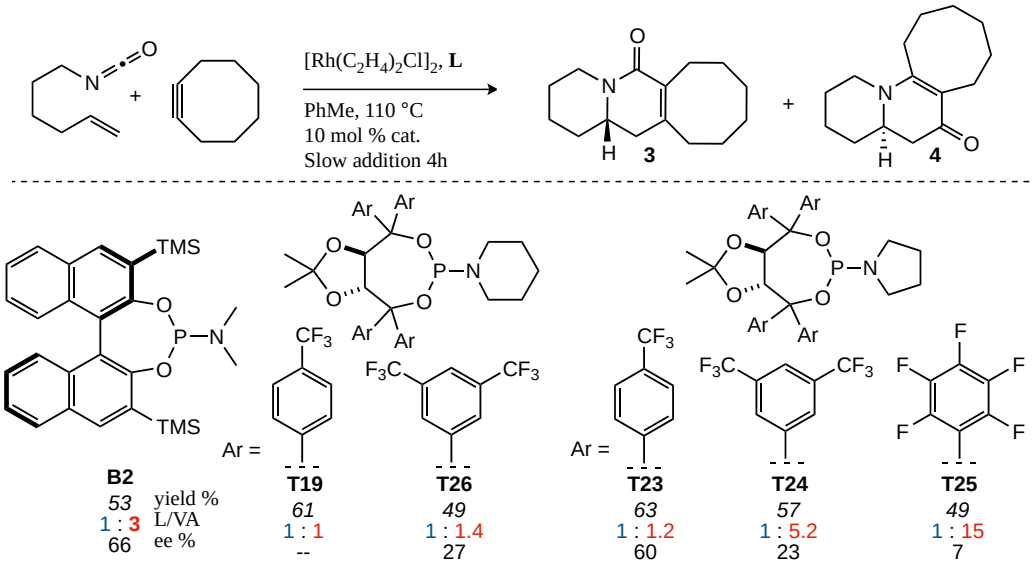

As will be discussed briefly in Chapter 6, we found that exchange of the chloride in the $[Rh(C_2H_4)_2Cl]_2$•CKphos catalyst with a tosylate counterion provided an increase in enantioselectivity in the cycloaddition with 1,1-disubstituted alkenyl isocyanates and terminal alkynes. Curious to see whether this catalyst system would also give enhanced enantioselectivity with internal symmetrical alkynes, such

as the notoriously difficult internal symmetrical alkynes (cyclic alkynes, 5-decyne) we tried the catalyst system with pentenyl isocyanate and commercially available 5-decyne. As discussed previously, $Rh(C_2H_4)_2Cl$•Guiphos provides a 1:3 mixture of lactam and vinylogous amide products in 88% yield and 9% ee (Chapter 2, Table 2.6). By comparison, $Rh(C_2H_4)_2OTs$•CKphos in DCE provides exclusively the vinylogous amide product in 35% ee (Table 4.4).

Interested to know what the affects of manipulation of the acetonide and amine would have on the perfluoroaryl Taddol backbone, we synthesized a variety of perfluoroaryl Taddol ligands and investigated them in the cycloaddition with 5-decyne and pentenyl isocyanate. Because we were focused on improving the enantioselectivity of the reaction, we reported only the ee's in Table 4.4. Amine modification decreased enantioselectivity in all instances (**T28**, **T29**, **T30** and **T31**). Secondary benzyl amine **T31** and methyl phosphonite **T32** provide low yields (>30%) and 16% ee.

Table 4.4 Screen of Taddol amine and acetonide changes on enantioselectivity.

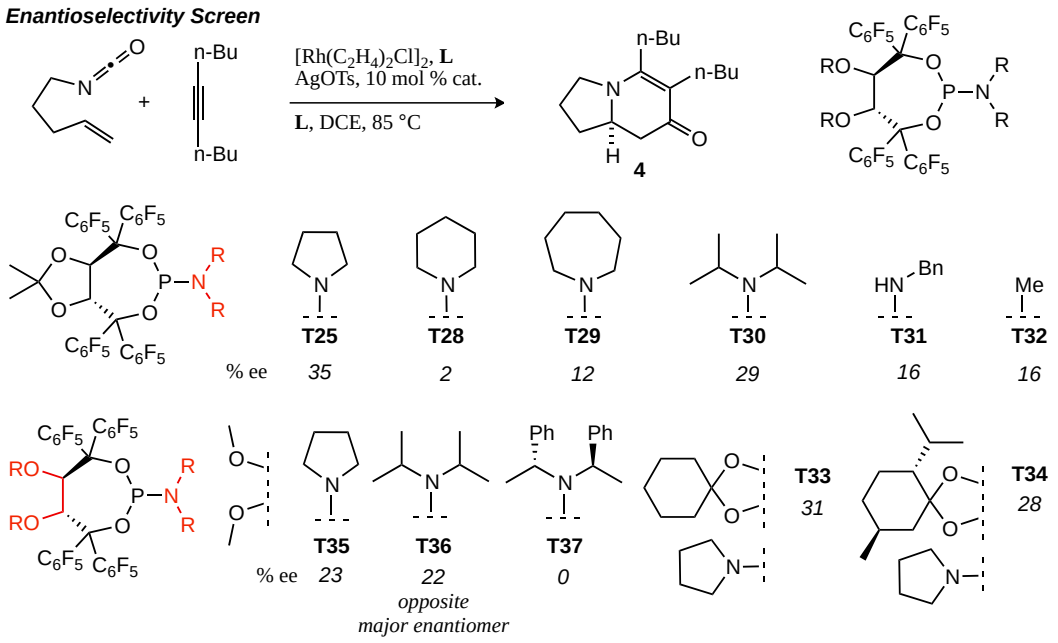

Johnson and coworkers see a pronounced increase in enantioselectivity with a menthone-derived Taddol phosphite in the metallophosphite-catalyzed asymmetric acylation of α,β-unsaturated amides.[17] They attribute the increase in ee to a gearing effect, in which the steric bulk of the isopropyl of the menthone-acetonide pushes one Taddol phenyl in closer proximity to the metal, increasing

enantioselectivity. Evidence for gearing of the aryl rings toward the metals was provided by X-ray analysis of metallophosphite catalysts. We investigated cyclohexanone derived **T33** and menthone-derived **T34** in the [2+2+2] to see if a similar gearing effect was found to increase enantioselectivity. Both **T33** and **T34** behave almost identically to CKphos **T25** in terms of yield and product selectivity. Enantioselectivity is only slightly decreased. This suggests that there is little aryl movement in the Taddol phosphoramidite backbone when bound to rhodium. This provides evidence for a Rh(I)–C_6F_5 interaction with one C_6F_5 aryl of the Taddol and will be discussed in chapter 5.

To test the other extreme, we synthesized monocyclic methyl-ether Taddol phosphoramidites **T35**, **T36** and **T37**. Fürstner and coworkers found that acyclic monodentate Taddol phosphoramidites improve enantioselectivity in Au(I) catalyzed [2+2] cycloaddition reactions of alkene tethered allenes to form substituted cyclobutanes.[18] Fürstner and coworkers propose that the increased ee comes from interaction between the Taddol phenyls and cationic Au(I). We found that monocyclic perfluoroaryl phosphoramidites **T35-T37** in the Rh(I) catalyzed [2+2+2] cycloaddition provide vinylogous amide in low yields (>25%) and low enantioselectivities (0-23%). Interestingly diisopropyl monocyclic Taddol **T36** provides the opposite major enantiomer as that seen with other Taddol phosphoramidites of the same enantiomer backbone. It is not clear what contributes to the low yield and enantioselectivity seen in the reaction of pentenyl isocyanate and 5-decyne but rigidity is necessary for good yield and selectivities.

4.2.4 Isocyanate Tether Elongation

Alkenyl isocyanate tethers of 3 to 5 methylene units are tolerated by the $Rh(C_2H_4)_2Cl$•CKphos catalyst (Scheme 4.2). Rh(I)•CKphos catalyzed cycloaddition of pentenyl isocyanate and 1-octyne works very well to give indolizinone **4a** in excellent yield, product selectivity and enantioselectivity. The excellent reactivity and selectivity is also seen with hexenyl isocyanate in the formation of quinolizinone **4m**.

Previous attempts to catalyze the cycloaddition of heptenyl isocyanate and an alkyne have failed and only 2-pyridone is isolated. However, we found that cycloaddition of heptenyl isocyanate and 1-octyne with Rh(I)•CKphos provides 7,6-bicyclic vinylogous amide **4n** in poor yield and enantioselectivity but excellent product selectivity. These are the first conditions reported to form the 7,6-bicyclic system under

Rh(I) [2+2+2] catalysis. Dilute conditions and prolonged reaction times are necessary for the cycloaddition to occur. Increased yields were found at 0.004M compared with 0.02M; this result is further mechanistic evidence that the alkene is the last π-component incorporated. 2-pyridone is also a byproduct of the reaction.

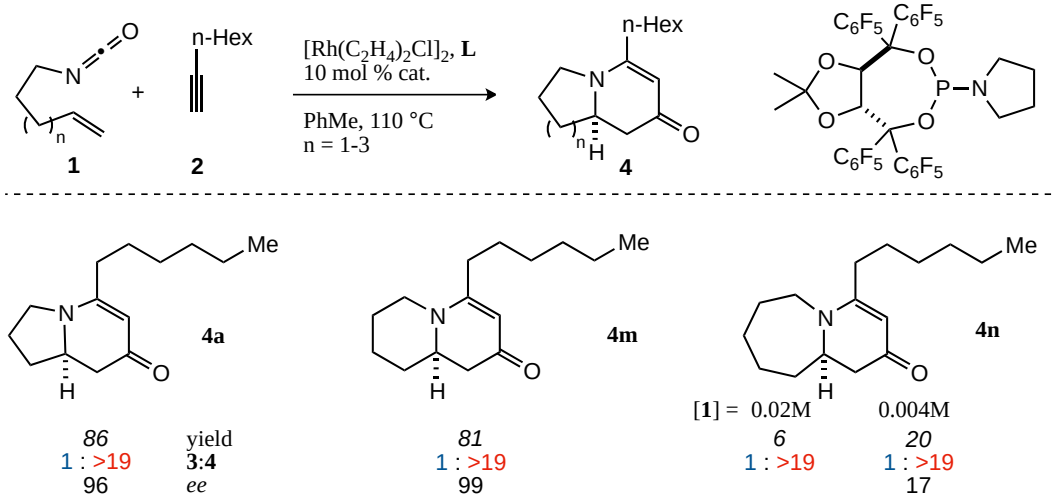

Scheme 4.2 Tether elongation in [2+2+2] cycloadditions.

4.2.5 Competition Experiment

To ascertain whether perfluoroaryl Taddol CKphos was altering the proposed mechanistic cycle by promoting alkene isocyanate cyclization first (for example); a competition experiment was carried out. We found Rh(I)•CKphos catalyzed cycloaddition of a 1:1:1 molar ratio of pentenyl isocyanate (**1a**), 1,1-disubstituted alkenyl isocyanate **1b** and benzyl acetylene affords a 1:1 mixture of vinylogous amide products **4i** and **4o**. This suggests that the alkene is not involved in the product determining step when CKphos is present. CKphos appears to be controlling the irreversible oxidative cyclization event that dictates which product pathway the reaction will undergo. How we believe that CKphos affects oxidative cyclization is the subject of Chapter 5.

Competition Experiment

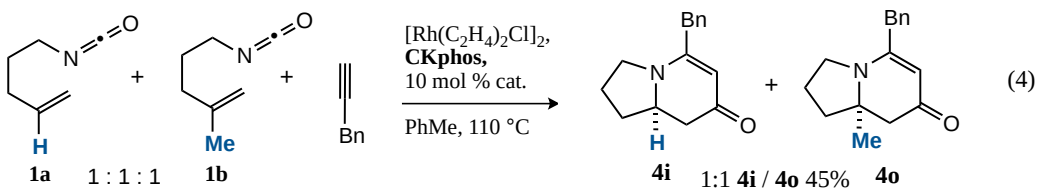

(4)

4.3 Conclusion

In conclusion, we have found that electronic manipulation of the aryls of Taddol phosphoramidite ligands may be used to control product selectivity in the Rh(I) catalyzed cycloaddition of alkenyl isocyanates and alkynes. Electron-rich aryl Taddol phosphoramidite **T22** was found to shift product selectivity with alkyl alkynes toward the lactam product in low yields, but excellent product selectivity and good enantioselectivity. Electron-deficient perfluoroaryl Taddol phosphoramidites were found to alter product selectivity with alkyl alkynes in favor the vinylogous amide **4** in excellent yield, product selectivity and enantioselectivity. Perfluoroaryl Taddol CKphos (**T25**) was found to improve product selectivity for a wide range of alkyl and aryl acetylenes, improving the utility of the transformation. Manipulation of the amine and acetonide portion of the Taddol found that CKphos **T25** is the optimal ligand for the transformation. Finally, a control experiment between mono and 1,1-disubstituted alkenyl isocyanates suggests that CKphos has not altered the proposed mechanistic cycle.

4.4 References

(1) Daly, J. W.; Spande, T. F.; Garraffo, H. M. *J. Nat. Prod.* **2005**, *68*, 1556–1575.

(2) Michael, J. *Nat. Prod. Rep.* **2005**, *22*, 603–626.

(3) Michael, J. P. *Nat. Prod. Rep.* **2007**, *24*, 191–222.

(4) Michael, J. P. *Nat. Prod. Rep.* **2008**, *25*, 139–165.

(5) Pivavarchyk, M.; Smith, A. M.; Zhang, Z.; Zhou, D.; Wang, X.; Toyooka, N.; Tsuneki, H.; Sasaoka, T.; McIntosh, J. M.; Crooks, P. A.; Dwoskin, L. P. *Eur. J. Pharmacol.* **2011**, *658*, 132–139.

(6) Michael, J. *Nat. Prod. Rep.* **2004**, *21*, 625–649.

(7) Samoylenko, V.; Ashfaq, M. K.; Jacob, M. R.; Tekwani, B. L.; Khan, S. I.; Manly, S. P.; Joshi, V. C.; Walker, L. A.; Muhammad, I. *J. Nat. Prod.* **2009**, *72*, 92–98.

(8) Michael, J. *Nat. Prod. Rep.* **2007**, *24*, 191–222.

(9) Michael, J. P. *Nat. Prod. Rep.* **2001**, *18*, 520–542.

(10) Samoylenko, V.; Ashfaq, M. K.; Jacob, M. R.; Tekwani, B. L.; Khan, S. I.; Manly, S. P.; Joshi, V. C.; Walker, L. A.; Muhammad, I. *J. Nat. Prod.* **2009**, *72*, 1, 92-98.

(11) Michael, J. P. *Beilstein J. Org. Chem.* **2007**, *3*, 27.

(12) Kim, G.; Jung, S.; Kim, W. *Org. Lett.* **2001**, *3*, 2985–2987.

(13) Meyer, A. M.; Katz, C. E.; Li, S.-W.; Velde, D. V.; Aube, J. *Org. Lett.* **2010**, *12*, 1244–1247.

(14) Perry, M. A.; Morin, M. D.; Slafer, B. W.; Wolckenhauer, S. A.; Rychnovsky, S. D. *J. Am. Chem. Soc.* **2010**, *132*, 9591–9593.

(15) Yu, R. T.; Rovis, T. *J. Am. Chem. Soc.* **2008**, *130*, 3262–3263.

(16) Yu, R. T.; Lee, E. E.; Malik, G.; Rovis, T. *Angew. Chem. Int. Ed.* **2009**, *48*, 2379–2382.

(17) Nahm, M. R.; Potnick, J. R.; White, P. S.; Johnson, J. S. *J. Am. Chem. Soc.* **2006**, *128*, 2751–2756.

(18) Teller, H.; Flügge, S.; Goddard, R.; Fürstner, A. *Angew. Chem. Int. Ed.* **2010**, *122*, 1993–1997.

CHAPTER 5

Perfluoroaryl Taddol Phosphoramidites as L,Z-Ligands on Rh(I) and Co(-I)

5.1 Introduction

5.1.1 Z-Type Organometallic Ligands

Development of chemical tools to rapidly, efficiently and selectively synthesize biologically active molecules is of utmost importance to the discovery of new drug candidates for future pharmaceuticals.[1,2] Transition metal catalysis is one of the most powerful chemical synthesis tools. Not only are metal catalysts robust synthetic tools with high catalyst turnover numbers, but they can quickly and efficiently bring together complex molecules from simple starting materials with high levels of selectivity.[3] Proper choice of the metal ligand for a reaction can be crucial both for reactivity and selectivity.[4] A wide array of ligand scaffolds have been developed to tune metal reactivity and transfer stereochemical information to the desired products. The vast majority of metal ligating groups that ligand scaffolds capitalize upon are L-type, two electron-donor groups (Figure 5.1).[5]

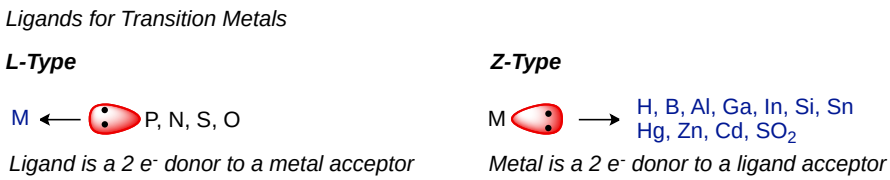

Figure 5.1 L and Z-type ligands for transition metals.

Privileged chiral ligand scaffolds[6] for metals are frequently bidentate L, L scaffolds: N,N-(Box),[7] O,O-(Binol, Taddol, Salen),[8] P,P-(Binap, Duphos, Dipamp, Diop),[9,10] P,N-(Phox),[11] N,O-(Cinchona), but may also be monodentate L-type, such as phosphoramidites (Figure 5.2).[12,13] Although typically monodentate, a few phosphoramidite ligands have been shown to coordinate in L, L fashion with P, Aryl[14,15] and P, Alkyl[16] electron donation to the metal center.

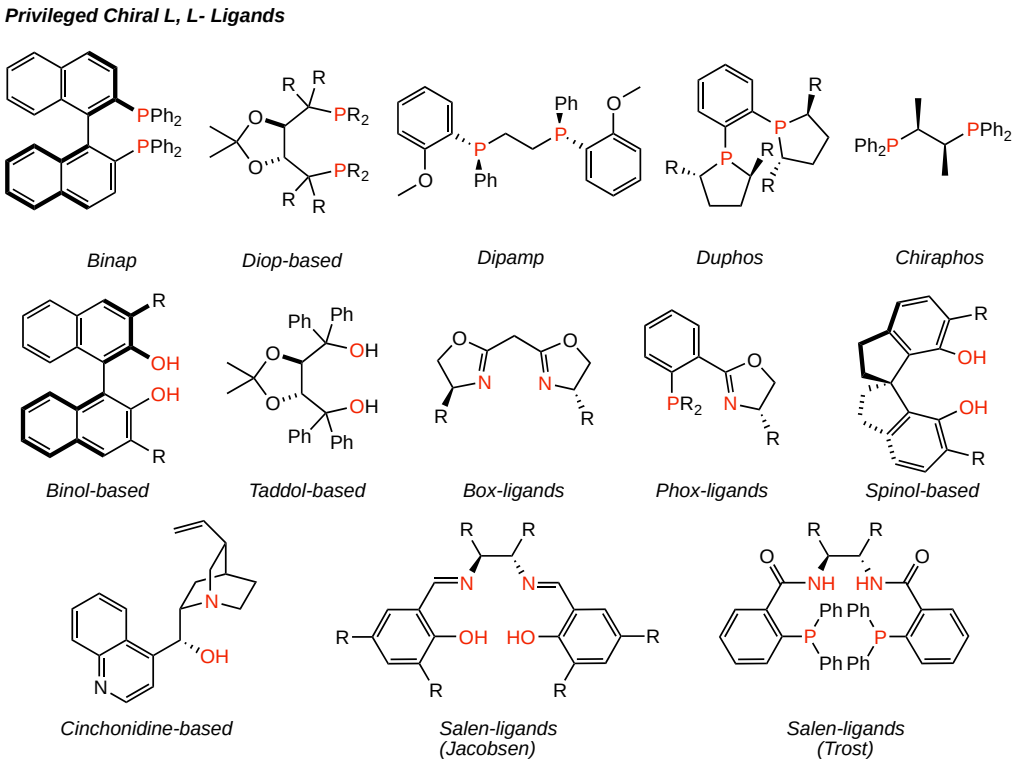

Figure 5.2 Privileged chiral ligand scaffolds for metal catalysis.

Sterically there is wide variation between these ligand scaffolds; electronically each serves as a two-electron donor to a metal center. On the other hand, complementary Lewis acidic, Z-type, two-electron acceptor groups are rare. A few ligand scaffolds have been developed that incorporate Z-type interactions and exist as L, Z-ligands, requiring at least one donor ligand for effective coordination along with one Lewis acid (Figure 5.3).[17-22] To our knowledge, perfluoroaryls have not yet been reported to act as Z-type ligands and furthermore, Z-type ligands have not yet been incorporated into a chiral ligand scaffold. Phosphoramidites are poor σ-donor ligands but bind strongly to transition metals through enhanced π-acceptor abilities, as evidenced by C–O IR stretching frequencies.[12,13,23]

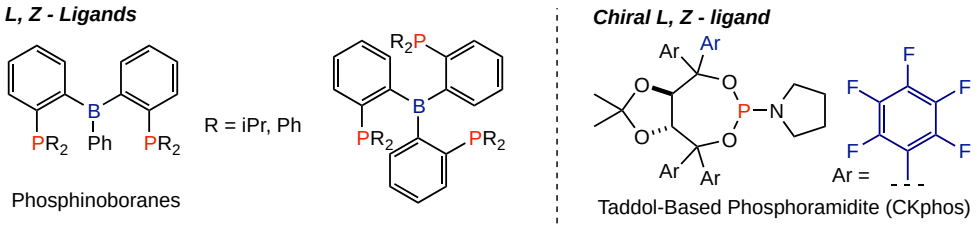

Figure 5.3 L, Z-ligands for transition metals.

5.1.2 Perfluoroaryls as Z-type Ligands

Perfluoroaryls, such as C_6F_6, have a permanent quadrupole equal in magnitude and opposite in sign to C_6H_6 and have been shown to interact with electron-rich Lewis bases through lone pair–π[24-26] and anion–π[27-29] interactions (Figure 5.4). The strength of anion–π interactions is comparable to a moderate to strong hydrogen bond (~20-50 kJ/mol).[28] Theoretical studies reveal that anion–π interactions with π-acidic aromatics are dominated by electrostatic interactions.[30] The importance of these counterintuitive, non-covalent attractive interactions is being explored in chemical and biological processes.

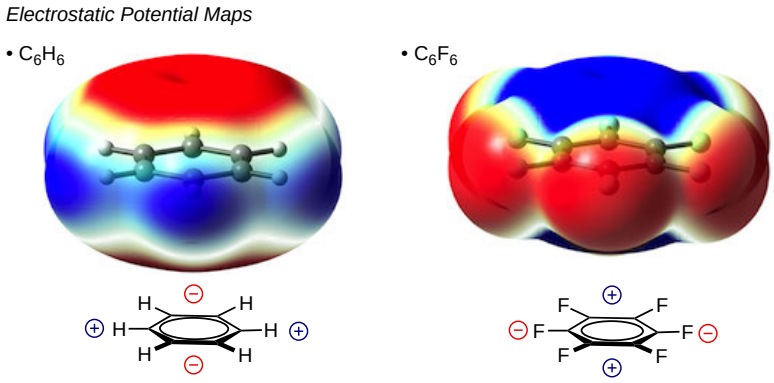

Figure 5.4 Calculated electrostatic potential maps (DFT) for benzene and hexafluorobenzene. Blue indicates net positive potential and net negative potential is red. The 0.004 au magnitude isovalue is plotted for the electron density. Mapping of the electrostatic potential ranges from -0.008 to 0.01 au.

Analogous metal–C_6F_5 interactions are rare. Only a handful of metal-C_6F_n complexes have been reported: Cr,[31] Rh,[32] Ir,[33] W,[34] Ru,[35] Ni,[36] and Re (Figure 5.5).[37] DFT calculations reveal that electron density in perfluoroaryls localizes on the fluorines, leaving a large, positive electrostatic potential on the π-system. Perfluoroaryls can be seen as accepting electron density from electron-rich metal centers. C_6F_n-metal interactions are markedly different from C_6H_n-metal interactions, where the aryl donates electrons to a metal (L-type, Aryl→M). Lewis acidic, aryl-metal interactions (Z-type, M→Aryl) where the metal donates electrons to an aryl acceptor are few and remain relatively unexplored.

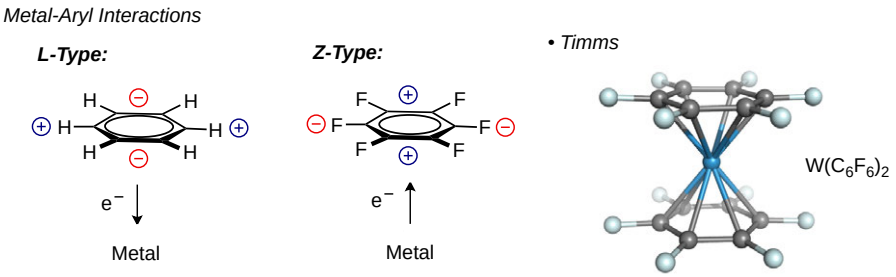

Figure 5.5 Perfluoroaryl as Z-type transition metal ligand.

5.2 Results

5.2.1 X-ray Analysis of Rh(I)•CKphos Complexes

Perfluoroaryl Taddol-derived phosphoramidite, CKphos, was synthesized from the perfluorinated diol and dichloropyridylphosphine. Treatment of $[Rh(cod)Cl]_2$ with *racemic* CKphos ligand in the presence of DCM results in the Rh(cod)Cl•CKphos complex, which readily forms X-ray quality crystals after slow evaporation in DCM/heptanes. X-ray analysis revealed a short, in comparison to other Rh(cod)Cl•Phosphoramidite, Rh–P bond distance. This shortened bond distance is attributed to increased *d*→P–O σ* backdonation seen with the more electron-deficient C_6F_5 Taddol, CKphos, in comparison to the C_6H_5 Taddol **T1** (Figure 5.6).

Additionally, Rh(cod)Cl•CKphos shows a significant trans effect in comparison to the phenyl Taddol-derived phosphoramidite, **T1**, with C=C bond distances of 1.365 Å (CKphos) and 1.378 Å (**T5**) seen. This is significantly shorter than C=C bond distance of 1.409 Å for **T5** or 1.424 Å reported for $[Rh(cod)Cl_2]_2$ and closer to the bond distance of the free alkene, 1.337 Å.[38] This suggests that the coordinated cyclooctadiene (cod) alkene trans to the phosphoramidite phosphorus has more C_{sp}^2 character, implying that there is less π-backbonding from rhodium to the alkene. Decreased π-backbonding to the alkene is likely the consequence of increased backdonation from filled rhodium *d* orbitals to lower lying P–O σ* of the electron-deficient phosphoramidite.[9] Incorporation of the C_6F_5 aryls into the Taddol phosphoramidite serves to lower the P–O σ*, increase backdonation from rhodium and shorten the C=C bond trans to the phosphoramidite. Overall, the shortened Rh–P and C=C bond distances suggest that perfluoroaryl

CKphos acts as a better π-acceptor ligand than phenyl-Taddol **T1** on rhodium, decreasing the π-basicity of Rh(I).

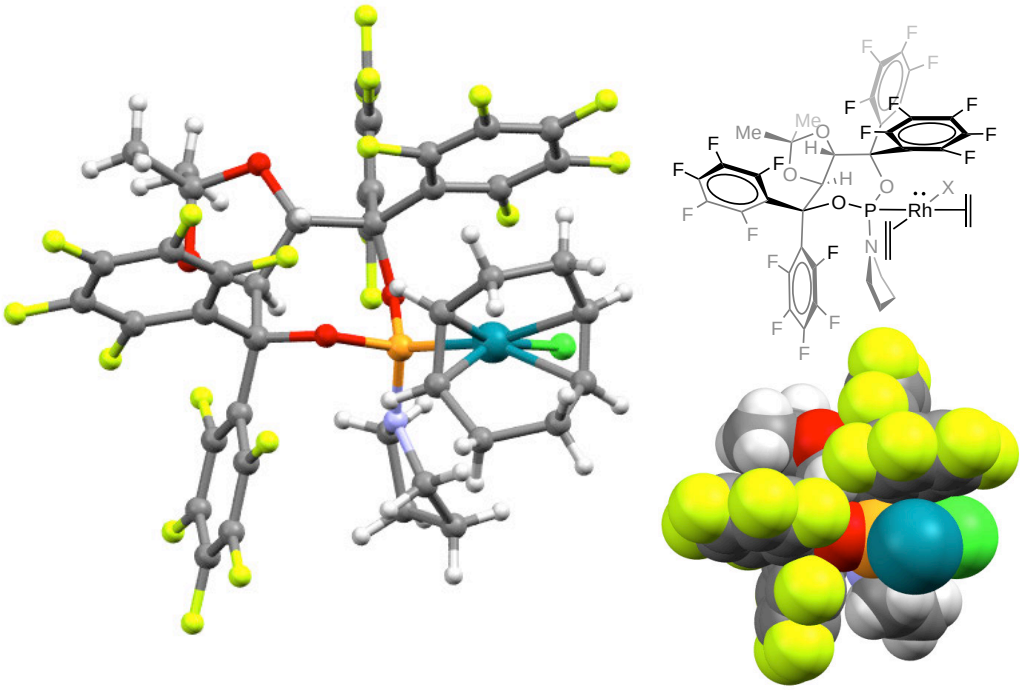

Ligand	Ar	X	L : VA[a]	Rh–P (Å)	Rh–Apical Ar	C=C trans to P
T25	C_6F_5	Cl	1: **>19**	2.2423(6)	***3.728***	1.365(4)
T1[b]	C_6H_5	Cl	**2.4** : 1	2.2547(3)	4.039	1.3781(18)
T5[b]	m-Xylyl	Cl	**12.5** : 1	2.2703(4)	4.025	1.409(2)

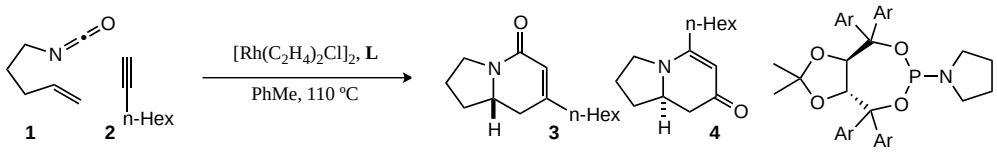

Figure 5.6 Ball and stick and spacefilling model of X-ray structure of Rh(cod)Cl•CKphos complex. C = grey, H = white, N = light blue, O = red, P = orange, Cl = green, Rh = teal, F = yellow. Ethylene bridge of cod on the chemdraw structure has been omitted for clarity. (a) product selectivity seen in reaction of pentenyl isocyanate and 1-octyne catalyzed by $[Rh(C_2H_4)_2Cl]_2$•**L** (10 mol %) in PhMe at 110 °C. (b) results previously reported.[39]

Previously reported X-ray analyses of Rh(cod)Cl•Phosphoramidite complexes revealed that one Taddol-phosphoramidite aryl is situated above rhodium hindering one face of the rhodium square plane (Figure 5.6).[39] In the Rh(cod)Cl•CKphos complex one aryl also sits directly above the rhodium square plane but it is significantly closer to rhodium than in Rh(cod)Cl•**T1**. The Rh–C_6F_5 centroid bond distance in the Rh(cod)Cl•CKphos complex is 3.728 Å, which is 0.3 Å closer to rhodium than the 4.039 Å Rh–

C_6H_5 centroid distance seen with **T1**. A search of the Cambridge Crystallographic Data Center (CCDC) found X-ray structures of C_6H_6–C_6F_6[40] and $Me_nC_6H_n$–C_6F_6[41-43] complexes with intercentroidal distances between 3.5 and 3.7 Å. These distances suggest that the Taddol C_6F_5 is in close enough proximity to be interacting with rhodium in the ground state.

To determine if the close Rh–C_6F_5 centroid distance was an isolated occurrence, we examined Rh(cod)X•CKphos complexes with different counterions (Figure 5.7). X-ray analysis of Rh(cod)OTs•CKphos found that the Rh–C_6F_5 centroid distance with the tosylate counterion decreases from 3.728 Å (chloride) to 3.687 Å. Rh(cod)OTf•CKphos has a longer Rh–C_6F_5 distance and the C_6F_5 has shifted from being directly over rhodium, as seen with chloride and tosylate, to being situated over the oxygen of the triflate. Presumably this change is due to the highly ionic nature of the Rh–OTf bond, which is less tightly bound to rhodium than chloride or tosylate, and the anionic OTf–C_6F_5 interaction is more favorable than the Rh–C_6F_5 when the rhodium is less electron rich. This suggests that the perfluoroaryl is acting as a Lewis acid and for the interaction to occur the metal involved needs to be relatively Lewis basic.

Rh(cod)OTs-CKphos

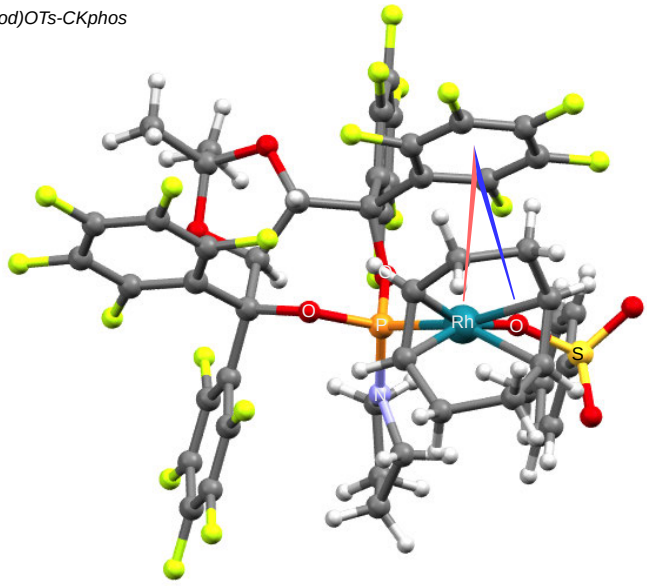

Rh(cod)OTf-CKphos

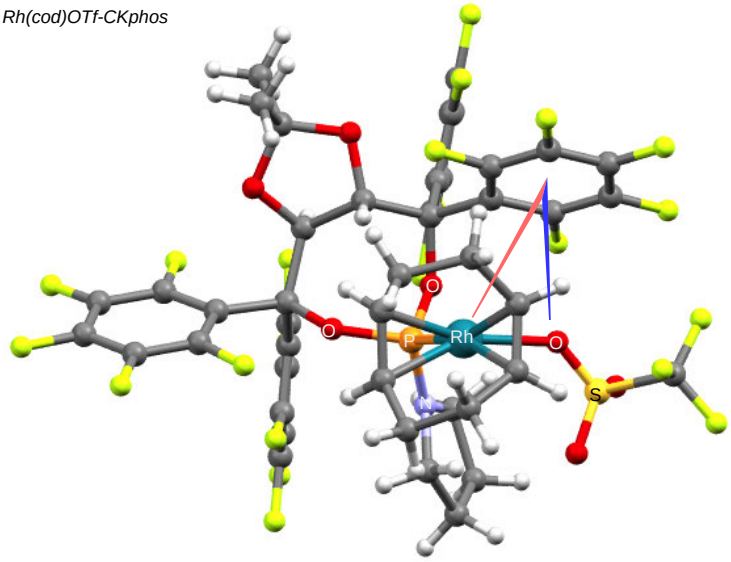

Ligand	Counterion (X)	L:VA[a]	Rh-P (Å)	Rh-Apical Ar	Apical Ar-X
CKphos	-Cl	1: **>19**	2.2421(10)	3.728	3.958
CKphos	-OTs	1: **>19**	2.2423(6)	3.687	3.775
CKphos	-OTf	1: **>19**	2.2366(10)	3.887	*3.279*

Figure 5.7 X-ray structures of Rh(cod)X•CKphos. C = grey, H = white, N = light blue, O = red, P = orange, Cl = green, Rh = teal, F = yellow. (a) product selectivity seen in reaction of pentenyl isocyanate and 1-octyne catalyzed by $[Rh(C_2H_4)_2X]_2$•**CKphos** (10 mol %) in DCE at 80 ºC.

5.2.2 DFT Calculations

DFT computational analyses of Rh(cod)Cl•CKphos and Rh(cod)Cl•**T1** were used to verify and better understand the Rh–C_6F_5 interaction implied by the ground state X-ray structure. Beginning with the X-ray

structures, energy minimizations were performed, and significantly, the Rh–C_6F_5 interaction was found to be a persistent, favorable interaction in gas phase and not the result of crystal packing forces. Calculated bond distances were found to agree with those in the X-ray crystal data for both Rh(cod)Cl•CKphos and Rh(cod)Cl•**T1** (Figure 5.8). With three different basis sets the calculated Rh–C_6F_5 centroid bond distance is found to be shorter than that observed in the X-ray data by 0.311 to 0.516 Å. Agreement between computational and X-ray data provides further support for the Rh–C_6F_5 interaction.

Electrostatic potential maps were generated from the DFT calculations of Rh(cod)Cl•CKphos and Rh(cod)Cl•**T1**. The maps show significant inversion of electrostatic potential between the perfluoroaryl and phenyl rhodium phosphoramidite complexes (Figure 5.8). In the Rh(cod)Cl•**T1** potential map significant negative potential (red) is found above and below each of the aryl rings while positive potential (blue) gathers around the hydrogens of the phenyl. Rh(cod)Cl•CKphos map shows a clear inversion of electrostatic potential. Positive potential (blue) is now found above and below each perfluoroaryl and significant negative potential (red) is on the fluorines. An interesting observation is that the electrostatic potential of the C_6F_5 above rhodium, proposed to be interacting with it, is less electropositive (blue) and has more negative electrostatic potential (red) on its fluorines (Top view).

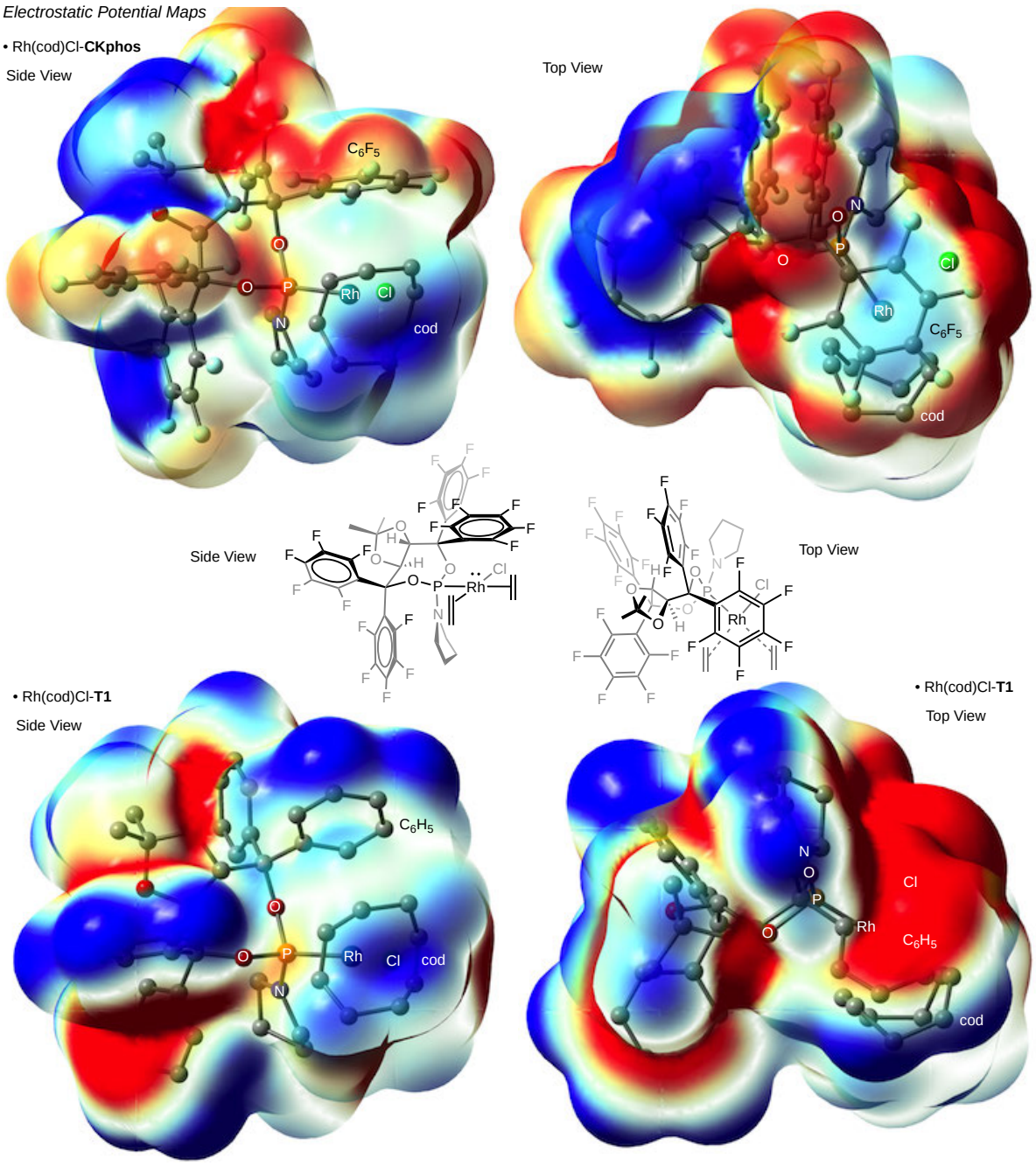

Figure 5.8 DFT calculations of the electrostatic potential maps for Rh(cod)Cl•CKphos and Rh(cod)Cl•**T1**. Blue indicates net positive potential; net negative potential is red. The 0.004 au magnitude isovalue is plotted for the electron density. Mapping of the electrostatic potential ranges from -0.008 to 0.01 au.

Furthermore, DFT calculations found that the HOMO for Rh(cod)Cl•CKphos is predominately on the rhodium d_z^2 orbital. As depicted in Figure 5.9, clearly the HOMO extends into the electropositive region below the highly electron deficient perfluoroaryl. This supports the notion that rhodium has significant

electron density that is properly located to interact with the C_6F_5. Together these results support the proposal that perfluoroaryl C_6F_5 functions as a Lewis acid to accept electron density from electron rich rhodium(I) as a Z-type ligand.

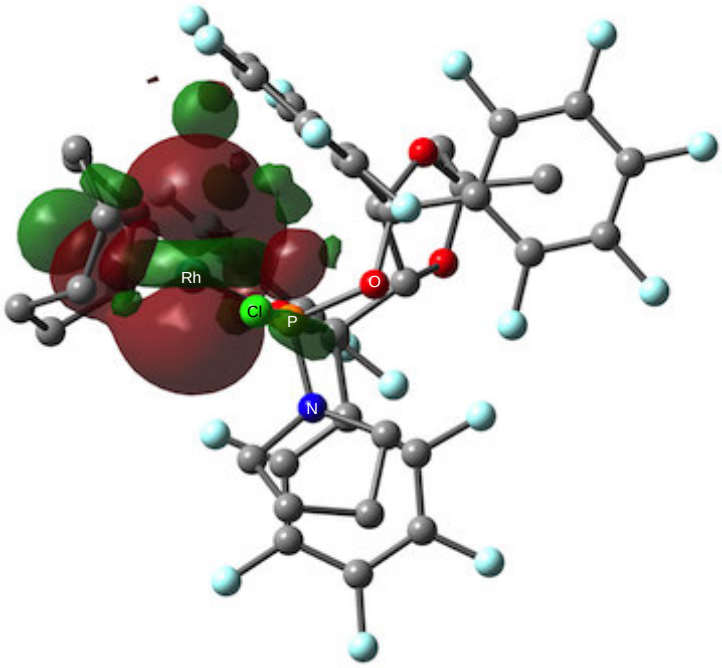

Figure 5.9 DFT calculation of Rh(cod)Cl•CKphos HOMO as depicted looking down Rh–Cl. C = grey, H = white, N = blue, O = red, P = orange, Cl = green, Rh = teal, F = light blue.

5.2.3 NMR Studies

To investigate the Rh–C_6F_5 interaction in solution, we analyzed Rh(cod)Cl•phosphoramidite complexes by NMR spectroscopy. ^{31}P-NMR shows coupling between phosphorus and rhodium (Figure 5.10). Rh(cod)Cl•**T1** has a $J_{Rh–P}$ coupling constant of 234 Hz and Rh(cod)Cl•CKphos has a $J_{Rh–P}$ of 243 Hz. Roodt, Varshavsky and coworkers found a correlation between solid-state bond lengths from X-ray crystal data and coupling constants observed in solution by ^{31}P-NMR.[44] The difference in coupling constants between C_6F_5 and C_6H_5 may be correlated to the bond distance seen in the solid state and corresponds to the electronegativity of the aryl substituents on the Taddol phosphoramidite. Interestingly, ^{31}P-NMR of Rh(cod)Cl•CKphos revealed phosphorus splitting into a doublet of doublet with J values of 243 Hz (J_{Rh-P}) and 5 Hz. A ^{19}F-decoupled ^{31}P-NMR study provided a broad doublet, suggesting that at least one fluorine on CKphos is coupling to phosphorus. Attempts to determine which fluorine is coupled

to phosphorus by ^{31}P-decoupled ^{19}F-NMR have been unfruitful. As a result, we calculated J_{P-F} coupling constants based on the Rh(cod)Cl•CKphos X-ray structure.

DFT spin-spin calculations [B3LYP, 6-311(d,p) basis on P and F] on the optimized Rh(cod)Cl•CKphos structure identified three fluorines with J_{P-F} coupling constants greater than 1 Hz (Figure 5.10). Each is an ortho fluorine, two (F_1, F_3) are within 5 Å of phosphorus and one (F_2) is more than 5 Å. In the static DFT calculations, ortho fluorines F_1, F_2 and F_3 appear to be coupling to phosphorus through long-range (5-bond) coupling,[45] but in solution, aryl rotation may disrupt long-range coupling for F_1 and F_2 because such coupling is sensitive to the molecule's conformation.[46,47] However, coordination of the C_6F_5 bearing F_3 to rhodium will limit rotation of this C_6F_5 and rigidify the phosphoramidite overall. Rigidification of the phosphoramidite through Rh–C_6F_5 interaction may allow ^{31}P-^{19}F coupling to occur either through-bond or through-space. The magnitude of through-space coupling between NMR active nuclei diminishes as the sum of the Van-der Waals radii is exceeded.[48,49] This would make through-space coupling unlikely; however, through-space ^{31}P–^{19}F coupling is reported on 3,3'-bistriflone-BINOL phosphoramidites and J_{P-F} values of 5 Hz are seen between atoms 6 bonds apart.[50] At this point, we cannot with certainty say which fluorine is the source of the ^{31}P-^{19}F coupling, however, we believe that the Rh–C_6F_5 interaction may facilitate P–F coupling through rigidification of the phosphoramidite.

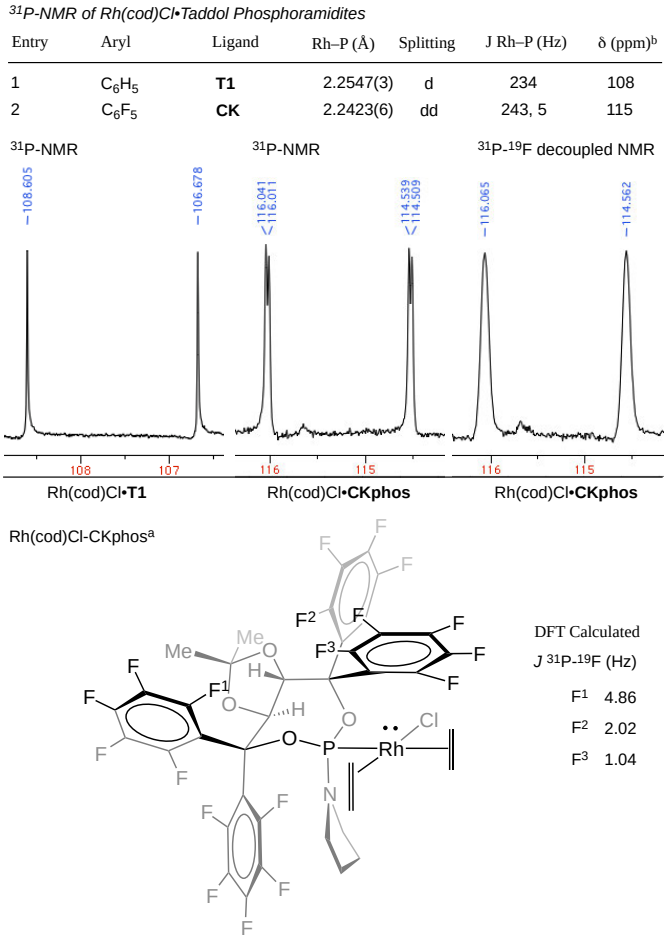

Figure 5.10 ^{31}P-NMR of Rh(cod)Cl•Phosphoramidites. [a] ethylene bridge of cod omitted for clarity. [b] ^{31}P-NMR shift of ligand.

5.2.4 Perfluoroaryl CKphos as a Ligand on Anionic Cobalt

To provide further evidence of the Metal–C_6F_5 interaction, we investigated CKphos as a ligand on highly Lewis basic, anionic cobalt. $Co(CO)_3$*n*-Bu_4N•CKphos was synthesized and analyzed by X-ray diffraction (Figure 5.11). Surprisingly, X-ray analysis revealed two Co–C_6F_5 interactions with Co–C_6F_5 centroid distances of 3.925 and 4.032 Å, which is longer than the Rh–centroid distance seen in Rh(cod)Cl•CKphos. We attribute the increased distance to steric interactions between the perfluoroaryls and CO ligands, which limit how close the aryl may approach. To accommodate a second Co–C_6F_5 interaction the phosphoramidite seven-membered ring changes its ring conformation in comparison to the ring conformation seen in Rh(cod)Cl•CKphos.

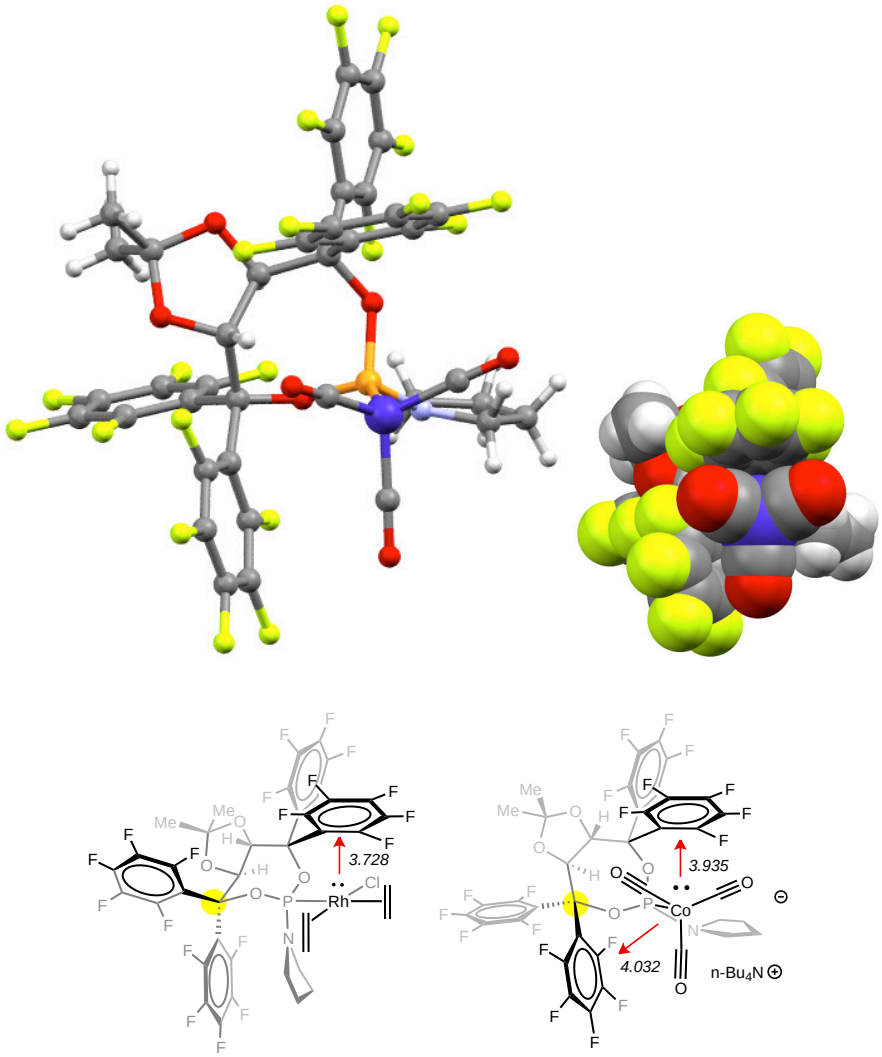

Figure 5.11 X-ray structure of *n*-$Bu_4NCo(CO)_3$•CKphos, comparison of phosphoramidite ring conformations with rhodium and cobalt. Tetrabutylammonium cation has been omitted for clarity, see appendix 5 for further details. C = grey, H = white, N = blue, O = red, P = orange, Cl = green, Co = purple, F = yellow.

The geometry of cobalt in anionic tetracarbonyl cobaltate complexes with a wide range of non-coordinating cations is tetrahedral.[51,52] Deviations from tetrahedral geometry are found when cobalt is strongly ligated by L-type ligands or through strong hydrogen bonding with large ammonium cations.[53-55] Weak hydrogen bonds with large ammonium cations do not distort cobalt's tetrahedral geometry.[55] $Co(CO)_3$*n*Bu_4N•CKphos adopts a distorted tetrahedral geometry at cobalt rather than a tetrahedral geometry, suggesting that the Co–C_6F_5 interaction may be similar to a strong hydrogen bond.

Furthermore, Brammer and coworkers found that $Co(CO)_3PPh_2(C_6H_4CH_2NHMe_2)$, a cobaltate complex with an intramolecular N^+–H---Co^- bond, adopts a similar distorted tetrahedral geometry (Figure 5.12).[55] In comparison, one coordinating C_6F_5 of $Co(CO)_3$*n*Bu_4•CKphos is in the same apical position above cobalt as the N–H bond seen in $Co(CO)_3PPh_2(C_6H_4CH_2NHMe_2)$. Also, in $Co(CO)_3PPh_2(C_6H_4CH_2NHMe_2)$ the distance between cobalt and the amine methyls is 4.075 and 4.124Å, similar to the Co–C_6F_5 centroid distance (3.925, 4.032) in $Co(CO)_3$*n*Bu_4N•CKphos. Overall, the Co-C_6F_5 bond distances, change in phosphoramidite ring conformations and distorted tetrahedral geometry at cobalt provide reasonable evidence that anionic cobalt is interacting with two perfluoroaryls of CKphos as Lewis acidic, Z-type ligands.

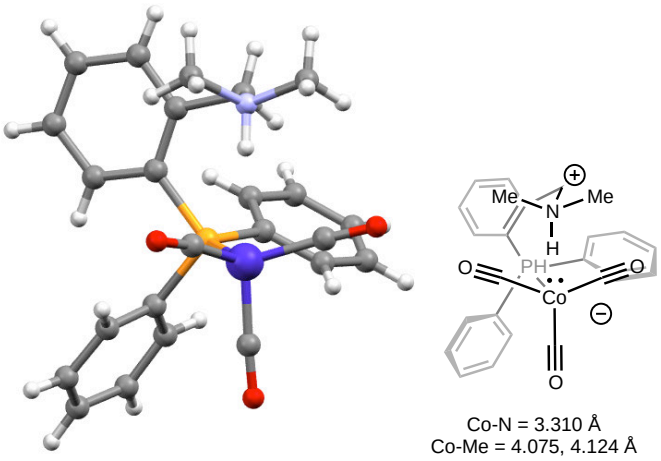

Figure 5.12 X-ray structure of $Co(CO)_3$·$PPh_2(C_6H_4CH_2NHMe_2)$.

5.2.5 Effects of Rh–P and Rh–C6F5 on [2+2+2] Cycloadditions

Product distribution between lactam **3** and vinylogous amide **4** is determined from the direction of the irreversible oxidative cyclization of alkyne and isocyanate from coordination complex **I**, as previously reported[39] and discussed in Chapter 3. The phosphoramidite ligand environment organizes the coordination of alkyne and isocyanate so that smaller substituents (C–H, C=O) are on the hindered side of the rhodium square plane (Scheme 5.1). Oxidative cyclization with the small substituents cyclizing away from rhodium via **TSa** results in C–C bond formation and metallacycle **IIa** and leads to lactam **3**. Cyclization with the large substituents moving away from rhodium via **TSb** results in C–N bond formation, metallacycle **IIb** and eventually vinylogous amide **4**.

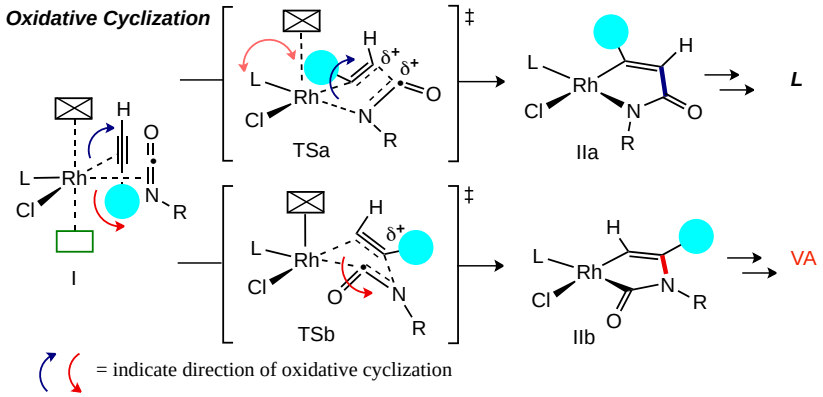

Scheme 5.1 Mechanistic model for lactam and vinylogous amide formation.

In the absence of ligand-substrate steric interactions, the LUMO coefficient of the isocyanate controls the direction of oxidative cyclization in accord with the calculations of Stockis and Hoffman, who found that oxidative cyclization places the largest LUMO coefficients β to the metal.[56] Electronic control of oxidative cyclization can be overridden by steric interactions during the oxidative cyclization event.[57]

5.2.6 Relationship Between Ground State Analyses and Product Selectivity

We have found that manipulation of the aryl portion of Taddol phosphoramidites conclusively affects product selectivity with electron-rich aryls providing lactam **3** and electron-deficient giving vinylogous amide **4**. X-ray analysis of Taddol phosphoramidites and CKphos reveal notable differences in Rh–P, C=C trans to phosphorus and Rh–aryl centroid distances. For example, the Rh–P difference between **T5** and **T1** is 0.015 Å and corresponds to a 12.5:1 to 2.4:1 (L:VA) shift in product selectivity (Figure 5.13) while the Rh–P difference between **T1** and CKphos is 0.012 Å and relates to a 2.4:1 to 1:>19 (L:VA) change in product selectivity. For the difference in Rh–P to account completely for the change in product selectivity, the difference would be expected to be greater than 0.015 Å. A plot of Rh–P versus L:VA ratio shows a strong linear relationship with an R^2 value of 0.90. When CKphos is removed from this plot R^2 increases to 0.95, suggesting another factor affects product selectivity other than Rh–P with CKphos. Because there is a weak correlation between C=C trans to phosphorus and L:VA, and each of the other Rh(cod)Cl•Taddol phosphoramidites has approximately the same Rh–Aryl distance except CKphos, we suggest that the Rh–C_6F_5 interaction corroborated with the Rh-P interaction accounts for the increase in product selectivity seen.

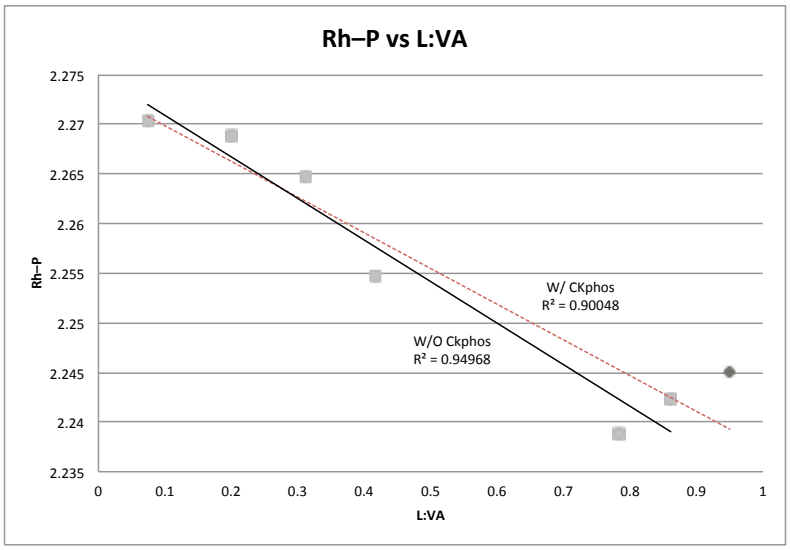

Figure 5.13 Graph of product selectivity versus Rh–P.

Rh(cod)Cl•CKphos has the shortest Rh–P and Rh–aryl centroid distances of the phosphoramidite complexes studied; a result of which is an augmented steric environment on Rh(I) and an amplification of ligand-substrate steric interactions during coordination and oxidative cyclization, favoring vinylogous amide **4** via **TSb** (Scheme 5.1). Additionally, a shortened C=C trans to phosphorus indicates that the π-basicity of Rh(I) is decreased, a result of increased rhodium backdonation to lower lying P–O σ* and a Lewis acidic, Z-type interaction between the π* of C_6F_5 and d_z^2 on Rh(I). Both serve to lower rhodium's HOMO, which disfavors electronic control of cyclization by increasing the energy gap between the rhodium HOMO and isocyanate LUMO. In summary, CKphos favors vinylogous amide through enhanced ligand-substrate steric interactions seen in the ground state and felt in the transition state for oxidative cyclization caused by a shortened Rh–P and a Rh–C_6F_5 interaction. Steric effects are amplified by a lower rhodium HOMO that lessens electronic control of oxidative cyclization.

5.3 Conclusion

In conclusion, we have found that perfluorinated Taddol phosphoramidites are capable of acting at chiral L,Z-bidentate ligands on electron rich transition metals rhodium and cobalt. In the case of Rh(I), C_6F_5 ligand, CKphos, provides excellent product and enantioselectivity in the [2+2+2] cycloaddition of alkene tethered isocyanates and exogenous alkynes. Evidence for the Z-type interaction between Rh(I) and one C_6F_5 Taddol aryl was provided by X-ray, NMR and DFT calculations and corroborated with

selectivity results in the cycloaddition. Increases in product and enantioselectivity in the [2+2+2] are attributed to the Z-type interaction affecting oxidative cyclization and possibly alkene 1,2-migratory insertion.

5.4 References

(1) Nicolaou, K. C.; Vourloumis, D.; Winssinger, N.; Baran, P. S. *Angew. Chem. Int. Ed.* **2000**, *39*, 44–122.

(2) Bennani, Y. L. *Drug Discov. Today* **2011**, *16*, 779–792.

(3) D'Souza, D. M.; Müller, T. J. J. *Chem. Soc. Rev.* **2007**, *36*, 1095–1108.

(4) Fors, B. P.; Buchwald, S. L. *J. Am. Chem. Soc.* **2010**, *132*, 15914–15917.

(5) Green, M. L. H. *J. Organomet. Chem.* **1995**, *500*, 127–148.

(6) Yoon, T. P.; Jacobsen, E. N. *Science* **2003**, *299*, 1691–1693.

(7) Desimoni, G. G.; Faita, G. G.; Jørgensen, K. A. K. *Chem. Rev.* **2011**, *111*, PR284–PR437.

(8) Seebach, D.; Beck, A. K.; Heckel, A. *Angew. Chem. Int. Ed.* **2001**, *40*, 92–138.

(9) Tolman, C. A. *Chem. Rev.* **1977**, *77*, 313–348.

(10) Kamer, P. C. J.; Van Leeuwen, P. W. N. M.; Reek, J. N. H. *Acc. Chem. Res.* **2001**, *34*, 895–904.

(11) Pfaltz, A.; Drury, W. J. *Proc. Natl. Acad. Sci. U.S.A.* **2004**, *101*, 5723–5726.

(12) Feringa, B. L. *Acc. Chem. Res.* **2000**, *33*, 346–353.

(13) Teichert, J. F.; Feringa, B. L. *Angew. Chem. Int. Ed.* **2010**, *49*, 2486–2528.

(14) Huber, D.; Kumar, P. G. A.; Pregosin, P. S.; Mezzetti, A. *Organometallics* **2005**, *24*, 5221–5223.

(15) Mikhel, I. S.; Rüegger, H.; Butti, P.; Camponovo, F.; Huber, D.; Mezzetti, A. *Organometallics* **2008**, *27*, 2937–2948.

(16) Leitner, A.; Shekhar, S.; Pouy, M. J.; Hartwig, J. F. *J. Am. Chem. Soc.* **2005**, *127*, 15506–15514.

(17) Amgoune, A.; Bourissou, D. *Chem. Commun.* **2011**, *47*, 859–871.

(18) Kameo, H.; Hashimoto, Y.; Nakazawa, H. *Organometallics* **2012**, *31*, 3155–3162.

(19) Bauer, J.; Braunschweig, H.; Radacki, K. *Chem. Commun.* **2012**, *48*, 10407–10409.

(20) Harman, W. H.; Peters, J. C. *J. Am. Chem. Soc.* **2012**, *134*, 5080–5082.

(21) Bauer, J.; Braunschweig, H.; Dewhurst, R. D. *Chem. Rev.* **2012**, *112*, 4329–4346.

(22) Ma, M.; Sidiropoulos, A.; Ralte, L.; Stasch, A.; Jones, C. *Chem. Commun.* **2013**, *49*, 48–50.

(23) Tolman, C. *J. Am. Chem. Soc.* **1974**, *96*, 2780–2789.

(24) Egli, M.; Sarkhel, S. *Acc. Chem. Res.* **2007**, *40*, 197–205.

(25) Nelyubina, Y. V.; Barzilovich, P. Y.; Antipin, M. Y.; Aldoshin, S. M.; Lyssenko, K. A. *ChemPhysChem* **2011**, *12*, 2895–2898.

(26) Amicangelo, J. C.; Irwin, D. G.; Lee, C. J.; Romano, N. C.; Saxton, N. L. *J. Phys. Chem. A* **2012**, *117*, 1336-1350.

(27) de Hoog, P.; Gamez, P.; Mutikainen, I.; Turpeinen, U.; Reedijk, J. *Angew. Chem. Int. Ed.* **2004**, *43*, 5815–5817.

(28) Schottel, B. L.; Chifotides, H. T.; Dunbar, K. R. *Chem. Soc. Rev.* **2008**, *37*, 68–83.

(29) Frontera, A.; Gamez, P.; Mascal, M.; Mooibroek, T. J.; Reedijk, J. *Angew. Chem. Int. Ed.* **2011**, *50*, 9564–9583.

(30) Garau, C.; Frontera, A.; Quiñonero, D.; Ballester, P.; Costa, A.; Deyà, P. M. *ChemPhysChem* **2003**, *4*, 1344–1348.

(31) Faggiani, R.; Hao, N.; Lock, C. J. L.; Sayer, B. G.; McGlinchey, M. J. *Organometallics* **1983**, *2*, 96–100.

(32) Belt, S. T.; Duckett, S. B.; Helliwell, M.; Perutz, R. N. *J. Chem. Soc., Chem. Commun.* **1989**, 928–930.

(33) Bell, T. W.; Helliwell, M.; Partridge, M. G.; Perutz, R. N. *Organometallics* **1992**, *11*, 1911–1918.

(34) Barker, J. J.; Orpen, A. G.; Seeley, A. J.; Timms, P. L. *J. Chem. Soc., Dalton Trans.* **1993**, 3097–3102.

(35) Martin, A.; Orpen, A. G.; Seeley, A. J.; Timms, P. L. *J. Chem. Soc., Dalton Trans.* **1994**, 2251–2255.

(36) Johnson, S. A.; Taylor, E. T.; Cruise, S. J. *Organometallics* **2009**, *28*, 3842–3855.

(37) Higgitt, C. L.; Hugo Klahn, A.; Moore, M. H.; Oelckers, B.; Partridge, M. G.; Perutz, R. N. *J. Chem. Soc., Dalton Trans.* **1997**, 1269–1280.

(38) De Ridder, D. J. A.; Imhoff, P. *Acta Crystallogr. E* **1994**, *50*, 1569–1572.

(39) Dalton, D. M.; Oberg, K. M.; Yu, R. T.; Lee, E. E.; Perreault, S.; Oinen, M. E.; Pease, M. L.; Malik, G.; Rovis, T. *J. Am. Chem. Soc.* **2009**, *131*, 15717–15728.

(40) Williams, J. H.; Cockcroft, J. K.; Fitch, A. N. *Angew. Chem. Int. Ed.* **1992**, *31*, 1655–1657.

(41) Dahl, T. *Acta Chem. Scand.* **1971**, *25*, 1031–1039.

(42) Dahl, T. *Acta Chem. Scand.* **1973**, *27*, 995–1003.

(43) Dahl, T. *Acta Chem. Scand A* **1975**, *29*, 2, 170-174.

(44) Steyn, G. J. J.; Roodt, A.; Poletaeva, I.; Varshavsky, Y. S. *J. Organomet. Chem.* **1997**, *536-537*, 197–205.

(45) Barfield, M.; Chakrabarti, B. *Chem. Rev.* **1969**, *69*, 757–778.

(46) Guenther, H.; Jikeli, G. *Chem. Rev.* **1977**, *77*, 599–637.

(47) Parr, W. J. E.; Schaefer, T.; Marat, K. *Can. J. Chem.* **1977**, *55*, 3243–3247.

(48) Tuttle, T.; Gräfenstein, J.; Cremer, D. *Chem. Phys. Lett.* **2004**, *394*, 5–13.

(49) Dračínský, M.; Jansa, P.; Bouř, P. *Chem.-Eur. J.* **2012**, *18*, 981–986.

(50) Kruck, M.; Muñoz, M. P.; Bishop, H. L.; Frost, C. G.; Chapman, C. J.; Kociok-Köhn, G.; Butts, C. P.; Lloyd-Jones, G. C. *Chem.-Eur. J.* **2008**, *14*, 7808–7812.

(51) Schmidt, J. A. R.; Lobkovsky, E. B.; Coates, G. W. *J. Am. Chem. Soc.* **2005**, *127*, 11426–11435.

(52) Deng, F.-G.; Hu, B.; Sun, W.; Chen, J.; Xia, C.-G. *Dalton Trans.* **2007**, *38*, 4262–4267.

(53) Brammer, L.; McCann, M. C.; Bullock, R. M.; McMullan, R. K.; Sherwood, P. *Organometallics* **1992**, *11*, 2339–2341.

(54) Mareque Rivas, J. C.; Brammer, L. *Acta Crystallogr. C* **1998**, *54*, 757–760.

(55) Brammer, L.; Mareque Rivas, J. C.; Spilling, C. D. *J. Organomet. Chem.* **2000**, *609*, 36–43.

(56) Stockis, A.; Hoffmann, R. *J. Am. Chem. Soc.* **1980**, *102*, 2952–2962.

(57) Wakatsuki, Y.; Nomura, O.; Kitaura, K.; Morokuma, K.; Yamazaki, H. *J. Am. Chem. Soc.* **1983**, *105*, 1907–1912.

CHAPTER 6

Rh(I)-Catalyzed [2+2+2] with Alkyl Alkynes to form Aza-Quaternary N-Stereocenters: Synthesis of Cylindricine Core

6.1 Introduction

6.1.1 5,9-Alkyl Substituted Indolizidine Alkaloids

Rapid, selective N-heterocycle synthesis is currently a vital area of research due to the biological importance of molecules that contain these motifs. Transition metal catalysis offers efficient access to complex N-heterocycles through [2+2+2] cycloadditions with N-containing π-components, such as isocyanates, to form indolizinones and quinolizinones. Rh(I)•phosphoramidite catalyzed cycloadditions can form two products: lactam and vinylogous amide, depending on the substrate and ligand. We found previously that there is an element of substrate control of product selectivity with Rh(I) and Taddol phosphoramidites, where alkyl alkynes favor lactam product and aryl alkynes provide vinylogous amide with 1,1-disubstituted alkenyl isocyanates (Scheme 6.1).[1] Consequently, a limitation of our methodology was the synthesis of vinylogous amide cycloadducts with alkyl alkynes.[2] Such alkyl susbstituted vinylogous amides indolizinones are desirable synthetic targets as a large number of indolizidine and quinolizidine natural products[3] have alkyl substituents at the indolizidine 5-carbon, including the cylindricine[4] and lepadiformine [5,6] alkaloids (Figure 6.1).

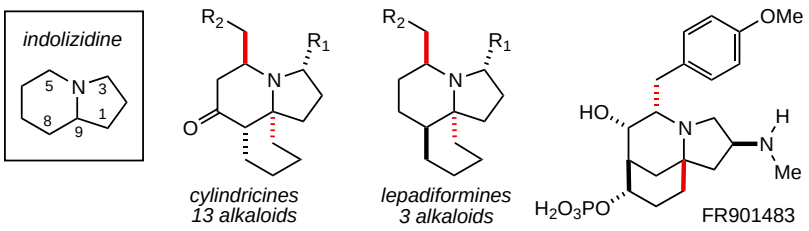

Figure 6.1 5,9-alkyl substituted indolizidine alkaloids.

We found that Rh(I)•CKphos provides a selective means of forming vinylogous amides from alkyl alkynes and 1,1-disubstituted alkenes. This is a valuable contribution to the synthetic community as there are a number of biologically active 5,9-alkyl substituted indolizidine alkaloids. This is evidenced by the myriad of synthetic methods that have already been developed for the synthesis of these alkaloids.

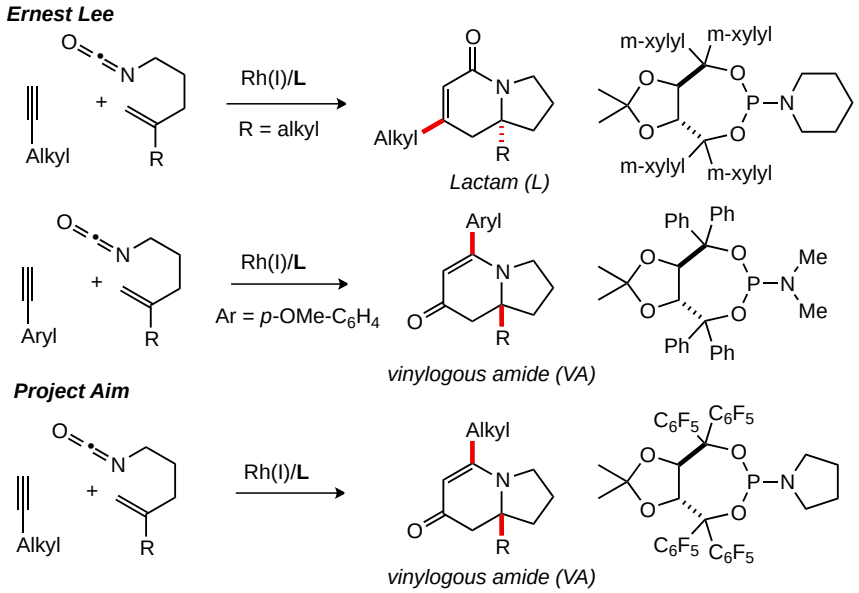

Scheme 6.1 Proposed application of [2+2+2] cycloaddition to the synthesis of 5,9-alkyl substituted indolizidinones.

6.1.2 Application of Rh(I)-Catalyzed [2+2+2] to Alkaloid Synthesis

Rh(I)•phosphoramidite catalysts efficiently and asymmetrically synthesize cores valuable to natural product total synthesis via [2+2+2] cycloaddition of alkenyl isocyanates and alkynes. Yu and Rovis used Rh(I) catalyzed cycloadditions in the rapid asymmetric syntheses of indolizidine 209-D and (–)-Lasubine II (chapter one).[2,7] Perreault and Rovis employed $Rh(C_2H_4)_2Cl$•CKphos as the catalyst for the cycloaddition of 1,1-disubstituted alkenyl isocyanate **1a** and p-MeO-benzyl acetylene en route to the total synthesis of (–)-FR901483 (Scheme 6.2).[8]

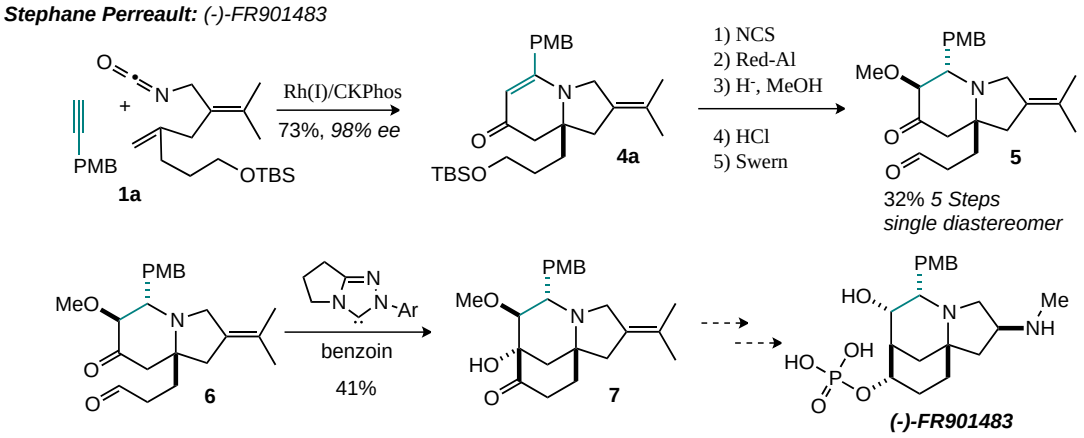

Scheme 6.2 Progress towards the synthesis of (–)-FR901483

Friedman and Rovis also found that $Rh(C_2H_4)_2Cl$•CKphos was the optimal catalyst in their efforts toward the total synthesis of Secu'amamine A (Scheme 6.3, unpublished results). In both cases, $Rh(C_2H_4)_2Cl$•CKphos provided vinylogous amide indolizinone in good yield and excellent product and enantioselectivity.

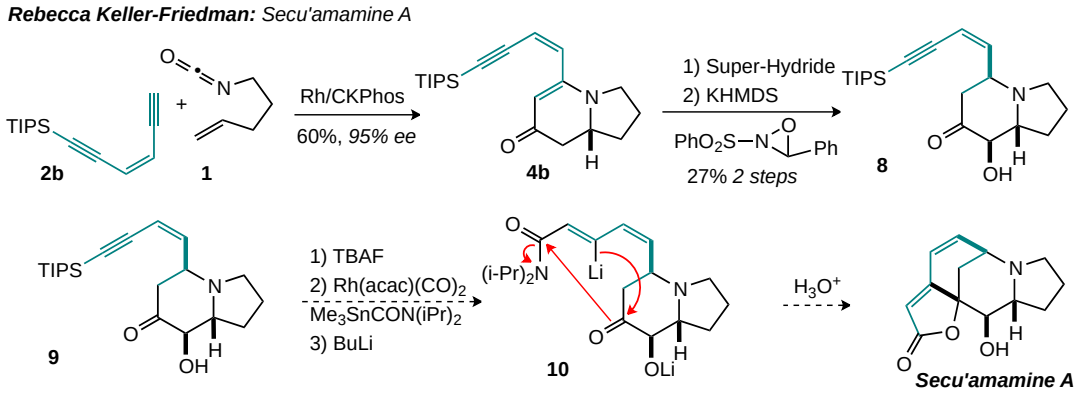

Scheme 6.3 Progress towards the synthesis of Secu'amamine A.

6.1.3 Synthetic Approaches to the Cylindricine and Lepadiformine Alkaloids

In the early 1990's, Blackman and co-workers isolated a series of tricyclic alkaloids from the marine ascidian (sea squirt) *clavelina cylindrica* off Tasmania's eastern coast.[9,10] This family of tricyclic amines was aptly named the cylindricine alkaloids and of the eleven isolated, cylindricines A and B are the most prevalent (Table 6.1). The structures of these compounds were elucidated by spectral analysis and confirmed by X-ray analysis of the picrate salts.

Table 6.1 Selected ascidian alkaloids.

Tricyclic Ascidian Alkaloids

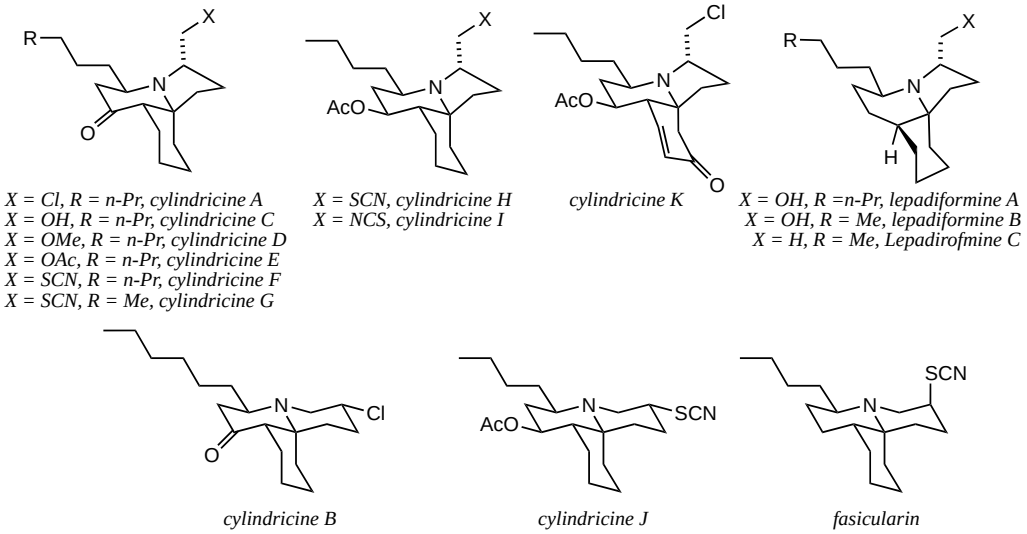

Blackman and coworkers found that after purification cylindricine A equilibrates to a 3:2 mixture of cylindricines A and B (Scheme 6.4); the same equilibration occurs with cylindricine B.[9,10] Protonation of the tertiary amine as the picrate salt prevents this equilibration. For this reason, Blackman presumed that interconversion between A and B occurs via aziridinium intermediate **11**.

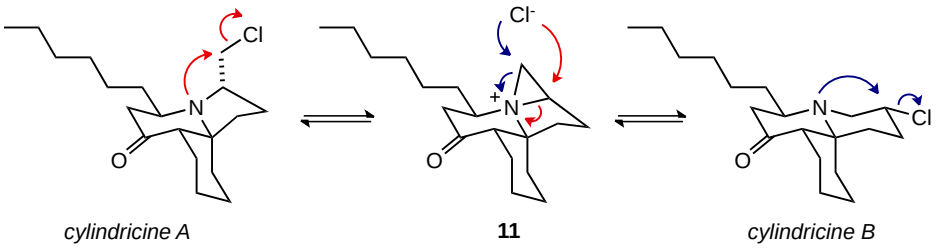

Scheme 6.4 Equilibration of cylindricine A and B alkaloids.

In 1994, Baird and coworkers isolated a related tricyclic alkaloid, lepadiformine, from marine tunicate *clavelina lepadiformis* off the coast of Tunisia[5] and then again off the coast of Djibouti[11] from *clavelina moluccensis*. Of the tricyclic ascidian alkaloids discussed, lepadiformine is the only alkaloid whose absolute configuration is known and confirmed through synthesis and X-ray analysis. X-ray analysis revealed the B ring of lepadiformine exists in the boat conformation (Table 6.2). In 2006, Baird and coworkers reported the isolation and characterization of lepadiformines B and C; lepadiformine was

then designated lepadiformine A (Table 6.1).[12] Biological activity of the lepadiformine alkaloids A-C was assessed with frog atrial myocytes and all three were found to inhibit inward rectifying K^+ ion channels. Lepadiformine A is proposed to bind two-thirds of the way down the K^+ ion channel. Of the lepadiformines studied, lepadiformine A has the greatest inhibitory effect, followed by B then C, suggesting that both the pendent alcohol and longer alkyl side chain (hexyl vs butyl) promote binding within the channel, increasing cytotoxicity.

6.1.4 Racemic Synthetic Approaches to the Cylindricine Alkaloids

In 1997 Snider/Liu[13] reported the first total synthesis of (±)-cylindricine alkaloids A, D and E (Scheme 6.5). In 1999 Liu/Heathcock[14] contributed a similar synthesis of (±)-cylindricine A. Both Snider and Heathcock elaborate cyclohexanone into cyclodienone aza-Michael precursor **12**. Double aza-Michael reaction gives a mixture of three diastereomers (**13a**, **13b**, **13c**) with the desired **13a** as the major product. Copper catalyzed radical cyclization of the chloroamine of **13a** provides a 1:1 mixture of (±)-cylindricine A and (±)-epi-cylindricine A in 84% yield. Snider converts (±)-cylindricine A into (±)-cylindricines D and E. From cyclohexanone Snider's synthesis of (±)-cylindricine A is 10 steps while Heathcock's is 8.

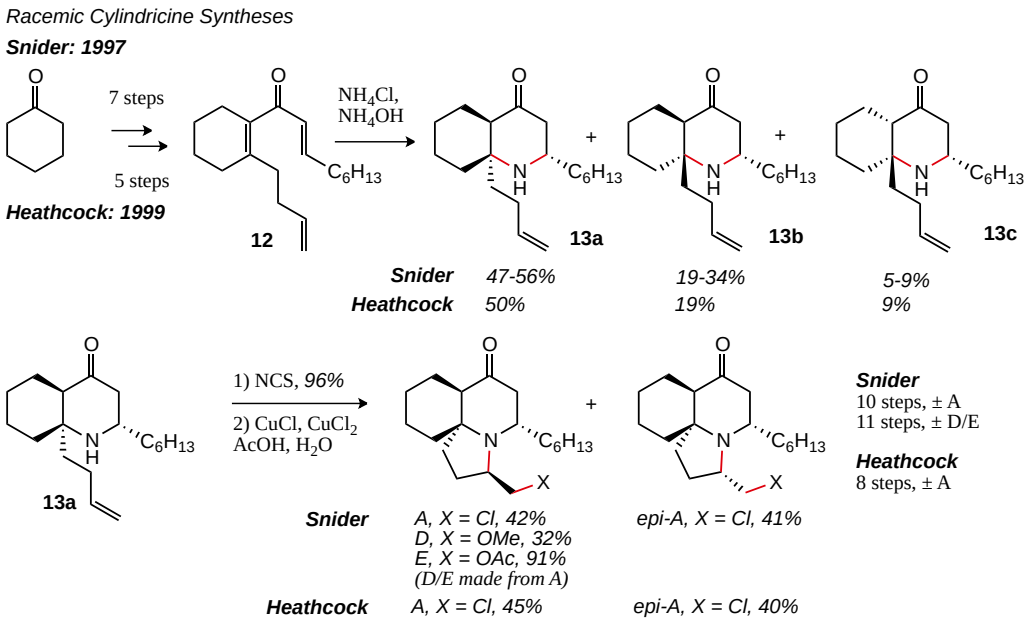

Scheme 6.5 Racemic cylindricine syntheses.

In 2008, Padwa and coworkers[15,16] reported a racemic total synthesis of the (±)-cylindricine C, which takes advantage of an oxime (**15**) Michael addition/dipolar cyclization to form the tetrasubstituted aza-stereocenter (**17**) and piperidone ring of **18**. He further functionalized **18** into (±)-cylindricine C and (±)-2-*epi*-cylindricine C in 15 steps (Scheme 6.6, eq 1). In 2010, Donohoe and coworkers[17] reported a 13 step racemic synthesis of (±)-cylindricine C and a formal synthesis of (±)-cylindricine A (eq 2); both use a regioselective Grignard addition to pyridinium salts (**20**) as key synthetic strategies. In 2011, Renaud and coworkers[18] reported a racemic synthesis of (±)-cylindricine C that features a radical alkene functionalization of **23** to form azido ketone **25**, followed by a Lewis acid catalyzed reductive amination cyclization to form (±)-cylindricine C in 16 steps (eq 3).

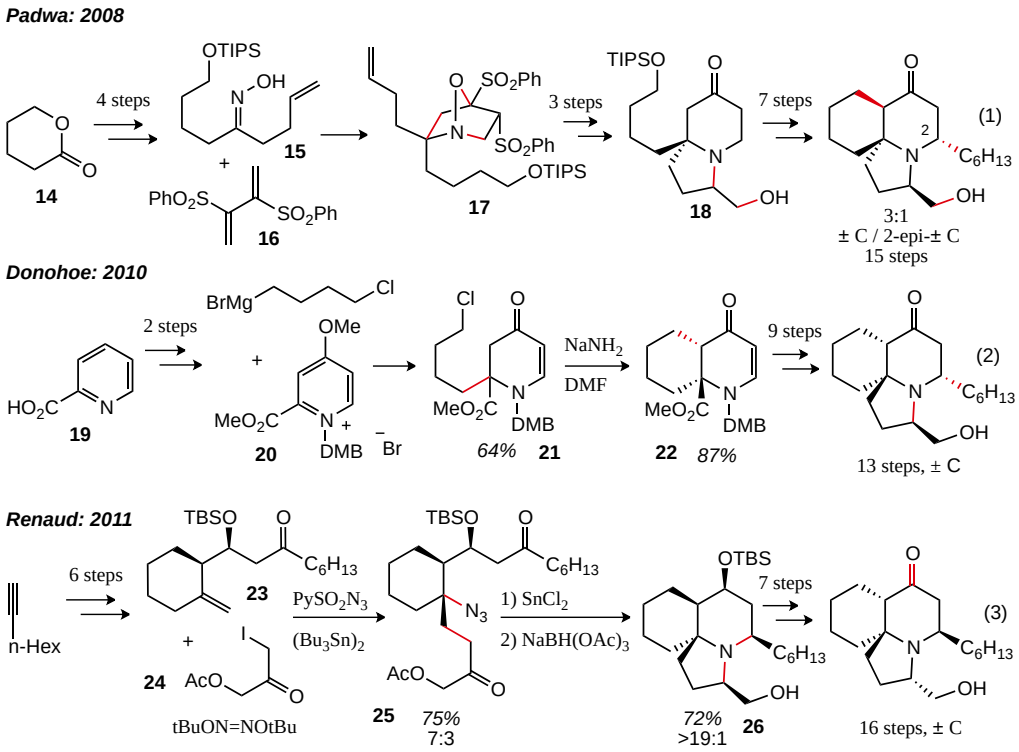

Scheme 6.6 Recent racemic cylindricine syntheses. DMB is 3,4-dimethoxybenzyl.

In 2003, Hunter[19] and in 2005, Ishibashi[20] published synthetic approaches to the cylindricine/ lepadiformine ring skeleton. In a departure from traditional synthetic routes to the cylindricines, Ishibashi synthesized the racemic tricyclic core via a 6-endo selective radical cyclization in 4 steps, establishing 2

of the 4 stereocenters of the cylindricine skeleton. Hunter/Richards employ a dialkylation strategy to form the tetrasubstituted aza-stereocenter racemically followed by ring closing metathesis and N-alkylation to form the tricycle in 14 steps. In 2009, Tanner and coworkers[21] reported the racemic synthesis of the tricyclic cylindricine core via a transannular Mannich reaction in 10 steps from cycloheptanone.

6.1.5 Enantioenriched Syntheses of Cylindricine Alkaloids

Taking advantage of chiral pool materials, Molander/Rohn,[22] Trost/Rudd,[23] Kibayashi,[24,25] Hsung[26-28] and Ciufolini[29] reported diastereoselective syntheses of enantioenriched cylindricines C, D, and E (Scheme 6.7). Molander and Trost both use a double aza-Michael reaction to access the tricyclic framework. Molander takes advantage of chiral butenolide **28** to form the aza-Michael precursor **29** (eq 4), while Trost uses a ruthenium catalyzed hydrative diyne coupling of serine-derived diyne **30** (eq 5). Elaborating D-homotyrosine, Ciufolini featured an oxidative spirocyclization of sulfonamide **32** to form the tetrasubstituted aza-stereocenter in spirocycle **33**, which was functionalized to (–)-cylindricine C with a total of 16 steps (eq 6).

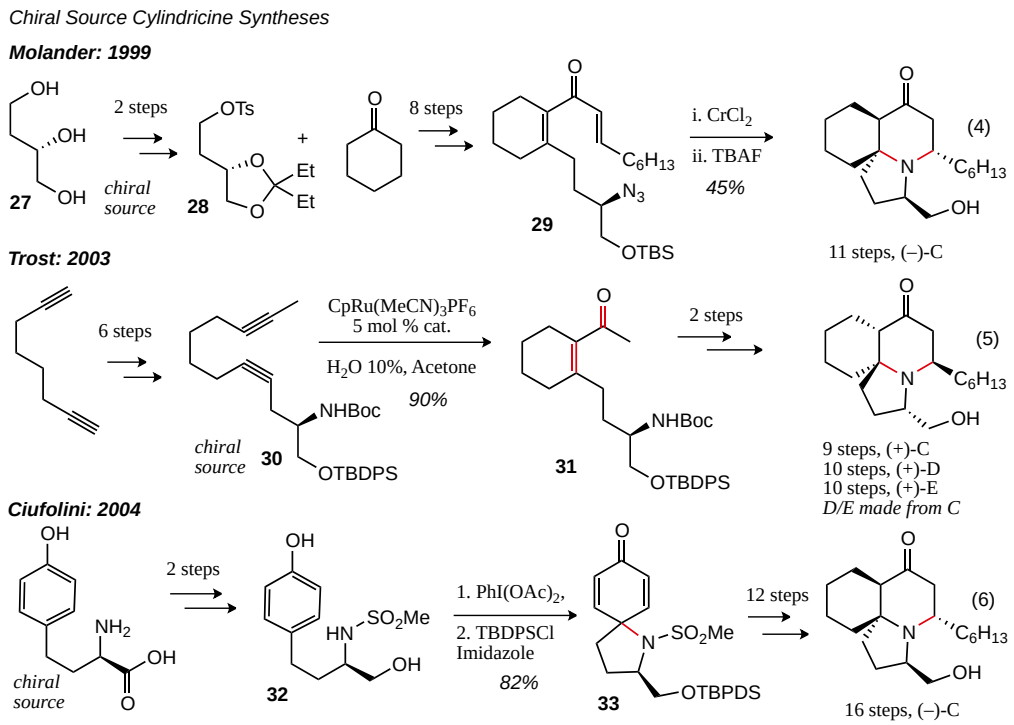

Scheme 6.7 Diastereoselective total syntheses of cylindricine alkaloids.

In 2004, Kibayashi and coworkers established that an allylmagnesium bromide addition to an L-pyroglutamic acid derived imine **34**, followed by ring closing metathesis and aza-Michael addition forms aza-spirocycle **36**, which is elaborated into cylindricine C with a total of 21 steps[24] (Scheme 6.8, eq 7). As reported in 2004 and 2005, Hsung and coworkers developed L-pyroglutamic acid into unsymmetrical ketone **37** that was then converted to aza-spirocycle **38** via an aza-Prins cyclization. Hsung and coworkers make **38** into an α-epoxy ketone that undergoes Wharton's rearrangement and allows an aza-Michael addition to form the cylindricine and lepadiformine frameworks in 13 steps[26,27] (eq 8). In 2005, Kibayashi and coworkers reported a similar aza-Prins spirocyclization strategy to synthesize three tricyclic marine alkaloids: cylindricine C (18 steps), lepadiformine A, and fasicularin[25] (eq 8). In 2005, Hsung and coworkers reported another approach to the cylindricine alkaloids featuring an aza-iminium [3+3] annulation strategy to access cylindricine C in 20 steps (eq 9).

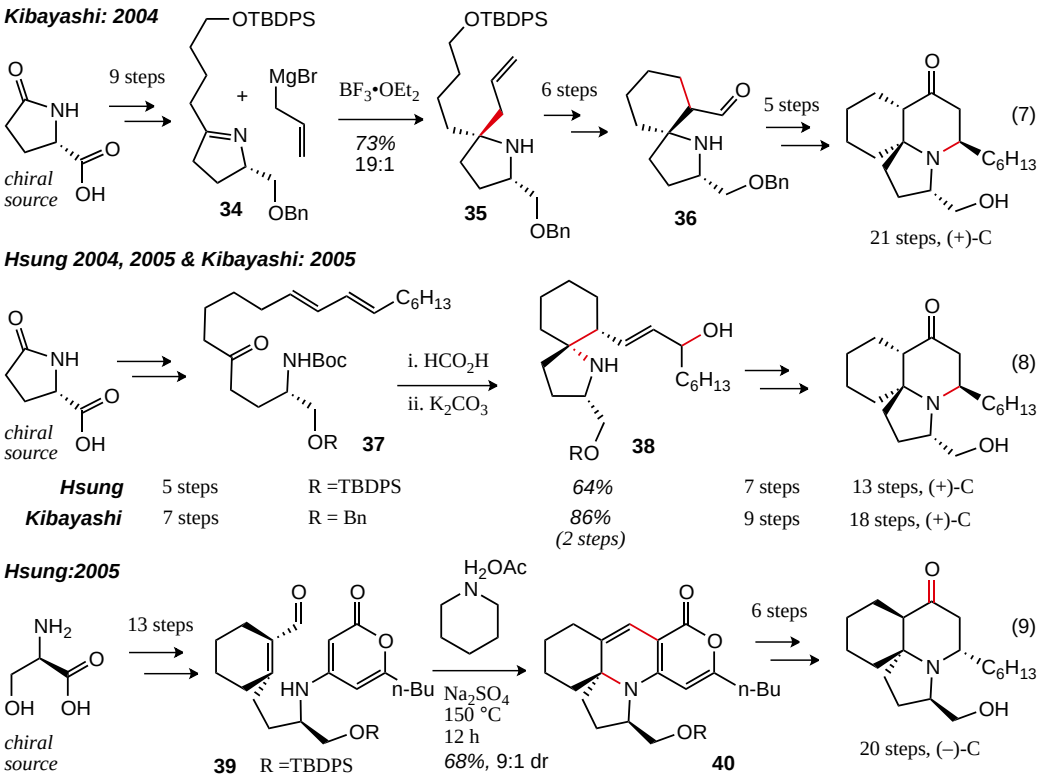

Scheme 6.8 Chiral source total syntheses of cylindricine alkaloids.

In 2010, Mariano[30] reported a tandem dienyne metathesis based approach to the cylindricine tricyclic framework building the core from proline in 14 steps.

6.1.6 Catalytic Asymmetric Approaches to the Cylindricine Alkaloids

In 2006, Shibasaki and coworkers[31] reported the first catalytic asymmetric synthesis of a cylindricine alkaloid (Scheme 6.9, eq 10). Using a dicationic chiral phase transfer catalyst, TaDiAS, they accomplish an asymmetric Michael addition in 84% yield and 82% ee to form cyclization precursor **42**. Further manipulation arrives at (+)-cylindricine C in 9 steps overall. In 2008, Tu, Zhang and coworkers[32] reported a catalytic asymmetric prolinamide catalyzed Hajos-Parrish annulation to form **45** and intramolecular Schmidt reaction of **46** for the enantioenriched synthesis of the tricyclic core of the cylindricine alkaloids in 87% ee and a total of 11 steps (eq 11).

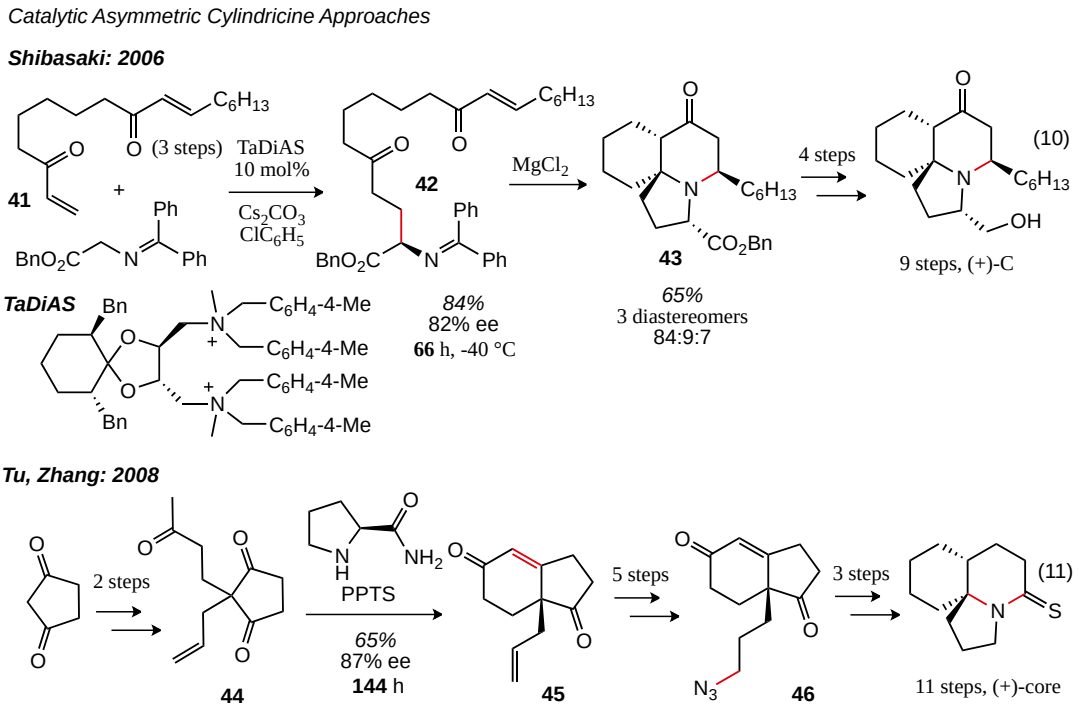

Scheme 6.9 Catalytic asymmetric cylindricine syntheses.

6.2 Results

6.2.1 Rh(I)-Catalyzed [2+2+2] Cycloaddition with 1,1-Disubstituted Alkenyl Isocyanates

Rhodium(I) catalyzed [2+2+2] cycloadditions are ideally suited for the catalytic asymmetric synthesis of the cylindricine molecules. Specifically, the syntheses of these molecules using our methodology requires formation of the vinylogous amide cycloadduct with an alkyl alkyne and a 1,1-disubstituted alkenyl isocyanate for the formation of the aza-quaternary stereocenter. As reported by Lee and Rovis in 2008,[1] 1,1-disubstituted alkenes are competent π-components in the cycloaddition and afford indolizidinone cycloadducts in high yields and ee's. As Lee and Rovis previously reported vinylogous amide cycloadduct formation required aryl acetylenes. Alkyl alkynes give lactam product in high product selectivity (Table 6.2) and unfortunately the lactam scaffold does not have the correct substitution pattern for the synthesis of the cylindricine family of alkaloids. With the development of perfluoroaryl Taddol phosphoramidite ligands that favor vinylogous amide with alkyl alkynes, we were able to apply these catalysts in the synthesis of the cylindricine molecules' core.

Yu and Lee have previously investigated the rhodium catalyzed [2+2+2] with 1,1-disubstituted alkenyl isocyanates (Table 6.2, eq 12). Yu found that Binol **B2** and Biaryl **B1** favor vinylogous amide with 1-octyne with modest product and enantioselectivities[2]. Lee reported[1] that m-xylyl Taddol **T5** provides lactam **3** with moderate product and excellent enantioselectivity. Fortuitously, we found that Rh(I)•CKphos (**T25**) provides a highly selective means of forming vinylogous amides from alkyl alkynes and 1,1-disubstituted alkenes with 1:>19 product selectivity and 90% enantioselectivity.

Table 6.2 Ligand screen of phosphoramidites with 1,1-disubstituted alkenyl isocyanates.

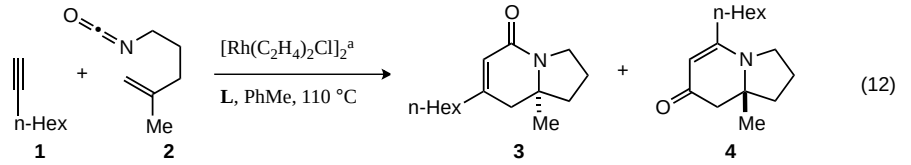

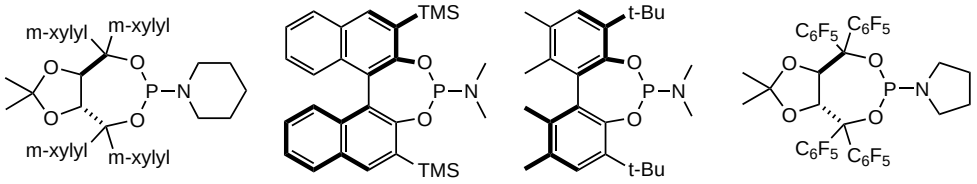

T5	B2	B1	T25 CKphos
88	*53*	*72*	*61*
6.5 : 1	1 : **3.4**	1 : **6.3**	1 : **>19**
91	72	27	90

The substrate scope of the cycloaddition with 1,1-disubstituted alkenyl isocyanates (**2**) to form indolizidinones with aza-quaternary stereocenters is large and varied (Table 6.3). Many functional groups are tolerated on the alkyne, including esters, chlorides, silylethers, aryls and alkenes. Product selectivities with alkyl, alkenyl and aryl alkynes are 1: >19 (L/VA). Additionally, enantioselectivities range from 88 (**4l**) to 98% (**4d**, **4e**, **4m**). Alkenes with large substituents are tolerated but result in lower yields (**4l**, **4m**), which are attributed to the competitive formation of pyridone side-product. The increased steric bulk on the alkene likely slows its coordination and subsequent 1,2-migratory insertion, allowing a second alkyne to incorporate.

Table 6.3 Substrate scope of cycloaddition with 1,1-disubstituted alkenyl isocyanates and alkyl alkynes.

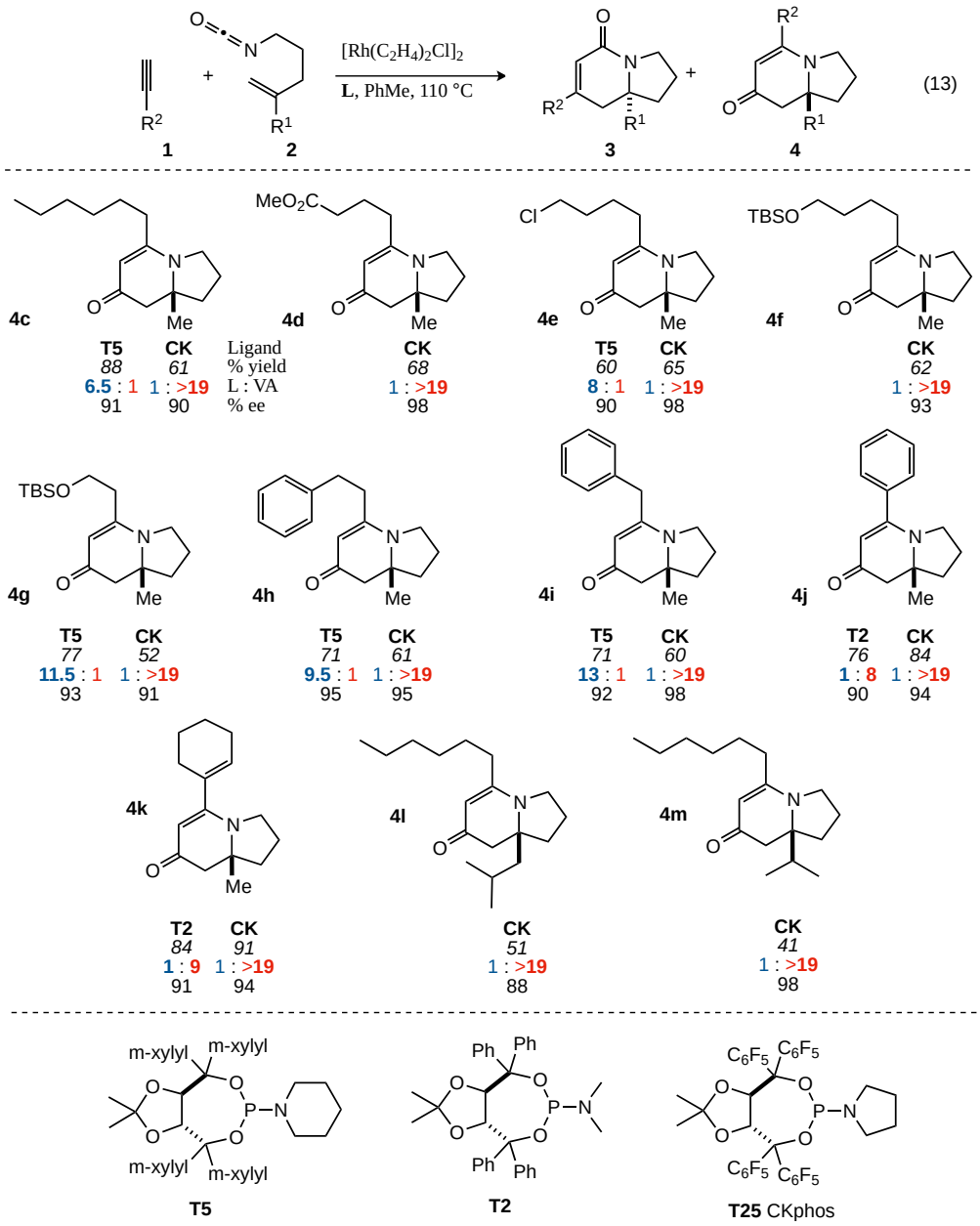

6.2.2 Application of Rh(I)-Catalyzed [2+2+2] to the Synthesis of the Cylindricine Core

To showcase the ability of this methodology to rapidly and enantioselectively assemble indolizidines from simple starting materials, we sought to apply the Rh(I)CKphos catalyzed cycloaddition of a 1,1-disubstituted alkenyl isocyanates with an alkyl alkyne in the synthesis of the cylindricine alkaloids

(Scheme 6.10). Reduction of the vinylogous amide and base induced alkylation would provide the tricyclic core, which could be further functionalized to introduce the C3 alkyl side chain.

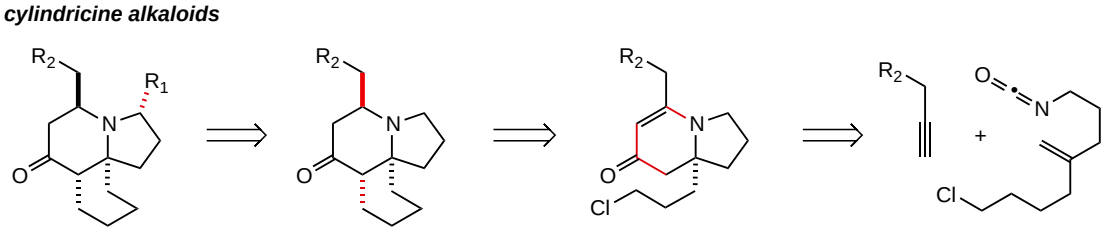

Scheme 6.10 Retrosynthesis of cylindricine alkaloids using Rh(I) catalyzed [2+2+2] cycloaddition.

Lee and Rovis developed an efficient route to the synthesis of the pendent alkyl chloride alkenyl isocyanate **2c** required for cylindricine synthesis (Scheme 6.11).[33] Iodoboration of 1-chlorohexyne provides vinyl iodide **47** in excellent yield. Negishi coupling of vinyl iodide **47** and iodoalkyl zinc reagent **48** provides ester **49** in 90% yield. Hydrolysis of the ester and treatment with diphenylphosphorylazide (DPPA) forms the acyl azide that undergoes a Curtius rearrangement to give isocyanate **1c** in 5 steps and 60% overall yield.

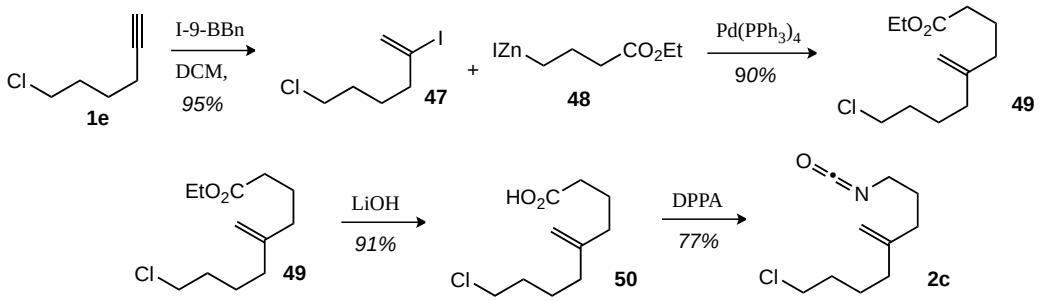

Scheme 6.11 Synthesis of alkyl chloride 1,1-disubstituted alkenyl isocyanate **1c**.

To assess the utility of using the cycloaddition for the synthesis of the cylindricine alkaloids, we started with alkyl chloride isocyanate **2c** and 1-octyne, using standard conditions (Scheme 6.12). Lee and Rovis (unpublished results) previously investigated Guiphos **B2** as a ligand for this transformation and found that it provides the vinylogous amide with moderate product and enantioselectivity (1:4 L/VA, 49% ee). Fortunately, CKphos gives vinylogous amide **4n** in excellent product and enantioselectivity (1: >19, 90%) with moderate yield.

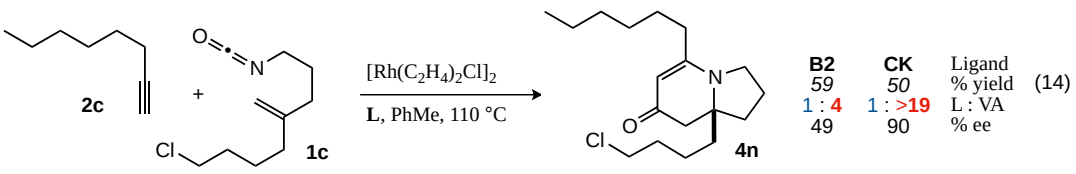

Scheme 6.12 Ligand screen with isocyanate **1c**.

6.2.3 Rh(I)•CKphos Catalyst Optimization

For a general approach to the cylindricine and lepadiformine alkaloids, 1-hexyne was chosen as the alkyne component because *n*-butyl is the smallest alkyl chain found in the these alkaloids, and we supposed it would be the most challenging to incorporate due to its low boiling point. Indeed, its low boiling point proved problematic under our standard reaction conditions. Attempts to run the reaction in a sealed tube or at lower temperatures were not effective (Table 6.4). To improve yields a variety of precatalysts and additives were screened. We found that cyclooctadiene (cod) precatalysts give little to no product conversion after 16 h based on ^{1}H–NMR (entries 4-6). Rhodium biscyclooctene (coe, entry 7) provides a modest increase in conversion to 10%. Rhodium bisethylene complex is the most reactive at 33% conversion (entry 1). We next examine the effect of different counterions with the Rh bisethylene complex by premixing with silver salts. We found decreased conversion with triflate (entry 2) while tosylate was found to provide the most reactive catalyst, increasing conversion to 69% in 16 h at 70 ºC and enantioselectivity to 95% (entry 3).

Table 6.4 Optimization of catalyst conditions for [2+2+2] cycloaddition at 70 °C. (a) % conversion after 16 is reported based on ^{1}H-NMR of product in reference to an internal standard.

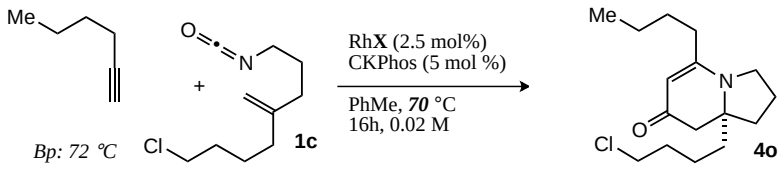

Entry	Precatalyst	Additive	L:VA	% Conversion[b]	% ee
1	$[Rh(C_2H_4)_2Cl]_2$		1:>19	33	90
2	$[Rh(C_2H_4)_2Cl]_2$	AgOTf[a]	1:>19	28	96
3	$[Rh(C_2H_4)_2Cl]_2$	AgOTs[a]	1:>19	***69***	***95***
4	$[Rh(cod)Cl]_2$		1:>19	4	
5	$[Rh(cod)OTf]_2$			0	
6	$[Rh(cod)_2BF_4]$			0	
7	$[Rh(coe)_2Cl]_2$		1:>19	10	

Having identified a more active catalyst for the cycloaddition, we increased the scale of the reaction with RhOTs$(C_2H_4)_2$•CKphos to afford gram scale quantities of vinylogous amide **4o** in 52% yield, 1: > 19 (L/VA) and 95% ee after 48 h (Scheme 6.13). The yield may be increased with a longer reaction time. Additionally, we found it imperative that the isocyanate be distilled (Kugelrohr) and that the reaction vessel and reagents be stringently dried and free of oxygen to prevent catalyst death over prolonged reaction times. Presence of insoluble AgCl salts in the reaction do not appear to affect yield or selectivity.

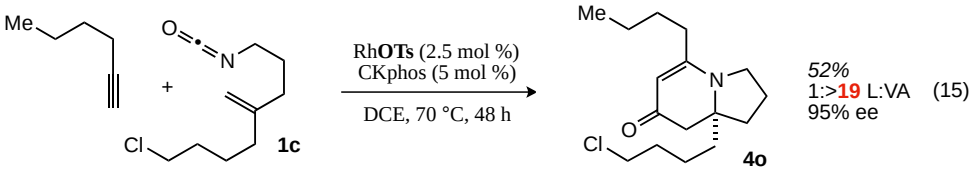

Scheme 6.13 Results of large scale [2+2+2] cycloaddition with optimized Rh(OTs)•CKphos catalyst.

6.2.4 Reduction and Alkylation of Indolizidinone Products

Inspired by Donohoe's enolate alkylation of vinylogous amide **21** (Scheme 6.6), we investigated similar conditions with indolizidinone **4o**. A wide variety of conditions were examined, including variation of base, temperature and solvent, but tricyclic product was not observed (Scheme 6.14, eq 16). We converted the alkyl chloride to the iodide by means of a Finkelstein reaction to enhance the leaving group ability of the chloride; however, cyclization still did not occur. Physical models of possible

transition states for the enolate alkylation suggest that formation of the *cis*-decalin system would proceed through an unfavorable twist boat conformation (**TSI**). Alkylation to give the *trans*-decalin would have to occur with a strained, potentially inaccessible geometry (**TSII**). The rigidity of the flat 5,6-fused ring system and the need for the alkyl chloride to approach from the opposite enolate face both may be causes of the unsuccessful reaction.

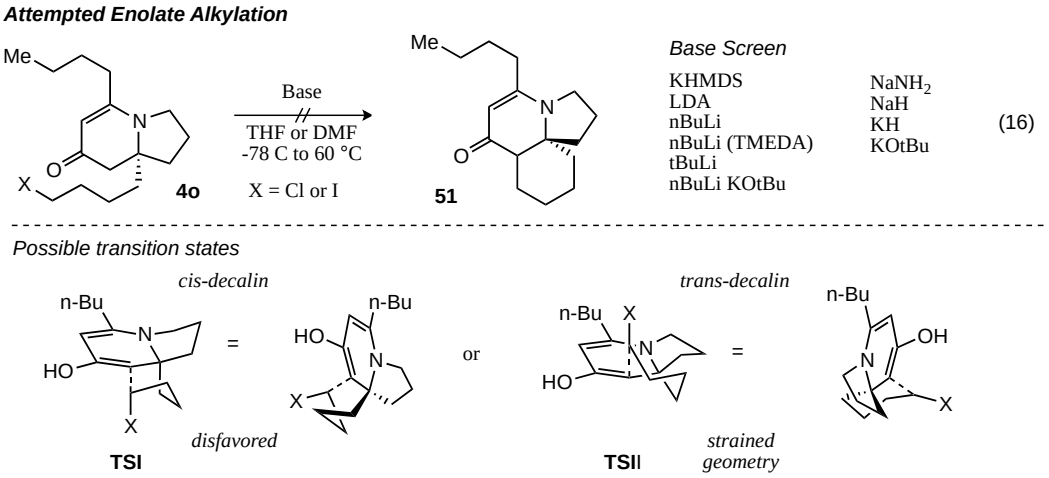

Scheme 6.14 Attempted enolate alkylation to form tricyclic alkaloids.

We hypothesized that increasing the flexibility of the system would favor the desired alkylation. Thus, we investigated a variety of 1,4-reduction conditions form indolizidinone **53** (Scheme 6.15). Under acidic conditions, borohydrides (sodium cyanoborohydride, sodium triacetoxyborohydride and lithium triethylborohydride (Superhydride)) doubly reduce vinylogous amide **4o** to provide a tertiary amine that is N-alkylated by the pendent alkyl chloride to form indolizidinium chloride **52**. Fortunately, aluminum hydrides (diisobutylaluminum hydride (DIBAL-H) and sodium bis(2-methoxyethoxy)aluminum hydride (Red-Al)) provide the 1,4-reduction product **53** selectively in moderate yields and good diastereoselectivity (dr) (12:1, and 4:1 dr respectively). Diastereoselectivity of the DIBAL-H reduction is proposed to be controlled by aluminum coordination to the carbonyl and delivery of the hydride to the more accessible face of the vinylogous amide opposite the pyrrolidine ring (**TSIII**).

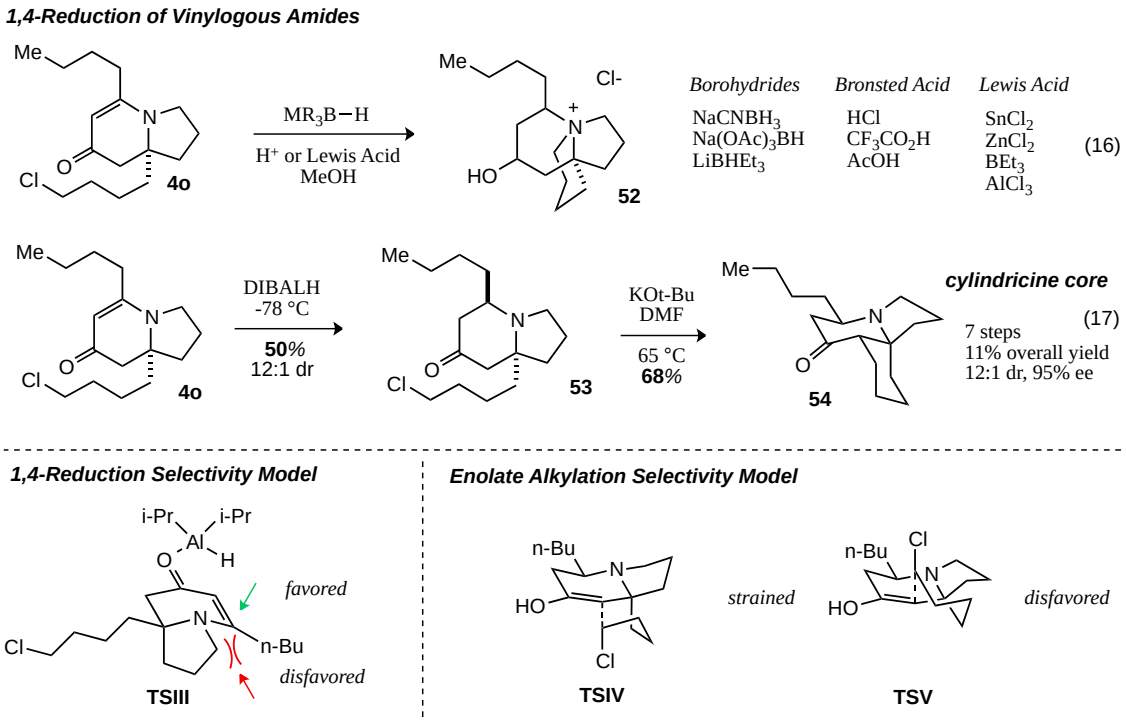

Scheme 6.15 1,4-reduction of indolizidinone **4o** and enolate alkylation.

Once isolated, **53** slowly undergoes undesired N-alkylation (Scheme 6.15, eq 16). However, if **53** is immediately subjected to potassium *tert*-butoxide (KO*t*-Bu) in polar protic (*t*-BuOH) or aprotic (DMSO, DMF) solvents with heat (65 °C) the *cis*-decalin system **54** is obtained (eq 17). Use of other solvents (THF, Et_2O, Toluene) or temperatures (-78 °C to rt) results in recovery of **53** or decomposition. DMF provides the highest yield of the cylindricine core **54** in 68% yield as a single diastereomer **54** after 12 h. In a related system, Padwa and coworkers reported that enolate alkylation first generates the kinetically favored *trans*-decalin system, which epimerizes under the reaction conditions to the thermodynamically favored *cis*-decalin.[16] Formation of the *trans*-decalin is explained by a favorable chair geometry of the alkyl chloride tether in the proposed transition state **TSIV** while alkylation of the other enolate face requires the tether to adopt a twist boat geometry (**TSV**). We see complete epimerization after 6 h at 65 ^{o}C.

Both the relative and absolute stereochemistry of the tricyclic core were confirmed by X-ray analysis of the hydrochloride salt of **54** (Figure 6.2). Overall, the cylindricine core was synthesized

enantioselectively in 7 steps, 95% ee and 11% overall yield from simple commercially available starting materials.

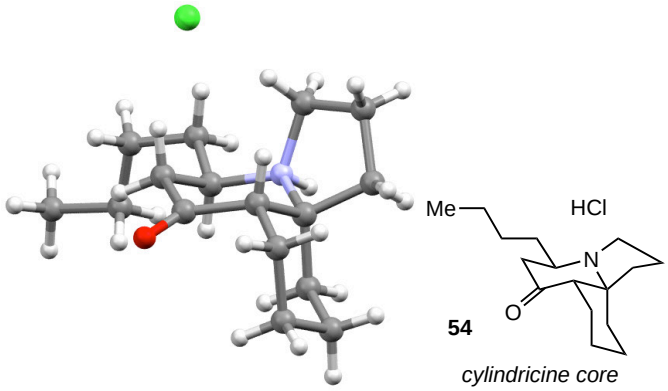

Figure 6.2 X-ray structure of HCl salt of tricycle **54** . Grey = C, Blue = N, Red = O, White = H, Green = Cl.

6.3 Conclusion

In summary, we have investigated the use of Rh(I)•CKphos as a catalyst for the asymmetric synthesis of indolizidines with aza-quaternary stereocenters. We found that the catalyst gives excellent product and enantioselectivity for a wide range of substrates. This enabled the stereoselective synthesis of the tricyclic core of the cylindricine alkaloids in an efficient and highly selective manner.

6.4 References

(1) Lee, E. E.; Rovis, T. *Org. Lett.* **2008**, *10*, 1231–1234.

(2) Yu, R. T.; Lee, E. E.; Malik, G.; Rovis, T. *Angew. Chem. Int. Ed.* **2009**, *48*, 2379–2382.

(3) Daly, J. W.; Spande, T. F.; Garraffo, H. M. *J. Nat. Prod.* **2005**, *68*, 1556–1575.

(4) Weinreb, S. *Chem. Rev.* **2006**, *106*, 2531–2549.

(5) Biard, J. F.; Guyot, S.; Roussakis, C.; Verbist, J. F.; Vercauteren, J.; Weber, J. F.; Boukef, K. *Tetrahedron Lett.* **1994**, *35*, 2691–2694.

(6) Weinreb, S. *Acc. Chem. Res.* **2003**, *36*, 59–65.

(7) Yu, R. T.; Rovis, T. *J. Am. Chem. Soc.* **2006**, *128*, 12370–12371.

(8) Perreault, S.; Rovis, T. *Synthesis* **2013**, *45*, 719–728.

(9) Li, C.; Blackman, A. *Aust. J. Chem.* **1994**, *47*, 1355–1361.

(10) Li, C.; Blackman, A. *Aust. J. Chem.* **1995**, *48*, 955–965.

(11) Jugé, M.; Grimaud, N.; Biard, J.-F.; Sauviat, M.-P.; Nabil, M.; Verbist, J.-F.; Petit, J.-Y. *Toxicon* **2001**, *39*, 1231–1237.

(12) Sauviat, M.; Vercauteren, J.; Grimaud, N.; Juge, M.; Nabil, M.; Petit, J.; Biard, J. *J. Nat. Prod.* **2006**, *69*, 558–562.

(13) Snider, B. B.; Liu, T. *J. Org. Chem.* **1997**, *62*, 5630–5633.

(14) Liu, J. F.; Heathcock, C. H. *J. Org. Chem.* **1999**, *64*, 8263–8266.

(15) Flick, A. C.; Caballero, M. J. A.; Padwa, A. *Org. Lett.* **2008**, *10*, 1871–1874.

(16) Flick, A. C.; Arevalo Caballero, M. J.; Padwa, A. *Tetrahedron* **2010**, *66*, 3643–3650.

(17) Donohoe, T. J.; Brian, P. M.; Hargaden, G. C.; O'Riordan, T. J. C. *Tetrahedron* **2010**, *66*, 6411–6420.

(18) Lapointe, G.; Schenk, K.; Renaud, P. *Org. Lett.* **2011**, *13*, 4774–4777.

(19) Hunter, R.; Richards, P. *Synlett* **2003**, 271–273.

(20) Taniguchi, T.; Tamura, O.; Uchiyama, M.; Muraoka, O.; Tanabe, G.; Ishibashi, H. *Synlett* **2005**, 1179–1181.

(21) Vital, P.; Hosseini, M.; Shanmugham, M. S.; Gotfredsen, C. H.; Harris, P.; Tanner, D. *Chem. Commun.* **2009**, 1888–1890.

(22) Molander, G. A.; Rönn, M. *J. Org. Chem.* **1999**, *64*, 5183–5187.

(23) Trost, B. M.; Rudd, M. T. *Org. Lett.* **2003**, *5*, 4599–4602.

(24) Arai, T.; Abe, H.; Aoyagi, S.; Kibayashi, C. *Tetrahedron Lett.* **2004**, *45*, 5921–5924.

(25) Abe, H.; Aoyagi, S.; Kibayashi, C. *J. Am. Chem. Soc.* **2005**, *127*, 1473–1480.

(26) Liu, J.; Hsung, R. P.; Peters, S. D. *Org. Lett.* **2004**, *6*, 3989–3992.

(27) Liu, J.; Swidorski, J. J.; Peters, S. D.; Hsung, R. P. *J. Org. Chem.* **2005**, *70*, 3898–3902.

(28) Swidorski, J.; Wang, J.; Hsung, R. P. *Org. Lett.* **2005**, *8*, 777–780.

(29) Canesi, S.; Bouchu, D.; Ciufolini, M. A. *Angew. Chem. Int. Ed.* **2004**, *43*, 4336–4338.

(30) Zou, J.; Cho, D. W.; Mariano, P. S. *Tetrahedron* **2010**, *66*, 5955–5961.

(31) Shibuguchi, T.; Mihara, H.; Kuramochi, A.; Sakuraba, S.; Ohshima, T.; Shibasaki, M. *Angew. Chem. Int. Ed.* **2006**, *45*, 4635–4637.

(32) Zhang, X.-M.; Wang, M.; Tu, Y.-Q.; Fan, C.-A.; Jiang, Y.-J.; Zhang, S.-Y.; Zhang, F.-M. *Synlett* **2008**, *18*, 2831–2835.

(33) Dalton, D. M.; Oberg, K. M.; Yu, R. T.; Lee, E. E.; Perreault, S.; Oinen, M. E.; Pease, M. L.; Malik, G.; Rovis, T. *J. Am. Chem. Soc.* **2009**, *131*, 15717–15728.

CHAPTER 7

Zn(II)-Catalyzed [4+2] Cycloadditions to Form Tetrahydropyridines

7.1 Introduction

7.1.1 3-Aminopiperidine Prevalence in Natural and Medicinal Compounds

3-aminopiperidines are an important class of nitrogen containing heterocycles that make up the core structure of a wide variety of natural products and current pharmaceuticals. The majority of 3-aminopiperidine containing natural products exist as tryptophan derived pyridoindoles (Figure 7.1).[1-8] Current approaches to the synthesis of this class of natural products rely on the Pictet-Spengler reaction. The Zn(II) catalyzed [4+2] cycloaddition of α,β-unsaturated imines and nitro olefins described in this chapter complements the Pictet–Spengler approach to pyridoindoles. Moreover it accesses piperidine cores not easily accessed with the Pictet-Spengler, such as the Saraine alkaloids, which do not contain an indole core.[9]

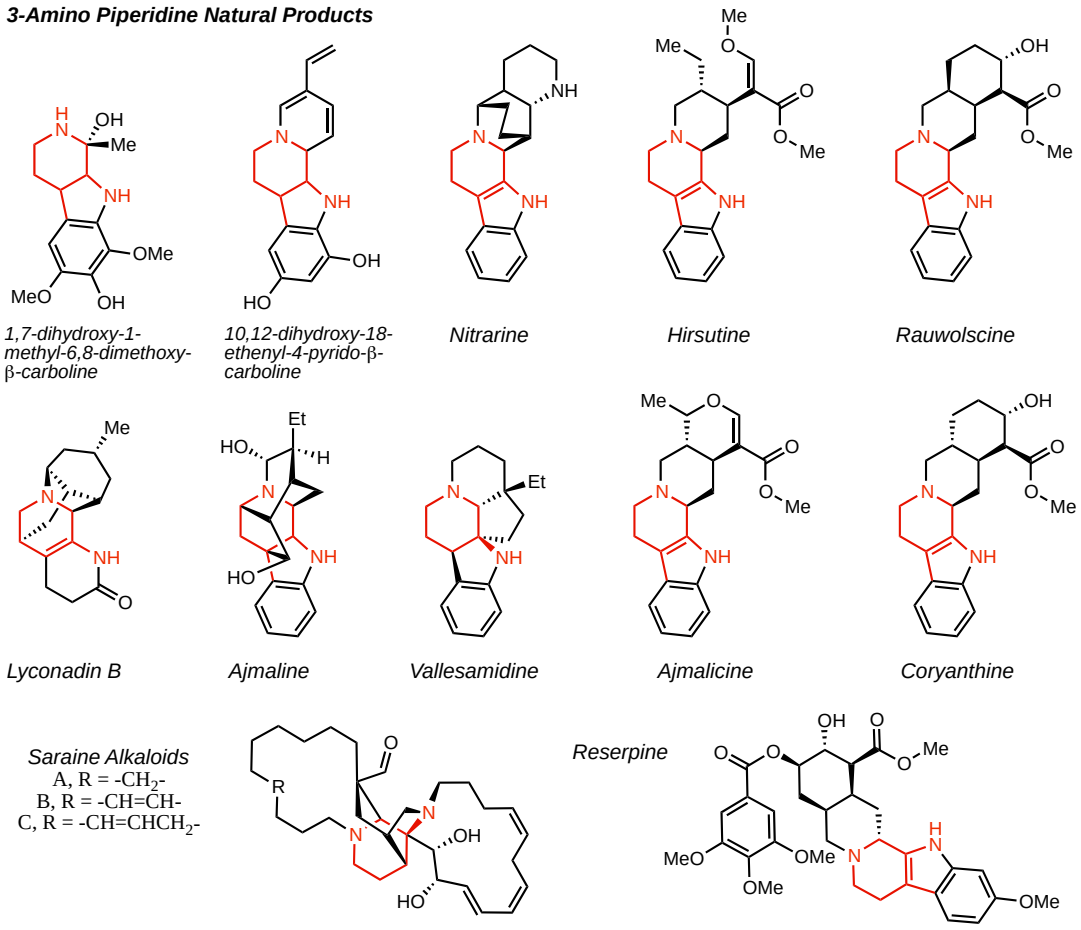

Figure 7.1 3-amino-piperidine containing natural products.

A number of pharmaceutical agents contain 3-aminopiperidines and display unique biological activity (Figure 7.2). For example, Xeljanx (Tofacitinib, Pfizer) is a JAK3 inhibitor, which is a novel mode of action for treatment of rheumatoid arthritis. Aloxi (Palonosetron, Eisai) is a 5-HT_3 antagonist used in treatment and prevention of chemotherapy induced nausea and vomiting. Tedalafil (Cialis, Adcirca) is a PDE5 inhibitor used to alleviate erectile dysfunction and pulmonary arterial hypertension. Maropitant (Cerenia, Zoetis) is a neurokinin (NK1) receptor antagonist. Alogliptin (Nesina, Takeda) is a DPP-4 inhibitor used as a type 2 anti-diabetic. Revlimid (Lenalidomide, Celgene) treats multiple myeloma and has shown efficacy in a class of myelodysplastic syndromes. We believe that Zn(II) catalyzed [4+2] cycloadditions of 1-azabutadienes and nitro olefins provide an inexpensive, efficient method for synthesizing a wide range of biologically active molecules.

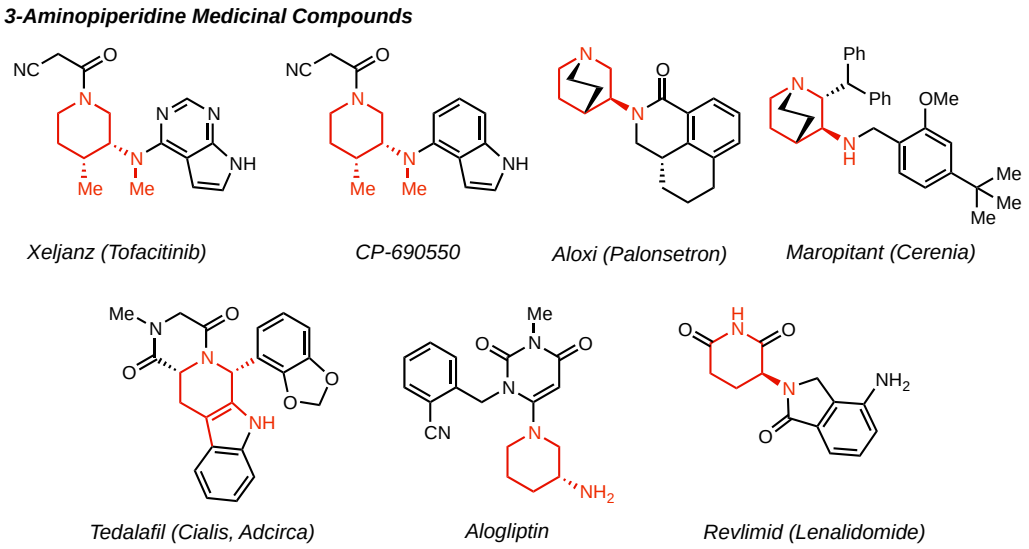

Figure 7.2 3-aminopiperidine containing medicinal compounds.

7.1.2 General Considerations Regarding 1-Azadiene [4+2] Cycloadditions

Discovered in 1928, the Diels-Alder cycloaddition is one of the most utilized reactions in organic synthesis. It offers the simple and effective assembly six membered rings from readily accessible materials (dienes and alkenes). High levels of selectivity (chemo-, regio-, diastereo- and enantioselectivity) can be achieved and the reaction has exceptional atom efficiency. Not surprisingly, extensions of the all carbon Diels-Alder reaction to heteroatom containing substrates (carbonyls, imines, 1-oxodienes, 1-azadienes, 2-azadienes) have been investigated. What is presented herein is a glance at 1-azadiene hetero-Diels–Alder (HDA) reactions.

HDA [4+2] cycloadditions with 1-azadienes (**1**) are considerably less developed than their 2-azadiene counterparts.[10] One reason 1-azadiene cycloadditions are underdeveloped is that the cycloaddition has less of a thermodynamic driving force than butadienes or 2-azadienes (Figure 7.3). Jung and Shapiro calculated the thermodynamic driving force of cycloadditions with 1-azadienes.[11] With butadiene and 2-azadiene, the net bond change is the conversion of 2 C=C bonds (2 x -146 kcal/mol) to 4 C–C (4 x -83 kcal/mol), resulting in a -40 kcal/mol change in enthalpy. On the other hand, the cycloaddition with 1-azadiene has a net bond change of 1 C=C (-146 kcal/mol) and 1 C=N (-147 kcal/mol) bond to 2 C–C (2 x 146 kcal/mol) and 2 C–N (2 x -73 kcal/mol), which has a corresponding change in enthalpy of -19 kcal/mol. Thus, the cycloaddition with 1-azabutadiene has a 21 kcal/mol lower enthalpic driving force.

Ultimately, the difference in ΔH is caused by the formation of 2 new C–N bonds, which have less bond strength than a C–C bond. As a result, [4+2] cycloadditions with 1-azadienes require high temperatures, specialized substrates and/or activating catalysts to favor product formation.

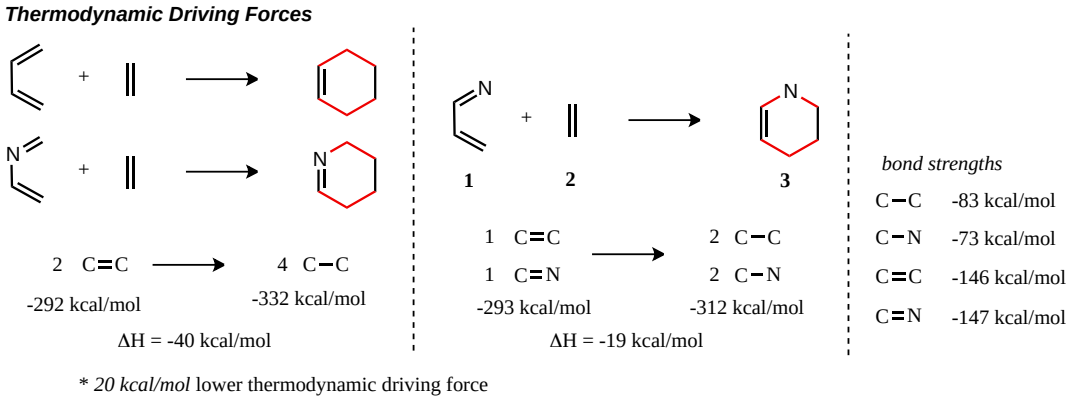

Figure 7.3 Thermodynamic driving force for [4+2] reactions.

HDA [4+2] cycloadditions are classified in an analogous manner to their Diels-Alder counterparts. Both regular demand and inverse demand cycloadditions have been reported.[12,13] The inverse demand [4+2] is better development and consists on an electron deficient 1-azadiene reacting with an electron-rich dienophile (Scheme 7.1, eq 1). Typical 1-azadienes have electron-deficient N-substituents (tosyl, tert-butyloxycarbonyl (Boc)) and potentially have at least one additional electron-withdrawing group (cyano, carbonyl, aryl). Dienophiles are electron-rich with at least one electron donating group (OR, NR_2, carbene catalyst). Regular demand 1-azadiene [4+2] cycloadditions consist of an electron-rich diene reacting with an electron-deficient dienophile (eq 2). Typical electron-rich 1-azadienes contain electron-releasing substituents (Aryl, OR, NR_2, SR) on the diene (1-4 positions) and electron deficient dienophiles contain electron-withdrawing groups, such as carbonyls (ketene) or cyano functionalities.

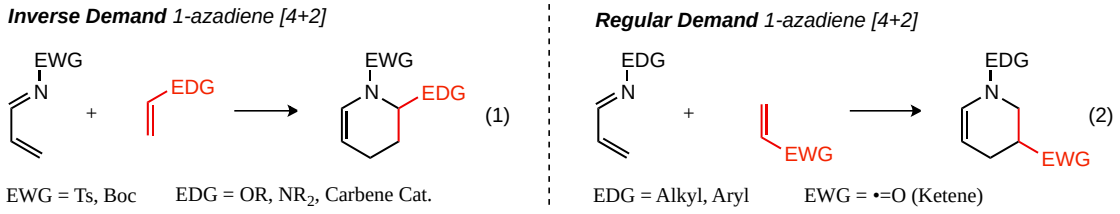

Scheme 7.1 Regular versus inverse demand 1-azadiene [4+2] reactions.

The regular and inverse demand Diels–Alder reactions are classified this way based on the relative energies of the diene and dienophile frontier molecular orbitals (FMO) (Figure 7.4). Regular demand 1-azadiene [4+2] reaction is controlled by interaction of the highest occupied molecular orbital (HOMO) of the diene (electron-rich) and the lowest unoccupied molecular orbital (LUMO) of the dienophile (electron-deficient), eq 3. The inverse demand 1-azadiene [4+2] consists of a favorable interaction between the LUMO of the diene (electron-deficient) and the HOMO of the dienophile (electron-rich), eq 4. Strategies for promoting regular demand [4+2] cycloadditions thus consist of either raising the energy of the diene HOMO by adding electron releasing substituents or lowering the LUMO of the dienophile by further withdrawing electron density (Lewis acid coordination). Likewise the inverse demand [4+2] is promoted by decreasing the HOMO of the diene or increasing the LUMO of the dienophile.

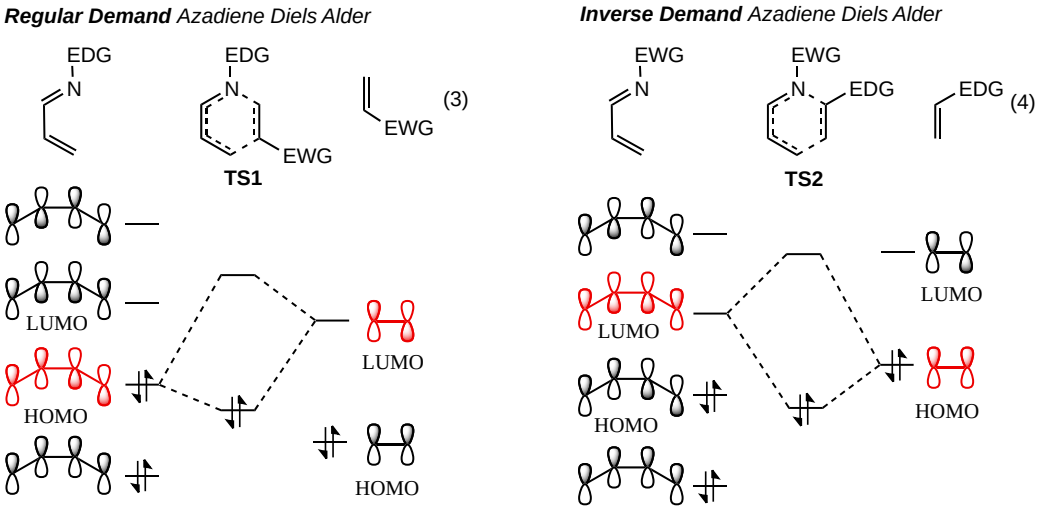

Figure 7.4 Simple depiction of frontier molecular orbitals in 1-azadiene [4+2].

7.1.3 Asymmetric Inverse Demand 1-Azadiene [4+2]

The inverse demand 1-azadiene hetero-Diels–Alder (HDA) has been developed to a greater extent than the regular demand 1-azadiene HDA. Only the most interesting examples of the inverse demand HDA will be discussed. To that end, Boger and coworkers reported in 2006 an intermolecular asymmetric inverse demand HDA coupling of sulfonyl 1-azadienes (**1a**) and enol ethers (**2a**) by covalently attaching a chiral auxiliary to the enol to make enantiopure tetrahydropyridines (**3a**).[14,15] This strategy is quite

effective at providing endo selective products in excellent yield (80-93%) and diastereomeric excess (Scheme 7.2).

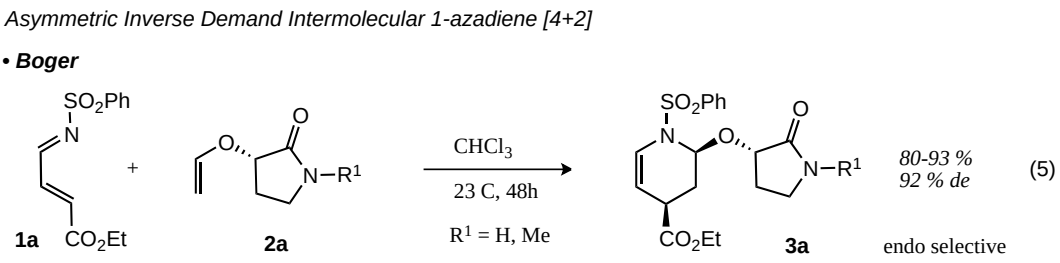

Scheme 7.2 Asymmetric inverse demand 1-azadiene [4+2].

Also in 2006, Bode and coworkers disclosed an N-heterocyclic carbene (**4**) catalyzed activation of α,β-unsaturated aldehydes and 1-azadienes to form *syn*-lactam pyridones (**4x**) in good yields and excellent enantioselectivities as single diastereomers (Scheme 7.3, eq 6).[16] Carretero in 2007 described a Ni(II)•DBFox-Ph Lewis acid catalyzed [4+2] cycloaddition with quinoline sulfonyl imines and enol ethers in good yields and enantioselectivities for the endo hemiaminal products (eq 7).[17] A quinoline directing group is required on the sulfonyl imine for reactivity and selectivity in this transformation. In 2012, Rovis revealed another carbene catalyzed synthesis of pyridones (**4d**) in an oxidative HDA of 1-azadiene **1d** and alkyl aldehyde **2d** that proceeds in good yields and excellent selectivities to form the anti diastereomer (eq 8).[18] In the reaction, a riboflavin derivative **5** oxidizes the Breslow intermediate (formed by addition of the carbene catalyst **4** into the aldehyde and subsequent proton transfer) to give the acyl azolium, which is deprotonated to provide an enolate that does an inverse demand HDA.

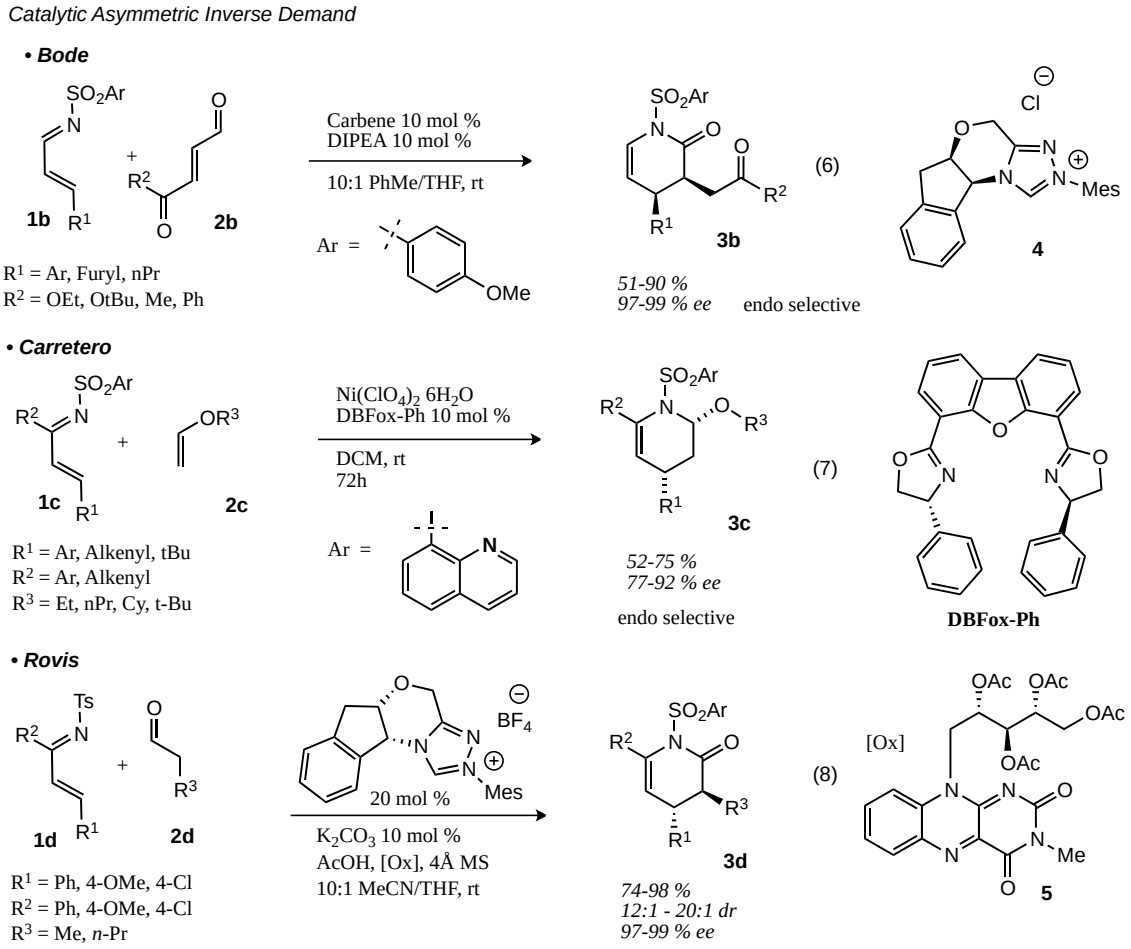

Scheme 7.3 Catalytic asymmetric inverse demand 1-azadiene [4+2].

7.1.4 Intramolecular Regular Demand 1-Azadiene [4+2]

Early work on the intramolecular 1-azadiene HDA was done by Fowler in 1983. Fowler and coworkers found that under flash vacuum pyrolysis at 650 ºC bi- and tricyclic tetrahydropyridines could be formed in good to excellent yields (Scheme 7.4, eq 9).[19] In 1999, Grierson investigated the thermal intramolecular cycloaddition of enol ether tethered 2-cyano-1-azabutadienes (**8**) for the synthesis of cyclic tetrahydropyridines and found that most cyclizations occur in moderate to good yields after 24 h (eq 10). [20] In 2008, Masson and Zhu reported a microwave facilitated reaction at 160 ºC to induce cyclization of 2-cyano-1-azabutadiene **10** with a tethered unactivated alkene into bicyclic tetrahydropyridine **11** in excellent yield (eq 11).[21]

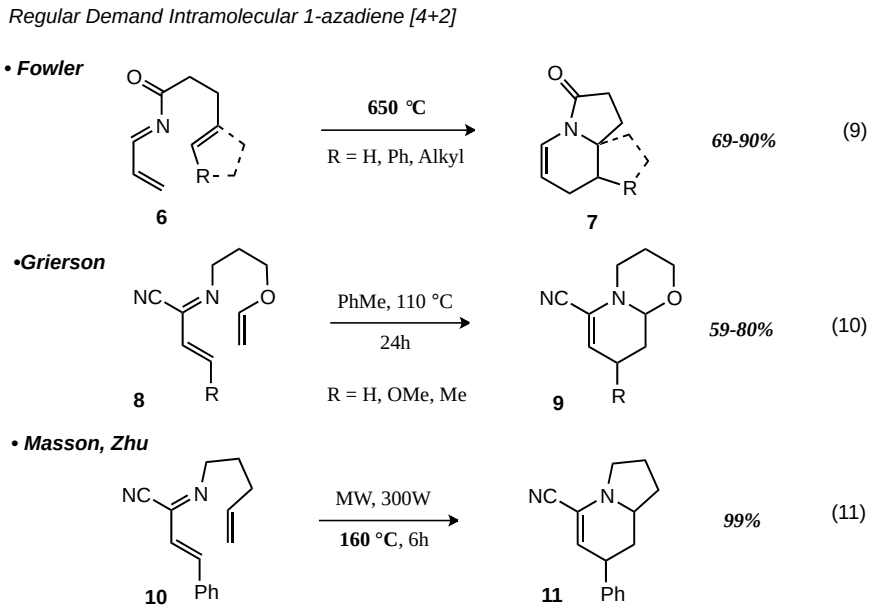

Scheme 7.4 Regular demand intramolecular 1-azadiene [4+2].

7.1.5 Intermolecular Regular Demand 1-Azadiene [4+2]

Intermolecular 1-azadiene HDA reactions were championed by Ghosez and coworkers as early as 1982. [22] Their pioneering work was focused on α,β-unsaturated hydrazones as reagent in HDA cycloadditions. Remarkably the cycloadducts (**3e**) derived from [4+2] with hydrazones display the opposite regioselectivity as that expected from a regular demand HDA; they suggest that the shift in regioselectivity is due to a push of electrons from the dimethyl amine of the hydrazone (**1e**) into the conjugated diene placing electron density at the 4-position, making it the most nucleophilic position and thus responsible for controlling regioselectivity (Scheme 7.5, eq 12). In 1986, Alberola and coworkers reported that at 80 ºC siloxyacrylonitrile **2e** will participate in a [4+2] cycloaddition with N-phenyl imine **1e** to provide the dihydropyridine **12** in excellent yield in 15 min (eq 13).[23] In 2004, Deniaud and coworkers disclosed the synthesis of pyridones (**13**) and piperidines (**14**) by [4+2] cycloaddition of aminothiobutadienes (**1h**) and electron deficient olefins (**2h**) in moderate to good yields (eq 14).[24] In 2008, Ishar and coworkers revealed a regular demand HDA of N-aryl α,β-unsaturated imines (**1i**) and electron-deficient allenes (**2i**) under thermal or microwave conditions to form dihydropyridines (**15**) or at room temperature, azetidine **16** (eq 15).[25]

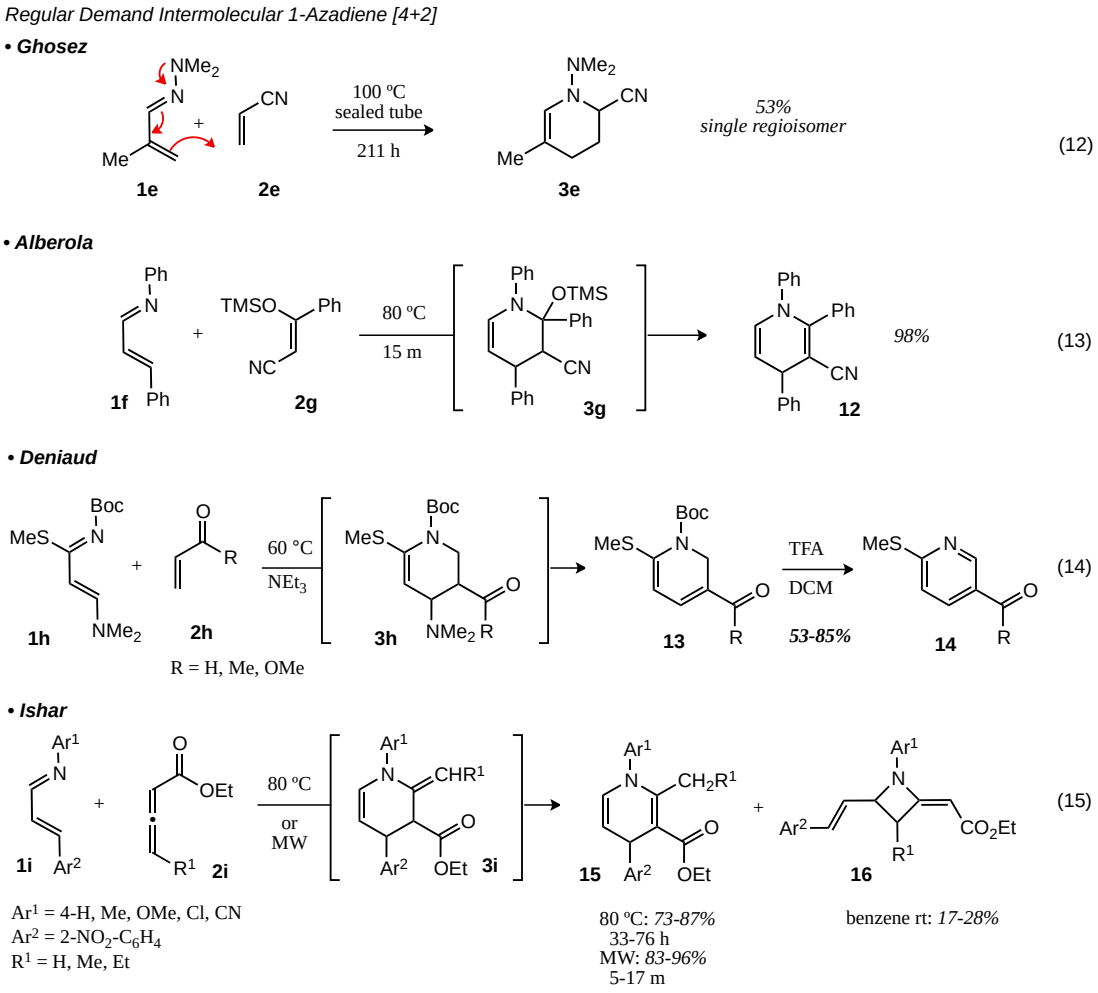

Scheme 7.5 Regular demand intermolecular 1-azadiene [4+2] examples.

Ketenes are one of the more widely used dienophiles in the 1-azadiene HDA, presumably due to their enhanced electrophilicity and reactivity compared to vinyl ketones or aldehydes. In 1970, Ghosez pioneered the use of ketenes as dienophiles in the [4+2] cycloaddition with 1-azabutadienes by generating them in situ from dihaloacyl chlorides (**17**) in the presence triethylamine to afford pyridone products (**18**) in modest yields.[26] In 1984, Singh and coworkers reported a one-pot synthesis of pyridone **20** by a [4+2] cycloaddition of N-phenyl azadiene **1f** and α-bromoesters, which form ketenes in situ in the presence of zinc in good yield (eq 17).[27] In 1991, Sandhu and coworkers disclosed the [4+2] cycloaddition of N-phenyl azadiene **1f** with benzylacetic acid **21**, which in the presence of triethylamine and dehydrating reagent, chlorosulfinyliminium **23**, generates ketene in situ as well as SO_2, HCl and dimethylformamide (DMF) (eq 18).[28]

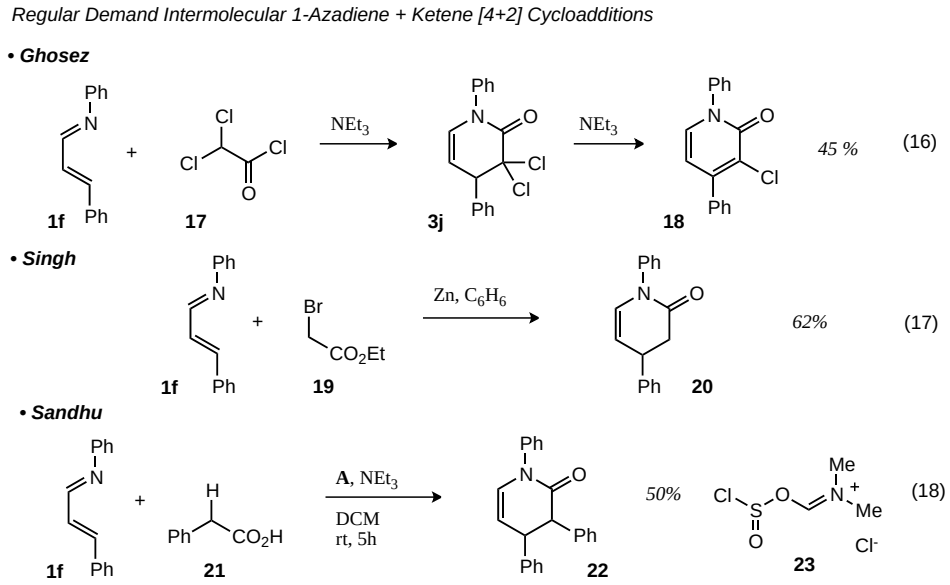

Scheme 7.6 Regular demand intermolecular 1-azadiene/ketene [4+2] cycloadditions.

Ghosez and coworkers in 1994 disclosed what is arguably the most useful asymmetric 1-azadiene HDA using chiral proline derived hydrazones (**1k**) and coupling them with electron deficient maleic anhydride derivatives (**2k**) to make enantioenriched tetrahydropyridines (**3k**)(Scheme 7.7, eq 19).[29] Good yields and diastereomeric excesses are achieved for a handful of substrates. In 2005 Barluenga reported a [4+2] cycloaddition of N-propyl azadiene (**1l**) and tungsten Fischer carbene **24** containing a menthol derived chiral auxiliary to form dihydropyridines (**26**) in two steps in excellent enantioselectivity (eq 20). [30] Catalytic asymmetric regular demand 1-azadiene HDA reactions have not yet been reported and would be a useful contribution to the scientific community.

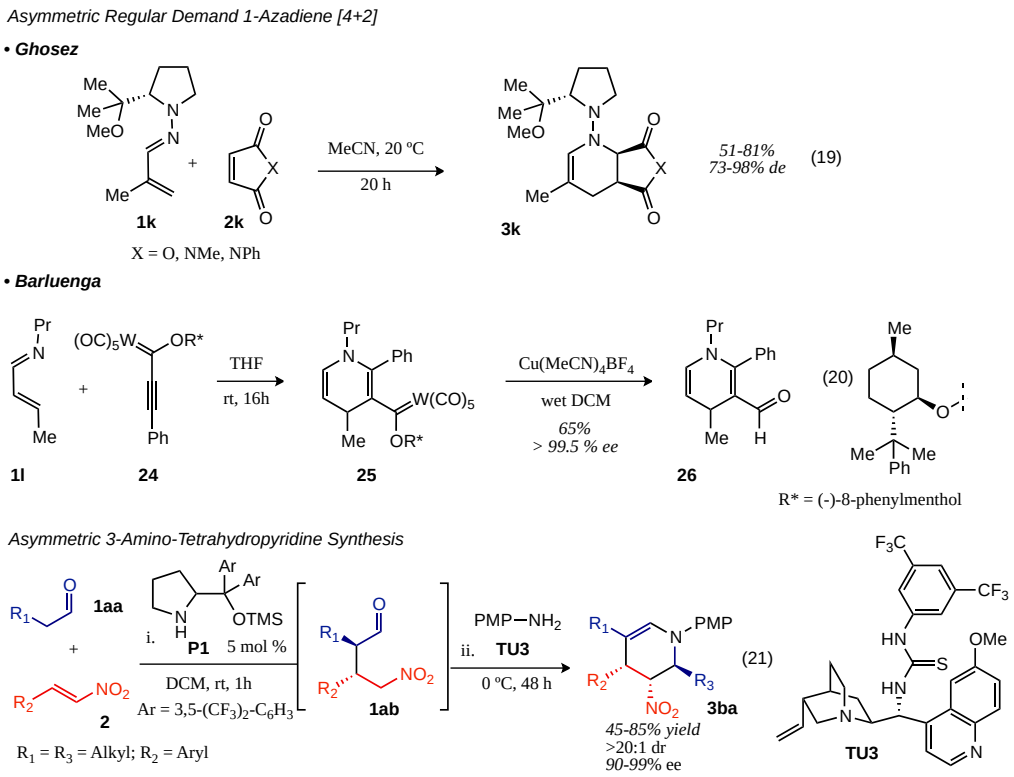

Scheme 7.7 Asymmetric regular demand intermolecular 1-azadiene [4+2].

In 2013, Lin and coworkers reported an efficient asymmetric cascade cyclization reaction to access 3-nitro-tetrahydropyridines from nitro olefins, aldehydes and amines (Scheme 7.8).[31] The two-step one pot procedure begins with a prolinol (**P1**) catalyzed Mannich addition into the nitroolefin. Addition of amine and a chiral quinone-derived thiourea catalyst (**TU3**) forms an imine that then undergoes a Henry reaction to arrive at tetrahydropyridine **3ba** with excellent enantioselectivity as the *cis*, *trans* isomer.

7.2 Results

7.2.1 Development of Lewis Acid Catalyzed 1-Azadiene Regular Demand [4+2]

During our studies of the Rh(I) catalyzed [2+2+2] cycloaddition of alkene tethered isocyanates and exogenous alkynes, we made many attempts to enact a fully intermolecular alkene, isocyanate and alkyne cycloaddition for the asymmetric synthesis of piperidines. A fully intermolecular [2+2+2] cycloaddition would increase the utility of the method and greatly expand the number compounds accessible. Furthermore, piperidines are one of the most prevalent N-heterocycles found in medicinal agents and are ubiquitous in biologically active naturally occurring alkaloids. Two other limitations of the method that

we sought to address in our investigations were the use of earth-abundant metals as catalysts and readily available starting materials. To this end we began investigating CoI_2/Zn catalyzed cycloadditions using imines as the nitrogen source (Scheme 7.8, eq 21). We were very excited to find that a $CoCl_2$, Zn, $Zn(OTf)_2$ catalyst system provided 8% yield of the desired tetrahydropyridine **3** (eq 22). Control experiments revealed that only $Zn(OTf)_2$ was needed for the reaction to occur. In the absence of $Zn(OTf)_2$ none of the tetrahydropyridine was observed. With this promising result we optimized the reaction using high throughput experimentation (HTE) methods.

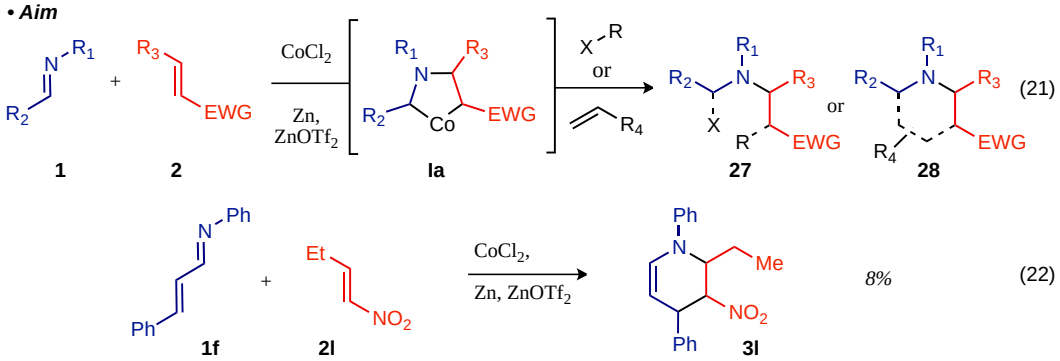

Scheme 7.8 Project aim and initial hit for reaction development

Taking advantage of the high throughput screen facilities at the CSU catalysis center, a variety of solvents and Lewis acid catalysts were investigated (Figure 7.5). $Zn(OTf)_2$, $CeCl_3$, $Sc(OTf)_3$ and $Ti(OiPr)_4$ were found to induce the HDA cycloaddition, while BF_3•OEt_2, $CrCl_2$ and $AlCl_3$ do not. Ethereal solvents: dimethoxyethane and 1,4-dioxanes gave the highest conversions especially when coupled with $Zn(OTf)_2$. A second screen of catalysts including: thiourea catalysts and Rh(I)•phosphoramidite **T4** revealed that ZnI_2 is the optimal catalyst under these conditions.

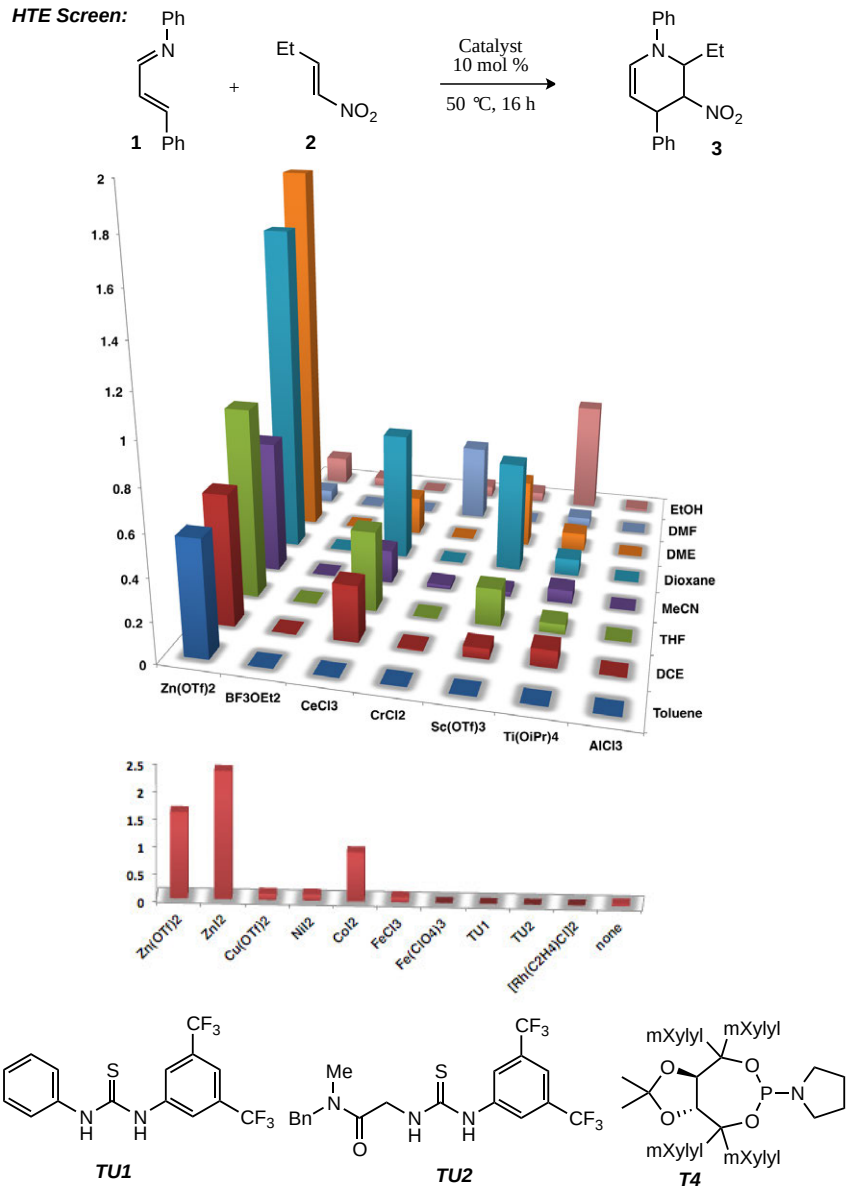

Figure 7.5 High-throughput experimentation (HTE) screening of Lewis acids and solvents.

Benchtop optimization beginning with the best results from the HTE screen is shown in Table 7.1. A screen of N-substituents on the 1-azadiene found phenyl and p-methoxyphenyl (PMP) to be the best substituents (entries 2, 3). PMP was chosen because it may be removed easily. [0.1] molar in 1-azadiene is the optimal concentration in DME (entry 6). A boost in yield is seen with the addition of drying agents (entry 9). A screen of equivalents of **1** and **2** found that 1.5 equivalents of **2** is best, providing 62% yield (entry 13). Increasing the temperature to 80 ºC gives no desired product.

Optimization

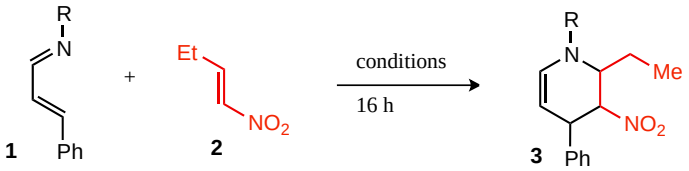

(23)

entry	R	2[a]	1[a]	catalyst	solvent	temp.	[M]	additive	yield (%)[b]
1	**PMB**	1.5	1	$Zn(OTf)_2$	DME	rt	0.07	--	ND
2	**Ph**	1.5	1	ZnI_2	DME	50	0.07	--	~ 10
3	**PMP**	1.5	1	ZnI_2	DME	50	0.07	--	~ 10
4	**PCF_3**	1.5	1	ZnI_2	DME	50	0.07	--	~ 8
5	PMP	2	1	ZnI_2	DME	50	**0.05**	--	12
6	PMP	2	1	ZnI_2	DME	50	**0.1**	--	15
7	PMP	2	1	ZnI_2	DME	50	**0.3**	--	0
8	PMP	2	1	ZnI_2	DME	50	0.1	**$MgSO_4$**	18
9	PMP	2	1	ZnI_2	DME	50	0.1	**4 A MS**	28
10	PMP	1	**1**	ZnI_2	DME	50	0.1	4 A MS	30
11	PMP	1	**1.5**	ZnI_2	DME	50	0.1	4 A MS	24
12	PMP	1	**2**	ZnI_2	DME	50	0.1	4 A MS	22
13	PMP	**1.5**	1	ZnI_2	DME	50	0.1	4 A MS	62
14	PMP	**2**	1	ZnI_2	DME	50	0.1	4 A MS	31
15	PMP	1.5	1	ZnI_2	DME	**80**	0.1	4 A MS	0

Table 7.1 Optimization of reaction conditions after HTE screen.

7.2.2 Reaction Scope of Zn(II)-Catalyzed [4+2]

We investigated a variety of nitrogen substituents on the α,β-unsaturated imine (**1**, Table 7.2). N-phenylazadiene **1m** provides tetrahydropyridine **3m** in good yield and excellent diastereoselectivity as the *cis*, *trans* endo cyclization product. Although the N-phenyl tetrahydropyridine **3m** contains a reactive enamine, it is relatively stable and isolated easily. Electron releasing *p*-methoxyphenyl (PMP) azadiene **1n** provides high conversion to clean products. However the resultant enamine of the tetrahydropyridine is more reactive, while this does make isolation tricky, it readily enables further functionalization of the enamine portion of the tetrahydropyridine. Additionally, the N-PMP may be easily removed with cerric ammonium nitrate (CAN), increasing the utility of the N-substituent. *p*-Methoxybenzyl azadiene **1s** forms a complex mixture of products, including tetrahydropyridine **3s**. Electron-withdrawing *p*-CF_3-phenyl azadiene **1o** gives tetrahydropyridine 3c in modest yield (55%) after 16 h. Increasing the electron-

deficiency of the N-substituent with tosyl **1r** or oxime **1q** inhibit cyclization. Additionally, ortho-substitution of the N-aryl is not tolerated (**3pa)** even with an electron-donating substituent.

Table 7.2 Nitrogen substituents tolerated in Zn(II) catalyzed 4+2 cycloaddition.

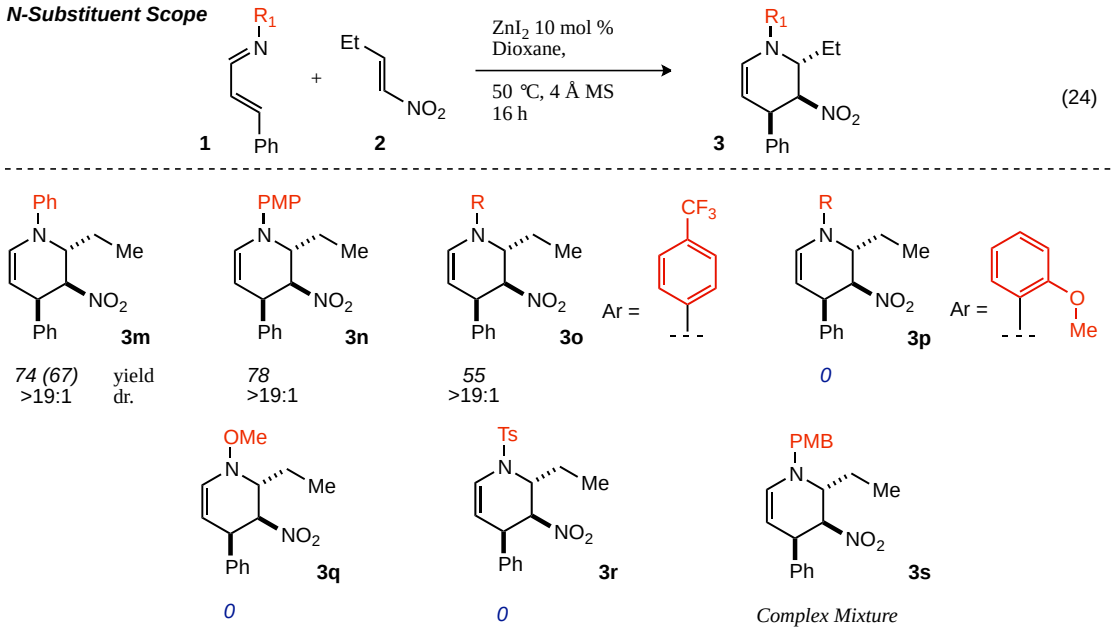

A variety of substituents on the nitro olefin are tolerated in the cycloaddition (Table 7.3). In general, the best nitro olefin substrates are small and relatively electron-rich. Small substituents, such as methyl **3t**, ethyl **3u** and cyclopropyl **3ab**, provide tetrahydropyridines in good yields and excellent diastereoselectivity (>19:1). However, the number of equivalents of nitro olefin needs to be decreased from 1.5 to 1.3. It was found that under the reaction conditions a second cycloaddition can occur between the enamine of the tetrahydropyridine (**3**) and a second nitro olefin. Similar 4+2 cycloadditions between nitro-olefins and electron rich alkenes have been reported and reviewed by Denmark and coworkers in the context of tandem [4+2]/[3+2] cycloadditions.[32,33] Pendant aromatic and silyl ether groups are well-tolerated (**3w**, 75% and **3x**, 69%). Large nitro olefin substituents inhibit cyclization as seen with isopropyl **3z** (35%) and tertbutyl **3aa** (0%). Alkenyl and aryl substituents are either not tolerated (styrenyltetrahydropyridine **3ac**) or cyclize poorly (**3ad**, 12%).

Table 7.3 Nitro olefin scope for Zn(II) catalyzed [4+2]. (a) 1.3 equivalents of **2** were used. (b) 2 equivalents of **2** were used.

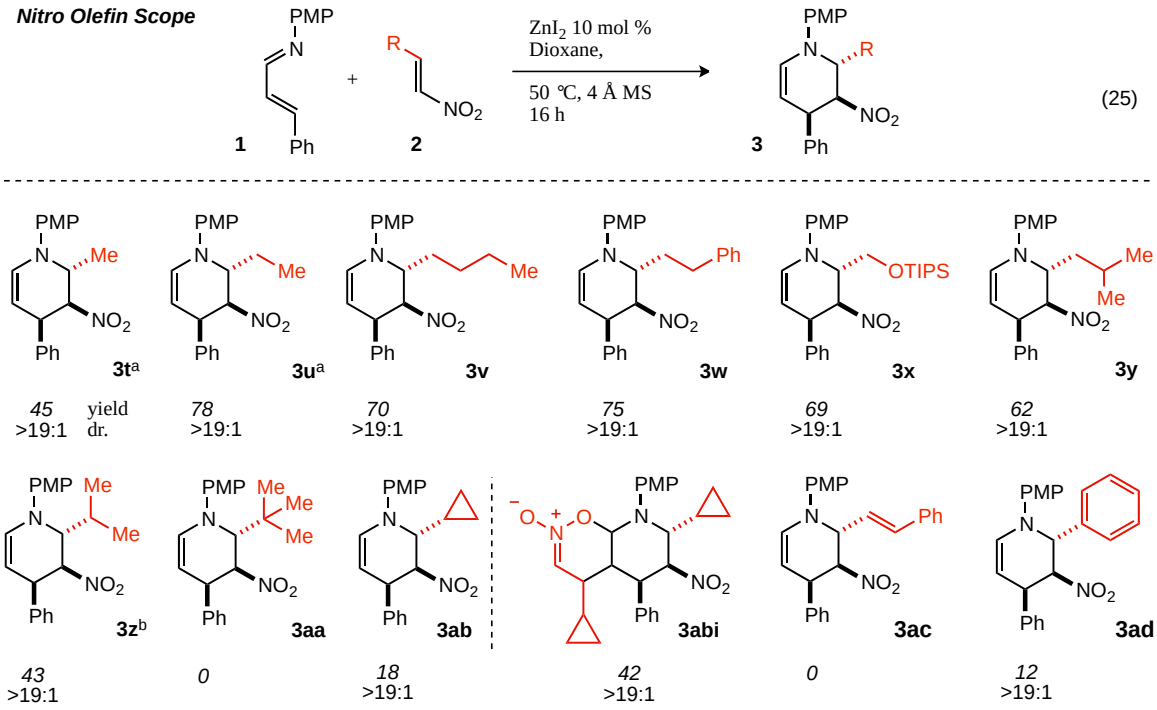

A range of functional groups are tolerated at the tetrahydropyridine 4 position (Table 7.4). Electron releasing substituents (**3ae**, **3ag**, **3aj**) generally give higher yields. Sterically bulky ortho-methoxy phenyl **3af** (35%) or electron deficient substituents, p-NO_2-phenyl **3ah**, provide lower yields (55%). Furyl imine **1ao** does not cyclize while methyl pyrazole imine does participate in the cyclization, albeit poorly (5% yield). Pyrazoles have a higher resonance energy (29.3 kcal/mol)[34] than those reported for furan (23.0 kcal/mol)[35]. The yield with N-Ph imines may be increased ~10-15% by use of N-PMP substituent. Imines with hydrogen at the 4-position do not cyclize under the reaction conditions (**3ap**, **3aq**).

Table 7.4 Imine scope for Zn(II) catalyzed [4+2].

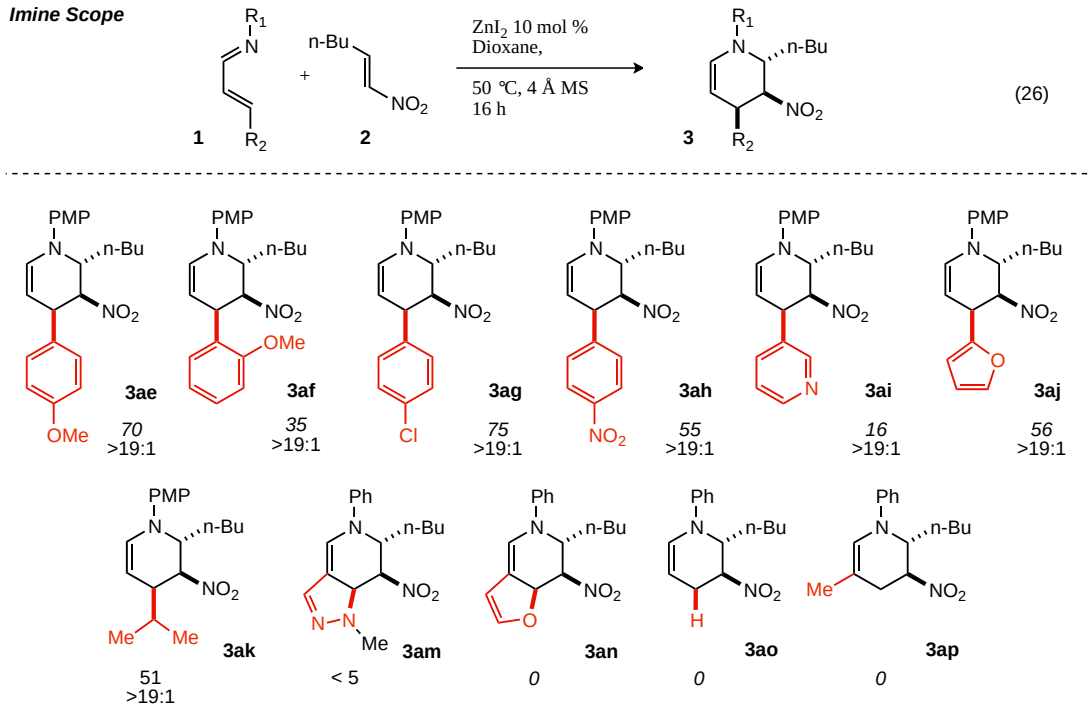

Initially relative stereochemistry was proposed to be *cis-trans* as depicted in equation 26. X-ray analysis of tetrahydropyridine 3ar confirmed the relative stereochemistry as *cis-trans* (Figure 7.6). Regiochemistry of the nitro-olefin addition was confirmed by X-ray analysis.

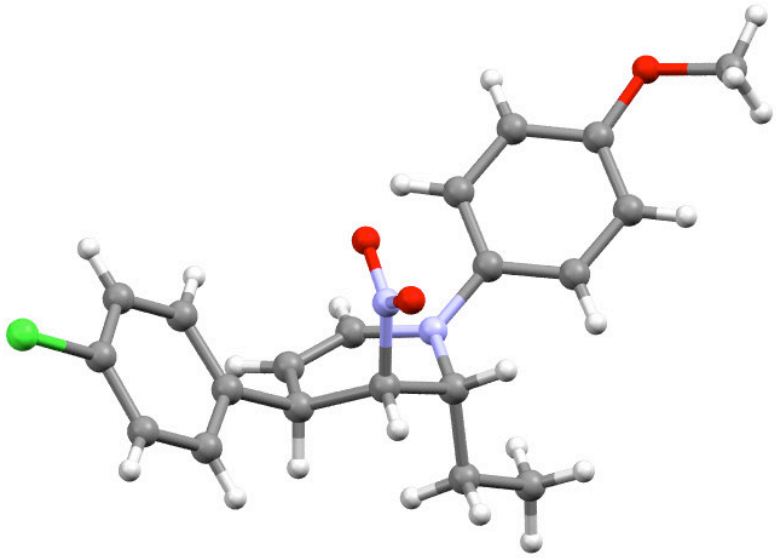

Figure 7.6 X-ray structure of tetrahydropyridine **3ar**. Thermal ellipsoids are shown in Appendix 7.

7.2.3 Mechanistic Discussion of Regiochemistry and Diastereoselectivity

Zn(II) catalyzed [4+2] cycloaddition of α,β-unsaturated imines and nitro olefins forms tetrahydropyridines with excellent control of regiochemistry and diastereoselectivity. High levels of regio and diastereoselectivity without a chiral environment imply that the cycloaddition occurs through a highly ordered transition state. These results are consistent with selectivities seen in other hetero-Diels–Alder (HDA) reactions.[36] In general, HDA reactions proceed through unsymmetrical transition states (concerted asynchronous). Houk and coworkers calculated transition states for a variety of HDA cycloadditions and found, in the case of formaldehyde and butadiene, C–O and C–C bond distances of 1.998 and 2.133 Å respectively.[37] Similar results were found with ketimines and diazenes.[38] Because of the excellent regio and diastereoselectivity, we suggest that the Zn(II) catalyzed [4+2] cycloaddition of α,β-unsaturated imines (**1**) and nitro olefins (**2**) is a hetero-Diels–Alder reaction operating through a concerted transition state with zinc acting as a Lewis acid to lower the LUMO of the nitro olefin.

Excellent regiochemistry may be explained using frontier molecular orbital (FMO) diagrams of imine **1** and nitro olefin **2**. The most favorable HOMO-LUMO interaction in the transition state will be between the atomic orbitals with the greatest HOMO coefficient of the diene (nitrogen of imine) and the largest LUMO coefficient of the dienophile (*beta* carbon of nitro olefin). Because regiochemistry is controlled by the atomic orbital HOMO-LUMO coefficients the number of diastereoselectivity models that needs to be considered is narrowed to two: endo versus exo (Scheme 7.9). Endo selectivity would give the *cis, trans* tetrahydropyridine **3**endo as depicted in transition state **TSI** (eq 27) and exo selectivity would provide *trans*, *trans* tetrahydropyridine **3**exo, as shown in **TSII** (eq 28). Endo selectivity may be the result of favorable secondary orbital interactions between the azadiene π-system and the nitroso of the nitro (**TSI**), which is absent in the exo transition state **TSII**.

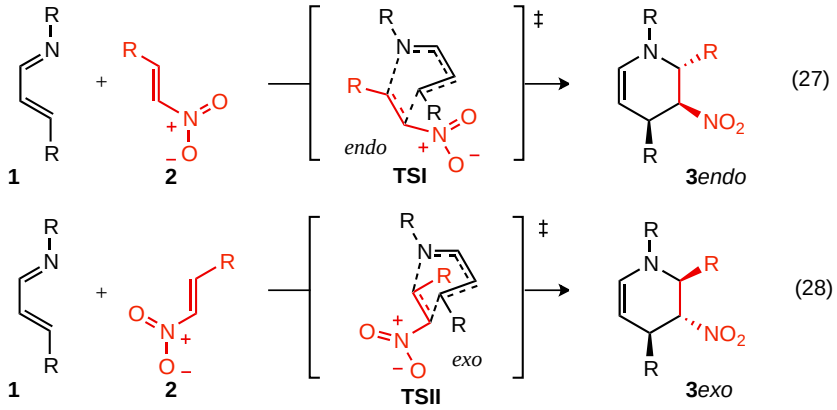

Scheme 7.9 Diastereoselectivity models.

7.2.4 Investigation of the Catalytic Asymmetric Zn(II) Regular Demand HDA

Preliminary investigations have begun to render the Zn(II) regular demand HDA or N-PMP azadienes and nitro olefins asymmetric through use of a chiral ligand on zinc. Many chiral scaffolds, proven to be successful in other reactions that use Zn catalysis have been investigated including: bisoxazoline (Box) **(L1-L5)**, chiral diamine **L6**, Jaconsen Salen **L7**, Trost Prophenol **L8** and Sharpless dihydroquinoline **L11** manifolds have been investigated in both HTE screens and benchtop follow up reactions (Figure 7.6). Additionally, various Zn precatalysts have been investigated for both reactivity and selectivity. At this point the focus has been on optimization of enantioselectivity. To date, the highest levels of enantioinduction have been reproducibly achieved with $Zn(PF_6)_2$•prophenol **L8** system yielding 47% ee.

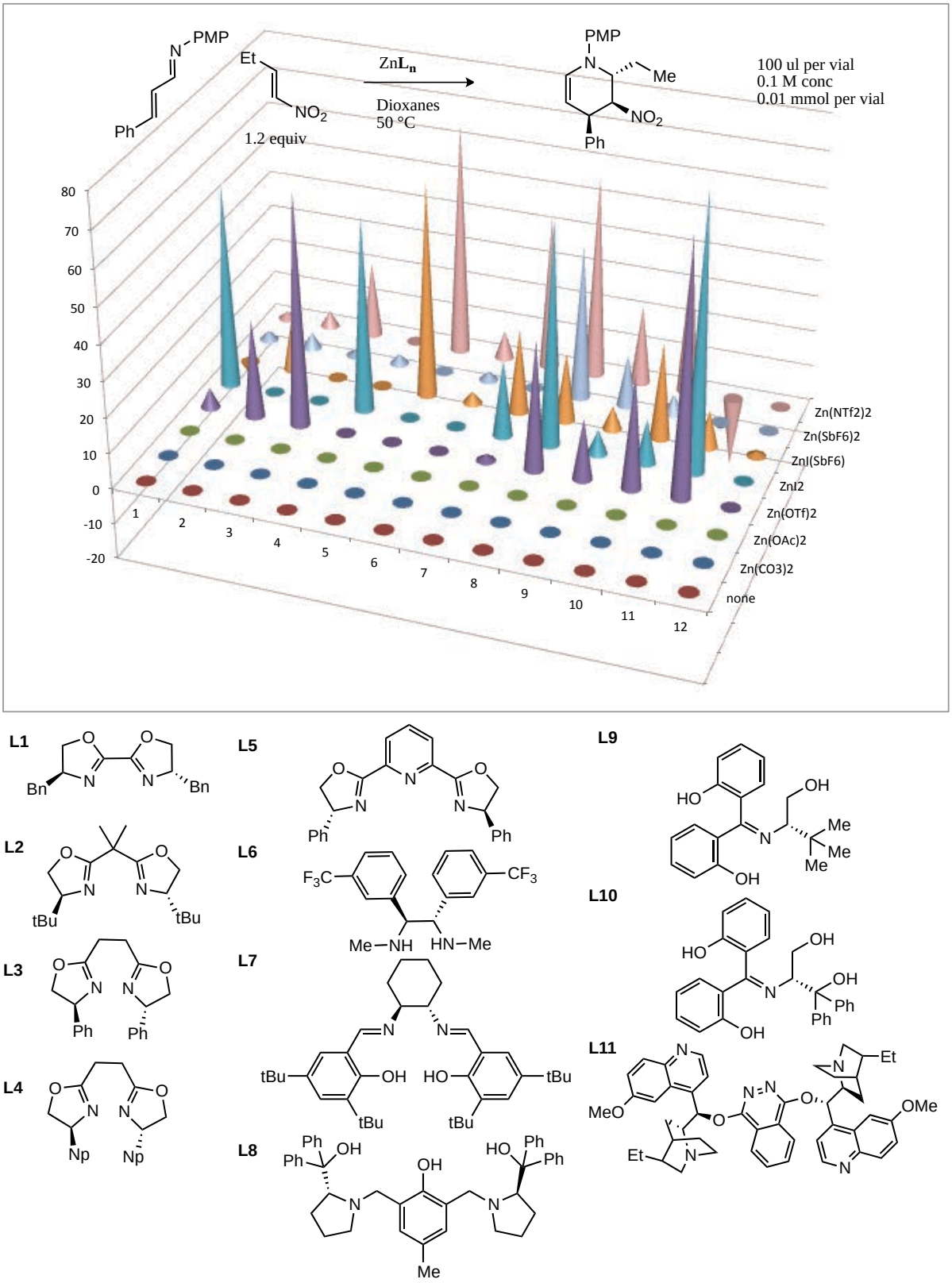

Figure 7.7 HTE screen of chiral ligands.

7.3 Conclusion

In summary, we have developed a facile highly diastereoselective method to synthesize biologically and medicinally relevant scaffolds in two steps from commercially available materials using earth abundant metal catalysts in a highly atom economical reaction. Efforts to render the reaction enantioselective are ongoing and will be the subject of a research communication in collaboration with Chun Kit Chu.

7.4 References

(1) Okwu, D. E.; Njoku, E. E. *Der Chemica Sinica* **2011**, *2*, 2, 261-267.

(2) Okwu, D. E.; Igara, E. C. *Int. J. Pharm. Tech. Res*. **2010**, *2*, 1, 910-913.

(3) Tulyganov, T. S.; Ibragimov, A. A. *Chem. Nat. Compd.* **1993**, *29*, 512–515.

(4) Wu, L. X.; Gu, X. F.; Zhu, Y. C.; Zhu, Y. Z. *Eur. J. Pharmacol.* **2011**, *650*, 290–297.

(5) Henry, J.-P.; Scherman, D. *Biochemical Pharmacology* **1989**, *38*, 2395–2404.

(6) Brown, S. H.; Djerassi, C.; Simpson, P. G. *J. Am. Chem. Soc.* **1968**, *90*, 2445–2446.

(7) Kurz, W.; Chatson, K.; Constabel, F.; Kutney, J.; Choi, L.; Kolodziejczyk, P.; Sleigh, S.; Stuart, K.; Worth, B. *Planta Medica* **2007**, *42*, 22–31.

(8) Ishiuchi, K.; Kubota, T.; Ishiyama, H.; Hayashi, S.; Shibata, T.; Kobayashi, J. *Tetrahedron Lett.* **2011**, *52*, 289–292.

(9) Defant, A.; Mancini, I.; Raspor, L.; Guella, G.; Turk, T.; Sepčić, K. *Eur. J. Org. Chem.* **2011**, *2011*, 3761–3767.

(10) Daniels, P. H.; Wong, J. L.; Atwood, J. L.; Canada, L. G.; Rogers, R. D. *J. Org. Chem.* **1980**, *45*, 435–440.

(11) Jung, M. E.; Shapiro, J. J. *J. Am. Chem. Soc.* **1980**, *102*, 7862–7866.

(12) Behforouz, M.; Ahmadian, M. *Tetrahedron* **2000**, *56*, 5259–5288.

(13) Groenendaal, B.; Ruijter, E.; Orru, R. V. A. *Chem. Commun.* **2008**, 5474–5489.

(14) Boger, D.; Panek, J. *J. Org. Chem.* **1981**, *46*, 2179–2182.

(15) Clark, R. C.; Pfeiffer, S. S.; Boger, D. L. *J. Am. Chem. Soc.* **2006**, *128*, 2587–2593.

(16) He, M.; Struble, J. R.; Bode, J. W. *J. Am. Chem. Soc.* **2006**, *128*, 8418–8420.

(17) Esquivias, J.; Arrayás, R. G.; Carretero, J. C. *J. Am. Chem. Soc.* **2007**, *129*, 1480–1481.

(18) Zhao, X.; Ruhl, K. E.; Rovis, T. *Angew. Chem. Int. Ed.* **2012**, *51*, 12330–12333.

(19) Cheng, Y. S.; Lupo, A. T.; Fowler, F. W. *J. Am. Chem. Soc.* **1983**, *105*, 7696–7703.

(20) Motorina, I. A.; Grierson, D. S. *Tetrahedron Lett.* **1999**, *40*, 7211–7214.

(21) Fontaine, P.; Chiaroni, A.; Masson, G.; Zhu, J. *Org. Lett.* **2008**, *10*, 1509–1512.

(22) Serckx-Poncin, B.; Hesbain-Frisque, A.-M.; Ghosez, L. *Tetrahedron Lett.* **1982**, *23*, 3261–3264.

(23) Alberola, A.; González, A. M.; González, B.; Laguna, M. A.; Pulido, F. J. *Tetrahedron Lett.* **1986**, *27*, 2027–2030.

(24) Robin, A.; Julienne, K.; Meslin, J. C.; Deniaud, D. *Tetrahedron Lett.* **2004**, *45*, 9557–9559.

(25) Singh, L.; Singh Ishar, M. P.; Elango, M.; Subramanian, V.; Gupta, V.; Kanwal, P. *J. Org. Chem.* **2008**, *73*, 2224–2233.

(26) Duran, F.; Ghosez, L. *J. Organomet. Chem.* **1970**, *11*, 245–248.

(27) Krishan, K.; Singh, A.; Singh, B.; Kumar, S. *Synthetic Comm.* **1984**, *14*, 219–225.

(28) Singh, S. P.; Mahajan, A. R.; Prajapati, D.; Sandhu, J. S. *Synthesis* **1991**, *1991*, 1026–1028.

(29) Beaudegnies, R.; Ghosez, L. *Tetrahedron: Asymmetry* **1994**, *5*, 557–560.

(30) Barluenga, J.; la Rúa, de, R. B.; de Sáa, D.; Ballesteros, A.; Tomás, M. *Angew. Chem. Int. Ed.* **2005**, *44*, 4981–4983.

(31) Lin, H.; Tan, Y.; Liu, W.-J.; Zhang, Z.-C.; Sun, X.-W.; Lin, G. *Chem. Commun.* **2013**, *49*, 4024–4026.

(32) Denmark, S. E.; Guagnano, V.; Dixon, J. A.; Stolle, A. *J. Org. Chem.* **1997**, *62*, 4610–4628.

(33) Denmark, S. E.; Thorarensen, A. *Chem. Rev.* **1996**, *96*, 137–166.

(34) Bansal, R. K. *Heterocyclic Chemistry*; 3rd ed. New Age International, 1999; p. 393.

(35) Eicher, T.; Hauptmann, S.; Speicher, A. *The Chemistry of Heterocycles: Structures, Reactions, Synthesis, and Applications*; John Wiley & Sons, 2013.

(36) Jørgensen, K. A. *Angew. Chem. Int. Ed.* **2000**, *39*, 3558–3588.

(37) McCarrick, M. A.; Wu, Y. D.; Houk, K. N. *J. Am. Chem. Soc.* **1992**, *114*, 1499–1500.

(38) McCarrick, M. A.; Wu, Y. D.; Houk, K. N. *J. Org. Chem.* **1993**, *58*, 3330–3343.

APPENDIX 1

A.1 Legend of Ligands

Taddol Ligand Screen

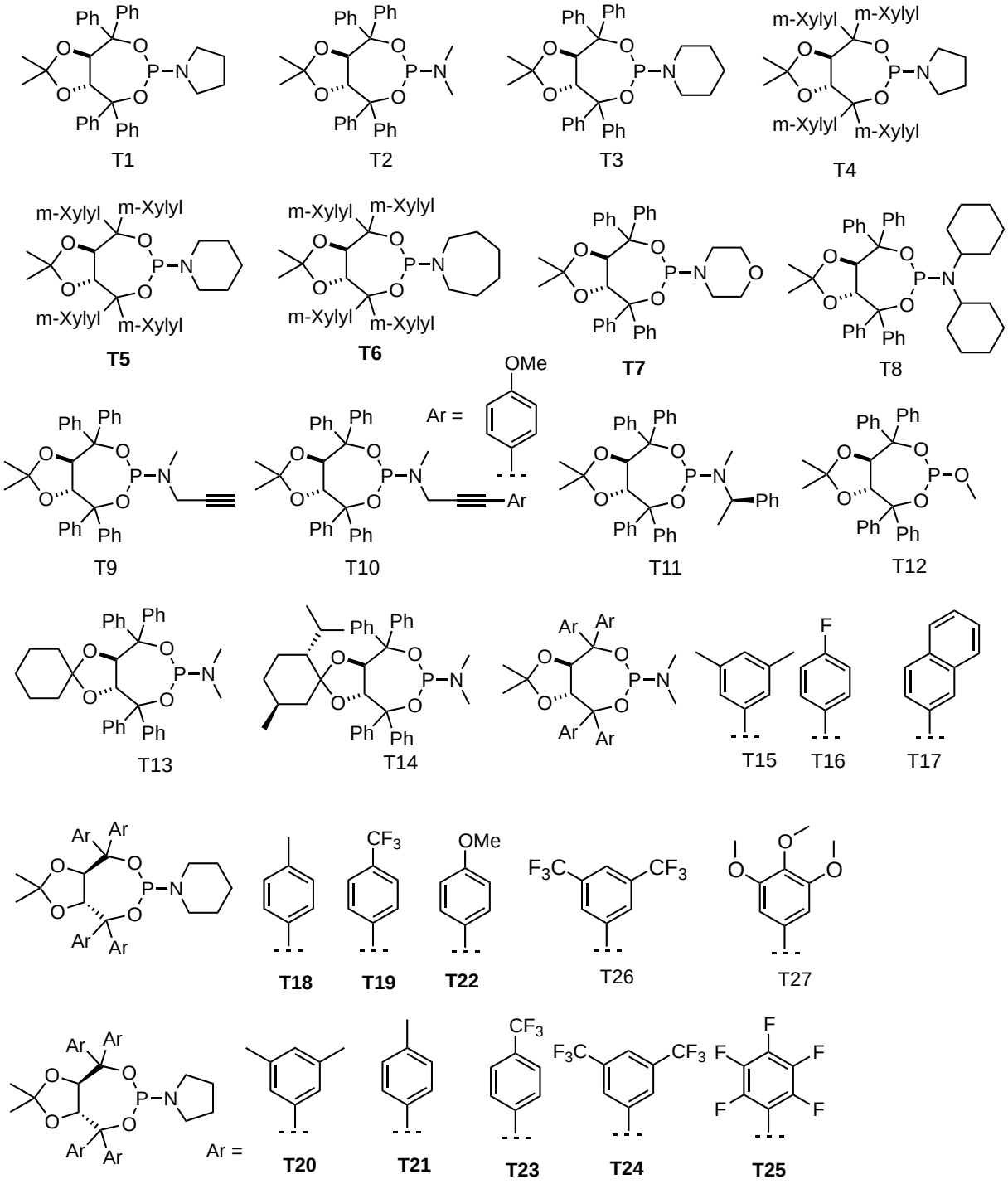

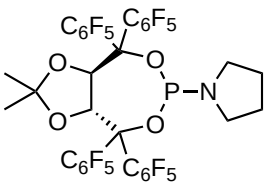

T25

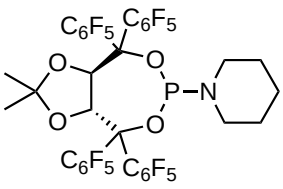

T28

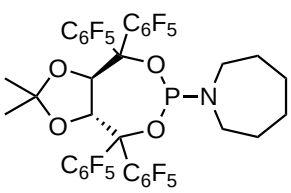

T29

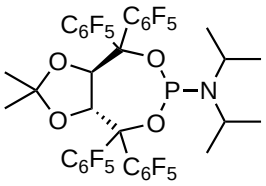

T30

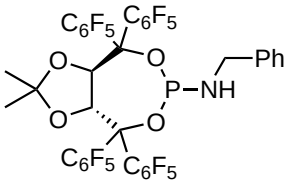

T31

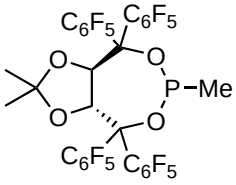

T32

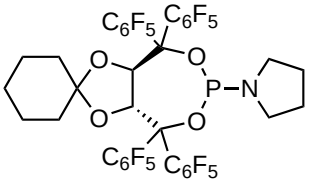

T33

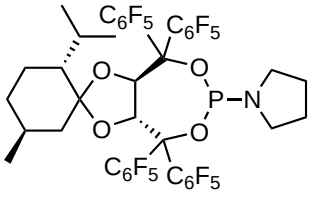

T34

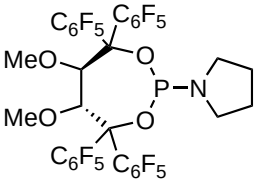

T35

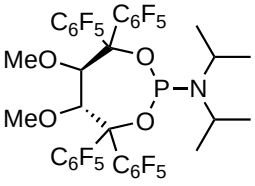

T36

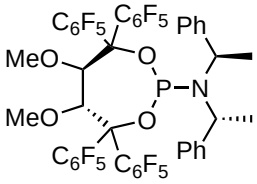

T37

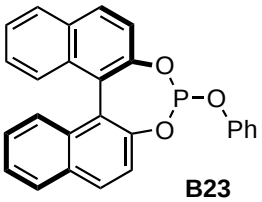

B23

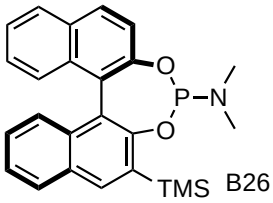

B26

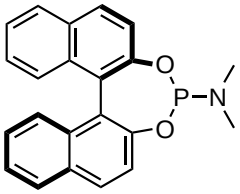

Monophos

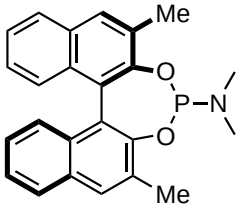

B0

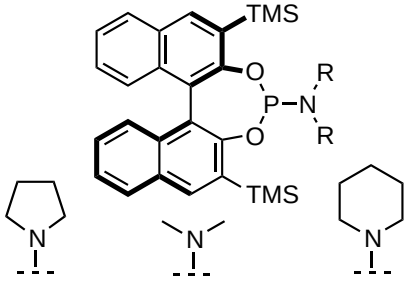

B24 **B2** **B25**

Binol Ligands

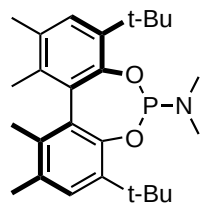

B1

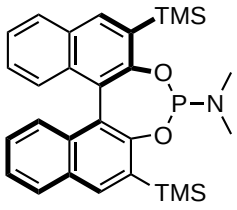

B2

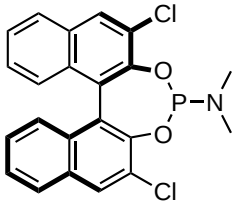

B3

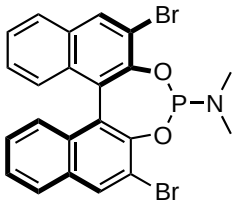

B4

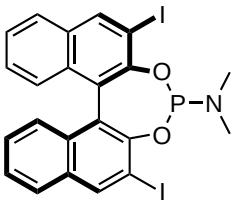

B5

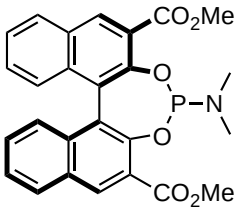

B6

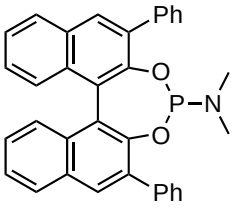

B7

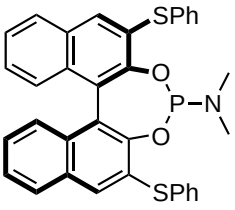

B8

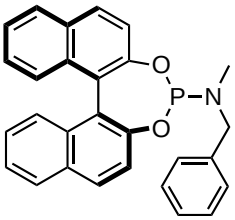

B9

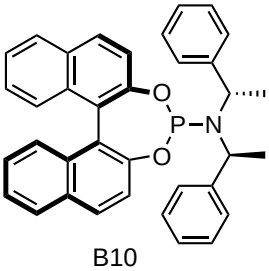

B10

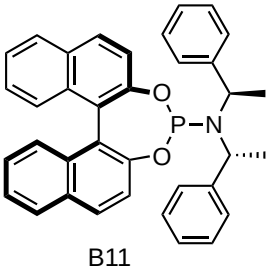

B11

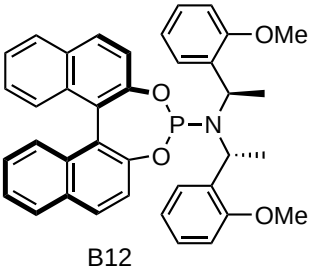

B12

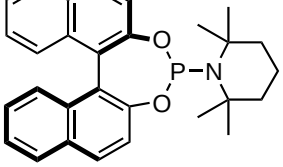

B13

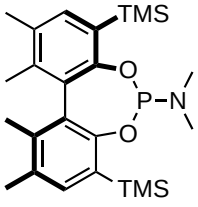

B14

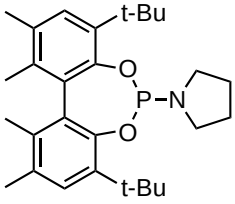

B15

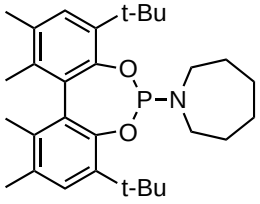

B16

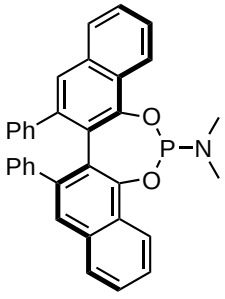

B17

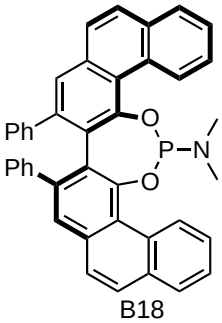

B18

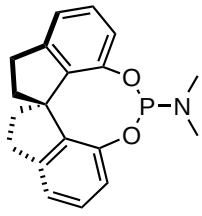

B19

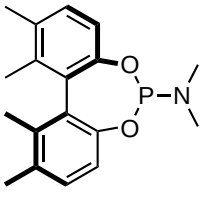

B20

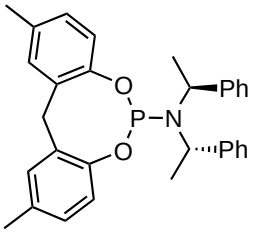

B21

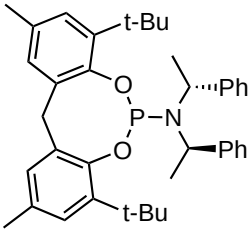

B22

APPENDIX 2

Rhodium Catalyzed [2+2+2] Cycloadditions of Alkenyl Isocyanates and Strained Cyclic Alkynes

A.2.1 Methods and Materials

Toluene, tetrahydrofuran, ether, and dichloromethane were degassed with argon and passed through one column of neutral alumina and one column of Q5 reactant. Triethylamine (peptide synthesis grade) was purchased from Fisher Scientific, dried over calcium hydride and freshly distilled prior to use. Flash column chromatography was carried out on silica gel (60 Å, 230 - 400 mesh, obtained from Silicycle Inc.) and was performed with reagent grade solvents. Analytical thin-layer chromatography (TLC) was performed on Silicycle glass-backed silica gel plates (60 Å, 0.25 mm, purchased from Silicycle Inc.) and visualized with a UV lamp (254 nm), and potassium permanganate or cerric ammonium molybdate.

Infrared spectra (IR) were obtained on a Nicolet Avatar 320 FT-IR spectrometer and Bruker Tensor 27 FT-IR spectrometer. ^{1}H NMR and ^{13}C NMR were obtained on Varian Unity 300 and Unity 400 spectrometers. Chemical shifts are expressed in parts per million values (δ, ppm). Proton chemical shifts in $CDCl_3$ were referenced to 7.26 ppm ($CHCl_3$). Carbon chemical shifts were referenced to 77.2 ppm ($CDCl_3$). Peak multiplicities are designated by the following abbreviations: s, singlet; d, doublet; t, triplet; q, quartet; m, multiplet; dd, doublet of doublets; dt, doublet of triplets; b, broad; *J*, coupling constant in Hz. Low resolution mass spectra (MS) and high resolution mass spectra (HRMS) were recorded on a Fisons VG Autospec spectrometer. HPLC spectra were obtained on an Agilent 1100 series system. Optical rotation was obtained with an Autopol-III automatic polarimeter. Melting points were obtained on a Fisher-Johns melting point apparatus and are uncorrected. References following the compound names indicate literature articles where the compound has been previously been reported.

Unless indicated, commercially available starting materials were purchased from Aldrich Chemicals and used without further purification. $[Rh(ethylene)_2Cl]_2$ was purchased from Strem Chemicals or Alfa Aesar and used without further purification. Phosphoramidite ligands were synthesized as previously reported: **B1** and **B2**[1], **T2**[2], CKphos [3]

A.2.2 [2+2+2] Cycloadditions of cyclic alkynes and isocyanates

Isocyanates and vinylogous amide indolizinone products not listed below were synthesized according to previously reported literature procedures.[4]

An oven-dried round bottom flask was charged with $[Rh(C_2H_4)_2Cl]_2$ (2 mg, 0.005 mmol) and ligand (5.5 mg, 0.001 mmol) and fitted with an oven-dried reflux condenser in an inert atmosphere (Ar) glove box. Upon removal from the glove box, 2 ml of toluene was added via syringe and the resulting yellow solution was stirred at ambient temperature for 5 min. To this solution, alkyne **1** (0.20 mmol, 1 equiv) and isocyanate **2** (0.22 mmol, 1.2 equiv) in 10 ml of toluene was added via syringe pump over 4 h. The reaction mixture was heated to 110 °C in an oil bath and kept at reflux for 16 h. The reaction mixture was cooled to 23 °C, concentrated in *vacuo*, and purified by flash column chromatography (19:1 EtOAc:MeOH). Evaporation of solvent afforded the analytically pure products. Absolute stereochemistry was established as previously reported.[5,6]

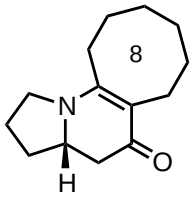

(S)-2,3,3a,4,6,7,8,9,10,11-decahydrocycloocta[e]indolizin-5(1H)-one

General procedure yielded a brown solid (43%). 81% ee by HPLC (Chiralcel OC, Hex:iPrOH 80:20, 1 ml/min). ^{1}H-NMR (300 MHz; CD_3OD): δ 3.79-3.63 (m, 2H), 3.61-3.54 (m, 1H), 2.63 (ddd, *J* = 7.7, 5.0, 2.6 Hz, 2H), 2.43 (dt, *J* = 11.4, 5.5 Hz, 2H),

[1] Yu, R. T.; Lee, E. E.; Malik, G.; Rovis, T. *Angew. Chem. Int. Ed.* **2009**, *48*, 2379–2382

[2] Dalton, D. M.; Oberg, K. M.; Yu, R. T.; Lee, E. E.; Perreault, S.; Oinen, M. E.; Pease, M. L.; Malik, G.; Rovis, T. *J. Am. Chem. Soc.* **2009**, *131*, 43, 15717-15728.

[3] Dalton, D. M.; Rappé, A. K.; Rovis, T. *Chem. Sci.* **2013**, *4*, 5, 2062-2070.

[4] a) Dalton, D. M.; Oberg, K. M.; Yu, R. T.; Lee, E. E.; Perreault, S.; Oinen, M. E.; Pease, M. L.; Malik, G.; Rovis, T. *J. Am. Chem. Soc.* **2009**, *131*, 43, 15717-15728. b) Yu, R. T.; Lee, E. E.; Malik, G.; Rovis, T. *Angew. Chem. Int. Ed.* **2009**, *48*, 2379-2382. c) Lee, E. E.; Rovis, T. *Org. Lett.* **2008**, 10, 6, 1231-1234.

[5] Yu, R. T.; Rovis, T. *J. Am. Chem. Soc.* **2006**, *128*, 12370-12371

[6] Yu, R. T.; Lee, E. E.; Malik, G.; Rovis, T. *Angew. Chem. Int. Ed.* **2009**, *48*, 2379-2382.

2.36-2.33 (m, 2H), 2.31-2.26 (m, 1H), 2.12 (dtt, *J* = 12.5, 7.2, 1.8 Hz, 1H), 1.95-1.78 (m, 2H), 1.72-1.57 (m, 4H), 1.51-1.42 (m, 3H), 1.41-1.30 (m, 2H).

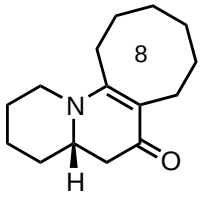

(S)-3,4,4a,5,7,8,9,10,11,12-decahydro-1H-cycloocta[c]quinolizin-6(2H)-one

^{1}H-NMR (300 MHz; $CDCl_3$): δ 3.86-3.82 (m, 1H), 3.30-3.20 (m, 1H), 2.78 (td, *J* = 12.7, 2.8 Hz, 1H), 2.61-2.54 (m, 2H), 2.50 (d, *J* = 5.6 Hz, 1H), 2.43 (s, 1H), 2.28 (dd, *J* = 16.3, 10.8 Hz, 1H), 1.85-1.80 (m, 1H), 1.76-1.71 (m, 1H), 1.65-1.57 (m, 5H), 1.54-1.40 (m, 9H), 1.24 (s, 1H).

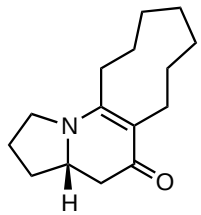

(S)-2,3,3a,4,7,8,9,10,11,12-decahydro-1H-cyclonona[e]indolizin-5(6H)-one

^{1}H-NMR (300 MHz; $CDCl_3$): δ 3.70-3.44 (m, 3H), 2.63-2.39 (m, 4H), 2.32-2.19 (m, 3H), 2.10-2.05 (m, 1H), 1.92-1.76 (m, 2H), 1.72-1.58 (m, 3H), 1.55-1.34 (m, 8H).

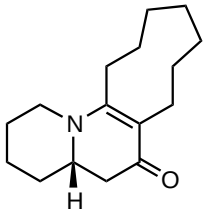

(S)-1,2,3,4,4a,5,8,9,10,11,12,13-dodecahydrocyclononona[c]quinolizin-6(7H)-one

^{1}H-NMR (300 MHz; $CDCl_3$): δ 3.79-3.75 (m, 1H), 3.26-3.16 (m, 1H), 2.74 (td, *J* = 12.6, 2.6 Hz, 1H), 2.58-2.53 (m, 2H), 2.48 (d, *J* = 5.5 Hz, 1H), 2.41 (s, 1H), 2.26 (dd, *J* = 16.2, 10.6 Hz, 1H), 1.80 (d, *J* = 11.8 Hz, 1H), 1.74-1.69 (m, 1H), 1.60-1.43 (m, 15H), 3.79-3.75 (m, 1H), 3.26-3.16 (m, 1H), 2.74 (td, *J* = 12.6, 2.6 Hz, 1H), 2.58-2.53 (m, 2H), 2.48 (d, *J* = 5.5 Hz, 1H), 2.41 (s, 1H), 2.26 (dd, *J* = 16.2, 10.6 Hz, 1H), 1.80 (d, *J* = 11.8 Hz, 1H), 1.74-1.69 (m, 1H), 1.60-1.43 (m, 15H).

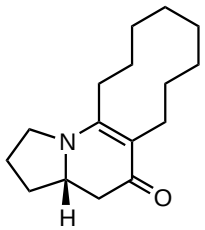

(S)-2,3,3a,4,6,7,8,9,10,11,12,13-dodecahydrocyclodeca[e]indolizin-5(1H)-one

^{1}H-NMR (300 MHz; $CDCl_3$): δ 3.76-3.58 (m, 2H), 3.49 (q, J = 8.5 Hz, 1H), 2.68 (dt, J = 13.6, 7.2 Hz, 1H), 2.49-2.33 (m, 5H), 2.28-2.16 (m, 2H), 2.09-1.98 (m, 1H), 1.92-1.79 (m, 1H), 1.73-1.57 (m, 6H), 1.45-1.33 (m, 8H), 1.24 (dt, J = 15.2, 7.3 Hz, 2H). ^{13}C–NMR (101 MHz; $CDCl_3$): δ 22.04, 23.11, 24.05, 24.97, 25.06, 26.38, 27.20, 27.33, 28.38, 32.16, 42.27, 47.82, 57.76, 109.01, 109.03, 109.06, 161.19, 190.79. IR (Thin Film) v 2922,

2852, 1618, 1475, 1445, 1340, 1299, 1276, 1135. LRMS (ESI) *m/z* $[C_{16}H_{26}NO]^+$ calculated 248.2, found 248.2.

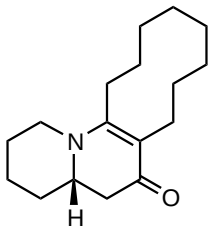

(S)-3,4,4a,5,7,8,9,10,11,12,13,14-dodecahydro-1H-cyclodeca[c]quinolizin-6(2H)-one

^{1}H-NMR (400 MHz; $CDCl_3$): δ 3.80 (d, J = 12.9 Hz, 1H), 3.22-3.14 (m, 1H), 2.50 (s, 5H), 2.28 (t, J = 12.1 Hz, 1H), 2.05 (d, J = 6.1 Hz,), 1.80 (d, J = 9.6 Hz, 1H), 1.68 (s, 5H), 1.54 (s, 3H), 1.43 (s, 10H), 1.34 (d, J = 78.0 Hz, 11H), 0.84 (t, J = 8.5 Hz, 2H). IR (Thin Film) v 2926, 2852, 1637, 1489, 1444, 1410, 1353, 1305, 1241, 1190, 1136, 1116. LRMS (ESI) *m/z* $[C_{17}H_{28}NO]^+$ calculated 262.2, found 262.2

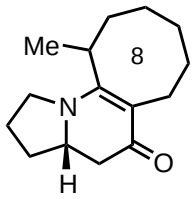

(3aS)-11-methyl-2,3,3a,4,6,7,8,9,10,11-decahydrocycloocta[e]indolizin-5(1H)-one .

Characterized as an inseparable mixture of diastereomers (2:1).

^{1}H-NMR (300 MHz; $CDCl_3$): δ 3.69-3.60 (m, 3H), 3.57-3.43 (m, 3H), 2.43 (dd, *J* = 15.6, 4.2 Hz, 2H), 2.29 (d, *J* = 16.4 Hz, 2H), 2.18 (dt, *J* = 11.7, 5.7 Hz, 2H), 2.06 (dt, *J* = 12.8, 6.6 Hz, 3H), 1.83-1.52 (m, 15H), 1.29 (d, *J* = 7.2 Hz, 6H), 1.24-1.12 (m, 8H).

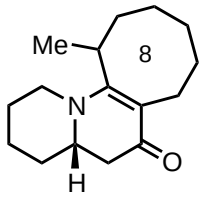

(4aS)-12-methyl-3,4,4a,5,7,8,9,10,11,12-decahydro-1H-cycloocta[c]quinolizin-6(2H)-one

Characterized as an inseparable mixture of diastereomers (2:1)

^{1}H-NMR (400 MHz; $CDCl_3$): δ 3.90 (d, *J* = 12.7 Hz, 1H), 3.83 (d, *J* = 13.2 Hz,), 3.25 (s, 1H), 3.20-3.12 (m, 1H), 3.07 (d, *J* = 10.1 Hz, 1H), 2.98 (q, *J* = 10.0 Hz, 1H), 2.64 (t, *J* = 11.9 Hz, 1H), 2.43 (t, *J* = 12.1 Hz, 1H), 2.29 (dd, *J* = 20.8, 9.6 Hz, 3H), 1.86-1.74 (m, 7H), 1.66 (d, *J* = 15.9 Hz, 3H), 1.54 (dd, *J* = 26.6, 12.8 Hz, 5H), 1.37 (dd, *J* = 25.5, 10.6 Hz, 5H), 1.26-1.15 (m, 10H). ^{13}C-NMR (101 MHz; $CDCl_3$): δ 191.1, 167.3, 98.7, 57.7, 50.2, 43.1, 37.6, 34.5, 32.97, 32.94, 31.9, 26.35, 26.30, 25.7, 24.6, 24.0, 23.7, 19.0.

A.2.3 ^{1}H-NMR and ^{13}C-NMR Spectra

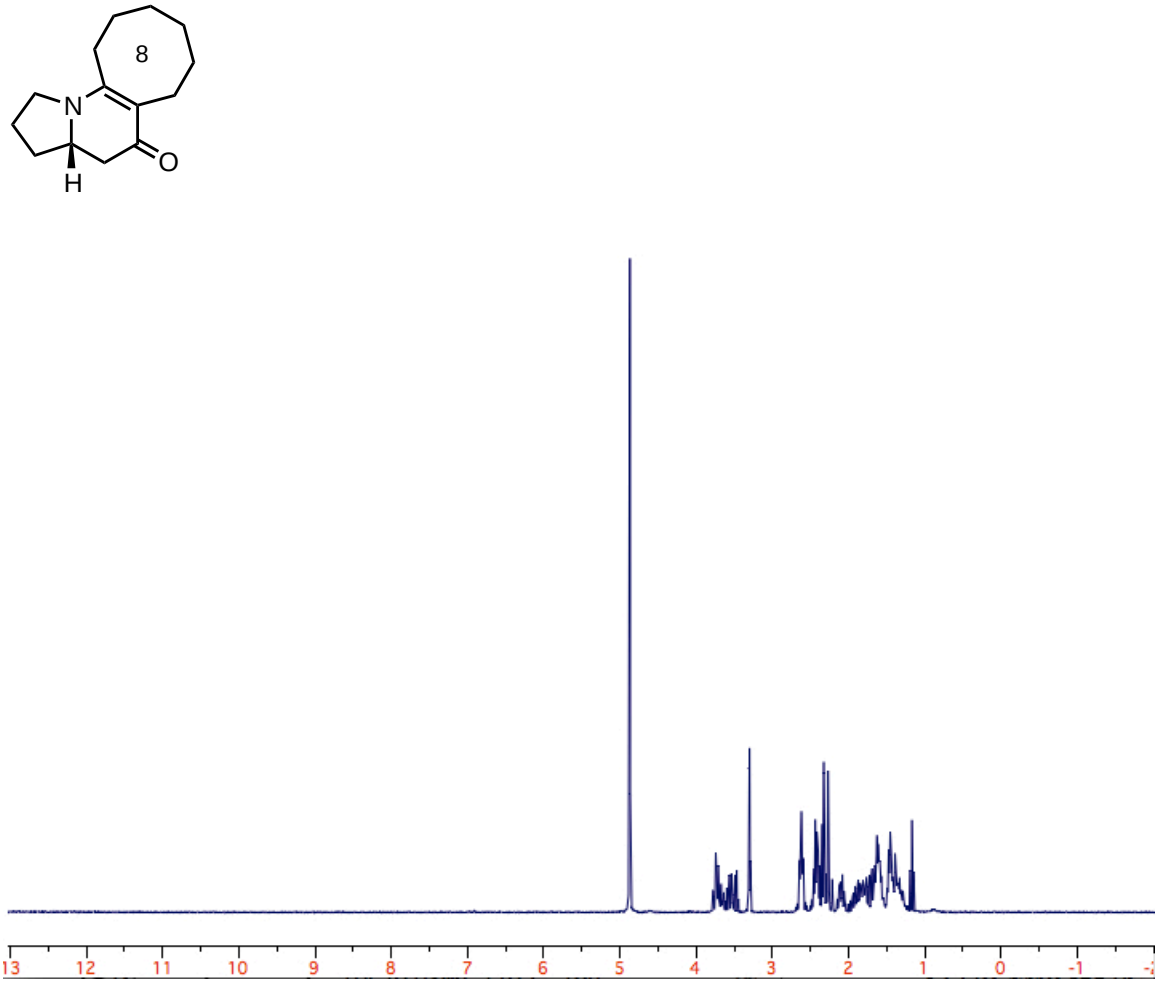

Figure A.2.1

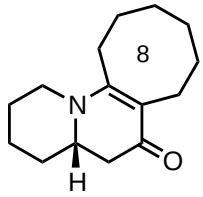

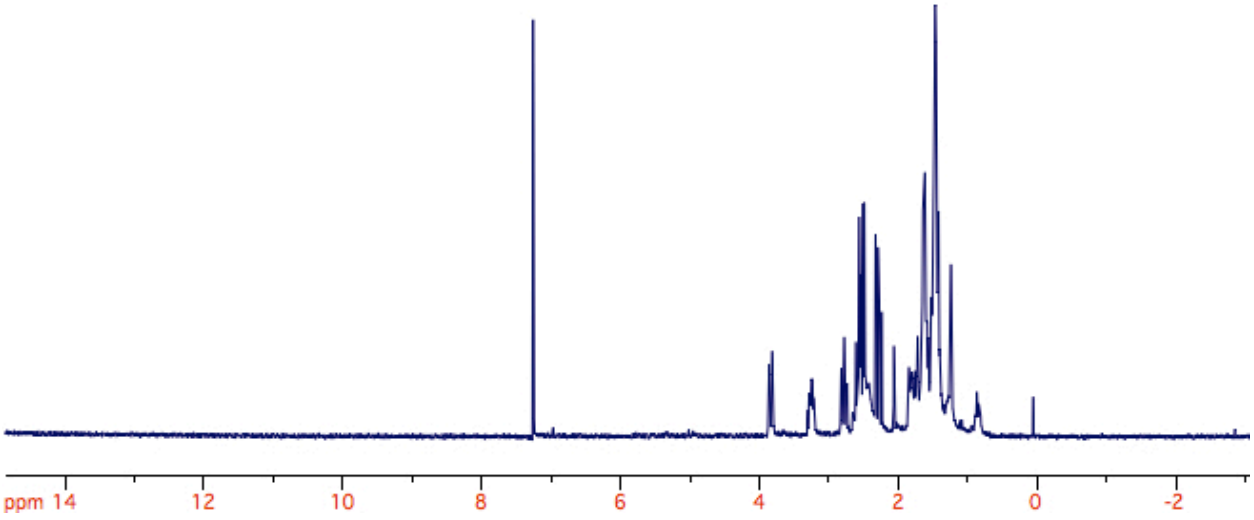

Figure A.2.2

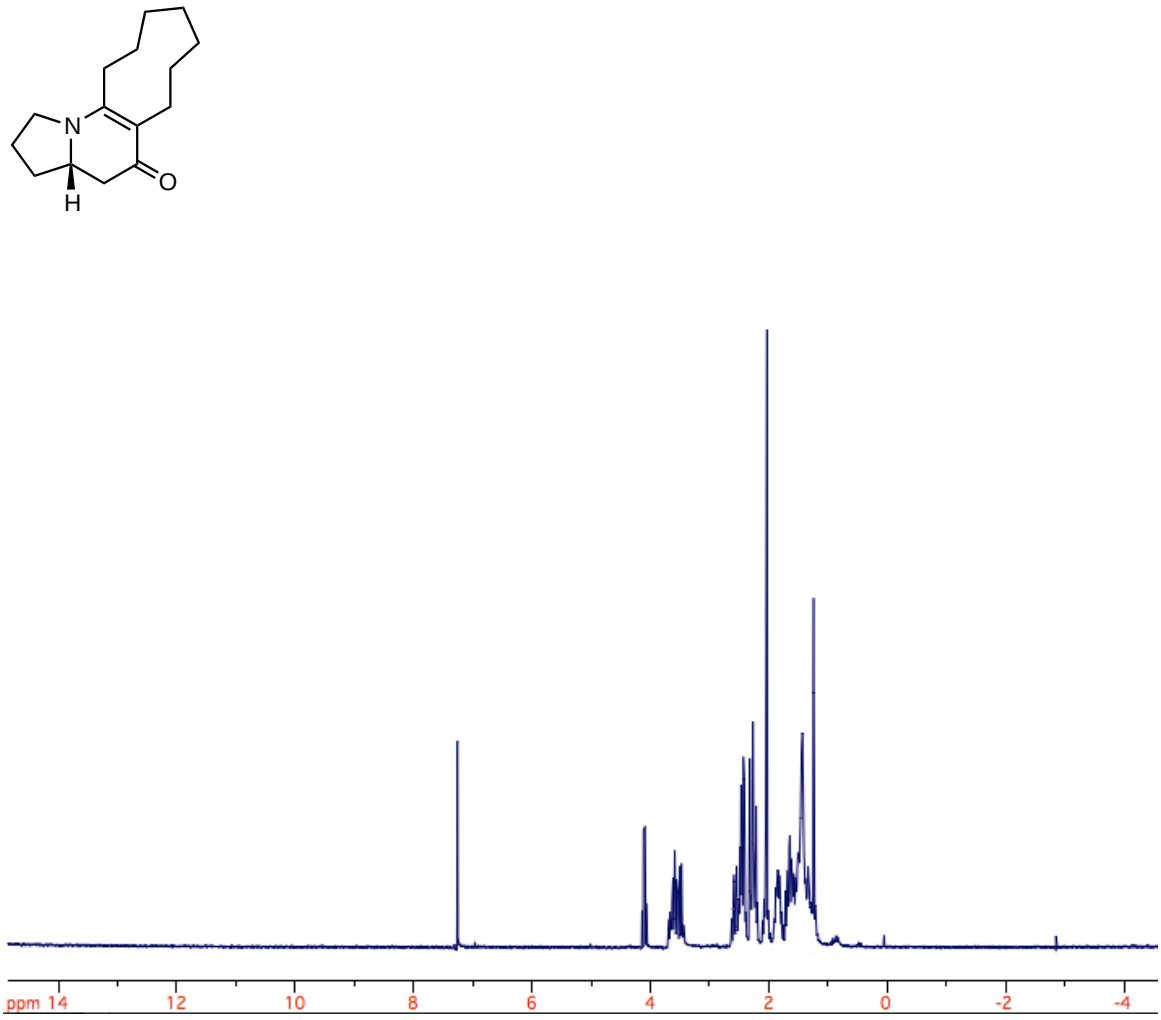

Figure A.2.3

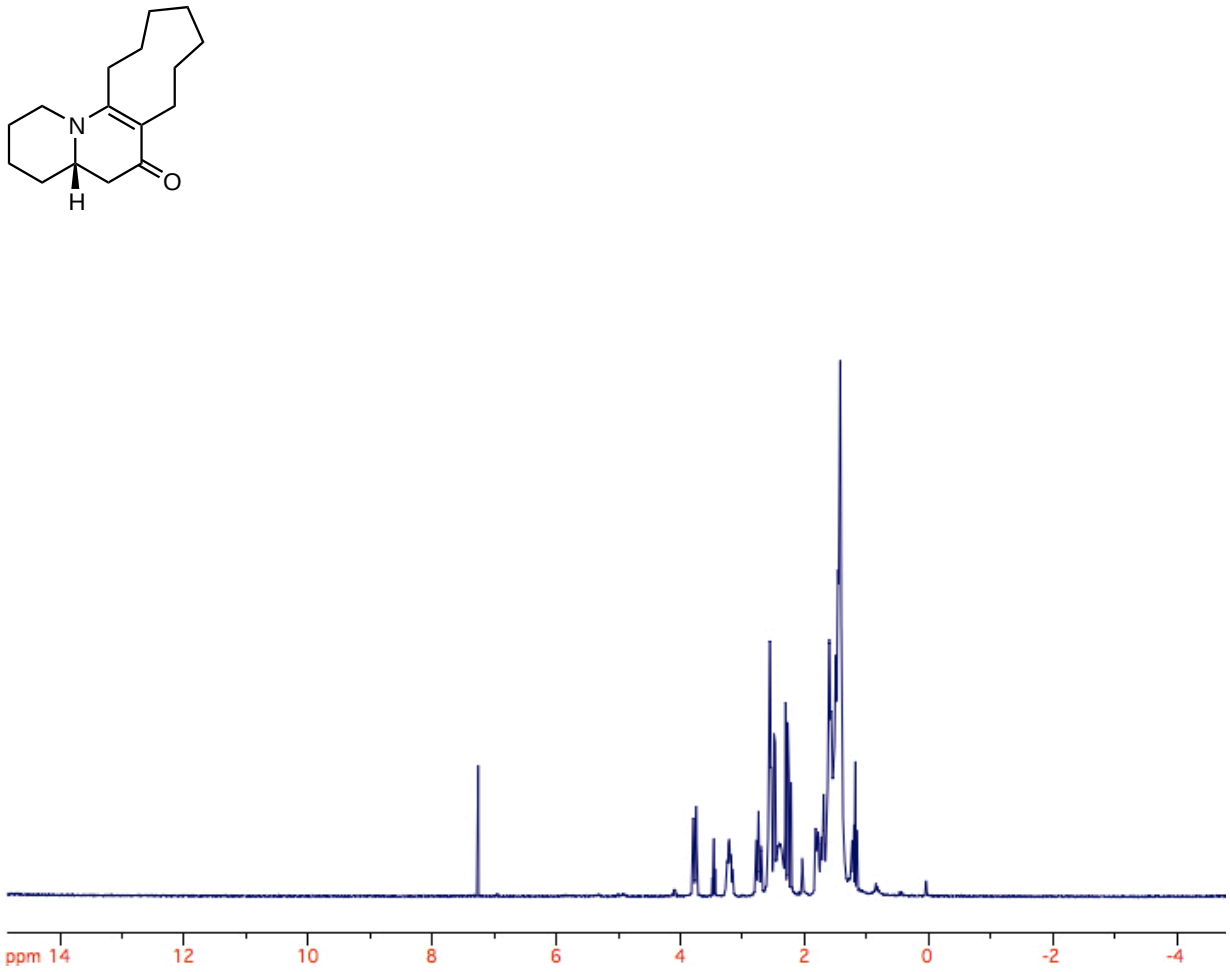

Figure A.2.4

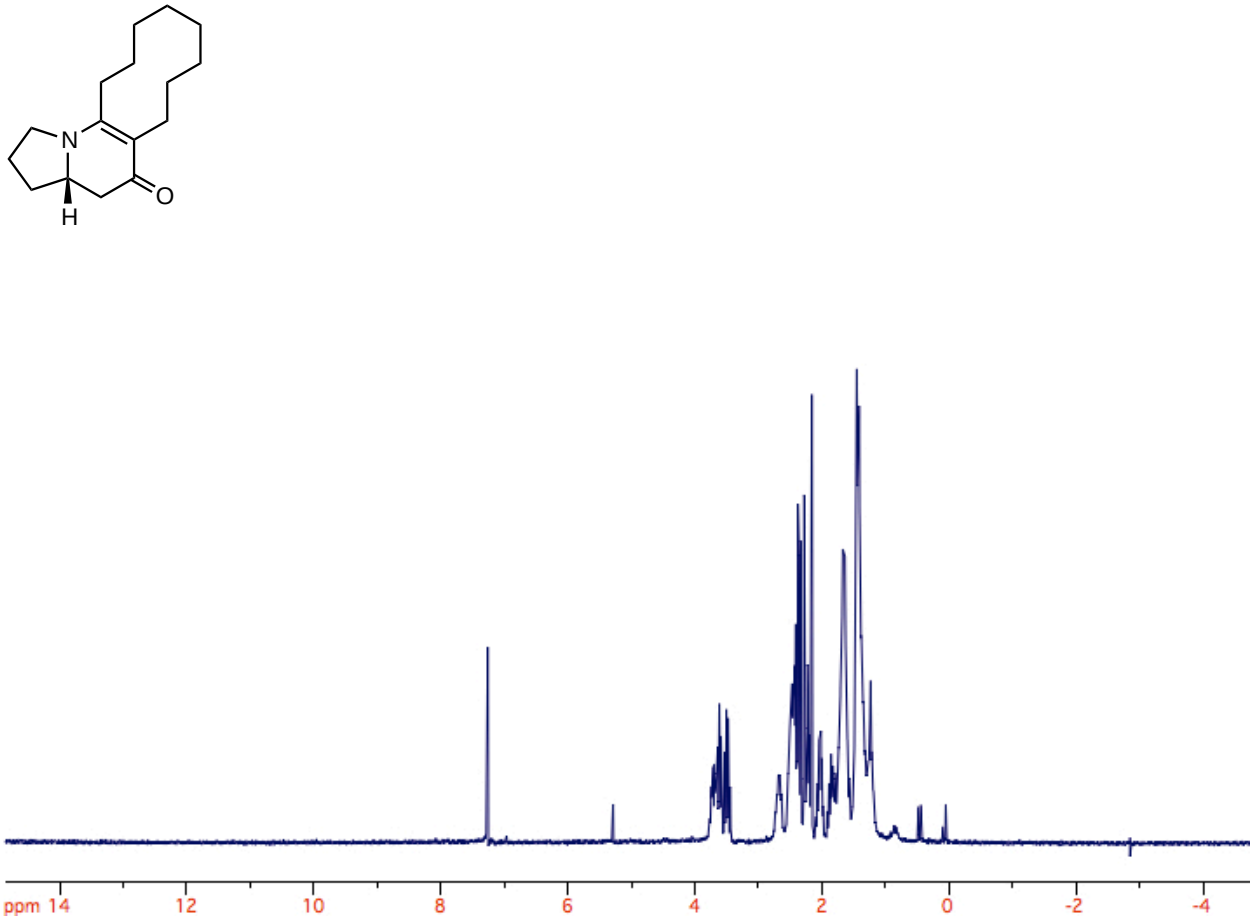

Figure A.2.5

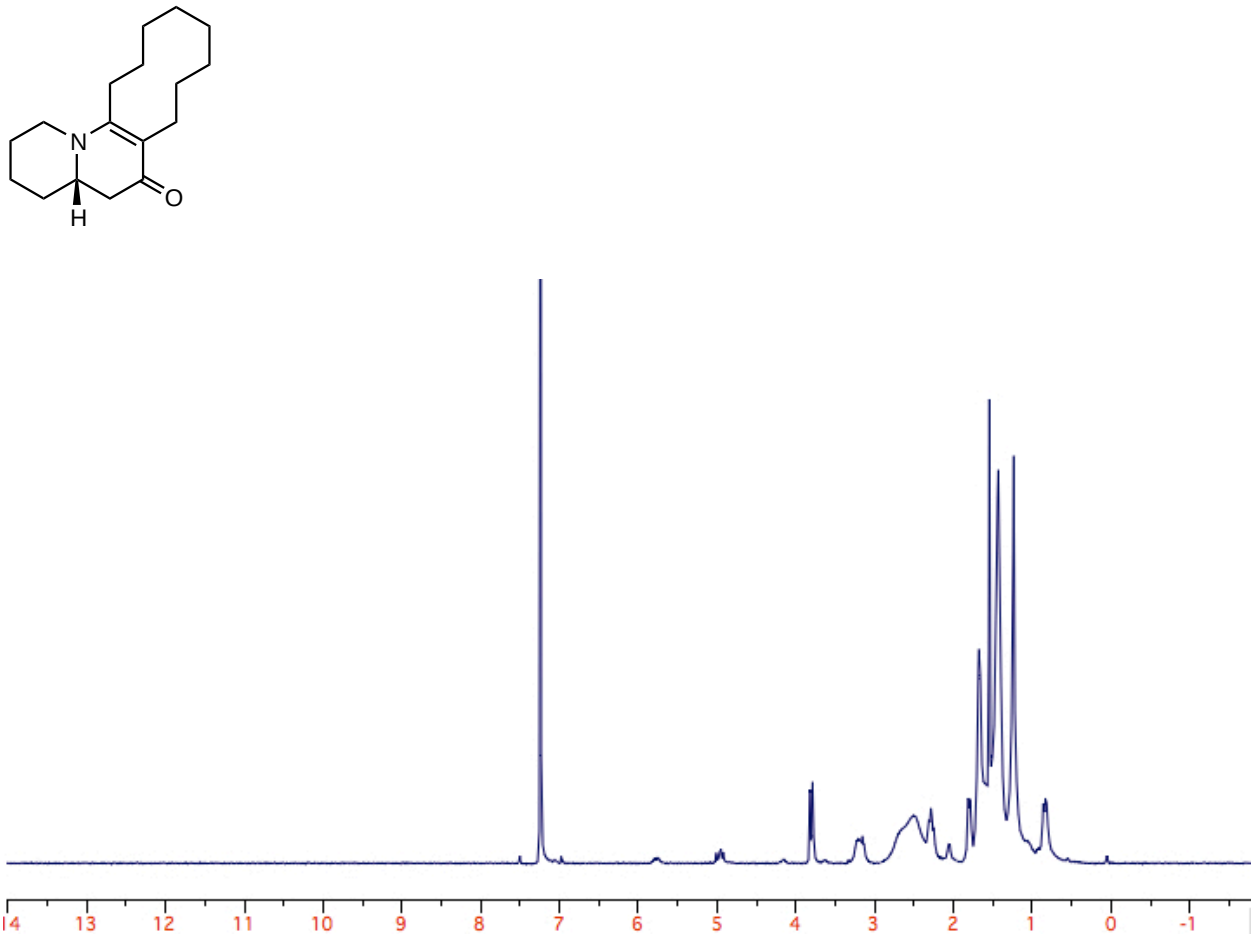

Figure A.2.6

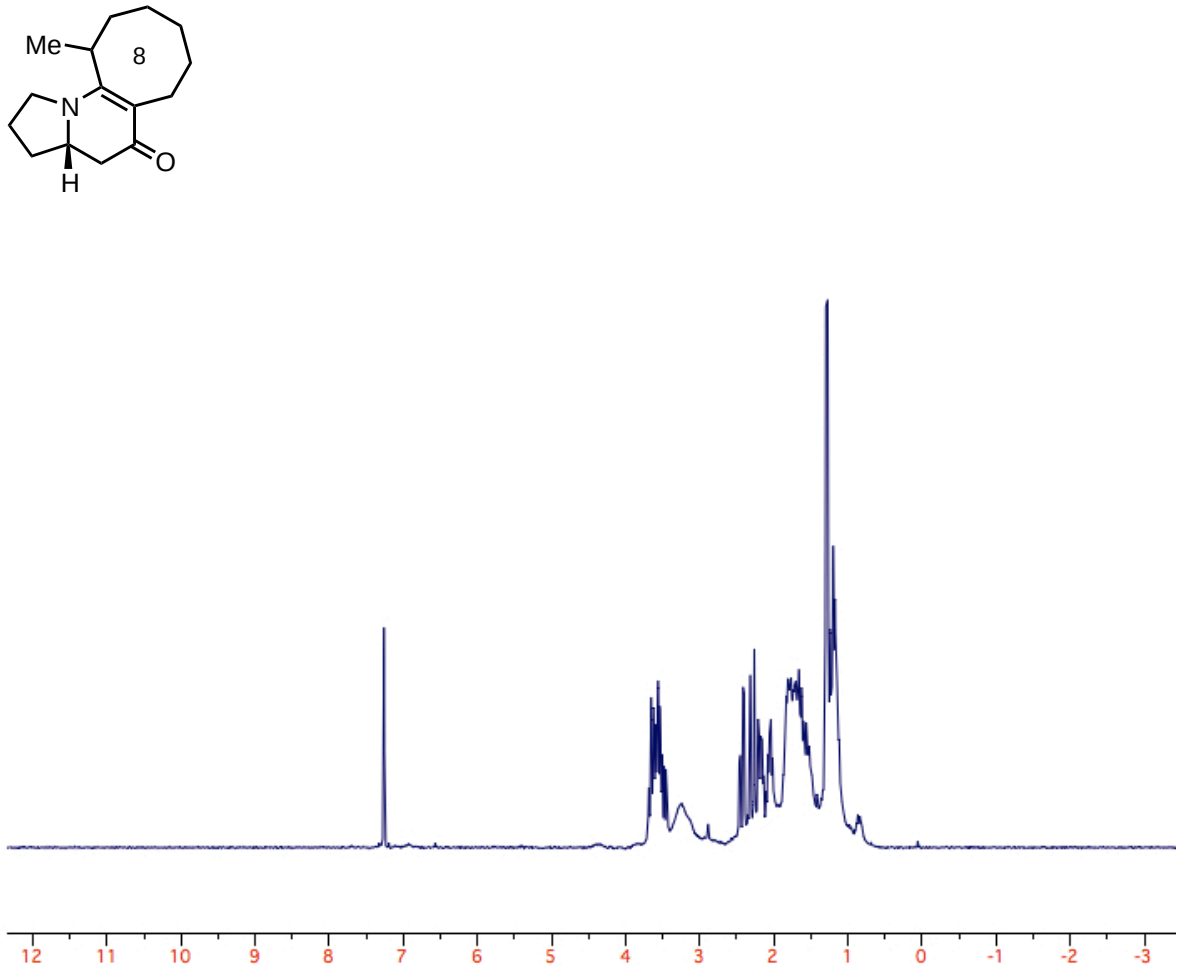

Figure A.2.7

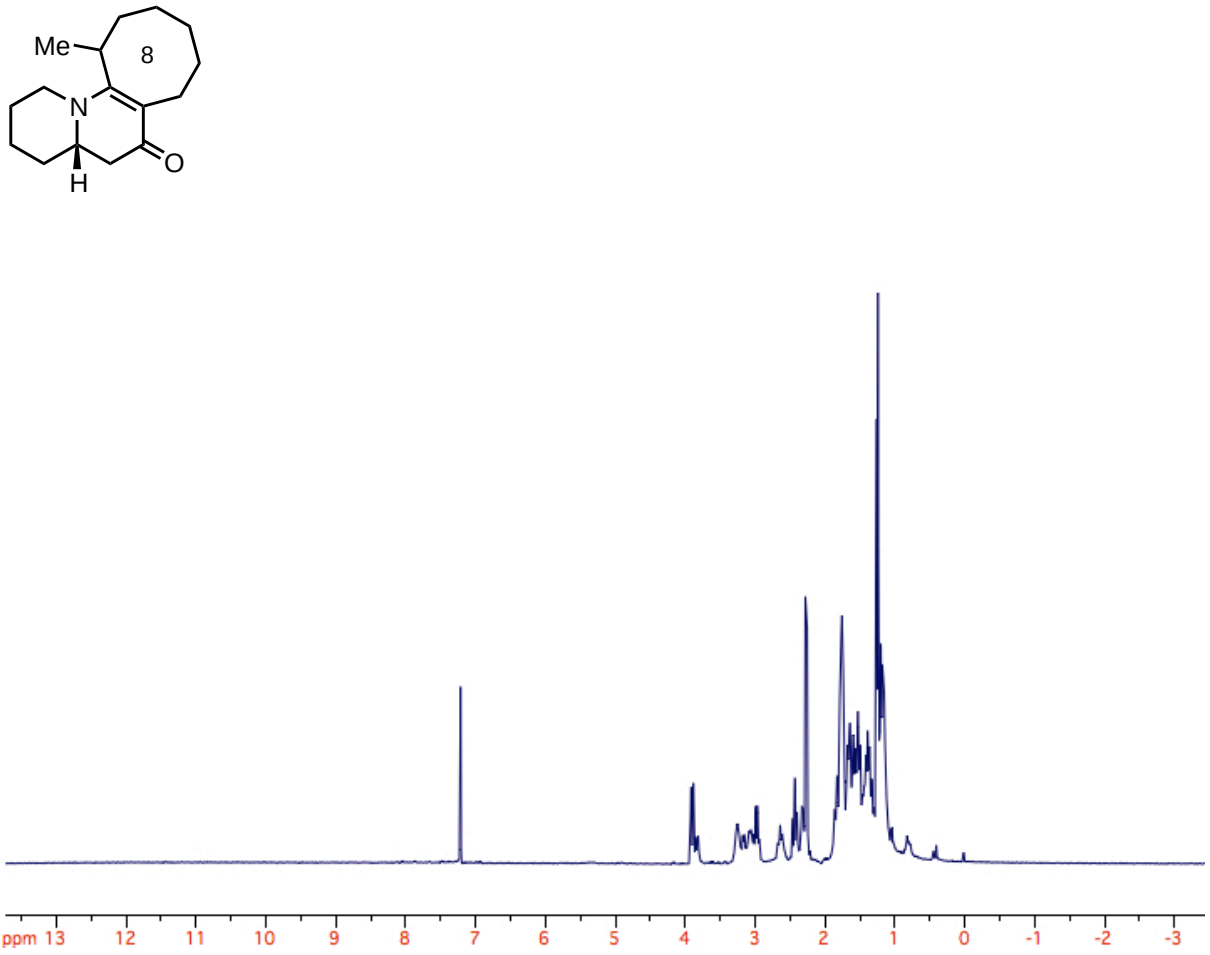

Figure A.2.8

APPENDIX 3

Mechanistic Proposal for Rh(I) Catalyzed [2+2+2] Cycloadditions

A.3.1 Methods and Materials

Toluene, tetrahydrofuran, ether, and dichloromethane were degassed with argon and passed through one column of neutral alumina and one column of Q5 reactant. Triethylamine (peptide synthesis grade) was purchased from Fisher Scientific, dried over calcium hydride and freshly distilled prior to use. Flash column chromatography was carried out on silica gel (60 Å, 230 - 400 mesh, obtained from Silicycle Inc.) and was performed with reagent grade solvents. Analytical thin-layer chromatography (TLC) was performed on Silicycle glass-backed silica gel plates (60 Å, 0.25 mm, purchased from Silicycle Inc.) and visualized with a UV lamp (254 nm), and potassium permanganate or cerric ammonium molybdate.

Infrared spectra (IR) were obtained on a Nicolet Avatar 320 FT-IR spectrometer and Bruker Tensor 27 FT-IR spectrometer. ^{1}H NMR and ^{13}C NMR were obtained on Varian Unity 300 and Unity 400 spectrometers. Chemical shifts are expressed in parts per million values (δ, ppm). Proton chemical shifts in $CDCl_3$ were referenced to 7.26 ppm ($CHCl_3$). Carbon chemical shifts were referenced to 77.2 ppm ($CDCl_3$). Peak multiplicities are designated by the following abbreviations: s, singlet; d, doublet; t, triplet; q, quartet; m, multiplet; dd, doublet of doublets; dt, doublet of triplets; b, broad; *J*, coupling constant in Hz. Low resolution mass spectra (MS) and high resolution mass spectra (HRMS) were recorded on a

Fisons VG Autospec spectrometer. HPLC spectra were obtained on an Agilent 1100 series system. Optical rotation was obtained with an Autopol-III automatic polarimeter. Melting points were obtained on a Fisher-Johns melting point apparatus and are uncorrected. References following the compound names indicate literature articles where the compound has been previously been reported.

Unless indicated, commercially available starting materials were purchased from Aldrich Chemicals and used without further purification. Alkynes were purchased from Aldrich Chemicals Co. and used without further purification or synthesized as previously reported.[1] $[Rh(C_2H_4)_2Cl]_2$ was purchased from Strem Chemicals, Inc. and used without further purification. Unless stated, isocyanates were prepared as previously reported.[2]

A.3.2 General Procedure for Ligand Synthesis:

The diol (0.27 mmol) was dissolved in THF in an oven-dried round bottom flask with a magnetic stir bar. Et_3N (3.5 eq, 0.95 mmol) was added and the reaction mixture was cooled to 0 °C before dropwise addition of phosphorous trichloride (1.1 eq, 0.30 mmol). The reaction mixture was stirred for 1 h and the amine (10 eq, 2.70 mmol) was added slowly at 0 °C. The reaction was stirred overnight at 23 °C, diluted with ether, and filtered. The filtrate was concentrated in *vacuo* and the resulting crude material was purified by flash column chromatography (98:2 Hex:EtOAc) to afford the desired phosphoramidite.

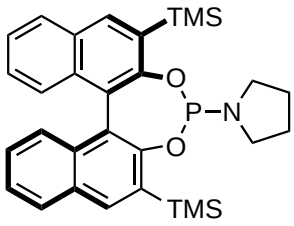

O,O-(R)-3,3'-bis(trimethylsilyl)-1,1'-binapthyl-2,2'-diyl-pyrrolidinephosphoramidite. General procedure yielded a white solid (85%). $[\alpha]^{20}_D$ = -550.4°, c = 0.01 g/ml $CHCl_3$. ^1H NMR (400 MHz, $CDCl_3$) δ 8.07 (m, 2H), 7.90 (m, 2H), 7.32 (m, 2H), 7.18 (m, 4H), 3.18 (m, 2H), 2.84 (bs, 2H), 1.65 (m, 4H), 0.45 (s, 9H), 0.44 (s, 9H). ^{13}C NMR (75 MHz, $CDCl_3$) δ 137.8, 136.6, 134.0, 133.7, 132.5, 132.2, 130.7, 130.1, 128.5, 128.3, 128.1, 127.5, 126.8, 126.7, 126.1, 124.2, 123.9, 123.6, 45.9, 45.7, 25.9, 25.8, 0.1, 0.0, -0.1, -0.9. ^{31}P NMR (75 MHz, $CDCl_3$) δ 149.82. R_f = 0.62 (98:2 Hex:EtOAc). IR (NaCl, Thin Film) 3534, 3053, 3032, 2960, 2899, 2858, 1578, 1388, 1255, 1086, 968, 835, 753 cm^{-1}. HRMS (ESI) *m/z* $[C_{30}H_{37}NO_2PSi_2]^+$ calcd 530.2095, found 530.2104.

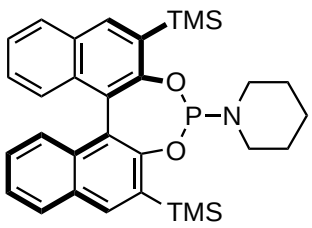

O,O-(R)-3,3'-bis(trimethylsilyl)-1,1'-binapthyl-2,2'-diyl-piperidinephosphoramidite. General procedure yielded a white solid (89%). $[\alpha]_D$ = -505.4°, c = 0.01 g/ml $CHCl_3$. ^1H NMR (400 MHz, $CDCl_3$) δ 8.07 (m, 2H), 7.91 (m, 2H), 7.39 (m, 3H), 7.17 (m, 3H), 2.92 (m, 2H), 1.53 (m, 4H), 1.32 (m, 2H), 0.51 (s, 9H), 0.45 (s, 9H). ^{13}C NMR (75 MHz, $CDCl_3$) δ 153.6, 136.7, 133.9, 133.7, 132.6, 132.1, 130.7, 130.0, 128.3, 128.2, 126.8, 126.7, 126.1, 126.0, 124.3, 124.1, 30.3, 27.2, 24.8. ^{31}P NMR (75 MHz, $CDCl_3$) δ 146.25. R_f = 0.40 (98:2 Hex:EtOAc). IR (NaCl, Thin Film) 3052, 2935, 2853, 1368, 1240, 1091, 1055, 979, 943, 840, 748 cm^{-1}. HRMS (ESI) m/z $[C_{31}H_{39}NO_2PSi_2]^+$ calcd 544.2251, found 544.2263.

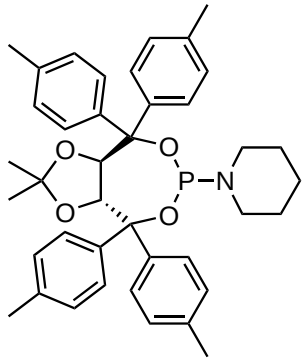

1-((3aR,8aR)-2,2-dimethyl-4,4,8,8-tetrap-tolyltetrahydro-[1,3]dioxolo[4,5-e][1,3,2]dioxaphosphepin-6-yl)piperidine. General procedure yielded a white solid (69%). $[\alpha]^{20}_D$ = -95.9º, c = 0.01g/ml, CH_2Cl_2. ^1H NMR (300 MHz, $CDCl_3$) δ 7.596 (d, *J* = 8.25 Hz, 2H), 7.425 (d, *J* = 8.14 Hz, 2H), 7.254 (dd, *J* = 18.02, 8.16, 4H), 7.028 (dd, *J* = 7.98, 4.14 Hz, 6H), 6.979 (d, *J* = 8.19 Hz, 2H), 5.039 (dd, *J* = 8.56 Hz, 1H), 4.645 (d, *J* = 8.55 Hz, 1H), 3.210 (m, 2H), 3.086 (m, 2H), 2.236 (d, *J* = 2.34 Hz, 9H), 2.202 (s, 3H), 1.509 (m, 6H), 1.269 (s, 3H), 0.211 (s, 3H). ^{13}C NMR (100 MHz, $CDCl_3$) δ 144.8, 144.3, 139.6, 139.5, 136.9, 136.8, 136.7, 136.6, 129.1, 128.9, 128.8, 128.5, 128.4, 128.0, 127.2, 111.4, 83.1, 82.9, 82.7, 81.4, 81.1, 45.3, 45.1, 27.9, 27.3, 25.6, 25.5, 21.4, 21.3, 21.2. ^{31}P NMR (75 MHz, $CDCl_3$) δ 138.7. R_f = 0.34 (19:1 Hex:EtOAc). IR (NaCl, Thin Film) 3027, 2986, 2940, 2853, 2361, 1506, 1445, 1378, 1255, 1209, 1168, 1050, 1030, 958, 830, 738 cm^{-1}. HRMS (ESI) *m/z* calcd $(C_{40}H_{46}NO_4P)^+$ 635.3164, found 635.3174.

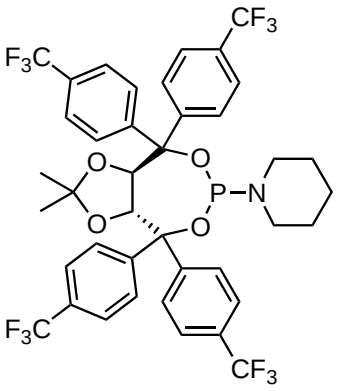

1-((3aR,8aR)-2,2-dimethyl-4,4,8,8-tetrakis(4-(trifluoromethyl)phenyl)tetrahydro-[1,3]dioxolo[4,5-e][1,3,2]dioxaphosphepin-6-yl)piperidine. General procedure yielded a white solid (51%). $[\alpha]^{20}_D$ = -84.5°, c = 0.01g/ml CH_2Cl_2. ^{1}H NMR (300 MHz, $CDCl_3$) δ 7.88 (d, *J* = 8.3 Hz, 2H), 7.72 (d, *J* = 8.3 Hz, 2H), 7.66-7.49 (m, 13H), 5.08 (dd, *J* = 8.6, 3.5 Hz, 1H), 4.58 (d, *J* = 8.6 Hz, 1H), 3.25 (d, *J* = 26.5, 6.6 Hz, 4H), 1.71-1.57 (m, 6H), 1.37 (s, 3H), 0.31 (s, 3H). ^{13}C NMR (75 MHz, $CDCl_3$) δ 150.1, 149.3, 129.4, 129.1, 129.0, 127.6, 127.4, 126.0, 125.7, 125.6, 125.2, 124.5, 112.3, 82.5, 82.3, 82.0, 80.9, 45.4, 45.1, 27.7, 27.3, 27.2, 25.5, 25.2. ^{31}P NMR (75 MHz, $CDCl_3$) δ 138.6. R_f = 0.44 (19:1 Hex:EtOAc). IR (NaCl, Thin Film) 3581, 2991, 2935, 2848, 2366, 2330, 1782, 1716, 1619, 1450, 1409, 1368, 1322, 1158, 1117, 845, 728 cm^{-1}. HRMS (ESI) *m/z* calcd $[C_{40}H_{34}F_{12}NO_4P]^+$ 851.2034, found 851.2032.

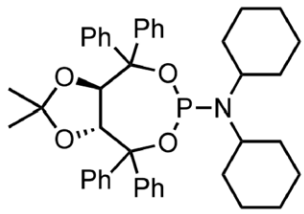

(3aR,8aR)-N,N-dicyclohexyl-2,2-dimethyl-4,4,8,8-tetraphenyltetrahydro-[1,3]dioxolo[4,5-e][1,3,2]dioxaphosphepin-6-amine. General procedure yielded a white solid. $[\alpha]^{20}_D$ = -60.6°, c = 0.01g/ml, CH_2Cl_2. ^{1}H NMR (400 MHz, $CDCl_3$) δ 7.80 (d, *J* = 7.4 Hz, 2H), 7.60 (d, *J* = 7.6 Hz, 2H), 7.42 (dd, *J* = 7.7, 2.3 Hz, 4H), 7.29-7.14 (m. 12H), 5.13 (dd, *J* = 8.6, 3.3 Hz, 1H), 4.60 (d, *J* = 8.6 Hz, 1H), 3.45 (s, 2H), 1.86-1.74 (m, 8H), 1.59-1.28 (m, 15H), 1.02 (d, *J* = 13.1 Hz, 2H) 0.20 (s, 3H). ^{13}C NMR (100 MHz, $CDCl_3$) δ 147.7, 147.1, 143.0, 142.4, 129.2, 128.9, 128.8, 127.9, 127.7, 127.6, 127.5, 127.4, 127.1, 126.9, 111.2, 83.3, 83.0, 82.8, 54.0, 53.9, 35.5, 35.4, 35.2, 35.1, 27.9, 27.1, 27.0, 25.7, 25.2. ^{31}P NMR (75 MHz, $CDCl_3$) δ 141.2. R_f = 0.30 (19:1 Hex:EtOAc). IR (NaCl, Thin Film) 2991, 2919, 2843, 2356, 2331, 2249, 1783, 1711, 1440, 1327, 1168, 1025, 907. HRMS (ESI) *m/e* calcd ($C_{43}H_{50}NO_4P$+H^+) 675.3477, found 675.3472.

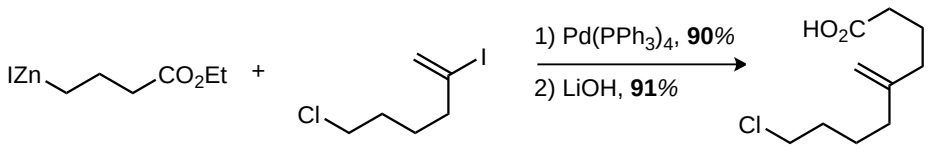

Scheme A.3.1

In a flame dried flask containing a suspension of zinc powder (204 mg, 3.12 mmol) in THF (0.5 mL) under Ar atmosphere, dibromoethane (23 mg, 0.12 mmol) was added. The solution was heated to 65 °C for 1 minute and cooled to room temperature. TMSCl (10 mg, 0.1 mmol) was then added, and the reaction stirred for 15 minutes. A solution of iodobutyrate (726 mg, 3.00 mmol) in THF (1.0 mL) was then added. The reaction was then stirred at 45 °C for 16 hours, cooled, and diluted with toluene/Et_2NH (10 mL/1 mL). The solution was then transferred by cannula into a flask containing palladium (116 mg, 0.1 mmol) and vinyl iodide (500 mg, 2.04 mmol). The reaction was stirred at 65 °C for 2 hours. The reaction was cooled to 23 °C, concentrated, loaded onto silica gel, and purified by flash chromatography (99:1 Hex:EtOAc). The resulting ester (0.2 M) was added to a stirring suspension of LiOH (5 eq) in MeOH:H_2O (3:1) and stirred at room temperature for 16 hours. The reaction was quenched with 1M HCl, extracted (Et_2O x 3), dried over $MgSO_4$, filtered, and concentrated in *vacuo*. The acid was then purified by silica gel flash chromatography (4:1 Hex:EtOAc).

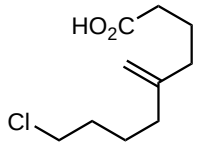

9-Chloro-5-methylene-nonanoic acid. Preceding procedure yielded a clear liquid (85%). ^{1}H NMR (400 MHz, $CDCl_3$) δ 4.74 (s, 1H), 4.74 (s, 1H), 3.52 (t, *J* = 6.5 Hz, 2H), 2.34 (t, *J* = 7.0 Hz, 2H), 2.04 (t, *J* = 7.5 Hz, 2H), 2.01 (t, *J* = 7.5 Hz, 2H), 1.80-1.71 (m, 4H), 1.56 (tt, *J* = 7.5, 7.5 Hz, 2H). ^{13}C NMR (100 MHz, $CDCl_3$) δ 179.6, 147.9, 110.4, 45.1, 35.2, 35.2, 33.5, 32.3, 25.0, 22.7. R_f = 0.25 (3:1 Hex:EtOAc). IR (NaCl, Thin Film) 2940, 1709, 1413, 1273 cm^{-1}.

A.3.2 General Procedure for Rh(I)-Catalyzed [2+2+2] Cycloadditions:

An oven-dried round bottom flask was charged with $[Rh(C_2H_4)_2Cl]_2$ (2.3 mg, 0.006 mmol) and ligand (0.012 mmol) and fitted with an oven-dried reflux condenser in an inert atmosphere (N_2) glove box. Upon removal from the glove box, 1 ml of toluene was added via syringe and the resulting yellow solution was stirred at ambient temperature for 15 min. To this solution, alkyne **1** (0.48 mmol) and isocyanate **2** (0.24 mmol) in 2 ml of toluene was added via syringe. An additional 4 ml of toluene was used to wash down the residue and added to the reaction mixture. The reaction mixture was heated to 110 °C in an oil bath and kept at reflux for 16 h. The reaction mixture was cooled to 23 °C, concentrated in *vacuo*, and purified

by flash column chromatography (typically 20:1 EtOAc:MeOH). Evaporation of solvent afforded the analytically pure products. Absolute stereochemistry was established as previously reported.[1,3]

A.3.3 Linear Free Energy Relationship

A plot of the Hammett values was made against the log of the ratio of **4**/**3** using Numbers software. *p*-dimethylaminophenylacetylene was not included in the plot because the sensitivity of the NMR restricted the detection of ratios as it was >20:1. **p*-trifluoromethylphenylacetylene was run with ligand **T3**.

Table A.3.1

	Hammett Value	**Log (4/3)**	**3**	**4**
-pNMe2	-0.83	1.27875360095283	5	95
-pOMe	-0.27	1.27875360095283	5	95
-mMe	-0.07	0.916941098889173	10.8	89.2
-H	0.00	0.845098040014257	12.5	87.5
-pCl	0.23	0.580661846626732	20.8	79.2
-pBr	0.23	0.505378014283088	23.8	76.2
-mF	0.34	0.255542756812029	35.7	64.3
-pC(O)Me	0.47	0.176091259055681	40	60
-pCF3*	0.54	-0.39946118179257	71.5	28.5

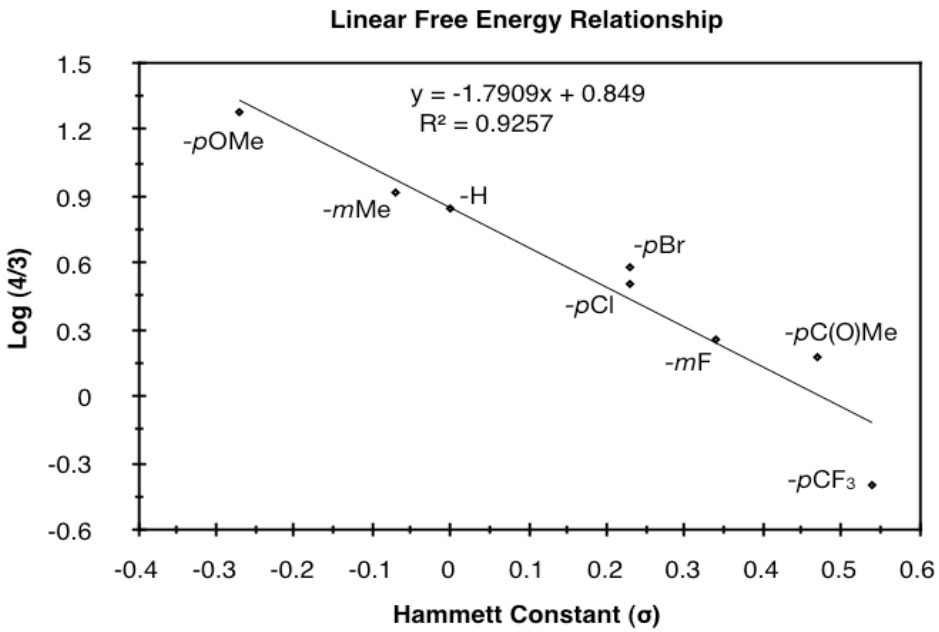
Linear Free Energy Relationship
y = -1.7909x + 0.849
R² = 0.9257
-pOMe
-mMe
-H
-pBr
-pCl
-mF
-pC(O)Me
-pCF3
Log (4/3)
Hammett Constant (σ)
1.5
1.2
0.9
0.6
0.3
0
-0.3
-0.6
-0.4
-0.3
-0.2
-0.1
0
0.1
0.2
0.3
0.4
0.5
0.6

Figure A.3.1

A.3.4 ^{1}H–NMR and ^{13}C–NMR Spectra

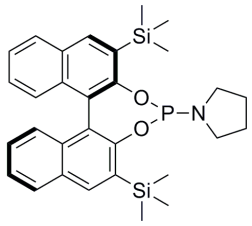

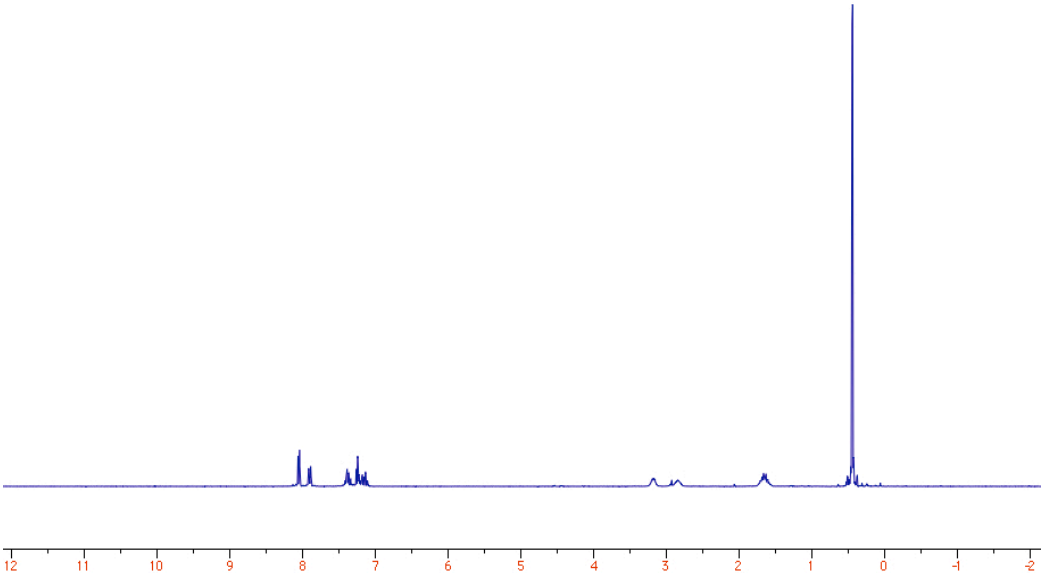

Figure A.3.2

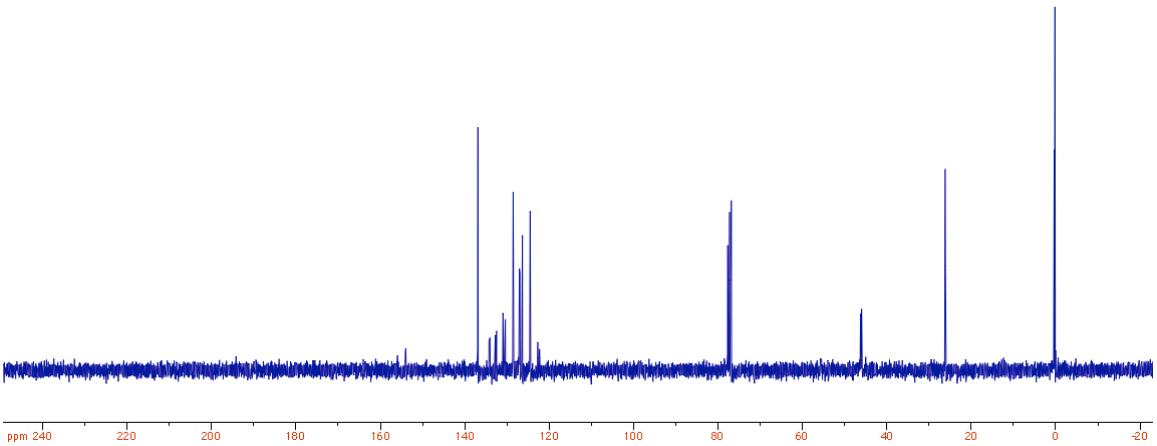

Figure A.3.3

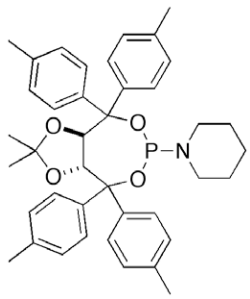

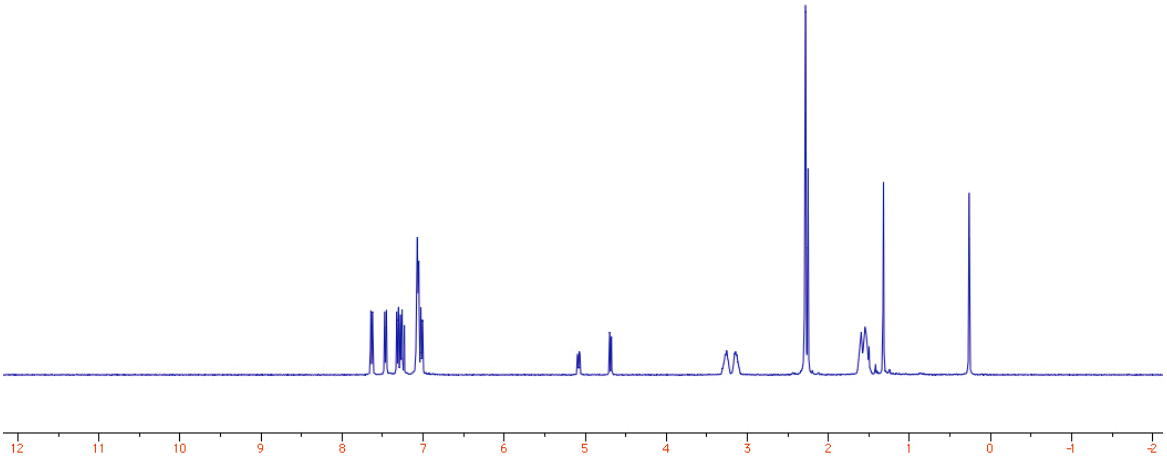

Figure A.3.4

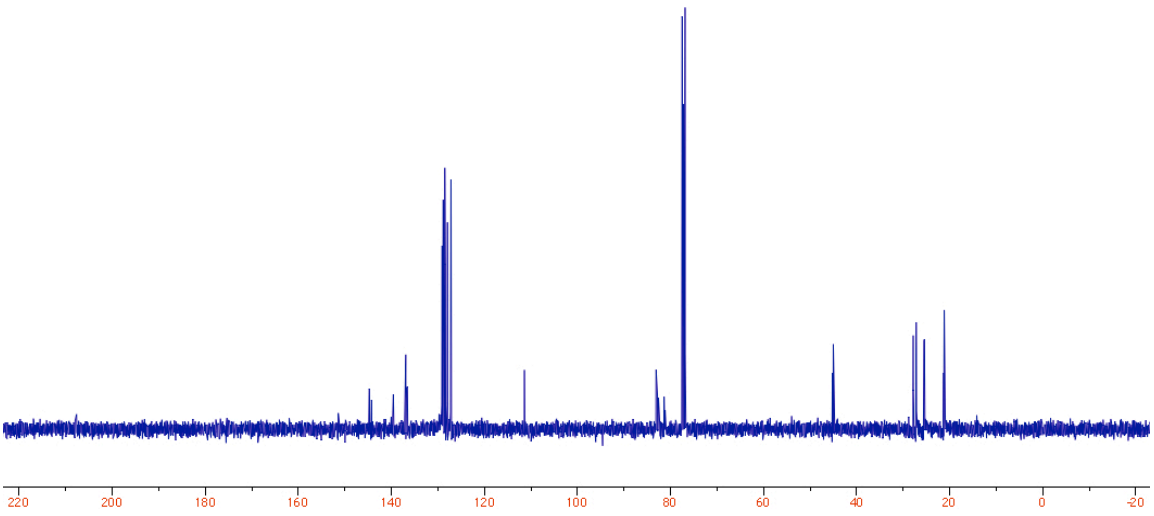

Figure A.3.5

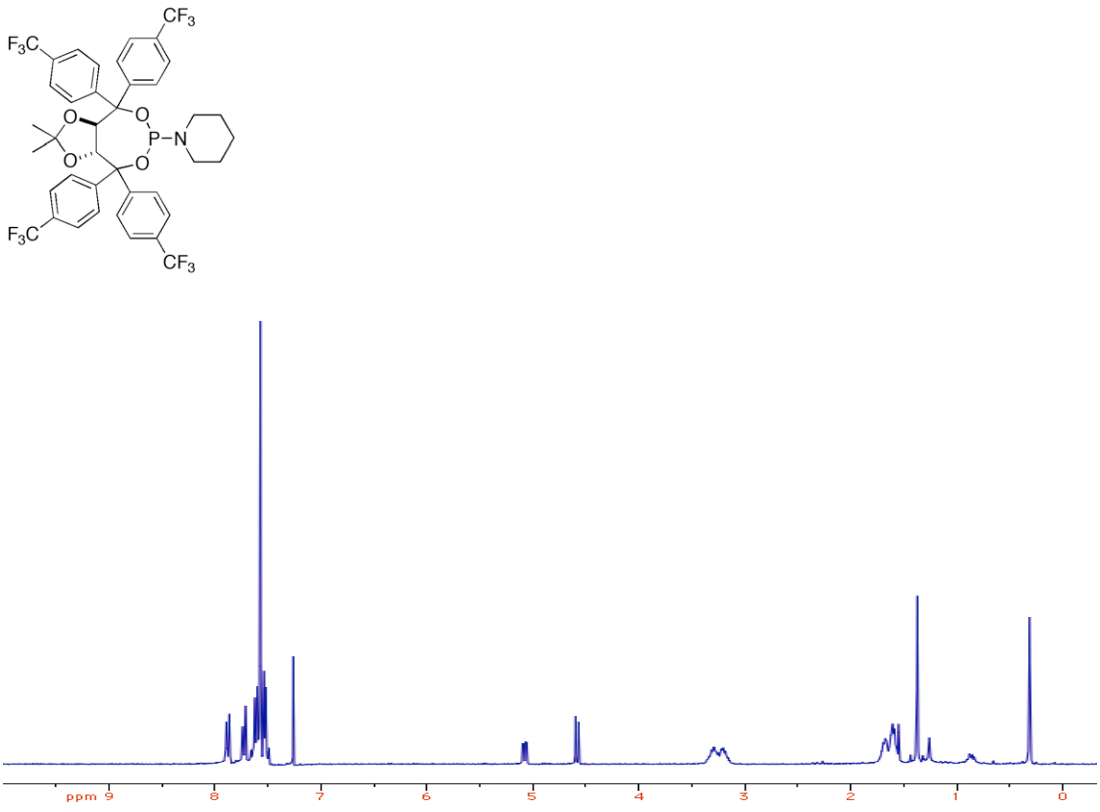

Figure A.3.6

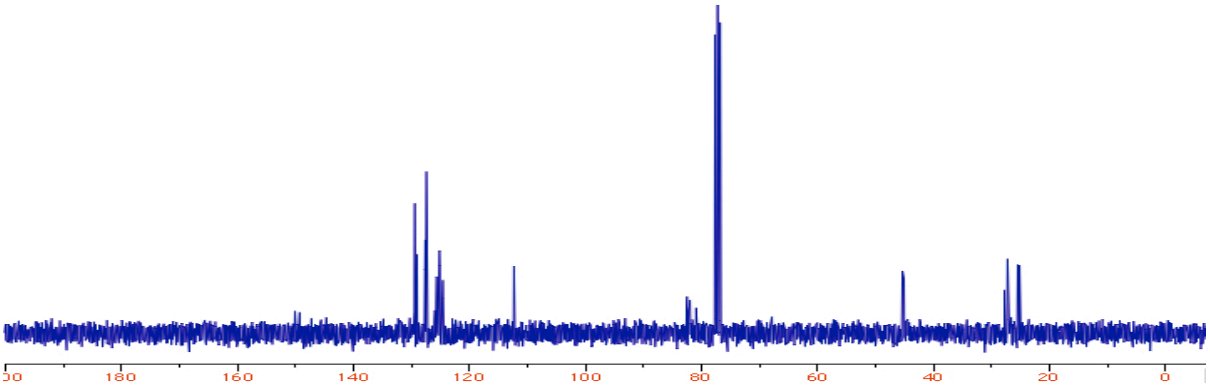

Figure A.3.7

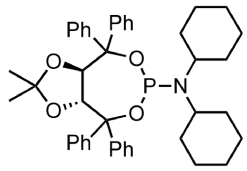

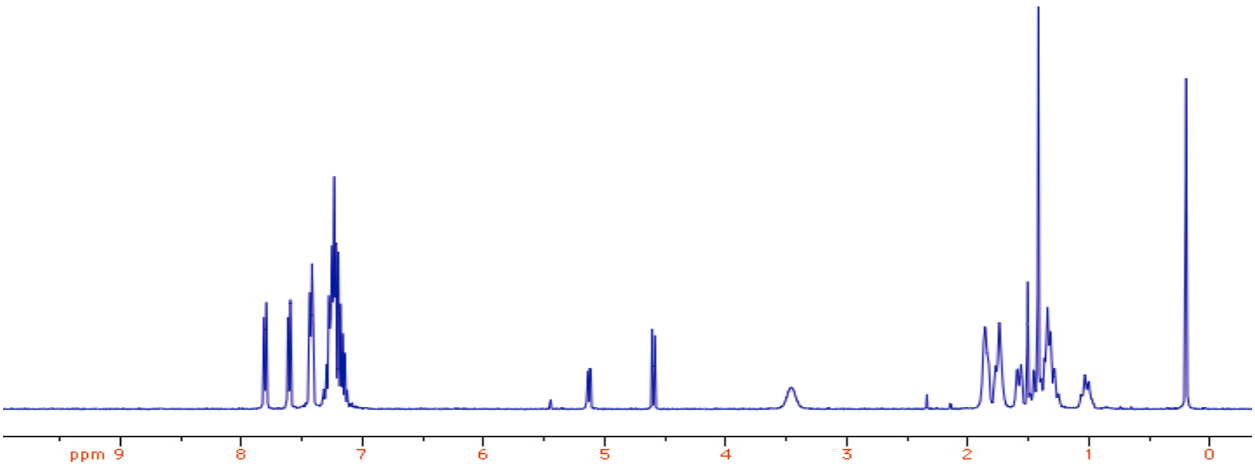

Figure A.3.8

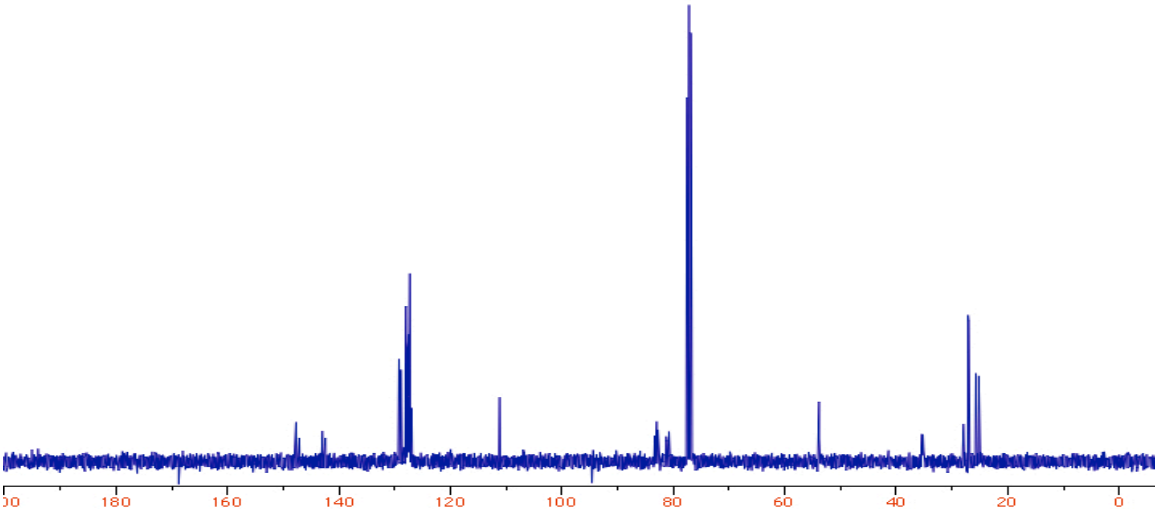

Figure A.3.9

A.3.5 Synthesis of Rhodium(cod)Cl•Phosphoramidite Complexes:

A 10 ml vial was charged with $[Rh(cod)Cl]_2$ (28 mg, 0.057 mmol) and ligand (0.114 mmol) in an inert atmosphere (N_2) glove box. Upon removal from the glove box, 1 ml of CH_2Cl_2 was added via syringe and the resulting yellow solution was layered with heptanes (~2 ml). The cap was loosely sealed and the solvent was allowed to evaporated slowly, yielding X-ray quality crystals.

A.3.6 Crystallographic Data:

All single crystals were coated in oil, transferred to a goniometer head, and mounted on a Bruker Kappa Apex CCD diffractometer under a stream of dinitrogen. All data collections were performed with Mo Kα radiation and a graphite monochromator. Data sets were taken with complete coverage and fourfold redundancy at 120K. Data was integrated and corrected for absorption effects with the Apex 2 software package.[1] Structures were solved with the SHELXTL software package.[2] All non-hydrogen atoms were refined with anisotropic thermal parameters and hydrogen atoms placed in idealized positions. Crystal data and structure parameters are provided as CIF files. Rhodium alkene bond distances were generated in XP using cent/x and join.

---

[1] Bruker AXS Inc., 5465 East Chervl Parkway, Madison, WI 53711-5373 USA

[2] Sheldrick, G. (1997) *SHELXL-97 Program for Crystal Structure Refinement*, Institüt für Anorganische Chemie
der Universität, Göttingen, Germany.

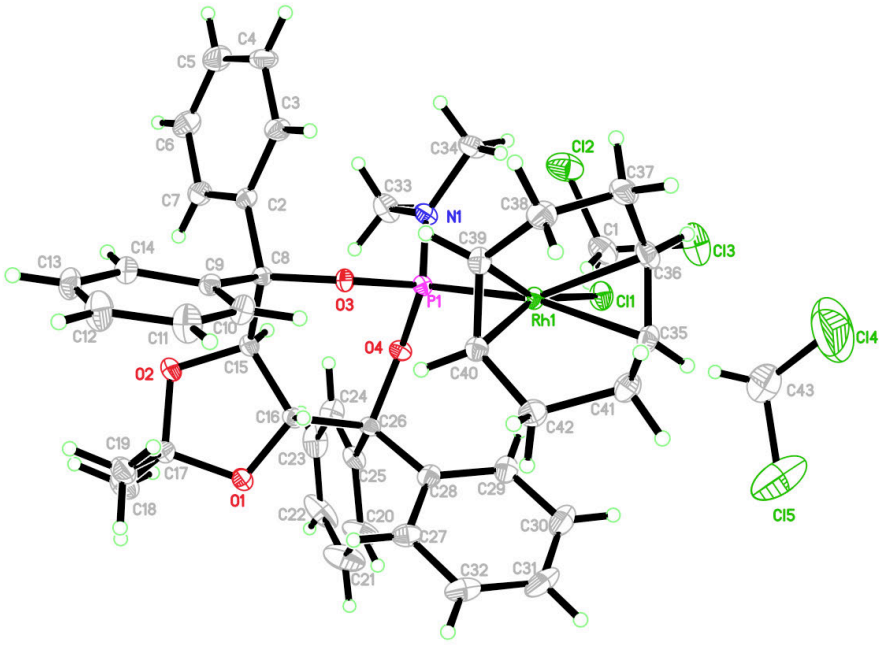

Table A.3.2. Crystal data and structure refinement for **T2**.

Identification code	rovis53_0m	
Empirical formula	C_{43} H_{50} Cl_5 N O_4 P Rh	
Formula weight	955.97	
Temperature	120 K	
Wavelength	0.71073 Å	
Crystal system	Monoclinic	
Space group	P 2_1	
Unit cell dimensions	*a* = 10.8877(3) Å	α = 90°
	b = 18.0279(5) Å	β = 91.9240(10)°
	c = 11.1484(3) Å	γ = 90°
Volume	2187.00(10) $Å^3$	
Z	2	
Density (calculated)	1.452 Mg/m^3	
Absorption coefficient	0.774 mm^{-1}	
F(000)	984	

Crystal size	0.39 x 0.13 x 0.11 mm^3
Theta range for data collection	1.83 to 40.55°.
Index ranges	-19<=h<=19, -26<=k<=32, -19<=l<=20
Reflections collected	54541
Independent reflections	23417 [R(int) = 0.0421]
Completeness to theta = 40.55°	98.0 %
Absorption correction	Multi-scan
Max. and min. transmission	0.9197 and 0.7512
Refinement method	Full-matrix least-squares on F^2
Data / restraints / parameters	23417 / 1 / 500
Goodness-of-fit on F^2	1.005
Final R indices [I>2sigma(I)]	R1 = 0.0511, wR2 = 0.1067
R indices (all data)	R1 = 0.0786, wR2 = 0.1195
Absolute structure parameter	-0.018(16)
Largest diff. peak and hole	1.854 and -1.097 e.$Å^{-3}$

Table A.3.3. Atomic coordinates (x 10^4) and equivalent isotropic displacement parameters ($Å^2$x 10^3) for **T2**. U(eq) is defined as one third of the trace of the orthogonalized U^{ij} tensor.

	x	y	z	U(eq)
C(1)	3074(3)	6207(2)	7166(3)	29(1)
C(2)	1226(2)	5493(1)	507(2)	14(1)
C(3)	2484(2)	5460(2)	292(2)	18(1)
C(4)	3092(2)	4786(2)	259(3)	23(1)
C(5)	2441(3)	4130(2)	424(3)	26(1)
C(6)	1199(3)	4155(2)	620(3)	24(1)
C(7)	585(2)	4834(1)	653(2)	19(1)
C(8)	590(2)	6245(1)	512(2)	12(1)
C(9)	402(2)	6528(1)	-775(2)	14(1)
C(10)	727(2)	7236(1)	-1124(2)	18(1)
C(11)	464(3)	7485(2)	-2298(2)	26(1)
C(12)	-134(3)	7017(2)	-3111(2)	28(1)
C(13)	-445(2)	6302(2)	-2783(2)	22(1)
C(14)	-162(2)	6053(2)	-1626(2)	18(1)
C(15)	-645(2)	6235(1)	1178(2)	13(1)
C(16)	-1006(2)	7012(1)	1583(2)	14(1)
C(17)	-2642(2)	6527(2)	462(2)	17(1)
C(18)	-3816(2)	6144(2)	798(3)	27(1)
C(19)	-2745(2)	6924(2)	-739(2)	22(1)
C(20)	-2564(2)	7261(2)	4162(3)	30(1)
C(21)	-3472(3)	6945(2)	4864(3)	38(1)
C(22)	-3436(2)	6196(2)	5135(3)	34(1)
C(23)	-2489(3)	5767(2)	4745(3)	27(1)
C(24)	-1567(2)	6084(2)	4054(2)	22(1)
C(25)	-1614(2)	6831(2)	3743(2)	16(1)
C(26)	-654(2)	7170(1)	2923(2)	13(1)
C(27)	-1118(2)	8524(2)	2479(2)	20(1)
C(28)	-497(2)	7996(2)	3178(2)	16(1)
C(29)	192(2)	8227(2)	4184(2)	20(1)
C(30)	242(3)	8973(2)	4504(3)	27(1)
C(31)	-413(3)	9495(2)	3817(3)	30(1)

C(32)	-1077(3)	9275(2)	2789(3)	26(1)
C(33)	1872(2)	5422(2)	3435(3)	23(1)
C(34)	3801(2)	6066(2)	3106(3)	22(1)
C(35)	3710(2)	9042(1)	3233(2)	19(1)
C(36)	4657(2)	8550(2)	3073(2)	20(1)
C(37)	5357(2)	8446(2)	1933(3)	23(1)
C(38)	4525(2)	8412(2)	801(2)	23(1)
C(39)	3283(2)	8043(1)	1008(2)	17(1)
C(40)	2226(2)	8450(1)	1316(2)	15(1)
C(41)	3249(2)	9587(2)	2281(2)	22(1)
C(42)	2153(2)	9276(2)	1524(2)	20(1)
C(43)	3397(4)	8641(3)	7535(5)	56(1)
Cl(1)	3137(1)	7566(1)	4920(1)	21(1)
Cl(2)	3749(1)	5357(1)	6704(1)	38(1)
Cl(3)	4118(1)	6716(1)	8085(1)	47(1)
Cl(4)	4889(2)	8948(1)	7369(2)	119(1)
Cl(5)	2367(2)	9333(1)	7852(2)	83(1)
N(1)	2454(2)	6106(1)	3050(2)	16(1)
O(1)	-2308(2)	7035(1)	1402(2)	19(1)
O(2)	-1664(2)	5988(1)	450(2)	17(1)
O(3)	1374(1)	6787(1)	1137(1)	12(1)
O(4)	493(1)	6771(1)	3220(1)	13(1)
P(1)	1779(1)	6862(1)	2553(1)	12(1)
Rh(1)	2923(1)	7898(1)	2860(1)	13(1)

Table A.3.4. Bond lengths [Å] and angles [°] for **T2**.

C(1)-Cl(3)	1.763(3)	C(24)-C(25)	1.392(4)
C(1)-Cl(2)	1.784(4)	C(25)-C(26)	1.537(3)
C(2)-C(7)	1.391(3)	C(26)-O(4)	1.468(3)
C(2)-C(3)	1.400(3)	C(26)-C(28)	1.525(4)
C(2)-C(8)	1.521(3)	C(27)-C(28)	1.391(4)
C(3)-C(4)	1.385(4)	C(27)-C(32)	1.399(4)
C(4)-C(5)	1.395(4)	C(28)-C(29)	1.393(3)
C(5)-C(6)	1.378(4)	C(29)-C(30)	1.392(4)
C(6)-C(7)	1.396(4)	C(30)-C(31)	1.393(5)
C(8)-O(3)	1.460(3)	C(31)-C(32)	1.392(5)
C(8)-C(9)	1.530(3)	C(33)-N(1)	1.459(3)
C(8)-C(15)	1.558(3)	C(34)-N(1)	1.468(3)
C(9)-C(10)	1.384(3)	C(35)-C(36)	1.376(4)
C(9)-C(14)	1.404(3)	C(35)-C(41)	1.520(4)
C(10)-C(11)	1.404(3)	C(35)-Rh(1)	2.266(2)
C(11)-C(12)	1.385(4)	C(36)-C(37)	1.516(4)
C(12)-C(13)	1.386(4)	C(36)-Rh(1)	2.230(2)
C(13)-C(14)	1.390(3)	C(37)-C(38)	1.528(4)
C(15)-O(2)	1.424(3)	C(38)-C(39)	1.531(3)
C(15)-C(16)	1.527(3)	C(39)-C(40)	1.417(3)
C(16)-O(1)	1.425(3)	C(39)-Rh(1)	2.130(2)
C(16)-C(26)	1.556(3)	C(40)-C(42)	1.509(4)
C(17)-O(1)	1.429(3)	C(40)-Rh(1)	2.107(2)
C(17)-O(2)	1.442(3)	C(41)-C(42)	1.544(4)
C(17)-C(18)	1.511(4)	C(43)-Cl(5)	1.721(5)
C(17)-C(19)	1.519(4)	C(43)-Cl(4)	1.732(5)
C(20)-C(25)	1.386(4)	Cl(1)-Rh(1)	2.3777(6)
C(20)-C(21)	1.402(4)	N(1)-P(1)	1.637(2)
C(21)-C(22)	1.383(5)	O(3)-P(1)	1.6300(16)
C(22)-C(23)	1.372(5)	O(4)-P(1)	1.6153(16)
C(23)-C(24)	1.406(4)	P(1)-Rh(1)	2.2648(6)
Cl(3)-C(1)-Cl(2)	110.53(16)		
C(7)-C(2)-C(3)	118.8(2)		
C(7)-C(2)-C(8)	122.0(2)		

C(3)-C(2)-C(8)	119.1(2)	C(25)-C(24)-C(23)	120.6(3)
C(4)-C(3)-C(2)	120.9(2)	C(20)-C(25)-C(24)	118.6(2)
C(3)-C(4)-C(5)	119.7(2)	C(20)-C(25)-C(26)	120.6(2)
C(6)-C(5)-C(4)	120.0(3)	C(24)-C(25)-C(26)	120.8(2)
C(5)-C(6)-C(7)	120.3(3)	O(4)-C(26)-C(28)	110.26(17)
C(2)-C(7)-C(6)	120.3(2)	O(4)-C(26)-C(25)	105.20(18)
O(3)-C(8)-C(2)	109.83(17)	C(28)-C(26)-C(25)	110.54(19)
O(3)-C(8)-C(9)	106.34(17)	O(4)-C(26)-C(16)	107.92(17)
C(2)-C(8)-C(9)	109.85(18)	C(28)-C(26)-C(16)	112.29(19)
O(3)-C(8)-C(15)	106.30(17)	C(25)-C(26)-C(16)	110.36(18)
C(2)-C(8)-C(15)	113.08(18)	C(28)-C(27)-C(32)	120.9(3)
C(9)-C(8)-C(15)	111.15(17)	C(27)-C(28)-C(29)	119.0(3)
C(10)-C(9)-C(14)	118.8(2)	C(27)-C(28)-C(26)	121.0(2)
C(10)-C(9)-C(8)	123.0(2)	C(29)-C(28)-C(26)	119.8(2)
C(14)-C(9)-C(8)	118.2(2)	C(30)-C(29)-C(28)	120.7(3)
C(9)-C(10)-C(11)	120.8(2)	C(29)-C(30)-C(31)	119.8(3)
C(12)-C(11)-C(10)	119.5(3)	C(32)-C(31)-C(30)	120.1(3)
C(11)-C(12)-C(13)	120.5(2)	C(31)-C(32)-C(27)	119.4(3)
C(12)-C(13)-C(14)	119.8(2)	C(36)-C(35)-C(41)	123.8(2)
C(13)-C(14)-C(9)	120.5(2)	C(36)-C(35)-Rh(1)	70.77(15)
O(2)-C(15)-C(16)	104.60(17)	C(41)-C(35)-Rh(1)	110.26(16)
O(2)-C(15)-C(8)	113.61(18)	C(35)-C(36)-C(37)	126.1(2)
C(16)-C(15)-C(8)	111.45(18)	C(35)-C(36)-Rh(1)	73.61(14)
O(1)-C(16)-C(15)	104.45(18)	C(37)-C(36)-Rh(1)	106.97(17)
O(1)-C(16)-C(26)	110.04(18)	C(36)-C(37)-C(38)	113.4(2)
C(15)-C(16)-C(26)	113.16(18)	C(37)-C(38)-C(39)	113.3(2)
O(1)-C(17)-O(2)	105.60(17)	C(40)-C(39)-C(38)	122.7(2)
O(1)-C(17)-C(18)	108.0(2)	C(40)-C(39)-Rh(1)	69.58(13)
O(2)-C(17)-C(18)	108.9(2)	C(38)-C(39)-Rh(1)	112.99(16)
O(1)-C(17)-C(19)	110.7(2)	C(39)-C(40)-C(42)	126.5(2)
O(2)-C(17)-C(19)	109.98(19)	C(39)-C(40)-Rh(1)	71.36(13)
C(18)-C(17)-C(19)	113.3(2)	C(42)-C(40)-Rh(1)	111.08(16)
C(25)-C(20)-C(21)	120.7(3)	C(35)-C(41)-C(42)	112.2(2)
C(22)-C(21)-C(20)	120.2(3)	C(40)-C(42)-C(41)	113.5(2)
C(23)-C(22)-C(21)	119.8(3)	Cl(5)-C(43)-Cl(4)	114.2(3)
C(22)-C(23)-C(24)	120.1(3)	C(33)-N(1)-C(34)	112.9(2)

C(33)-N(1)-P(1)	127.56(16)	C(39)-Rh(1)-P(1)	94.17(6)
C(34)-N(1)-P(1)	119.52(17)	C(36)-Rh(1)-P(1)	155.60(7)
C(16)-O(1)-C(17)	108.22(17)	C(40)-Rh(1)-C(35)	81.04(9)
C(15)-O(2)-C(17)	110.19(18)	C(39)-Rh(1)-C(35)	89.20(9)
C(8)-O(3)-P(1)	130.68(14)	C(36)-Rh(1)-C(35)	35.62(9)
C(26)-O(4)-P(1)	126.17(14)	P(1)-Rh(1)-C(35)	168.73(7)
O(4)-P(1)-O(3)	103.16(8)	C(40)-Rh(1)-Cl(1)	158.25(7)
O(4)-P(1)-N(1)	98.40(10)	C(39)-Rh(1)-Cl(1)	162.17(6)
O(3)-P(1)-N(1)	111.29(10)	C(36)-Rh(1)-Cl(1)	88.55(7)
O(4)-P(1)-Rh(1)	119.67(7)	P(1)-Rh(1)-Cl(1)	88.50(2)
O(3)-P(1)-Rh(1)	110.11(6)	C(35)-Rh(1)-Cl(1)	91.57(7)
N(1)-P(1)-Rh(1)	113.35(8)		
C(40)-Rh(1)-C(39)	39.06(9)		
C(40)-Rh(1)-C(36)	96.83(9)		
C(39)-Rh(1)-C(36)	81.75(9)		
C(40)-Rh(1)-P(1)	94.83(7)		

Symmetry transformations used to generate equivalent atoms:

Table A.3.5. Anisotropic displacement parameters ($Å^2 x\ 10^3$)for **T2**. The anisotropic displacement factor exponent takes the form: $-2p^2[\ h^2 a^{*2} U^{11} + ... + 2\ h\ k\ a^*\ b^*\ U^{12}\ ]$

	U^{11}	U^{22}	U^{33}	U^{23}	U^{13}	U^{12}
C(1)	24(1)	34(2)	30(1)	8(1)	-1(1)	-1(1)
C(2)	15(1)	12(1)	15(1)	0(1)	1(1)	0(1)
C(3)	16(1)	19(1)	20(1)	-1(1)	5(1)	-1(1)
C(4)	17(1)	20(1)	32(1)	-4(1)	3(1)	6(1)
C(5)	30(1)	17(1)	31(1)	-2(1)	-2(1)	6(1)
C(6)	30(1)	13(1)	28(1)	-1(1)	3(1)	0(1)
C(7)	20(1)	15(1)	21(1)	0(1)	0(1)	-1(1)
C(8)	11(1)	11(1)	13(1)	0(1)	1(1)	-1(1)
C(9)	15(1)	14(1)	12(1)	0(1)	1(1)	2(1)
C(10)	24(1)	16(1)	15(1)	1(1)	0(1)	-3(1)
C(11)	34(1)	26(1)	17(1)	7(1)	-2(1)	-6(1)
C(12)	34(1)	36(2)	13(1)	4(1)	-2(1)	-6(1)
C(13)	26(1)	27(1)	13(1)	-2(1)	-3(1)	-1(1)
C(14)	19(1)	18(1)	17(1)	0(1)	-1(1)	-2(1)
C(15)	12(1)	15(1)	12(1)	0(1)	0(1)	-1(1)
C(16)	13(1)	15(1)	14(1)	1(1)	-1(1)	2(1)
C(17)	14(1)	20(1)	17(1)	-3(1)	-1(1)	0(1)
C(18)	15(1)	35(2)	31(1)	2(1)	2(1)	-2(1)
C(19)	18(1)	28(1)	19(1)	1(1)	-4(1)	2(1)
C(20)	18(1)	40(2)	32(1)	15(1)	9(1)	7(1)
C(21)	21(1)	53(2)	41(2)	17(2)	17(1)	8(1)
C(22)	15(1)	59(2)	28(1)	23(1)	2(1)	-7(1)
C(23)	31(1)	29(2)	22(1)	7(1)	1(1)	-14(1)
C(24)	24(1)	23(1)	18(1)	0(1)	5(1)	-6(1)
C(25)	12(1)	23(1)	14(1)	5(1)	1(1)	-3(1)
C(26)	11(1)	16(1)	13(1)	0(1)	1(1)	1(1)
C(27)	19(1)	20(1)	21(1)	2(1)	7(1)	3(1)
C(28)	15(1)	19(1)	16(1)	-2(1)	5(1)	-1(1)
C(29)	20(1)	22(1)	18(1)	-2(1)	3(1)	-5(1)
C(30)	31(1)	23(1)	28(1)	-9(1)	7(1)	-5(1)

C(31)	36(2)	17(1)	38(2)	-10(1)	18(1)	-3(1)
C(32)	26(1)	18(1)	34(1)	4(1)	12(1)	5(1)
C(33)	22(1)	17(1)	28(1)	10(1)	-5(1)	-3(1)
C(34)	14(1)	24(1)	28(1)	2(1)	1(1)	3(1)
C(35)	20(1)	15(1)	20(1)	-3(1)	1(1)	-5(1)
C(36)	14(1)	19(1)	26(1)	2(1)	-3(1)	-4(1)
C(37)	14(1)	23(1)	32(1)	-1(1)	3(1)	-3(1)
C(38)	19(1)	23(1)	27(1)	-2(1)	9(1)	-4(1)
C(39)	17(1)	19(1)	14(1)	0(1)	2(1)	-4(1)
C(40)	16(1)	16(1)	14(1)	0(1)	2(1)	-1(1)
C(41)	26(1)	12(1)	27(1)	-1(1)	1(1)	-2(1)
C(42)	22(1)	16(1)	23(1)	2(1)	0(1)	1(1)
C(43)	53(2)	53(3)	61(3)	-22(2)	0(2)	-1(2)
Cl(1)	23(1)	25(1)	14(1)	0(1)	-1(1)	-3(1)
Cl(2)	29(1)	36(1)	51(1)	10(1)	12(1)	0(1)
Cl(3)	43(1)	52(1)	45(1)	7(1)	-12(1)	-17(1)
Cl(4)	67(1)	161(2)	131(2)	-45(2)	11(1)	-50(1)
Cl(5)	118(1)	44(1)	90(1)	-13(1)	38(1)	11(1)
N(1)	12(1)	15(1)	20(1)	3(1)	-1(1)	0(1)
O(1)	13(1)	24(1)	17(1)	-5(1)	-2(1)	3(1)
O(2)	12(1)	19(1)	20(1)	-2(1)	-3(1)	-1(1)
O(3)	13(1)	12(1)	12(1)	0(1)	-1(1)	-3(1)
O(4)	12(1)	14(1)	14(1)	3(1)	2(1)	0(1)
P(1)	11(1)	13(1)	11(1)	1(1)	0(1)	-1(1)
Rh(1)	12(1)	13(1)	13(1)	-1(1)	1(1)	-2(1)

Table A.3.6. Hydrogen coordinates (x 10^4) and isotropic displacement parameters ($Å^2$x 10^3) for **T2**.

	x	y	z	U(eq)
H(1A)	2838	6499	6465	35
H(1B)	2339	6103	7605	35
H(3)	2917	5897	169	22
H(4)	3931	4772	129	28
H(5)	2845	3676	402	31
H(6)	767	3716	730	28
H(7)	-256	4845	774	22
H(10)	1123	7550	-575	22
H(11)	691	7960	-2527	31
H(12)	-330	7185	-3883	34
H(13)	-841	5989	-3335	26
H(14)	-349	5568	-1414	21
H(15)	-556	5913	1884	15
H(16)	-625	7384	1073	17
H(18A)	-3702	5917	1573	40
H(18B)	-4021	5769	213	40
H(18C)	-4469	6500	822	40
H(19A)	-3383	7290	-717	33
H(19B)	-2938	6571	-1362	33
H(19C)	-1978	7161	-897	33
H(20)	-2599	7763	3976	35
H(21)	-4100	7240	5148	45
H(22)	-4052	5985	5580	40
H(23)	-2456	5265	4937	33
H(24)	-921	5791	3803	26
H(27)	-1566	8375	1796	24
H(29)	625	7880	4648	24
H(30)	709	9123	5174	33
H(31)	-405	9991	4045	36
H(32)	-1491	9625	2314	31

H(33A)	2179	5012	2983	34
H(33B)	999	5459	3304	34
H(33C)	2057	5343	4274	34
H(34A)	4079	5957	3914	33
H(34B)	4136	6533	2863	33
H(34C)	4069	5682	2580	33
H(35)	3630	9214	4061	22
H(36)	5138	8438	3809	24
H(37A)	5828	7990	1996	28
H(37B)	5932	8852	1856	28
H(38A)	4944	8138	187	27
H(38B)	4385	8912	507	27
H(39)	3113	7605	508	20
H(40)	1457	8236	990	18
H(41A)	3914	9704	1755	26
H(41B)	3001	10043	2666	26
H(42A)	1398	9386	1927	24
H(42B)	2116	9526	753	24
H(43A)	3121	8394	6801	67
H(43B)	3394	8277	8176	67

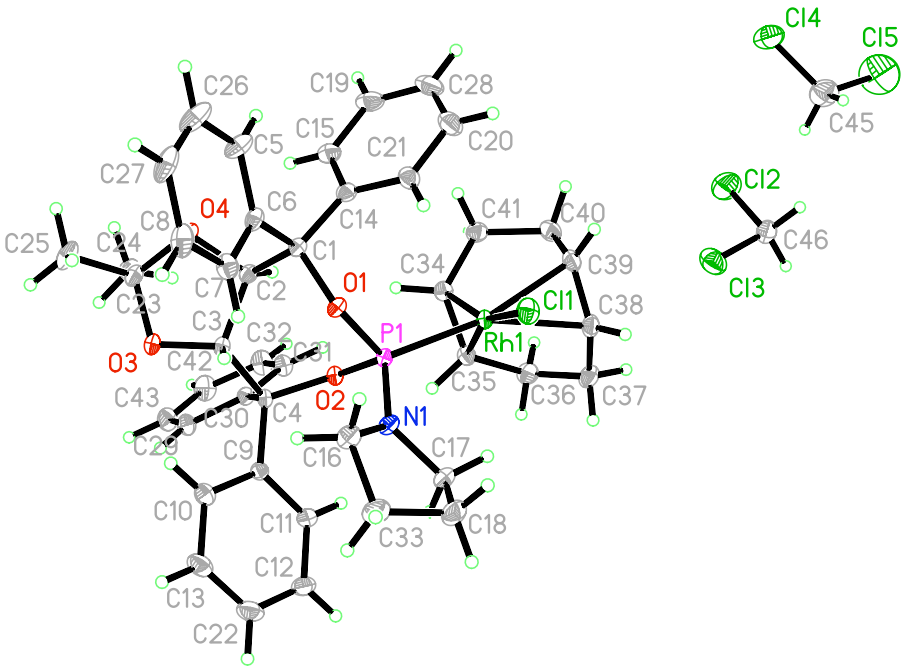

Table A.3.7. Crystal data and structure refinement for **T1**.

Identification code	**T1**	
Empirical formula	$C_{45}H_{52}Cl_5NO_4PRh$	
Formula weight	982.01	
Temperature	120 K	
Wavelength	0.71073 Å	
Crystal system	Monoclinic	
Space group	$P2_1$	
Unit cell dimensions	a = 10.8926(7) Å	α= 90°.
	b = 18.1189(11) Å	β= 91.835(3)°.
	c = 11.2230(7) Å	γ = 90°.
Volume	2213.9(2) $Å^3$	
Z	2	
Density (calculated)	1.473 Mg/m^3	
Absorption coefficient	0.767 mm^{-1}	
F(000)	1012	

Crystal size	0.32 x 0.30 x 0.26 mm^3
Theta range for data collection	2.14 to 35.63°.
Index ranges	-17<=h<=17, -29<=k<=29, -18<=l<=17
Reflections collected	77157
Independent reflections	20295 [R(int) = 0.0257]
Completeness to theta = 35.63°	100.0 %
Absorption correction	Semi-empirical from equivalents
Max. and min. transmission	0.8249 and 0.7898
Refinement method	Full-matrix least-squares on F^2
Data / restraints / parameters	20295 / 1 / 517
Goodness-of-fit on F^2	1.018
Final R indices [I>2sigma(I)]	R1 = 0.0232, wR2 = 0.0574
R indices (all data)	R1 = 0.0246, wR2 = 0.0581
Absolute structure parameter	-0.016(8)
Largest diff. peak and hole	1.092 and -0.978 e.$Å^{-3}$

Table A.3.8. Atomic coordinates (x 10^4) and equivalent isotropic displacement parameters ($Å^2$x 10^3) for **T1**. U(eq) is defined as one third of the trace of the orthogonalized U^{ij} tensor.

	x	y	z	U(eq)
C(1)	-688(1)	709(1)	7937(1)	13(1)
C(2)	-1052(1)	547(1)	6607(1)	14(1)
C(3)	-697(1)	-230(1)	6211(1)	13(1)
C(4)	541(1)	-227(1)	5541(1)	12(1)
C(5)	-2589(1)	816(1)	9192(1)	23(1)
C(6)	-1638(1)	378(1)	8768(1)	15(1)
C(7)	-1592(1)	-365(1)	9092(1)	18(1)
C(8)	-2481(1)	-667(1)	9816(1)	24(1)
C(9)	1168(1)	-978(1)	5536(1)	13(1)
C(10)	534(1)	-1632(1)	5753(1)	19(1)
C(11)	2408(1)	-1018(1)	5240(1)	16(1)
C(12)	3007(1)	-1692(1)	5198(1)	21(1)
C(13)	1139(1)	-2312(1)	5707(1)	24(1)
C(14)	-517(1)	1527(1)	8181(1)	15(1)
C(15)	-1110(1)	2061(1)	7475(1)	19(1)
C(16)	1754(1)	-987(1)	8671(1)	19(1)
C(17)	3694(1)	-502(1)	7975(1)	18(1)
C(18)	3942(1)	-1072(1)	8945(1)	24(1)
C(19)	-1039(1)	2806(1)	7778(1)	25(1)
C(20)	244(1)	2499(1)	9491(1)	26(1)
C(21)	178(1)	1753(1)	9187(1)	19(1)
C(22)	2373(1)	-2343(1)	5435(1)	24(1)
C(23)	-2683(1)	64(1)	5503(1)	17(1)
C(24)	-2777(1)	458(1)	4309(1)	21(1)
C(25)	-3867(1)	-315(1)	5834(1)	27(1)
C(26)	-3469(1)	511(1)	9928(1)	30(1)
C(27)	-3415(1)	-228(1)	10237(1)	28(1)
C(28)	-372(1)	3025(1)	8793(1)	28(1)
C(29)	-213(1)	-429(1)	3421(1)	17(1)
C(30)	348(1)	44(1)	4262(1)	13(1)
C(31)	674(1)	753(1)	3905(1)	16(1)

C(32)	416(1)	990(1)	2737(1)	22(1)
C(33)	2784(1)	-1552(1)	8874(1)	25(1)
C(34)	2212(1)	1947(1)	6321(1)	15(1)
C(35)	3278(1)	1549(1)	6034(1)	15(1)
C(36)	4523(1)	1910(1)	5841(1)	21(1)
C(37)	5339(1)	1941(1)	6985(1)	22(1)
C(38)	4626(1)	2057(1)	8100(1)	19(1)
C(39)	3669(1)	2544(1)	8237(1)	19(1)
C(40)	3218(1)	3082(1)	7284(1)	22(1)
C(41)	2140(1)	2771(1)	6521(1)	20(1)
C(42)	-179(1)	526(1)	1926(1)	24(1)
C(43)	-484(1)	-187(1)	2273(1)	21(1)
C(45)	6689(2)	7108(1)	7423(2)	40(1)
C(46)	6900(1)	4752(1)	7696(1)	26(1)
Cl(1)	3102(1)	1037(1)	9901(1)	20(1)
Cl(2)	5966(1)	5338(1)	6808(1)	46(1)
Cl(3)	6182(1)	3878(1)	7841(1)	35(1)
Cl(4)	5091(1)	7280(1)	7392(1)	58(1)
Cl(5)	7571(1)	7914(1)	7400(1)	78(1)
N(1)	2348(1)	-391(1)	8009(1)	14(1)
O(1)	445(1)	305(1)	8221(1)	13(1)
O(2)	1332(1)	315(1)	6140(1)	12(1)
O(3)	-1714(1)	-479(1)	5494(1)	16(1)
O(4)	-2352(1)	567(1)	6438(1)	19(1)
P(1)	1729(1)	384(1)	7545(1)	11(1)
Rh(1)	2890(1)	1400(1)	7862(1)	12(1)

Table A.3.9. Bond lengths [Å] and angles [°] for **T1**.

C(1)-O(1)	1.4607(13)	C(20)-C(21)	1.3953(19)
C(1)-C(14)	1.5188(15)	C(23)-O(4)	1.4275(15)
C(1)-C(6)	1.5371(15)	C(23)-O(3)	1.4429(15)
C(1)-C(2)	1.5594(15)	C(23)-C(25)	1.5171(17)
C(2)-O(4)	1.4228(13)	C(23)-C(24)	1.5188(18)
C(2)-C(3)	1.5291(16)	C(26)-C(27)	1.386(2)
C(3)-O(3)	1.4210(13)	C(29)-C(43)	1.3844(17)
C(3)-C(4)	1.5655(14)	C(29)-C(30)	1.4001(15)
C(4)-O(2)	1.4569(12)	C(30)-C(31)	1.3938(16)
C(4)-C(9)	1.5214(15)	C(31)-C(32)	1.3987(16)
C(4)-C(30)	1.5260(14)	C(32)-C(42)	1.3847(19)
C(5)-C(26)	1.3994(19)	C(34)-C(35)	1.4131(16)
C(5)-C(6)	1.3999(17)	C(34)-C(41)	1.5125(17)
C(6)-C(7)	1.3947(17)	C(34)-Rh(1)	2.1071(11)
C(7)-C(8)	1.3959(17)	C(35)-C(36)	1.5270(16)
C(8)-C(27)	1.385(2)	C(35)-Rh(1)	2.1252(11)
C(9)-C(10)	1.3960(16)	C(36)-C(37)	1.5387(19)
C(9)-C(11)	1.4029(15)	C(37)-C(38)	1.5086(19)
C(10)-C(13)	1.4004(18)	C(38)-C(39)	1.3781(18)
C(11)-C(12)	1.3877(17)	C(38)-Rh(1)	2.2439(11)
C(12)-C(22)	1.396(2)	C(39)-C(40)	1.5171(18)
C(13)-C(22)	1.389(2)	C(39)-Rh(1)	2.2749(12)
C(14)-C(15)	1.3948(16)	C(40)-C(41)	1.5382(18)
C(14)-C(21)	1.4004(16)	C(42)-C(43)	1.392(2)
C(15)-C(19)	1.3941(18)	C(45)-Cl(5)	1.750(2)
C(16)-N(1)	1.4724(15)	C(45)-Cl(4)	1.769(2)
C(16)-C(33)	1.5300(18)	C(46)-Cl(2)	1.7585(16)
C(17)-N(1)	1.4824(14)	C(46)-Cl(3)	1.7756(16)
C(17)-C(18)	1.5176(18)	Cl(1)-Rh(1)	2.3842(3)
C(18)-C(33)	1.532(2)	N(1)-P(1)	1.6355(10)
C(19)-C(28)	1.389(2)	O(1)-P(1)	1.6184(8)
C(20)-C(28)	1.392(2)	O(2)-P(1)	1.6263(8)
		P(1)-Rh(1)	2.2547(3)

O(1)-C(1)-C(14)	110.61(8)	N(1)-C(17)-C(18)	103.12(10)
O(1)-C(1)-C(6)	104.68(8)	C(17)-C(18)-C(33)	102.80(10)
C(14)-C(1)-C(6)	110.60(9)	C(28)-C(19)-C(15)	119.97(13)
O(1)-C(1)-C(2)	107.60(8)	C(28)-C(20)-C(21)	120.37(13)
C(14)-C(1)-C(2)	112.42(9)	C(20)-C(21)-C(14)	120.14(12)
C(6)-C(1)-C(2)	110.63(9)	C(13)-C(22)-C(12)	119.76(12)
O(4)-C(2)-C(3)	104.09(9)	O(4)-C(23)-O(3)	105.76(9)
O(4)-C(2)-C(1)	110.14(9)	O(4)-C(23)-C(25)	107.79(10)
C(3)-C(2)-C(1)	113.08(9)	O(3)-C(23)-C(25)	108.72(10)
O(3)-C(3)-C(2)	104.92(8)	O(4)-C(23)-C(24)	110.93(10)
O(3)-C(3)-C(4)	113.35(9)	O(3)-C(23)-C(24)	110.08(10)
C(2)-C(3)-C(4)	111.53(8)	C(25)-C(23)-C(24)	113.25(10)
O(2)-C(4)-C(9)	110.20(8)	C(27)-C(26)-C(5)	120.36(13)
O(2)-C(4)-C(30)	106.18(8)	C(8)-C(27)-C(26)	119.69(12)
C(9)-C(4)-C(30)	109.46(8)	C(19)-C(28)-C(20)	119.75(12)
O(2)-C(4)-C(3)	106.61(8)	C(43)-C(29)-C(30)	120.61(11)
C(9)-C(4)-C(3)	113.16(8)	C(31)-C(30)-C(29)	118.67(10)
C(30)-C(4)-C(3)	110.97(8)	C(31)-C(30)-C(4)	122.59(9)
C(26)-C(5)-C(6)	120.29(13)	C(29)-C(30)-C(4)	118.71(9)
C(7)-C(6)-C(5)	118.70(11)	C(30)-C(31)-C(32)	120.44(11)
C(7)-C(6)-C(1)	120.95(10)	C(42)-C(32)-C(31)	120.35(12)
C(5)-C(6)-C(1)	120.33(11)	C(16)-C(33)-C(18)	103.11(10)
C(6)-C(7)-C(8)	120.65(12)	C(35)-C(34)-C(41)	125.80(10)
C(27)-C(8)-C(7)	120.30(13)	C(35)-C(34)-Rh(1)	71.19(6)
C(10)-C(9)-C(11)	118.87(10)	C(41)-C(34)-Rh(1)	111.17(8)
C(10)-C(9)-C(4)	122.22(9)	C(34)-C(35)-C(36)	123.59(10)
C(11)-C(9)-C(4)	118.81(9)	C(34)-C(35)-Rh(1)	69.81(6)
C(9)-C(10)-C(13)	120.34(11)	C(36)-C(35)-Rh(1)	113.34(8)
C(12)-C(11)-C(9)	120.71(11)	C(35)-C(36)-C(37)	112.91(10)
C(11)-C(12)-C(22)	120.08(12)	C(38)-C(37)-C(36)	113.47(10)
C(22)-C(13)-C(10)	120.21(12)	C(39)-C(38)-C(37)	126.37(12)
C(15)-C(14)-C(21)	118.96(11)	C(39)-C(38)-Rh(1)	73.48(7)
C(15)-C(14)-C(1)	121.54(10)	C(37)-C(38)-Rh(1)	106.32(8)
C(21)-C(14)-C(1)	119.34(10)	C(38)-C(39)-C(40)	124.23(12)
C(19)-C(15)-C(14)	120.79(12)	C(38)-C(39)-Rh(1)	71.02(7)
N(1)-C(16)-C(33)	103.50(10)	C(40)-C(39)-Rh(1)	110.17(8)

C(39)-C(40)-C(41)	112.42(10)
C(34)-C(41)-C(40)	113.73(10)
C(32)-C(42)-C(43)	119.36(11)
C(29)-C(43)-C(42)	120.52(11)
Cl(5)-C(45)-Cl(4)	113.10(11)
Cl(2)-C(46)-Cl(3)	110.00(8)
C(16)-N(1)-C(17)	111.36(9)
C(16)-N(1)-P(1)	127.40(8)
C(17)-N(1)-P(1)	120.45(8)
C(1)-O(1)-P(1)	126.14(7)
C(4)-O(2)-P(1)	129.39(7)
C(3)-O(3)-C(23)	109.69(9)
C(2)-O(4)-C(23)	108.02(8)
O(1)-P(1)-O(2)	103.96(4)
O(1)-P(1)-N(1)	97.37(4)
O(2)-P(1)-N(1)	109.63(5)
O(1)-P(1)-Rh(1)	119.13(3)
O(2)-P(1)-Rh(1)	110.27(3)
N(1)-P(1)-Rh(1)	115.28(4)
C(34)-Rh(1)-C(35)	39.01(4)
C(34)-Rh(1)-C(38)	96.89(4)
C(35)-Rh(1)-C(38)	81.64(4)
C(34)-Rh(1)-P(1)	94.27(3)
C(35)-Rh(1)-P(1)	94.55(3)
C(38)-Rh(1)-P(1)	156.70(3)
C(34)-Rh(1)-C(39)	80.89(4)
C(35)-Rh(1)-C(39)	88.75(4)
C(38)-Rh(1)-C(39)	35.50(5)
P(1)-Rh(1)-C(39)	167.77(3)
C(34)-Rh(1)-Cl(1)	159.72(3)
C(35)-Rh(1)-Cl(1)	160.95(3)
C(38)-Rh(1)-Cl(1)	88.66(3)
P(1)-Rh(1)-Cl(1)	87.891(11)
C(39)-Rh(1)-Cl(1)	92.84(3)

Symmetry transformations used to generate equivalent atoms:

Table A.3.10. Anisotropic displacement parameters ($Å^2$x 10^3)for **T1**. The anisotropic displacement factor exponent takes the form: $-2\pi^2[h^2a^{*2}U^{11} + ... + 2 h k a^* b^* U^{12}]$

	U^{11}	U^{22}	U^{33}	U^{23}	U^{13}	U^{12}
C(1)	11(1)	15(1)	12(1)	1(1)	1(1)	1(1)
C(2)	12(1)	16(1)	13(1)	0(1)	0(1)	1(1)
C(3)	11(1)	15(1)	13(1)	0(1)	-1(1)	-2(1)
C(4)	11(1)	12(1)	12(1)	0(1)	0(1)	-2(1)
C(5)	15(1)	32(1)	22(1)	7(1)	5(1)	5(1)
C(6)	12(1)	21(1)	12(1)	2(1)	1(1)	-2(1)
C(7)	20(1)	21(1)	15(1)	1(1)	2(1)	-6(1)
C(8)	23(1)	30(1)	18(1)	5(1)	1(1)	-11(1)
C(9)	14(1)	12(1)	13(1)	0(1)	-1(1)	0(1)
C(10)	20(1)	14(1)	24(1)	0(1)	1(1)	-2(1)
C(11)	15(1)	16(1)	18(1)	-1(1)	2(1)	2(1)
C(12)	19(1)	22(1)	22(1)	-3(1)	0(1)	7(1)
C(13)	30(1)	13(1)	29(1)	0(1)	1(1)	-1(1)
C(14)	14(1)	16(1)	16(1)	-1(1)	3(1)	0(1)
C(15)	19(1)	17(1)	21(1)	2(1)	2(1)	3(1)
C(16)	18(1)	17(1)	23(1)	7(1)	2(1)	0(1)
C(17)	12(1)	21(1)	20(1)	1(1)	0(1)	3(1)
C(18)	20(1)	24(1)	27(1)	4(1)	-6(1)	4(1)
C(19)	26(1)	16(1)	34(1)	2(1)	9(1)	5(1)
C(20)	29(1)	24(1)	25(1)	-9(1)	6(1)	-5(1)
C(21)	20(1)	20(1)	17(1)	-3(1)	2(1)	-2(1)
C(22)	30(1)	16(1)	27(1)	-2(1)	-3(1)	7(1)
C(23)	11(1)	22(1)	18(1)	0(1)	-1(1)	0(1)
C(24)	18(1)	27(1)	18(1)	1(1)	-3(1)	2(1)
C(25)	12(1)	35(1)	33(1)	5(1)	2(1)	-4(1)
C(26)	15(1)	47(1)	27(1)	12(1)	7(1)	5(1)
C(27)	14(1)	48(1)	21(1)	10(1)	1(1)	-8(1)
C(28)	33(1)	17(1)	34(1)	-7(1)	13(1)	-1(1)
C(29)	18(1)	18(1)	14(1)	-1(1)	-2(1)	-2(1)
C(30)	13(1)	14(1)	11(1)	0(1)	0(1)	0(1)
C(31)	18(1)	17(1)	13(1)	2(1)	-1(1)	-2(1)

C(32)	26(1)	22(1)	16(1)	6(1)	-2(1)	-3(1)
C(33)	23(1)	18(1)	34(1)	9(1)	-1(1)	4(1)
C(34)	16(1)	15(1)	14(1)	1(1)	-1(1)	-1(1)
C(35)	16(1)	16(1)	14(1)	0(1)	2(1)	-2(1)
C(36)	18(1)	21(1)	23(1)	0(1)	6(1)	-3(1)
C(37)	13(1)	24(1)	30(1)	0(1)	2(1)	-2(1)
C(38)	15(1)	18(1)	24(1)	0(1)	-4(1)	-4(1)
C(39)	20(1)	15(1)	21(1)	-4(1)	-2(1)	-3(1)
C(40)	24(1)	14(1)	27(1)	-1(1)	-1(1)	-1(1)
C(41)	19(1)	16(1)	24(1)	2(1)	-1(1)	2(1)
C(42)	27(1)	29(1)	14(1)	3(1)	-4(1)	-1(1)
C(43)	22(1)	26(1)	15(1)	-3(1)	-4(1)	-1(1)
C(45)	41(1)	33(1)	47(1)	6(1)	0(1)	5(1)
C(46)	20(1)	32(1)	27(1)	-5(1)	-2(1)	0(1)
Cl(1)	22(1)	25(1)	13(1)	1(1)	-2(1)	-1(1)
Cl(2)	44(1)	46(1)	47(1)	-1(1)	-12(1)	16(1)
Cl(3)	35(1)	35(1)	36(1)	-12(1)	11(1)	-8(1)
Cl(4)	40(1)	77(1)	58(1)	-25(1)	-6(1)	24(1)
Cl(5)	83(1)	39(1)	110(1)	18(1)	11(1)	-15(1)
N(1)	11(1)	16(1)	16(1)	4(1)	2(1)	1(1)
O(1)	11(1)	16(1)	13(1)	2(1)	1(1)	0(1)
O(2)	12(1)	13(1)	11(1)	0(1)	0(1)	-2(1)
O(3)	11(1)	18(1)	20(1)	-2(1)	-2(1)	-2(1)
O(4)	12(1)	27(1)	17(1)	-3(1)	-2(1)	4(1)
P(1)	10(1)	12(1)	11(1)	1(1)	0(1)	-1(1)
Rh(1)	12(1)	13(1)	12(1)	0(1)	-1(1)	-2(1)

Table A.3.11. Hydrogen coordinates (x 10^4) and isotropic displacement parameters ($Å^2$x 10^3) for **T1**.

	x	y	z	U(eq)
H(2)	-675	914	6092	16
H(3)	-609	-547	6916	15
H(5)	-2635	1313	8983	27
H(7)	-962	-662	8823	22
H(8)	-2446	-1164	10017	29
H(10)	-294	-1615	5930	23
H(11)	2832	-587	5070	20
H(12)	3832	-1711	5011	25
H(13)	713	-2745	5859	29
H(15)	-1559	1918	6795	23
H(16A)	1074	-1198	8208	23
H(16B)	1454	-808	9423	23
H(17A)	4133	-47	8146	21
H(17B)	3930	-686	7203	21
H(18A)	4042	-839	9721	29
H(18B)	4670	-1359	8787	29
H(19)	-1438	3157	7300	30
H(20)	702	2646	10163	31
H(21)	596	1405	9654	22
H(22)	2775	-2795	5411	29
H(24A)	-3468	787	4299	31
H(24B)	-2883	101	3682	31
H(24C)	-2039	735	4192	31
H(25A)	-3749	-559	6588	40
H(25B)	-4092	-671	5233	40
H(25C)	-4508	46	5889	40
H(26)	-4094	807	10211	35
H(27)	-4002	-430	10725	33
H(28)	-337	3521	9006	33
H(29)	-405	-910	3637	20

H(31)	1066	1070	4446	19
H(32)	646	1461	2505	26
H(33A)	2813	-1898	8216	30
H(33B)	2681	-1823	9609	30
H(34)	1451	1733	5983	18
H(35)	3117	1112	5538	18
H(36A)	4392	2408	5546	25
H(36B)	4948	1636	5237	25
H(37A)	5796	1483	7061	27
H(37B)	5927	2339	6914	27
H(38)	5094	1949	8840	23
H(39)	3572	2717	9056	23
H(40A)	3890	3201	6771	26
H(40B)	2960	3536	7663	26
H(41A)	1378	2883	6908	24
H(41B)	2118	3018	5753	24
H(42)	-374	689	1158	28
H(43)	-873	-503	1728	25
H(45A)	6909	6829	8137	49
H(45B)	6885	6806	6741	49
H(46A)	7038	4970	8478	32
H(46B)	7690	4691	7334	32

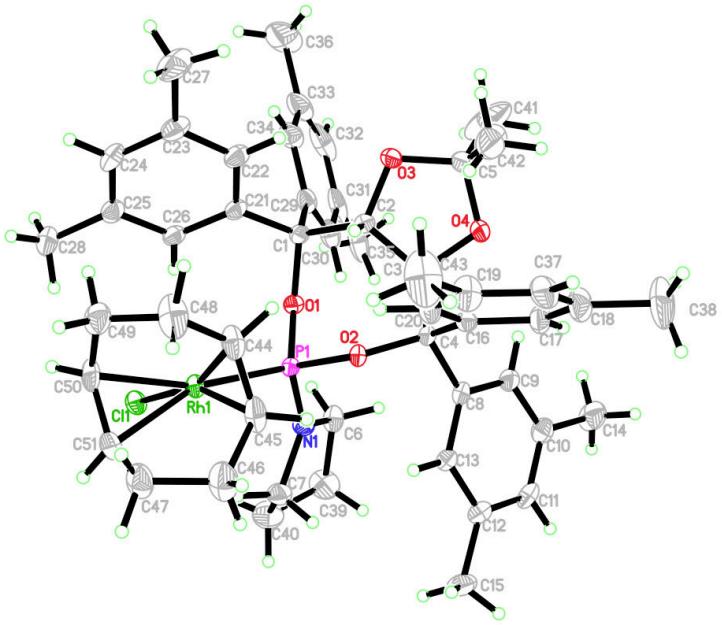

Table A.3.12. Crystal data and structure refinement for **T4**.

Identification code	rovis73_0m	
Empirical formula	C_{51} H_{64} Cl N O_4 P Rh	
Formula weight	924.36	
Temperature	120 K	
Wavelength	0.71073 Å	
Crystal system	Orthorhombic	
Space group	P $2_12_12_1$	
Unit cell dimensions	*a* = 15.3754(4) Å	α = 90°
	b = 17.3853(4) Å	β = 90°
	c = 18.1214(4) Å	γ = 90°
Volume	4844.0(2) $Å^3$	
Z	4	
Density (calculated)	1.268 Mg/m^3	
Absorption coefficient	0.483 mm^{-1}	
F(000)	1944	

Crystal size	0.31 x 0.26 x 0.19 mm^3
Theta range for data collection	2.10 to 36.43°.
Index ranges	-25<=h<=25, -28<=k<=25, -30<=l<=28
Reflections collected	52621
Independent reflections	23450 [R(int) = 0.0546]
Completeness to theta = 36.43°	99.5 %
Absorption correction	Multi-Scan
Max. and min. transmission	0.9159 and 0.8658
Refinement method	Full-matrix least-squares on F^2
Data / restraints / parameters	23450 / 0 / 542
Goodness-of-fit on F^2	1.006
Final R indices [I>2sigma(I)]	R1 = 0.0532, wR2 = 0.1024
R indices (all data)	R1 = 0.0916, wR2 = 0.1182
Absolute structure parameter	-0.030(17)
Largest diff. peak and hole	1.864 and -0.936 e.$Å^{-3}$

Table A.3.13. Atomic coordinates (x 10^4) and equivalent isotropic displacement parameters ($Å^2$x 10^3) for **T4**. U(eq) is defined as one third of the trace of the orthogonalized U^{ij} tensor.

	x	y	z	U(eq)
C(1)	115(2)	5573(1)	-839(1)	17(1)
C(2)	527(2)	4751(1)	-800(1)	18(1)
C(3)	120(2)	4265(1)	-177(1)	18(1)
C(4)	697(1)	4268(1)	527(1)	16(1)
C(5)	244(2)	3536(2)	-1257(2)	36(1)
C(6)	-1015(2)	5763(2)	1276(2)	23(1)
C(7)	162(2)	6373(2)	1953(2)	26(1)
C(8)	181(2)	4065(1)	1222(1)	17(1)
C(9)	-527(2)	3559(1)	1194(2)	21(1)
C(10)	-943(2)	3322(2)	1836(2)	24(1)
C(11)	-654(2)	3611(2)	2508(2)	25(1)
C(12)	33(2)	4131(2)	2553(2)	23(1)
C(13)	453(2)	4344(1)	1898(1)	19(1)
C(14)	-1687(2)	2759(2)	1810(2)	37(1)
C(15)	327(2)	4463(2)	3276(2)	33(1)
C(16)	1486(2)	3731(1)	456(1)	18(1)
C(17)	1388(2)	2939(1)	580(2)	26(1)
C(18)	2094(2)	2444(2)	503(2)	34(1)
C(19)	3008(2)	3517(2)	178(2)	33(1)
C(20)	2295(2)	4005(2)	251(2)	26(1)
C(21)	721(2)	6148(1)	-1216(1)	19(1)
C(22)	1323(2)	5918(2)	-1741(2)	24(1)
C(23)	1814(2)	6454(2)	-2126(2)	29(1)
C(24)	1704(2)	7238(2)	-1971(2)	26(1)
C(25)	1103(2)	7481(2)	-1444(2)	23(1)
C(26)	614(2)	6932(1)	-1076(1)	20(1)
C(27)	2452(2)	6205(2)	-2717(2)	45(1)
C(28)	992(2)	8326(2)	-1273(2)	33(1)
C(29)	-768(2)	5543(1)	-1231(2)	23(1)
C(30)	-1532(2)	5450(1)	-837(2)	26(1)
C(31)	-2339(2)	5401(2)	-1186(2)	35(1)

C(32)	-2349(2)	5438(2)	-1957(2)	45(1)
C(33)	-1597(3)	5526(2)	-2367(2)	39(1)
C(34)	-806(2)	5585(2)	-1996(2)	30(1)
C(35)	-3166(2)	5342(2)	-746(2)	47(1)
C(36)	-1622(3)	5568(2)	-3203(2)	60(1)
C(37)	2903(2)	2736(2)	310(2)	34(1)
C(38)	1982(3)	1595(2)	641(3)	60(1)
C(39)	-1329(2)	6069(2)	2014(2)	39(1)
C(40)	-700(2)	6709(2)	2207(2)	39(1)
C(41)	-492(4)	3227(3)	-1692(2)	115(3)
C(42)	1122(3)	3114(2)	-1364(2)	65(1)
C(43)	3898(2)	3838(2)	-40(3)	61(1)
C(44)	2693(2)	6106(2)	216(2)	29(1)
C(45)	2612(2)	6028(2)	980(2)	29(1)
C(46)	3169(2)	6399(2)	1571(2)	42(1)
C(47)	3379(2)	7236(2)	1405(2)	37(1)
C(48)	3434(2)	6544(2)	-151(2)	45(1)
C(49)	3226(2)	7394(2)	-280(2)	32(1)
C(50)	2602(2)	7729(2)	264(2)	26(1)
C(51)	2644(2)	7648(2)	1019(2)	25(1)
Cl(1)	554(1)	7756(1)	653(1)	21(1)
N(1)	-78(1)	5980(1)	1258(1)	18(1)
O(1)	-70(1)	5823(1)	-90(1)	16(1)
O(2)	1061(1)	5036(1)	596(1)	15(1)
O(3)	363(1)	4325(1)	-1449(1)	23(1)
O(4)	37(1)	3517(1)	-489(1)	23(1)
P(1)	618(1)	5885(1)	583(1)	14(1)
Rh(1)	1663(1)	6806(1)	588(1)	17(1)

Table A.3.14. Bond lengths [Å] and angles [°] for **T4**.

C(1)-O(1)	1.454(3)	C(18)-C(38)	1.508(4)
C(1)-C(21)	1.528(3)	C(19)-C(37)	1.388(4)
C(1)-C(29)	1.533(3)	C(19)-C(20)	1.392(4)
C(1)-C(2)	1.564(3)	C(19)-C(43)	1.531(5)
C(2)-O(3)	1.413(3)	C(21)-C(22)	1.387(4)
C(2)-C(3)	1.542(3)	C(21)-C(26)	1.396(3)
C(3)-O(4)	1.425(3)	C(22)-C(23)	1.387(4)
C(3)-C(4)	1.553(3)	C(23)-C(24)	1.403(4)
C(4)-O(2)	1.454(3)	C(23)-C(27)	1.516(4)
C(4)-C(8)	1.531(3)	C(24)-C(25)	1.393(4)
C(4)-C(16)	1.536(3)	C(25)-C(26)	1.387(4)
C(5)-O(3)	1.428(3)	C(25)-C(28)	1.510(4)
C(5)-O(4)	1.428(3)	C(29)-C(30)	1.384(4)
C(5)-C(41)	1.480(5)	C(29)-C(34)	1.389(4)
C(5)-C(42)	1.548(5)	C(30)-C(31)	1.397(4)
C(6)-N(1)	1.489(3)	C(31)-C(32)	1.399(5)
C(6)-C(39)	1.517(4)	C(31)-C(35)	1.504(5)
C(7)-N(1)	1.479(3)	C(32)-C(33)	1.383(5)
C(7)-C(40)	1.520(4)	C(33)-C(34)	1.393(4)
C(8)-C(13)	1.382(3)	C(33)-C(36)	1.516(5)
C(8)-C(9)	1.400(3)	C(39)-C(40)	1.514(5)
C(9)-C(10)	1.391(4)	C(44)-C(45)	1.395(4)
C(10)-C(11)	1.390(4)	C(44)-C(48)	1.524(4)
C(10)-C(14)	1.507(4)	C(44)-Rh(1)	2.108(3)
C(11)-C(12)	1.392(4)	C(45)-C(46)	1.516(4)
C(12)-C(13)	1.401(4)	C(45)-Rh(1)	2.113(3)
C(12)-C(15)	1.501(4)	C(46)-C(47)	1.521(4)
C(16)-C(20)	1.384(4)	C(47)-C(51)	1.510(4)
C(16)-C(17)	1.402(3)	C(48)-C(49)	1.530(4)
C(17)-C(18)	1.392(4)	C(49)-C(50)	1.495(4)
C(18)-C(37)	1.387(5)	C(50)-C(51)	1.377(4)
		C(50)-Rh(1)	2.236(3)
		C(51)-Rh(1)	2.242(3)
		Cl(1)-Rh(1)	2.3765(6)
		N(1)-P(1)	1.633(2)

O(1)-P(1)	1.6188(18)	C(9)-C(10)-C(14)	121.1(2)
O(2)-P(1)	1.6260(15)	C(10)-C(11)-C(12)	121.9(2)
P(1)-Rh(1)	2.2688(6)	C(11)-C(12)-C(13)	118.2(2)
		C(11)-C(12)-C(15)	121.9(2)
O(1)-C(1)-C(21)	109.92(19)	C(13)-C(12)-C(15)	119.9(3)
O(1)-C(1)-C(29)	105.58(19)	C(8)-C(13)-C(12)	121.2(2)
C(21)-C(1)-C(29)	110.8(2)	C(20)-C(16)-C(17)	118.6(2)
O(1)-C(1)-C(2)	108.03(17)	C(20)-C(16)-C(4)	121.5(2)
C(21)-C(1)-C(2)	111.9(2)	C(17)-C(16)-C(4)	119.9(2)
C(29)-C(1)-C(2)	110.39(19)	C(18)-C(17)-C(16)	120.4(3)
O(3)-C(2)-C(3)	104.53(19)	C(37)-C(18)-C(17)	119.9(3)
O(3)-C(2)-C(1)	111.59(19)	C(37)-C(18)-C(38)	120.1(3)
C(3)-C(2)-C(1)	111.8(2)	C(17)-C(18)-C(38)	120.0(3)
O(4)-C(3)-C(2)	104.21(19)	C(37)-C(19)-C(20)	119.3(3)
O(4)-C(3)-C(4)	112.37(19)	C(37)-C(19)-C(43)	120.3(3)
C(2)-C(3)-C(4)	111.6(2)	C(20)-C(19)-C(43)	120.4(3)
O(2)-C(4)-C(8)	109.89(19)	C(16)-C(20)-C(19)	121.5(3)
O(2)-C(4)-C(16)	105.19(17)	C(22)-C(21)-C(26)	119.1(2)
C(8)-C(4)-C(16)	109.82(19)	C(22)-C(21)-C(1)	121.6(2)
O(2)-C(4)-C(3)	107.06(17)	C(26)-C(21)-C(1)	119.1(2)
C(8)-C(4)-C(3)	112.29(19)	C(23)-C(22)-C(21)	121.0(3)
C(16)-C(4)-C(3)	112.31(19)	C(22)-C(23)-C(24)	119.1(3)
O(3)-C(5)-O(4)	106.7(2)	C(22)-C(23)-C(27)	121.1(3)
O(3)-C(5)-C(41)	108.5(3)	C(24)-C(23)-C(27)	119.8(3)
O(4)-C(5)-C(41)	109.9(3)	C(25)-C(24)-C(23)	120.8(3)
O(3)-C(5)-C(42)	108.2(3)	C(26)-C(25)-C(24)	118.7(2)
O(4)-C(5)-C(42)	107.7(3)	C(26)-C(25)-C(28)	120.6(3)
C(41)-C(5)-C(42)	115.5(4)	C(24)-C(25)-C(28)	120.7(2)
N(1)-C(6)-C(39)	103.8(2)	C(25)-C(26)-C(21)	121.4(2)
N(1)-C(7)-C(40)	102.6(2)	C(30)-C(29)-C(34)	119.0(2)
C(13)-C(8)-C(9)	119.3(2)	C(30)-C(29)-C(1)	121.1(2)
C(13)-C(8)-C(4)	119.4(2)	C(34)-C(29)-C(1)	119.8(2)
C(9)-C(8)-C(4)	121.2(2)	C(29)-C(30)-C(31)	121.9(3)
C(10)-C(9)-C(8)	120.9(2)	C(30)-C(31)-C(32)	117.4(3)
C(11)-C(10)-C(9)	118.6(2)	C(30)-C(31)-C(35)	121.0(3)
C(11)-C(10)-C(14)	120.4(2)	C(32)-C(31)-C(35)	121.6(3)

C(33)-C(32)-C(31)	122.2(3)	C(4)-O(2)-P(1)	132.18(13)
C(32)-C(33)-C(34)	118.6(3)	C(2)-O(3)-C(5)	108.87(19)
C(32)-C(33)-C(36)	121.3(3)	C(3)-O(4)-C(5)	110.29(19)
C(34)-C(33)-C(36)	120.1(4)	O(1)-P(1)-O(2)	102.94(9)
C(29)-C(34)-C(33)	121.0(3)	O(1)-P(1)-N(1)	98.27(9)
C(18)-C(37)-C(19)	120.3(3)	O(2)-P(1)-N(1)	110.82(10)
C(40)-C(39)-C(6)	105.0(2)	O(1)-P(1)-Rh(1)	120.87(7)
C(39)-C(40)-C(7)	101.8(2)	O(2)-P(1)-Rh(1)	110.09(6)
C(45)-C(44)-C(48)	123.2(3)	N(1)-P(1)-Rh(1)	112.94(8)
C(45)-C(44)-Rh(1)	70.90(17)	C(44)-Rh(1)-C(45)	38.60(11)
C(48)-C(44)-Rh(1)	114.36(19)	C(44)-Rh(1)-C(50)	81.13(11)
C(44)-C(45)-C(46)	127.6(3)	C(45)-Rh(1)-C(50)	95.83(12)
C(44)-C(45)-Rh(1)	70.50(17)	C(44)-Rh(1)-C(51)	89.05(12)
C(46)-C(45)-Rh(1)	110.8(2)	C(45)-Rh(1)-C(51)	80.59(10)
C(45)-C(46)-C(47)	112.8(3)	C(50)-Rh(1)-C(51)	35.81(10)
C(51)-C(47)-C(46)	112.7(3)	C(44)-Rh(1)-P(1)	97.06(8)
C(44)-C(48)-C(49)	113.2(3)	C(45)-Rh(1)-P(1)	92.20(8)
C(50)-C(49)-C(48)	114.2(2)	C(50)-Rh(1)-P(1)	164.27(8)
C(51)-C(50)-C(49)	125.9(3)	C(51)-Rh(1)-P(1)	159.80(8)
C(51)-C(50)-Rh(1)	72.33(17)	C(44)-Rh(1)-Cl(1)	162.98(9)
C(49)-C(50)-Rh(1)	107.96(18)	C(45)-Rh(1)-Cl(1)	157.50(10)
C(50)-C(51)-C(47)	122.9(3)	C(50)-Rh(1)-Cl(1)	88.75(8)
C(50)-C(51)-Rh(1)	71.85(17)	C(51)-Rh(1)-Cl(1)	90.70(8)
C(47)-C(51)-Rh(1)	110.82(18)	P(1)-Rh(1)-Cl(1)	88.970(19)
C(7)-N(1)-C(6)	109.9(2)		
C(7)-N(1)-P(1)	121.38(18)		
C(6)-N(1)-P(1)	128.62(18)		
C(1)-O(1)-P(1)	126.59(15)		

Symmetry transformations used to generate equivalent atoms:

Table A.3.15. Anisotropic displacement parameters ($Å^2 x\ 10^3$)for **T4**. The anisotropic displacement factor exponent takes the form: $-2p^2[\ h^2a^{*2}U^{11} + ... + 2\ h\ k\ a^*\ b^*\ U^{12}\ ]$

	U^{11}	U^{22}	U^{33}	U^{23}	U^{13}	U^{12}
C(1)	19(1)	16(1)	16(1)	2(1)	-2(1)	2(1)
C(2)	20(1)	18(1)	15(1)	1(1)	-1(1)	0(1)
C(3)	21(1)	15(1)	18(1)	0(1)	-2(1)	-2(1)
C(4)	19(1)	12(1)	16(1)	1(1)	0(1)	-2(1)
C(5)	62(2)	27(2)	20(1)	-5(1)	5(1)	-14(1)
C(6)	17(1)	20(1)	33(1)	3(1)	4(1)	0(1)
C(7)	28(1)	28(1)	20(1)	-2(1)	4(1)	-3(1)
C(8)	17(1)	15(1)	20(1)	4(1)	1(1)	1(1)
C(9)	24(1)	19(1)	21(1)	2(1)	-2(1)	-3(1)
C(10)	22(1)	24(1)	27(1)	5(1)	1(1)	-3(1)
C(11)	25(1)	24(1)	24(1)	11(1)	3(1)	0(1)
C(12)	25(1)	26(1)	18(1)	5(1)	1(1)	1(1)
C(13)	19(1)	19(1)	18(1)	3(1)	0(1)	-1(1)
C(14)	34(2)	39(2)	37(2)	9(1)	3(2)	-14(2)
C(15)	38(2)	41(2)	18(1)	3(1)	0(1)	-8(1)
C(16)	22(1)	18(1)	15(1)	-1(1)	-2(1)	1(1)
C(17)	30(1)	17(1)	29(1)	2(1)	2(1)	2(1)
C(18)	41(2)	20(1)	42(2)	2(1)	8(2)	8(1)
C(19)	22(1)	31(2)	45(2)	1(1)	5(1)	8(1)
C(20)	26(1)	19(1)	34(2)	1(1)	2(1)	3(1)
C(21)	21(1)	21(1)	15(1)	4(1)	-1(1)	2(1)
C(22)	27(1)	25(1)	19(1)	5(1)	2(1)	6(1)
C(23)	30(2)	35(2)	21(1)	6(1)	8(1)	5(1)
C(24)	27(1)	26(1)	26(1)	12(1)	1(1)	0(1)
C(25)	26(1)	24(1)	20(1)	4(1)	-4(1)	0(1)
C(26)	22(1)	21(1)	16(1)	3(1)	0(1)	2(1)
C(27)	47(2)	48(2)	39(2)	11(2)	25(2)	15(2)
C(28)	44(2)	23(2)	33(2)	7(1)	-1(1)	-6(1)
C(29)	25(1)	15(1)	28(1)	0(1)	-10(1)	2(1)
C(30)	20(1)	18(1)	39(2)	0(1)	-8(1)	-1(1)
C(31)	25(1)	12(1)	66(2)	-5(1)	-16(1)	3(1)

C(32)	41(2)	22(1)	72(3)	-13(2)	-38(2)	9(1)
C(33)	53(2)	25(1)	39(2)	-8(1)	-25(2)	8(2)
C(34)	36(2)	24(1)	30(2)	-2(1)	-14(1)	2(1)
C(35)	22(1)	20(1)	100(3)	1(2)	-20(2)	-4(1)
C(36)	83(3)	55(2)	41(2)	-8(2)	-39(2)	12(2)
C(37)	39(2)	26(1)	38(2)	-5(1)	2(1)	14(1)
C(38)	62(2)	21(1)	97(3)	7(2)	15(3)	12(2)
C(39)	31(2)	45(2)	39(2)	-7(2)	19(1)	-6(1)
C(40)	42(2)	42(2)	35(2)	-6(2)	12(1)	4(2)
C(41)	175(6)	133(5)	37(2)	36(3)	-47(3)	-126(5)
C(42)	111(4)	35(2)	48(2)	8(2)	32(2)	29(2)
C(43)	28(2)	46(2)	109(4)	2(2)	22(2)	6(2)
C(44)	21(1)	18(1)	46(2)	-2(1)	10(1)	1(1)
C(45)	20(1)	18(1)	49(2)	4(1)	-11(1)	-1(1)
C(46)	35(2)	33(2)	58(2)	7(2)	-18(2)	-6(1)
C(47)	36(2)	30(1)	46(2)	4(1)	-17(2)	-11(1)
C(48)	30(2)	32(2)	72(2)	-4(2)	28(2)	-2(1)
C(49)	29(2)	30(1)	37(2)	3(1)	9(1)	-6(1)
C(50)	22(1)	16(1)	40(2)	3(1)	6(1)	-7(1)
C(51)	24(1)	19(1)	31(2)	-2(1)	-2(1)	-6(1)
Cl(1)	21(1)	17(1)	25(1)	-2(1)	1(1)	2(1)
N(1)	18(1)	20(1)	17(1)	-2(1)	4(1)	-1(1)
O(1)	16(1)	17(1)	15(1)	0(1)	0(1)	1(1)
O(2)	16(1)	12(1)	18(1)	2(1)	1(1)	-1(1)
O(3)	37(1)	17(1)	15(1)	-2(1)	-4(1)	4(1)
O(4)	34(1)	16(1)	20(1)	-1(1)	-5(1)	-3(1)
P(1)	14(1)	13(1)	15(1)	1(1)	1(1)	0(1)
Rh(1)	15(1)	14(1)	21(1)	0(1)	1(1)	-1(1)

Table A.3.16. Hydrogen coordinates (x 10^4) and isotropic displacement parameters ($Å^2$x 10^3) for **T4**.

	x	y	z	U(eq)
H(2)	1155	4794	-721	21
H(3)	-458	4467	-56	21
H(6A)	-1085	5210	1248	28
H(6B)	-1329	6000	872	28
H(7A)	588	6774	1866	31
H(7B)	392	6012	2312	31
H(9)	-721	3379	740	25
H(11)	-927	3453	2940	30
H(13)	923	4680	1918	22
H(14A)	-1467	2245	1859	55
H(14B)	-1986	2808	1347	55
H(14C)	-2084	2865	2207	55
H(15A)	65	4958	3345	49
H(15B)	949	4515	3274	49
H(15C)	156	4126	3670	49
H(17)	848	2744	715	31
H(20)	2365	4528	160	32
H(22)	1399	5397	-1837	29
H(24)	2035	7601	-2223	32
H(26)	205	7089	-729	24
H(27A)	2459	5653	-2748	68
H(27B)	3023	6387	-2594	68
H(27C)	2278	6416	-3184	68
H(28A)	541	8536	-1579	50
H(28B)	1528	8591	-1368	50
H(28C)	837	8387	-763	50
H(30)	-1506	5421	-325	31
H(32)	-2879	5401	-2203	54
H(34)	-296	5654	-2264	36
H(35A)	-3464	5827	-757	71

H(35B)	-3030	5209	-245	71
H(35C)	-3532	4951	-956	71
H(36A)	-1422	6065	-3361	90
H(36B)	-2208	5490	-3370	90
H(36C)	-1253	5177	-3406	90
H(37)	3376	2406	269	41
H(38A)	2423	1315	379	90
H(38B)	1418	1435	473	90
H(38C)	2035	1493	1160	90
H(39A)	-1917	6265	1974	46
H(39B)	-1316	5668	2386	46
H(40A)	-698	6811	2733	47
H(40B)	-838	7179	1944	47
H(41A)	-986	3561	-1639	172
H(41B)	-639	2723	-1516	172
H(41C)	-330	3198	-2203	172
H(42A)	1273	3111	-1878	97
H(42B)	1072	2595	-1189	97
H(42C)	1567	3376	-1090	97
H(43A)	3937	3871	-568	91
H(43B)	4347	3503	142	91
H(43C)	3970	4341	170	91
H(44)	2501	5652	-61	34
H(45)	2369	5531	1130	34
H(46A)	3708	6113	1618	50
H(46B)	2867	6369	2040	50
H(47A)	3509	7500	1864	45
H(47B)	3895	7259	1097	45
H(48A)	3566	6303	-621	53
H(48B)	3948	6505	157	53
H(49A)	3764	7685	-262	38
H(49B)	2986	7452	-772	38
H(50)	2326	8207	100	31
H(51)	2396	8078	1298	30

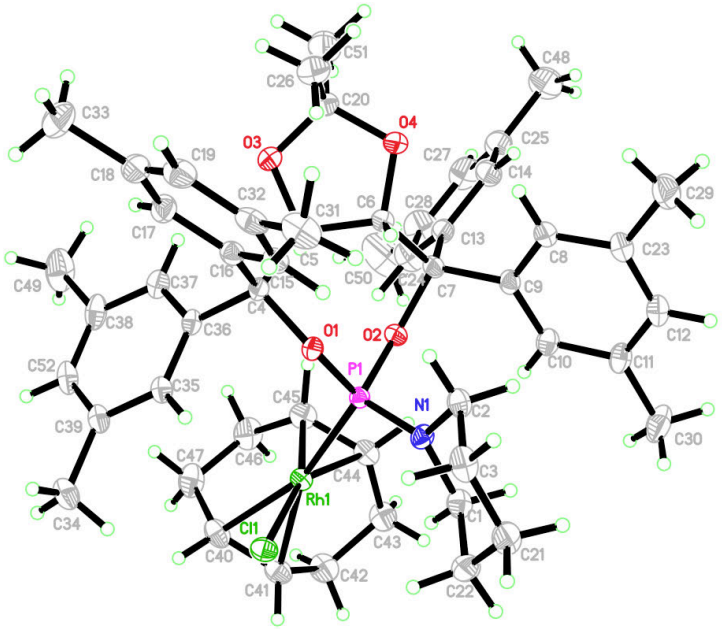

Table A.3.17. Crystal data and structure refinement for **T5**.

Identification code	rovis36_0m	
Empirical formula	C_{52} H_{66} Cl N O_4 P Rh	
Formula weight	938.39	
Temperature	120 K	
Wavelength	0.71073 Å	
Crystal system	Orthorhombic	
Space group	P $2_12_12_1$	
Unit cell dimensions	*a* = 15.3932(6) Å	α = 90°
	b = 17.5850(7) Å	β = 90°
	c = 18.0197(8) Å	γ = 90°
Volume	4877.7(3) $Å^3$	
Z	4	
Density (calculated)	1.278 Mg/m^3	
Absorption coefficient	0.481 mm^{-1}	
F(000)	1976	

Crystal size	0.63 x 0.45 x 0.30 mm^3
Theta range for data collection	2.09 to 33.49°.
Index ranges	-21<=h<=23, -26<=k<=27, -27<=l<=27
Reflections collected	138707
Independent reflections	18942 [R(int) = 0.0541]
Completeness to theta = 33.49°	99.3 %
Absorption correction	Multi-scan
Max. and min. transmission	0.8683 and 0.7527
Refinement method	Full-matrix least-squares on F^2
Data / restraints / parameters	18942 / 0 / 568
Goodness-of-fit on F^2	1.029
Final R indices [I>2sigma(I)]	R1 = 0.0333, wR2 = 0.0761
R indices (all data)	R1 = 0.0434, wR2 = 0.0811
Absolute structure parameter	-0.014(12)
Largest diff. peak and hole	0.709 and -0.589 e.$Å^{-3}$

Table A.3.18. Atomic coordinates (x 10^4) and equivalent isotropic displacement parameters ($Å^2$x 10^3) for **T5**. U(eq) is defined as one third of the trace of the orthogonalized U^{ij} tensor.

	x	y	z	U(eq)
C(1)	158(1)	6132(1)	2978(1)	23(1)
C(2)	-1028(1)	5493(1)	3623(1)	21(1)
C(3)	-1684(1)	6058(1)	3313(1)	27(1)
C(4)	19(1)	5558(1)	5821(1)	16(1)
C(5)	421(1)	4739(1)	5820(1)	18(1)
C(6)	21(1)	4233(1)	5219(1)	19(1)
C(7)	611(1)	4193(1)	4521(1)	18(1)
C(8)	-607(1)	3502(1)	3843(1)	21(1)
C(9)	132(1)	3957(1)	3823(1)	18(1)
C(10)	478(1)	4166(1)	3141(1)	21(1)
C(11)	91(1)	3940(1)	2479(1)	24(1)
C(12)	-642(1)	3476(1)	2513(1)	25(1)
C(13)	1388(1)	3654(1)	4632(1)	21(1)
C(14)	1257(2)	2867(1)	4593(1)	28(1)
C(15)	-1641(1)	5510(1)	5821(1)	20(1)
C(16)	-862(1)	5565(1)	6212(1)	19(1)
C(17)	-886(1)	5604(1)	6988(1)	24(1)
C(18)	-1677(1)	5578(1)	7366(1)	28(1)
C(19)	-2443(1)	5508(1)	6967(1)	28(1)
C(20)	-109(2)	3614(1)	6349(1)	27(1)
C(21)	-1385(1)	6359(1)	2565(1)	30(1)
C(22)	-484(1)	6708(1)	2635(1)	29(1)
C(23)	-998(1)	3249(1)	3187(1)	24(1)
C(24)	2222(1)	3923(1)	4747(1)	31(1)
C(25)	1953(2)	2366(1)	4665(1)	34(1)
C(26)	-1056(2)	3632(1)	6604(1)	35(1)
C(27)	2780(2)	2655(1)	4770(1)	39(1)
C(28)	2926(2)	3425(2)	4811(2)	40(1)
C(29)	-1774(2)	2728(1)	3200(1)	38(1)
C(30)	461(2)	4190(2)	1744(1)	40(1)
C(31)	-3277(1)	5440(1)	5767(1)	32(1)

C(32)	-2438(1)	5479(1)	6191(1)	24(1)
C(33)	-1677(2)	5626(2)	8209(1)	42(1)
C(34)	809(1)	8301(1)	6194(1)	28(1)
C(35)	476(1)	6908(1)	6024(1)	18(1)
C(36)	618(1)	6146(1)	6179(1)	17(1)
C(37)	1238(1)	5939(1)	6703(1)	23(1)
C(38)	1715(1)	6499(1)	7071(1)	27(1)
C(39)	961(1)	7474(1)	6375(1)	21(1)
C(40)	2502(1)	7599(1)	4709(1)	26(1)
C(41)	2551(1)	7548(1)	3949(1)	25(1)
C(42)	3277(1)	7164(1)	3529(1)	31(1)
C(43)	3057(1)	6337(1)	3336(1)	29(1)
C(44)	2499(1)	5939(1)	3906(1)	22(1)
C(45)	2610(1)	5999(1)	4683(1)	24(1)
C(46)	3361(1)	6420(1)	5043(1)	32(1)
C(47)	3122(1)	7238(1)	5252(1)	32(1)
C(48)	1795(2)	1517(1)	4634(2)	48(1)
C(49)	2356(2)	6278(2)	7672(2)	45(1)
C(50)	3840(2)	3741(2)	4927(3)	74(1)
C(51)	411(2)	3000(1)	6718(1)	41(1)
C(52)	1574(1)	7256(1)	6899(1)	25(1)
Cl(1)	456(1)	7628(1)	4288(1)	21(1)
N(1)	-162(1)	5843(1)	3678(1)	18(1)
O(1)	-162(1)	5763(1)	5051(1)	16(1)
O(2)	981(1)	4949(1)	4424(1)	17(1)
O(3)	275(1)	4342(1)	6495(1)	23(1)
O(4)	-65(1)	3509(1)	5563(1)	24(1)
P(1)	527(1)	5784(1)	4376(1)	14(1)
Rh(1)	1566(1)	6700(1)	4344(1)	16(1)

Table A.3.19. Bond lengths [Å] and angles [°] for **T5**.

C(1)-N(1)	1.447(2)	C(18)-C(33)	1.520(3)
C(1)-C(22)	1.545(3)	C(19)-C(32)	1.401(3)
C(2)-N(1)	1.471(2)	C(20)-O(4)	1.431(2)
C(2)-C(3)	1.523(3)	C(20)-O(3)	1.433(2)
C(3)-C(21)	1.519(3)	C(20)-C(51)	1.499(3)
C(4)-O(1)	1.4606(19)	C(20)-C(26)	1.529(3)
C(4)-C(36)	1.528(2)	C(21)-C(22)	1.523(3)
C(4)-C(16)	1.529(2)	C(23)-C(29)	1.507(3)
C(4)-C(5)	1.567(2)	C(24)-C(28)	1.398(3)
C(5)-O(3)	1.421(2)	C(25)-C(27)	1.384(4)
C(5)-C(6)	1.531(2)	C(25)-C(48)	1.515(3)
C(6)-O(4)	1.421(2)	C(27)-C(28)	1.375(4)
C(6)-C(7)	1.553(2)	C(28)-C(50)	1.526(4)
C(7)-O(2)	1.458(2)	C(31)-C(32)	1.502(3)
C(7)-C(9)	1.516(2)	C(34)-C(39)	1.508(3)
C(7)-C(13)	1.539(2)	C(35)-C(36)	1.387(3)
C(8)-C(9)	1.391(3)	C(35)-C(39)	1.396(2)
C(8)-C(23)	1.398(2)	C(36)-C(37)	1.390(2)
C(9)-C(10)	1.389(2)	C(37)-C(38)	1.397(3)
C(10)-C(11)	1.391(3)	C(38)-C(52)	1.384(3)
C(11)-C(12)	1.394(3)	C(38)-C(49)	1.517(3)
C(11)-C(30)	1.507(3)	C(39)-C(52)	1.389(3)
C(12)-C(23)	1.392(3)	C(40)-C(41)	1.374(3)
C(13)-C(24)	1.384(3)	C(40)-C(47)	1.506(3)
C(13)-C(14)	1.400(3)	C(40)-Rh(1)	2.2373(19)
C(14)-C(25)	1.393(3)	C(41)-C(42)	1.510(3)
C(15)-C(16)	1.393(2)	C(41)-Rh(1)	2.2430(19)
C(15)-C(32)	1.397(3)	C(42)-C(43)	1.533(3)
C(16)-C(17)	1.400(3)	C(43)-C(44)	1.510(3)
C(17)-C(18)	1.397(3)	C(44)-C(45)	1.413(3)
C(18)-C(19)	1.388(3)	C(44)-Rh(1)	2.1155(19)
		C(45)-C(46)	1.519(3)
		C(45)-Rh(1)	2.1152(19)
		C(46)-C(47)	1.532(3)
		Cl(1)-Rh(1)	2.3654(4)

N(1)-P(1)	1.6477(15)	C(24)-C(13)-C(7)	122.01(16)
O(1)-P(1)	1.6149(13)	C(14)-C(13)-C(7)	119.33(18)
O(2)-P(1)	1.6283(12)	C(25)-C(14)-C(13)	120.6(2)
P(1)-Rh(1)	2.2703(4)	C(16)-C(15)-C(32)	121.17(16)
		C(15)-C(16)-C(17)	119.04(16)
N(1)-C(1)-C(22)	111.20(15)	C(15)-C(16)-C(4)	122.06(15)
N(1)-C(2)-C(3)	110.65(15)	C(17)-C(16)-C(4)	118.87(16)
C(21)-C(3)-C(2)	110.61(16)	C(18)-C(17)-C(16)	120.60(18)
O(1)-C(4)-C(36)	110.47(13)	C(19)-C(18)-C(17)	119.41(17)
O(1)-C(4)-C(16)	105.39(13)	C(19)-C(18)-C(33)	121.51(19)
C(36)-C(4)-C(16)	109.64(13)	C(17)-C(18)-C(33)	119.1(2)
O(1)-C(4)-C(5)	107.50(12)	C(18)-C(19)-C(32)	121.05(18)
C(36)-C(4)-C(5)	112.59(14)	O(4)-C(20)-O(3)	106.10(15)
C(16)-C(4)-C(5)	110.99(14)	O(4)-C(20)-C(51)	108.68(18)
O(3)-C(5)-C(6)	104.78(13)	O(3)-C(20)-C(51)	109.99(18)
O(3)-C(5)-C(4)	112.89(13)	O(4)-C(20)-C(26)	110.15(17)
C(6)-C(5)-C(4)	112.15(14)	O(3)-C(20)-C(26)	108.71(17)
O(4)-C(6)-C(5)	104.52(13)	C(51)-C(20)-C(26)	112.99(19)
O(4)-C(6)-C(7)	111.47(14)	C(3)-C(21)-C(22)	110.09(16)
C(5)-C(6)-C(7)	111.30(14)	C(21)-C(22)-C(1)	110.59(17)
O(2)-C(7)-C(9)	109.83(13)	C(12)-C(23)-C(8)	118.50(17)
O(2)-C(7)-C(13)	105.88(14)	C(12)-C(23)-C(29)	119.99(17)
C(9)-C(7)-C(13)	108.47(13)	C(8)-C(23)-C(29)	121.49(17)
O(2)-C(7)-C(6)	106.56(13)	C(13)-C(24)-C(28)	121.2(2)
C(9)-C(7)-C(6)	113.60(14)	C(27)-C(25)-C(14)	119.2(2)
C(13)-C(7)-C(6)	112.20(14)	C(27)-C(25)-C(48)	121.0(2)
C(9)-C(8)-C(23)	120.88(17)	C(14)-C(25)-C(48)	119.8(2)
C(10)-C(9)-C(8)	119.25(16)	C(28)-C(27)-C(25)	121.3(2)
C(10)-C(9)-C(7)	118.42(16)	C(27)-C(28)-C(24)	119.0(2)
C(8)-C(9)-C(7)	122.22(16)	C(27)-C(28)-C(50)	121.1(2)
C(9)-C(10)-C(11)	121.24(17)	C(24)-C(28)-C(50)	119.8(2)
C(10)-C(11)-C(12)	118.50(17)	C(15)-C(32)-C(19)	118.71(18)
C(10)-C(11)-C(30)	120.56(18)	C(15)-C(32)-C(31)	120.98(18)
C(12)-C(11)-C(30)	120.93(17)	C(19)-C(32)-C(31)	120.28(18)
C(23)-C(12)-C(11)	121.60(17)	C(36)-C(35)-C(39)	120.92(16)
C(24)-C(13)-C(14)	118.63(18)	C(35)-C(36)-C(37)	119.84(16)

C(35)-C(36)-C(4)	118.26(15)	C(4)-O(1)-P(1)	126.59(10)
C(37)-C(36)-C(4)	121.60(16)	C(7)-O(2)-P(1)	131.43(10)
C(36)-C(37)-C(38)	119.96(18)	C(5)-O(3)-C(20)	110.34(13)
C(52)-C(38)-C(37)	119.33(18)	C(6)-O(4)-C(20)	108.63(13)
C(52)-C(38)-C(49)	120.58(18)	O(1)-P(1)-O(2)	102.74(6)
C(37)-C(38)-C(49)	120.1(2)	O(1)-P(1)-N(1)	98.83(6)
C(52)-C(39)-C(35)	118.33(17)	O(2)-P(1)-N(1)	111.92(7)
C(52)-C(39)-C(34)	121.26(16)	O(1)-P(1)-Rh(1)	119.87(5)
C(35)-C(39)-C(34)	120.40(17)	O(2)-P(1)-Rh(1)	109.79(4)
C(41)-C(40)-C(47)	125.9(2)	N(1)-P(1)-Rh(1)	112.95(6)
C(41)-C(40)-Rh(1)	72.37(13)	C(45)-Rh(1)-C(44)	39.03(7)
C(47)-C(40)-Rh(1)	107.56(14)	C(45)-Rh(1)-C(40)	80.67(8)
C(40)-C(41)-C(42)	124.6(2)	C(44)-Rh(1)-C(40)	96.82(8)
C(40)-C(41)-Rh(1)	71.91(12)	C(45)-Rh(1)-C(41)	88.06(8)
C(42)-C(41)-Rh(1)	111.17(14)	C(44)-Rh(1)-C(41)	80.98(7)
C(41)-C(42)-C(43)	112.04(17)	C(40)-Rh(1)-C(41)	35.72(7)
C(44)-C(43)-C(42)	114.17(17)	C(45)-Rh(1)-P(1)	96.58(6)
C(45)-C(44)-C(43)	124.86(19)	C(44)-Rh(1)-P(1)	92.26(6)
C(45)-C(44)-Rh(1)	70.48(12)	C(40)-Rh(1)-P(1)	161.33(6)
C(43)-C(44)-Rh(1)	110.32(13)	C(41)-Rh(1)-P(1)	162.90(6)
C(44)-C(45)-C(46)	123.42(19)	C(45)-Rh(1)-Cl(1)	164.48(6)
C(44)-C(45)-Rh(1)	70.50(12)	C(44)-Rh(1)-Cl(1)	155.62(6)
C(46)-C(45)-Rh(1)	114.63(14)	C(40)-Rh(1)-Cl(1)	89.47(6)
C(45)-C(46)-C(47)	112.35(17)	C(41)-Rh(1)-Cl(1)	90.90(6)
C(40)-C(47)-C(46)	112.80(17)	P(1)-Rh(1)-Cl(1)	88.919(14)
C(38)-C(52)-C(39)	121.59(17)		
C(1)-N(1)-C(2)	113.37(14)		
C(1)-N(1)-P(1)	117.90(12)		
C(2)-N(1)-P(1)	127.45(12)		

Symmetry transformations used to generate equivalent atoms:

Table A.3.20. Anisotropic displacement parameters ($Å^2 x\ 10^3$)for **T5**. The anisotropic displacement factor exponent takes the form: $-2p^2[\ h^2a^{*2}U^{11} + ... + 2\ h\ k\ a^*\ b^*\ U^{12}\ ]$

	U^{11}	U^{22}	U^{33}	U^{23}	U^{13}	U^{12}
C(1)	18(1)	27(1)	25(1)	-3(1)	0(1)	-3(1)
C(2)	16(1)	23(1)	23(1)	-4(1)	-2(1)	-2(1)
C(3)	19(1)	29(1)	34(1)	-9(1)	-6(1)	5(1)
C(4)	18(1)	18(1)	14(1)	-1(1)	0(1)	1(1)
C(5)	22(1)	17(1)	16(1)	-1(1)	0(1)	1(1)
C(6)	22(1)	16(1)	18(1)	0(1)	1(1)	-1(1)
C(7)	20(1)	14(1)	19(1)	-1(1)	-1(1)	1(1)
C(8)	25(1)	18(1)	21(1)	-2(1)	1(1)	-2(1)
C(9)	20(1)	16(1)	17(1)	-3(1)	0(1)	3(1)
C(10)	21(1)	24(1)	19(1)	-4(1)	2(1)	2(1)
C(11)	24(1)	28(1)	19(1)	-7(1)	2(1)	3(1)
C(12)	27(1)	27(1)	22(1)	-7(1)	-3(1)	0(1)
C(13)	28(1)	19(1)	18(1)	-1(1)	-1(1)	7(1)
C(14)	37(1)	19(1)	27(1)	-1(1)	-2(1)	7(1)
C(15)	22(1)	17(1)	23(1)	-1(1)	2(1)	0(1)
C(16)	20(1)	16(1)	21(1)	-1(1)	4(1)	0(1)
C(17)	24(1)	26(1)	22(1)	-2(1)	3(1)	-2(1)
C(18)	33(1)	25(1)	26(1)	-2(1)	11(1)	-3(1)
C(19)	26(1)	23(1)	35(1)	1(1)	13(1)	0(1)
C(20)	41(1)	20(1)	20(1)	3(1)	-4(1)	-2(1)
C(21)	29(1)	28(1)	32(1)	-2(1)	-13(1)	5(1)
C(22)	35(1)	26(1)	26(1)	3(1)	-10(1)	-1(1)
C(23)	26(1)	22(1)	25(1)	-5(1)	-2(1)	-2(1)
C(24)	25(1)	26(1)	41(1)	-1(1)	-5(1)	7(1)
C(25)	50(1)	23(1)	28(1)	0(1)	-3(1)	14(1)
C(26)	41(1)	35(1)	29(1)	3(1)	6(1)	-7(1)
C(27)	46(1)	36(1)	35(1)	0(1)	-6(1)	23(1)
C(28)	29(1)	40(1)	52(1)	1(1)	-8(1)	13(1)
C(29)	42(1)	40(1)	33(1)	-6(1)	-2(1)	-16(1)
C(30)	38(1)	61(2)	19(1)	-6(1)	3(1)	-15(1)
C(31)	20(1)	26(1)	49(1)	0(1)	3(1)	1(1)

C(32)	21(1)	15(1)	36(1)	1(1)	6(1)	1(1)
C(33)	49(2)	49(1)	28(1)	-4(1)	16(1)	-5(1)
C(34)	29(1)	23(1)	33(1)	-7(1)	0(1)	-4(1)
C(35)	16(1)	21(1)	19(1)	-4(1)	1(1)	-1(1)
C(36)	16(1)	21(1)	15(1)	-4(1)	1(1)	0(1)
C(37)	22(1)	27(1)	20(1)	-4(1)	-2(1)	4(1)
C(38)	18(1)	40(1)	23(1)	-13(1)	-3(1)	1(1)
C(39)	19(1)	22(1)	23(1)	-7(1)	2(1)	-3(1)
C(40)	18(1)	23(1)	36(1)	-6(1)	1(1)	-6(1)
C(41)	21(1)	22(1)	31(1)	1(1)	3(1)	-5(1)
C(42)	24(1)	32(1)	36(1)	-1(1)	8(1)	-5(1)
C(43)	23(1)	32(1)	31(1)	-4(1)	9(1)	-1(1)
C(44)	16(1)	21(1)	29(1)	-2(1)	0(1)	1(1)
C(45)	17(1)	26(1)	30(1)	2(1)	-4(1)	2(1)
C(46)	20(1)	41(1)	36(1)	-3(1)	-10(1)	1(1)
C(47)	21(1)	43(1)	31(1)	-8(1)	-4(1)	-5(1)
C(48)	71(2)	23(1)	49(1)	1(1)	-2(1)	16(1)
C(49)	39(1)	53(2)	43(1)	-16(1)	-23(1)	13(1)
C(50)	31(2)	57(2)	134(4)	-2(2)	-18(2)	12(1)
C(51)	58(2)	28(1)	38(1)	4(1)	-10(1)	8(1)
C(52)	20(1)	30(1)	26(1)	-13(1)	1(1)	-2(1)
Cl(1)	19(1)	19(1)	24(1)	2(1)	0(1)	1(1)
N(1)	15(1)	22(1)	16(1)	0(1)	-3(1)	-2(1)
O(1)	15(1)	17(1)	15(1)	-1(1)	-1(1)	0(1)
O(2)	17(1)	14(1)	19(1)	0(1)	1(1)	1(1)
O(3)	31(1)	21(1)	17(1)	1(1)	-1(1)	-1(1)
O(4)	38(1)	16(1)	19(1)	1(1)	4(1)	-3(1)
P(1)	14(1)	15(1)	14(1)	0(1)	-1(1)	0(1)
Rh(1)	13(1)	18(1)	19(1)	0(1)	-1(1)	-1(1)

Table A.3.21. Hydrogen coordinates (x 10^4) and isotropic displacement parameters (Å^{2}x 10^3) for **T5**.

	x	y	z	U(eq)
H(1A)	246	5704	2629	28
H(1B)	727	6383	3057	28
H(2A)	-1218	5322	4121	25
H(2B)	-998	5042	3295	25
H(3A)	-2255	5806	3257	33
H(3B)	-1754	6487	3664	33
H(5)	1061	4779	5732	22
H(6)	-566	4431	5079	22
H(8)	-849	3362	4308	26
H(10)	988	4470	3126	25
H(12)	-905	3311	2064	30
H(14)	688	2673	4516	33
H(15)	-1629	5494	5294	25
H(17)	-359	5649	7259	29
H(19)	-2981	5480	7225	34
H(21A)	-1800	6748	2385	36
H(21B)	-1372	5939	2200	36
H(22A)	-514	7168	2951	35
H(22B)	-274	6864	2138	35
H(24)	2318	4456	4783	37
H(26A)	-1370	4028	6331	52
H(26B)	-1080	3741	7136	52
H(26C)	-1326	3137	6507	52
H(27)	3256	2315	4814	47
H(29A)	-2214	2915	2851	57
H(29B)	-2020	2715	3702	57
H(29C)	-1595	2214	3055	57
H(30A)	486	3754	1406	59
H(30B)	1047	4393	1818	59
H(30C)	89	4585	1529	59

H(31A)	-3582	5927	5809	48
H(31B)	-3641	5034	5971	48
H(31C)	-3155	5334	5243	48
H(33A)	-1384	6095	8365	63
H(33B)	-1369	5186	8414	63
H(33C)	-2277	5629	8390	63
H(34A)	308	8488	6476	42
H(34B)	694	8355	5662	42
H(34C)	1325	8597	6326	42
H(35)	42	7047	5675	22
H(37)	1336	5417	6810	28
H(42A)	3812	7174	3834	37
H(42B)	3393	7449	3066	37
H(43A)	2751	6328	2853	34
H(43B)	3605	6049	3277	34
H(46A)	3860	6428	4697	39
H(46B)	3543	6143	5495	39
H(47A)	2854	7240	5752	38
H(47B)	3658	7548	5277	38
H(48A)	2230	1279	4311	71
H(48B)	1213	1418	4436	71
H(48C)	1841	1302	5134	71
H(49A)	2935	6468	7542	68
H(49B)	2375	5722	7716	68
H(49C)	2174	6499	8146	68
H(50A)	4241	3322	5030	111
H(50B)	3837	4095	5347	111
H(50C)	4027	4010	4478	111
H(51A)	161	2503	6595	62
H(51B)	398	3074	7257	62
H(51C)	1013	3022	6542	62
H(52)	1905	7636	7146	30
H(40)	2103(17)	8005(15)	4886(14)	31(7)
H(41)	2203(17)	7873(15)	3659(14)	30(7)
H(44)	2204(18)	5499(16)	3700(15)	36(7)
H(45)	2348(17)	5594(15)	4956(14)	30(6)

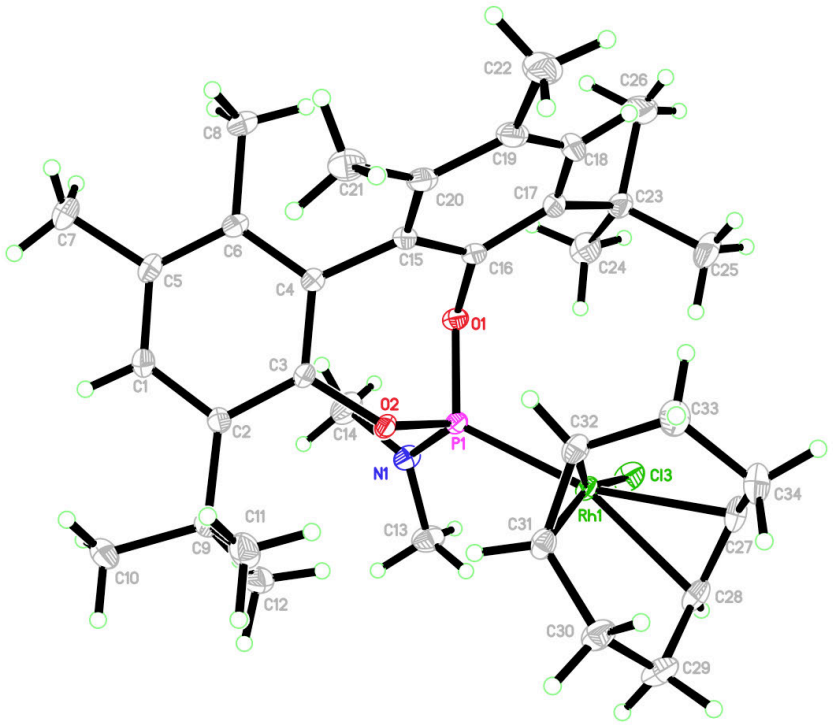

Table A.3.22. Crystal data and structure refinement for **B1.**

Identification code	rovis41_0m	
Empirical formula	C_{34} H_{50} Cl N O_2 P Rh	
Formula weight	674.08	
Temperature	120 K	
Wavelength	0.71073 Å	
Crystal system	Triclinic	
Space group	P-1	
Unit cell dimensions	*a* = 10.4105(5) Å	α = 77.003(3)°
	b = 10.8685(6) Å	β = 76.360(2)°
	c = 16.5368(10) Å	γ = 64.354(2)°
Volume	1622.99(15) $Å^3$	
Z	2	
Density (calculated)	1.379 Mg/m^3	

Absorption coefficient	0.688 mm^{-1}
F(000)	708
Crystal size	0.70 x 0.37 x 0.17 mm^3
Theta range for data collection	2.10 to 33.37°.
Index ranges	-16<=h<=13, -16<=k<=15, -25<=l<=25
Reflections collected	19235
Independent reflections	12140 [R(int) = 0.0176]
Completeness to theta = 33.37°	96.3 %
Absorption correction	Multi-scan
Max. and min. transmission	0.8890 and 0.6455
Refinement method	Full-matrix least-squares on F^2
Data / restraints / parameters	12140 / 0 / 389
Goodness-of-fit on F^2	1.104
Final R indices [I>2sigma(I)]	R1 = 0.0336, wR2 = 0.0761
R indices (all data)	R1 = 0.0410, wR2 = 0.0792
Largest diff. peak and hole	1.056 and -0.844 e.$Å^{-3}$

Table A.3.23. Atomic coordinates (x 10^4) and equivalent isotropic displacement parameters ($Å^2$x 10^3) for **B1**. U(eq) is defined as one third of the trace of the orthogonalized U^{ij} tensor.

	x	y	z	U(eq)
C(1)	2679(2)	6412(2)	4177(1)	18(1)
C(2)	3711(2)	5600(2)	3586(1)	13(1)
C(3)	3191(2)	4967(2)	3167(1)	12(1)
C(4)	1725(2)	5267(2)	3240(1)	13(1)
C(5)	1231(2)	6611(2)	4340(1)	19(1)
C(6)	728(2)	6061(2)	3855(1)	16(1)
C(7)	212(2)	7467(2)	5014(1)	29(1)
C(8)	-842(2)	6305(2)	4004(1)	22(1)
C(9)	5251(2)	5552(2)	3354(1)	17(1)
C(10)	5482(2)	6415(2)	3879(1)	23(1)
C(11)	5462(2)	6175(2)	2427(1)	24(1)
C(12)	6416(2)	4076(2)	3485(1)	23(1)
C(13)	6577(2)	718(2)	3606(1)	22(1)
C(14)	4216(2)	1871(2)	4453(1)	25(1)
C(15)	1241(2)	4796(2)	2630(1)	14(1)
C(16)	1684(2)	3384(2)	2628(1)	14(1)
C(17)	1071(2)	2863(2)	2194(1)	18(1)
C(18)	164(2)	3863(2)	1646(1)	22(1)
C(19)	-161(2)	5260(2)	1545(1)	21(1)
C(20)	342(2)	5760(2)	2065(1)	17(1)
C(21)	-45(2)	7279(2)	1987(1)	22(1)
C(22)	-1070(2)	6240(2)	893(1)	28(1)
C(23)	1264(2)	1357(2)	2277(1)	22(1)
C(24)	1991(2)	396(2)	3020(1)	27(1)
C(25)	2139(2)	773(2)	1460(2)	33(1)
C(26)	-240(2)	1330(2)	2412(2)	36(1)
C(27)	6145(2)	815(2)	289(1)	19(1)
C(28)	7404(2)	550(2)	552(1)	19(1)
C(29)	8267(2)	1418(2)	274(1)	24(1)
C(30)	7346(2)	2971(2)	255(1)	22(1)
C(31)	6010(2)	3301(2)	932(1)	16(1)

C(32)	4641(2)	3464(2)	823(1)	16(1)
C(33)	4271(2)	3234(2)	57(1)	21(1)
C(34)	5448(2)	2006(2)	-359(1)	23(1)
Cl(3)	5896(1)	-687(1)	2247(1)	21(1)
N(1)	5070(2)	1691(2)	3620(1)	16(1)
O(1)	2774(1)	2508(1)	3105(1)	14(1)
O(2)	4135(1)	4065(1)	2599(1)	12(1)
P(1)	4404(1)	2437(1)	2749(1)	12(1)
Rh(1)	5602(1)	1536(1)	1559(1)	12(1)

Table A.3.24. Bond lengths [Å] and angles [°] for **B1**.

C(1)-C(5)	1.394(2)	C(27)-Rh(1)	2.2678(17)
C(1)-C(2)	1.400(2)	C(28)-C(29)	1.501(3)
C(2)-C(3)	1.399(2)	C(28)-Rh(1)	2.2432(17)
C(2)-C(9)	1.538(2)	C(29)-C(30)	1.536(3)
C(3)-C(4)	1.397(2)	C(30)-C(31)	1.526(2)
C(3)-O(2)	1.3982(18)	C(31)-C(32)	1.409(2)
C(4)-C(6)	1.407(2)	C(31)-Rh(1)	2.1299(17)
C(4)-C(15)	1.492(2)	C(32)-C(33)	1.508(2)
C(5)-C(6)	1.400(2)	C(32)-Rh(1)	2.1182(17)
C(5)-C(7)	1.513(2)	C(33)-C(34)	1.534(3)
C(6)-C(8)	1.505(2)	Cl(3)-Rh(1)	2.3485(4)
C(9)-C(10)	1.533(2)	N(1)-P(1)	1.6337(15)
C(9)-C(11)	1.536(3)	O(1)-P(1)	1.6333(12)
C(9)-C(12)	1.540(3)	O(2)-P(1)	1.6359(12)
C(13)-N(1)	1.462(2)	P(1)-Rh(1)	2.2451(4)
C(14)-N(1)	1.457(2)		
C(15)-C(16)	1.399(2)	C(5)-C(1)-C(2)	123.69(15)
C(15)-C(20)	1.403(2)	C(3)-C(2)-C(1)	114.97(14)
C(16)-C(17)	1.397(2)	C(3)-C(2)-C(9)	123.15(14)
C(16)-O(1)	1.402(2)	C(1)-C(2)-C(9)	121.57(14)
C(17)-C(18)	1.403(3)	C(4)-C(3)-O(2)	116.60(13)
C(17)-C(23)	1.538(3)	C(4)-C(3)-C(2)	122.91(14)
C(18)-C(19)	1.383(3)	O(2)-C(3)-C(2)	120.33(13)
C(19)-C(20)	1.407(2)	C(3)-C(4)-C(6)	119.67(14)
C(19)-C(22)	1.512(3)	C(3)-C(4)-C(15)	119.01(14)
C(20)-C(21)	1.503(3)	C(6)-C(4)-C(15)	121.25(14)
C(23)-C(24)	1.534(3)	C(1)-C(5)-C(6)	119.50(15)
C(23)-C(25)	1.536(3)	C(1)-C(5)-C(7)	119.57(16)
C(23)-C(26)	1.541(3)	C(6)-C(5)-C(7)	120.88(16)
C(27)-C(28)	1.369(3)	C(5)-C(6)-C(4)	118.45(15)
C(27)-C(34)	1.510(3)	C(5)-C(6)-C(8)	120.17(15)
		C(4)-C(6)-C(8)	121.37(15)
		C(10)-C(9)-C(11)	107.65(15)
		C(10)-C(9)-C(2)	111.50(14)
		C(11)-C(9)-C(2)	107.96(14)

C(10)-C(9)-C(12)	107.42(15)
C(11)-C(9)-C(12)	109.48(15)
C(2)-C(9)-C(12)	112.70(14)
C(16)-C(15)-C(20)	120.09(15)
C(16)-C(15)-C(4)	119.49(14)
C(20)-C(15)-C(4)	120.42(15)
C(17)-C(16)-C(15)	122.79(15)
C(17)-C(16)-O(1)	121.46(15)
C(15)-C(16)-O(1)	115.74(14)
C(16)-C(17)-C(18)	114.22(16)
C(16)-C(17)-C(23)	127.09(17)
C(18)-C(17)-C(23)	118.68(16)
C(19)-C(18)-C(17)	124.55(16)
C(18)-C(19)-C(20)	119.32(16)
C(18)-C(19)-C(22)	120.29(17)
C(20)-C(19)-C(22)	120.39(18)
C(15)-C(20)-C(19)	117.89(16)
C(15)-C(20)-C(21)	121.95(16)
C(19)-C(20)-C(21)	120.13(16)
C(24)-C(23)-C(25)	108.90(17)
C(24)-C(23)-C(17)	115.06(15)
C(25)-C(23)-C(17)	109.30(17)
C(24)-C(23)-C(26)	106.14(18)
C(25)-C(23)-C(26)	108.87(17)
C(17)-C(23)-C(26)	108.39(15)
C(28)-C(27)-C(34)	124.64(17)
C(28)-C(27)-Rh(1)	71.35(10)
C(34)-C(27)-Rh(1)	110.21(11)
C(27)-C(28)-C(29)	125.78(17)
C(27)-C(28)-Rh(1)	73.31(10)
C(29)-C(28)-Rh(1)	107.07(11)
C(28)-C(29)-C(30)	113.71(15)
C(31)-C(30)-C(29)	113.04(15)
C(32)-C(31)-C(30)	124.82(16)
C(32)-C(31)-Rh(1)	70.19(10)
C(30)-C(31)-Rh(1)	113.59(11)
C(31)-C(32)-C(33)	126.44(15)
C(31)-C(32)-Rh(1)	71.09(10)
C(33)-C(32)-Rh(1)	109.09(11)
C(32)-C(33)-C(34)	113.89(15)
C(27)-C(34)-C(33)	111.41(15)
C(14)-N(1)-C(13)	115.22(14)
C(14)-N(1)-P(1)	123.53(12)
C(13)-N(1)-P(1)	121.16(12)
C(16)-O(1)-P(1)	117.76(10)
C(3)-O(2)-P(1)	122.20(10)
O(1)-P(1)-N(1)	97.23(7)
O(1)-P(1)-O(2)	101.98(6)
N(1)-P(1)-O(2)	109.12(7)
O(1)-P(1)-Rh(1)	119.26(5)
N(1)-P(1)-Rh(1)	118.68(5)
O(2)-P(1)-Rh(1)	108.89(4)
C(32)-Rh(1)-C(31)	38.73(7)
C(32)-Rh(1)-C(28)	96.83(7)
C(31)-Rh(1)-C(28)	81.16(7)
C(32)-Rh(1)-P(1)	91.19(5)
C(31)-Rh(1)-P(1)	95.11(5)
C(28)-Rh(1)-P(1)	161.50(5)
C(32)-Rh(1)-C(27)	80.89(7)
C(31)-Rh(1)-C(27)	88.00(7)
C(28)-Rh(1)-C(27)	35.34(7)
P(1)-Rh(1)-C(27)	163.15(5)
C(32)-Rh(1)-Cl(3)	157.29(5)
C(31)-Rh(1)-Cl(3)	162.92(5)
C(28)-Rh(1)-Cl(3)	88.04(5)
P(1)-Rh(1)-Cl(3)	90.953(16)
C(27)-Rh(1)-Cl(3)	90.81(5)

Symmetry transformations used to generate equivalent atoms:

Table A.3.25. Anisotropic displacement parameters ($Å^2 x\ 10^3$)for **B1**. The anisotropic displacement factor exponent takes the form: $-2p^2[\ h^2 a^{*2} U^{11} + ... + 2\ h\ k\ a^*\ b^*\ U^{12}\ ]$

	U^{11}	U^{22}	U^{33}	U^{23}	U^{13}	U^{12}
C(1)	19(1)	18(1)	17(1)	-7(1)	-3(1)	-7(1)
C(2)	14(1)	13(1)	14(1)	-2(1)	-3(1)	-5(1)
C(3)	12(1)	11(1)	11(1)	-3(1)	0(1)	-4(1)
C(4)	12(1)	13(1)	14(1)	-3(1)	-2(1)	-5(1)
C(5)	17(1)	18(1)	18(1)	-9(1)	2(1)	-5(1)
C(6)	12(1)	16(1)	18(1)	-5(1)	0(1)	-4(1)
C(7)	23(1)	35(1)	30(1)	-22(1)	5(1)	-8(1)
C(8)	12(1)	25(1)	27(1)	-10(1)	2(1)	-5(1)
C(9)	14(1)	20(1)	18(1)	-6(1)	-1(1)	-9(1)
C(10)	22(1)	31(1)	25(1)	-10(1)	-4(1)	-14(1)
C(11)	30(1)	29(1)	20(1)	-6(1)	2(1)	-21(1)
C(12)	15(1)	22(1)	33(1)	-7(1)	-6(1)	-5(1)
C(13)	16(1)	23(1)	21(1)	0(1)	-4(1)	-4(1)
C(14)	26(1)	28(1)	14(1)	-2(1)	-1(1)	-6(1)
C(15)	11(1)	16(1)	14(1)	-4(1)	-1(1)	-5(1)
C(16)	10(1)	17(1)	15(1)	-5(1)	0(1)	-5(1)
C(17)	14(1)	22(1)	20(1)	-11(1)	2(1)	-8(1)
C(18)	18(1)	31(1)	21(1)	-12(1)	-3(1)	-10(1)
C(19)	13(1)	31(1)	17(1)	-5(1)	-3(1)	-6(1)
C(20)	11(1)	20(1)	18(1)	-3(1)	-2(1)	-4(1)
C(21)	19(1)	18(1)	25(1)	1(1)	-7(1)	-4(1)
C(22)	21(1)	40(1)	22(1)	-4(1)	-9(1)	-8(1)
C(23)	16(1)	23(1)	33(1)	-16(1)	4(1)	-9(1)
C(24)	27(1)	20(1)	37(1)	-8(1)	2(1)	-13(1)
C(25)	29(1)	33(1)	37(1)	-23(1)	5(1)	-10(1)
C(26)	20(1)	31(1)	65(2)	-22(1)	1(1)	-14(1)
C(27)	27(1)	15(1)	15(1)	-7(1)	-1(1)	-7(1)
C(28)	20(1)	14(1)	18(1)	-5(1)	3(1)	-3(1)
C(29)	18(1)	20(1)	26(1)	-4(1)	6(1)	-5(1)
C(30)	20(1)	20(1)	23(1)	-4(1)	5(1)	-9(1)
C(31)	19(1)	12(1)	16(1)	-3(1)	1(1)	-7(1)

C(32)	18(1)	13(1)	15(1)	-2(1)	-2(1)	-3(1)
C(33)	24(1)	19(1)	18(1)	-2(1)	-7(1)	-4(1)
C(34)	32(1)	20(1)	17(1)	-5(1)	-5(1)	-8(1)
Cl(3)	22(1)	12(1)	25(1)	-1(1)	2(1)	-6(1)
N(1)	14(1)	16(1)	13(1)	-1(1)	-2(1)	-4(1)
O(1)	11(1)	14(1)	16(1)	-2(1)	0(1)	-5(1)
O(2)	12(1)	12(1)	13(1)	-4(1)	1(1)	-4(1)
P(1)	11(1)	11(1)	12(1)	-3(1)	0(1)	-4(1)
Rh(1)	12(1)	10(1)	13(1)	-3(1)	0(1)	-3(1)

Table A.3.26. Hydrogen coordinates (x 10^4) and isotropic displacement parameters (Å^{2}x 10^3) for **B1**.

	x	y	z	U(eq)
H(1)	2976	6842	4478	21
H(7A)	739	7761	5279	44
H(7B)	-220	6923	5427	44
H(7C)	-528	8260	4765	44
H(8A)	-977	5748	3683	33
H(8B)	-1408	7260	3834	33
H(8C)	-1141	6061	4591	33
H(10A)	5377	6035	4462	35
H(10B)	4779	7347	3804	35
H(10C)	6433	6403	3700	35
H(11A)	6423	6144	2266	36
H(11B)	4777	7115	2353	36
H(11C)	5319	5656	2083	36
H(12A)	6231	3656	4051	35
H(12B)	7348	4109	3385	35
H(12C)	6396	3545	3099	35
H(13A)	7027	984	3940	33
H(13B)	7074	721	3038	33
H(13C)	6619	-191	3831	33
H(14A)	3942	1106	4667	38
H(14B)	3365	2711	4419	38
H(14C)	4777	1913	4823	38
H(18)	-247	3567	1328	26
H(21A)	527	7429	2302	34
H(21B)	-1049	7738	2203	34
H(21C)	140	7640	1406	34
H(22A)	-1369	5738	620	43
H(22B)	-513	6671	483	43
H(22C)	-1905	6933	1161	43
H(24A)	1942	-481	3073	41

H(24B)	1504	796	3527	41
H(24C)	2983	272	2926	41
H(25A)	1661	1339	995	49
H(25B)	2216	-150	1498	49
H(25C)	3086	765	1378	49
H(26A)	-726	1885	1947	54
H(26B)	-793	1690	2922	54
H(26C)	-138	398	2450	54
H(29A)	8802	1246	-283	28
H(29B)	8961	1138	652	28
H(30A)	7932	3417	329	26
H(30B)	7044	3349	-292	26
H(33A)	4094	4061	-352	26
H(33B)	3384	3087	216	26
H(34A)	5027	1709	-702	28
H(34B)	6177	2291	-724	28
H(5)	3810(20)	4010(20)	1165(14)	17(5)
H(3)	7840(20)	-300(20)	836(13)	14(5)
H(2)	6040(20)	3770(20)	1363(14)	19(5)
H(4)	5750(30)	180(30)	435(16)	29(6)

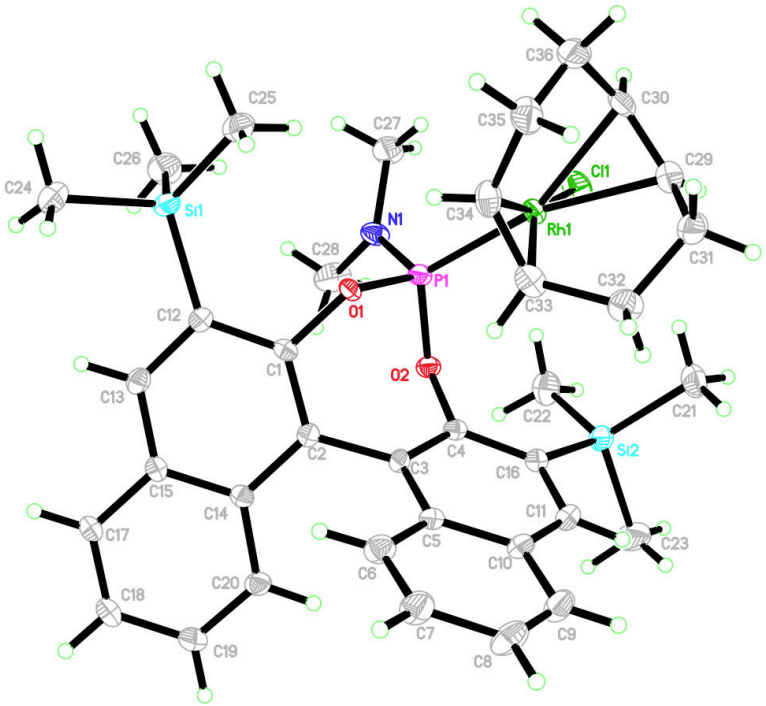

Table A.3.27. Crystal data and structure refinement for **B2**.

Identification code	rovis45_0m	
Empirical formula	C_{36} H_{46} Cl N O_2 P Rh Si_2	
Formula weight	750.25	
Temperature	120 K	
Wavelength	0.71073 Å	
Crystal system	Orthorhombic	
Space group	P $2_12_12_1$	
Unit cell dimensions	*a* = 11.2417(5) Å	α = 90°
	b = 14.6792(6) Å	β = 90°
	c = 21.3614(9) Å	γ = 90°
Volume	3525.0(3) $Å^3$	
Z	4	
Density (calculated)	1.414 Mg/m^3	
Absorption coefficient	0.706 mm^{-1}	
F(000)	1560	

Crystal size	0.23 x 0.09 x 0.07 mm^3
Theta range for data collection	1.68 to 33.27°.
Index ranges	-17<=h<=9, -22<=k<=13, -32<=l<=32
Reflections collected	31400
Independent reflections	12869 [R(int) = 0.0581]
Completeness to theta = 33.27°	99.8 %
Absorption correction	Multi-scan
Max. and min. transmission	0.9535 and 0.8516
Refinement method	Full-matrix least-squares on F^2
Data / restraints / parameters	12869 / 0 / 422
Goodness-of-fit on F^2	0.996
Final R indices [I>2sigma(I)]	R1 = 0.0453, wR2 = 0.0863
R indices (all data)	R1 = NaN, wR2 = 0.1035
Absolute structure parameter	-0.02(2)
Largest diff. peak and hole	0.606 and -0.511 e.$Å^{-3}$

Table A.3.28. Atomic coordinates (x 10^4) and equivalent isotropic displacement parameters ($Å^2$x 10^3) for **B2**. U(eq) is defined as one third of the trace of the orthogonalized U^{ij} tensor.

	x	y	z	U(eq)
C(1)	2668(3)	9520(2)	7963(1)	13(1)
C(2)	2739(3)	9780(2)	8586(1)	13(1)
C(3)	3808(3)	9550(2)	8970(1)	14(1)
C(4)	4184(3)	8655(2)	9024(1)	14(1)
C(5)	4491(3)	10242(2)	9275(1)	16(1)
C(6)	4291(3)	11185(2)	9180(1)	21(1)
C(7)	5006(3)	11826(2)	9464(2)	25(1)
C(8)	5938(4)	11561(2)	9862(2)	28(1)
C(9)	6161(3)	10659(2)	9959(2)	25(1)
C(10)	5458(3)	9979(2)	9667(1)	18(1)
C(11)	5676(3)	9047(2)	9765(1)	20(1)
C(12)	1735(3)	9766(2)	7554(1)	14(1)
C(13)	822(3)	10266(2)	7815(1)	16(1)
C(14)	1739(3)	10247(2)	8852(1)	13(1)
C(15)	779(3)	10498(2)	8459(1)	15(1)
C(16)	5064(3)	8364(2)	9455(1)	18(1)
C(17)	-202(3)	10975(2)	8712(2)	19(1)
C(18)	-256(3)	11172(2)	9337(2)	25(1)
C(19)	660(3)	10898(2)	9735(2)	22(1)
C(20)	1644(3)	10454(2)	9501(1)	18(1)
C(21)	6948(3)	6855(3)	9421(2)	30(1)
C(22)	4290(3)	6298(2)	9382(2)	29(1)
C(23)	5371(4)	7106(3)	10556(2)	35(1)
C(24)	719(3)	10386(2)	6319(2)	29(1)
C(25)	3102(3)	9395(3)	6291(2)	28(1)
C(26)	888(4)	8363(2)	6575(2)	31(1)
C(27)	3357(3)	6739(2)	7088(2)	28(1)
C(28)	1950(3)	7068(3)	7938(2)	31(1)
C(29)	7986(3)	7731(2)	7648(2)	22(1)
C(30)	7579(3)	7587(2)	7054(2)	22(1)
C(31)	8513(3)	8598(3)	7896(2)	26(1)

C(32)	7583(3)	9197(2)	8227(2)	27(1)
C(33)	6394(3)	9198(2)	7905(2)	22(1)
C(34)	6176(3)	9175(2)	7261(2)	23(1)
C(35)	7115(3)	9224(3)	6747(2)	28(1)
C(36)	7507(3)	8280(3)	6531(2)	30(1)
Cl(1)	5810(1)	6265(1)	7811(1)	27(1)
N(1)	3063(2)	7296(2)	7631(1)	19(1)
O(1)	3630(2)	9053(1)	7708(1)	15(1)
O(2)	3651(2)	7999(1)	8639(1)	15(1)
P(2)	4043(1)	8027(1)	7902(1)	14(1)
Rh(1)	5961(1)	7841(1)	7651(1)	15(1)
Si(1)	1647(1)	9484(1)	6693(1)	18(1)
Si(3)	5400(1)	7133(1)	9681(1)	20(1)

—

Table A.3.29. Bond lengths [Å] and angles [°] for **B2**.

C(1)-C(2)	1.387(4)
C(1)-O(1)	1.392(3)
C(1)-C(12)	1.411(4)
C(2)-C(14)	1.433(4)
C(2)-C(3)	1.494(4)
C(3)-C(4)	1.385(4)
C(3)-C(5)	1.430(4)
C(4)-O(2)	1.402(3)
C(4)-C(16)	1.417(4)
C(5)-C(6)	1.417(4)
C(5)-C(10)	1.426(4)
C(6)-C(7)	1.378(5)
C(7)-C(8)	1.404(5)
C(8)-C(9)	1.363(5)
C(9)-C(10)	1.417(4)
C(10)-C(11)	1.406(4)
C(11)-C(16)	1.385(4)
C(12)-C(13)	1.380(4)
C(12)-Si(1)	1.888(3)
C(13)-C(15)	1.418(4)
C(14)-C(15)	1.415(4)
C(14)-C(20)	1.424(4)
C(15)-C(17)	1.414(4)
C(16)-Si(3)	1.907(3)
C(17)-C(18)	1.367(5)
C(18)-C(19)	1.394(5)
C(19)-C(20)	1.377(4)
C(21)-Si(3)	1.872(4)
C(22)-Si(3)	1.863(4)
C(23)-Si(3)	1.870(3)
C(24)-Si(1)	1.866(4)
C(25)-Si(1)	1.852(4)
C(26)-Si(1)	1.871(4)
C(27)-N(1)	1.457(4)
C(28)-N(1)	1.452(4)
C(29)-C(30)	1.365(5)
C(29)-C(31)	1.500(5)
C(29)-Rh(1)	2.282(3)
C(30)-C(36)	1.513(5)
C(30)-Rh(1)	2.252(3)
C(31)-C(32)	1.539(5)
C(32)-C(33)	1.503(5)
C(33)-C(34)	1.396(5)
C(33)-Rh(1)	2.120(3)
C(34)-C(35)	1.525(5)
C(34)-Rh(1)	2.141(3)
C(35)-C(36)	1.525(5)
Cl(1)-Rh(1)	2.3455(8)
N(1)-P(2)	1.643(3)
O(1)-P(2)	1.630(2)
O(2)-P(2)	1.634(2)
P(2)-Rh(1)	2.2388(9)

		C(4)-C(16)-Si(3)	126.0(2)
C(2)-C(1)-O(1)	117.8(3)	C(18)-C(17)-C(15)	120.8(3)
C(2)-C(1)-C(12)	124.5(3)	C(17)-C(18)-C(19)	120.1(3)
O(1)-C(1)-C(12)	117.5(2)	C(20)-C(19)-C(18)	120.6(3)
C(1)-C(2)-C(14)	117.8(3)	C(19)-C(20)-C(14)	120.9(3)
C(1)-C(2)-C(3)	120.7(3)	C(30)-C(29)-C(31)	126.2(3)
C(14)-C(2)-C(3)	121.5(2)	C(30)-C(29)-Rh(1)	71.30(19)
C(4)-C(3)-C(5)	118.2(3)	C(31)-C(29)-Rh(1)	109.4(2)
C(4)-C(3)-C(2)	120.4(3)	C(29)-C(30)-C(36)	126.9(3)
C(5)-C(3)-C(2)	121.4(3)	C(29)-C(30)-Rh(1)	73.67(19)
C(3)-C(4)-O(2)	118.1(3)	C(36)-C(30)-Rh(1)	105.3(2)
C(3)-C(4)-C(16)	123.6(3)	C(29)-C(31)-C(32)	112.3(3)
O(2)-C(4)-C(16)	118.2(3)	C(33)-C(32)-C(31)	113.2(3)
C(6)-C(5)-C(10)	118.0(3)	C(34)-C(33)-C(32)	127.3(3)
C(6)-C(5)-C(3)	123.0(3)	C(34)-C(33)-Rh(1)	71.7(2)
C(10)-C(5)-C(3)	118.9(3)	C(32)-C(33)-Rh(1)	108.7(2)
C(7)-C(6)-C(5)	120.7(3)	C(33)-C(34)-C(35)	125.9(3)
C(6)-C(7)-C(8)	120.8(3)	C(33)-C(34)-Rh(1)	70.0(2)
C(9)-C(8)-C(7)	119.9(3)	C(35)-C(34)-Rh(1)	113.6(2)
C(8)-C(9)-C(10)	121.0(3)	C(36)-C(35)-C(34)	112.0(3)
C(11)-C(10)-C(9)	121.5(3)	C(30)-C(36)-C(35)	113.7(3)
C(11)-C(10)-C(5)	119.0(3)	C(28)-N(1)-C(27)	115.2(3)
C(9)-C(10)-C(5)	119.5(3)	C(28)-N(1)-P(2)	124.7(2)
C(16)-C(11)-C(10)	123.2(3)	C(27)-N(1)-P(2)	119.7(2)
C(13)-C(12)-C(1)	116.0(3)	C(1)-O(1)-P(2)	125.26(19)
C(13)-C(12)-Si(1)	118.1(2)	C(4)-O(2)-P(2)	115.68(17)
C(1)-C(12)-Si(1)	125.8(2)	O(1)-P(2)-O(2)	101.02(11)
C(12)-C(13)-C(15)	123.0(3)	O(1)-P(2)-N(1)	108.82(13)
C(15)-C(14)-C(20)	117.7(3)	O(2)-P(2)-N(1)	98.22(12)
C(15)-C(14)-C(2)	119.2(2)	O(1)-P(2)-Rh(1)	108.99(8)
C(20)-C(14)-C(2)	123.1(3)	O(2)-P(2)-Rh(1)	119.14(8)
C(17)-C(15)-C(14)	119.8(3)	N(1)-P(2)-Rh(1)	118.83(10)
C(17)-C(15)-C(13)	121.1(3)	C(33)-Rh(1)-C(34)	38.25(13)
C(14)-C(15)-C(13)	119.1(3)	C(33)-Rh(1)-P(2)	92.62(10)
C(11)-C(16)-C(4)	116.0(3)	C(34)-Rh(1)-P(2)	95.22(10)
C(11)-C(16)-Si(3)	117.8(2)	C(33)-Rh(1)-C(30)	96.59(14)

C(34)-Rh(1)-C(30)	80.79(13)	P(2)-Rh(1)-C(30)	159.00(9)
C(33)-Rh(1)-C(29)	80.71(13)		
C(34)-Rh(1)-C(29)	87.19(13)		
P(2)-Rh(1)-C(29)	165.96(9)		
C(30)-Rh(1)-C(29)	35.02(12)		
C(33)-Rh(1)-Cl(1)	154.96(10)		
C(34)-Rh(1)-Cl(1)	165.24(10)		
P(2)-Rh(1)-Cl(1)	90.89(3)		
C(30)-Rh(1)-Cl(1)	88.71(9)		
C(29)-Rh(1)-Cl(1)	90.14(9)		
C(25)-Si(1)-C(24)	110.21(17)		
C(25)-Si(1)-C(26)	106.13(18)		
C(24)-Si(1)-C(26)	108.07(18)		
C(25)-Si(1)-C(12)	114.94(15)		
C(24)-Si(1)-C(12)	106.95(15)		
C(26)-Si(1)-C(12)	110.39(15)		
C(22)-Si(3)-C(23)	108.46(19)		
C(22)-Si(3)-C(21)	112.20(17)		
C(23)-Si(3)-C(21)	107.93(18)		
C(22)-Si(3)-C(16)	113.88(15)		
C(23)-Si(3)-C(16)	105.61(16)		
C(21)-Si(3)-C(16)	108.39(16)		

Symmetry transformations used to generate equivalent atoms:

Table A.3.30. Anisotropic displacement parameters ($Å^2 x\ 10^3$)for **B2**. The anisotropic displacement factor exponent takes the form: $-2p^2[\ h^2a^{*2}U^{11} + ... + 2\ h\ k\ a^*\ b^*\ U^{12}\ ]$

	U^{11}	U^{22}	U^{33}	U^{23}	U^{13}	U^{12}
C(1)	14(1)	11(1)	14(1)	-1(1)	3(1)	1(1)
C(2)	14(1)	12(1)	14(1)	0(1)	-1(1)	-1(1)
C(3)	14(2)	16(1)	12(1)	2(1)	-1(1)	2(1)
C(4)	15(2)	15(1)	12(1)	-1(1)	2(1)	0(1)
C(5)	18(2)	18(1)	13(1)	-3(1)	0(1)	3(1)
C(6)	26(2)	17(1)	20(1)	-1(1)	-2(1)	0(1)
C(7)	31(2)	18(2)	27(2)	-2(1)	-6(1)	-1(1)
C(8)	32(2)	25(2)	26(2)	-4(1)	-10(2)	-10(2)
C(9)	25(2)	27(2)	22(1)	-2(1)	-8(1)	-2(1)
C(10)	19(2)	20(2)	14(1)	-2(1)	-3(1)	-1(1)
C(11)	20(2)	24(2)	18(1)	-3(1)	-5(1)	3(1)
C(12)	14(1)	14(1)	14(1)	1(1)	-1(1)	-2(1)
C(13)	15(2)	16(1)	17(1)	-1(1)	-4(1)	-2(1)
C(14)	15(1)	11(1)	14(1)	1(1)	2(1)	1(1)
C(15)	14(2)	14(1)	17(1)	0(1)	0(1)	1(1)
C(16)	18(2)	23(2)	14(1)	-2(1)	-1(1)	5(1)
C(17)	18(2)	18(2)	21(1)	-3(1)	0(1)	6(1)
C(18)	24(2)	25(2)	26(2)	-4(1)	0(1)	11(2)
C(19)	24(2)	26(2)	17(1)	-3(1)	3(1)	5(1)
C(20)	24(2)	15(1)	14(1)	0(1)	-1(1)	2(1)
C(21)	24(2)	30(2)	35(2)	-3(2)	-4(2)	9(2)
C(22)	30(2)	22(2)	34(2)	6(2)	-3(2)	2(2)
C(23)	54(2)	33(2)	19(1)	3(2)	-5(2)	13(2)
C(24)	33(2)	34(2)	21(2)	-1(1)	-7(2)	5(2)
C(25)	24(2)	43(2)	18(1)	0(2)	0(1)	1(2)
C(26)	32(2)	29(2)	32(2)	-8(2)	-3(2)	-3(2)
C(27)	28(2)	28(2)	29(2)	-16(2)	-5(2)	0(2)
C(28)	26(2)	41(2)	26(2)	-4(2)	4(1)	-16(2)
C(29)	19(1)	23(2)	25(1)	2(2)	0(1)	1(1)
C(30)	15(2)	25(2)	24(2)	-6(1)	4(1)	3(1)
C(31)	19(2)	35(2)	24(2)	-2(2)	-2(1)	-3(2)

C(32)	25(2)	28(2)	29(2)	-6(2)	0(2)	-6(2)
C(33)	19(2)	15(2)	32(2)	-3(1)	3(1)	-4(1)
C(34)	20(2)	17(1)	31(2)	5(1)	-2(1)	2(1)
C(35)	22(2)	35(2)	29(2)	10(2)	3(2)	1(2)
C(36)	22(2)	47(2)	20(2)	1(2)	4(1)	-2(2)
Cl(1)	26(1)	15(1)	38(1)	-2(1)	2(1)	2(1)
N(1)	17(1)	21(1)	20(1)	-7(1)	3(1)	-4(1)
O(1)	14(1)	17(1)	13(1)	0(1)	2(1)	5(1)
O(2)	18(1)	15(1)	13(1)	-2(1)	0(1)	1(1)
P(2)	14(1)	15(1)	14(1)	-2(1)	1(1)	0(1)
Rh(1)	14(1)	14(1)	19(1)	-2(1)	1(1)	1(1)
Si(1)	18(1)	23(1)	14(1)	-3(1)	-2(1)	0(1)
Si(3)	23(1)	19(1)	18(1)	1(1)	-2(1)	6(1)

Table A.3.31. Hydrogen coordinates (x 10^4) and isotropic displacement parameters (Å^{2}x 10^3) for **B2**.

	x	y	z	U(eq)
H(6)	3669	11374	8924	25
H(7)	4870	12442	9391	30
H(8)	6403	11999	10059	33
H(9)	6783	10487	10220	30
H(11)	6260	8881	10052	25
H(13)	206	10460	7557	19
H(17)	-818	11158	8450	23
H(18)	-904	11489	9497	30
H(19)	607	11016	10162	27
H(20)	2254	10286	9771	21
H(21A)	6980	6848	8972	44
H(21B)	7171	6268	9579	44
H(21C)	7488	7308	9578	44
H(22A)	3502	6509	9476	43
H(22B)	4417	5718	9579	43
H(22C)	4377	6235	8937	43
H(23A)	5537	6499	10698	53
H(23B)	4600	7290	10701	53
H(23C)	5962	7516	10717	53
H(24A)	765	10328	5872	44
H(24B)	1006	10975	6442	44
H(24C)	-93	10318	6450	44
H(25A)	3546	9946	6355	43
H(25B)	2976	9304	5851	43
H(25C)	3539	8888	6459	43
H(26A)	1386	7882	6730	46
H(26B)	742	8272	6136	46
H(26C)	146	8360	6797	46
H(27A)	2769	6827	6768	43
H(27B)	3374	6109	7208	43

H(27C)	4124	6913	6931	43
H(28A)	2039	6504	8161	47
H(28B)	1334	7005	7630	47
H(28C)	1741	7542	8227	47
H(31A)	8860	8938	7552	32
H(31B)	9144	8452	8188	32
H(32A)	7481	8982	8653	33
H(32B)	7878	9818	8247	33
H(35A)	6795	9557	6393	34
H(35B)	7802	9555	6902	34
H(36A)	6951	8062	6218	36
H(36B)	8281	8329	6334	36
H(29)	8080(30)	7230(20)	7882(15)	16(8)
H(30)	7440(30)	7020(20)	6941(14)	8(8)
H(33)	5790(40)	9430(30)	8163(18)	31(11)
H(34)	5530(30)	9340(30)	7133(17)	20(10)

APPENDIX 4

Ligand Development for Rh(I)-Catalyzed [2+2+2] Cycloadditions with Terminal Alkynes

A.4.1 Materials and Methods

Toluene, tetrahydrofuran, ether, and dichloromethane were degassed with argon and passed through one column of neutral alumina and one column of Q5 reactant. Triethylamine (peptide synthesis grade) was purchased from Fisher Scientific, dried over calcium hydride and freshly distilled prior to use. Flash column chromatography was carried out on silica gel (60 Å, 230 - 400 mesh, obtained from Silicycle Inc.) and was performed with reagent grade solvents. Analytical thin-layer chromatography (TLC) was performed on Silicycle glass-backed silica gel plates (60 Å, 0.25 mm, purchased from Silicycle Inc.) and visualized with a UV lamp (254 nm), and potassium permanganate or cerric ammonium molybdate.

Infrared spectra (IR) were obtained on a Nicolet Avatar 320 FT-IR spectrometer and Bruker Tensor 27 FT-IR spectrometer. ^{1}H NMR and ^{13}C NMR were obtained on Varian Unity 300 and Unity 400 spectrometers. Chemical shifts are expressed in parts per million values (δ, ppm). Proton chemical shifts in $CDCl_3$ were referenced to 7.26 ppm ($CHCl_3$). Carbon chemical shifts were referenced to 77.2 ppm ($CDCl_3$). Peak multiplicities are designated by the following abbreviations: s, singlet; d, doublet; t, triplet; q, quartet; m, multiplet; dd, doublet of doublets; dt, doublet of triplets; b, broad; *J*, coupling constant in Hz. Low resolution mass spectra (MS) and high resolution mass spectra (HRMS) were recorded on a Fisons VG Autospec spectrometer. HPLC spectra were obtained on an Agilent 1100 series system. Optical rotation was obtained with an Autopol-III automatic polarimeter. Melting points were obtained on a

Fisher-Johns melting point apparatus and are uncorrected. References following the compound names indicate literature articles where the compound has been previously been reported.

Unless indicated, commercially available starting materials were purchased from Aldrich Chemicals and used without further purification. $[Rh(ethylene)_2Cl]_2$ and cobalt carbonyl were purchased from Strem Chemicals or Alfa Aesar and used without further purification.

A.4.2 General Procedure for Ligand Synthesis

Taddol diols were prepared from diethyl-tartrate according to literature procedures.[1]

To a flame-dried round bottom flask equipped with a magnetic stirbar under an Ar atmosphere was added the desired amine (pyrrolidine: 0.20 ml, 2.42 mmol, 1 equiv.) and tetrahydrofuran (THF, anhydrous, 40 ml). The reaction vessel is cooled to 0 °C and *n*-butyl lithium (1.6 ml, 1.6 M in hexanes) is added dropwise via syringe. The solution is stirred for 30 minutes at 0 °C before phosphorous trichloride (0.22 ml, 2.52 mmol, 1.0 equiv.) is added in one portion via syringe. After stirring an additional 15 minutes, a solution of Taddol diol (2.0 g, 2.42 mmol, 1 equiv.), and triethylamine (1.0 ml, 7.19 mmol, 3.0 equiv.) in THF (10 ml) is added via syringe. The flask is allowed to warm to room temperature, stirred for 3 hours, and solvent is removed by rotary evaporation. Toluene (50 ml) is then added to the resultant residue and the slurry is filtered through alumina and washed with toluene (2x). Solvent is removed from the combined filtrates by rotary evaporation. If necessary, the product can be further purified by column chromatography (19:1 Hexanes/EtOAc) to yield a white foam powder (1.1g, 51% yield, CKPhos).

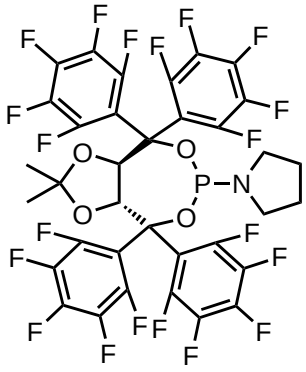

1-((3aR,8aR)-2,2-dimethyl-4,4,8,8-tetrakis(perfluorophenyl)tetrahydro-[1,3]dioxolo[4,5-e][1,3,2]dioxaphosphepin-6-yl)pyrrolidine (CKphos).

General procedure yielded a white solid (51 %). $[\alpha]^{20}_D$ = -109°, c = 0.01 g/ml $CHCl_3$. Rf = 0.46 (19:1, Hex/EtOAc). ^{1}H-NMR (400 MHz; $CDCl_3$): δ 5.59 (1H, d, *J* = 7.8 Hz), 5.31 (1H, d, *J* = 8.2 Hz), 3.12 (2H, dd, *J* = 9.7, 5.7 Hz), 2.79 (2H, dd, *J* = 9.4, 5.4 Hz), 1.70-1.59 (4H, m), 1.08 (3H, s), 0.72 (3H, s).

[1] For the synthesis of the Taddol diol precursors see: Seebach, D.; Beck, A.K.; Keckel, A. *Angew. Chem. Int. Ed.* **2001**, *40*, 92. Burks, H.E.; Shubin, L.; Morken, J.P. *J. Am. Chem. Soc.* **2007**, 129, 28, 8766.

^{13}C-NMR (100 MHZ; $CDCl_3$): δ 146.3, 143.8, 142.3, 139.7, 139.0, 136.5, 117.7, 113.3, 80.6, 80.5, 80.4, 45.6, 45.4, 45.1, 26.3, 26.2, 26.0, 25.9, 25.8. ^{31}P-NMR (75 MHz; $CDCl_3$): δ 138.6. ^{19}F-NMR (376 MHz; $CDCl_3$): δ −131.2 (1F, d), -133.7 (1F, m), -135.8 (1F, d), -137.6 (2F, m), -139.2 (1F, d), -140.1 (1F, d), -151.8 (1F, t), -152.1 (1F, t), -152.3 (1F, t), -152.9 (1F, t), -160.4 (1F, m), -160.7 (1F, m), -161.1 to -161.4 (5F, m), -161.8 (1F, dt), -162.1 (1F, m). IR (Thin Film) v 2988, 2876, 1651, 1525, 1487, 1409, 1384, 1374, 1346, 1308, 1240, 1131, 985, 862, 807, 743, 703. HRMS (ESI) m/z $[C_{35}H_{17}F_{20}NO_4P]$+ calculated 925.0498, found 925.0508.

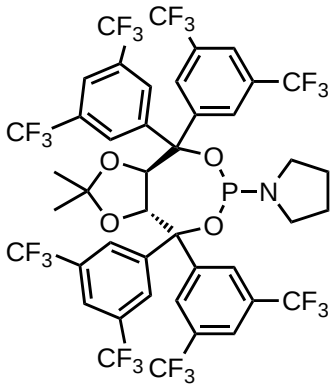

1-((3aR,8aR)-4,4,8,8-tetrakis(3,5-bistrifluoromethylphenyl)-2,2-dimethyltetrahydro-[1,3]dioxolo[4,5-e][1,3,2]dioxaphosphepin-6-yl)pyrollidine (T8)

General procedure yielded a white solid (72 %). $[\alpha]^{20}_D$ = -65°, c = 0.01 g/ml $CHCl_3$. Rf = 0.5 (19:1, Hex/EtOAc). ^{1}H-NMR (400 MHz; $CDCl_3$): δ 8.26 (2H, s), 8.01 (2H, s), 7.84 (8H, q, J = 8.7 Hz), 4.96-4.93 (1H, dd, J = 8.7, 3.8 Hz), 4.30 (dd, J = 8.7, 1.1 Hz), 3.41 (2H, quintet, J = 6.9 Hz), 3.30 (2H, quintet, J = 7.0 Hz), 1.97-1.89 (4H, m) 1.49 (3H, s) 0.310 (3H, s). ^{13}C-NMR (100 MHz; $CDCl_3$): δ 147.3, 146.4, 142.6, 141.8, 131.8 (m), 128.5 (d), 126.9, 126.6, 124.3, 122.7 (m), 122.3 (m), 121.6, 118.9, 82.8, 81.8, 81.5, 80.0, 79.9, 79.3, 45.0, 26.9, 26.0, 25.1. ^{19}F-NMR (376 MHz; $CDCl_3$): δ 63.1 (q). ^{31}P-NMR (75 MHz; $CDCl_3$) δ 139.4. IR (Thin Film) v 3103, 2969, 2879, 1625, 1467, 1374, 1338, 1279, 1176, 1133, 1047, 1014, 904, 879, 848, 779, 709, 683. HRMS (ESI) *m/z* $[C_{43}H_{29}F_{24}NO_4P]^+$ calculated 1109.1373, found 1109.1364.

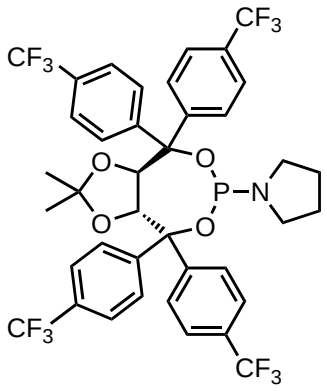

1-((3aR,8aR)-2,2-dimethyl-4,4,8,8-tetrakis(4-(trifluoromethyl)phenyl)tetrahydro-[1,3]dioxolo[4,5-e][1,3,2]dioxaphosphepin-6-yl)pyrrolidine (T7)

General procedure yielded a white solid (56%). $[\alpha]^{20}_{D}$ = -87°, c = 0.01 g/ml $CHCl_3$. Rf = 0.34 (19:1, Hex/EtOAc). ^{1}H-NMR (400 MHz; $CDCl_3$): δ 7.87 (2H, d, *J* = 8.3 Hz), 7.70 (2H, d, *J* = 8.4 Hz), 7.63-7.50 (12H, m), 5.12 (1H, dd, *J* = 8.6, 3.4 Hz), 4.64 (1H, d, *J* = 8.6 Hz), 3.40 (2H, quintet, 7.2 Hz), 3.26 (2H, quintet, 7.3 Hz), 1.87 (4H, m), 1.34 (3H, s), 0.32 (3H, s). ^{13}C-NMR (100 MHz; $CDCl_3$): δ 147.8, 147.1, 143.3, 142.7, 128.4, 128.2, 128.1, 128.0, 127.9 127.8, 127.7, 127.6, 127.3, 127.0, 126.9, 126.7, 125.8 125.4, 125.3, 123.5, 123.5, 123.4, 123.3, 123.0, 123.0, 122.9, 122.9, 122.8, 122.3, 122.3, 120.7, 120.6, 110.4, 80.3, 80.3, 80.1, 79.8, 79.0, 18.7, 78.6, 43.1, 43.0, 25.5, 24.1, 24.0, 23.3. ^{19}F-NMR (376 MHz; $CDCl_3$): δ -62.7 (q). ^{31}P-NMR (75 MHz; $CDCl_3$): δ 139.0. IR (Thin Film) v 2991, 2939, 2876, 1929, 1619, 1458, 1375, 1166, 1126, 1070, 1009, 909, 881, 851, 780, 733. HRMS (ESI) *m/z* $[C_{39}H_{33}F_{12}NO_4P]^+$ calculated 837.1877, found 837.1877.

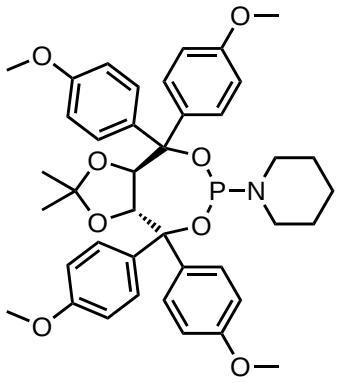

1-((3aR,8aR)-4,4,8,8-tetrakis(4-methoxyphenyl)-2,2-dimethyltetrahydro-[1,3]dioxolo[4,5-e][1,3,2]dioxaphosphepin-6-yl)piperidine (T4)

Synthesized according to the general ligand procedure with the following modifications to yield a white solid (35 %). After removal of THF, the product was further purified by column chromatography on neutral alumina (19:1 to 9:1 Hex/EtOAc). $[\alpha]^{20}_{D}$ = -94.5°, c = 0.01 g/ml $CHCl_3$. Rf = 0.10 (9:1, Hex/EtOAc). ^{1}H-NMR (400 MHz; $CDCl_3$): δ 7.69 (2H, d, *J* = 8.8 Hz), 7.51 (2H, d, *J* = 8.8 Hz), 7.34 (4H, dd, *J* = 18.0, 8.8 Hz), 6.81 (8H, td, *J* = 9.6, 5.9 Hz), 5.06 (1H, dd, *J* = 8.5, 3.3 Hz), 4.70 (1H, d, *J* = 8.5 Hz), 3.78 (12H, m), 3.27 (2H, m), 3.16 (2H, m), 1.59 (3H, s), 1.33 (3H, s). ^{13}C-NMR (100 MHZ; $CDCl_3$): δ 158.6, 158.5, 158.4, 158.3, 139.7, 139.3, 134.7, 134.4, 130.1, 130.0, 129.9, 128.2, 113.3, 112.9, 112.7, 112.4, 111.3, 98.3, 82.9, 82.8, 82.6, 82.4, 55.1, 45.0, 44.9, 27.6, 27.0, 25.5, 25.2. ^{31}P-NMR (75 MHZ; $CDCl_3$): δ 138.6. IR (Thin Film) v 2994, 2934, 2836, 1609,

1582, 1509, 1462, 1372, 1301, 1251, 1214, 1176, 1092, 1035, 949, 880, 787, 739, 712. MS (LR-ES) *m/z* $[C_{40}H_{46}NO_8P]^+$ calculated 700.3, found 700.4.

A.4.3 General Procedure for Rh(I)-Catalyzed [2+2+2] Cycloadditions

Isocyanates and vinylogous amide indolizinone products not listed below were synthesized according to previously reported literature procedures.[2]

An oven-dried round bottom flask was charged with $[Rh(C_2H_4)_2Cl]_2$ (4 mg, 0.01 mmol) and ligand (20 mg, 0.02 mmol) and fitted with an oven-dried reflux condenser in an inert atmosphere (Ar) glove box. Upon removal from the glove box, 2 ml of toluene was added via syringe and the resulting yellow solution was stirred at ambient temperature for 5 min. To this solution, alkyne **1** (0.20 mmol, 1 equiv) and isocyanate **2** (0.26 mmol, 1.3 equiv) in 6 ml of toluene was added via syringe. An additional 2 ml of toluene was used to wash down the residue and added to the reaction mixture. The reaction mixture was heated to 110 °C in an oil bath and kept at reflux for 16 h. The reaction mixture was cooled to 23 °C, concentrated in *vacuo*, and purified by flash column chromatography (19:1 EtOAc:MeOH). Evaporation of solvent afforded the analytically pure products. Absolute stereochemistry was established as previously reported.[3,4]

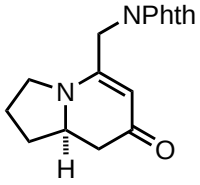

2-((7-oxo-1,2,3,7,8,8a-hexahydroindolizin-5-yl)methyl)isoindoline-1,3-dione

General procedure yielded a brown solid (71%). 98% ee by HPLC (Chiralcel ODH, Hex:iPrOH 70:30, 1 ml/min, RTmajor = 41.6 min, RTminor = 26.8 min). $[\alpha]^{20}_D$ = 152°, c = 0.01 g/ml $CHCl_3$. Rf = 0.14 (EtOAc). ^{1}H NMR (400 MHz, $CDCl_3$) δ 7.81 (2H, dd, *J* = 5.4, 3.1 Hz), 7.69 (2H, dd, *J* = 5.4, 3.0 Hz), 4.66 (1H, s), 4.41 (2H, q, *J* = 13.6 Hz), 3.75 (1H, ddt, *J* = 15.5, 10.3, 5.2 Hz), 3.61 (2H, dq, *J* = 24.9, 8.5 Hz), 2.34 (1H, dd, *J* = 16.0, 5.0 Hz), 2.24 (2H m), 2.13 (1H, dt, *J* = 12.7, 6.4 Hz), 1.90 (1H, m), 1.64 (1H, m). ^{13}C NMR (100 MHz, $CDCl_3$) δ 191.7, 167.3, 157.3, 134.4, 131.7, 123.7, 98.3, 94.7, 59.5, 46.5, 41.2, 37.9, 32.2, 24.1. IR (Thin Film) v 2964, 2875, 2360, 1778, 1716, 1620, 1562, 1500, 1469, 1422, 1394, 1351, 1330, 1300, 1273, 1250, 1198, 1167, 1112, 1086, 989, 952, 859, 756. HRMS (ESI) *m/z* $[C_{17}H_{17}N_2O_3]^+$ calculated 297.1234, found 297.1234.

---

[2] a) Dalton, D. M.; Oberg, K. M.; Yu, R. T.; Lee, E. E.; Perreault, S.; Oinen, M. E.; Pease, M. L.; Malik, G.; Rovis, T. *J. Am. Chem. Soc.* **2009**, *131*, 43, 15717-15728. b) Yu, R. T.; Lee, E. E.; Malik, G.; Rovis, T. *Angew. Chem. Int. Ed.* **2009**, *48*, 2379-2382. c) Lee, E. E.; Rovis, T. *Org. Lett.* **2008**, 10, 6, 1231-1234.

[3] Yu, R. T.; Rovis, T. *J. Am. Chem. Soc.* **2006**, *128*, 12370-12371

[4] Yu, R. T.; Lee, E. E.; Malik, G.; Rovis, T. *Angew. Chem. Int. Ed.* **2009**, *48*, 2379-2382.

A.4.4 ^{1}H–NMR, ^{13}C–NMR, ^{19}F–NMR, and ^{31}P–NMR Spectra

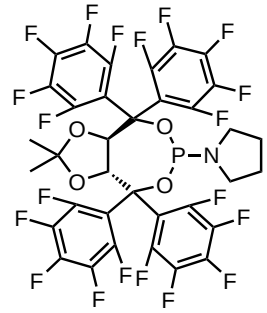

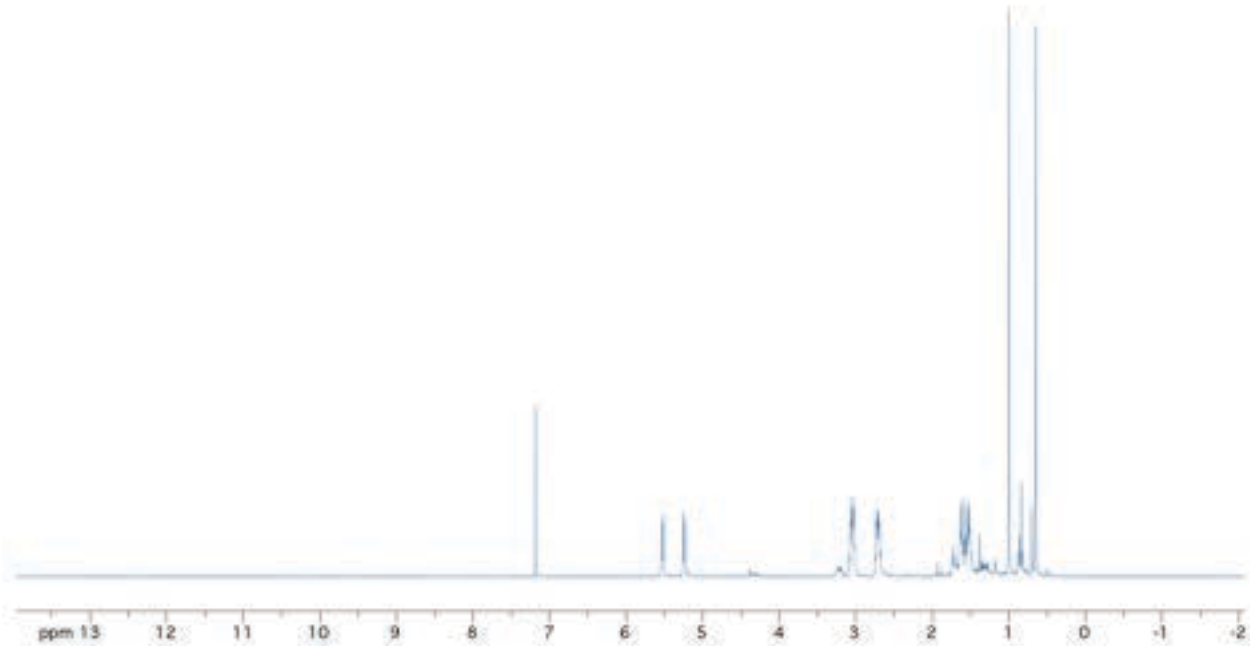

Figure A.4.1 ^{1}H-NMR CKphos

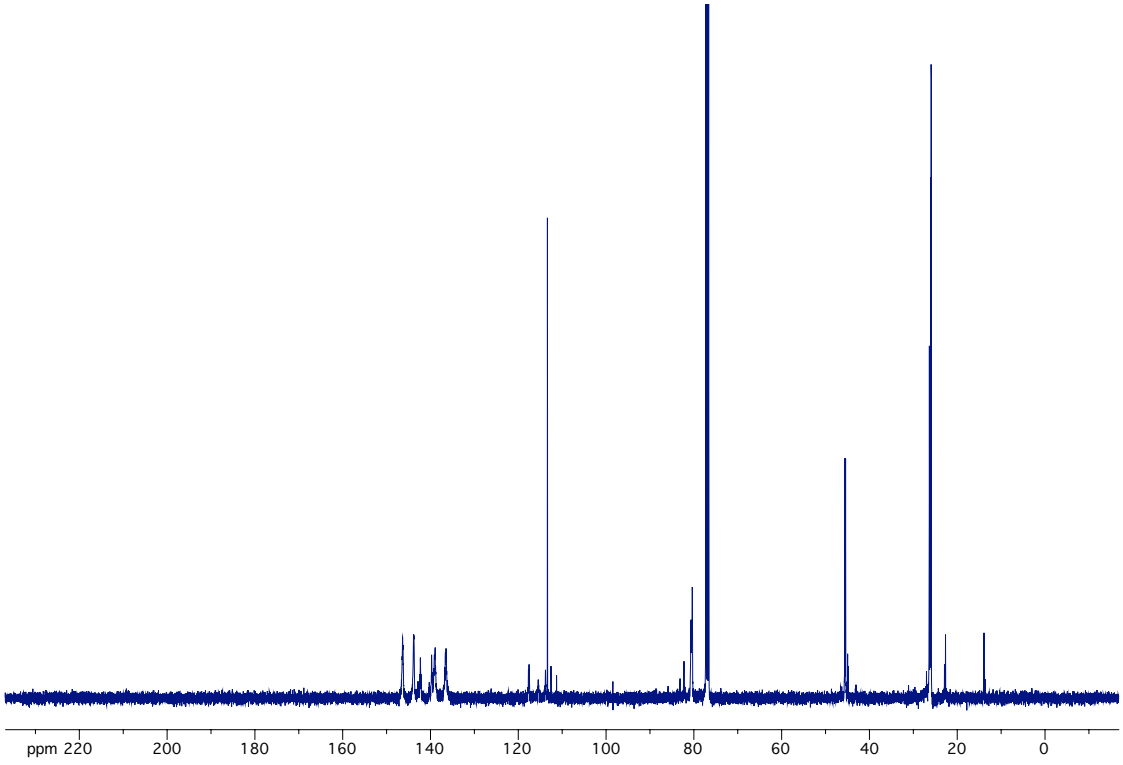

Figure A.4.2 ^{13}C-NMR

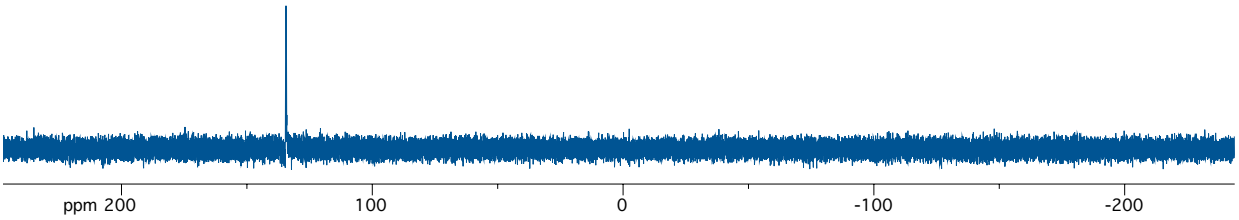

Figure A.4.3 ^{31}P-NMR

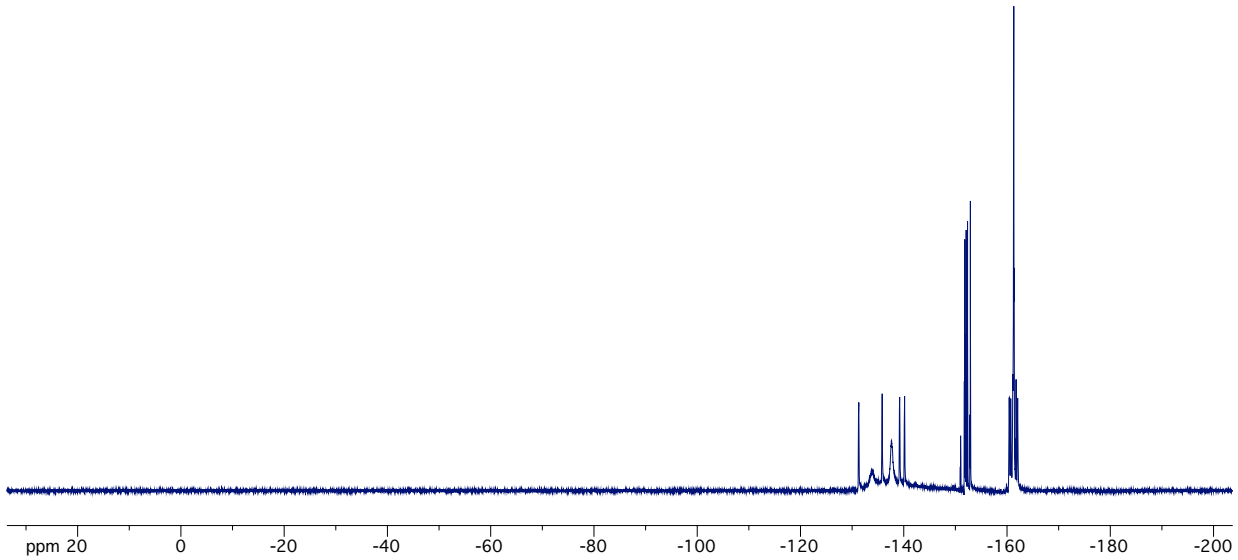

Figure A.4.4 ^{19}F-NMR

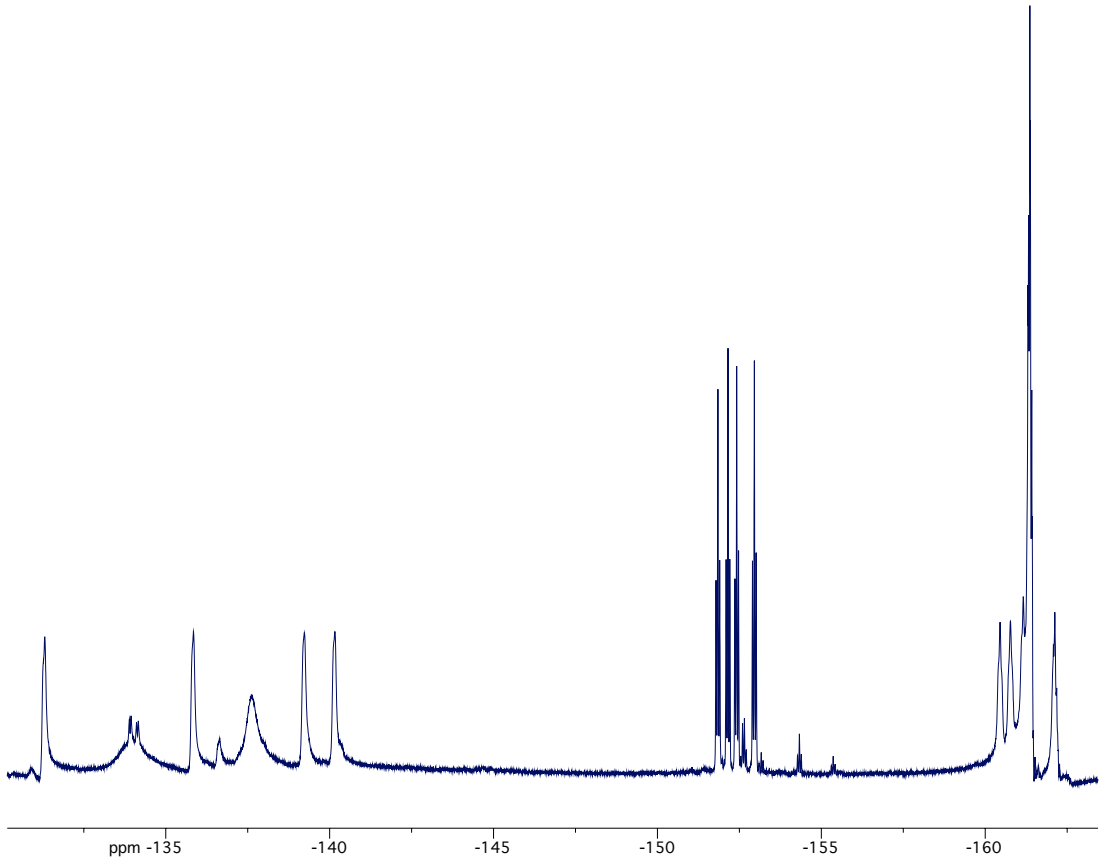

Figure A.4.5 ^{19}F-NMR

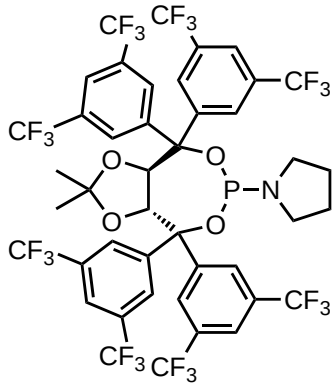

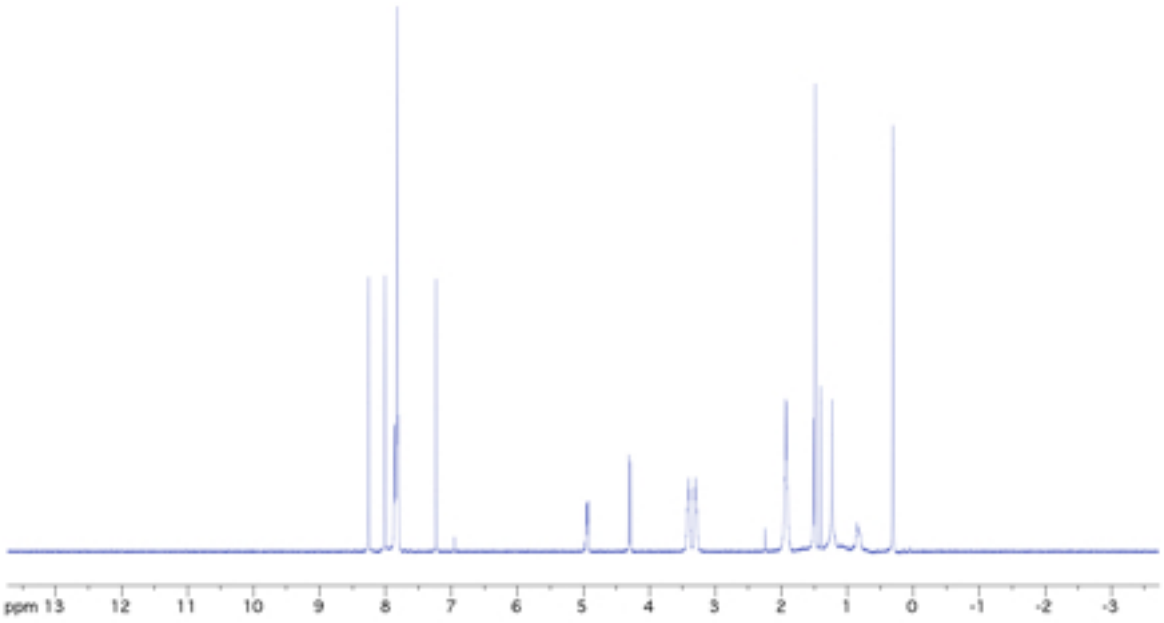

Figure A.4.6 ^{1}H-NMR

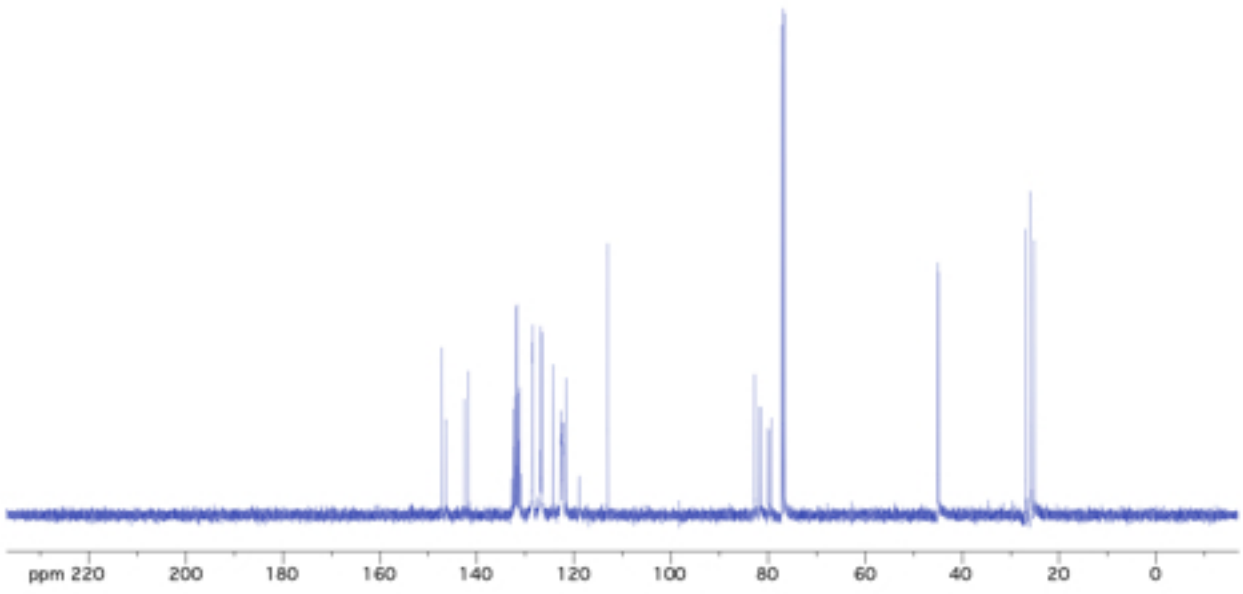

Figure A.4.7 ^{13}C-NMR

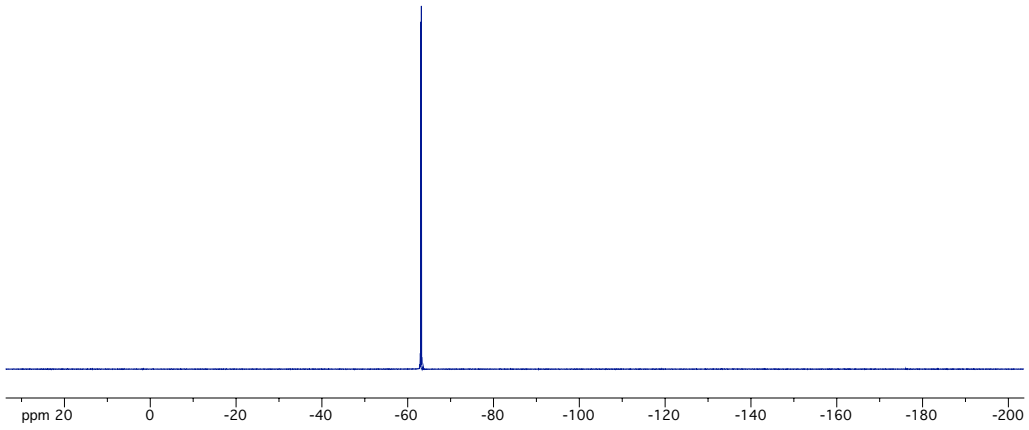

Figure A.4.8 ^{19}F-NMR

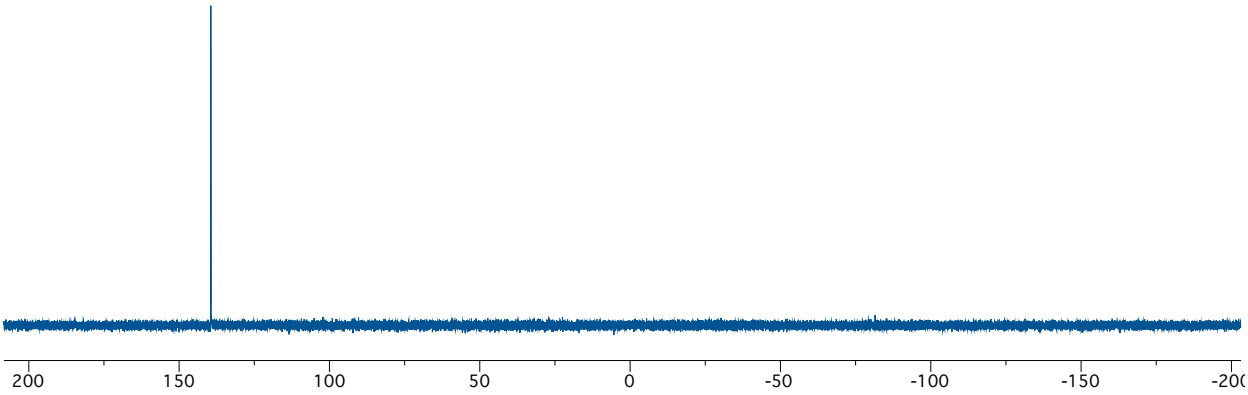

Figure A.4.9 ^{31}P-NMR

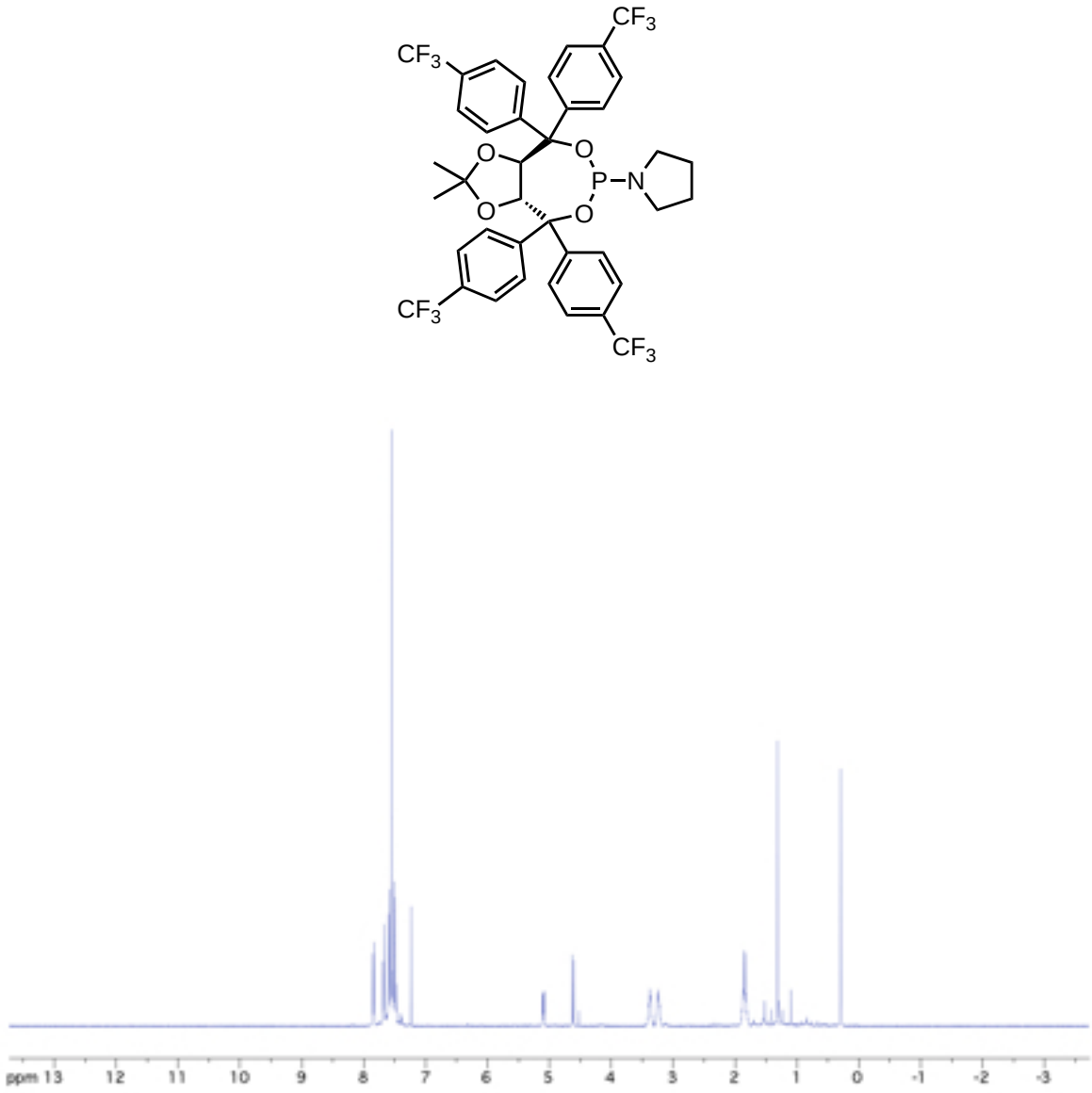

Figure A.4.10 ^{1}H-NMR

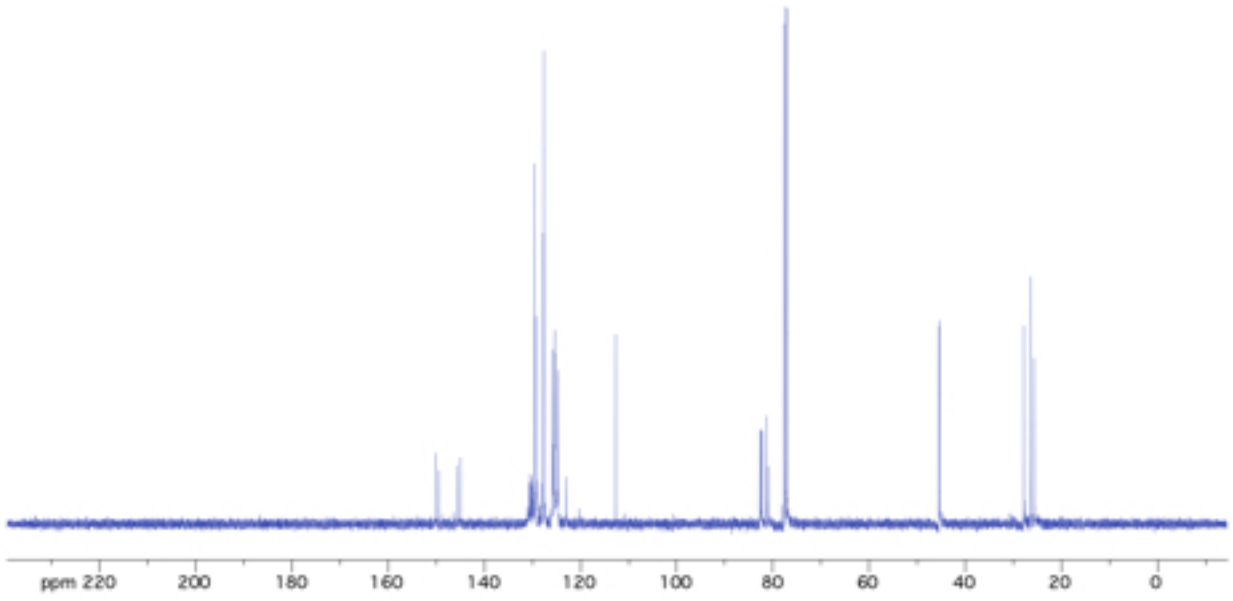

Figure A.4.11 ^{13}C-NMR

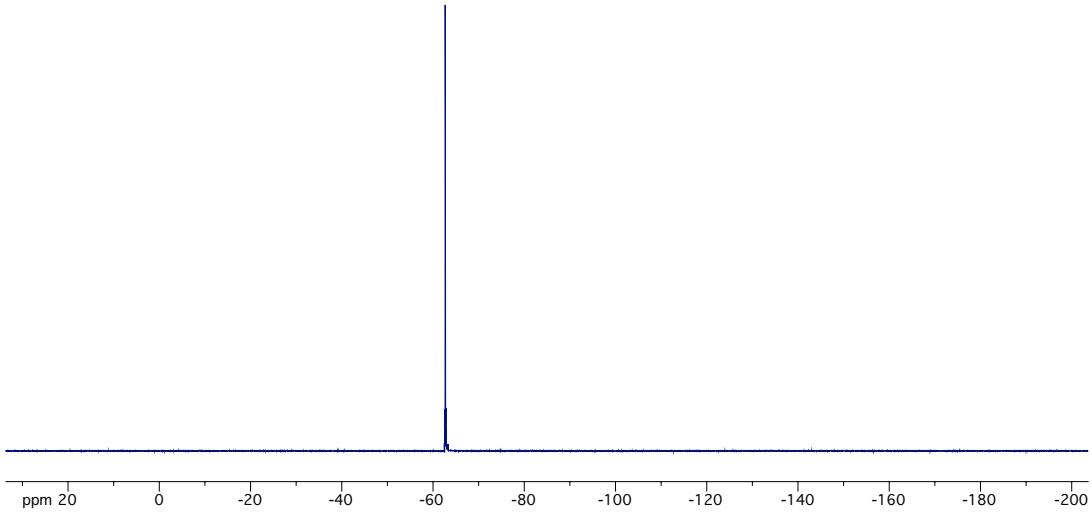

Figure A.4.12 ^{19}F-NMR

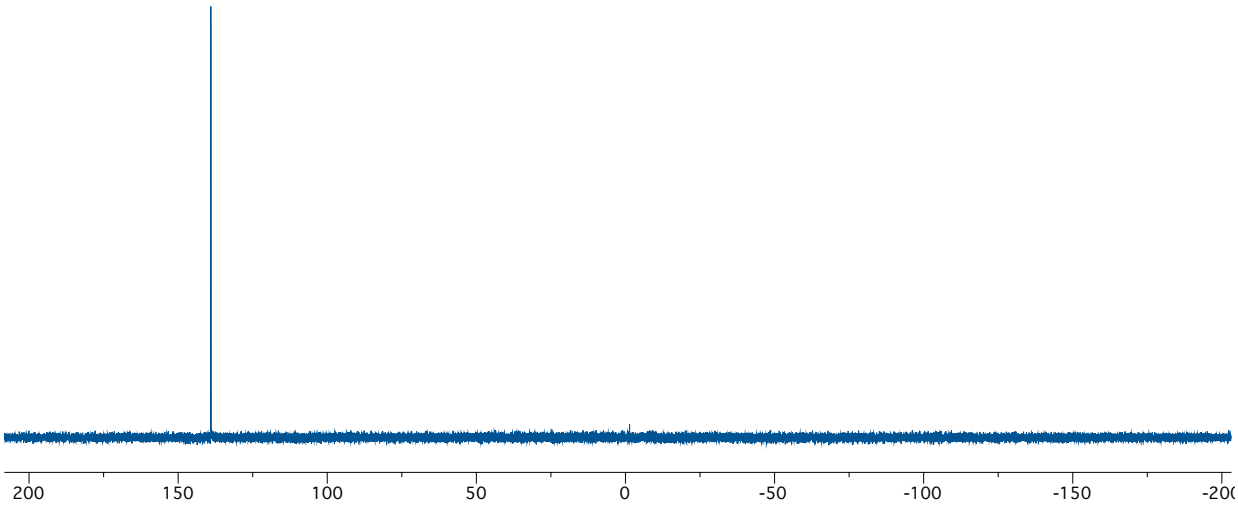

Figure A.4.13 ^{31}P-NMR

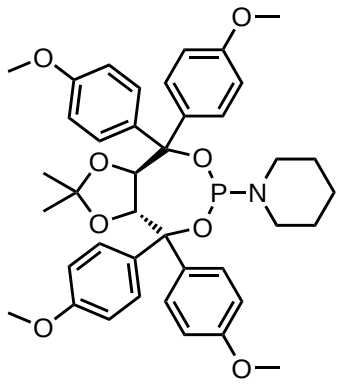

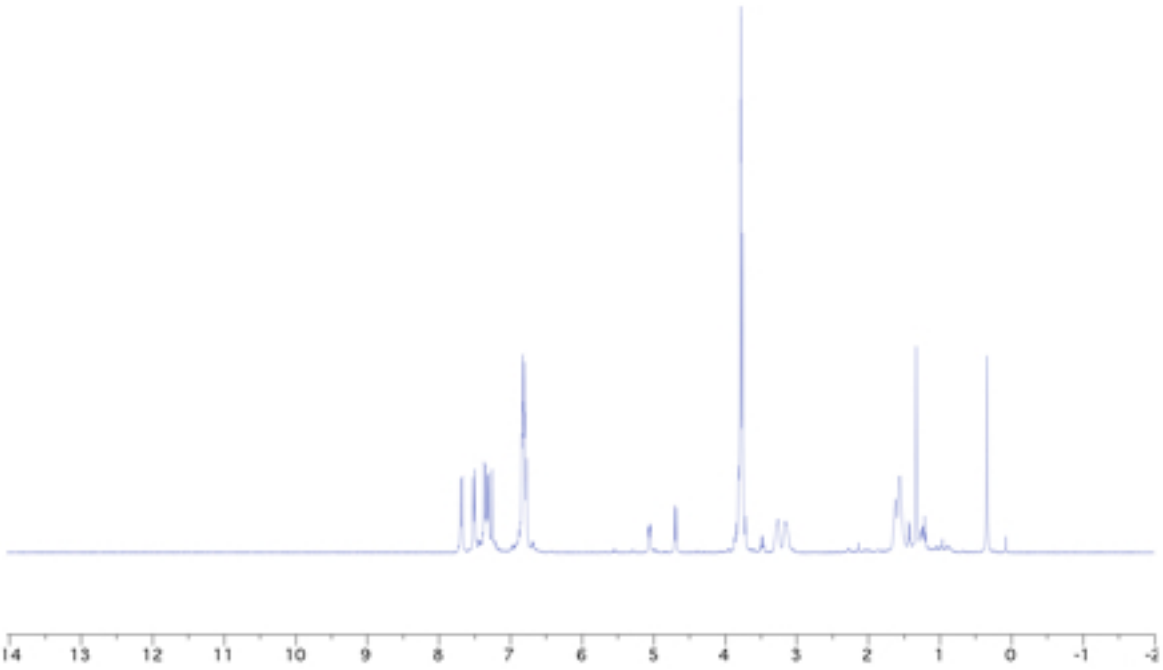

Figure A.4.14 ^{1}H-NMR

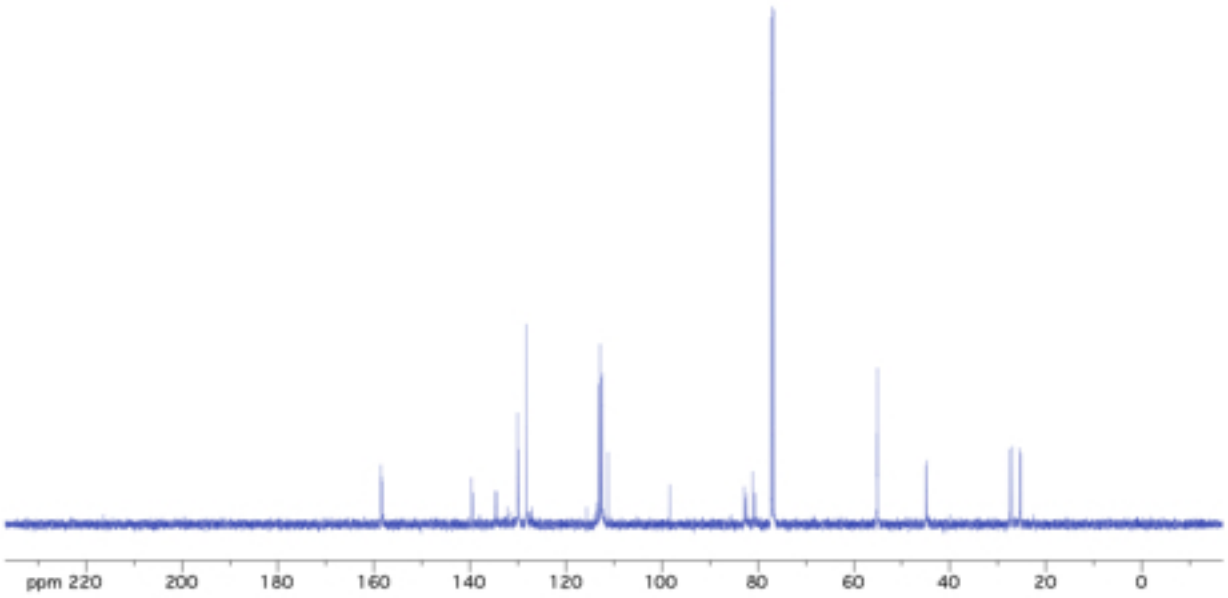

Figure A.4.15 ^{13}C-NMR

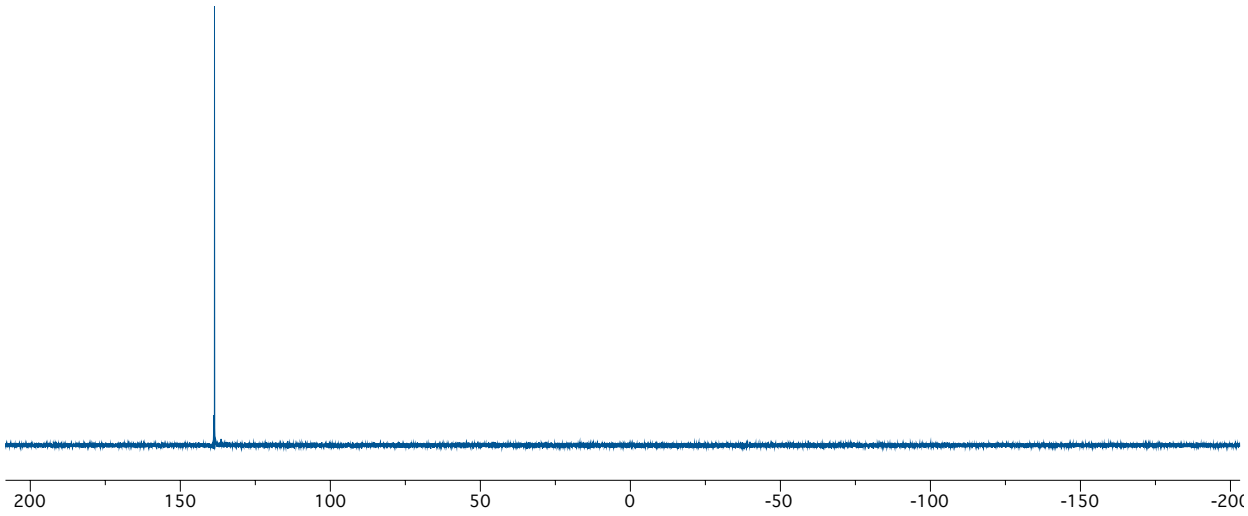

Figure A.4.16 ^{31}P-NMR

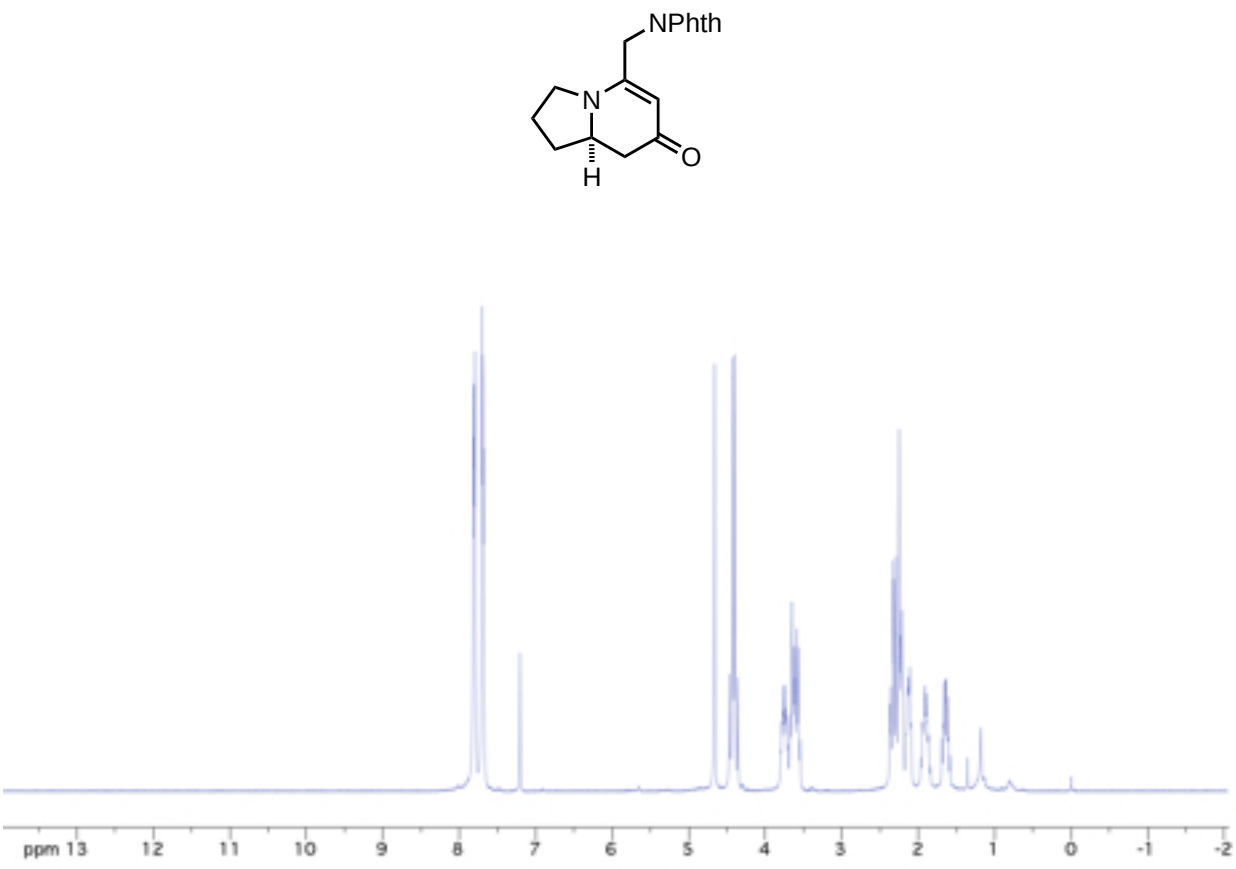

Figure A.4.17 ^{1}H-NMR

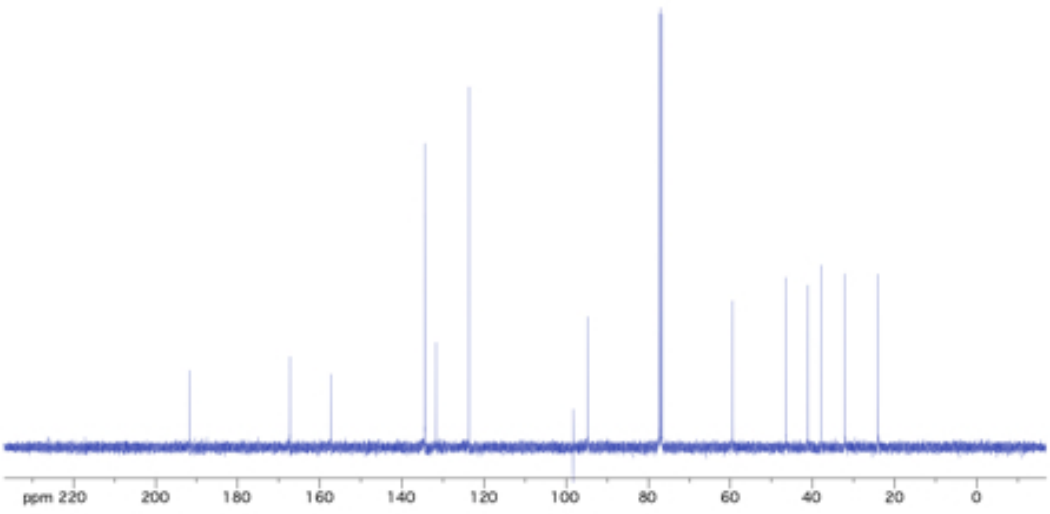

Figure A.4.18 ^{13}C-NMR

APPENDIX 5

Perfluoroaryl Taddol Phosphoramidites as L,Z-Ligands on Rh(I) and Co(-1)

A.5.1 Materials and Methods

Toluene, tetrahydrofuran, ether, and dichloromethane were degassed with argon and passed through one column of neutral alumina and one column of Q5 reactant. Triethylamine (peptide synthesis grade) was purchased from Fisher Scientific, dried over calcium hydride and freshly distilled prior to use. Flash column chromatography was carried out on silica gel (60 Å, 230 - 400 mesh, obtained from Silicycle Inc.) and was performed with reagent grade solvents. Analytical thin-layer chromatography (TLC) was performed on Silicycle glass-backed silica gel plates (60 Å, 0.25 mm, purchased from Silicycle Inc.) and visualized with a UV lamp (254 nm), and potassium permanganate or cerric ammonium molybdate.

Infrared spectra (IR) were obtained on a Nicolet Avatar 320 FT-IR spectrometer and Bruker Tensor 27 FT-IR spectrometer. ^{1}H NMR and ^{13}C NMR were obtained on Varian Unity 300 and Unity 400 spectrometers. Chemical shifts are expressed in parts per million values (δ, ppm). Proton chemical shifts in $CDCl_3$ were referenced to 7.26 ppm ($CHCl_3$). Carbon chemical shifts were referenced to 77.2 ppm ($CDCl_3$). Peak multiplicities are designated by the following abbreviations: s, singlet; d, doublet; t, triplet; q, quartet; m, multiplet; dd, doublet of doublets; dt, doublet of triplets; b, broad; *J*, coupling constant in Hz. Low resolution mass spectra (MS) and high resolution mass spectra (HRMS) were recorded on a Fisons VG Autospec spectrometer. HPLC spectra were obtained on an Agilent 1100 series system. Optical

rotation was obtained with an Autopol-III automatic polarimeter. Melting points were obtained on a Fisher-Johns melting point apparatus and are uncorrected. References following the compound names indicate literature articles where the compound has been previously been reported.

Unless indicated, commercially available starting materials were purchased from Aldrich Chemicals and used without further purification. $[Rh(ethylene)_2Cl]_2$ and cobalt carbonyl were purchased from Strem Chemicals or Alfa Aesar and used without further purification.

A.5.2 X-ray Crystallography Data

All single crystals were coated in oil, transferred to a goniometer head, and mounted on a Bruker Kappa Apex CCD diffractometer under a stream of N_2. All data collections were performed with Mo Kα radiation and a graphite monochromator. Data sets were taken with complete coverage and fourfold redundancy at 120 °K. Data was integrated and corrected for absorption effects with the Apex 2 software package.[1] Structures were solved with the SHELXTL software package.[2] All non-hydrogen atoms were refined with anisotropic thermal parameters and hydrogen atoms placed in idealized positions. Crystal data and structure parameters are provided as CIF files. Rhodium alkene bond distances were generated in XP using the cent/x, join and bang commands.

Rh(cod)X-CKphos complexes were synthesized by adding Rh(cod)Cl (1 equiv.), racemic CKphos (1 equiv), and Ag salt of desired counterion (OTs, OTf, 1 equiv) to an oven dried vial equipped with a magnetic stirbar in an Ar atmosphere glove box. After removal of vial from the glove box, DCM (1 ml) is added and the solution stirred at rt under Ar flow for 1 h. A white precipitate forms and the solution is filtered through a plug of cotton or glass wool. The clear yellow solution is layered with hexanes and slow evaporation provided yellow X-ray quality crystals.

---

[1] Bruker AXS Inc., 5465 East Chervl Parkway, Madison, WI 53711-5373 USA

[2] Sheldrick, G. (1997) *SHELXL-97 Program for Crystal Structure Refinement*, Institüt für Anorganische Chemie der Universität, Göttingen, Germany.

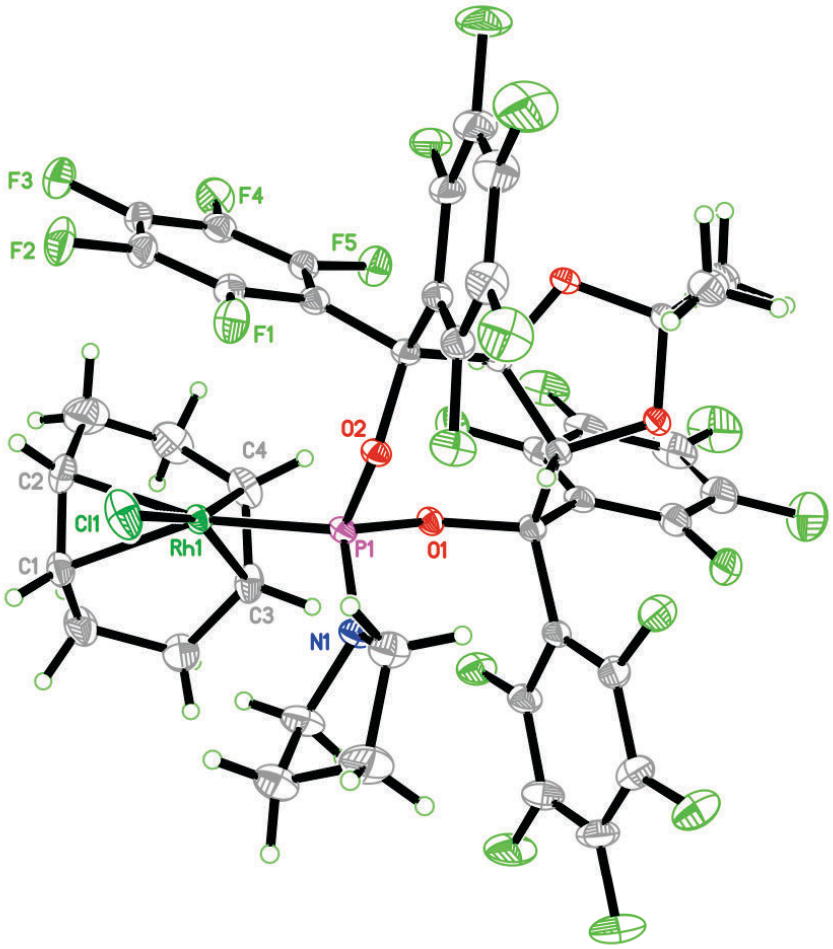

Table A.5.1. Crystal data and structure refinement for Rh(cod)Cl•CKphos.

Identification code	rovis106_0m	
Empirical formula	C_{44} H_{28} Cl_3 F_{20} N O_4 P Rh	
Formula weight	1254.90	
Temperature	120(2) K	
Wavelength	0.71073 Å	
Crystal system	Triclinic	
Space group	*P* -1	
Unit cell dimensions	*a* = 11.5246(6) Å	α = 68.867(2)°
	b = 12.6819(7) Å	β = 84.990(3)°
	c = 17.2832(9) Å	γ = 77.050(3)°
Volume	2296.1(2) $Å^3$	
Z	2	
Density (calculated)	1.815 Mg/m^3	

Absorption coefficient	0.709 mm^{-1}
F_{000}	1244
Crystal size	0.37 x 0.11 x 0.09 mm^3
Theta range for data collection	1.76 to 33.21°.
Index ranges	-17≤h≤17, -18≤k≤19, -26≤l≤26
Reflections collected	64119
Independent reflections	17541 [R(int) = 0.0432]
Completeness to theta = 33.21°	99.5 %
Absorption correction	Multi-scan
Max. and min. transmission	0.9364 and 0.7794
Refinement method	Full-matrix least-squares on F^2
Data / restraints / parameters	17541 / 0 / 669
Goodness-of-fit on F^2	1.091
Final R indices [I>2sigma(I)]	R1 = 0.0495, wR2 = 0.1323
R indices (all data)	R1 = 0.0742, wR2 = 0.1536
Largest diff. peak and hole	2.036 and -1.839 $e.Å^{-3}$

Table A.5.2. Atomic coordinates (x 10^4) and equivalent isotropic displacement parameters ($Å^2$x 10^3) for Rh(cod)Cl·CKphos. U(eq) is defined as one third of the trace of the orthogonalized U^{ij} tensor.

	x	y	z	U(eq)
C(1)	5785(2)	6845(2)	4563(1)	22(1)
C(2)	5018(3)	6309(3)	5139(2)	30(1)
C(3)	5884(3)	8412(2)	5378(2)	24(1)
C(4)	4968(2)	7962(2)	5891(2)	26(1)
C(5)	3792(3)	7928(3)	5568(2)	36(1)
C(6)	3816(3)	6852(4)	5370(2)	43(1)
C(7)	5479(3)	8124(3)	4049(2)	30(1)
C(8)	5908(3)	8863(2)	4439(2)	30(1)
C(9)	7699(2)	7879(2)	7747(1)	16(1)
C(10)	7939(2)	6743(2)	8524(1)	15(1)
C(11)	6847(2)	6179(2)	8670(1)	15(1)
C(12)	7100(2)	5156(2)	8328(1)	15(1)
C(13)	7407(2)	6263(2)	9914(1)	19(1)
C(14)	6617(3)	7017(3)	10338(2)	28(1)
C(15)	8284(3)	5271(3)	10493(2)	29(1)
C(16)	6032(2)	4877(2)	8018(1)	17(1)
C(17)	6272(2)	3936(2)	7743(1)	19(1)
C(18)	5415(3)	3621(2)	7416(2)	23(1)
C(19)	4255(2)	4239(2)	7356(2)	23(1)
C(20)	3984(2)	5170(2)	7619(1)	21(1)
C(21)	4850(2)	5472(2)	7953(1)	19(1)
C(22)	7721(2)	4049(2)	9015(1)	16(1)
C(23)	8924(2)	3559(2)	9055(1)	19(1)
C(24)	9409(2)	2546(2)	9690(2)	26(1)
C(25)	8685(3)	2005(2)	10314(2)	30(1)
C(26)	7483(3)	2470(2)	10300(2)	27(1)
C(27)	7021(2)	3473(2)	9662(2)	21(1)
C(28)	9140(2)	7214(3)	5547(2)	27(1)
C(29)	10301(3)	6530(3)	5345(2)	32(1)
C(30)	10996(3)	6137(3)	6129(2)	36(1)

C(31)	10075(2)	5812(2)	6816(2)	25(1)
C(32)	8786(2)	8368(2)	7323(1)	17(1)
C(33)	8600(2)	9307(2)	6582(2)	22(1)
C(34)	9504(3)	9836(2)	6147(2)	29(1)
C(35)	10644(3)	9443(3)	6457(2)	30(1)
C(36)	10864(2)	8532(2)	7197(2)	25(1)
C(37)	9942(2)	8012(2)	7620(1)	20(1)
C(38)	6825(2)	8818(2)	7997(1)	20(1)
C(39)	5599(2)	9127(2)	7875(2)	22(1)
C(40)	4870(3)	9957(2)	8142(2)	29(1)
C(41)	5345(3)	10504(3)	8553(2)	37(1)
C(42)	6545(3)	10227(3)	8696(2)	35(1)
C(43)	7262(3)	9403(2)	8424(2)	25(1)
C(44)	-79(4)	2612(3)	7082(3)	52(1)
Cl(1)	7565(1)	4779(1)	5899(1)	31(1)
Cl(2)	-362(2)	1290(1)	7594(2)	125(1)
Cl(3)	1320(1)	2673(2)	6615(1)	83(1)
F(1)	7370(1)	3288(1)	7803(1)	25(1)
F(2)	5702(2)	2712(2)	7167(1)	32(1)
F(3)	3406(2)	3927(2)	7062(1)	32(1)
F(4)	2857(1)	5764(2)	7575(1)	30(1)
F(5)	4477(1)	6357(1)	8226(1)	26(1)
F(6)	9705(1)	4029(1)	8484(1)	26(1)
F(7)	10576(2)	2102(2)	9680(1)	36(1)
F(8)	9142(2)	1030(2)	10924(1)	45(1)
F(9)	6762(2)	1962(2)	10899(1)	40(1)
F(10)	5848(1)	3880(1)	9685(1)	26(1)
F(11)	10224(1)	7159(1)	8349(1)	25(1)
F(12)	11956(2)	8168(2)	7518(1)	34(1)
F(13)	11516(2)	9956(2)	6046(1)	42(1)
F(14)	9265(2)	10729(2)	5435(1)	41(1)
F(15)	7501(1)	9753(1)	6262(1)	27(1)
F(16)	8424(2)	9176(2)	8589(1)	29(1)
F(17)	7015(2)	10762(2)	9095(1)	52(1)
F(18)	4635(2)	11320(2)	8803(2)	56(1)
F(19)	3698(2)	10233(2)	7988(1)	37(1)

F(20)	5041(1)	8634(1)	7494(1)	26(1)
N(1)	8959(2)	6605(2)	6449(1)	19(1)
O(1)	7124(1)	7617(1)	7148(1)	15(1)
O(2)	7907(1)	5434(1)	7635(1)	15(1)
O(3)	8013(2)	6984(2)	9250(1)	20(1)
O(4)	6672(2)	5800(2)	9538(1)	20(1)
P(1)	7595(1)	6561(1)	6790(1)	14(1)
Rh(1)	6382(1)	6592(1)	5832(1)	16(1)

Table A.5.3. Bond lengths [Å] and angles [°] for Rh(cod)Cl·CKphos.

C(1)-C(2)	1.365(4)	C(13)-O(4)	1.441(3)
C(1)-C(7)	1.518(4)	C(13)-C(14)	1.511(4)
C(1)-Rh(1)	2.245(2)	C(13)-C(15)	1.518(4)
C(2)-C(6)	1.491(5)	C(16)-C(21)	1.394(3)
C(2)-Rh(1)	2.219(3)	C(16)-C(17)	1.401(3)
C(3)-C(4)	1.403(4)	C(17)-F(1)	1.336(3)
C(3)-C(8)	1.514(4)	C(17)-C(18)	1.376(4)
C(3)-Rh(1)	2.110(3)	C(18)-F(2)	1.336(3)
C(4)-C(5)	1.524(4)	C(18)-C(19)	1.382(4)
C(4)-Rh(1)	2.125(3)	C(19)-F(3)	1.333(3)
C(5)-C(6)	1.516(5)	C(19)-C(20)	1.377(4)
C(7)-C(8)	1.515(4)	C(20)-F(4)	1.341(3)
C(9)-O(1)	1.445(3)	C(20)-C(21)	1.381(4)
C(9)-C(32)	1.533(3)	C(21)-F(5)	1.341(3)
C(9)-C(38)	1.541(3)	C(22)-C(23)	1.384(3)
C(9)-C(10)	1.564(3)	C(22)-C(27)	1.397(3)
C(10)-O(3)	1.409(3)	C(23)-F(6)	1.341(3)
C(10)-C(11)	1.541(3)	C(23)-C(24)	1.392(3)
C(11)-O(4)	1.413(3)	C(24)-F(7)	1.337(3)
C(11)-C(12)	1.571(3)	C(24)-C(25)	1.376(4)
C(12)-O(2)	1.440(2)	C(25)-F(8)	1.336(3)
C(12)-C(16)	1.541(3)	C(25)-C(26)	1.378(4)
C(12)-C(22)	1.545(3)	C(26)-F(9)	1.337(3)
C(13)-O(3)	1.425(3)	C(26)-C(27)	1.379(3)

C(27)-F(10)	1.337(3)	C(2)-C(1)-C(7)	122.2(3)
C(28)-N(1)	1.489(3)	C(2)-C(1)-Rh(1)	71.18(15)
C(28)-C(29)	1.511(4)	C(7)-C(1)-Rh(1)	110.13(17)
C(29)-C(30)	1.500(5)	C(1)-C(2)-C(6)	127.1(3)
C(30)-C(31)	1.525(4)	C(1)-C(2)-Rh(1)	73.21(16)
C(31)-N(1)	1.473(3)	C(6)-C(2)-Rh(1)	108.7(2)
C(32)-C(37)	1.388(4)	C(4)-C(3)-C(8)	126.5(3)
C(32)-C(33)	1.392(3)	C(4)-C(3)-Rh(1)	71.24(15)
C(33)-F(15)	1.344(3)	C(8)-C(3)-Rh(1)	109.84(18)
C(33)-C(34)	1.383(3)	C(3)-C(4)-C(5)	123.8(2)
C(34)-F(14)	1.338(3)	C(3)-C(4)-Rh(1)	70.06(15)
C(34)-C(35)	1.378(4)	C(5)-C(4)-Rh(1)	113.3(2)
C(35)-F(13)	1.332(3)	C(6)-C(5)-C(4)	114.1(3)
C(35)-C(36)	1.377(4)	C(2)-C(6)-C(5)	114.1(3)
C(36)-F(12)	1.334(3)	C(8)-C(7)-C(1)	112.7(2)
C(36)-C(37)	1.389(3)	C(3)-C(8)-C(7)	114.5(2)
C(37)-F(11)	1.339(3)	O(1)-C(9)-C(32)	107.81(17)
C(38)-C(39)	1.393(4)	O(1)-C(9)-C(38)	108.55(19)
C(38)-C(43)	1.407(4)	C(32)-C(9)-C(38)	108.55(18)
C(39)-F(20)	1.337(3)	O(1)-C(9)-C(10)	106.04(17)
C(39)-C(40)	1.383(4)	C(32)-C(9)-C(10)	116.94(19)
C(40)-F(19)	1.343(4)	C(38)-C(9)-C(10)	108.68(17)
C(40)-C(41)	1.371(5)	O(3)-C(10)-C(11)	104.46(17)
C(41)-F(18)	1.344(3)	O(3)-C(10)-C(9)	111.13(19)
C(41)-C(42)	1.371(5)	C(11)-C(10)-C(9)	108.50(19)
C(42)-F(17)	1.339(4)	O(4)-C(11)-C(10)	104.44(18)
C(42)-C(43)	1.376(4)	O(4)-C(11)-C(12)	112.39(17)
C(43)-F(16)	1.337(3)	C(10)-C(11)-C(12)	110.19(18)
C(44)-Cl(2)	1.681(4)	O(2)-C(12)-C(16)	106.41(17)
C(44)-Cl(3)	1.743(4)	O(2)-C(12)-C(22)	108.60(18)
Cl(1)-Rh(1)	2.3645(7)	C(16)-C(12)-C(22)	107.92(18)
N(1)-P(1)	1.636(2)	O(2)-C(12)-C(11)	107.52(16)
O(1)-P(1)	1.6390(17)	C(16)-C(12)-C(11)	117.72(19)
O(2)-P(1)	1.6309(16)	C(22)-C(12)-C(11)	108.39(18)
P(1)-Rh(1)	2.2423(6)	O(3)-C(13)-O(4)	106.27(17)
		O(3)-C(13)-C(14)	107.8(2)

O(4)-C(13)-C(14)	109.0(2)	C(25)-C(26)-C(27)	119.6(2)
O(3)-C(13)-C(15)	110.9(2)	F(10)-C(27)-C(26)	116.6(2)
O(4)-C(13)-C(15)	108.9(2)	F(10)-C(27)-C(22)	120.5(2)
C(14)-C(13)-C(15)	113.6(2)	C(26)-C(27)-C(22)	122.9(2)
C(21)-C(16)-C(17)	115.4(2)	N(1)-C(28)-C(29)	104.0(2)
C(21)-C(16)-C(12)	127.8(2)	C(30)-C(29)-C(28)	102.7(2)
C(17)-C(16)-C(12)	116.8(2)	C(29)-C(30)-C(31)	103.9(2)
F(1)-C(17)-C(18)	116.8(2)	N(1)-C(31)-C(30)	103.6(2)
F(1)-C(17)-C(16)	120.1(2)	C(37)-C(32)-C(33)	115.5(2)
C(18)-C(17)-C(16)	123.0(2)	C(37)-C(32)-C(9)	126.9(2)
F(2)-C(18)-C(17)	120.1(2)	C(33)-C(32)-C(9)	117.5(2)
F(2)-C(18)-C(19)	120.2(2)	F(15)-C(33)-C(34)	116.7(2)
C(17)-C(18)-C(19)	119.7(2)	F(15)-C(33)-C(32)	120.2(2)
F(3)-C(19)-C(20)	120.4(2)	C(34)-C(33)-C(32)	123.1(3)
F(3)-C(19)-C(18)	120.6(2)	F(14)-C(34)-C(35)	120.5(2)
C(20)-C(19)-C(18)	119.0(2)	F(14)-C(34)-C(33)	120.0(3)
F(4)-C(20)-C(19)	119.4(2)	C(35)-C(34)-C(33)	119.5(2)
F(4)-C(20)-C(21)	119.9(2)	F(13)-C(35)-C(36)	120.6(3)
C(19)-C(20)-C(21)	120.8(2)	F(13)-C(35)-C(34)	120.0(3)
F(5)-C(21)-C(20)	115.8(2)	C(36)-C(35)-C(34)	119.4(2)
F(5)-C(21)-C(16)	122.1(2)	F(12)-C(36)-C(35)	120.0(2)
C(20)-C(21)-C(16)	122.1(2)	F(12)-C(36)-C(37)	120.1(2)
C(23)-C(22)-C(27)	115.7(2)	C(35)-C(36)-C(37)	119.9(3)
C(23)-C(22)-C(12)	126.0(2)	F(11)-C(37)-C(32)	121.3(2)
C(27)-C(22)-C(12)	118.2(2)	F(11)-C(37)-C(36)	116.1(2)
F(6)-C(23)-C(22)	122.3(2)	C(32)-C(37)-C(36)	122.6(2)
F(6)-C(23)-C(24)	115.4(2)	C(39)-C(38)-C(43)	114.7(2)
C(22)-C(23)-C(24)	122.4(2)	C(39)-C(38)-C(9)	126.2(2)
F(7)-C(24)-C(25)	120.8(2)	C(43)-C(38)-C(9)	119.0(2)
F(7)-C(24)-C(23)	119.3(2)	F(20)-C(39)-C(40)	115.2(3)
C(25)-C(24)-C(23)	119.9(3)	F(20)-C(39)-C(38)	122.2(2)
F(8)-C(25)-C(24)	120.3(3)	C(40)-C(39)-C(38)	122.7(3)
F(8)-C(25)-C(26)	120.1(3)	F(19)-C(40)-C(41)	120.2(3)
C(24)-C(25)-C(26)	119.5(2)	F(19)-C(40)-C(39)	119.7(3)
F(9)-C(26)-C(25)	120.7(2)	C(41)-C(40)-C(39)	120.1(3)
F(9)-C(26)-C(27)	119.8(3)	F(18)-C(41)-C(42)	120.3(3)

F(18)-C(41)-C(40)	120.0(3)	O(2)-P(1)-Rh(1)	120.99(7)
C(42)-C(41)-C(40)	119.7(3)	N(1)-P(1)-Rh(1)	112.80(8)
F(17)-C(42)-C(41)	120.0(3)	O(1)-P(1)-Rh(1)	112.84(7)
F(17)-C(42)-C(43)	120.4(3)	C(3)-Rh(1)-C(4)	38.69(11)
C(41)-C(42)-C(43)	119.6(3)	C(3)-Rh(1)-C(2)	95.88(11)
F(16)-C(43)-C(42)	116.3(3)	C(4)-Rh(1)-C(2)	81.07(12)
F(16)-C(43)-C(38)	120.6(2)	C(3)-Rh(1)-P(1)	93.08(8)
C(42)-C(43)-C(38)	123.2(3)	C(4)-Rh(1)-P(1)	99.74(8)
Cl(2)-C(44)-Cl(3)	116.8(2)	C(2)-Rh(1)-P(1)	166.24(8)
C(31)-N(1)-C(28)	109.80(19)	C(3)-Rh(1)-C(1)	81.50(10)
C(31)-N(1)-P(1)	128.56(16)	C(4)-Rh(1)-C(1)	89.82(10)
C(28)-N(1)-P(1)	117.95(17)	C(2)-Rh(1)-C(1)	35.60(10)
C(9)-O(1)-P(1)	127.67(15)	P(1)-Rh(1)-C(1)	157.25(7)
C(12)-O(2)-P(1)	123.75(14)	C(3)-Rh(1)-Cl(1)	155.33(8)
C(10)-O(3)-C(13)	109.76(17)	C(4)-Rh(1)-Cl(1)	164.91(8)
C(11)-O(4)-C(13)	110.40(16)	C(2)-Rh(1)-Cl(1)	89.33(9)
O(2)-P(1)-N(1)	97.71(9)	P(1)-Rh(1)-Cl(1)	86.84(2)
O(2)-P(1)-O(1)	102.68(8)	C(1)-Rh(1)-Cl(1)	89.08(7)
N(1)-P(1)-O(1)	108.16(10)		

Symmetry transformations used to generate equivalent atoms:

Table A.5.4. Anisotropic displacement parameters ($Å^2 x\ 10^3$) for Rh(cod)Cl·CKphos. The anisotropic displacement factor exponent takes the form: $-2p^2[\ h^2a^{*2}U^{11} + ... + 2\ h\ k\ a^*\ b^*\ U^{12}\ ]$

	U^{11}	U^{22}	U^{33}	U^{23}	U^{13}	U^{12}
C(1)	31(1)	20(1)	16(1)	-7(1)	-4(1)	-5(1)
C(2)	35(2)	34(2)	29(1)	-16(1)	-5(1)	-16(1)
C(3)	32(1)	15(1)	25(1)	-9(1)	-8(1)	0(1)
C(4)	23(1)	28(1)	22(1)	-10(1)	-5(1)	8(1)
C(5)	20(1)	52(2)	30(1)	-13(1)	-5(1)	3(1)
C(6)	28(2)	66(2)	34(2)	-7(2)	-4(1)	-20(2)
C(7)	42(2)	27(1)	18(1)	-5(1)	-6(1)	-5(1)
C(8)	46(2)	18(1)	24(1)	-2(1)	-3(1)	-9(1)
C(9)	21(1)	12(1)	13(1)	-3(1)	1(1)	-4(1)

C(10)	21(1)	14(1)	12(1)	-5(1)	2(1)	-6(1)
C(11)	18(1)	14(1)	13(1)	-4(1)	2(1)	-6(1)
C(12)	17(1)	13(1)	13(1)	-3(1)	1(1)	-3(1)
C(13)	26(1)	19(1)	13(1)	-6(1)	3(1)	-9(1)
C(14)	33(1)	29(1)	26(1)	-16(1)	9(1)	-10(1)
C(15)	32(1)	25(1)	23(1)	0(1)	-5(1)	-7(1)
C(16)	20(1)	14(1)	15(1)	-4(1)	0(1)	-4(1)
C(17)	23(1)	15(1)	18(1)	-4(1)	-2(1)	-4(1)
C(18)	34(1)	17(1)	20(1)	-7(1)	-2(1)	-8(1)
C(19)	28(1)	28(1)	17(1)	-7(1)	-2(1)	-14(1)
C(20)	20(1)	25(1)	17(1)	-4(1)	-1(1)	-6(1)
C(21)	21(1)	19(1)	16(1)	-5(1)	1(1)	-5(1)
C(22)	21(1)	13(1)	15(1)	-3(1)	-1(1)	-4(1)
C(23)	23(1)	17(1)	18(1)	-5(1)	0(1)	-4(1)
C(24)	25(1)	21(1)	27(1)	-4(1)	-7(1)	0(1)
C(25)	41(2)	15(1)	25(1)	5(1)	-10(1)	-4(1)
C(26)	34(1)	21(1)	21(1)	3(1)	-2(1)	-10(1)
C(27)	25(1)	19(1)	18(1)	-1(1)	-1(1)	-9(1)
C(28)	21(1)	33(2)	21(1)	-4(1)	6(1)	-3(1)
C(29)	28(1)	38(2)	29(1)	-13(1)	9(1)	-6(1)
C(30)	20(1)	43(2)	38(2)	-10(1)	6(1)	-2(1)
C(31)	20(1)	27(1)	24(1)	-5(1)	-1(1)	-2(1)
C(32)	23(1)	15(1)	14(1)	-4(1)	2(1)	-7(1)
C(33)	28(1)	18(1)	18(1)	-2(1)	2(1)	-7(1)
C(34)	36(2)	24(1)	22(1)	1(1)	5(1)	-13(1)
C(35)	30(1)	29(1)	31(1)	-9(1)	12(1)	-16(1)
C(36)	21(1)	24(1)	32(1)	-11(1)	2(1)	-7(1)
C(37)	25(1)	16(1)	18(1)	-5(1)	0(1)	-6(1)
C(38)	29(1)	14(1)	16(1)	-5(1)	6(1)	-7(1)
C(39)	29(1)	16(1)	17(1)	-4(1)	5(1)	-2(1)
C(40)	35(2)	16(1)	28(1)	-5(1)	12(1)	1(1)
C(41)	56(2)	18(1)	38(2)	-17(1)	20(2)	-5(1)
C(42)	54(2)	26(2)	32(1)	-19(1)	14(1)	-16(1)
C(43)	37(1)	18(1)	21(1)	-9(1)	5(1)	-9(1)
C(44)	55(2)	38(2)	57(2)	-13(2)	12(2)	-7(2)
Cl(1)	46(1)	18(1)	24(1)	-10(1)	-6(1)	7(1)

Cl(2)	118(1)	32(1)	198(2)	-25(1)	73(1)	-15(1)
Cl(3)	50(1)	118(1)	85(1)	-43(1)	16(1)	-22(1)
F(1)	26(1)	19(1)	30(1)	-12(1)	-6(1)	1(1)
F(2)	44(1)	25(1)	36(1)	-17(1)	-7(1)	-9(1)
F(3)	33(1)	41(1)	31(1)	-15(1)	-6(1)	-17(1)
F(4)	19(1)	42(1)	30(1)	-13(1)	-2(1)	-4(1)
F(5)	21(1)	27(1)	34(1)	-18(1)	0(1)	-1(1)
F(6)	20(1)	27(1)	23(1)	-2(1)	0(1)	-1(1)
F(7)	28(1)	31(1)	37(1)	-4(1)	-10(1)	7(1)
F(8)	51(1)	26(1)	38(1)	13(1)	-14(1)	-2(1)
F(9)	45(1)	34(1)	27(1)	10(1)	1(1)	-19(1)
F(10)	22(1)	28(1)	22(1)	-2(1)	2(1)	-10(1)
F(11)	26(1)	23(1)	23(1)	0(1)	-6(1)	-7(1)
F(12)	22(1)	34(1)	46(1)	-11(1)	-1(1)	-10(1)
F(13)	35(1)	40(1)	46(1)	-4(1)	14(1)	-22(1)
F(14)	46(1)	35(1)	28(1)	11(1)	4(1)	-16(1)
F(15)	27(1)	23(1)	23(1)	3(1)	-3(1)	-6(1)
F(16)	40(1)	28(1)	27(1)	-13(1)	2(1)	-16(1)
F(17)	76(2)	45(1)	59(1)	-43(1)	16(1)	-26(1)
F(18)	72(2)	34(1)	68(1)	-37(1)	31(1)	-5(1)
F(19)	32(1)	27(1)	39(1)	-6(1)	13(1)	6(1)
F(20)	23(1)	28(1)	26(1)	-13(1)	-1(1)	2(1)
N(1)	16(1)	19(1)	16(1)	-2(1)	1(1)	-2(1)
O(1)	19(1)	13(1)	13(1)	-5(1)	0(1)	-2(1)
O(2)	17(1)	14(1)	12(1)	-3(1)	1(1)	-3(1)
O(3)	31(1)	21(1)	12(1)	-5(1)	2(1)	-14(1)
O(4)	27(1)	22(1)	13(1)	-6(1)	5(1)	-12(1)
P(1)	16(1)	12(1)	12(1)	-4(1)	1(1)	-2(1)
Rh(1)	19(1)	13(1)	13(1)	-5(1)	0(1)	-2(1)

Table A.5.5. Hydrogen coordinates (x 10^4) and isotropic displacement parameters ($Å^2$x 10^3) for Rh(cod)Cl·CKphos.

	x	y	z	U(eq)

H(1)	6299	6360	4285	27
H(2)	5091	5497	5205	35
H(3)	6332	8784	5623	28
H(4)	4899	8078	6425	31
H(5A)	3176	7981	5979	43
H(5B)	3580	8600	5070	43
H(6A)	3526	6289	5850	52
H(6B)	3275	7050	4917	52
H(7A)	5836	8248	3502	36
H(7B)	4623	8366	3981	36
H(8A)	6717	8923	4252	36
H(8B)	5415	9635	4241	36
H(10)	8661	6212	8444	18
H(11)	6150	6756	8393	18
H(14A)	7099	7350	10574	41
H(14B)	6165	6558	10770	41
H(14C)	6083	7622	9941	41
H(15A)	8814	4878	10177	43
H(15B)	7857	4740	10889	43
H(15C)	8735	5567	10779	43
H(28A)	9194	8008	5436	33
H(28B)	8492	7209	5226	33
H(29A)	10176	5878	5220	38
H(29B)	10702	7011	4879	38
H(30A)	11335	6753	6163	43
H(30B)	11632	5476	6162	43
H(31A)	10015	5012	6958	30
H(31B)	10276	5926	7309	30
H(44A)	-177	3023	7468	62
H(44B)	-676	3026	6655	62

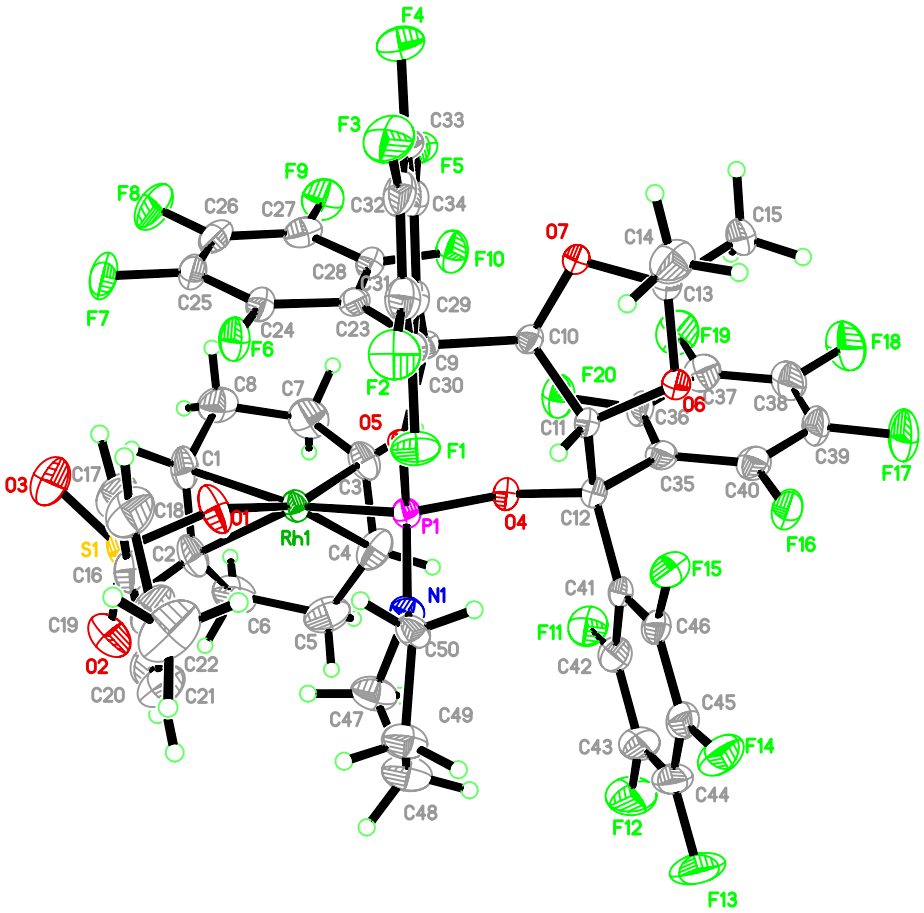

Table A.5.6. Crystal data and structure refinement for Rh(cod)OTs·CKphos.

Identification code	Rovis117_0m	
Empirical formula	C_{50} H_{33} F_{20} N O_7 P Rh S	
Formula weight	1305.71	
Temperature	120 K	
Wavelength	0.71073 Å	
Crystal system	Triclinic	
Space group	*P* -1	
Unit cell dimensions	*a* = 11.7155(4) Å	α = 70.901(2)°.
	b = 12.1131(4) Å	β = 89.025(2)°.
	c = 18.2303(6) Å	γ = 83.198(2)°.
Volume	2426.82(14) Å^3	
Z	2	
Density (calculated)	1.787 Mg/m^3	
Absorption coefficient	0.561 mm^{-1}	
F_{000}	1304	

Crystal size	0.29 x 0.13 x 0.07 mm^3
Theta range for data collection	1.75 to 26.52°.
Index ranges	-14≤h≤14, -15≤k≤15, -22≤l≤22
Reflections collected	36213
Independent reflections	9971 [R_{int} = 0.0596]
Completeness to theta = 26.52°	98.8 %
Absorption correction	Multi-scan
Max. and min. transmission	0.9597 and 0.8538
Refinement method	Full-matrix least-squares on F^2
Data / restraints / parameters	9971 / 0 / 733
Goodness-of-fit on F^2	1.059
Final R indices [I>2sigma(I)]	R1 = 0.0457, wR2 = 0.1109
R indices (all data)	R1 = 0.0782, wR2 = 0.1451
Largest diff. peak and hole	0.740 and -1.029 e.$Å^{-3}$

Table A.5.7. Atomic coordinates (x 10^4) and equivalent isotropic displacement parameters ($Å^2$x 10^3) for Rh(cod)OTs·CKphos. U(eq) is defined as one third of the trace of the orthogonalized U^{ij} tensor.

	x	y	z	U(eq)
C(1)	9955(4)	8455(4)	5518(3)	32(1)
C(2)	9206(4)	8425(4)	4954(3)	33(1)
C(3)	9865(4)	6004(4)	6177(2)	29(1)
C(4)	8957(4)	6007(4)	5686(3)	33(1)
C(5)	8938(4)	6495(4)	4805(3)	41(1)
C(6)	9476(5)	7642(5)	4471(3)	42(1)
C(7)	11032(4)	6404(4)	5907(3)	40(1)
C(8)	11091(4)	7704(4)	5751(3)	36(1)
C(9)	7958(3)	6393(3)	8449(2)	18(1)
C(10)	8051(3)	5016(3)	8765(2)	19(1)
C(11)	6914(3)	4585(3)	8627(2)	19(1)
C(12)	7028(3)	4175(3)	7902(2)	20(1)
C(13)	7459(4)	3732(3)	9927(2)	24(1)
C(14)	6685(4)	4193(4)	10454(3)	37(1)
C(15)	8130(4)	2543(3)	10323(3)	33(1)
C(16)	5996(4)	10401(3)	6383(2)	27(1)

C(17)	6073(4)	10656(4)	7070(3)	36(1)
C(18)	5093(4)	10811(4)	7467(3)	41(1)
C(19)	4013(4)	10768(4)	7181(3)	36(1)
C(20)	3948(4)	10554(4)	6485(3)	39(1)
C(21)	4916(4)	10360(4)	6090(3)	33(1)
C(22)	2962(5)	10933(5)	7623(3)	54(2)
C(23)	9072(3)	6931(3)	8169(2)	21(1)
C(24)	9007(4)	8167(3)	7898(2)	23(1)
C(25)	9936(4)	8761(3)	7603(2)	27(1)
C(26)	10979(4)	8147(4)	7568(2)	28(1)
C(27)	11093(4)	6940(4)	7832(2)	27(1)
C(28)	10152(4)	6352(3)	8133(2)	24(1)
C(29)	7445(3)	6876(3)	9080(2)	19(1)
C(30)	6311(3)	7337(3)	9111(2)	22(1)
C(31)	5911(4)	7751(4)	9702(2)	26(1)
C(32)	6646(4)	7711(3)	10290(2)	28(1)
C(33)	7771(4)	7260(4)	10286(2)	27(1)
C(34)	8153(4)	6855(3)	9689(2)	23(1)
C(35)	7766(4)	2964(3)	8133(2)	23(1)
C(36)	8931(4)	2760(3)	8022(2)	26(1)
C(37)	9546(4)	1659(4)	8316(3)	31(1)
C(38)	9008(4)	709(4)	8741(3)	36(1)
C(39)	7858(4)	868(4)	8856(3)	33(1)
C(40)	7252(4)	1968(4)	8559(2)	28(1)
C(41)	5900(4)	4088(3)	7514(2)	21(1)
C(42)	5962(4)	3875(4)	6803(3)	28(1)
C(43)	5001(4)	3757(4)	6423(3)	35(1)
C(44)	3952(4)	3829(4)	6736(3)	35(1)
C(45)	3852(4)	4014(4)	7441(3)	30(1)
C(46)	4809(4)	4143(3)	7818(2)	24(1)
C(47)	5788(4)	7086(4)	5831(2)	35(1)
C(48)	4530(4)	7033(5)	5785(3)	41(1)
C(49)	4034(4)	7417(4)	6430(3)	33(1)
C(50)	4991(3)	7160(4)	7043(2)	23(1)
F(1)	5517(2)	7395(2)	8573(1)	30(1)
F(2)	4813(2)	8215(2)	9687(1)	35(1)

F(3)	6264(2)	8131(2)	10856(1)	37(1)
F(4)	8511(2)	7237(2)	10843(1)	38(1)
F(5)	9269(2)	6428(2)	9719(1)	28(1)
F(6)	8016(2)	8811(2)	7939(1)	29(1)
F(7)	9812(2)	9940(2)	7358(2)	38(1)
F(8)	11884(2)	8716(2)	7289(2)	42(1)
F(9)	12113(2)	6333(2)	7806(2)	38(1)
F(10)	10377(2)	5175(2)	8406(2)	33(1)
F(11)	6991(2)	3755(2)	6480(1)	36(1)
F(12)	5119(3)	3567(3)	5737(2)	52(1)
F(13)	3018(3)	3714(3)	6375(2)	55(1)
F(14)	2821(2)	4058(2)	7768(2)	40(1)
F(15)	4644(2)	4294(2)	8509(1)	28(1)
F(16)	6125(2)	2043(2)	8712(1)	31(1)
F(17)	7315(3)	-46(2)	9265(2)	46(1)
F(18)	9611(3)	-360(2)	9034(2)	49(1)
F(19)	10677(2)	1518(2)	8181(2)	44(1)
F(20)	9548(2)	3624(2)	7621(2)	34(1)
N(1)	6022(3)	6783(3)	6670(2)	22(1)
O(1)	7647(3)	8838(2)	6361(2)	35(1)
O(2)	6922(3)	10208(3)	5127(2)	41(1)
O(3)	8068(3)	10843(3)	5986(2)	44(1)
O(4)	7644(2)	5019(2)	7334(2)	20(1)
O(5)	7160(2)	6791(2)	7790(1)	18(1)
O(6)	6794(2)	3630(2)	9305(2)	23(1)
O(7)	8242(2)	4566(2)	9576(2)	25(1)
P(1)	7347(1)	6446(1)	7004(1)	19(1)
Rh(1)	8577(1)	7393(1)	6135(1)	22(1)
S(1)	7254(1)	10085(1)	5906(1)	29(1)

Table A.5.8. Bond lengths [Å] and angles [°] for Rh(cod)OTs·CKphos.

C(1)-C(2)	1.376(6)	C(2)-C(6)	1.496(6)
C(1)-C(8)	1.503(6)	C(2)-Rh(1)	2.269(4)
C(1)-Rh(1)	2.239(4)	C(3)-C(4)	1.401(6)

C(3)-C(7)	1.525(6)	C(26)-C(27)	1.372(6)
C(3)-Rh(1)	2.105(4)	C(27)-F(9)	1.335(5)
C(4)-C(5)	1.517(6)	C(27)-C(28)	1.391(6)
C(4)-Rh(1)	2.098(4)	C(28)-F(10)	1.342(4)
C(5)-C(6)	1.529(7)	C(29)-C(30)	1.387(6)
C(7)-C(8)	1.515(7)	C(29)-C(34)	1.390(6)
C(9)-O(5)	1.449(4)	C(30)-F(1)	1.342(4)
C(9)-C(23)	1.534(5)	C(30)-C(31)	1.383(6)
C(9)-C(29)	1.535(5)	C(31)-F(2)	1.338(5)
C(9)-C(10)	1.567(5)	C(31)-C(32)	1.372(6)
C(10)-O(7)	1.410(4)	C(32)-F(3)	1.341(5)
C(10)-C(11)	1.541(5)	C(32)-C(33)	1.367(6)
C(11)-O(6)	1.409(4)	C(33)-F(4)	1.338(5)
C(11)-C(12)	1.556(5)	C(33)-C(34)	1.379(6)
C(12)-O(4)	1.447(4)	C(34)-F(5)	1.343(5)
C(12)-C(41)	1.540(5)	C(35)-C(36)	1.380(6)
C(12)-C(35)	1.545(5)	C(35)-C(40)	1.402(6)
C(13)-O(7)	1.431(5)	C(36)-F(20)	1.346(4)
C(13)-O(6)	1.433(5)	C(36)-C(37)	1.380(6)
C(13)-C(14)	1.503(6)	C(37)-F(19)	1.345(5)
C(13)-C(15)	1.512(6)	C(37)-C(38)	1.376(6)
C(16)-C(17)	1.390(6)	C(38)-F(18)	1.344(5)
C(16)-C(21)	1.394(6)	C(38)-C(39)	1.360(7)
C(16)-S(1)	1.765(4)	C(39)-F(17)	1.340(5)
C(17)-C(18)	1.374(7)	C(39)-C(40)	1.375(6)
C(18)-C(19)	1.390(7)	C(40)-F(16)	1.343(5)
C(19)-C(20)	1.381(7)	C(41)-C(46)	1.387(6)
C(19)-C(22)	1.490(7)	C(41)-C(42)	1.401(6)
C(20)-C(21)	1.370(7)	C(42)-F(11)	1.347(5)
C(23)-C(28)	1.384(6)	C(42)-C(43)	1.377(6)
C(23)-C(24)	1.407(5)	C(43)-F(12)	1.345(5)
C(24)-F(6)	1.335(5)	C(43)-C(44)	1.351(7)
C(24)-C(25)	1.380(6)	C(44)-F(13)	1.332(5)
C(25)-F(7)	1.340(5)	C(44)-C(45)	1.376(6)
C(25)-C(26)	1.365(6)	C(45)-F(14)	1.340(5)
C(26)-F(8)	1.335(5)	C(45)-C(46)	1.376(6)

C(46)-F(15)	1.339(5)	C(29)-C(9)-C(10)	108.8(3)
C(47)-N(1)	1.474(5)	O(7)-C(10)-C(11)	104.9(3)
C(47)-C(48)	1.487(6)	O(7)-C(10)-C(9)	112.0(3)
C(48)-C(49)	1.485(6)	C(11)-C(10)-C(9)	110.9(3)
C(49)-C(50)	1.529(6)	O(6)-C(11)-C(10)	104.0(3)
C(50)-N(1)	1.475(5)	O(6)-C(11)-C(12)	110.9(3)
N(1)-P(1)	1.632(3)	C(10)-C(11)-C(12)	109.0(3)
O(1)-S(1)	1.487(3)	O(4)-C(12)-C(41)	107.9(3)
O(1)-Rh(1)	2.104(3)	O(4)-C(12)-C(35)	108.4(3)
O(2)-S(1)	1.434(3)	C(41)-C(12)-C(35)	108.7(3)
O(3)-S(1)	1.441(3)	O(4)-C(12)-C(11)	106.4(3)
O(4)-P(1)	1.629(3)	C(41)-C(12)-C(11)	116.6(3)
O(5)-P(1)	1.624(3)	C(35)-C(12)-C(11)	108.4(3)
P(1)-Rh(1)	2.2421(10)	O(7)-C(13)-O(6)	106.4(3)
		O(7)-C(13)-C(14)	109.1(3)
C(2)-C(1)-C(8)	125.9(4)	O(6)-C(13)-C(14)	109.9(4)
C(2)-C(1)-Rh(1)	73.4(2)	O(7)-C(13)-C(15)	109.3(4)
C(8)-C(1)-Rh(1)	107.8(3)	O(6)-C(13)-C(15)	107.4(3)
C(1)-C(2)-C(6)	122.1(4)	C(14)-C(13)-C(15)	114.4(4)
C(1)-C(2)-Rh(1)	71.0(2)	C(17)-C(16)-C(21)	119.3(4)
C(6)-C(2)-Rh(1)	110.6(3)	C(17)-C(16)-S(1)	120.3(3)
C(4)-C(3)-C(7)	125.0(4)	C(21)-C(16)-S(1)	120.4(3)
C(4)-C(3)-Rh(1)	70.3(3)	C(18)-C(17)-C(16)	119.7(4)
C(7)-C(3)-Rh(1)	113.8(3)	C(17)-C(18)-C(19)	121.4(5)
C(3)-C(4)-C(5)	125.8(4)	C(20)-C(19)-C(18)	118.1(5)
C(3)-C(4)-Rh(1)	70.8(2)	C(20)-C(19)-C(22)	121.4(4)
C(5)-C(4)-Rh(1)	109.5(3)	C(18)-C(19)-C(22)	120.5(5)
C(4)-C(5)-C(6)	114.5(4)	C(21)-C(20)-C(19)	121.6(4)
C(2)-C(6)-C(5)	111.1(4)	C(20)-C(21)-C(16)	119.9(4)
C(8)-C(7)-C(3)	114.3(4)	C(28)-C(23)-C(24)	114.7(4)
C(1)-C(8)-C(7)	113.9(4)	C(28)-C(23)-C(9)	128.0(3)
O(5)-C(9)-C(23)	106.8(3)	C(24)-C(23)-C(9)	117.2(4)
O(5)-C(9)-C(29)	108.1(3)	F(6)-C(24)-C(25)	117.4(3)
C(23)-C(9)-C(29)	109.1(3)	F(6)-C(24)-C(23)	119.5(3)
O(5)-C(9)-C(10)	107.2(3)	C(25)-C(24)-C(23)	123.0(4)
C(23)-C(9)-C(10)	116.5(3)	F(7)-C(25)-C(26)	120.3(4)

F(7)-C(25)-C(24)	119.8(4)	F(19)-C(37)-C(36)	119.5(4)
C(26)-C(25)-C(24)	120.0(4)	C(38)-C(37)-C(36)	120.4(4)
F(8)-C(26)-C(25)	120.3(4)	F(18)-C(38)-C(39)	120.6(4)
F(8)-C(26)-C(27)	120.3(4)	F(18)-C(38)-C(37)	120.3(5)
C(25)-C(26)-C(27)	119.4(4)	C(39)-C(38)-C(37)	119.1(4)
F(9)-C(27)-C(26)	119.8(4)	F(17)-C(39)-C(38)	120.1(4)
F(9)-C(27)-C(28)	120.1(4)	F(17)-C(39)-C(40)	119.8(4)
C(26)-C(27)-C(28)	120.1(4)	C(38)-C(39)-C(40)	120.1(4)
F(10)-C(28)-C(23)	122.3(3)	F(16)-C(40)-C(39)	115.9(4)
F(10)-C(28)-C(27)	114.8(4)	F(16)-C(40)-C(35)	121.3(4)
C(23)-C(28)-C(27)	122.8(4)	C(39)-C(40)-C(35)	122.8(4)
C(30)-C(29)-C(34)	115.1(4)	C(46)-C(41)-C(42)	115.4(4)
C(30)-C(29)-C(9)	126.0(3)	C(46)-C(41)-C(12)	126.3(4)
C(34)-C(29)-C(9)	118.9(4)	C(42)-C(41)-C(12)	118.2(4)
F(1)-C(30)-C(31)	115.2(4)	F(11)-C(42)-C(43)	118.0(4)
F(1)-C(30)-C(29)	122.2(4)	F(11)-C(42)-C(41)	119.7(4)
C(31)-C(30)-C(29)	122.6(4)	C(43)-C(42)-C(41)	122.3(4)
F(2)-C(31)-C(32)	120.2(4)	F(12)-C(43)-C(44)	120.4(4)
F(2)-C(31)-C(30)	119.8(4)	F(12)-C(43)-C(42)	119.2(5)
C(32)-C(31)-C(30)	120.0(4)	C(44)-C(43)-C(42)	120.4(4)
F(3)-C(32)-C(33)	120.5(4)	F(13)-C(44)-C(43)	120.9(4)
F(3)-C(32)-C(31)	120.0(4)	F(13)-C(44)-C(45)	119.6(5)
C(33)-C(32)-C(31)	119.4(4)	C(43)-C(44)-C(45)	119.4(4)
F(4)-C(33)-C(32)	120.5(4)	F(14)-C(45)-C(46)	119.6(4)
F(4)-C(33)-C(34)	119.8(4)	F(14)-C(45)-C(44)	120.1(4)
C(32)-C(33)-C(34)	119.7(4)	C(46)-C(45)-C(44)	120.3(4)
F(5)-C(34)-C(33)	116.5(4)	F(15)-C(46)-C(45)	116.6(4)
F(5)-C(34)-C(29)	120.2(4)	F(15)-C(46)-C(41)	121.1(3)
C(33)-C(34)-C(29)	123.2(4)	C(45)-C(46)-C(41)	122.2(4)
C(36)-C(35)-C(40)	115.1(4)	N(1)-C(47)-C(48)	103.4(4)
C(36)-C(35)-C(12)	126.4(4)	C(49)-C(48)-C(47)	105.4(4)
C(40)-C(35)-C(12)	118.3(4)	C(48)-C(49)-C(50)	106.9(4)
F(20)-C(36)-C(37)	115.2(4)	N(1)-C(50)-C(49)	104.0(3)
F(20)-C(36)-C(35)	122.3(4)	C(47)-N(1)-C(50)	109.5(3)
C(37)-C(36)-C(35)	122.5(4)	C(47)-N(1)-P(1)	119.7(3)
F(19)-C(37)-C(38)	120.1(4)	C(50)-N(1)-P(1)	128.5(3)

S(1)-O(1)-Rh(1)	136.05(19)	C(4)-Rh(1)-P(1)	93.91(12)
C(12)-O(4)-P(1)	128.1(2)	O(1)-Rh(1)-P(1)	80.50(8)
C(9)-O(5)-P(1)	124.5(2)	C(3)-Rh(1)-P(1)	101.05(12)
C(11)-O(6)-C(13)	109.5(3)	C(1)-Rh(1)-P(1)	165.74(13)
C(10)-O(7)-C(13)	110.3(3)	C(4)-Rh(1)-C(2)	81.08(17)
O(5)-P(1)-O(4)	103.02(14)	O(1)-Rh(1)-C(2)	96.39(14)
O(5)-P(1)-N(1)	98.25(16)	C(3)-Rh(1)-C(2)	89.00(16)
O(4)-P(1)-N(1)	109.15(16)	C(1)-Rh(1)-C(2)	35.55(16)
O(5)-P(1)-Rh(1)	117.86(10)	P(1)-Rh(1)-C(2)	157.25(13)
O(4)-P(1)-Rh(1)	115.15(11)	O(2)-S(1)-O(3)	116.2(2)
N(1)-P(1)-Rh(1)	111.79(12)	O(2)-S(1)-O(1)	111.50(19)
C(4)-Rh(1)-O(1)	159.38(16)	O(3)-S(1)-O(1)	110.6(2)
C(4)-Rh(1)-C(3)	38.94(17)	O(2)-S(1)-C(16)	107.4(2)
O(1)-Rh(1)-C(3)	161.58(15)	O(3)-S(1)-C(16)	107.2(2)
C(4)-Rh(1)-C(1)	96.45(17)	O(1)-S(1)-C(16)	102.97(18)
O(1)-Rh(1)-C(1)	92.95(15)		
C(3)-Rh(1)-C(1)	81.22(16)		

Symmetry transformations used to generate equivalent atoms:

Table A.5.9. Anisotropic displacement parameters ($Å^2 x\ 10^3$)for Rh(cod)OTs·CKphos. The anisotropic displacement factor exponent takes the form: $-2p^2[\ h^2a^{*2}U^{11} + ... + 2\ h\ k\ a^*\ b^*\ U^{12}\ ]$

	U^{11}	U^{22}	U^{33}	U^{23}	U^{13}	U^{12}
C(1)	28(2)	24(2)	36(3)	0(2)	13(2)	-9(2)
C(2)	34(3)	27(2)	27(2)	4(2)	9(2)	-1(2)
C(3)	31(3)	25(2)	26(2)	-4(2)	6(2)	3(2)
C(4)	31(3)	34(3)	43(3)	-23(2)	12(2)	-10(2)
C(5)	41(3)	55(3)	39(3)	-30(3)	1(2)	-7(3)
C(6)	45(3)	57(3)	21(2)	-9(2)	7(2)	-7(3)
C(7)	24(3)	45(3)	45(3)	-9(2)	5(2)	-1(2)
C(8)	25(2)	48(3)	35(3)	-13(2)	4(2)	-10(2)
C(9)	17(2)	16(2)	21(2)	-5(2)	-2(2)	-3(2)
C(10)	20(2)	15(2)	22(2)	-7(2)	-2(2)	-2(2)
C(11)	22(2)	14(2)	21(2)	-3(2)	-2(2)	-5(2)

C(12)	21(2)	18(2)	21(2)	-5(2)	0(2)	-6(2)
C(13)	31(2)	21(2)	20(2)	-4(2)	-2(2)	-9(2)
C(14)	39(3)	45(3)	35(3)	-21(2)	8(2)	-13(2)
C(15)	45(3)	19(2)	30(3)	1(2)	-10(2)	-7(2)
C(16)	33(3)	18(2)	30(2)	-7(2)	4(2)	-3(2)
C(17)	30(3)	30(2)	53(3)	-21(2)	-1(2)	-4(2)
C(18)	46(3)	37(3)	50(3)	-30(2)	4(3)	-2(2)
C(19)	35(3)	34(3)	50(3)	-26(2)	8(2)	-10(2)
C(20)	32(3)	43(3)	51(3)	-23(2)	-2(2)	-10(2)
C(21)	36(3)	32(2)	34(3)	-15(2)	3(2)	-7(2)
C(22)	40(3)	63(4)	74(4)	-43(3)	16(3)	-14(3)
C(23)	21(2)	23(2)	20(2)	-7(2)	-1(2)	-6(2)
C(24)	26(2)	19(2)	25(2)	-8(2)	2(2)	-5(2)
C(25)	35(3)	21(2)	26(2)	-6(2)	1(2)	-10(2)
C(26)	31(3)	33(2)	27(2)	-15(2)	5(2)	-16(2)
C(27)	24(2)	37(3)	26(2)	-16(2)	2(2)	-7(2)
C(28)	27(2)	19(2)	28(2)	-7(2)	-3(2)	-6(2)
C(29)	24(2)	12(2)	22(2)	-6(2)	4(2)	-4(2)
C(30)	23(2)	21(2)	21(2)	-5(2)	0(2)	-5(2)
C(31)	28(2)	24(2)	26(2)	-8(2)	8(2)	-6(2)
C(32)	41(3)	19(2)	28(2)	-13(2)	8(2)	-9(2)
C(33)	36(3)	26(2)	20(2)	-9(2)	-5(2)	-9(2)
C(34)	23(2)	17(2)	28(2)	-7(2)	1(2)	-2(2)
C(35)	26(2)	19(2)	24(2)	-9(2)	-5(2)	0(2)
C(36)	33(3)	17(2)	30(2)	-10(2)	1(2)	-7(2)
C(37)	30(3)	26(2)	41(3)	-18(2)	0(2)	4(2)
C(38)	49(3)	19(2)	39(3)	-9(2)	-7(2)	4(2)
C(39)	47(3)	17(2)	34(3)	-6(2)	-1(2)	-9(2)
C(40)	31(3)	24(2)	30(2)	-13(2)	-2(2)	-3(2)
C(41)	27(2)	12(2)	24(2)	-4(2)	-4(2)	-5(2)
C(42)	34(3)	24(2)	30(2)	-12(2)	-1(2)	-4(2)
C(43)	52(3)	32(2)	29(3)	-19(2)	-11(2)	-5(2)
C(44)	38(3)	29(2)	41(3)	-14(2)	-18(2)	-1(2)
C(45)	28(3)	19(2)	41(3)	-6(2)	-5(2)	-2(2)
C(46)	27(2)	15(2)	30(2)	-7(2)	-3(2)	-3(2)
C(47)	31(3)	49(3)	24(2)	-10(2)	-2(2)	-1(2)

C(48)	31(3)	52(3)	36(3)	-14(2)	-7(2)	3(2)
C(49)	25(2)	44(3)	28(2)	-9(2)	-2(2)	-2(2)
C(50)	16(2)	25(2)	23(2)	-2(2)	0(2)	2(2)
F(1)	21(1)	44(2)	28(1)	-17(1)	-1(1)	-1(1)
F(2)	31(2)	41(2)	37(2)	-19(1)	9(1)	2(1)
F(3)	48(2)	40(2)	33(2)	-25(1)	7(1)	-5(1)
F(4)	45(2)	43(2)	31(1)	-19(1)	-7(1)	-9(1)
F(5)	26(1)	32(1)	29(1)	-12(1)	-5(1)	-5(1)
F(6)	31(1)	18(1)	37(1)	-8(1)	5(1)	-2(1)
F(7)	51(2)	22(1)	44(2)	-9(1)	7(1)	-17(1)
F(8)	37(2)	46(2)	52(2)	-22(1)	17(1)	-27(1)
F(9)	21(1)	44(2)	49(2)	-17(1)	5(1)	0(1)
F(10)	23(1)	22(1)	50(2)	-8(1)	2(1)	1(1)
F(11)	46(2)	39(2)	29(1)	-19(1)	6(1)	-8(1)
F(12)	72(2)	57(2)	38(2)	-28(2)	-15(2)	-8(2)
F(13)	48(2)	57(2)	69(2)	-30(2)	-30(2)	-5(2)
F(14)	24(1)	38(2)	63(2)	-21(1)	-5(1)	-6(1)
F(15)	26(1)	35(1)	29(1)	-15(1)	3(1)	-10(1)
F(16)	30(1)	23(1)	39(2)	-9(1)	3(1)	-9(1)
F(17)	57(2)	19(1)	58(2)	-4(1)	6(2)	-9(1)
F(18)	56(2)	19(1)	63(2)	-9(1)	-5(2)	15(1)
F(19)	33(2)	37(2)	64(2)	-22(1)	1(1)	7(1)
F(20)	29(1)	25(1)	47(2)	-10(1)	7(1)	-1(1)
N(1)	21(2)	26(2)	19(2)	-6(2)	0(1)	-1(2)
O(1)	46(2)	21(2)	30(2)	0(1)	8(2)	7(1)
O(2)	47(2)	38(2)	30(2)	-4(2)	-1(2)	4(2)
O(3)	42(2)	41(2)	54(2)	-16(2)	8(2)	-18(2)
O(4)	22(2)	16(1)	22(2)	-6(1)	3(1)	-4(1)
O(5)	18(1)	16(1)	18(1)	-4(1)	-3(1)	1(1)
O(6)	28(2)	21(1)	19(2)	-4(1)	-2(1)	-9(1)
O(7)	32(2)	20(1)	22(2)	-2(1)	-6(1)	-10(1)
P(1)	19(1)	18(1)	19(1)	-5(1)	1(1)	-2(1)
Rh(1)	21(1)	20(1)	22(1)	-4(1)	2(1)	-3(1)
S(1)	31(1)	20(1)	30(1)	-1(1)	3(1)	-1(1)

Table A.5.10. Hydrogen coordinates (x 10^4) and isotropic displacement parameters ($Å^2$x 10^3) for Rh(cod)OTs·CKphos.

	x	y	z	U(eq)
H(1)	9925	9226	5587	38
H(2)	8736	9173	4690	39
H(3)	9905	5355	6671	35
H(4)	8493	5357	5898	40
H(5A)	8147	6629	4619	50
H(5B)	9344	5908	4609	50
H(6A)	10303	7465	4452	50
H(6B)	9185	8048	3945	50
H(7A)	11610	5957	6301	48
H(7B)	11222	6222	5436	48
H(8A)	11383	7810	6216	43
H(8B)	11634	7973	5342	43
H(10)	8676	4685	8507	22
H(11)	6269	5207	8559	23
H(14A)	6204	4885	10151	56
H(14B)	7144	4387	10816	56
H(14C)	6214	3603	10733	56
H(15A)	7607	1970	10527	50
H(15B)	8595	2586	10739	50
H(15C)	8616	2318	9954	50
H(17)	6785	10721	7259	43
H(18)	5154	10947	7937	49
H(20)	3231	10541	6279	47
H(21)	4852	10201	5628	40
H(22A)	2293	11066	7295	80
H(22B)	2994	11599	7794	80
H(22C)	2922	10241	8066	80
H(47A)	6219	6524	5624	42
H(47B)	5979	7869	5548	42
H(48A)	4207	7554	5289	49

H(48B)	4376	6238	5848	49
H(49A)	3392	6988	6648	40
H(49B)	3762	8251	6243	40
H(50A)	5090	7859	7172	27
H(50B)	4825	6541	7512	27

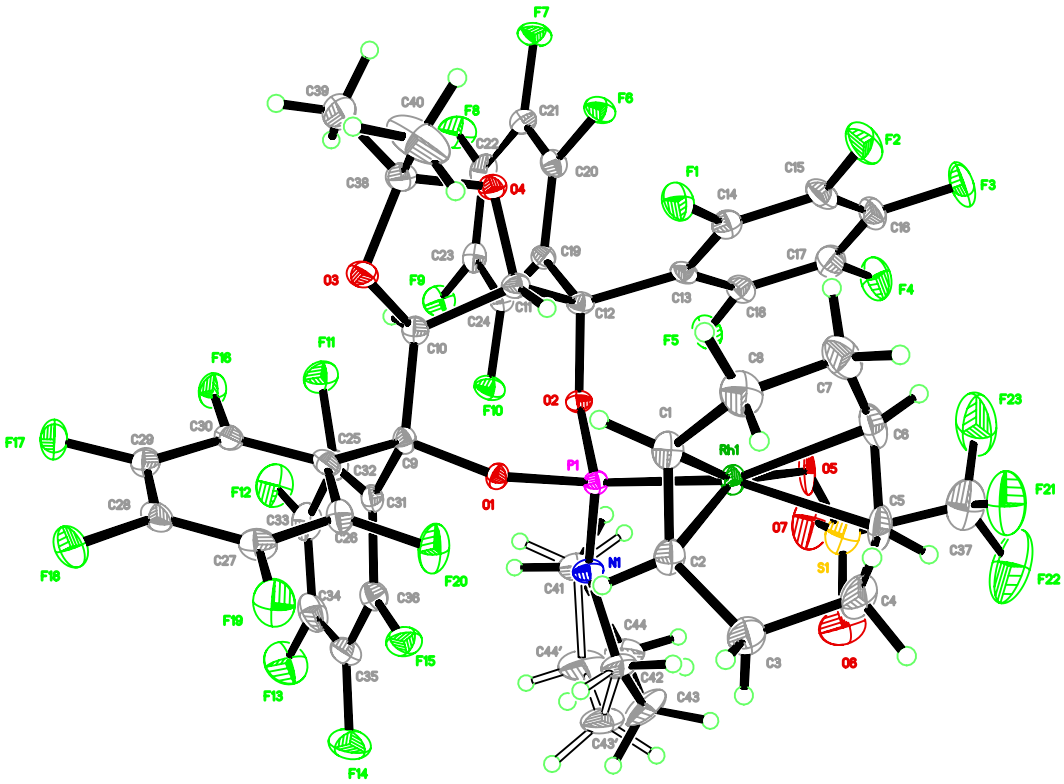

Table A.5.11. Crystal data and structure refinement for Rh(cod)OTf·CKphos.

Identification code	Rovis107	
Empirical formula	$C_{44}\ H_{28}\ F_{23}\ N\ O_7\ P\ Rh\ S$	
Formula weight	1285.61	
Temperature	120(2) K	
Wavelength	0.71073 Å	
Crystal system	Triclinic	
Space group	P-1	
Unit cell dimensions	*a* = 10.4903(10) Å	α= 78.012(3)°.
	b = 14.3946(14) Å	β= 84.045(3)°.
	c = 15.5781(15) Å	γ = 72.010(4)°.
Volume	2186.6(4) $Å^3$	
Z	2	
Density (calculated)	1.953 Mg/m^3	
Absorption coefficient	0.630 mm^{-1}	
F_{000}	1276	
Crystal size	0.23 x 0.06 x 0.06 mm^3	
Theta range for data collection	1.82 to 27.10°.	
Index ranges	-13≤h≤13, -17≤k≤18, -19≤l≤19	

Reflections collected	40057
Independent reflections	9632 [R_{int} = 0.0482]
Completeness to theta = 27.10°	99.9 %
Absorption correction	Multi-scan
Max. and min. transmission	0.9626 and 0.8687
Refinement method	Full-matrix least-squares on F^2
Data / restraints / parameters	9632 / 43 / 725
Goodness-of-fit on F^2	1.124
Final R indices [I>2sigma(I)]	R1 = 0.0453, wR2 = 0.1260
R indices (all data)	R1 = 0.0687, wR2 = 0.1592
Largest diff. peak and hole	0.851 and -1.335 e.Å^{-3}

Table A.5.12. Atomic coordinates (x 10^4) and equivalent isotropic displacement parameters (Å^{2}x 10^3) for Rh(cod)OTf·CKphos. U(eq) is defined as one third of the trace of the orthogonalized U^{ij} tensor.

	x	y	z	U(eq)
C(1)	5764(4)	5050(3)	7868(3)	18(1)
C(2)	4816(4)	5209(3)	7231(3)	19(1)
C(3)	4769(5)	4485(3)	6663(3)	28(1)
C(4)	6143(5)	3908(3)	6330(3)	30(1)
C(5)	7091(5)	4542(3)	6092(3)	25(1)
C(6)	7983(4)	4555(3)	6655(3)	25(1)
C(7)	8166(5)	3970(3)	7597(3)	30(1)
C(8)	6850(5)	4068(3)	8136(3)	29(1)
C(9)	3468(4)	7979(3)	8467(2)	13(1)
C(10)	4657(4)	8066(3)	8935(2)	14(1)
C(11)	6086(4)	7476(3)	8664(2)	14(1)
C(12)	6672(4)	7965(3)	7810(2)	13(1)
C(13)	8014(4)	7311(3)	7454(3)	14(1)
C(14)	8764(4)	6368(3)	7861(3)	17(1)
C(15)	9997(4)	5879(3)	7511(3)	21(1)
C(16)	10511(4)	6314(3)	6741(3)	23(1)
C(17)	9789(4)	7240(3)	6310(3)	23(1)
C(18)	8569(4)	7712(3)	6670(3)	18(1)
C(19)	6879(4)	8954(3)	7897(2)	13(1)

C(20)	7976(4)	8942(3)	8352(3)	16(1)
C(21)	8224(4)	9793(3)	8470(3)	17(1)
C(22)	7384(4)	10710(3)	8112(3)	18(1)
C(23)	6322(4)	10758(3)	7642(2)	16(1)
C(24)	6068(4)	9901(3)	7545(2)	13(1)
C(25)	2480(4)	7575(3)	9137(3)	15(1)
C(26)	2124(4)	6716(3)	9156(3)	17(1)
C(27)	1138(4)	6464(3)	9723(3)	19(1)
C(28)	455(4)	7074(3)	10309(3)	17(1)
C(29)	782(4)	7920(3)	10319(3)	18(1)
C(30)	1780(4)	8156(3)	9743(2)	15(1)
C(31)	2573(4)	8971(3)	7936(2)	15(1)
C(32)	2514(4)	9929(3)	7983(3)	21(1)
C(33)	1618(5)	10765(3)	7507(3)	24(1)
C(34)	727(5)	10646(3)	6985(3)	26(1)
C(35)	726(4)	9703(3)	6946(3)	23(1)
C(36)	1611(4)	8902(3)	7418(3)	17(1)
C(37)	8636(6)	6410(4)	4253(4)	42(1)
C(38)	5945(4)	7383(4)	10160(3)	25(1)
C(39)	6022(6)	8122(6)	10673(4)	62(2)
C(40)	6330(6)	6317(5)	10675(4)	56(2)
N(1)	4050(3)	8110(2)	6186(2)	15(1)
C(41)	4019(4)	9137(3)	5739(3)	21(1)
C(42)	3390(4)	7647(3)	5662(3)	21(1)
C(43)	3253(19)	8356(9)	4782(6)	32(4)
C(44)	3631(15)	9152(9)	4811(6)	24(3)
C(43')	2675(15)	8529(8)	4989(9)	31(3)
C(44')	3044(17)	9338(9)	5013(9)	35(4)
F(1)	8347(2)	5891(2)	8616(2)	23(1)
F(2)	10689(3)	4987(2)	7930(2)	31(1)
F(3)	11703(3)	5845(2)	6403(2)	33(1)
F(4)	10265(3)	7667(2)	5560(2)	33(1)
F(5)	7906(2)	8609(2)	6232(2)	21(1)
F(6)	8883(2)	8081(2)	8676(2)	18(1)
F(7)	9280(2)	9722(2)	8917(2)	23(1)
F(8)	7614(3)	11543(2)	8212(2)	28(1)

F(9)	5515(2)	11640(2)	7287(2)	22(1)
F(10)	5010(2)	10042(2)	7073(2)	18(1)
F(11)	3288(3)	10147(2)	8505(2)	24(1)
F(12)	1626(3)	11661(2)	7590(2)	33(1)
F(13)	-154(3)	11441(2)	6540(2)	39(1)
F(14)	-172(3)	9581(2)	6454(2)	33(1)
F(15)	1495(2)	7998(2)	7382(2)	23(1)
F(16)	2050(2)	8998(2)	9767(2)	20(1)
F(17)	111(2)	8532(2)	10851(2)	25(1)
F(18)	-528(2)	6848(2)	10848(2)	26(1)
F(19)	821(3)	5642(2)	9703(2)	29(1)
F(20)	2700(3)	6078(2)	8606(2)	28(1)
F(21)	8884(4)	5441(2)	4542(2)	53(1)
F(22)	8554(5)	6556(3)	3386(2)	74(1)
F(23)	9662(4)	6681(3)	4427(3)	72(1)
O(1)	4020(3)	7278(2)	7885(2)	12(1)
O(2)	5682(3)	8198(2)	7157(2)	13(1)
O(3)	4632(3)	7603(2)	9843(2)	24(1)
O(4)	6807(3)	7445(2)	9391(2)	15(1)
O(5)	7268(3)	6760(2)	5631(2)	22(1)
O(6)	6076(4)	6755(3)	4470(3)	51(1)
O(7)	7034(4)	8114(3)	4477(3)	50(1)
P(1)	4970(1)	7402(1)	6991(1)	12(1)
Rh(1)	6259(1)	5936(1)	6698(1)	14(1)
S(1)	7073(1)	7101(1)	4755(1)	33(1)

Table A.5.13. Bond lengths [Å] and angles [°] for Rh(cod)OTf·CKphos.

C(1)-C(2)	1.412(6)	C(5)-C(6)	1.352(6)
C(1)-C(8)	1.526(6)	C(5)-Rh(1)	2.282(4)
C(1)-Rh(1)	2.113(4)	C(6)-C(7)	1.532(7)
C(2)-C(3)	1.515(5)	C(6)-Rh(1)	2.244(4)
C(2)-Rh(1)	2.104(4)	C(7)-C(8)	1.523(7)
C(3)-C(4)	1.523(6)	C(9)-O(1)	1.443(4)
C(4)-C(5)	1.518(7)	C(9)-C(25)	1.548(5)

C(9)-C(10)	1.558(5)	C(27)-C(28)	1.388(6)
C(9)-C(31)	1.564(5)	C(28)-F(18)	1.337(5)
C(10)-O(3)	1.435(5)	C(28)-C(29)	1.367(6)
C(10)-C(11)	1.542(5)	C(29)-F(17)	1.326(4)
C(11)-O(4)	1.412(4)	C(29)-C(30)	1.383(6)
C(11)-C(12)	1.533(5)	C(30)-F(16)	1.336(4)
C(12)-O(2)	1.444(4)	C(31)-C(32)	1.378(6)
C(12)-C(19)	1.540(5)	C(31)-C(36)	1.395(5)
C(12)-C(13)	1.553(5)	C(32)-F(11)	1.348(5)
C(13)-C(18)	1.389(6)	C(32)-C(33)	1.399(6)
C(13)-C(14)	1.397(6)	C(33)-F(12)	1.325(5)
C(14)-F(1)	1.337(5)	C(33)-C(34)	1.370(6)
C(14)-C(15)	1.384(6)	C(34)-F(13)	1.339(5)
C(15)-F(2)	1.333(5)	C(34)-C(35)	1.373(6)
C(15)-C(16)	1.372(7)	C(35)-F(14)	1.346(5)
C(16)-F(3)	1.337(5)	C(35)-C(36)	1.364(6)
C(16)-C(17)	1.383(7)	C(36)-F(15)	1.356(5)
C(17)-F(4)	1.327(5)	C(37)-F(23)	1.322(7)
C(17)-C(18)	1.373(6)	C(37)-F(21)	1.324(6)
C(18)-F(5)	1.340(5)	C(37)-F(22)	1.331(7)
C(19)-C(24)	1.397(5)	C(37)-S(1)	1.828(6)
C(19)-C(20)	1.408(5)	C(38)-O(4)	1.428(5)
C(20)-F(6)	1.344(4)	C(38)-O(3)	1.431(5)
C(20)-C(21)	1.379(5)	C(38)-C(39)	1.482(7)
C(21)-F(7)	1.335(4)	C(38)-C(40)	1.527(7)
C(21)-C(22)	1.381(6)	N(1)-C(42)	1.488(5)
C(22)-F(8)	1.336(4)	N(1)-C(41)	1.489(5)
C(22)-C(23)	1.373(6)	N(1)-P(1)	1.629(3)
C(23)-F(9)	1.332(4)	C(41)-C(44')	1.527(10)
C(23)-C(24)	1.379(5)	C(41)-C(44)	1.537(10)
C(24)-F(10)	1.335(4)	C(42)-C(43')	1.515(10)
C(25)-C(30)	1.390(5)	C(42)-C(43)	1.520(10)
C(25)-C(26)	1.392(6)	C(43)-C(44)	1.333(12)
C(26)-F(20)	1.349(4)	C(43')-C(44')	1.344(12)
C(26)-C(27)	1.374(6)	O(1)-P(1)	1.639(3)
C(27)-F(19)	1.332(5)	O(2)-P(1)	1.623(3)

O(5)-S(1)	1.366(3)	C(11)-C(12)-C(19)	111.9(3)
O(5)-Rh(1)	2.210(3)	O(2)-C(12)-C(13)	108.1(3)
O(6)-S(1)	1.431(4)	C(11)-C(12)-C(13)	115.3(3)
O(7)-S(1)	1.421(4)	C(19)-C(12)-C(13)	107.9(3)
P(1)-Rh(1)	2.2366(10)	C(18)-C(13)-C(14)	115.8(4)
		C(18)-C(13)-C(12)	117.5(3)
C(2)-C(1)-C(8)	124.0(4)	C(14)-C(13)-C(12)	126.6(4)
C(2)-C(1)-Rh(1)	70.1(2)	F(1)-C(14)-C(15)	116.1(4)
C(8)-C(1)-Rh(1)	113.7(3)	F(1)-C(14)-C(13)	122.2(4)
C(1)-C(2)-C(3)	126.5(4)	C(15)-C(14)-C(13)	121.7(4)
C(1)-C(2)-Rh(1)	70.8(2)	F(2)-C(15)-C(16)	120.1(4)
C(3)-C(2)-Rh(1)	109.8(3)	F(2)-C(15)-C(14)	119.6(4)
C(2)-C(3)-C(4)	114.0(4)	C(16)-C(15)-C(14)	120.3(4)
C(5)-C(4)-C(3)	112.3(4)	F(3)-C(16)-C(15)	120.4(4)
C(6)-C(5)-C(4)	122.8(4)	F(3)-C(16)-C(17)	119.8(4)
C(6)-C(5)-Rh(1)	71.1(2)	C(15)-C(16)-C(17)	119.8(4)
C(4)-C(5)-Rh(1)	109.2(3)	F(4)-C(17)-C(18)	120.5(4)
C(5)-C(6)-C(7)	126.1(4)	F(4)-C(17)-C(16)	120.6(4)
C(5)-C(6)-Rh(1)	74.2(2)	C(18)-C(17)-C(16)	118.9(4)
C(7)-C(6)-Rh(1)	107.1(3)	F(5)-C(18)-C(17)	116.9(4)
C(8)-C(7)-C(6)	113.2(4)	F(5)-C(18)-C(13)	119.6(3)
C(7)-C(8)-C(1)	114.5(4)	C(17)-C(18)-C(13)	123.5(4)
O(1)-C(9)-C(25)	108.0(3)	C(24)-C(19)-C(20)	114.9(3)
O(1)-C(9)-C(10)	107.7(3)	C(24)-C(19)-C(12)	125.6(3)
C(25)-C(9)-C(10)	111.2(3)	C(20)-C(19)-C(12)	119.5(3)
O(1)-C(9)-C(31)	109.3(3)	F(6)-C(20)-C(21)	115.7(3)
C(25)-C(9)-C(31)	104.6(3)	F(6)-C(20)-C(19)	121.0(3)
C(10)-C(9)-C(31)	115.8(3)	C(21)-C(20)-C(19)	123.2(4)
O(3)-C(10)-C(11)	98.9(3)	F(7)-C(21)-C(20)	119.8(3)
O(3)-C(10)-C(9)	110.3(3)	F(7)-C(21)-C(22)	120.9(3)
C(11)-C(10)-C(9)	117.3(3)	C(20)-C(21)-C(22)	119.3(4)
O(4)-C(11)-C(12)	110.9(3)	F(8)-C(22)-C(23)	120.3(4)
O(4)-C(11)-C(10)	101.1(3)	F(8)-C(22)-C(21)	120.3(4)
C(12)-C(11)-C(10)	114.7(3)	C(23)-C(22)-C(21)	119.5(4)
O(2)-C(12)-C(11)	106.4(3)	F(9)-C(23)-C(22)	119.8(3)
O(2)-C(12)-C(19)	106.9(3)	F(9)-C(23)-C(24)	119.6(4)

C(22)-C(23)-C(24)	120.6(4)	C(36)-C(35)-C(34)	119.8(4)
F(10)-C(24)-C(23)	115.1(3)	F(15)-C(36)-C(35)	116.1(4)
F(10)-C(24)-C(19)	122.4(3)	F(15)-C(36)-C(31)	119.9(3)
C(23)-C(24)-C(19)	122.5(3)	C(35)-C(36)-C(31)	123.9(4)
C(30)-C(25)-C(26)	115.2(4)	F(23)-C(37)-F(21)	108.6(5)
C(30)-C(25)-C(9)	118.0(3)	F(23)-C(37)-F(22)	108.9(5)
C(26)-C(25)-C(9)	126.6(3)	F(21)-C(37)-F(22)	106.5(4)
F(20)-C(26)-C(27)	114.9(4)	F(23)-C(37)-S(1)	111.1(4)
F(20)-C(26)-C(25)	122.5(4)	F(21)-C(37)-S(1)	110.9(4)
C(27)-C(26)-C(25)	122.6(4)	F(22)-C(37)-S(1)	110.7(4)
F(19)-C(27)-C(26)	120.1(4)	O(4)-C(38)-O(3)	105.2(3)
F(19)-C(27)-C(28)	119.7(4)	O(4)-C(38)-C(39)	108.6(4)
C(26)-C(27)-C(28)	120.2(4)	O(3)-C(38)-C(39)	111.8(4)
F(18)-C(28)-C(29)	120.2(4)	O(4)-C(38)-C(40)	109.5(4)
F(18)-C(28)-C(27)	120.6(4)	O(3)-C(38)-C(40)	107.9(4)
C(29)-C(28)-C(27)	119.2(4)	C(39)-C(38)-C(40)	113.5(5)
F(17)-C(29)-C(28)	120.2(4)	C(42)-N(1)-C(41)	111.3(3)
F(17)-C(29)-C(30)	120.2(4)	C(42)-N(1)-P(1)	118.7(3)
C(28)-C(29)-C(30)	119.5(4)	C(41)-N(1)-P(1)	128.2(3)
F(16)-C(30)-C(29)	117.4(3)	N(1)-C(41)-C(44')	101.8(5)
F(16)-C(30)-C(25)	119.3(4)	N(1)-C(41)-C(44)	101.4(5)
C(29)-C(30)-C(25)	123.4(4)	C(44')-C(41)-C(44)	25.1(5)
C(32)-C(31)-C(36)	114.5(4)	N(1)-C(42)-C(43')	102.3(5)
C(32)-C(31)-C(9)	127.9(3)	N(1)-C(42)-C(43)	102.2(5)
C(36)-C(31)-C(9)	117.2(3)	C(43')-C(42)-C(43)	25.0(5)
F(11)-C(32)-C(31)	123.3(4)	C(44)-C(43)-C(42)	111.7(8)
F(11)-C(32)-C(33)	113.9(4)	C(43)-C(44)-C(41)	111.4(8)
C(31)-C(32)-C(33)	122.8(4)	C(44')-C(43')-C(42)	111.3(8)
F(12)-C(33)-C(34)	121.2(4)	C(43')-C(44')-C(41)	111.6(8)
F(12)-C(33)-C(32)	118.9(4)	C(9)-O(1)-P(1)	128.2(2)
C(34)-C(33)-C(32)	119.8(4)	C(12)-O(2)-P(1)	122.9(2)
F(13)-C(34)-C(33)	120.4(4)	C(38)-O(3)-C(10)	108.0(3)
F(13)-C(34)-C(35)	120.6(4)	C(11)-O(4)-C(38)	108.1(3)
C(33)-C(34)-C(35)	119.0(4)	S(1)-O(5)-Rh(1)	134.0(2)
F(14)-C(35)-C(36)	120.8(4)	O(2)-P(1)-N(1)	97.64(15)
F(14)-C(35)-C(34)	119.3(4)	O(2)-P(1)-O(1)	102.58(13)

N(1)-P(1)-O(1)	109.63(16)	C(1)-Rh(1)-C(5)	89.16(16)
O(2)-P(1)-Rh(1)	118.95(11)	O(5)-Rh(1)-C(5)	90.24(14)
N(1)-P(1)-Rh(1)	114.40(12)	P(1)-Rh(1)-C(5)	162.54(12)
O(1)-P(1)-Rh(1)	112.18(10)	C(6)-Rh(1)-C(5)	34.76(16)
C(2)-Rh(1)-C(1)	39.13(16)	O(5)-S(1)-O(7)	113.5(2)
C(2)-Rh(1)-O(5)	154.66(14)	O(5)-S(1)-O(6)	111.1(2)
C(1)-Rh(1)-O(5)	165.46(14)	O(7)-S(1)-O(6)	119.4(3)
C(2)-Rh(1)-P(1)	93.09(11)	O(5)-S(1)-C(37)	102.5(2)
C(1)-Rh(1)-P(1)	96.87(11)	O(7)-S(1)-C(37)	104.4(3)
O(5)-Rh(1)-P(1)	87.94(7)	O(6)-S(1)-C(37)	103.7(3)
C(2)-Rh(1)-C(6)	96.47(16)		
C(1)-Rh(1)-C(6)	81.63(17)		
O(5)-Rh(1)-C(6)	89.65(14)		
P(1)-Rh(1)-C(6)	162.45(12)		
C(2)-Rh(1)-C(5)	81.26(16)		

Symmetry transformations used to generate equivalent atoms:

Table A.5.14. Anisotropic displacement parameters ($Å^2 x\ 10^3$)for Rh(cod)OTf·CKphos. The anisotropic displacement factor exponent takes the form: $-2p^2[\ h^2a^{*2}U^{11} + ... + 2\ h\ k\ a^*\ b^*\ U^{12}\ ]$

	U^{11}	U^{22}	U^{33}	U^{23}	U^{13}	U^{12}
C(1)	22(2)	12(2)	19(2)	-1(2)	2(2)	-5(2)
C(2)	21(2)	16(2)	24(2)	-7(2)	4(2)	-10(2)
C(3)	26(2)	27(2)	38(3)	-16(2)	2(2)	-13(2)
C(4)	36(3)	22(2)	40(3)	-19(2)	4(2)	-12(2)
C(5)	27(2)	17(2)	33(2)	-15(2)	11(2)	-5(2)
C(6)	17(2)	17(2)	41(3)	-11(2)	8(2)	-3(2)
C(7)	25(2)	18(2)	41(3)	-3(2)	-4(2)	1(2)
C(8)	32(3)	18(2)	29(2)	3(2)	-4(2)	-1(2)
C(9)	13(2)	10(2)	16(2)	-5(2)	2(2)	-3(2)
C(10)	15(2)	14(2)	16(2)	-4(2)	2(2)	-6(2)
C(11)	15(2)	12(2)	15(2)	-3(2)	-4(2)	-3(2)
C(12)	14(2)	11(2)	15(2)	-2(1)	-4(2)	-4(2)
C(13)	11(2)	13(2)	22(2)	-6(2)	-4(2)	-4(2)
C(14)	19(2)	15(2)	17(2)	-3(2)	-2(2)	-6(2)
C(15)	14(2)	15(2)	34(2)	-6(2)	-6(2)	-1(2)

C(16)	12(2)	26(2)	35(2)	-15(2)	2(2)	-6(2)
C(17)	19(2)	31(2)	24(2)	-10(2)	6(2)	-14(2)
C(18)	15(2)	15(2)	23(2)	-4(2)	-2(2)	-5(2)
C(19)	12(2)	15(2)	14(2)	-3(2)	1(1)	-6(2)
C(20)	16(2)	13(2)	17(2)	-1(2)	-1(2)	-2(2)
C(21)	18(2)	18(2)	17(2)	-5(2)	-1(2)	-6(2)
C(22)	25(2)	11(2)	23(2)	-7(2)	3(2)	-10(2)
C(23)	20(2)	12(2)	14(2)	0(2)	3(2)	-3(2)
C(24)	13(2)	14(2)	12(2)	-3(2)	-1(1)	-4(2)
C(25)	10(2)	17(2)	17(2)	-2(2)	-2(2)	-3(2)
C(26)	15(2)	16(2)	18(2)	-5(2)	2(2)	-2(2)
C(27)	21(2)	19(2)	21(2)	0(2)	-2(2)	-12(2)
C(28)	13(2)	24(2)	15(2)	2(2)	0(2)	-9(2)
C(29)	16(2)	21(2)	15(2)	-4(2)	-2(2)	-2(2)
C(30)	12(2)	17(2)	15(2)	-2(2)	-2(2)	-5(2)
C(31)	12(2)	16(2)	14(2)	-4(2)	1(2)	-1(2)
C(32)	20(2)	24(2)	19(2)	-6(2)	2(2)	-7(2)
C(33)	29(2)	16(2)	25(2)	-2(2)	3(2)	-5(2)
C(34)	19(2)	25(2)	25(2)	3(2)	2(2)	2(2)
C(35)	14(2)	31(2)	23(2)	-5(2)	-3(2)	-5(2)
C(36)	16(2)	16(2)	19(2)	-3(2)	0(2)	-4(2)
C(37)	49(3)	36(3)	45(3)	-13(3)	13(3)	-18(3)
C(38)	16(2)	43(3)	16(2)	-6(2)	0(2)	-9(2)
C(39)	25(3)	116(6)	63(4)	-71(4)	0(3)	-11(3)
C(40)	28(3)	78(5)	41(3)	38(3)	-7(2)	-18(3)
N(1)	18(2)	14(2)	16(2)	-2(1)	-5(1)	-7(1)
C(41)	26(2)	14(2)	21(2)	3(2)	-8(2)	-9(2)
C(42)	23(2)	21(2)	22(2)	-7(2)	-6(2)	-10(2)
C(43)	57(10)	27(6)	11(5)	-1(4)	-13(5)	-7(6)
C(44)	27(6)	28(6)	17(5)	7(4)	-7(4)	-15(5)
C(43')	32(7)	30(6)	31(7)	-5(5)	-19(5)	-4(5)
C(44')	41(8)	31(6)	26(6)	9(5)	-25(6)	-3(6)
F(1)	22(1)	15(1)	25(1)	-1(1)	0(1)	0(1)
F(2)	23(1)	17(1)	45(2)	-5(1)	-5(1)	5(1)
F(3)	16(1)	33(2)	49(2)	-18(1)	10(1)	-1(1)
F(4)	25(1)	41(2)	29(1)	-5(1)	14(1)	-12(1)

F(5)	20(1)	18(1)	21(1)	2(1)	2(1)	-5(1)
F(6)	16(1)	13(1)	24(1)	-3(1)	-6(1)	-2(1)
F(7)	18(1)	23(1)	31(1)	-10(1)	-9(1)	-8(1)
F(8)	34(2)	15(1)	40(2)	-7(1)	-8(1)	-12(1)
F(9)	28(1)	11(1)	25(1)	0(1)	-6(1)	-2(1)
F(10)	16(1)	15(1)	23(1)	-1(1)	-7(1)	-2(1)
F(11)	29(1)	18(1)	28(1)	-8(1)	-3(1)	-9(1)
F(12)	42(2)	14(1)	38(2)	-4(1)	0(1)	-5(1)
F(13)	37(2)	25(2)	44(2)	6(1)	-12(1)	5(1)
F(14)	26(1)	40(2)	30(1)	-1(1)	-12(1)	-7(1)
F(15)	23(1)	21(1)	27(1)	-7(1)	-4(1)	-9(1)
F(16)	22(1)	20(1)	23(1)	-10(1)	6(1)	-11(1)
F(17)	23(1)	30(1)	24(1)	-12(1)	9(1)	-10(1)
F(18)	20(1)	33(2)	26(1)	-4(1)	7(1)	-14(1)
F(19)	33(2)	24(1)	38(2)	-9(1)	9(1)	-20(1)
F(20)	34(2)	19(1)	36(2)	-15(1)	15(1)	-14(1)
F(21)	59(2)	35(2)	62(2)	-14(2)	21(2)	-11(2)
F(22)	114(4)	62(3)	36(2)	-16(2)	31(2)	-19(2)
F(23)	48(2)	77(3)	109(3)	-53(3)	36(2)	-34(2)
O(1)	13(1)	12(1)	13(1)	-5(1)	2(1)	-5(1)
O(2)	13(1)	13(1)	13(1)	-2(1)	-2(1)	-6(1)
O(3)	14(2)	44(2)	12(1)	-3(1)	-1(1)	-10(1)
O(4)	14(1)	19(1)	12(1)	-1(1)	-2(1)	-6(1)
O(5)	22(2)	12(1)	35(2)	-11(1)	25(1)	-12(1)
O(6)	43(2)	75(3)	45(2)	-25(2)	-7(2)	-19(2)
O(7)	70(3)	32(2)	39(2)	-3(2)	10(2)	-8(2)
P(1)	13(1)	11(1)	13(1)	-3(1)	0(1)	-4(1)
Rh(1)	15(1)	12(1)	17(1)	-5(1)	1(1)	-3(1)
S(1)	35(1)	34(1)	31(1)	-11(1)	2(1)	-9(1)

Table A.5.15. Hydrogen coordinates (x 10^4) and isotropic displacement parameters ($Å^2$x 10^3) for Rh(cod)OTf·CKphos.

	x	y	z	U(eq)

H(1)	5415	5415	8349	22
H(2)	3936	5663	7356	23
H(3A)	4230	4849	6163	33
H(3B)	4328	4016	7000	33
H(4A)	6532	3340	6779	36
H(4B)	6037	3661	5816	36
H(5)	7371	4660	5469	30
H(6)	8803	4682	6365	30
H(7A)	8603	3274	7580	36
H(7B)	8751	4205	7886	36
H(8A)	7027	3994	8749	35
H(8B)	6511	3527	8083	35
H(10)	4601	8768	8885	17
H(11)	6106	6801	8622	17
H(39A)	5735	8777	10323	93
H(39B)	6930	7982	10835	93
H(39C)	5450	8086	11194	93
H(40A)	5803	6287	11216	83
H(40B)	7264	6108	10799	83
H(40C)	6166	5886	10333	83
H(41A)	4889	9243	5731	25
H(41B)	3354	9632	6017	25
H(41C)	4900	9166	5499	25
H(41D)	3689	9605	6137	25
H(42A)	2520	7617	5924	25
H(42B)	3943	6984	5604	25
H(42C)	2760	7347	6025	25
H(42D)	4045	7148	5383	25
H(43A)	3800	8010	4337	39
H(43B)	2327	8568	4616	39
H(44A)	2902	9748	4629	28
H(44B)	4391	9169	4403	28
H(43C)	2882	8365	4407	37
H(43D)	1713	8673	5103	37
H(44C)	2253	9878	5111	42
H(44D)	3465	9542	4451	42

A.5.3 Synthesis and X-ray Data for $Co(CO)_3Nn\text{-}Bu_4$·CKPhos Complex

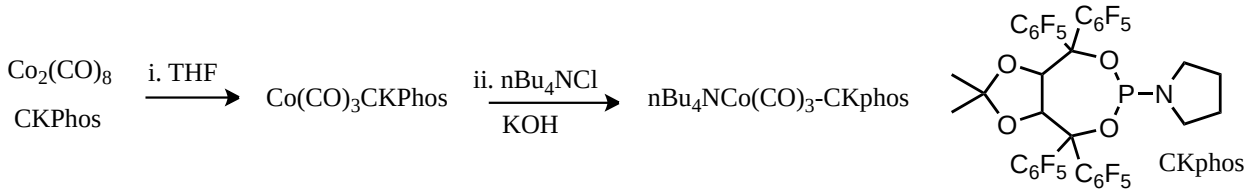

In an Ar atmosphere glove box to an oven-dried 20 ml scintillation vial equipped with a magnetic stirbar was added Co_2CO_8 (15 mg, 0.044 mmol, 1 equiv), racemic CKPhos (55 mg, 0.059 mmol) and THF (2 ml). Bubbling (release of CO) occurs and the resultant dark brown solution is stirred 30 minutes at room temperature. *n*-Bu_4NCl (37 mg, 0.133 mmol) and KOH (10 mg, 0.178 mmol) are then added and the heterogeneous solution is stirred overnight. Reaction mixture is then filtered through a plug of cotton in a glass pipette to remove solid. THF was removed under reduced pressure and DCM was added to solid residue. Layering with hexanes and slow evaporation provided tan crystals of X-ray quality (50 mg, 43 % yield).

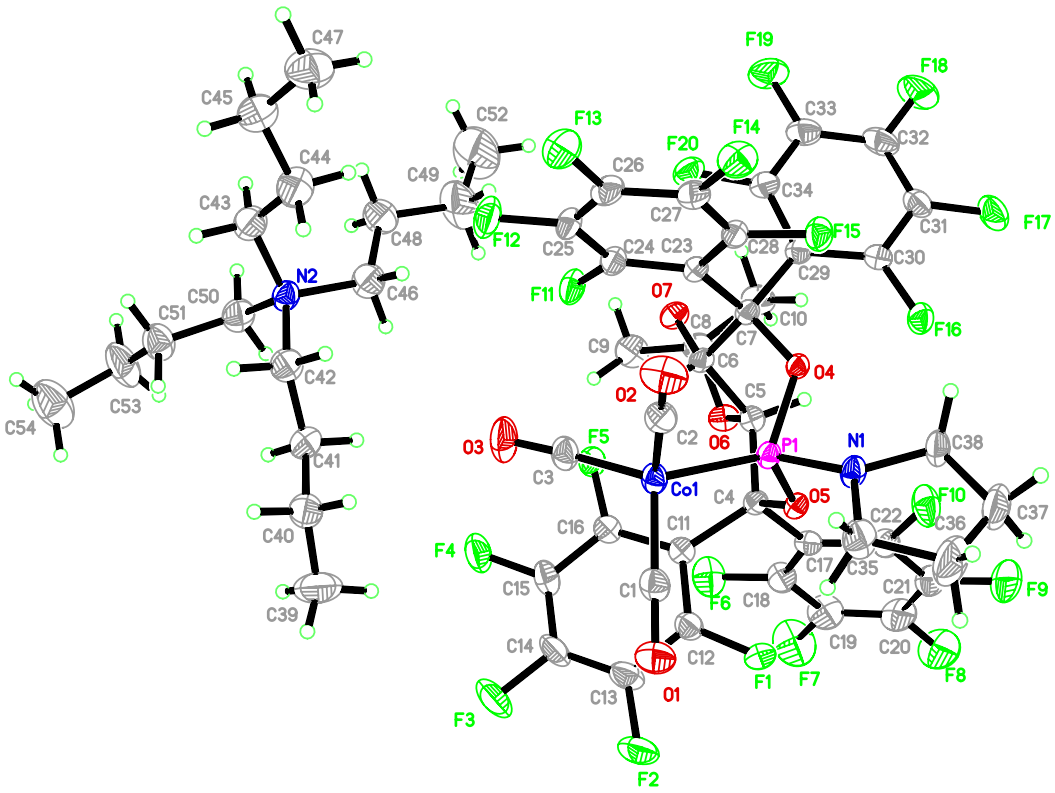

Table A.5.16. Crystal data and structure refinement for $Co(CO)_3$*n*-Bu_4N·CKphos.

Identification code	rovis141r_0m-sr	
Empirical formula	C_{54} H_{52} Co F_{20} N_2 O_7 P	
Formula weight	1310.88	
Temperature	120 K	
Wavelength	0.71073 Å	
Crystal system	Triclinic	
Space group	*P* -1	
Unit cell dimensions	*a* = 13.4123(5) Å	α= 94.268(2)°
	b = 14.8876(6) Å	β= 90.340(2)°
	c = 16.7728(7) Å	ɣ = 97.344(2)°
Volume	3312.1(2) $Å^3$	
Z	2	
Density (calculated)	1.314 Mg/m^3	
Absorption coefficient	0.385 mm^{-1}	
F_{000}	1336	
Crystal size	0.56 x 0.21 x 0.05 mm^3	
Theta range for data collection	1.22 to 26.45°.	

Index ranges	-16≤h≤15, -18≤k≤18, -20≤l≤20
Reflections collected	48968
Independent reflections	13496 [R_{int} = 0.0482]
Completeness to theta = 26.45°	98.8 %
Absorption correction	multi-scan
Max. and min. transmission	0.9795 and 0.8137
Refinement method	Full-matrix least-squares on F^2
Data / restraints / parameters	13496 / 0 / 772
Goodness-of-fit on F^2	0.934
Final R indices [I>2sigma(I)]	R1 = 0.0571, wR2 = 0.1458
R indices (all data)	R1 = 0.1172, wR2 = 0.1645
Largest diff. peak and hole	0.535 and -0.318 e.Å^{-3}

Table A.5.17. Atomic coordinates (x 10^4) and equivalent isotropic displacement parameters (Å^{2}x 10^3) for $Co(CO)_3$n-Bu_4N·CKphos. U(eq) is defined as one third of the trace of the orthogonalized U^{ij} tensor.

	x	y	z	U(eq)
C(1)	1347(3)	3478(2)	4123(2)	63(1)
C(2)	2441(3)	2324(2)	5031(2)	61(1)
C(3)	3367(3)	3303(2)	3786(2)	65(1)
C(4)	1574(2)	1869(2)	1843(2)	45(1)
C(5)	2393(2)	1244(2)	1700(2)	45(1)
C(6)	3280(2)	1306(2)	2299(2)	45(1)
C(7)	3085(2)	620(2)	2959(2)	43(1)
C(8)	3808(3)	1090(2)	982(2)	60(1)
C(9)	4583(3)	1708(3)	529(2)	84(1)
C(10)	3709(3)	97(3)	644(2)	76(1)
C(11)	1846(3)	2913(2)	1951(2)	49(1)
C(12)	1070(3)	3420(2)	2136(2)	61(1)
C(13)	1207(4)	4354(3)	2260(3)	79(1)
C(14)	2139(4)	4818(2)	2205(3)	85(1)
C(15)	2920(3)	4355(3)	2008(2)	73(1)
C(16)	2786(3)	3421(2)	1897(2)	56(1)
C(17)	825(3)	1642(2)	1123(2)	51(1)
C(18)	890(3)	2108(3)	446(2)	71(1)

C(19)	217(4)	1922(3)	-188(3)	92(2)
C(20)	-560(4)	1253(4)	-148(3)	90(2)
C(21)	-634(3)	754(3)	475(3)	75(1)
C(22)	63(3)	936(3)	1092(2)	61(1)
C(23)	3739(2)	846(2)	3721(2)	43(1)
C(24)	4556(3)	1497(2)	3850(2)	54(1)
C(25)	5051(3)	1677(2)	4569(2)	60(1)
C(26)	4742(3)	1197(3)	5200(2)	64(1)
C(27)	3948(3)	525(2)	5113(2)	58(1)
C(28)	3473(2)	358(2)	4376(2)	51(1)
C(29)	3219(2)	-340(2)	2617(2)	47(1)
C(30)	2449(3)	-1025(2)	2385(2)	51(1)
C(31)	2622(3)	-1861(2)	2057(2)	65(1)
C(32)	3580(4)	-2053(3)	1947(3)	81(1)
C(33)	4373(3)	-1404(3)	2179(3)	76(1)
C(34)	4185(3)	-580(2)	2508(2)	58(1)
C(35)	-136(3)	1495(3)	4340(3)	89(1)
C(36)	-1098(4)	916(4)	4325(4)	145(3)
C(37)	-1009(4)	104(4)	3846(4)	145(3)
C(38)	26(3)	113(2)	3551(2)	67(1)
C(39)	4645(5)	6448(4)	3510(4)	157(3)
C(40)	5267(3)	5971(3)	4012(3)	91(1)
C(41)	6051(3)	5517(3)	3546(3)	88(1)
C(42)	6737(3)	5105(3)	4048(3)	77(1)
C(43)	8287(3)	4400(3)	4275(3)	84(1)
C(44)	7878(4)	3750(3)	4855(3)	99(2)
C(45)	8584(4)	3563(4)	5483(3)	110(2)
C(46)	7054(3)	3759(3)	3187(3)	85(1)
C(47)	8192(4)	2849(4)	6013(3)	123(2)
C(48)	7704(4)	3147(3)	2787(3)	102(2)
C(49)	7164(5)	2306(4)	2381(4)	149(3)
C(50)	8127(3)	5216(3)	3064(3)	83(1)
C(51)	8563(4)	6143(3)	3357(3)	90(1)
C(52)	7691(6)	1695(5)	1896(5)	207(4)
C(53)	9021(4)	6702(3)	2746(4)	132(2)
C(54)	9303(5)	7652(4)	2919(4)	156(3)

Co(1)	2237(1)	2737(1)	4102(1)	51(1)
F(1)	118(2)	3014(1)	2181(1)	77(1)
F(2)	416(2)	4792(2)	2430(2)	114(1)
F(3)	2280(2)	5726(2)	2326(2)	130(1)
F(4)	3855(2)	4802(2)	1936(2)	101(1)
F(5)	3610(2)	3040(1)	1711(1)	67(1)
F(6)	1656(2)	2786(2)	367(1)	96(1)
F(7)	338(3)	2436(2)	-817(2)	147(1)
F(8)	-1230(2)	1084(2)	-759(2)	132(1)
F(9)	-1388(2)	66(2)	496(2)	112(1)
F(10)	-78(2)	359(2)	1675(1)	94(1)
F(11)	4929(2)	1986(1)	3250(1)	71(1)
F(12)	5847(2)	2321(2)	4653(2)	95(1)
F(13)	5232(2)	1361(2)	5912(1)	92(1)
F(14)	3645(2)	36(2)	5723(1)	79(1)
F(15)	2718(2)	-339(1)	4315(1)	64(1)
F(16)	1485(2)	-906(1)	2448(1)	65(1)
F(17)	1842(2)	-2491(1)	1834(1)	89(1)
F(18)	3754(2)	-2866(2)	1603(2)	118(1)
F(19)	5317(2)	-1582(2)	2067(2)	108(1)
F(20)	4996(2)	20(1)	2723(1)	72(1)
N(1)	543(2)	1016(2)	3850(2)	52(1)
N(2)	7549(2)	4620(2)	3657(2)	60(1)
O(1)	742(2)	3977(2)	4140(2)	97(1)
O(2)	2590(2)	2062(2)	5646(2)	91(1)
O(3)	4117(2)	3728(2)	3621(2)	105(1)
O(4)	2074(1)	626(1)	3198(1)	41(1)
O(5)	1021(1)	1602(1)	2529(1)	44(1)
O(6)	2864(2)	1417(2)	965(1)	56(1)
O(7)	4102(2)	1149(2)	1808(1)	55(1)
P(1)	1533(1)	1552(1)	3437(1)	43(1)

Table A.5.18. Bond lengths [Å] and angles [°] for $Co(CO)_3$n-Bu_4N·CKphos.

C(1)-O(1)	1.167(4)	C(1)-Co(1)	1.726(4)

C(2)-O(2)	1.153(4)	C(20)-C(21)	1.325(6)
C(2)-Co(1)	1.750(4)	C(20)-F(8)	1.346(5)
C(3)-O(3)	1.164(4)	C(21)-F(9)	1.347(4)
C(3)-Co(1)	1.743(4)	C(21)-C(22)	1.379(5)
C(4)-O(5)	1.427(4)	C(22)-F(10)	1.348(4)
C(4)-C(5)	1.537(4)	C(23)-C(24)	1.372(4)
C(4)-C(11)	1.548(4)	C(23)-C(28)	1.386(4)
C(4)-C(17)	1.555(4)	C(24)-F(11)	1.346(4)
C(5)-O(6)	1.413(3)	C(24)-C(25)	1.366(5)
C(5)-C(6)	1.542(4)	C(25)-F(12)	1.341(4)
C(6)-O(7)	1.414(3)	C(25)-C(26)	1.357(5)
C(6)-C(7)	1.562(4)	C(26)-F(13)	1.350(4)
C(7)-O(4)	1.417(3)	C(26)-C(27)	1.364(5)
C(7)-C(29)	1.532(4)	C(27)-F(14)	1.336(4)
C(7)-C(23)	1.537(4)	C(27)-C(28)	1.377(5)
C(8)-O(6)	1.415(4)	C(28)-F(15)	1.352(3)
C(8)-O(7)	1.430(4)	C(29)-C(30)	1.388(4)
C(8)-C(10)	1.532(5)	C(29)-C(34)	1.397(5)
C(8)-C(9)	1.541(5)	C(30)-F(16)	1.332(4)
C(11)-C(12)	1.386(5)	C(30)-C(31)	1.371(5)
C(11)-C(16)	1.392(5)	C(31)-F(17)	1.343(4)
C(12)-F(1)	1.346(4)	C(31)-C(32)	1.363(6)
C(12)-C(13)	1.378(5)	C(32)-F(18)	1.350(4)
C(13)-F(2)	1.337(4)	C(32)-C(33)	1.377(6)
C(13)-C(14)	1.355(6)	C(33)-F(19)	1.338(4)
C(14)-F(3)	1.341(4)	C(33)-C(34)	1.361(5)
C(14)-C(15)	1.355(6)	C(34)-F(20)	1.345(4)
C(15)-F(4)	1.354(4)	C(35)-N(1)	1.449(5)
C(15)-C(16)	1.376(5)	C(35)-C(36)	1.456(6)
C(16)-F(5)	1.333(4)	C(36)-C(37)	1.419(7)
C(17)-C(22)	1.367(5)	C(37)-C(38)	1.475(6)
C(17)-C(18)	1.371(5)	C(38)-N(1)	1.482(4)
C(18)-F(6)	1.360(4)	C(39)-C(40)	1.465(7)
C(18)-C(19)	1.379(6)	C(40)-C(41)	1.513(6)
C(19)-F(7)	1.349(5)	C(41)-C(42)	1.464(6)
C(19)-C(20)	1.350(6)	C(42)-N(2)	1.509(5)

C(43)-C(44)	1.481(6)	C(23)-C(7)-C(6)	115.5(2)
C(43)-N(2)	1.511(5)	O(6)-C(8)-O(7)	105.6(2)
C(44)-C(45)	1.477(6)	O(6)-C(8)-C(10)	110.3(3)
C(45)-C(47)	1.484(6)	O(7)-C(8)-C(10)	109.6(3)
C(46)-C(48)	1.470(6)	O(6)-C(8)-C(9)	109.8(3)
C(46)-N(2)	1.526(5)	O(7)-C(8)-C(9)	109.0(3)
C(48)-C(49)	1.480(6)	C(10)-C(8)-C(9)	112.3(3)
C(49)-C(52)	1.432(7)	C(12)-C(11)-C(16)	114.7(3)
C(50)-C(51)	1.476(5)	C(12)-C(11)-C(4)	117.0(3)
C(50)-N(2)	1.532(5)	C(16)-C(11)-C(4)	128.2(3)
C(51)-C(53)	1.458(6)	F(1)-C(12)-C(13)	116.1(4)
C(53)-C(54)	1.423(6)	F(1)-C(12)-C(11)	120.7(3)
Co(1)-P(1)	2.1254(8)	C(13)-C(12)-C(11)	123.2(4)
N(1)-P(1)	1.644(3)	F(2)-C(13)-C(14)	120.7(4)
O(4)-P(1)	1.663(2)	F(2)-C(13)-C(12)	119.4(4)
O(5)-P(1)	1.676(2)	C(14)-C(13)-C(12)	119.9(4)
O(1)-C(1)-Co(1)	179.6(4)	F(3)-C(14)-C(15)	120.5(4)
O(2)-C(2)-Co(1)	178.9(4)	F(3)-C(14)-C(13)	120.2(4)
O(3)-C(3)-Co(1)	175.0(3)	C(15)-C(14)-C(13)	119.2(4)
O(5)-C(4)-C(5)	108.3(2)	F(4)-C(15)-C(14)	120.5(4)
O(5)-C(4)-C(11)	107.0(2)	F(4)-C(15)-C(16)	118.6(4)
C(5)-C(4)-C(11)	121.0(3)	C(14)-C(15)-C(16)	120.9(4)
O(5)-C(4)-C(17)	105.7(2)	F(5)-C(16)-C(15)	115.6(3)
C(5)-C(4)-C(17)	105.9(2)	F(5)-C(16)-C(11)	122.3(3)
C(11)-C(4)-C(17)	108.1(3)	C(15)-C(16)-C(11)	122.1(4)
O(6)-C(5)-C(4)	109.3(2)	C(22)-C(17)-C(18)	113.6(3)
O(6)-C(5)-C(6)	103.7(2)	C(22)-C(17)-C(4)	123.1(3)
C(4)-C(5)-C(6)	119.7(2)	C(18)-C(17)-C(4)	123.3(3)
O(7)-C(6)-C(5)	103.4(2)	F(6)-C(18)-C(17)	120.2(3)
O(7)-C(6)-C(7)	113.4(3)	F(6)-C(18)-C(19)	116.3(4)
C(5)-C(6)-C(7)	112.7(2)	C(17)-C(18)-C(19)	123.5(4)
O(4)-C(7)-C(29)	108.7(2)	F(7)-C(19)-C(20)	122.1(4)
O(4)-C(7)-C(23)	106.5(2)	F(7)-C(19)-C(18)	118.6(5)
C(29)-C(7)-C(23)	108.6(3)	C(20)-C(19)-C(18)	119.3(4)
O(4)-C(7)-C(6)	107.1(2)	C(21)-C(20)-F(8)	120.8(5)
C(29)-C(7)-C(6)	110.2(2)	C(21)-C(20)-C(19)	119.8(4)

F(8)-C(20)-C(19)	119.4(5)	C(31)-C(32)-C(33)	119.4(4)
C(20)-C(21)-F(9)	119.5(4)	F(19)-C(33)-C(34)	120.8(4)
C(20)-C(21)-C(22)	119.9(4)	F(19)-C(33)-C(32)	119.8(4)
F(9)-C(21)-C(22)	120.6(4)	C(34)-C(33)-C(32)	119.4(4)
F(10)-C(22)-C(17)	122.4(3)	F(20)-C(34)-C(33)	116.1(3)
F(10)-C(22)-C(21)	113.9(4)	F(20)-C(34)-C(29)	120.3(3)
C(17)-C(22)-C(21)	123.7(4)	C(33)-C(34)-C(29)	123.6(4)
C(24)-C(23)-C(28)	114.4(3)	N(1)-C(35)-C(36)	107.1(4)
C(24)-C(23)-C(7)	128.1(3)	C(37)-C(36)-C(35)	108.6(4)
C(28)-C(23)-C(7)	117.5(3)	C(36)-C(37)-C(38)	110.3(4)
F(11)-C(24)-C(25)	116.2(3)	C(37)-C(38)-N(1)	104.3(3)
F(11)-C(24)-C(23)	120.5(3)	C(39)-C(40)-C(41)	113.0(5)
C(25)-C(24)-C(23)	123.2(3)	C(42)-C(41)-C(40)	113.7(4)
F(12)-C(25)-C(26)	119.8(3)	C(41)-C(42)-N(2)	119.2(4)
F(12)-C(25)-C(24)	120.2(4)	C(44)-C(43)-N(2)	115.9(4)
C(26)-C(25)-C(24)	120.1(3)	C(45)-C(44)-C(43)	116.2(4)
F(13)-C(26)-C(25)	120.6(4)	C(44)-C(45)-C(47)	115.5(5)
F(13)-C(26)-C(27)	119.3(4)	C(48)-C(46)-N(2)	118.4(4)
C(25)-C(26)-C(27)	120.1(3)	C(46)-C(48)-C(49)	114.8(4)
F(14)-C(27)-C(26)	120.9(3)	C(52)-C(49)-C(48)	120.8(6)
F(14)-C(27)-C(28)	120.8(3)	C(51)-C(50)-N(2)	117.9(3)
C(26)-C(27)-C(28)	118.3(3)	C(53)-C(51)-C(50)	115.0(4)
F(15)-C(28)-C(27)	115.7(3)	C(54)-C(53)-C(51)	120.4(5)
F(15)-C(28)-C(23)	120.3(3)	C(1)-Co(1)-C(3)	108.34(18)
C(27)-C(28)-C(23)	124.0(3)	C(1)-Co(1)-C(2)	113.38(17)
C(30)-C(29)-C(34)	114.5(3)	C(3)-Co(1)-C(2)	108.66(18)
C(30)-C(29)-C(7)	125.8(3)	C(1)-Co(1)-P(1)	104.31(12)
C(34)-C(29)-C(7)	119.8(3)	C(3)-Co(1)-P(1)	120.39(11)
F(16)-C(30)-C(31)	115.2(3)	C(2)-Co(1)-P(1)	101.83(11)
F(16)-C(30)-C(29)	122.0(3)	C(35)-N(1)-C(38)	109.6(3)
C(31)-C(30)-C(29)	122.8(3)	C(35)-N(1)-P(1)	121.9(2)
F(17)-C(31)-C(32)	119.9(3)	C(38)-N(1)-P(1)	124.7(2)
F(17)-C(31)-C(30)	119.8(4)	C(42)-N(2)-C(43)	110.8(3)
C(32)-C(31)-C(30)	120.3(4)	C(42)-N(2)-C(46)	108.6(3)
F(18)-C(32)-C(31)	120.5(4)	C(43)-N(2)-C(46)	111.2(3)
F(18)-C(32)-C(33)	120.1(4)	C(42)-N(2)-C(50)	110.3(3)

C(43)-N(2)-C(50)	108.3(3)	N(1)-P(1)-Co(1)	115.64(10)
C(46)-N(2)-C(50)	107.6(3)	O(4)-P(1)-Co(1)	124.99(8)
C(7)-O(4)-P(1)	125.24(17)	O(5)-P(1)-Co(1)	121.56(8)
C(4)-O(5)-P(1)	124.50(18)		
C(5)-O(6)-C(8)	107.5(2)		
C(6)-O(7)-C(8)	110.4(2)		
N(1)-P(1)-O(4)	95.44(12)		
N(1)-P(1)-O(5)	97.57(12)		
O(4)-P(1)-O(5)	95.50(10)		

Symmetry transformations used to generate equivalent atoms:

Table A.5.19. Anisotropic displacement parameters ($Å^2 x\ 10^3$)for $Co(CO)_3$n-Bu_4N·CKphos. The anisotropic displacement factor exponent takes the form: $-2p^2[\ h^2a^{*2}U^{11} + ... + 2\ h\ k\ a^*\ b^*\ U^{12}\ ]$

	U^{11}	U^{22}	U^{33}	U^{23}	U^{13}	U^{12}
C(1)	68(3)	58(2)	62(2)	-12(2)	11(2)	4(2)
C(2)	62(2)	60(2)	58(3)	-12(2)	2(2)	12(2)
C(3)	66(3)	56(2)	68(3)	-13(2)	-1(2)	-2(2)
C(4)	43(2)	47(2)	45(2)	-1(2)	0(2)	7(2)
C(5)	51(2)	47(2)	36(2)	-1(1)	5(2)	6(2)
C(6)	36(2)	48(2)	50(2)	-4(2)	8(2)	10(1)
C(7)	35(2)	48(2)	46(2)	0(2)	2(2)	5(1)
C(8)	54(2)	73(2)	54(2)	3(2)	12(2)	18(2)
C(9)	83(3)	91(3)	80(3)	12(2)	33(2)	15(2)
C(10)	87(3)	78(3)	65(3)	-12(2)	15(2)	29(2)
C(11)	54(2)	50(2)	43(2)	3(2)	5(2)	7(2)
C(12)	63(3)	50(2)	69(3)	2(2)	9(2)	9(2)
C(13)	89(3)	56(3)	95(3)	3(2)	25(3)	29(2)
C(14)	100(4)	36(2)	119(4)	1(2)	23(3)	9(2)
C(15)	84(3)	52(2)	79(3)	4(2)	12(2)	-12(2)
C(16)	62(2)	53(2)	53(2)	5(2)	8(2)	8(2)
C(17)	55(2)	51(2)	47(2)	1(2)	-2(2)	14(2)
C(18)	78(3)	69(3)	65(3)	6(2)	-6(2)	6(2)
C(19)	117(4)	106(4)	55(3)	18(3)	-26(3)	15(3)
C(20)	96(4)	106(4)	68(3)	-14(3)	-42(3)	20(3)
C(21)	72(3)	74(3)	76(3)	-11(2)	-17(2)	7(2)
C(22)	69(3)	61(2)	52(2)	-1(2)	-15(2)	7(2)
C(23)	38(2)	47(2)	44(2)	2(2)	0(2)	5(1)
C(24)	45(2)	58(2)	57(2)	5(2)	-3(2)	1(2)
C(25)	46(2)	64(2)	67(3)	-3(2)	-14(2)	-4(2)
C(26)	63(3)	73(3)	56(2)	-11(2)	-23(2)	16(2)
C(27)	59(2)	64(2)	52(2)	5(2)	-4(2)	16(2)
C(28)	43(2)	50(2)	58(2)	-1(2)	-2(2)	5(2)
C(29)	48(2)	47(2)	48(2)	2(2)	-1(2)	10(2)
C(30)	55(2)	49(2)	50(2)	5(2)	0(2)	13(2)

C(31)	82(3)	43(2)	69(3)	2(2)	-9(2)	9(2)
C(32)	109(4)	53(2)	83(3)	-10(2)	-3(3)	35(3)
C(33)	75(3)	74(3)	87(3)	-1(2)	5(2)	35(2)
C(34)	55(2)	63(2)	57(2)	0(2)	-4(2)	16(2)
C(35)	72(3)	81(3)	112(4)	-7(3)	41(3)	2(2)
C(36)	67(4)	135(5)	222(7)	-19(5)	54(4)	-13(3)
C(37)	58(3)	87(4)	277(8)	-33(4)	47(4)	-17(3)
C(38)	54(2)	60(2)	80(3)	5(2)	9(2)	-15(2)
C(39)	139(5)	150(5)	191(7)	-44(5)	-56(5)	88(5)
C(40)	73(3)	81(3)	117(4)	-20(3)	9(3)	13(2)
C(41)	58(3)	86(3)	118(4)	1(3)	-4(3)	10(2)
C(42)	62(3)	78(3)	91(3)	4(2)	17(2)	8(2)
C(43)	74(3)	89(3)	88(3)	-7(3)	-3(3)	13(2)
C(44)	95(4)	108(4)	91(3)	18(3)	-3(3)	0(3)
C(45)	110(4)	110(4)	113(4)	15(3)	-25(3)	17(3)
C(46)	82(3)	87(3)	84(3)	-18(2)	1(2)	15(2)
C(47)	136(5)	132(5)	110(4)	40(4)	-5(4)	30(4)
C(48)	105(4)	83(3)	117(4)	-23(3)	-4(3)	25(3)
C(49)	155(6)	103(4)	179(6)	-60(4)	50(5)	14(4)
C(50)	64(3)	87(3)	96(3)	-5(3)	16(2)	11(2)
C(51)	86(3)	79(3)	104(4)	-3(3)	20(3)	1(3)
C(52)	209(8)	152(6)	250(9)	-96(6)	23(7)	44(6)
C(53)	130(5)	66(3)	193(6)	3(3)	61(4)	-18(3)
C(54)	161(6)	103(5)	197(7)	7(4)	72(5)	-6(4)
Co(1)	52(1)	48(1)	50(1)	-10(1)	2(1)	0(1)
F(1)	50(1)	70(1)	114(2)	4(1)	7(1)	19(1)
F(2)	105(2)	72(2)	173(3)	7(2)	30(2)	45(2)
F(3)	148(3)	42(1)	196(3)	1(2)	30(2)	8(2)
F(4)	94(2)	61(1)	139(2)	4(1)	16(2)	-21(1)
F(5)	53(1)	61(1)	87(2)	4(1)	18(1)	2(1)
F(6)	121(2)	101(2)	63(2)	24(1)	-5(1)	-11(2)
F(7)	214(4)	154(3)	74(2)	40(2)	-42(2)	3(3)
F(8)	143(3)	154(3)	98(2)	-9(2)	-64(2)	23(2)
F(9)	95(2)	116(2)	111(2)	-18(2)	-36(2)	-22(2)
F(10)	110(2)	80(2)	81(2)	8(1)	-31(1)	-29(1)
F(11)	53(1)	81(1)	75(2)	16(1)	-3(1)	-17(1)

F(12)	73(2)	98(2)	104(2)	3(1)	-33(1)	-27(1)
F(13)	103(2)	102(2)	69(2)	-7(1)	-41(1)	9(1)
F(14)	85(2)	98(2)	57(1)	21(1)	-4(1)	14(1)
F(15)	60(1)	67(1)	62(1)	18(1)	-5(1)	-9(1)
F(16)	57(1)	55(1)	78(1)	-11(1)	-5(1)	-2(1)
F(17)	111(2)	46(1)	105(2)	-10(1)	-13(2)	0(1)
F(18)	145(3)	66(2)	147(2)	-26(2)	-1(2)	47(2)
F(19)	85(2)	101(2)	145(2)	-17(2)	6(2)	53(2)
F(20)	47(1)	79(1)	90(2)	-8(1)	0(1)	18(1)
N(1)	43(2)	55(2)	55(2)	-7(1)	16(1)	-2(1)
N(2)	47(2)	65(2)	65(2)	-3(2)	6(2)	3(2)
O(1)	88(2)	80(2)	127(3)	-5(2)	14(2)	32(2)
O(2)	122(3)	100(2)	57(2)	6(2)	2(2)	38(2)
O(3)	80(2)	89(2)	131(3)	-6(2)	21(2)	-32(2)
O(4)	34(1)	40(1)	48(1)	-2(1)	4(1)	3(1)
O(5)	37(1)	50(1)	43(1)	-1(1)	1(1)	4(1)
O(6)	60(2)	69(2)	42(1)	4(1)	10(1)	19(1)
O(7)	45(1)	69(2)	53(2)	2(1)	11(1)	12(1)
P(1)	38(1)	45(1)	43(1)	-3(1)	4(1)	1(1)

Table A.5.20. Hydrogen coordinates (x 10^4) and isotropic displacement parameters ($Å^2$x 10^3) for $Co(CO)_3$n-Bu_4N·CKphos.

	x	y	z	U(eq)
H(5)	2065	614	1656	54
H(6)	3401	1925	2555	53
H(9A)	4361	1712	-16	126
H(9B)	5222	1482	540	126
H(9C)	4650	2314	779	126
H(10A)	3192	-255	922	113
H(10B)	4336	-136	712	113
H(10C)	3536	62	85	113
H(35A)	-213	2071	4128	107
H(35B)	124	1611	4883	107

H(36A)	-1285	776	4863	174
H(36B)	-1617	1228	4104	174
H(37A)	-1476	47	3396	174
H(37B)	-1177	-414	4160	174
H(38A)	30	41	2972	80
H(38B)	346	-370	3762	80
H(39A)	5069	6827	3177	235
H(39B)	4253	6817	3843	235
H(39C)	4203	6013	3179	235
H(40A)	4836	5515	4277	109
H(40B)	5601	6401	4422	109
H(41A)	5714	5050	3168	105
H(41B)	6441	5964	3242	105
H(42A)	6332	4675	4359	93
H(42B)	7063	5581	4423	93
H(43A)	8837	4155	3998	101
H(43B)	8564	4962	4571	101
H(44A)	7308	3982	5114	119
H(44B)	7629	3179	4561	119
H(45A)	8783	4122	5812	132
H(45B)	9184	3386	5227	132
H(46A)	6629	3412	3551	102
H(46B)	6616	3941	2783	102
H(47A)	7675	3061	6342	185
H(47B)	8729	2712	6346	185
H(47C)	7919	2311	5693	185
H(48A)	8165	2979	3182	122
H(48B)	8103	3475	2396	122
H(49A)	6825	1961	2791	179
H(49B)	6643	2487	2046	179
H(50A)	8669	4900	2853	100
H(50B)	7676	5267	2619	100
H(51A)	8038	6449	3611	109
H(51B)	9069	6099	3763	109
H(52A)	7895	1965	1411	311
H(52B)	7257	1137	1769	311

H(52C)	8274	1573	2183	311
H(53A)	9620	6446	2570	159
H(53B)	8558	6629	2292	159
H(54A)	8711	7951	2957	233
H(54B)	9719	7889	2500	233
H(54C)	9670	7754	3418	233

A.5.4 Synthesis of Rh(cod)Cl•Phosphoramidite Complexes

To an oven-dried 3 ml vial flushed with argon was added rhodium(cod)chloride dimer (1 equiv.) and phosphoramidite ligand (2 equiv.). Solids were dissolved in $CDCl_3$ and stirred until homogenous under argon. Spectra were collected promptly after the solution was made. Complex in solution slowly decomposed over time (hours) when exposed to air.

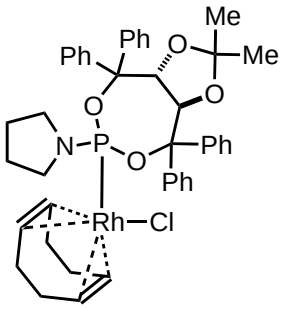

Rh(cod)Cl•T1 Complex

General procedure yielded a yellow solution. ^{1}H-NMR (400 MHz; $CDCl_3$): δ 7.96 (2H, d, *J* = 7.3 Hz) 7.51 (2H, t, *J* = 7.6 Hz) 7.42 (3H, m) 7.31 (2H, t, 7.6 Hz) 7.22 (3H, m) 7.13 (6H, m) 7.00 (2H, dt, *J* = 2.4, 5.0 Hz) 5.42 (1H, d, *J* = 8.0 Hz) 5.38 (1H, dd, *J* = 4.0, 7.5 Hz) 5.19 (1H, d, *J* = 8.0 Hz) 5.04 (1H, m) 4.00 (1H, m) 3.46 (1H, t, *J* = 6.9 Hz) 3.36 (2H, bs) 3.03 (2H, t, *J* = 6.7 Hz) 2.27 (1H, m) 2.17 (1H, m) 1.87 (2H, dd, *J* = 5.7, 13.2 Hz) 1.80 (1H, t, *J* = 9.0 Hz) 1.68 (2H, t, *J* = 9.0 Hz) 1.50 (1H, m) 1.33 (2H, m) 1.17 (2H, m) 0.44 (3H, s) 0.38 (3H, s). ^{13}C-NMR (100 MHz; $CDCl_3$): δ 144.6, 143.6, 142.0, 141.7, 129.2, 128.5, 128.0, 127.01, 126.83, 115.0, 109.1, 106.3, 98.4, 86.9, 86.1, 80.7, 78.7, 68.3, 67.6, 48.4, 33.3, 32.4, 28.6, 26.8, 26.4, 25.6. ^{31}P-NMR (75 MHz; $CDCl_3$): δ 144.6, 143.6.

Rh(cod)Cl•CKphos Complex

General procedure yielded a yellow solution. ^{1}H-NMR (400 MHz; $CDCl_3$): δ 5.76 (1H, d, *J* = 7.6 Hz) 5.64 (1H, d, *J* = 7.6 Hz) 5.49 (1H, m) 4.79 (1H, m) 4.13 (1H, bs) 3.84 (1H, bs) 3.02 (2H, bs) 2.41 (2H, m) 2.28 (1H, m) 2.18 (1H, dd *J* = 5.7, 15 Hz) 2.09 (3H, q, *J* = 7.4 Hz) 1.97 (1H, dt, *J* = 6.1, 13.0 Hz) 1.86 (1H, dt, *J* = 7.0, 14.2 Hz) 1.68 (1H, q, *J* = 7.8 Hz) 1.49 (6H, bs) 0.80 (3H, s) 0.73 (3H, s). ^{13}C-NMR (100 MHz; $CDCl_3$): δ 146.1, 143.6, 142.3, 138.9, 136.4, 116.0, 115.2, 113.4, 112.7, 109.7, 85.2, 83.3, 79.1, 78.7, 71.7, 69.2, 49.6, 34.4, 32.0, 30.8, 27.7, 26.4, 26.1. ^{31}P-NMR (75 MHz; $CDCl_3$): δ 116.5 (1P, dd, *J* =

5, 243 Hz). ^{19}F-NMR (376 MHz; $CDCl_3$): δ ^{19}F-NMR (376 MHz; $CDCl_3$): δ -124.63 (dd, *J* = 24.9, 4.8 Hz, 1F), -129.52 (d, *J* = 23.0 Hz, 1F), -131.90 (d, *J* = 23.0 Hz, 1F), -134.13 (d, *J* = 22.2 Hz, 1F), -138.01 (d, *J* = 22.0 Hz, 1F), -139.33 (d, *J* = 18.1 Hz, 1F), -140.30--140.34 (m, 1F), -143.66 (d, *J* = 22.8 Hz, 1F), -151.43--151.63 (m, 3F), -152.39 (t, *J* = 21.7 Hz, 1F), -157.19 (td, *J* = 23.3, 6.7 Hz, 1F), -160.44 (td, *J* = 22.2, 5.2 Hz, 1F), -160.68 (td, *J* = 21.7, 5.2 Hz, 1F), -160.89 (td, *J* = 21.5, 5.2 Hz, 1F), -161.71 (dddd, *J* = 40.0, 21.8, 20.3, 6.8 Hz, 3F), -162.99 (td, *J* = 22.3, 5.2 Hz, 1F).

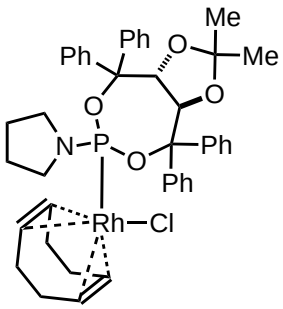

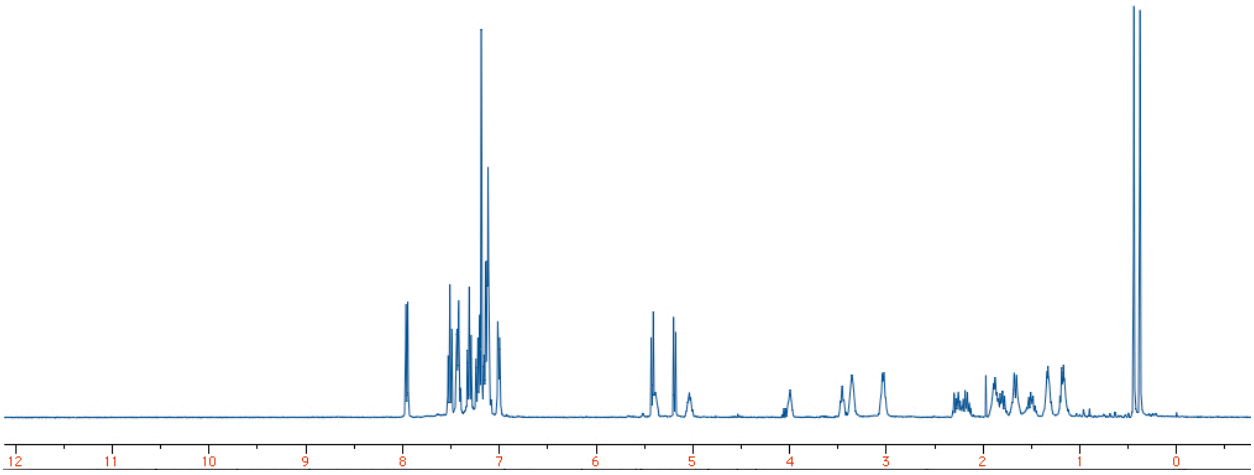

Figure A.5.1 ^{1}H-NMR Rh(cod)Cl•**T1**

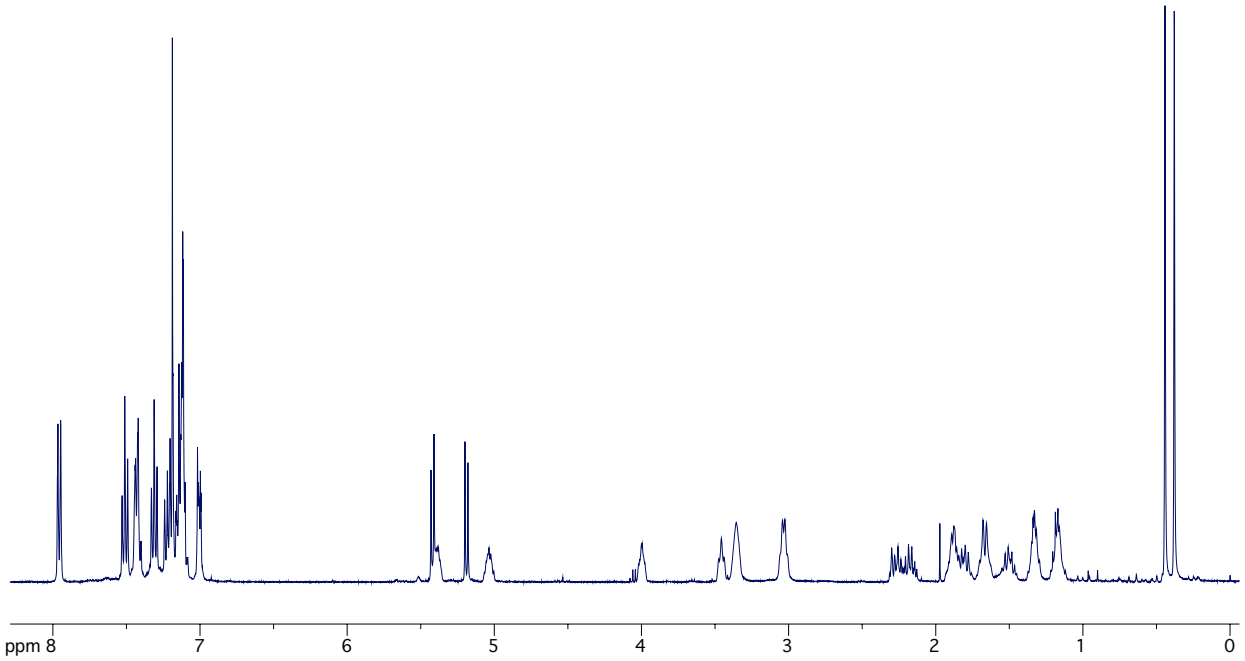

Figure A.5.2 ^{1}H-NMR Rh(cod)Cl•**T1**

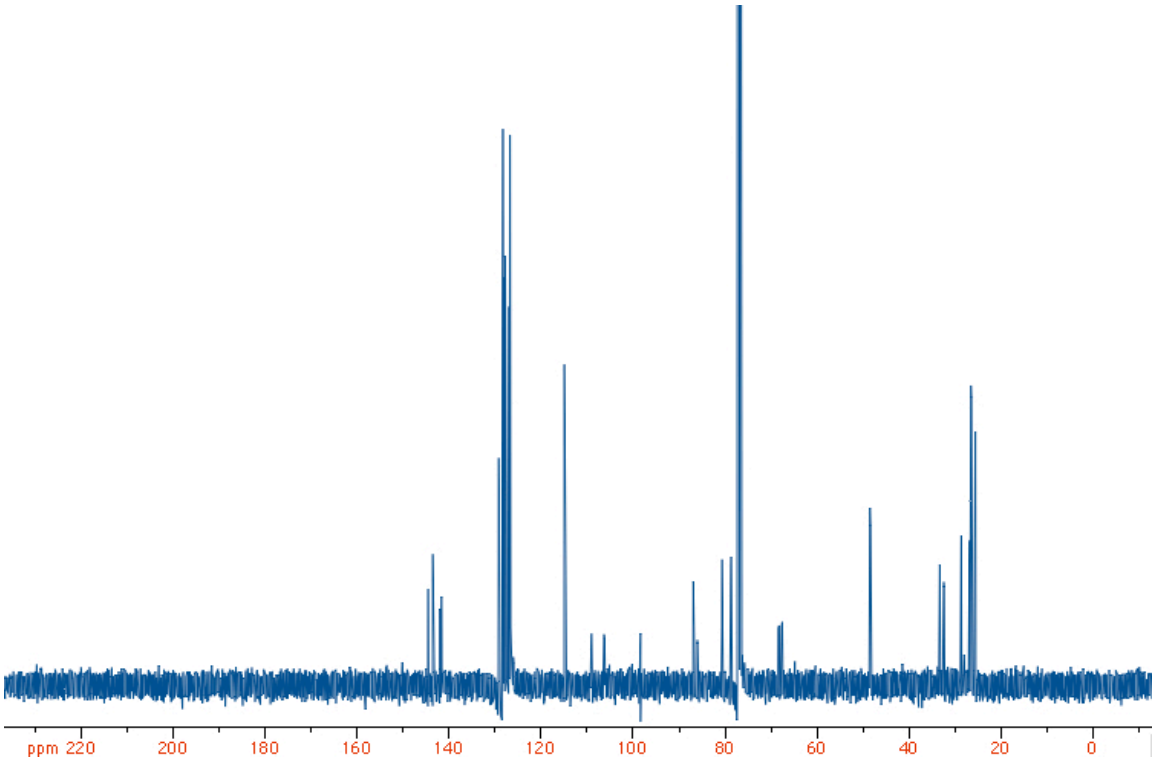

Figure A.5.3 ^{13}CNMR Rh(cod)Cl•**T1**

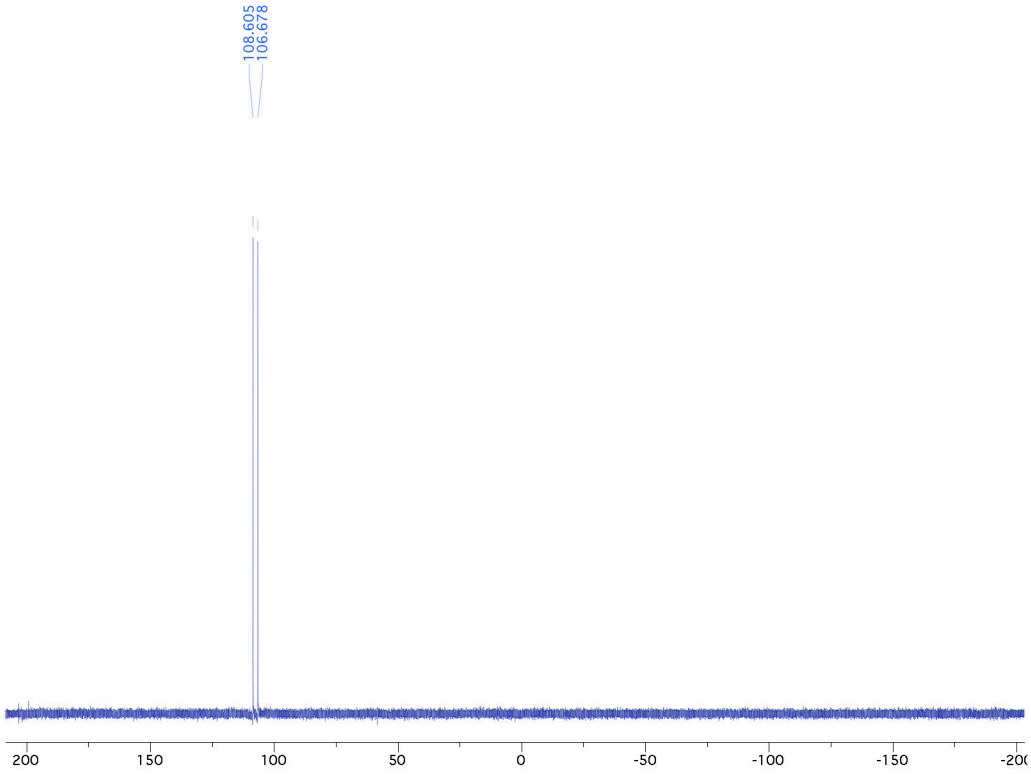

Figure A.5.4 ^{31}P-NMR Rh(cod)Cl•**T1**

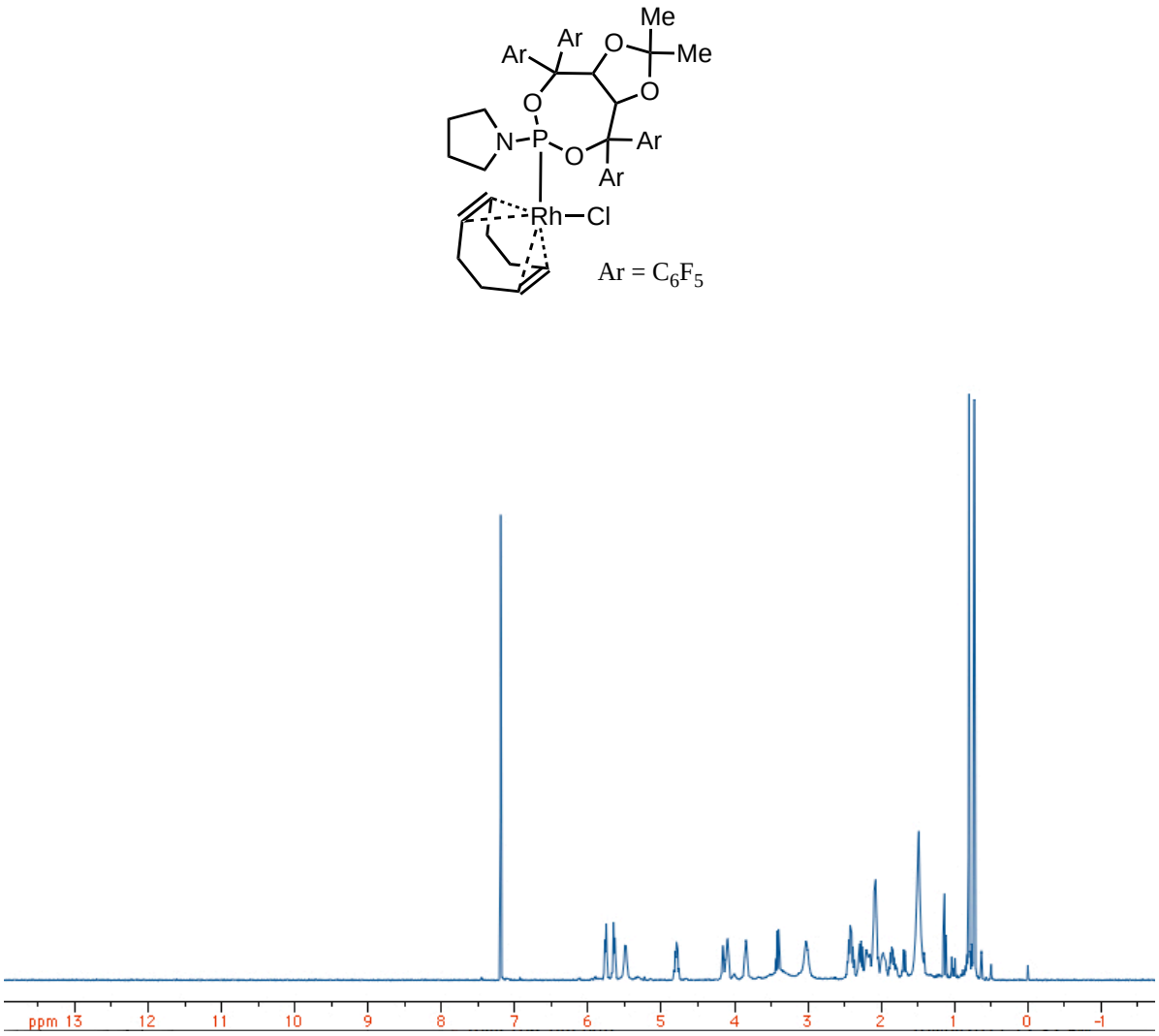

Figure A.5.5 [1]HNMR Rh(cod)Cl•CKphos

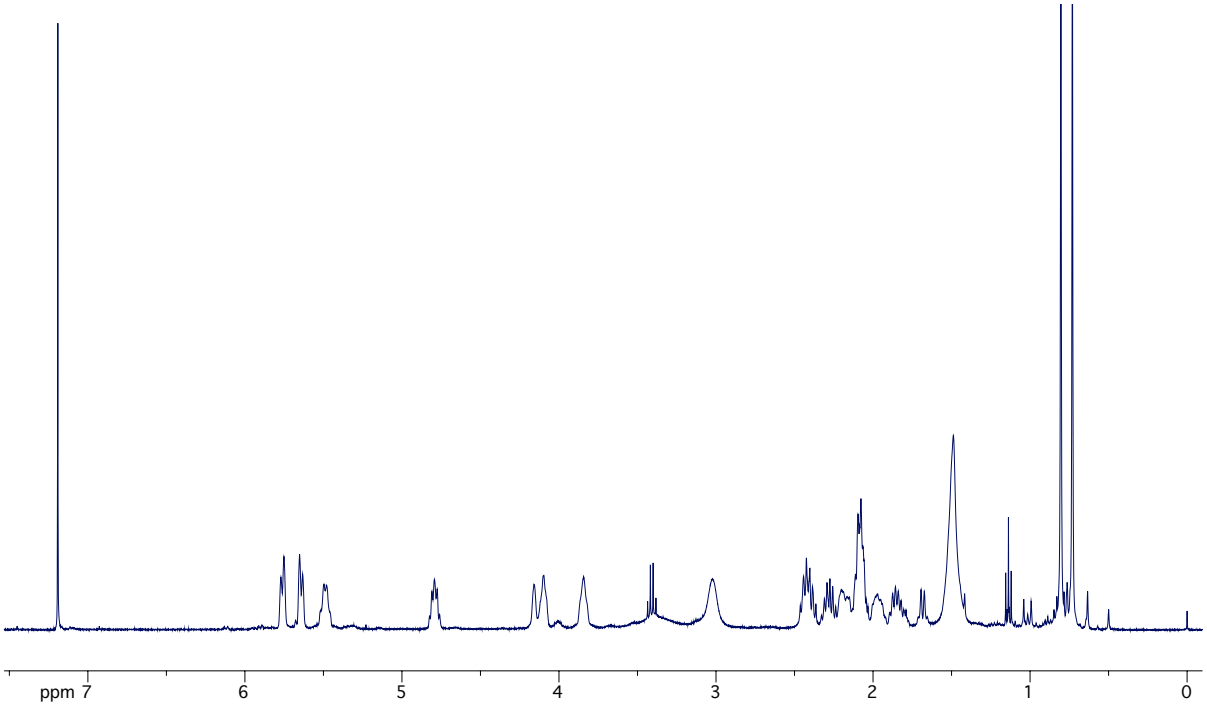

Figure A.5.6 [1]HNMR of Rh(cod)Cl•CKphos

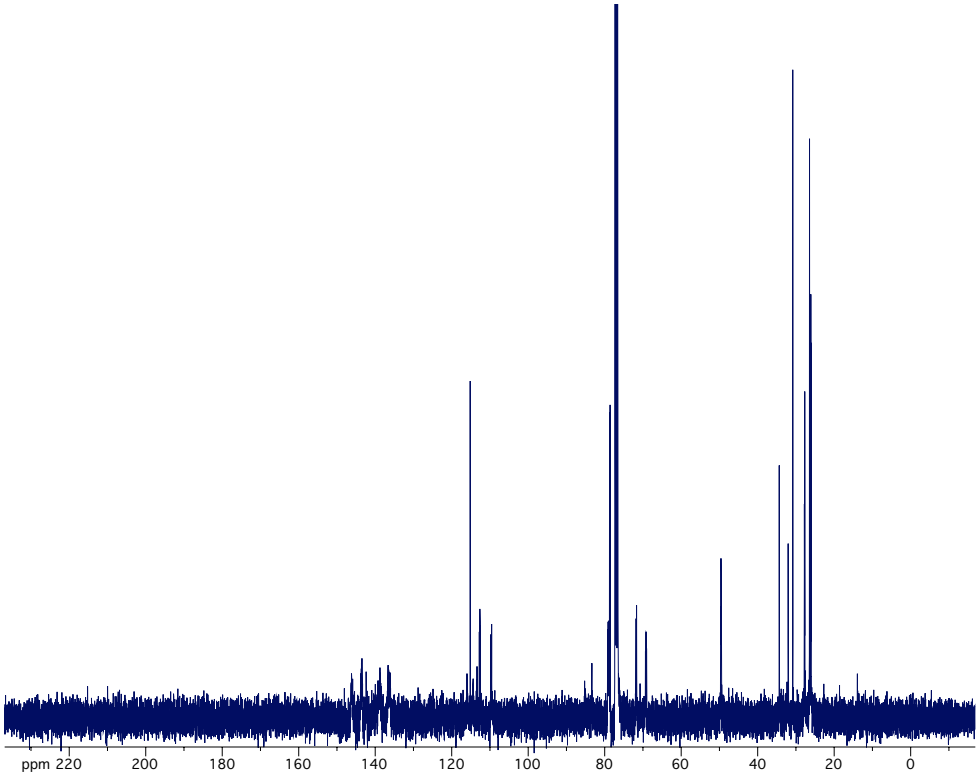

Figure A.5.7 [13]CNMR of Rh(cod)Cl•CKphos

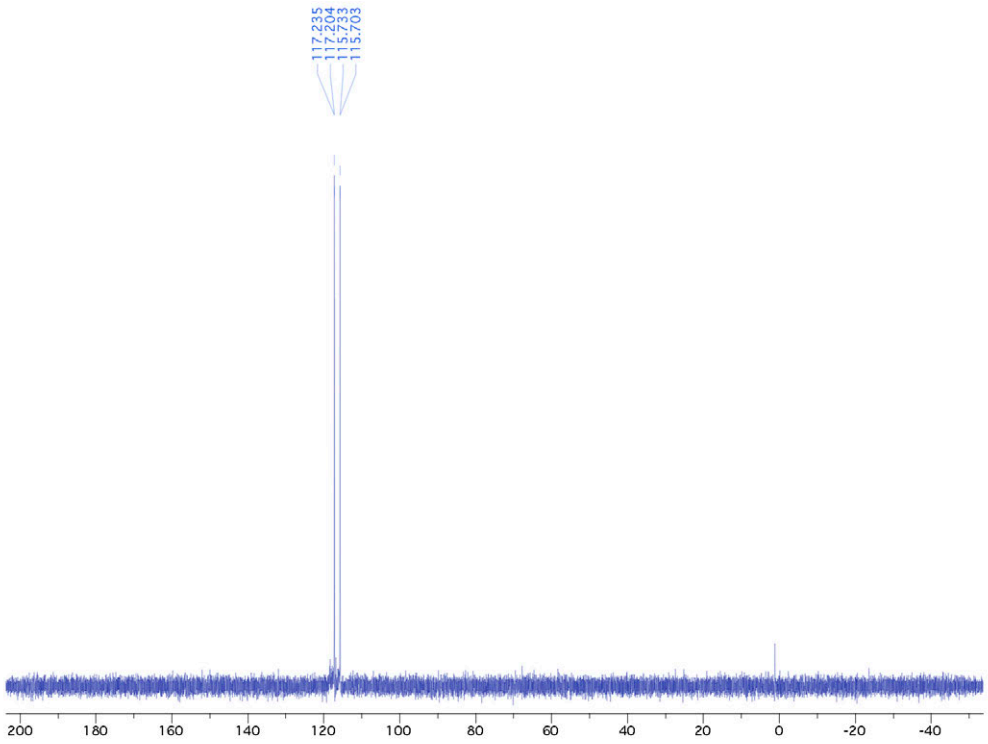

Figure A.5.8 ^{31}P-NMR Rh(cod)Cl•CKphos

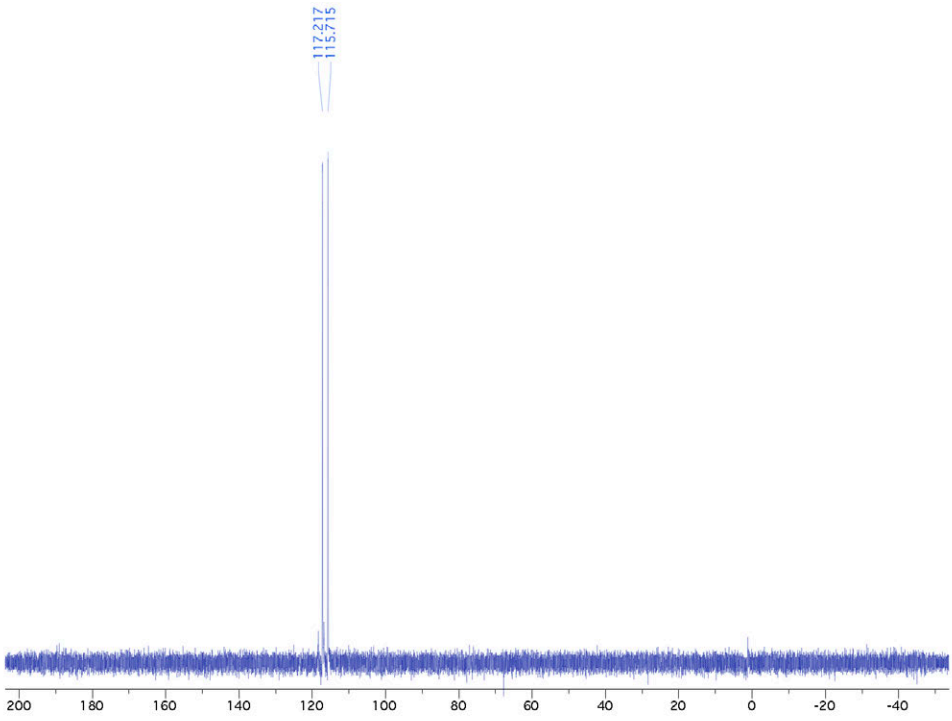

Figure A.5.9 ^{19}F-decoupled ^{31}P-NMR Rh(cod)Cl•CKphos

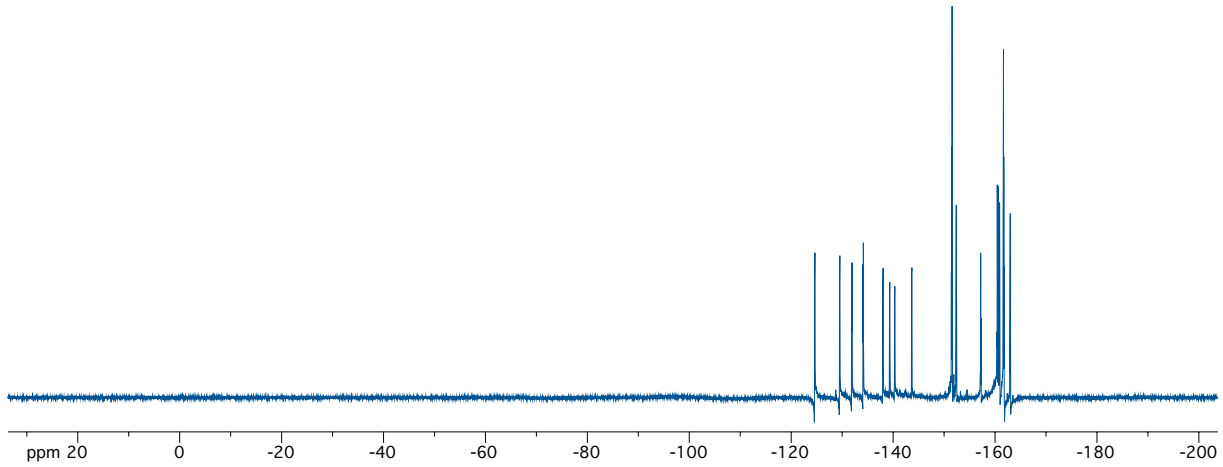

Figure A.5.10 ^{19}FNMR Rh(cod)Cl•CKphos

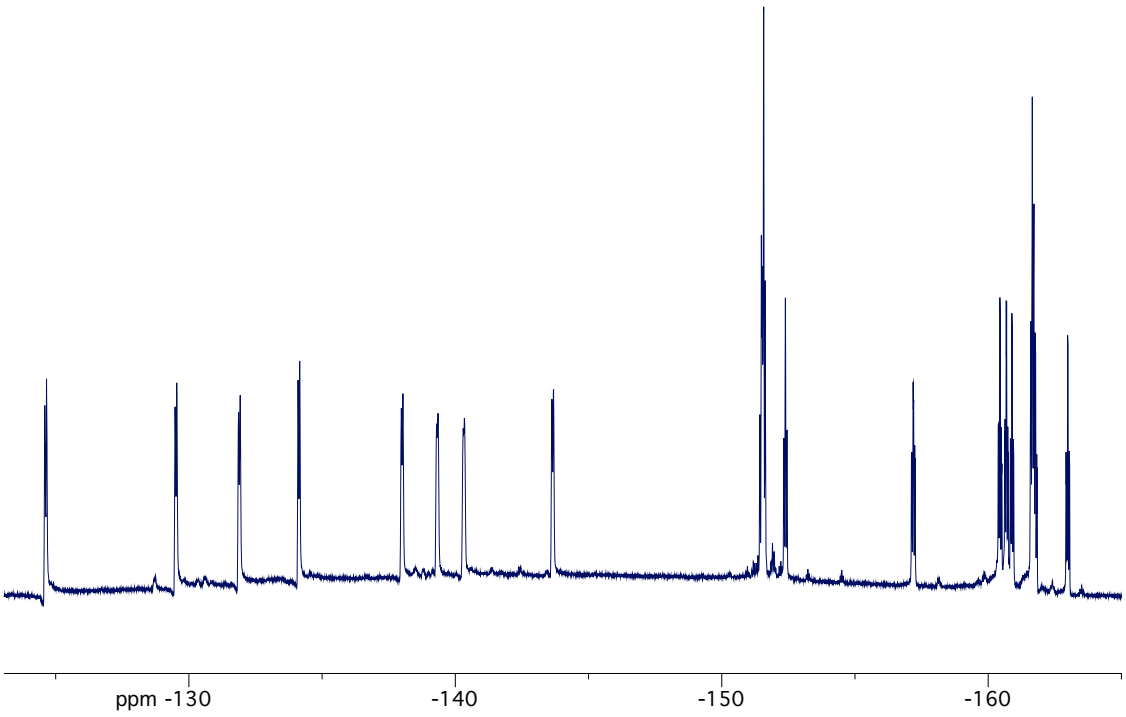

Figure A.5.11 ^{19}FNMR Rh(cod)Cl•CKphos

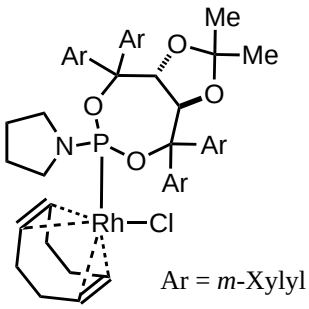

Ar = *m*-Xylyl

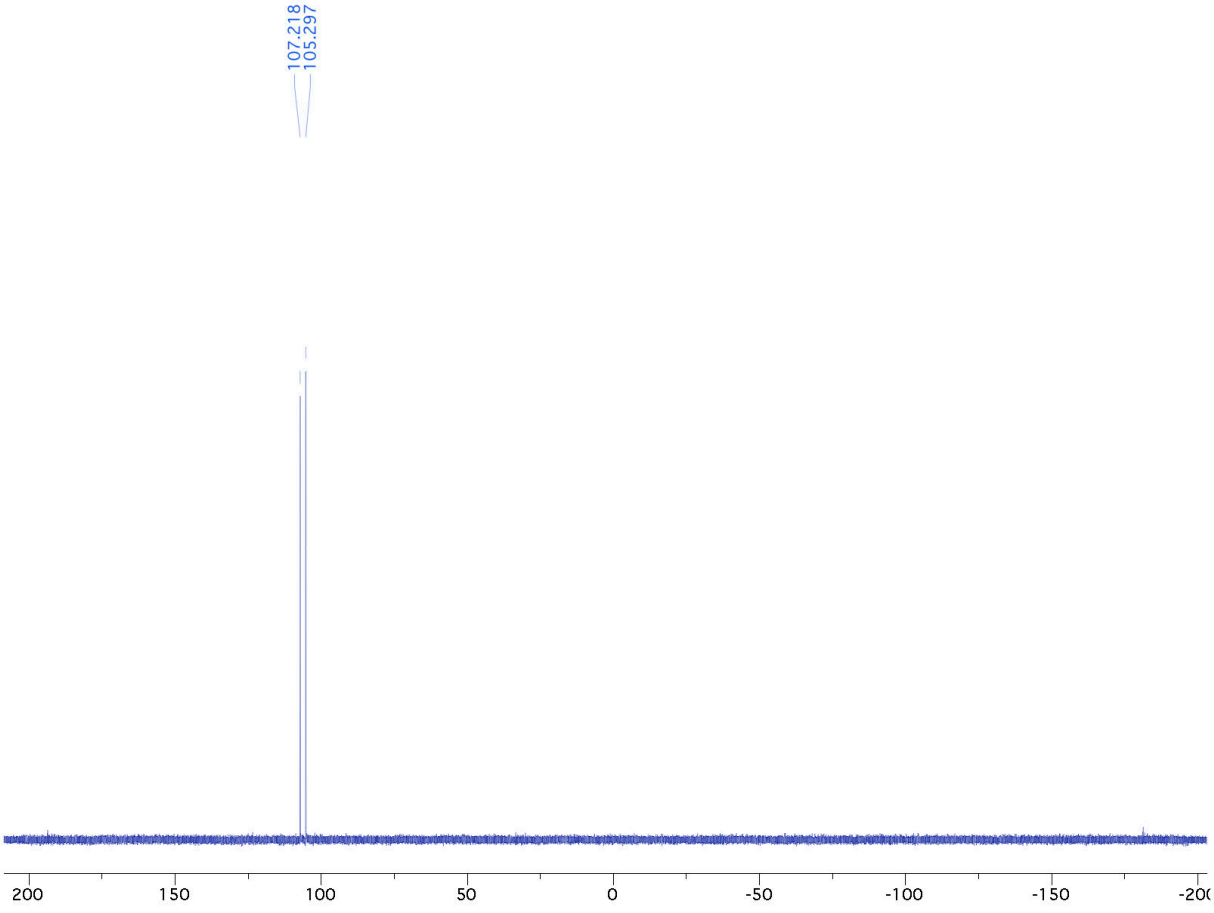

Figure A.5.12 ^{31}P-NMR Spectrum

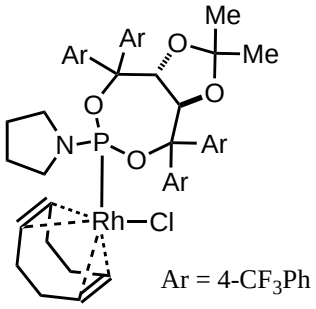

Ar = 4-CF_3Ph

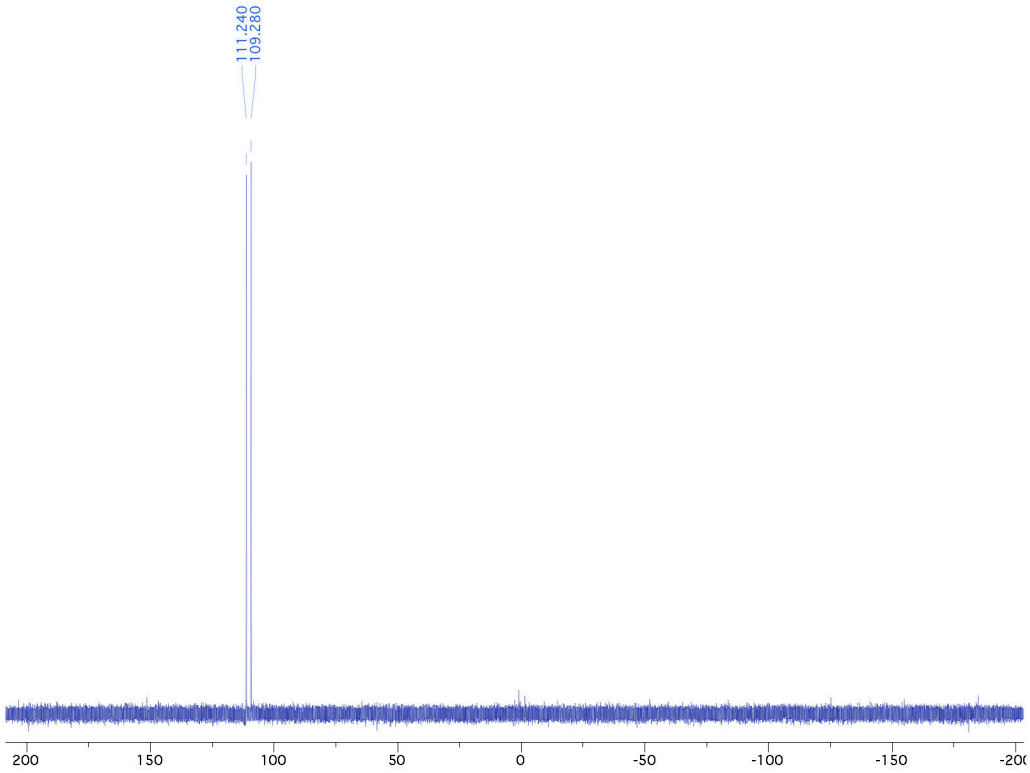

Figure A.5.13 ^{31}P-NMR Spectrum

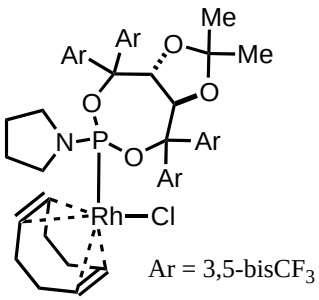

Ar = 3,5-bisCF_3

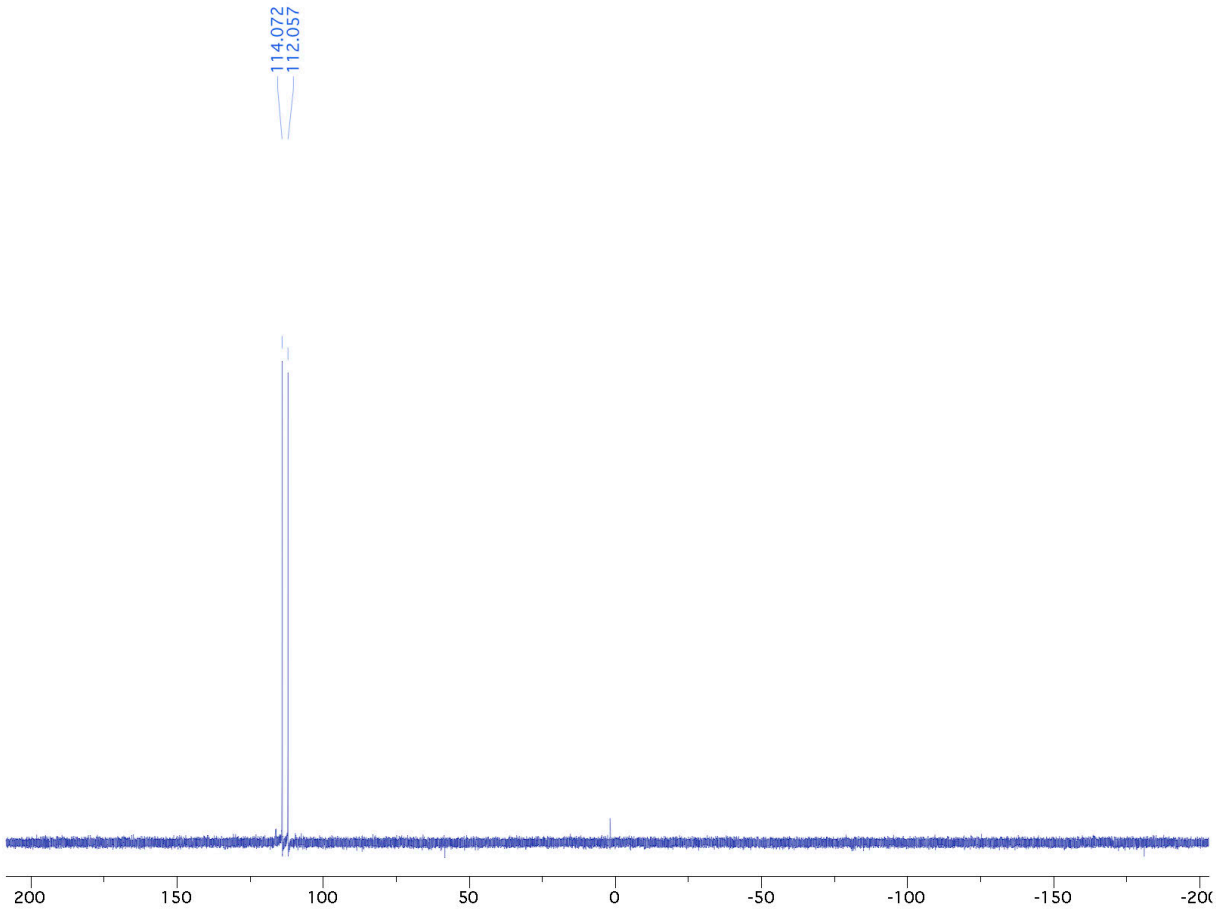

Figure A.5.14 ^{31}P-NMR Spectrum

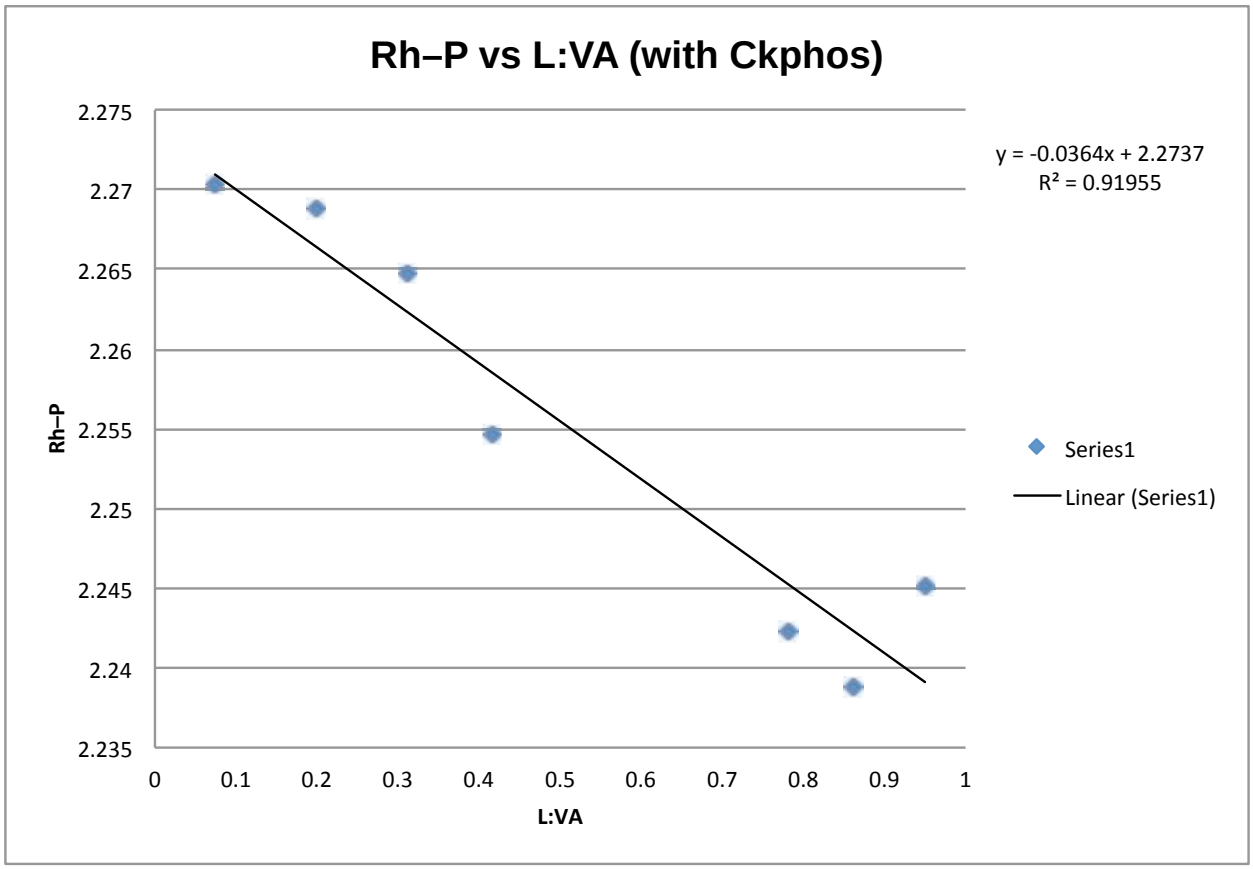

	L:VA	Rh–P (Å)
XylylTaddolpip	0.074	2.2703
XylylTaddolpyr	0.200	2.2688
PhTaddolNMe2	0.313	2.2648
PhTaddolpyr	0.417	2.2547
Guiphos	0.783	2.2423
tBuPhos	0.860	2.2388
CKphs	0.950	2.2451

Figure A.5.15 Graph of Rh–P versus product selectivity.

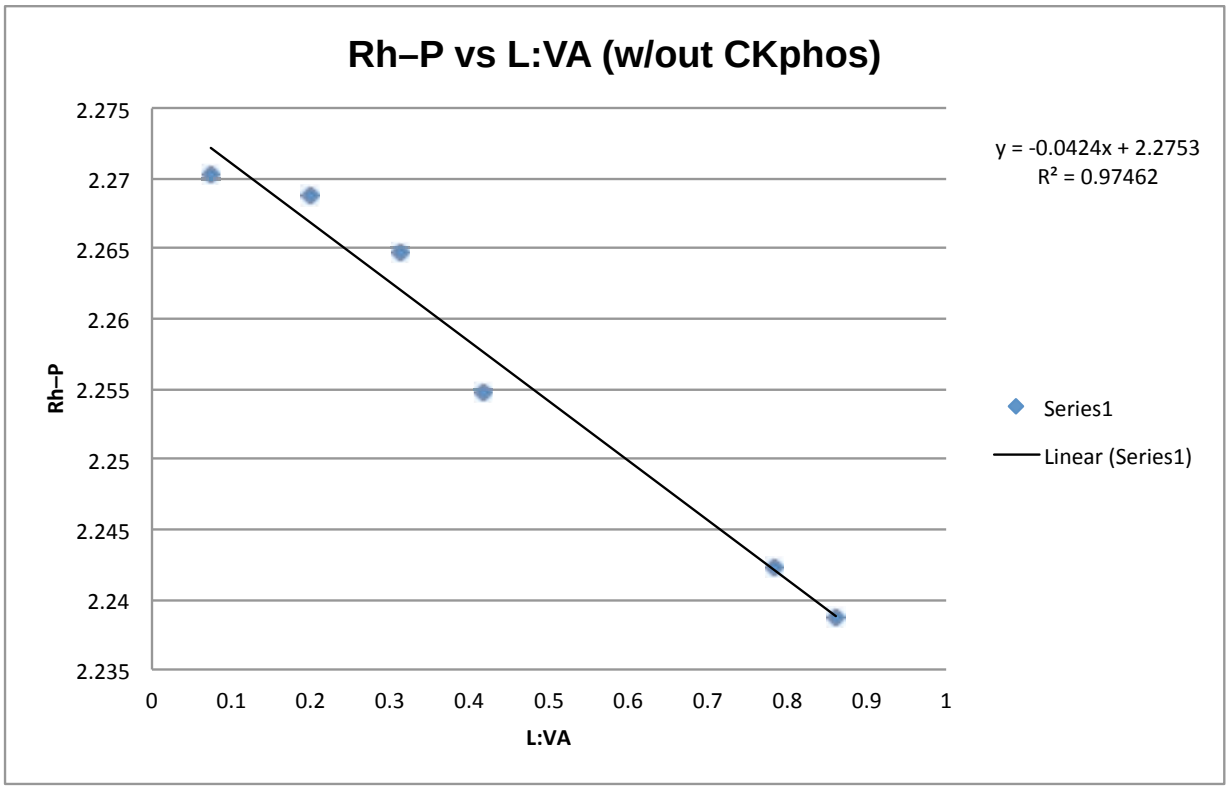

Figure A.5.16 Graph of Rh–P versus product selectivity with CKphos.

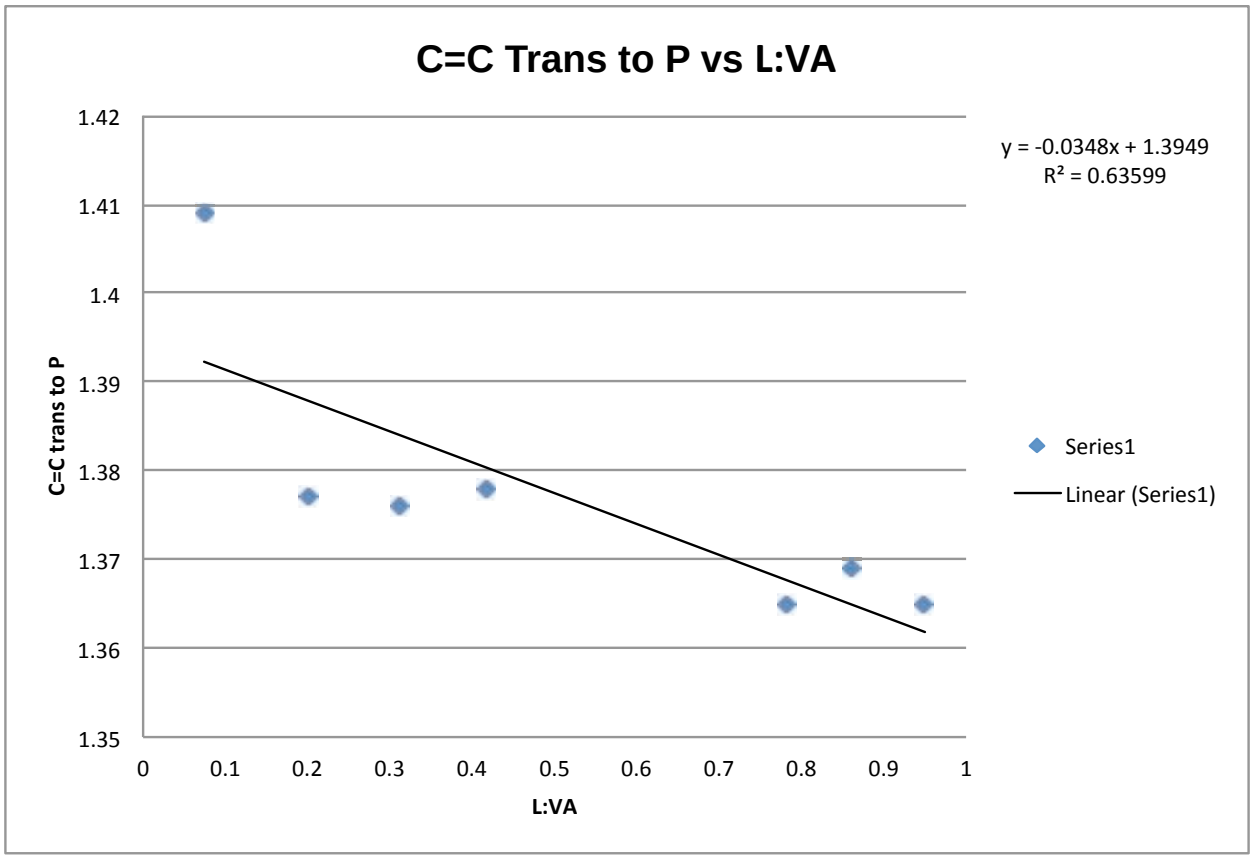

	L:VA	C=C trans to P (Å)
XylylTaddolpip	0.074	1.409
XylylTaddolpyr	0.200	1.377
PhTaddolNMe2	0.313	1.376
PhTaddolpyr	0.417	1.378
Guiphos	0.783	1.365
tBuPhos	0.861	1.369
CKphos	0.950	1.365

Figure A.5.17 Graph of C=C trans to phosphorus versus product selectivity.

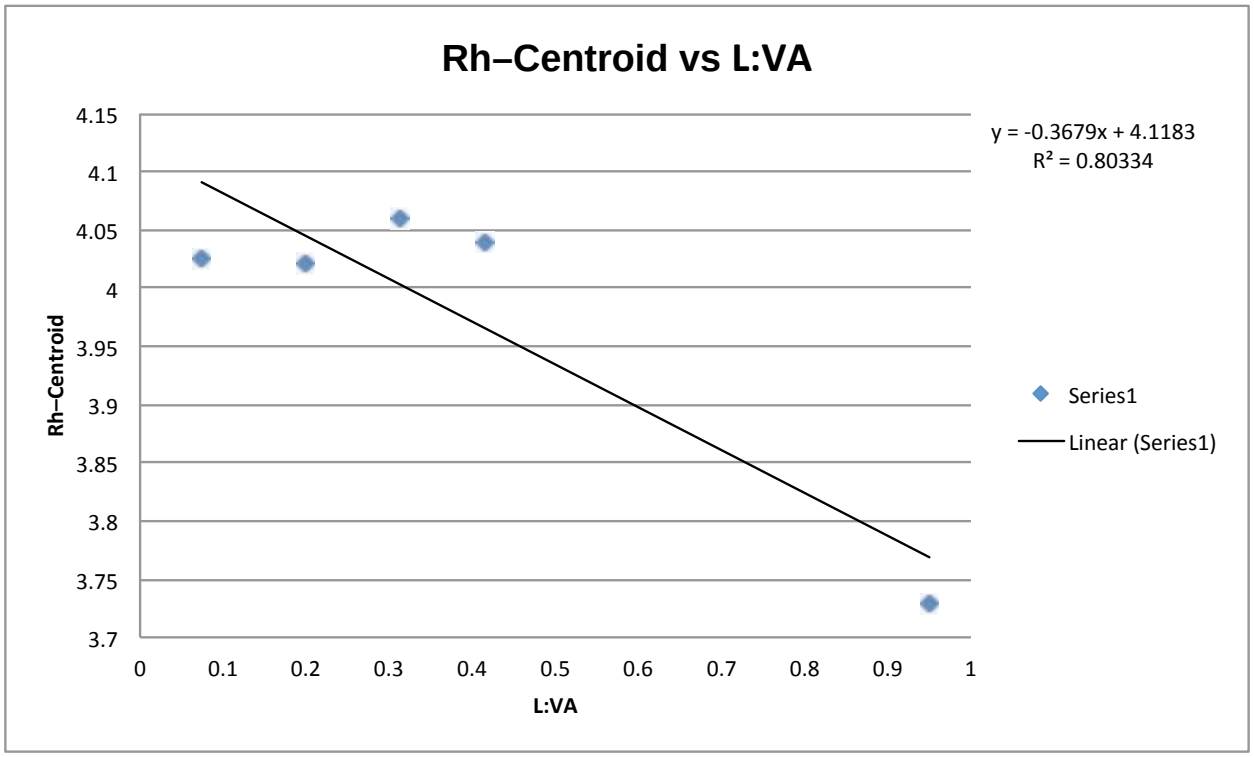

	L:VA	Rh–Centroid (Å)
XylylTaddolpip	0.074	4.025
XylylTaddolpyr	0.200	4.022
PhTaddolNMe2	0.313	4.059
PhTaddolpyr	0.417	4.039
CKphos	0.950	3.728

Figure A.5.18 Graph of Rh–Centroid versus product selectivity.

A.5.7 DFT Calculations on Rh(cod)Cl•Phosphoramidite Complexes

B3LYP hybrid[3] and B97D empirically corrected[4] density functional studies were carried out in the G09 suite of electronic structure codes.[5] Geometries were optimized for each complex starting from the X-ray coordinates for CK/Cl (starting guess C-H distances adjusted to 1.07 Å and 1.09Å for Csp^2-H and Csp^3-H distances, respectively). The LANL2 basis sets and effective core potentials were used for P and Cl, supplemented by double zeta d functions with exponents of 0.93,0.34 for P, and 1.5, 0.375 for Cl. A LANL08[6] basis set and effective core potentials was used for Rh, an f exponent of 1.35 was added as well. H, C, and N, and F were described with a 6-31g* model.[7]

---

[3] Becke, A. D. *J. Chem. Phys.* **1993**, *98*, 5648-5652

[4] Grimme, S. *J. Comp. Chem.* **2006**, 27, 1787-99

[5] Frisch, M. J.; et. al. *Gaussian 09, Revision A.1*, Gaussian, Inc.: Wallingford CT, 2009

[6] Hay, P. J.; Wadt, W. R. *J. Chem. Phys.* **1985**, *82*, 299-310. Roy, L. E.; Hay, P. J.; Martin, R. L. *J. Chem. Theory Comput.* **2008**, *4*, 1029–1031.

[7] (a) Binkley, J. S.; Pople, J. A.; Hehre, W. J. *J. Am. Chem. Soc.* **1980**, *102*, 939-947; (b) Ditchfield, R.; Hehre, W. J.; Pople, J. A. *J. Chem. Phys.* **1971**, *54*, 724-728; (c) Francl, M. M.; Pietro, W. J.; Hehre, W. J.; Binkley, J. S.; Gordon, M. S.; DeFrees, D. J.; Pople, J. A. *J. Chem. Phys.* **1982**, *77*, 3654-3665; (d) Hehre, W. J.; Ditchfield, R.; Pople, J. A. *J. Chem. Phys.* **1972**, *56*, 2257-2261.

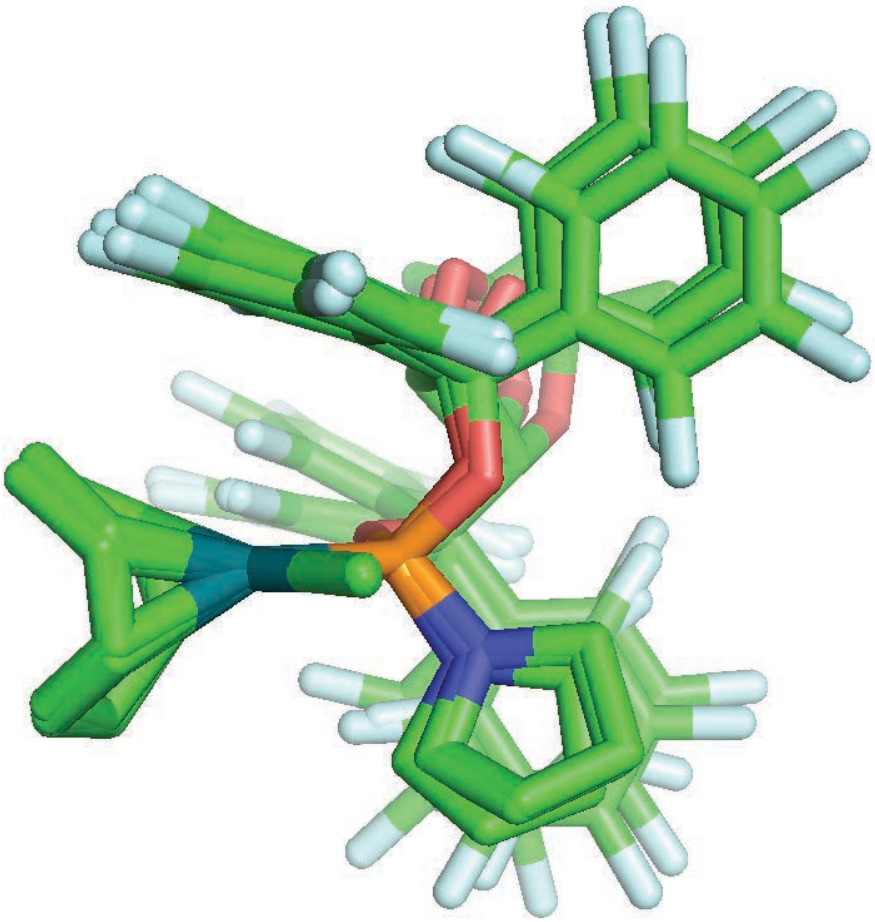

Figure A.5.19 Overlay of Rh(cod)Cl/CKphos structures.

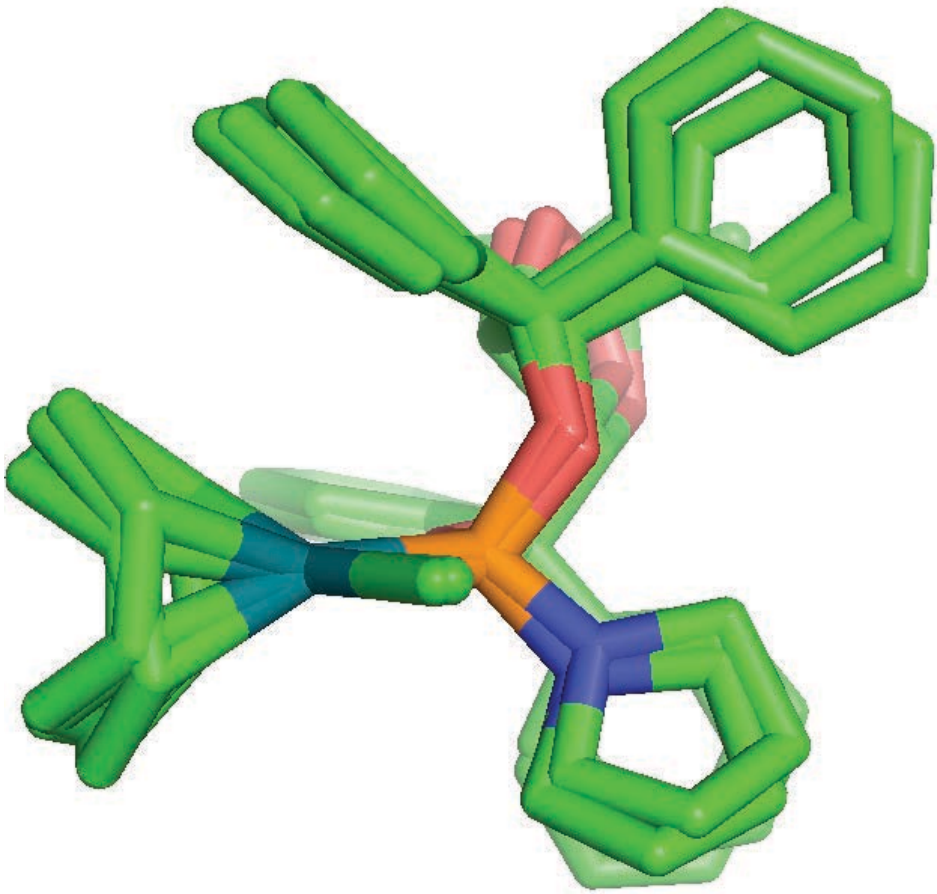

Figure A.5.20 Overlay of Rh(cod)Cl/**T1** structures.

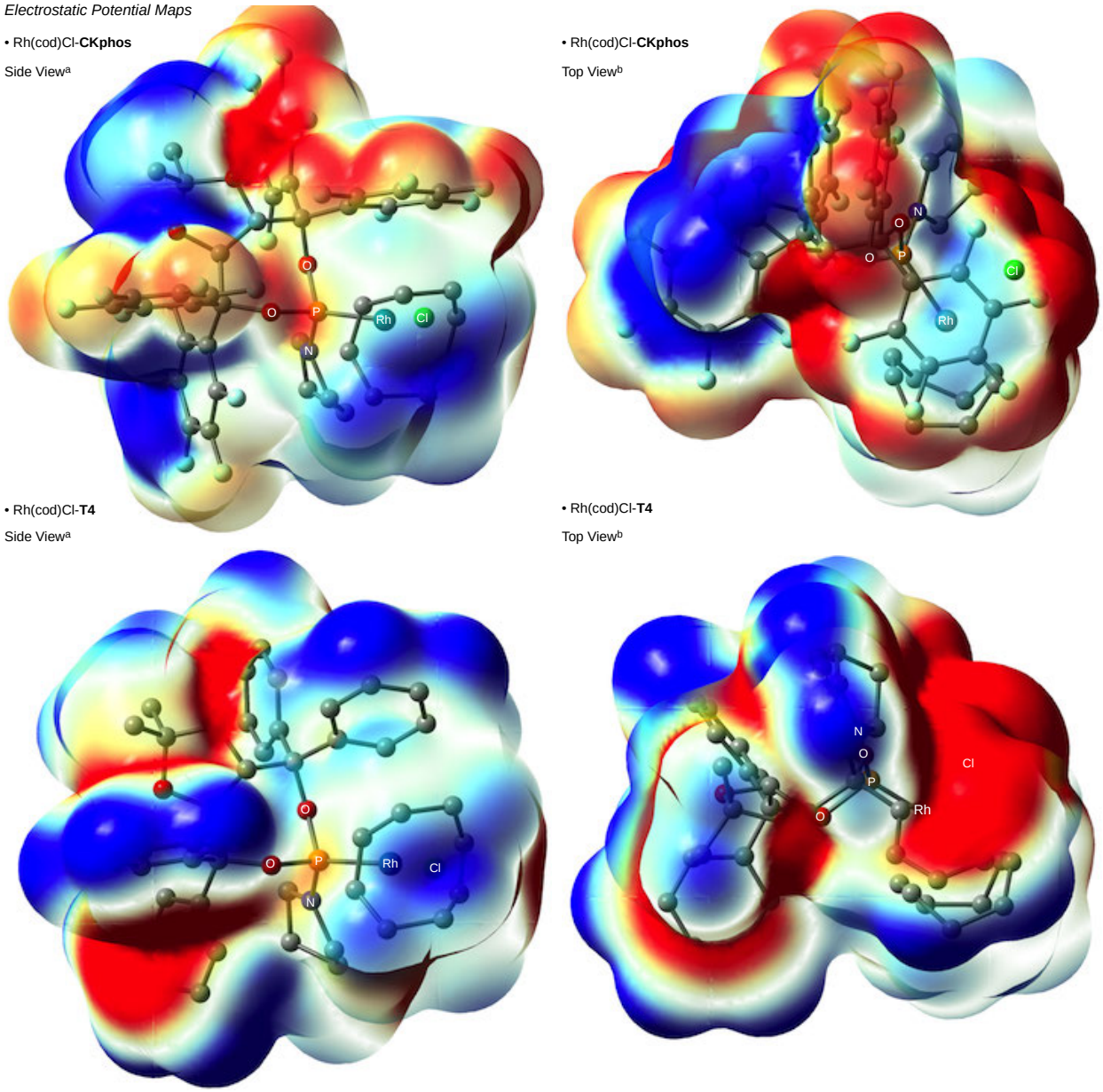

Figure A.5.21. Electrostatic potential maps of Rh(cod)Cl/CKphos and Rh(cod)Cl/**T1**

Table A.5.21. Select Computed bonded and non-bonded distances (Å).

	X-ray CK/Cl	B3LYP	B97D	X-ray **T1**	B3LYP	B97D
Rh-P	2.242	2.331	2.248	2.255	2.324	2.247
C=C	1.365	1.365	1.390	1.378	1.382	1.387
Rh-Aryl	3.728	3.790	3.492	4.039	4.257	4.008
Cl-Aryl	3.958	4.006	3.941	4.694	4.847	4.837

T1 B3LYP E(RB3LYP) = -2154.19845891 A.U.

Center Number	Atomic Number	Atomic Type	Coordinates (Angstroms) X	Y	Z
1	6	0	5.045794	-0.709029	0.140118
2	1	0	5.336739	-0.897483	-0.890895
3	6	0	4.807421	0.605102	0.495239
4	1	0	4.948817	1.357311	-0.277288
5	6	0	2.686513	-1.721306	1.411558
6	1	0	1.757228	-2.276254	1.296129
7	6	0	2.584396	-0.433934	1.985098
8	1	0	1.582829	-0.084244	2.225122
9	6	0	3.694430	0.255759	2.779176
10	1	0	3.236624	0.891212	3.545737
11	1	0	4.279995	-0.494036	3.323700
12	6	0	4.617718	1.134068	1.901613
13	1	0	4.175549	2.131541	1.816657
14	1	0	5.594076	1.268373	2.394256
15	6	0	5.235246	-1.850895	1.125124
16	1	0	5.970666	-2.553937	0.716869
17	1	0	5.667329	-1.467898	2.055215
18	6	0	3.919081	-2.608556	1.415063
19	1	0	3.773446	-3.372981	0.641854
20	1	0	3.999097	-3.154609	2.369428
21	6	0	-1.734299	-1.410808	0.503108
22	6	0	-2.442742	-0.044209	0.210475
23	1	0	-2.519655	0.079088	-0.873974

24	6	0	-1.688559	1.144135	0.824942
25	1	0	-1.036926	0.802030	1.634772
26	6	0	-0.802083	1.906523	-0.224642
27	6	0	-3.958440	1.286684	1.400703
28	6	0	-4.374543	1.061863	2.851649
29	1	0	-5.304315	0.485905	2.895005
30	1	0	-4.534514	2.024315	3.348145
31	1	0	-3.596024	0.509371	3.383672
32	6	0	-4.986077	2.081039	0.598513
33	1	0	-4.646951	2.203518	-0.433215
34	1	0	-5.125665	3.073199	1.038859
35	1	0	-5.947587	1.557341	0.600582
36	6	0	0.315631	2.717633	0.440180
37	6	0	1.423565	3.114129	-0.323265
38	6	0	2.404814	3.935004	0.231253
39	6	0	2.294719	4.375539	1.553249
40	6	0	1.197183	3.982347	2.319463
41	6	0	0.211943	3.158432	1.766926
42	6	0	-1.664020	2.828667	-1.107827
43	6	0	-2.110850	2.426231	-2.372022
44	6	0	-2.917677	3.264568	-3.147391
45	6	0	-3.291403	4.519927	-2.671714
46	6	0	-2.847727	4.931874	-1.412847
47	6	0	-2.042436	4.096881	-0.640697
48	6	0	1.289440	-2.322988	-2.626843
49	1	0	0.932213	-3.293018	-2.252054
50	1	0	2.292583	-2.137259	-2.233653
51	6	0	1.234916	-2.274912	-4.156764
52	1	0	1.913784	-1.494519	-4.517307

53	1	0	1.520660	-3.227563	-4.614239
54	6	0	-0.225680	-1.886324	-4.425745
55	1	0	-0.878905	-2.758610	-4.304353
56	1	0	-0.390226	-1.475417	-5.427009
57	6	0	-0.525409	-0.850447	-3.329283
58	1	0	-0.273554	0.161131	-3.665425
59	1	0	-1.578730	-0.869191	-3.029517
60	6	0	-2.160216	-2.520456	-0.467044
61	6	0	-1.397033	-3.696341	-0.531678
62	6	0	-1.772277	-4.745189	-1.367316
63	6	0	-2.928063	-4.643293	-2.148789
64	6	0	-3.704488	-3.488471	-2.075763
65	6	0	-3.325567	-2.433022	-1.238273
66	6	0	-1.983692	-1.872110	1.950117
67	6	0	-1.019570	-1.712593	2.951887
68	6	0	-1.275971	-2.124796	4.263496
69	6	0	-2.499677	-2.703366	4.593969
70	6	0	-3.466411	-2.871981	3.599109
71	6	0	-3.210591	-2.463582	2.291915
72	17	0	3.235279	0.630037	-2.359627
73	1	0	1.527846	2.767942	-1.345574
74	1	0	3.256628	4.229213	-0.375759
75	1	0	3.055914	5.023616	1.980179
76	1	0	1.096920	4.321783	3.347194
77	1	0	-0.652666	2.892676	2.367180
78	1	0	-1.812235	1.464186	-2.764335
79	1	0	-3.244104	2.932024	-4.129416
80	1	0	-3.914333	5.174201	-3.275821
81	1	0	-3.124794	5.910460	-1.029587

82	1	0	-1.703451	4.436304	0.331066
83	1	0	-3.962400	-1.556875	-1.170227
84	1	0	-4.613099	-3.402569	-2.665861
85	1	0	-3.223319	-5.462304	-2.799083
86	1	0	-1.165752	-5.646271	-1.406006
87	1	0	-0.503614	-3.783111	0.079121
88	1	0	-3.969514	-2.606280	1.531312
89	1	0	-4.423357	-3.327811	3.839476
90	1	0	-2.698163	-3.026663	5.612391
91	1	0	-0.508884	-1.995281	5.022651
92	1	0	-0.056944	-1.284688	2.706817
93	7	0	0.362900	-1.243757	-2.211946
94	8	0	-0.298403	-1.170734	0.392596
95	8	0	-0.245104	0.906648	-1.125698
96	8	0	-3.739492	0.012869	0.777360
97	8	0	-2.700728	1.975838	1.365456
98	15	0	0.599230	-0.446159	-0.782343
99	45	0	2.826405	-0.261857	-0.146318

T4 B97D: E(RB97D) = -2153.08504790 A.U.

Center Number	Atomic Number	Atomic Type	Coordinates (Angstroms) X	Y	Z
1	6	0	4.956396	-0.887400	0.305762
2	1	0	5.249127	-1.324622	-0.651965
3	6	0	4.790200	0.487867	0.372315
4	1	0	4.988892	1.069276	-0.531311

5	6	0	2.487499	-1.467614	1.667796
6	1	0	1.535772	-2.003651	1.660811
7	6	0	2.428335	-0.069237	1.931855
8	1	0	1.434312	0.369948	2.053548
9	6	0	3.548296	0.713713	2.628155
10	1	0	3.098967	1.560847	3.168542
11	1	0	4.015408	0.062185	3.384816
12	6	0	4.634923	1.275267	1.663485
13	1	0	4.362327	2.301300	1.392650
14	1	0	5.607193	1.325884	2.190234
15	6	0	5.046418	-1.768775	1.544429
16	1	0	5.766544	-2.581756	1.360105
17	1	0	5.442616	-1.176064	2.382851
18	6	0	3.675908	-2.384410	1.931722
19	1	0	3.517337	-3.295436	1.331924
20	1	0	3.689109	-2.702662	2.993361
21	6	0	-1.752942	-1.267428	0.670186
22	6	0	-2.385772	0.104504	0.236021
23	1	0	-2.468931	0.114590	-0.860318
24	6	0	-1.524404	1.282622	0.724240
25	1	0	-0.848219	0.970103	1.532355
26	6	0	-0.634649	1.854152	-0.451081
27	6	0	-3.776660	1.675892	1.252687
28	6	0	-4.301872	1.659542	2.688431
29	1	0	-5.307248	1.212831	2.713043
30	1	0	-4.357721	2.687296	3.077756
31	1	0	-3.626544	1.060072	3.314353
32	6	0	-4.648975	2.473789	0.279822
33	1	0	-4.227566	2.420752	-0.732726

34	1	0	-4.684848	3.528359	0.590354
35	1	0	-5.671152	2.064572	0.277440
36	6	0	0.582914	2.625037	0.061138
37	6	0	1.712916	2.753466	-0.770435
38	6	0	2.792337	3.551866	-0.372518
39	6	0	2.761244	4.223752	0.861202
40	6	0	1.650051	4.075096	1.705323
41	6	0	0.562697	3.279090	1.306642
42	6	0	-1.499583	2.723042	-1.375526
43	6	0	-2.112380	2.186011	-2.523521
44	6	0	-2.975855	2.971554	-3.304276
45	6	0	-3.239548	4.302208	-2.948080
46	6	0	-2.625351	4.844783	-1.807805
47	6	0	-1.762891	4.062201	-1.029451
48	6	0	1.090580	-2.756988	-2.355767
49	1	0	0.746966	-3.632346	-1.774605
50	1	0	2.141391	-2.542637	-2.118081
51	6	0	0.844479	-2.972176	-3.857734
52	1	0	1.485958	-2.282170	-4.427341
53	1	0	1.055177	-4.005226	-4.172549
54	6	0	-0.639057	-2.578829	-4.011073
55	1	0	-1.286703	-3.380458	-3.624014
56	1	0	-0.928822	-2.357682	-5.049374
57	6	0	-0.764317	-1.336933	-3.106322
58	1	0	-0.514224	-0.413234	-3.652639
59	1	0	-1.772752	-1.236480	-2.677896
60	6	0	-2.233724	-2.442495	-0.184789
61	6	0	-1.482150	-3.632721	-0.188871
62	6	0	-1.899447	-4.737622	-0.939507

63	6	0	-3.086564	-4.672241	-1.691168
64	6	0	-3.851470	-3.497320	-1.674953
65	6	0	-3.428958	-2.386511	-0.923370
66	6	0	-2.026886	-1.520929	2.159531
67	6	0	-1.089120	-1.177701	3.150388
68	6	0	-1.396793	-1.345572	4.510732
69	6	0	-2.644509	-1.855368	4.897366
70	6	0	-3.582186	-2.205955	3.911363
71	6	0	-3.274963	-2.041529	2.554857
72	17	0	3.307157	-0.034999	-2.503759
73	1	0	1.747592	2.226541	-1.721970
74	1	0	3.661233	3.638233	-1.027390
75	1	0	3.601662	4.851015	1.166758
76	1	0	1.619262	4.586755	2.669768
77	1	0	-0.310629	3.195616	1.954291
78	1	0	-1.904432	1.159107	-2.814351
79	1	0	-3.437357	2.539338	-4.194876
80	1	0	-3.910778	4.912716	-3.555707
81	1	0	-2.817047	5.881178	-1.521944
82	1	0	-1.291984	4.489742	-0.145755
83	1	0	-4.042712	-1.485537	-0.900477
84	1	0	-4.780432	-3.438915	-2.246000
85	1	0	-3.413491	-5.533018	-2.278067
86	1	0	-1.298701	-5.649530	-0.940537
87	1	0	-0.558284	-3.675768	0.388121
88	1	0	-4.006955	-2.312084	1.794798
89	1	0	-4.555823	-2.608843	4.198439
90	1	0	-2.883395	-1.985235	5.955090
91	1	0	-0.653467	-1.078604	5.265204

92	1	0	-0.111961	-0.798765	2.861785
93	7	0	0.245766	-1.580086	-2.047943
94	8	0	-0.302867	-1.126036	0.540667
95	8	0	-0.202966	0.724374	-1.268392
96	8	0	-3.666882	0.310775	0.806555
97	8	0	-2.440881	2.226899	1.253138
98	15	0	0.586977	-0.613944	-0.754030
99	45	0	2.744943	-0.392646	-0.166655

CKphos/Cl B3LYP: E(RB3LYP) = -4138.68423078 A.U.

Center Number	Atomic Number	Atomic Type	Coordinates (Angstroms) X	Y	Z
1	6	0	3.138142	-4.333540	-1.008653
2	1	0	3.249506	-4.286784	-2.089635
3	6	0	3.944889	-3.503100	-0.253178
4	1	0	4.652744	-2.877230	-0.791624
5	6	0	0.746546	-3.726187	0.450013
6	1	0	-0.275829	-3.358995	0.403084
7	6	0	1.608280	-3.071726	1.353959
8	1	0	1.187880	-2.233351	1.898756
9	6	0	2.812329	-3.722384	2.038470
10	1	0	2.950899	-3.252239	3.018078
11	1	0	2.588145	-4.776453	2.239962
12	6	0	4.137818	-3.597698	1.245515
13	1	0	4.672871	-2.703210	1.575835
14	1	0	4.799680	-4.444418	1.485734
15	6	0	2.359705	-5.511055	-0.445626

16	1	0	2.350917	-6.319428	-1.185764
17	1	0	2.879675	-5.907524	0.432564
18	6	0	0.904220	-5.138688	-0.083338
19	1	0	0.281746	-5.220223	-0.982863
20	1	0	0.494835	-5.867396	0.635032
21	6	0	-2.040450	-0.090862	0.328078
22	6	0	-1.510469	1.374011	0.594175
23	1	0	-1.462938	1.901331	-0.356206
24	6	0	-0.126832	1.358268	1.281644
25	1	0	0.023150	0.423703	1.817059
26	6	0	1.029890	1.556966	0.233876
27	6	0	-1.541313	2.754401	2.489186
28	6	0	-1.907439	2.221277	3.872639
29	1	0	-2.969621	2.390726	4.075248
30	1	0	-1.317377	2.732058	4.639653
31	1	0	-1.703459	1.148731	3.935202
32	6	0	-1.736151	4.261263	2.364410
33	1	0	-1.505760	4.586108	1.346162
34	1	0	-1.078304	4.786795	3.063541
35	1	0	-2.773329	4.526675	2.589970
36	6	0	2.429401	1.071629	0.655880
37	6	0	3.472629	1.232509	-0.270238
38	6	0	4.762798	0.769626	-0.039635
39	6	0	5.050039	0.120415	1.155878
40	6	0	4.048761	-0.038339	2.104788
41	6	0	2.764159	0.435667	1.855116
42	6	0	1.096842	3.054296	-0.147612
43	6	0	0.471044	3.633601	-1.257693
44	6	0	0.562074	4.997365	-1.542869

45	6	0	1.280052	5.840963	-0.705802
46	6	0	1.896944	5.305711	0.420160
47	6	0	1.794028	3.944220	0.685215
48	6	0	-0.341160	-2.163163	-3.238947
49	1	0	-1.342858	-2.607923	-3.152002
50	1	0	0.382327	-2.861452	-2.806401
51	6	0	-0.018682	-1.793185	-4.688307
52	1	0	1.067000	-1.706826	-4.800665
53	1	0	-0.392560	-2.534744	-5.401342
54	6	0	-0.684350	-0.418533	-4.835878
55	1	0	-1.764947	-0.535158	-4.986868
56	1	0	-0.291746	0.166205	-5.673279
57	6	0	-0.404974	0.267969	-3.488847
58	1	0	0.534539	0.825608	-3.513227
59	1	0	-1.202719	0.956947	-3.201764
60	6	0	-2.979898	-0.239400	-0.890263
61	6	0	-3.267028	-1.529046	-1.360912
62	6	0	-4.080339	-1.765259	-2.463142
63	6	0	-4.678959	-0.695643	-3.122761
64	6	0	-4.449474	0.595443	-2.662726
65	6	0	-3.620896	0.808604	-1.560380
66	6	0	-2.776931	-0.621385	1.580847
67	6	0	-2.226596	-1.484386	2.537049
68	6	0	-2.949703	-1.939170	3.642502
69	6	0	-4.257519	-1.520563	3.845626
70	6	0	-4.829601	-0.638823	2.934561
71	6	0	-4.092853	-0.201034	1.839125
72	17	0	3.120787	-1.349076	-2.532842
73	9	0	3.245876	1.849786	-1.434102

74	9	0	5.713764	0.928322	-0.959688
75	9	0	6.267558	-0.378687	1.381819
76	9	0	4.310603	-0.689992	3.246882
77	9	0	1.865378	0.230485	2.836488
78	9	0	-0.281437	2.924591	-2.113991
79	9	0	-0.050992	5.490590	-2.623538
80	9	0	1.368887	7.144729	-0.970762
81	9	0	2.580293	6.100481	1.249907
82	9	0	2.406636	3.510400	1.796017
83	9	0	-3.497993	2.081671	-1.157465
84	9	0	-5.035123	1.634095	-3.266205
85	9	0	-5.463505	-0.908274	-4.179741
86	9	0	-4.275020	-3.015969	-2.896040
87	9	0	-2.739376	-2.610110	-0.764342
88	9	0	-4.712648	0.662047	1.022085
89	9	0	-6.081313	-0.206416	3.116715
90	9	0	-4.951144	-1.948538	4.900604
91	9	0	-2.372529	-2.774170	4.512358
92	9	0	-0.961011	-1.919965	2.474115
93	7	0	-0.296850	-0.860575	-2.523593
94	8	0	-0.882517	-0.925307	0.105867
95	8	0	0.663921	0.811684	-0.950220
96	8	0	-2.336064	2.085882	1.494559
97	8	0	-0.177296	2.442528	2.185358
98	15	0	0.346705	-0.801541	-0.999944
99	45	0	2.019538	-2.386673	-0.652613

CKphos/Cl B97D: E(RB97D) = -4136.65357295 A.U.

Center Number	Atomic Number	Atomic Type	Coordinates (Angstroms) X	Y	Z
1	6	0	3.520765	-3.992548	-0.562303
2	1	0	3.606790	-4.049169	-1.650094
3	6	0	4.269639	-3.028025	0.101449
4	1	0	4.929404	-2.395416	-0.498419
5	6	0	1.096158	-3.413004	0.885738
6	1	0	0.036522	-3.156893	0.837581
7	6	0	1.914886	-2.585392	1.699561
8	1	0	1.430415	-1.730064	2.169431
9	6	0	3.164952	-3.089198	2.433311
10	1	0	3.294330	-2.496593	3.349555
11	1	0	2.985823	-4.129666	2.749159
12	6	0	4.483903	-3.008890	1.606193
13	1	0	5.022874	-2.092114	1.866719
14	1	0	5.147492	-3.846475	1.893453
15	6	0	2.851728	-5.158694	0.153341
16	1	0	2.895345	-6.051171	-0.490330
17	1	0	3.418186	-5.395757	1.066631
18	6	0	1.370208	-4.862613	0.507863
19	1	0	0.744945	-5.088913	-0.370925
20	1	0	1.031306	-5.538921	1.317412
21	6	0	-2.027373	-0.289585	0.323250
22	6	0	-1.662807	1.252386	0.399313
23	1	0	-1.583965	1.644367	-0.615780
24	6	0	-0.327753	1.435264	1.165619
25	1	0	-0.100517	0.555687	1.767468
26	6	0	0.839591	1.651079	0.107579

27	6	0	-1.928433	2.928294	1.995223
28	6	0	-2.510549	2.787674	3.401764
29	1	0	-3.583136	3.032443	3.387797
30	1	0	-1.994683	3.470978	4.092064
31	1	0	-2.378721	1.752698	3.748197
32	6	0	-2.040788	4.343303	1.421562
33	1	0	-1.653302	4.358301	0.394090
34	1	0	-1.455799	5.043154	2.036654
35	1	0	-3.093663	4.662118	1.414244
36	6	0	2.271054	1.296280	0.549965
37	6	0	3.287355	1.411727	-0.423569
38	6	0	4.599865	0.986130	-0.195858
39	6	0	4.939868	0.460236	1.055215
40	6	0	3.969279	0.373920	2.056998
41	6	0	2.656221	0.787258	1.800689
42	6	0	0.772784	3.113348	-0.377137
43	6	0	0.136316	3.557833	-1.551686
44	6	0	0.049894	4.920876	-1.884309
45	6	0	0.596899	5.888708	-1.034945
46	6	0	1.232269	5.480812	0.144242
47	6	0	1.312353	4.117761	0.454053
48	6	0	-0.103425	-2.542293	-2.928710
49	1	0	-1.032591	-3.109340	-2.743092
50	1	0	0.736664	-3.076704	-2.460719
51	6	0	0.112641	-2.297760	-4.429435
52	1	0	1.176814	-2.076844	-4.599080
53	1	0	-0.186655	-3.161525	-5.041414
54	6	0	-0.738917	-1.040260	-4.688770
55	1	0	-1.807565	-1.306202	-4.737948

56	1	0	-0.469247	-0.514857	-5.616546
57	6	0	-0.461843	-0.169870	-3.448639
58	1	0	0.436148	0.448082	-3.587219
59	1	0	-1.302461	0.488271	-3.193995
60	6	0	-2.859147	-0.733903	-0.899138
61	6	0	-2.985373	-2.117466	-1.139677
62	6	0	-3.596066	-2.630349	-2.287503
63	6	0	-4.148471	-1.752705	-3.229336
64	6	0	-4.103478	-0.375806	-2.988961
65	6	0	-3.480919	0.115150	-1.830254
66	6	0	-2.746822	-0.690238	1.629758
67	6	0	-2.123562	-1.256566	2.758253
68	6	0	-2.826880	-1.535767	3.943506
69	6	0	-4.187664	-1.228648	4.043420
70	6	0	-4.835231	-0.641022	2.949528
71	6	0	-4.115686	-0.376013	1.778203
72	17	0	3.201273	-1.287940	-2.453236
73	9	0	3.011198	1.929843	-1.631107
74	9	0	5.525196	1.073552	-1.158359
75	9	0	6.186733	0.017307	1.287660
76	9	0	4.295875	-0.128396	3.264323
77	9	0	1.789097	0.673098	2.831480
78	9	0	-0.445501	2.715786	-2.429050
79	9	0	-0.558025	5.296811	-3.021502
80	9	0	0.511500	7.189895	-1.344712
81	9	0	1.751192	6.397266	0.978106
82	9	0	1.936690	3.800945	1.604942
83	9	0	-3.512826	1.453460	-1.665730
84	9	0	-4.643852	0.476489	-3.875417

85	9	0	-4.695470	-2.227100	-4.358075
86	9	0	-3.609248	-3.955961	-2.514005
87	9	0	-2.457740	-3.016250	-0.282348
88	9	0	-4.800089	0.219477	0.782308
89	9	0	-6.137242	-0.320875	3.033157
90	9	0	-4.862698	-1.490235	5.171197
91	9	0	-2.190122	-2.095718	4.985590
92	9	0	-0.811801	-1.562089	2.787600
93	7	0	-0.224040	-1.168372	-2.368119
94	8	0	-0.768309	-1.013652	0.256829
95	8	0	0.546005	0.782281	-1.021314
96	8	0	-2.610584	1.997301	1.136449
97	8	0	-0.537137	2.539663	2.021862
98	15	0	0.435596	-0.857150	-0.878393
99	45	0	2.243371	-2.096171	-0.377433

APPENDIX 6

Rh(I)-Catalyzed [2+2+2] Cycloadditions with Alkyl Alkynes to Form Aza-Quaternary N-Stereocenters: Synthesis of Cylindricine Core

A.6.1 Methods and Materials

Toluene, tetrahydrofuran, ether, and dichloromethane were degassed with argon and passed through one column of neutral alumina and one column of Q5 reactant. Triethylamine (peptide synthesis grade) was purchased from Fisher Scientific, dried over calcium hydride and freshly distilled prior to use. Flash column chromatography was carried out on silica gel (60 Å, 230 - 400 mesh, obtained from Silicycle Inc.) and was performed with reagent grade solvents. Analytical thin-layer chromatography (TLC) was performed on Silicycle glass-backed silica gel plates (60 Å, 0.25 mm, purchased from Silicycle Inc.) and visualized with a UV lamp (254 nm), and potassium permanganate or cerric ammonium molybdate.

Infrared spectra (IR) were obtained on a Nicolet Avatar 320 FT-IR spectrometer and Bruker Tensor 27 FT-IR spectrometer. ^{1}H NMR and ^{13}C NMR were obtained on Varian Unity 300 and Unity 400 spectrometers. Chemical shifts are expressed in parts per million values (δ, ppm). Proton chemical shifts in CDCl3 were referenced to 7.26 ppm (CHCl3). Carbon chemical shifts were referenced to 77.2 ppm (CDCl3). Peak multiplicities are designated by the following abbreviations: s, singlet; d, doublet; t, triplet; q, quartet; m, multiplet; dd, doublet of doublets; dt, doublet of triplets; b, broad; *J*, coupling constant in Hz. Low resolution mass spectra (MS) and high resolution mass spectra (HRMS) were

recorded on a Fisons VG Autospec spectrometer. HPLC spectra were obtained on an Agilent 1100 series system. Optical rotation was obtained with an Autopol-III automatic polarimeter. Melting points were obtained on a Fisher-Johns melting point apparatus and are uncorrected. References following the compound names indicate literature articles where the compound has been previously been reported.

Unless indicated, commercially available starting materials were purchased from Aldrich Chemicals and used without further purification. $[Rh(ethylene)_2Cl]_2$ was purchased from Strem Chemicals or Alfa Aesar and used without further purification.

A.6.2 General Procedure for Rhodium Catalyzed [2+2+2] Cycloadditions

Isocyanates and vinylogous amide indolizinone products not listed below were synthesized as previously reported.[2,1]

An oven-dried round bottom flask was charged with $[Rh(C_2H_4)_2Cl]_2$ (4 mg, 0.01 mmol) and ligand (20 mg, 0.02 mmol) and fitted with an oven-dried reflux condenser in an inert atmosphere (Ar) glove box. Upon removal from the glove box, 2 ml of toluene was added via syringe and the resulting yellow solution was stirred at ambient temperature for 5 min. To this solution, alkyne **1** (0.20 mmol, 1 equiv) and isocyanate **2** (0.26 mmol, 1.3 equiv) in 6 ml of toluene was added via syringe. An additional 2 ml of toluene was used to wash down the residue and added to the reaction mixture. The reaction mixture was heated to 110 °C in an oil bath and kept at reflux for 16 h. The reaction mixture was cooled to 23 °C, concentrated in *vacuo*, and purified by flash column chromatography (19:1 EtOAc:MeOH). Evaporation of solvent afforded the analytically pure products. Absolute stereochemistry was established as previously reported.[1,2]

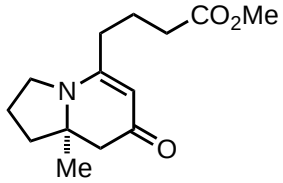

(R)-methyl 4-(8a-methyl-7-oxo-1,2,3,7,8,8a-hexahydroindolizin-5-yl)butanoate (4b)

General procedure yielded a yellow solid (68 %). 98% ee by HPLC (Chiralcel IA, Hex:iPrOH 90:10, 1 ml/min, RTmajor = 31.9 min, RTminor = 30.2 min). $[\alpha]^{20}_D = 43°$, c = 0.01 g/ml

[1] Lee, E. E.; Rovis, T. *Org. Lett.* **2008**, 10, 6, 1231-1234.

[2] Yu, R. T.; Rovis, T. *J. Am. Chem. Soc.* **2006**, *128*, 12370-12371

$CHCl_3$. Rf = 0.07 (EtOAc). ^{1}H NMR (400 MHz, $CDCl_3$) δ 4.89 (1H, s), 3.67 (3H, s), 3.64-3.58 (1H, m), 3.47 (1H, dt, *J* = 10.7, 8.5 Hz), 2.40 (2H, dd, *J* = 76.0, 15.9 Hz), 2.39 (t, *J* = 7.2 Hz), 2.26-2.22 (2H, m), 2.08-1.98 (3H, m), 1.89-1.80 (3H, m), 1.19 (3H, s). ^{13}C NMR (100 MHz, $CDCl_3$) δ 191.5, 173.7, 161.8, 96.6, 63.3, 52.0, 48.2, 46.7, 39.8, 33.4, 33.2, 22.6, 20.2. IR (Thin Film) v 2966, 2879, 1736, 1623, 1542, 1489, 1458, 1371, 1342, 1267, 1211, 1167, 1149, 1098, 1015, 929, 881, 767. HRMS (ESI) *m/z* $[C_{14}H_{22}NO_3]^+$ calculated 252.1594, found 252.16.

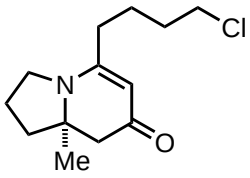

(R)-5-(4-chlorobutyl)-8a-methyl-2,3,8,8a-tetrahydroindolizin-7(1H)-one (4c)

General procedure yielded a yellow solid (68%). 98% ee by HPLC (Chiralcel IA, Hex:iPrOH 90:10, 1 ml/min, RTmajor = 24.6 min, RTminor = 23.4 min). $[\alpha]^{20}_D$ = 84°, c = 0.01 g/ml $CHCl_3$. Rf = 0.07 (EtOAc). ^{1}H NMR (400 MHz, $CDCl_3$) δ 4.91 (1H, s), 3.62-3.54 (3H, m), 3.50-3.43 (1H, m), 2.41 (2H, dd, *J* = 75.3, 15.9 Hz), 2.16-2.27 (2H, m), 2.10-1.98 (3H, m), 1.78-1.87 (3H, m) 1.70 (2H, quintet, *J* = 7.6 Hz), 1.20 (3H, s). ^{13}C NMR (100 MHz, $CDCl_3$) δ 191.4, 162.1, 96.6, 63.3, 48.2, 46.7, 44.8, 39.8, 33.4, 32.1, 24.6, 22.6, 20.2. IR (Thin Film) v 2965, 2873, 1718, 1623, 1540, 1491, 1372, 1270, 1214, 1166, 1098. HRMS (ESI) *m/z* $[C_{13}H_{20}ClNO]^+$ calculated 241.1233, found 241.1238.

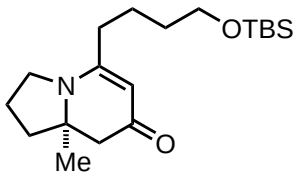

(*R*)-5-(4-((*tert*-butyldimethylsilyl)oxy)butyl)-8a-methyl-2,3,8,8a-tetrahydroindolizin-7(1*H*)-one (4d)

General procedure yielded a yellow solid (62%). 93% ee by HPLC (Chiralcel IA, Hex:iPrOH 90:10, 1 ml/min, RTmajor = 10.2 min, RTminor = 9.4 min). $[\alpha]^{20}_D$ = 32°, c = 0.01 g/ml $CHCl_3$.

Rf = 0.14 (EtOAc).^{1}H NMR (400 MHz, $CDCl_3$) δ 4.91 (1H, s), 3.59 (3H, dt, *J* = 16.6, 5.7 Hz), 3.45 (1H, dt, *J* = 10.6, 8.5 Hz), 2.40 (2H, dd, *J* = 77.9, 16.0 Hz), 2.24-2.15 (2H, m), 2.07-1.97 (3H, m), 1.85-1.77 (1H, m), 1.63-1.52 (4H, m), 1.19 (3H, s), 0.87 (9H, s), 0.03 (3H, s). ^{13}C NMR (100 MHz, $CDCl_3$) δ 191.3, 163.1, 96.4, 63.2, 62.8, 48.2, 46.7, 39.8, 33.9, 32.5, 26.3, 23.9, 22.6, 20.2, 18.6, -5.0. IR (Thin

Film) v 2936, 2874, 1720, 1604, 1525, 1493, 1459, 1372, 1297, 1216, 1166, 1099. HRMS (ESI) *m/z* $[C_{19}H_{36}NO_2Si]^+$ calculated 338.251, found 338.2514.

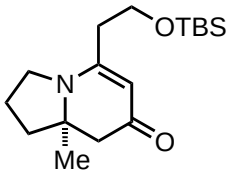

(R)-5-(2-((tert-butyldimethylsilyl)oxy)ethyl)-8a-methyl-2,3,8,8a-tetrahydroindolizin-7(1H)-one (4e)

General procedure yielded a brown solid (52%). 91% ee by HPLC (Chiralcel IA, Hex:iPrOH 90:10, 1 ml/min, RTmajor = 10.2 min, RTminor = 9.2 min). $[\alpha]^{20}_D$ = 68°, c = 0.01 g/ml $CHCl_3$. Rf = 0.14 (EtOAc). ^{1}H NMR (400 MHz, $CDCl_3$) δ 4.88 (1H, s), 3.80 (2H, t, *J* = 6.6 Hz), 3.67 (1H, dt, *J* = 10.6, 5.5 Hz), 3.55 (1H, dt, *J* = 10.9, 8.4 Hz), 2.44 (2H, t, *J* = 6.6 Hz), 2.39 (dd, *J* = 78.3, 15.9 Hz), 2.07-1.97 (4H, m) 1.86-1.80 (1H, m), 1.20 (3H, s), 0.87 (9H, s), 0.03 (6H, s). ^{13}C NMR (100 MHz, $CDCl_3$) δ 191.1, 161.0, 96.4, 63.3, 62.2, 48.1, 47.3, 39.9, 37.3, 26.2, 22.4, 20.2, 18.6. -5.1. IR (Thin Film) v 2960, 1608, 1536, 1492, 1371, 1341, 1267, 1213, 1150, 1097, 937, 837, 779. HRMS (ESI) *m/z* $[C_{17}H_{32}NO_2Si]^+$ calculated 310.2197, found 310.2197.

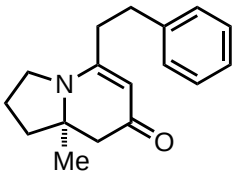

(*R*)-8a-methyl-5-phenethyl-2,3,8,8a-tetrahydroindolizin-7(1*H*)-one (4f)

General procedure yielded a yellow solid (61%). 95% ee by HPLC (Chiralcel IA, Hex:iPrOH 90:10, 1 ml/min, RTmajor = 28.0 min, RTminor = 24.2 min). $[\alpha]^{20}_D$ = +86°, c = 0.01 g/ml $CHCl_3$.

Rf = 0.11 (EtOAc). ^{1}H NMR (400 MHz, $CDCl_3$) δ 7.30-7.26 (2H, m), 7.23-7.17 (3H, m), 4.98 (1H, s), 3.46 (1H, dq, *J* = 10.3, 6.5 Hz), 3.33-3.27 (1H, m), 2.86-2.82 (2H, m), 2.52-2.48 (1H, m), 2.40 (2H, dd, *J* = 76.7, 15.9 Hz), 2.01-1.93 (3H, m), 1.82-1.73 (1H, m), 1.17 (3H, s). ^{13}C NMR (100 MHz, $CDCl_3$) δ 191.3, 162.2, 140.5, 128.9, 128.7, 126.8, 96.3, 63.3, 48.1, 46.8, 39.8, 35.9, 34.1, 22.5, 20.2. IR (Thin Film) v 3027, 2968, 2878, 1718, 1624, 1541, 1492, 1454, 1414, 1371, 1341, 1268, 1214, 1168, 1098, 1077, 1020, 753, 701. HRMS (ESI) *m/z* $[C_{17}H_{22}NO]^+$ calculated 256.1696, found 256.1701.

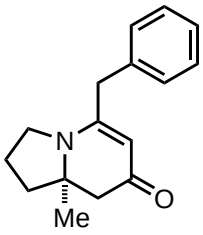

(R)-5-benzyl-8a-methyl-2,3,8,8a-tetrahydroindolizin-7(1H)-one (4g)

General procedure yielded a yellow solid (60%). 98% ee by HPLC (Chiralcel IA, Hex:iPrOH 90:10, 1 ml/min, RTmajor = 21.4 min, RTminor = 19.4 min). $[\alpha]^{20}_{D}$ = 93°, c = 0.01 g/ml $CHCl_3$.

Rf = 0.10 (EtOAc). ^{1}H NMR (400 MHz, $CDCl_3$) δ 7.26-7.12 (5H, m), 4.89 (1H, s), 3.49 (2H, s), 3.37-3.25 (2H, m), 2.38 (2H, dd, *J* = 77.0, 15.9 Hz), 1.93-1.84 (3H, m), 1.77-1.70 (1H, m), 1.14 (3H, s). ^{13}C NMR (100 MHz, $CDCl_3$) δ 191.6, 160.5, 135.9, 129.1, 128.8, 127.3, 98.6, 63.5, 48.3, 46.8, 40.8, 39.8, 22.6, 19.8. IR (Thin Film) v 3029, 2969, 2880, 1718, 1625, 1540, 1494, 1454, 1410, 1372, 1296, 1269, 1215, 1165, 1098, 1030, 933, 705. HRMS (ESI) *m/z* $[C_{16}H_{19}NO]^+$ calculated 241.1467, found 241.1469.

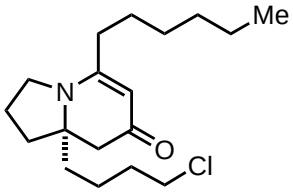

(R)-8a-(4-chlorobutyl)-5-hexyl-2,3,8,8a-tetrahydroindolizin-7(1H)-one (4j)

General procedure yielded a brown solid (50%). 90% ee by HPLC (Chiralcel IA, Hex:iPrOH 90:10, 1 ml/min, RTmajor = 15.0 min, RTminor = 12.7 min). $[\alpha]^{20}_{D}$ = +24°, c = 0.01 g/ml $CHCl_3$. Rf = 0.14 (EtOAc). ^{1}H NMR (400 MHz, $CDCl_3$) δ 4.93 (1H, s), 3.59-3.45 (4H, m), 2.44 (2H, s), 2.25-2.13 (3H, m), 2.03 (2H, qd, *J* = 8.2, 2.8 Hz), 1.83 (1H, dd, *J* = 11.6, 8.9 Hz), 1.76-1.66 (3H, m), 1.54-1.46 (2H, m), 1.42 (2H, t, *J* = 4.6 Hz), 1.38-1.24 (8H, m), 0.88 (3H, t, *J* = 6.7 Hz). ^{13}C NMR (100 MHz, $CDCl_3$) δ 190.8, 163.1, 96.6, 65.7, 46.8, 45.2, 44.6, 36.4, 34.1, 32.7, 31.4, 31.2, 28.9, 27.2, 22.7, 22.4, 21.7, 14.0. IR (Thin Film) v 2930, 2860, 1626, 1543, 1465, 1344, 1255, 1216, 1149, 1084, 768. HRMS (ESI) *m/z* $[C_{18}H_{31}ClNO]^+$ calculated 312.2022, found 312.2095.

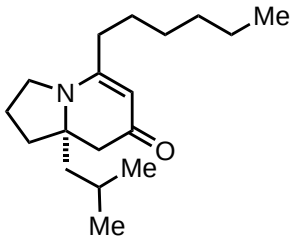

(S)-5-hexyl-8a-isobutyl-2,3,8,8a-tetrahydroindolizin-7(1H)-one (4k)

General procedure yielded a yellow solid (51%). 88% ee by HPLC (Chiralcel IA, Hex:iPrOH 90:10, 1 ml/min, RTmajor = 10.7 min, RTminor = 9.2 min). $[\alpha]^{20}_{D}$ = +46°, c = 0.01 g/ml $CHCl_3$. Rf = 0.19 (EtOAc). ^{1}H NMR (400 MHz, $CDCl_3$) δ 4.95 (1H, s), 3.54 (1H, dt, *J* = 9.4, 4.4 Hz), 3.49-3.43 (1H, m), 2.46 (2H, dd, *J* = 36.6, 18.3 Hz), 2.24-2.16 (4H, m), 2.06-2.00 (2H, m), 1.82 (1H, dd, *J* = 14.0, 4.8 Hz), 1.71 (1H, q, *J* = 10.8 Hz), 1.62 (1H, dt, *J* = 12.4, 6.3 Hz), 1.50 (2H, quintet, *J* = 7.4 Hz), 1.36-1.20 (8H, m), 0.92-0.86 (9H, m). ^{13}C NMR (100 MHz, $CDCl_3$) δ 190.8, 163.0, 96.5, 66.2, 46.5, 45.1, 39.8, 37.1, 34.1, 31.5, 28.9, 27.1, 25.0, 24.6, 24.2, 22.6, 22.4, 14.0. IR (Thin Film) v 2959, 2927, 2869, 1721, 1640, 1597, 1525, 1461, 1414, 1259, 1203, 1103. HRMS (ESI) *m/z* $[C_{18}H_{32}NO]^+$ calculated 278.2478, found 278.2488.

A.6.3 Synthesis of the cylindricine core

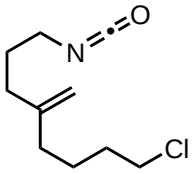

8-chloro-1-isocyanato-4-methyleneoctane (1)

Isocyanate **1** was synthesized as previously reported.[2a]

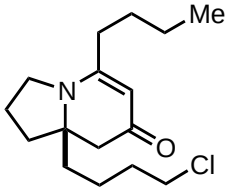

(R)-5-butyl-8a-(4-chlorobutyl)-2,3,8,8a-tetrahydroindolizin-7(1H)-one (4l)

An oven-dried 250ml round bottom flask was charged with $[Rh(C_2H_4)_2Cl]_2$ (48 mg, 0.12 mmol), CKphos (230 mg, 0.25 mmol), AgOTs (69 mg, 0.25 mmol) and 4 Å molecular sieves fitted with a rubber septum in an inert atmosphere (Ar) glove box. Upon removal from the glove box, 5 ml of 1,2-dichloroethane was added via syringe and the resulting yellow solution was stirred at ambient temperature for 30min. To this solution, alkyne **1** (5.1 mmol, 1 equiv) and isocyanate **2** (5.0 mmol, 1.0 equiv) in 5 ml of DCE was added via syringe under an Ar atmosphere. An additional 110 ml of DCE was added to the reaction mixture. The reaction mixture was heated to 70 °C in an oil bath until complete consumption of isocyanate was observed by HNMR (~48h). The reaction mixture was cooled to 23 °C, concentrated in *vacuo*, and purified by flash column chromatography (19:1 EtOAc:MeOH). Evaporation of solvent afforded a brown oil (730 mg, 2.58mmol,

52%). Absolute stereochemistry was established as previously reported. 95% ee by HPLC (Chiralcel IA, Hex:iPrOH 90:10, 1 ml/min, RTmajor = 15.5 min, RTminor = 14.4 min). $[\alpha]^{20}_D$ = -35.4°, c = 0.01 g/ml $CHCl_3$. Rf = 0.1 (EtOAc). ^{1}H NMR (400 MHz, $CDCl_3$) δ 4.88 (1H, s), 3.54-3.46 (4H, m), 2.41 (2H, d, J = 1.9), 2.24-2.11 (3H, m), 2.04-1.98 (2H, m), 1.81 (1H, dd, J = 11.8, 8.8), 1.74-1.66 (3H, m), 1.50-1.31 (8H, m), 0.90 (3H, t, J = 7.3). ^{13}C NMR (100 MHz, $CDCl_3$) δ 190.8, 163.0, 96.6, 65.7, 46.8, 45.2, 44.7, 36.5, 33.8, 32.7, 31.1, 29.4, 22.7, 22.4, 21.7, 13.8. IR (Thin Film) v 2956, 2869, 1626, 1543, 1464, 1255, 1093. LRMS (MM-ES) *m/z* $[C_{16}H_{26}ClNO]^+$ calculated 284.2, found 284.2.

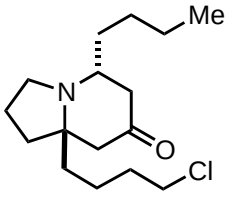

(5S,8aR)-5-butyl-8a-(4-chlorobutyl)hexahydroindolizin-7(1H)-one (7)

To a 50 ml oven-dried round bottom flask containing a magnetic stirbar was added a solution of indolizinone **4y** (201 mg, 0.70 mmol) in 15 ml THF and cooled to -78 °C. DIBALH (3.9 ml, 3.87 mmol, 1M in hexanes) was added dropwise via syringe. The yellow solution was stirred for 3h at -78 °C and then allowed to warm to 0 °C and stirred for 1h. The solution was quenched by very slow addition of a saturated solution of Rochelles salt (~3ml). *Caution!* Addition of the Rochelles salt solution causes vigorous bubbling. After addition of Rochelles salt, the solution was stirred until it becomes very chunky (~3h) at 0 °C. At this point ~10 ml of ethyl acetate is added, the solids are broken, the mixture is filtered through celite and the solids washed with ethyl acetate. The layers are then separated and the organic layer is washed with 3M HCl (3 x 10 ml). Ice is then added to the aqueous extracts, basified with 3M KOH, extracted with ethyl acetate (3 x 15 ml). Organic extracts washed with brine, dried over $MgSO_4$, filtered and condensed under reduced pressure. Residue was immediately purified by silica flash column chromatography by gradient elution from 9:1 to 1:1 Hexanes/Ethyl Acetate to produce a light yellow oil (100 mg, 350 mmol, 50 %). Rf = 0.32 (8:2 Hexanes/Ethyl Acetate). Upon isolation the product is used immediately in the next reaction to minimize decomposition.

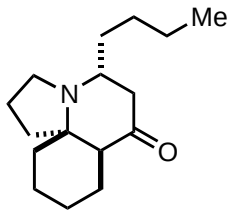

(5S,7aR,11aR)-5-butyloctahydro-1H-pyrrolo[2,1-j]quinolin-7(7aH)-one (9)

An oven dried flask charged with a magnetic stirbar and activated 4 Å molecular sieves was evacuated and backfilled with Ar. To the flask was added a solution of alkyl chloride 5 (62 mg, 0.22 mmol) in 10 ml DMF (dry, degassed) followed quickly by solid potassium tert-butoxide (100 mg, 0.89 mmol). The flask was purged with Ar and heated to 65 °C for 3h. During this time, the reaction goes from yellow to orange. After the flask cooled to rt, a saturated aqueous solution of NH_4Cl was added until the pH was ~8. EtOAc was added and the phases separated. Aqueous layer was extracted with EtOAc (2x) and the combined organic layers were washed with H_2O, brine, dried over $MgSO_4$ and rotovaped. Orange residue was purified immediately by flash chromatography by gradient elution from 9:1 to 1:1 Hex/EtOAc to yield a yellow oil (37 mg, 68%). $[\alpha]^{20}_D$ = +27°, c = 0.01 g/ml $CHCl_3$. Rf = 0.3 (19:1, DCM/MeOH). ^{1}H NMR (400 MHz, $CDCl_3$) δ 3.13 (1H, q, J = 8.4), 3.05 (1H, q, J = 8.2), 2.89 (1H, q, J = 7.3), 2.30 (1H, d, J = 8.0), 2.25-2.17 (3H, m), 1.95 (1H, dd, J = 9.1, 5.9), 1.85 (3H, quintet, J = 7.0), 1.69-1.64 (2H, m), 1.44-1.26 (12H, m), 0.89 (3H, t, J = 6.9). ^{13}C NMR (100 MHz, $CDCl_3$) δ 211.0, 67.2, 53.9, 50.9, 43.9, 42.8, 35.7, 34.9, 31.1, 28.3, 24.0, 22.8, 22.7, 21.8, 20.1, 14.0. IR (Thin Film) v 2934, 2862, 1705, 1559, 1449, 1355, 1328, 1211, 1170, 1125, 1104, 925. LRMS (MM-ES) *m/z* $[C_{16}H_{28}NO]^+$ calculated 250.2, found 250.2. Absolute and relative stereochemistry confirmed by X-ray analysis.

A.6.4 Competition Experiment of Alkenyl Isocyanates with 3-Phenyl Propyne

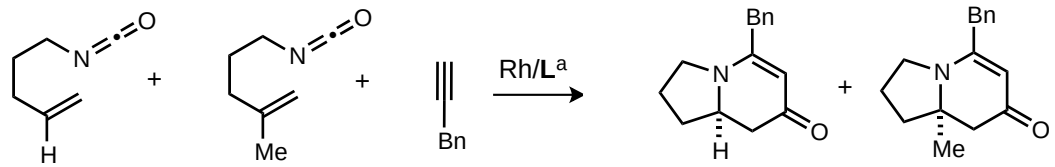

2m **2g** **4m** **4g**

1 equiv. 1 equiv. 1 equiv. 1:1 **4m** / **4g** 45%

An oven-dried round bottom flask was charged with $[Rh(C_2H_4)_2Cl]_2$ (4 mg, 0.01 mmol) and CKPhos (20 mg, 0.02 mmol) and fitted with an oven-dried reflux condenser topped with a rubber septum in an inert atmosphere (N_2) glove box. Upon removal from the glove box, 2 ml of toluene was added via syringe and the resulting yellow solution was stirred at ambient temperature for 15 min. To this solution, benzyl acetylene (0.20 mmol) and isocyanates **2m** and **2g** (0.20 mmol, 0.20 mmol) in 6 ml of toluene was added via syringe. An additional 2 ml of toluene was used to wash down the residue and added to the reaction mixture. The reaction mixture was heated to 110 °C in an oil bath. After refluxing for 16 hours, the reaction mixture was cooled to 23 °C, concentrated in *vacuo*, and purified by flash column chromatography (19:1 EtOAc:MeOH) to yield a 1:1 mixture of two vinylogous amide products **4m** and **4g** as shown above.

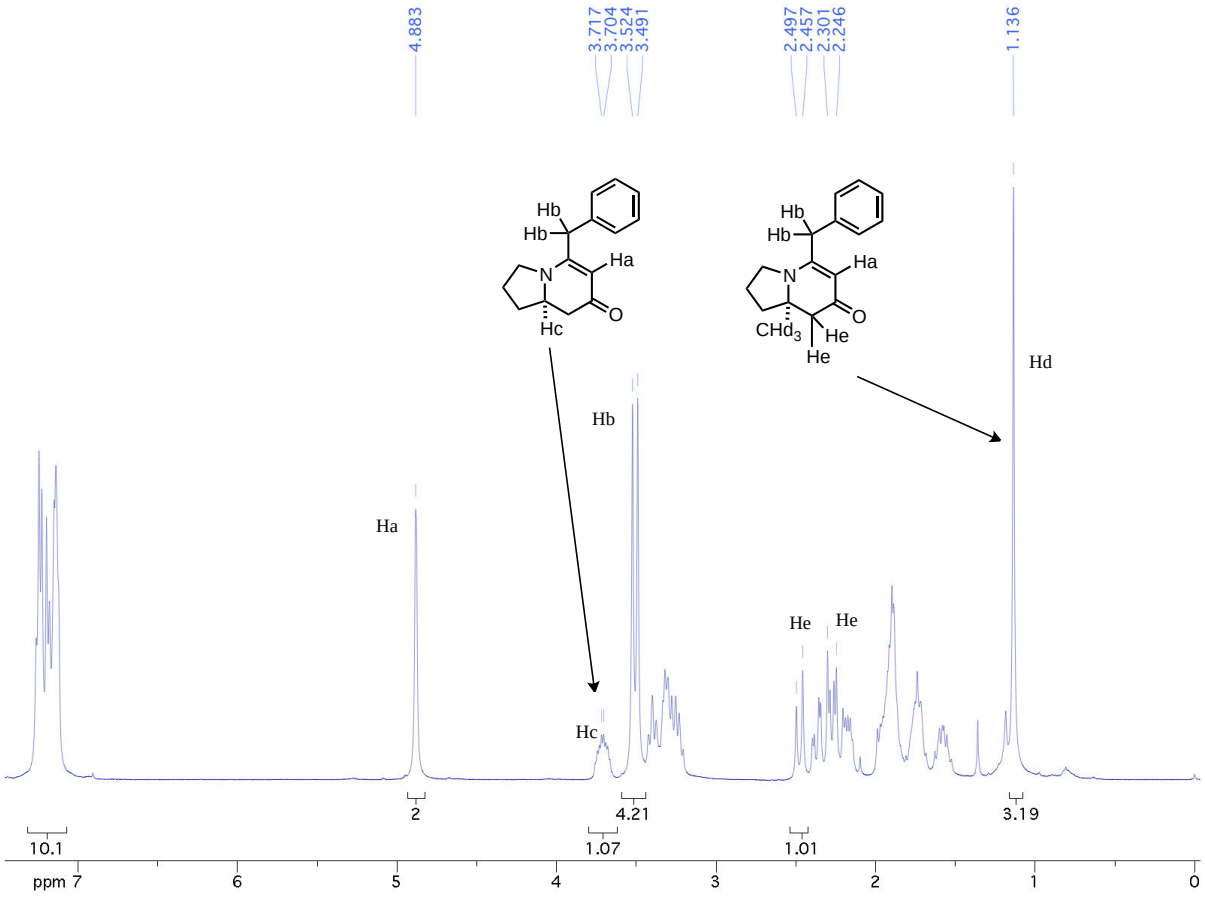
4.883
3.717
3.704
3.524
3.491
2.497
2.457
2.301
2.246
1.136
Hb
Hb
Ha
N
O
Hc
CHd3
He
He
Hd
Hb
Ha
Hc
He
He
2
4.21
3.19
10.1
1.07
1.01
ppm 7
6
5
4
3
2
1
0

Figure A.6.1

A.6.5 ^{1}H-NMR and ^{13}C-NMR Spectra

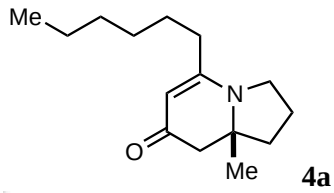

4a

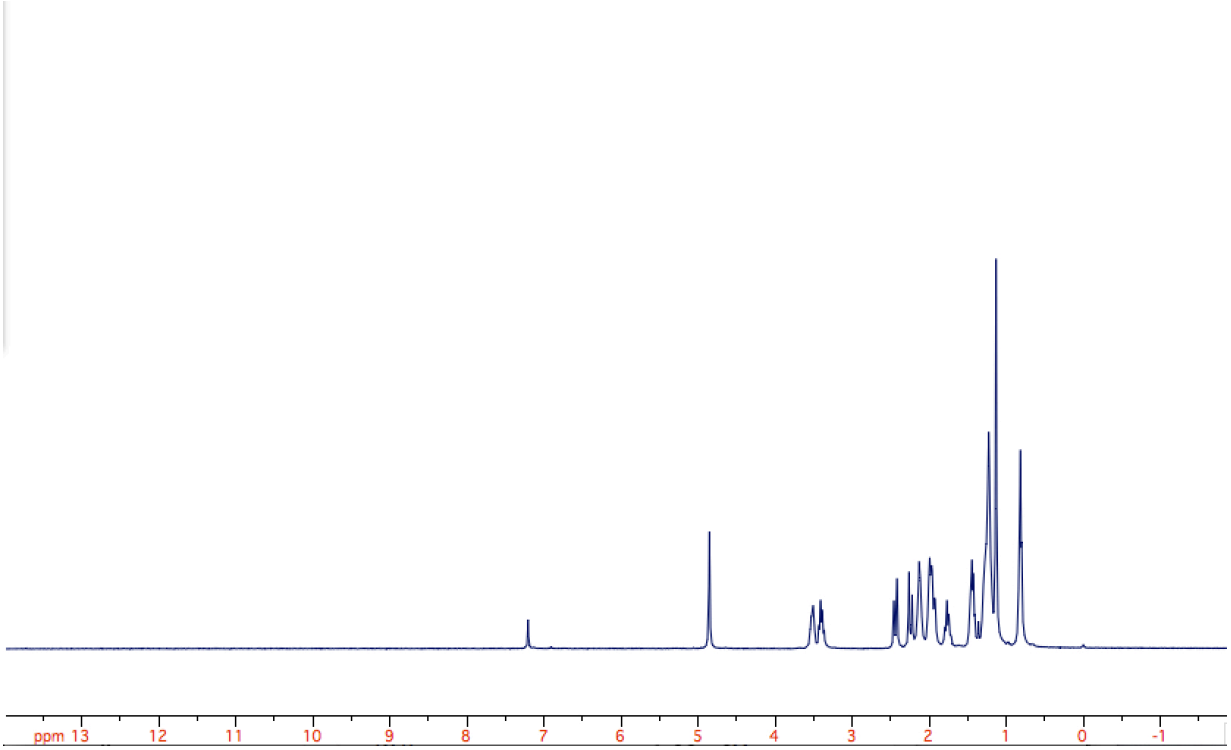

Figure A.6.2

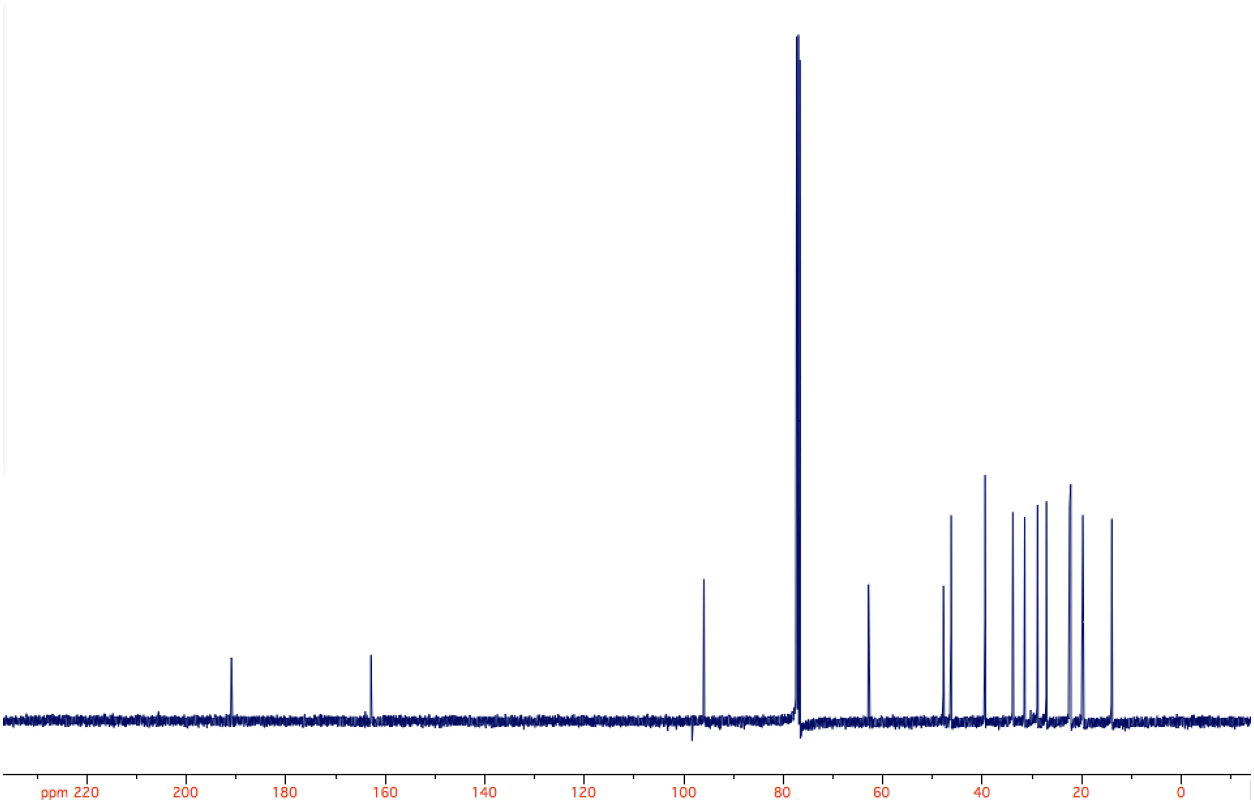

Figure A.6.3

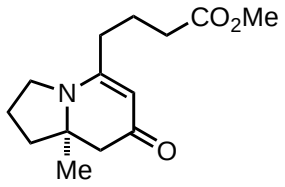

4b

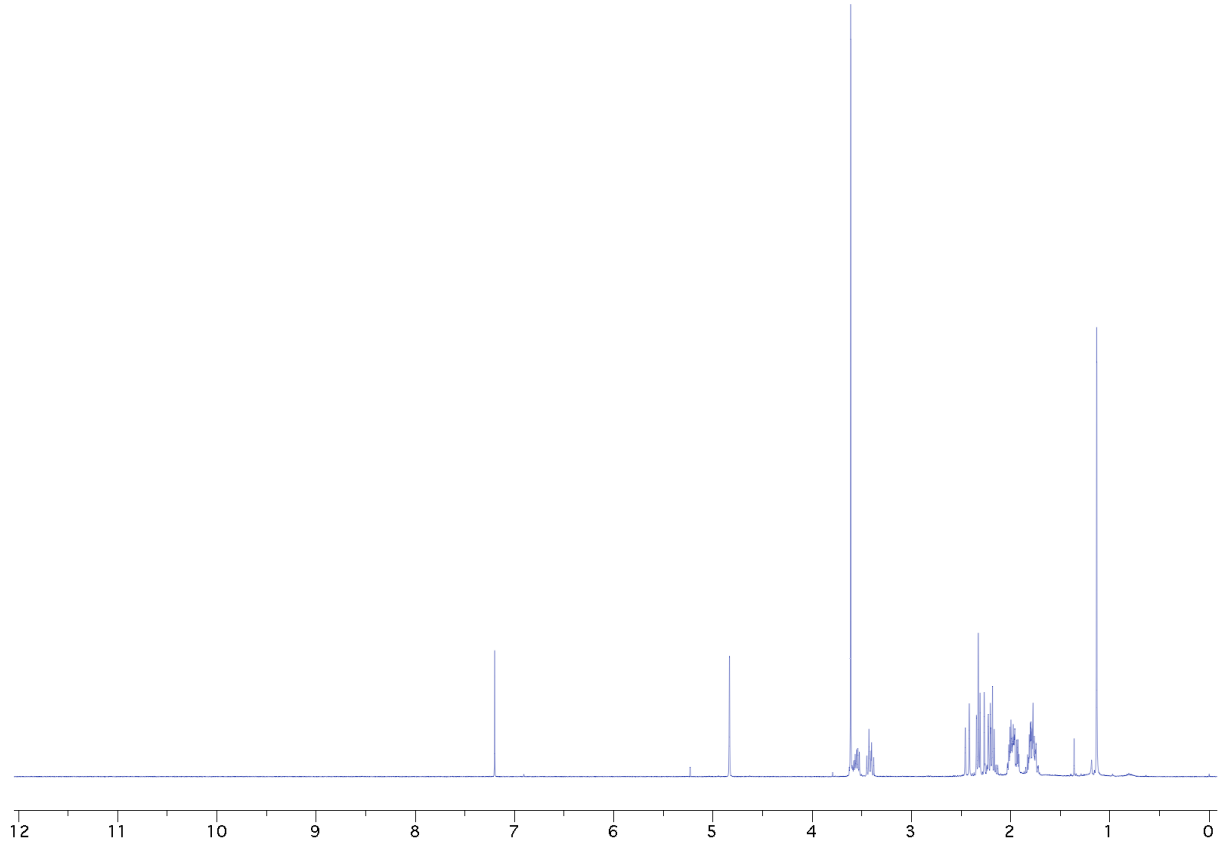

Figure A.6.4

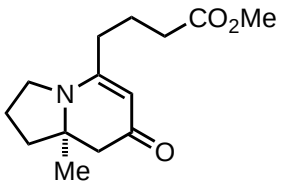

4b

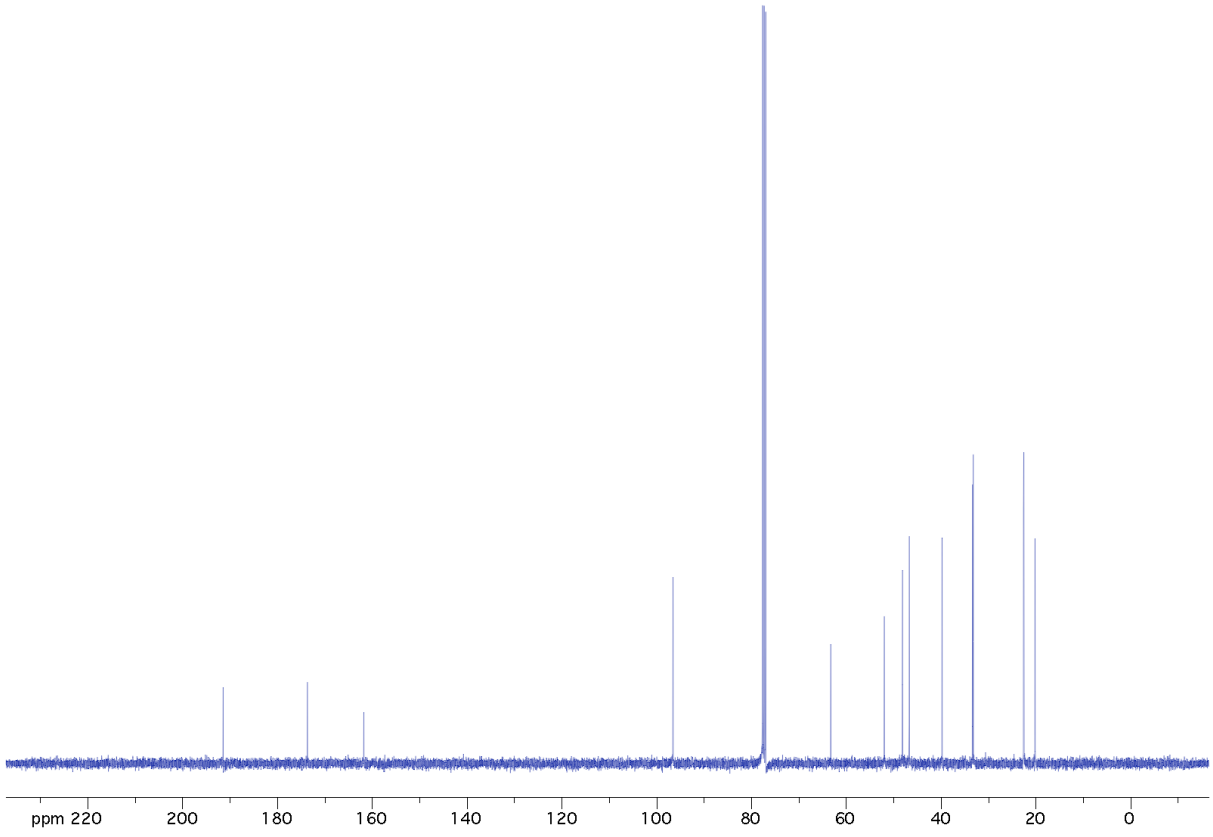

Figure A.6.5

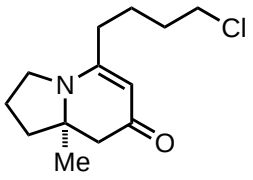

4c

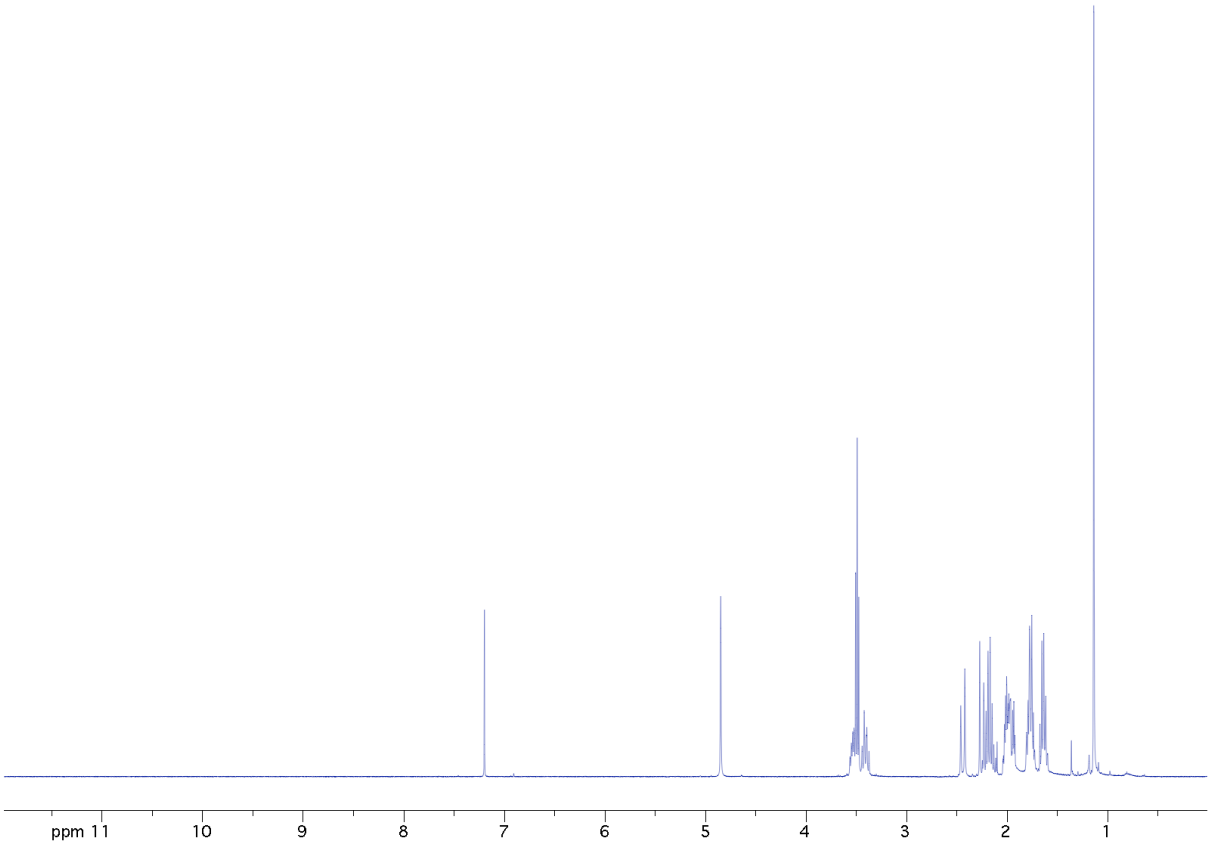

Figure A.6.6

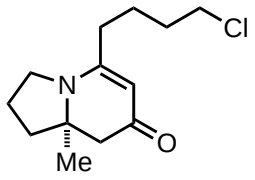

4c

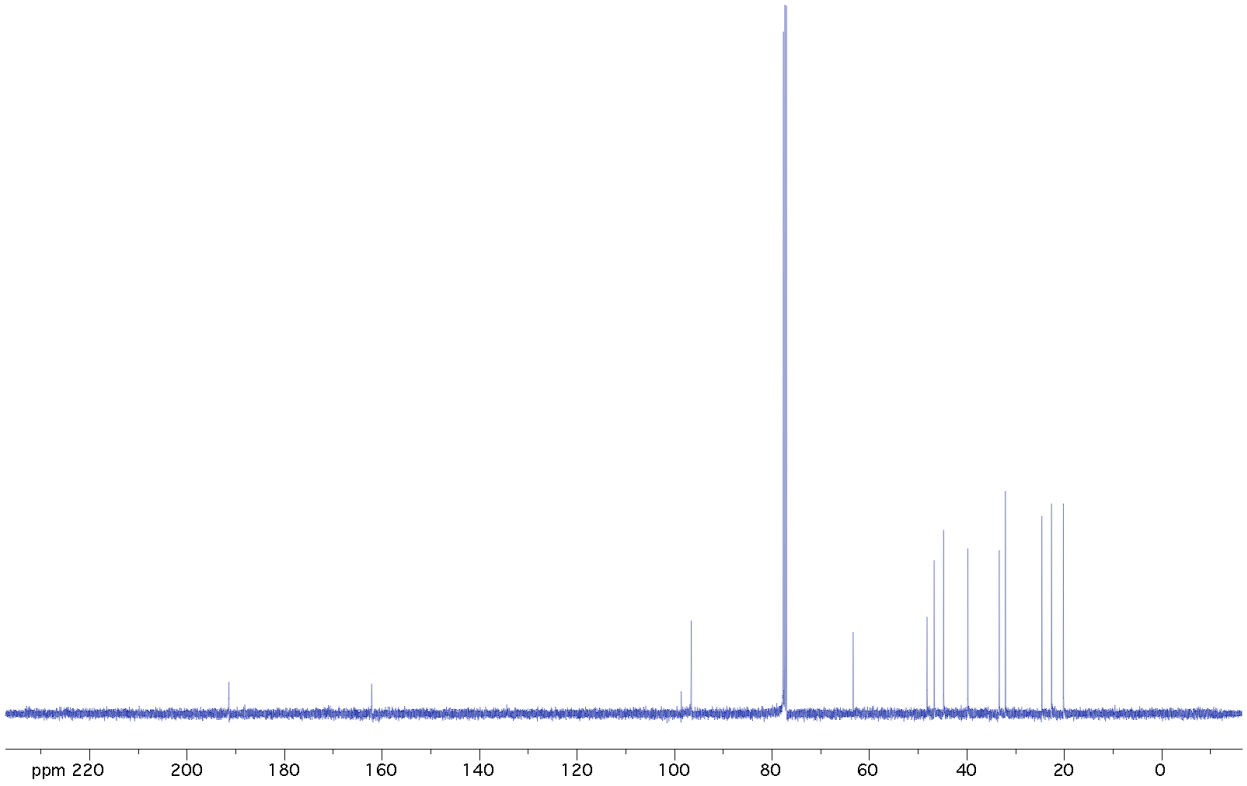

Figure A.6.7

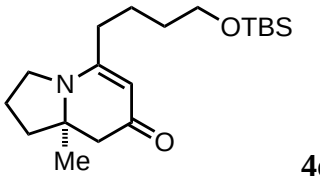

4d

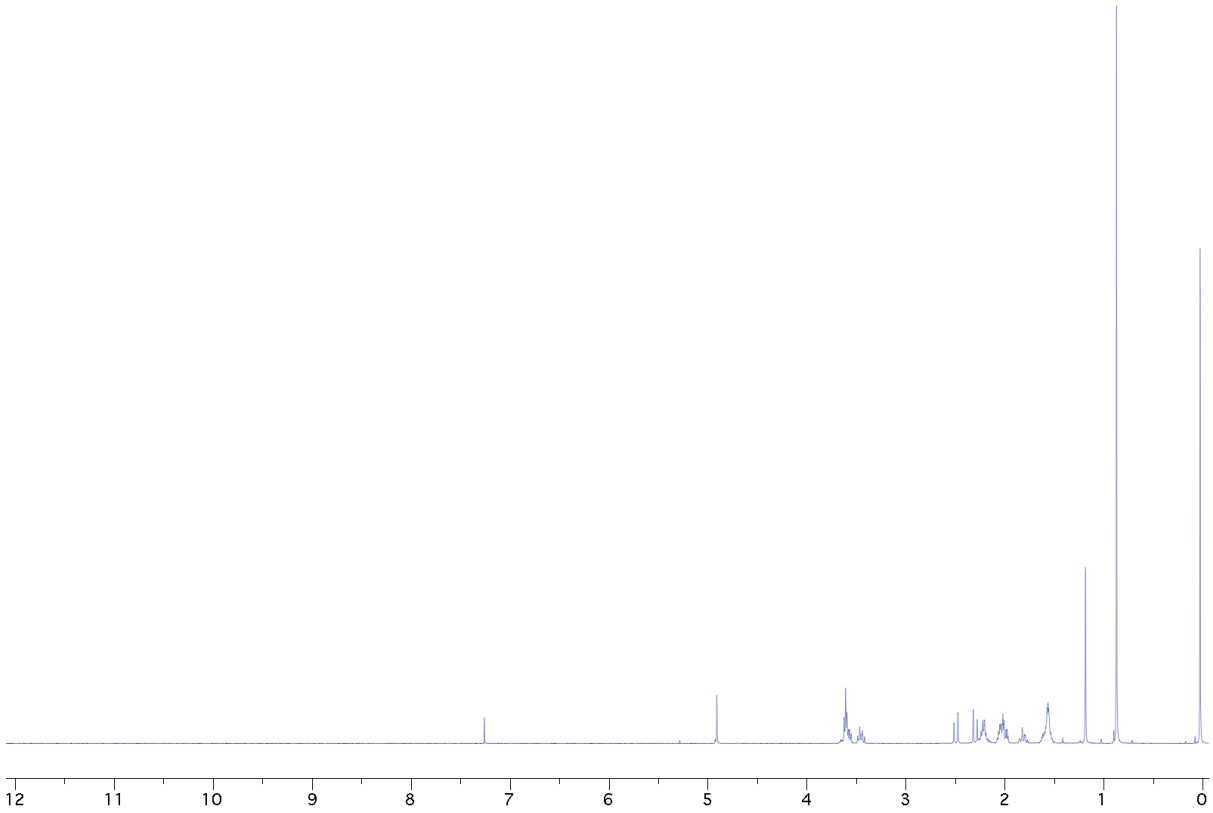

Figure A.6.8

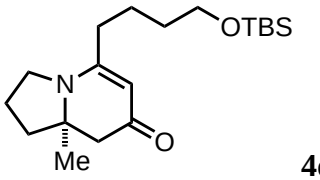

4d

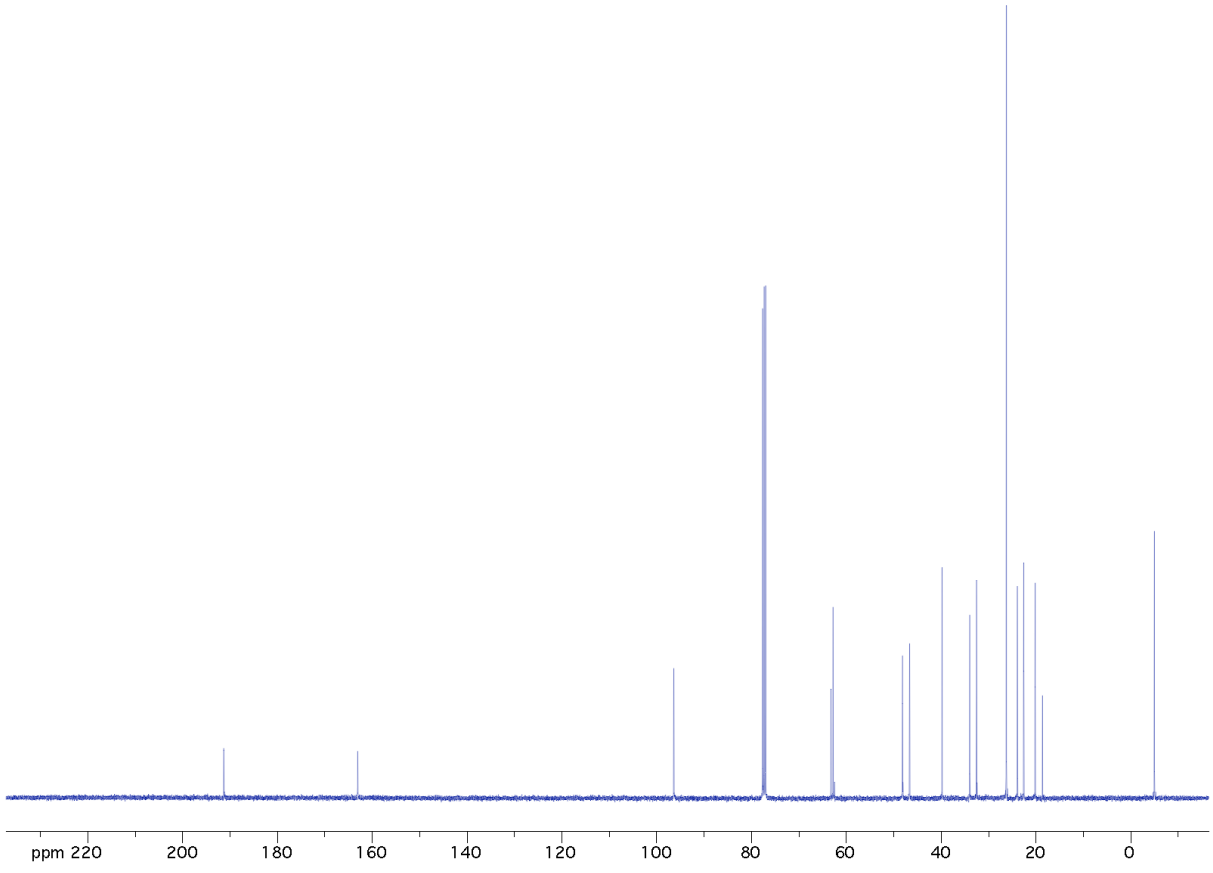

Figure A.6.9

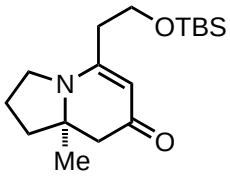

4e

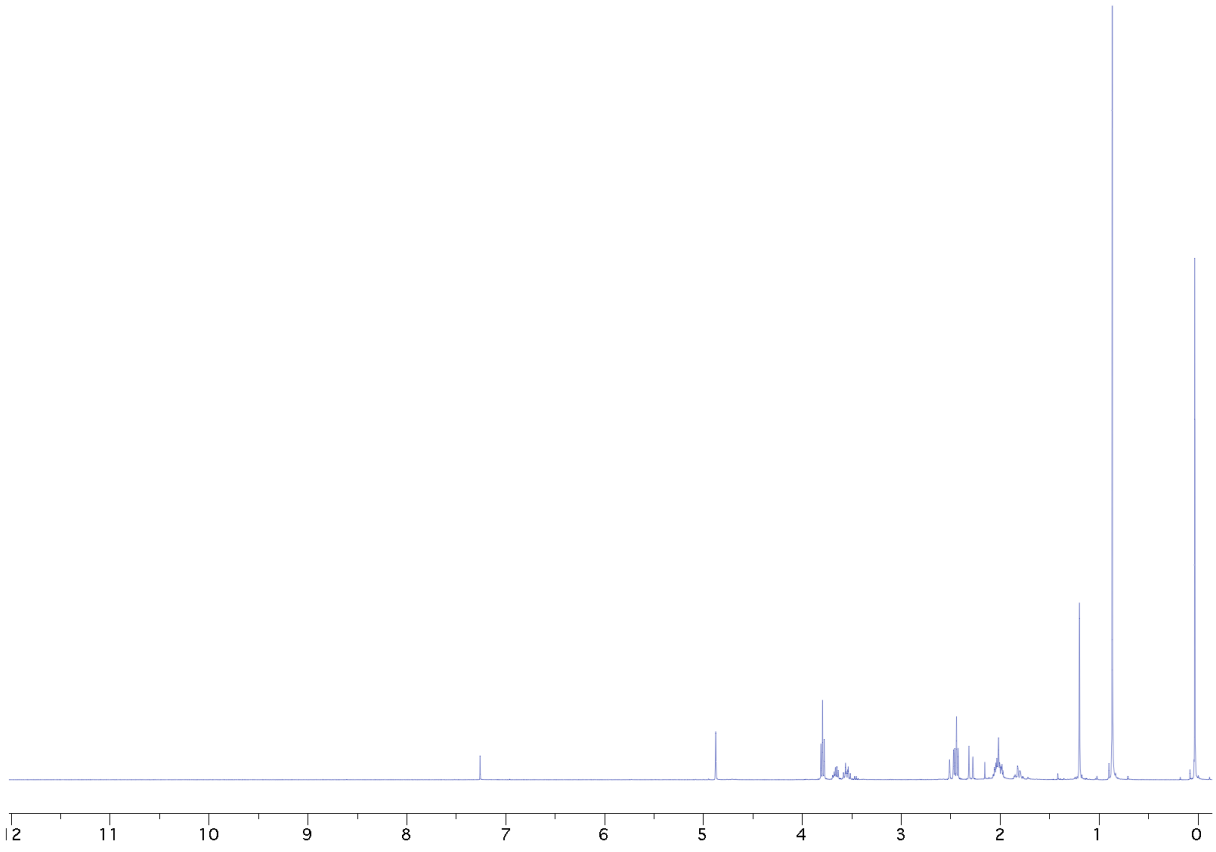

Figure A.6.10

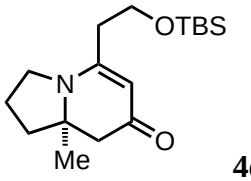

4e

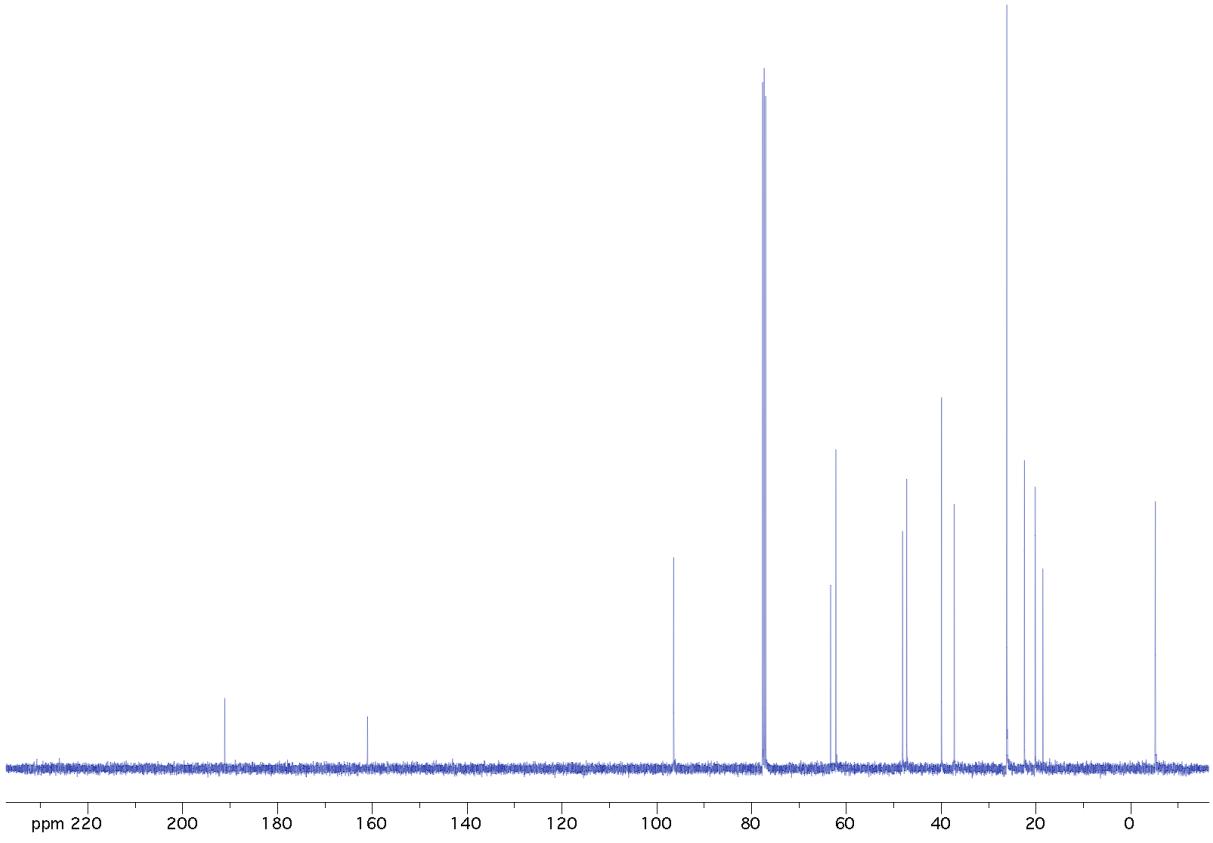

Figure A.6.11

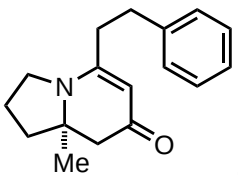

4f

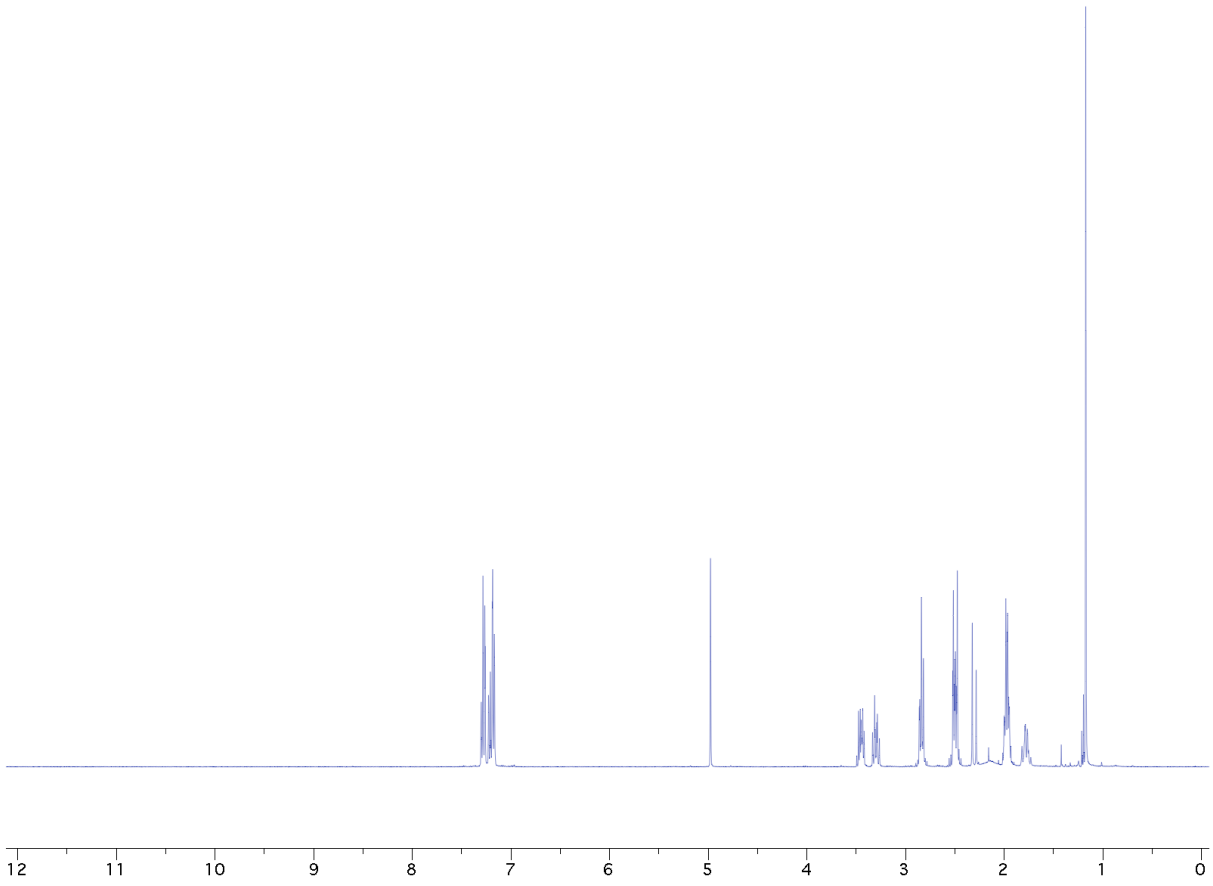

Figure A.6.12

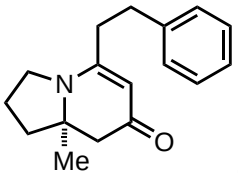

4f

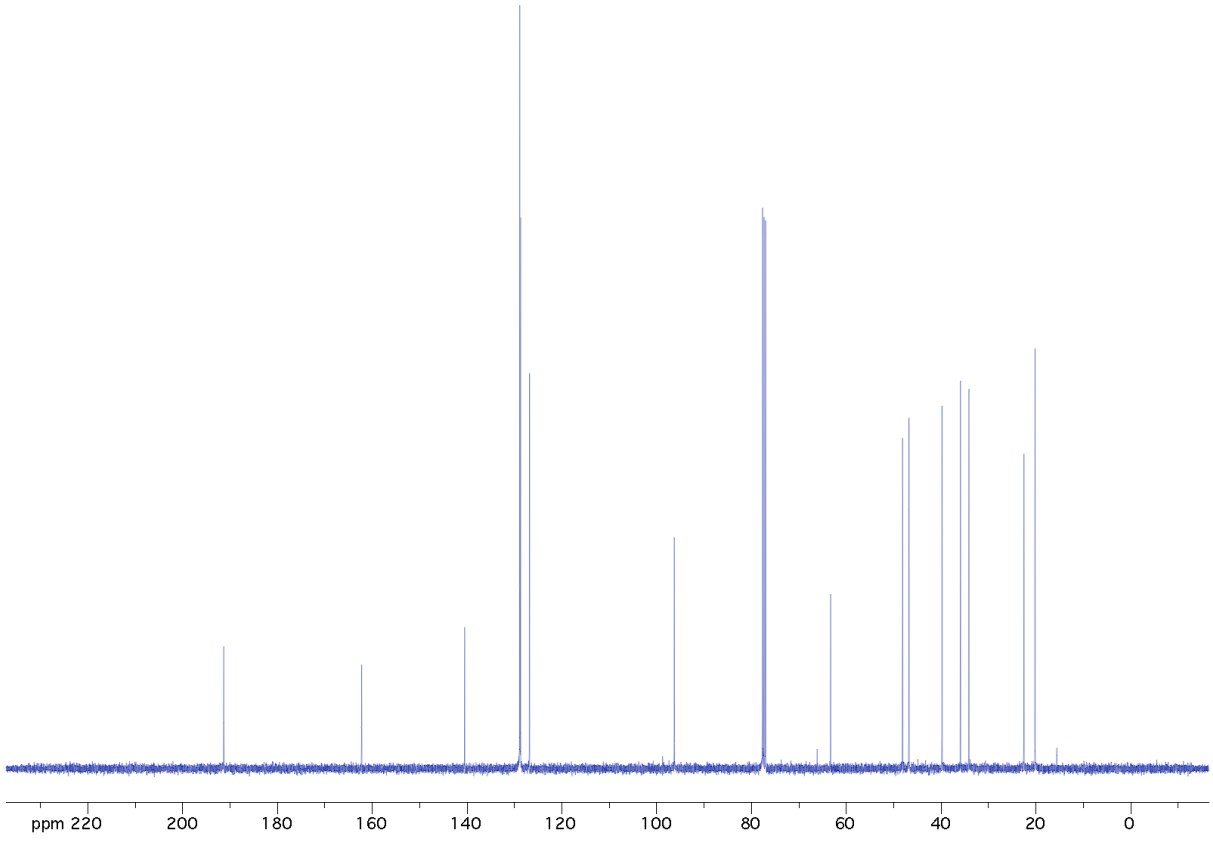

Figure A.6.13

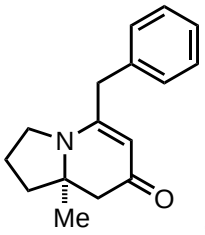

4g

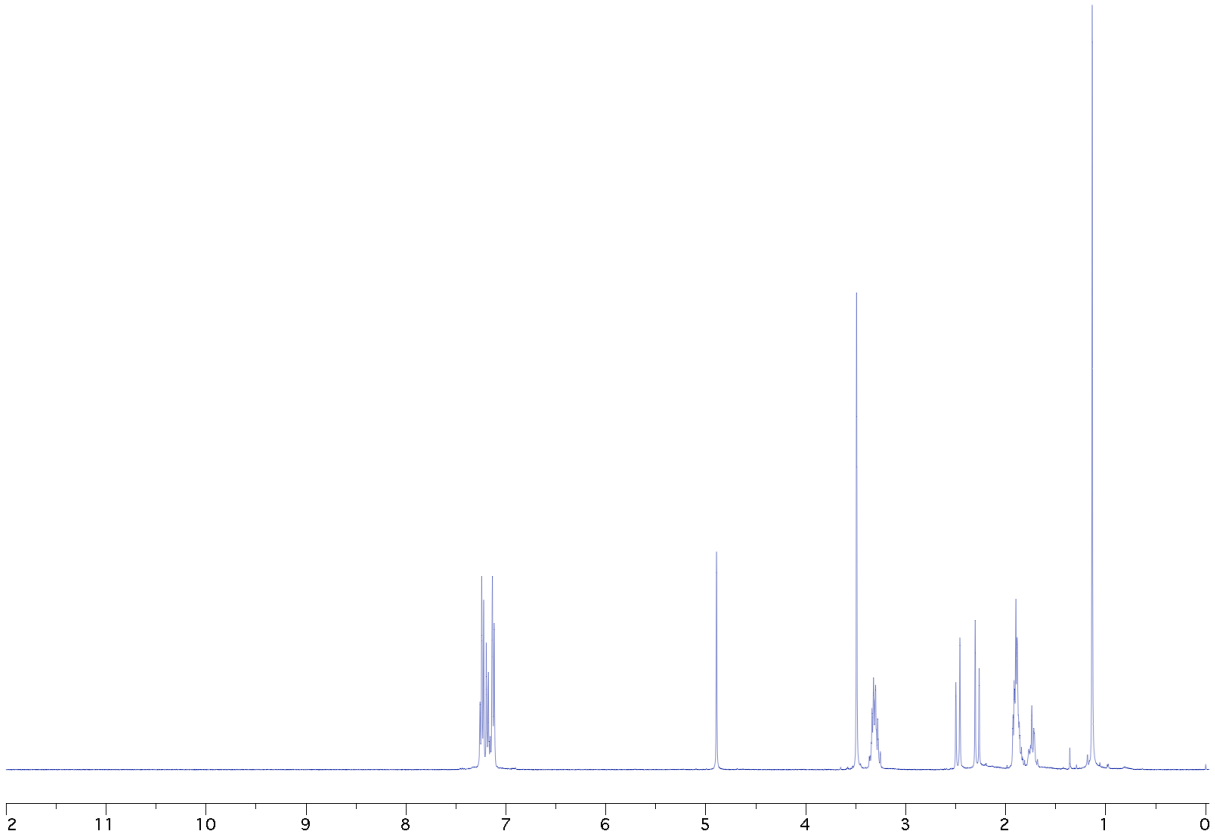

Figure A.6.14

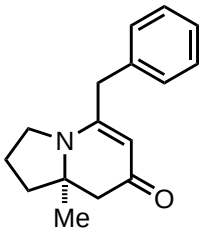

4g

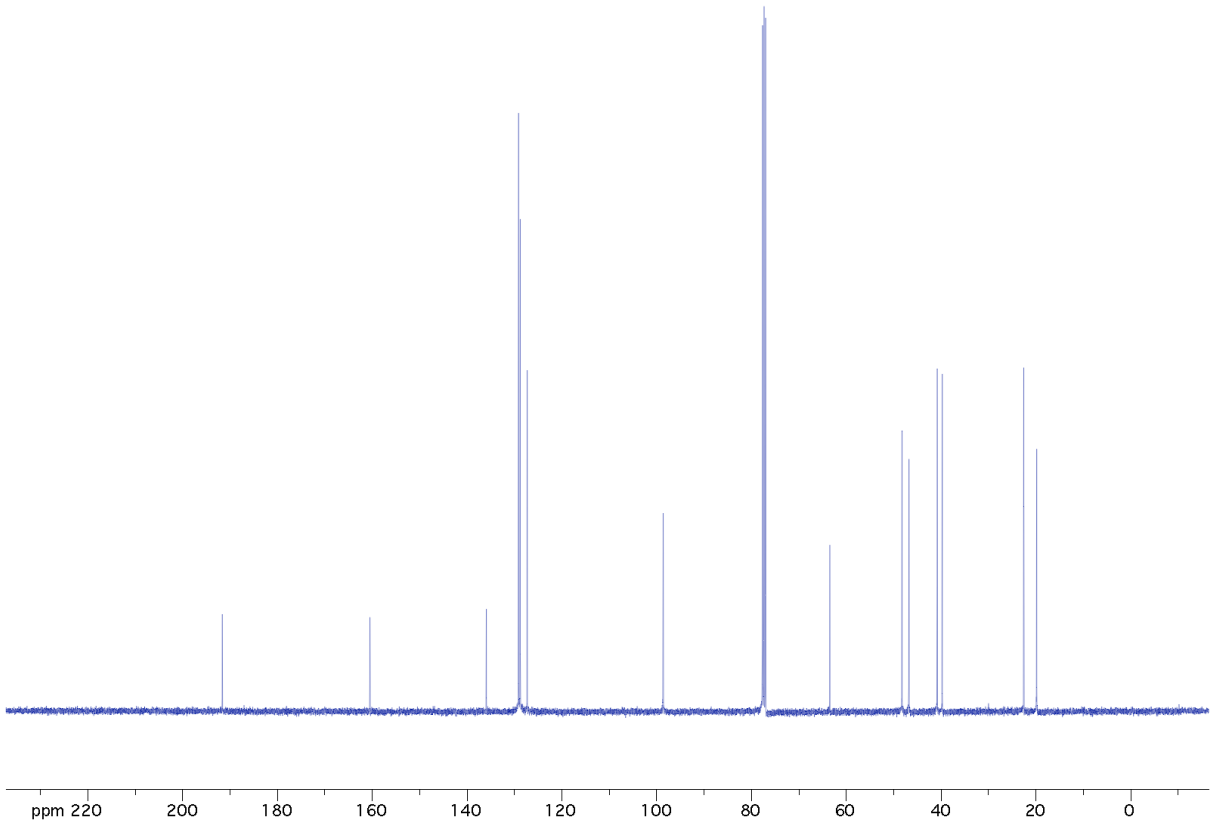

Figure A.6.15

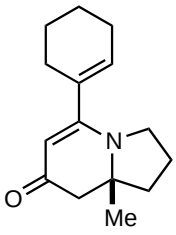

4h (crude 1HNMR)

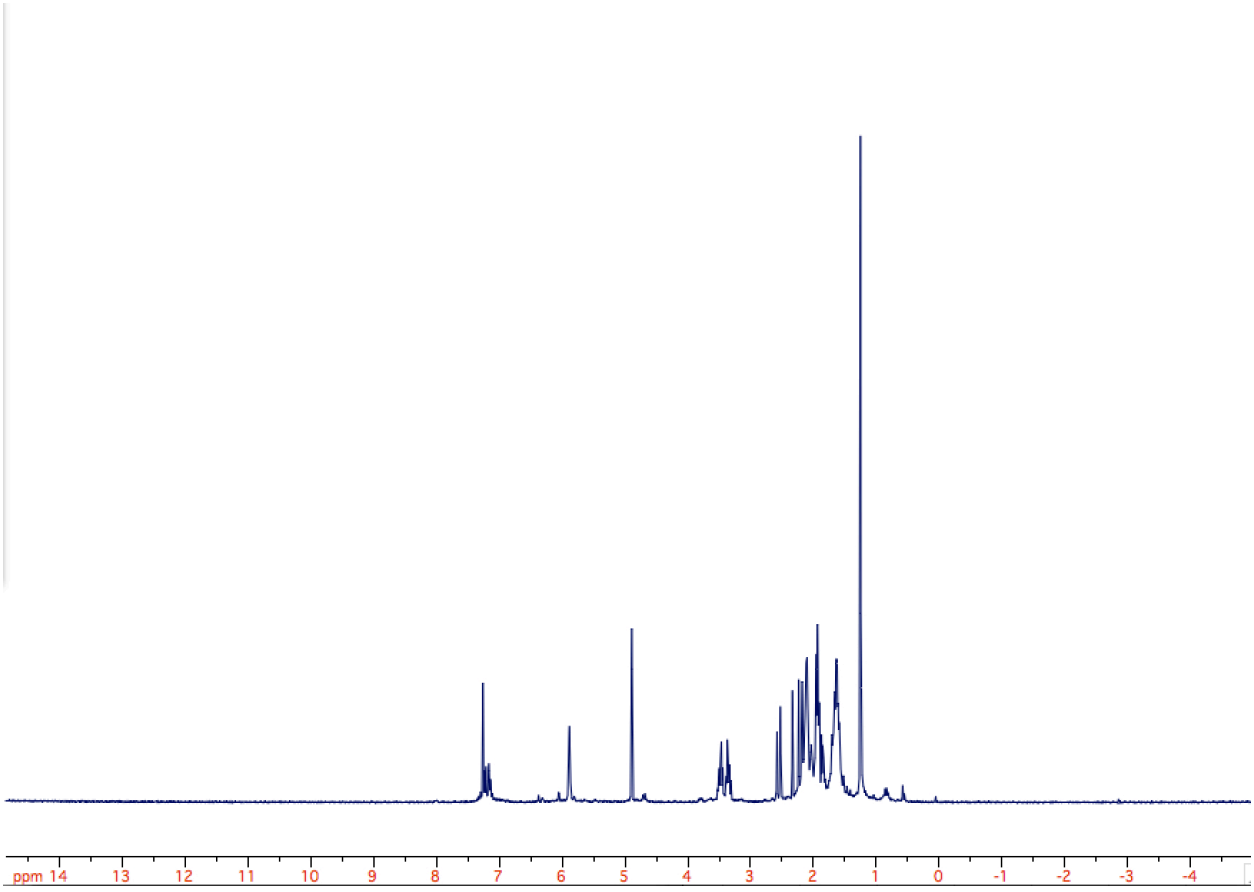

Figure A.6.16

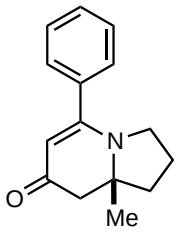

4i (crude 1HNMR)

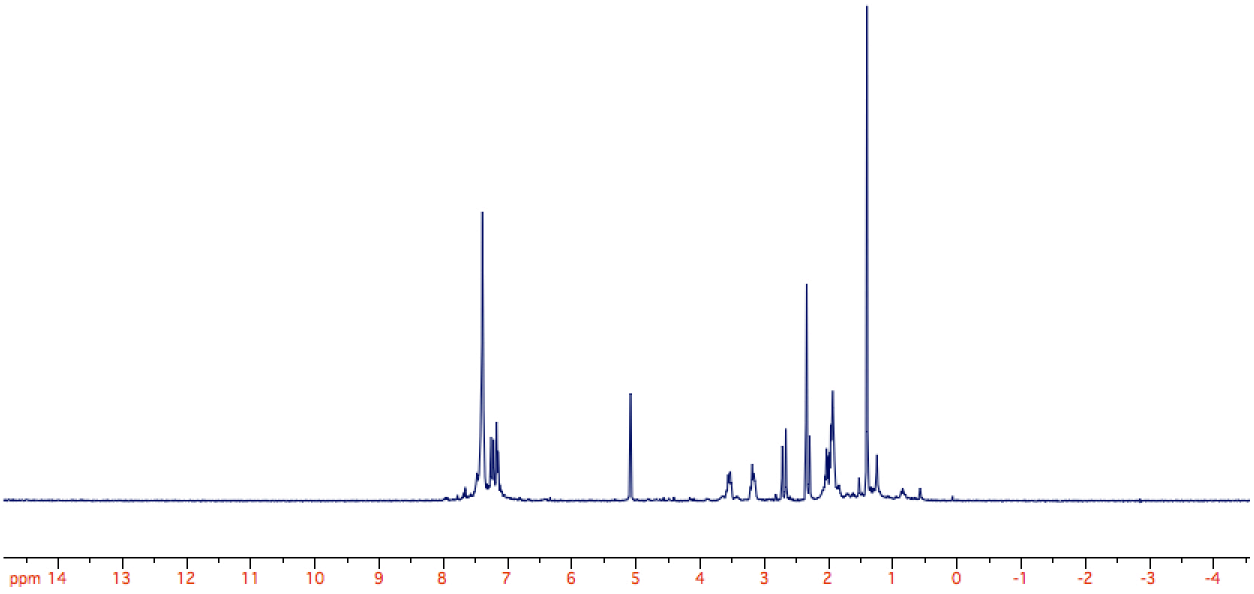

Figure A.6.17

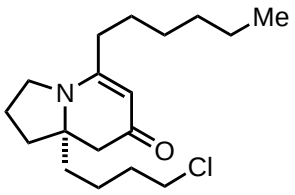

4j

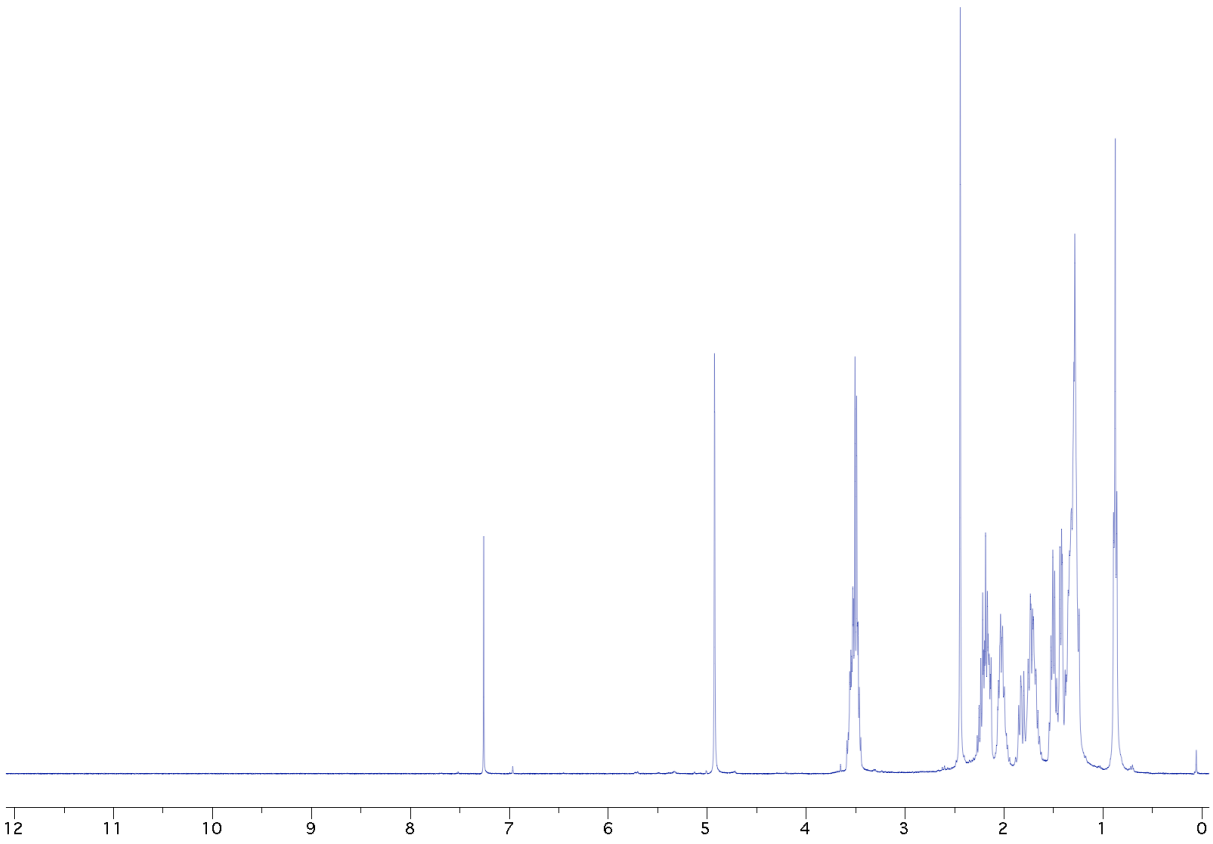

Figure A.6.18

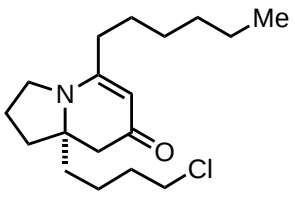

4j

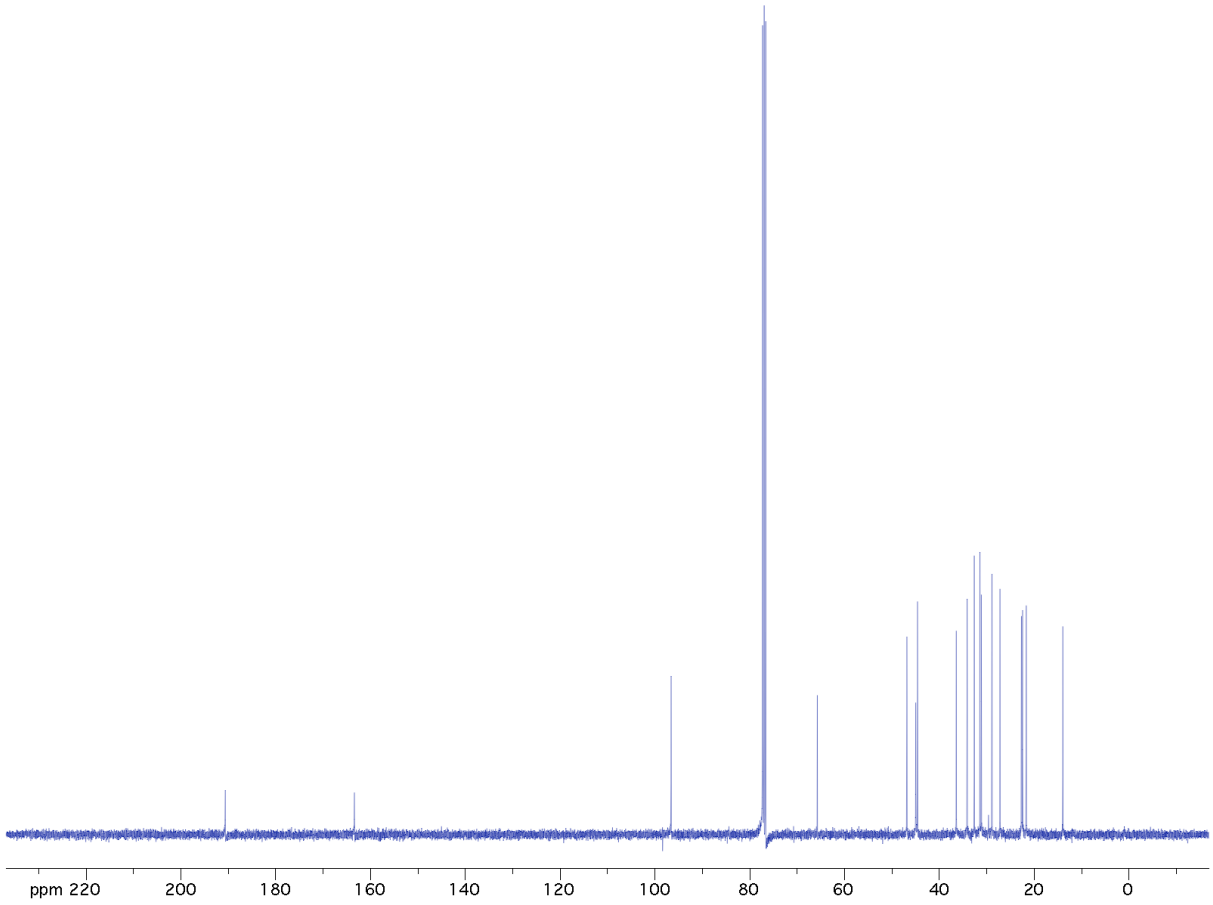

Figure A.6.19

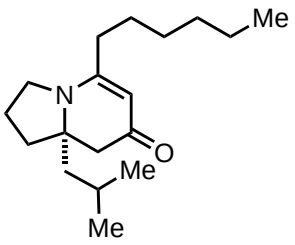

4k

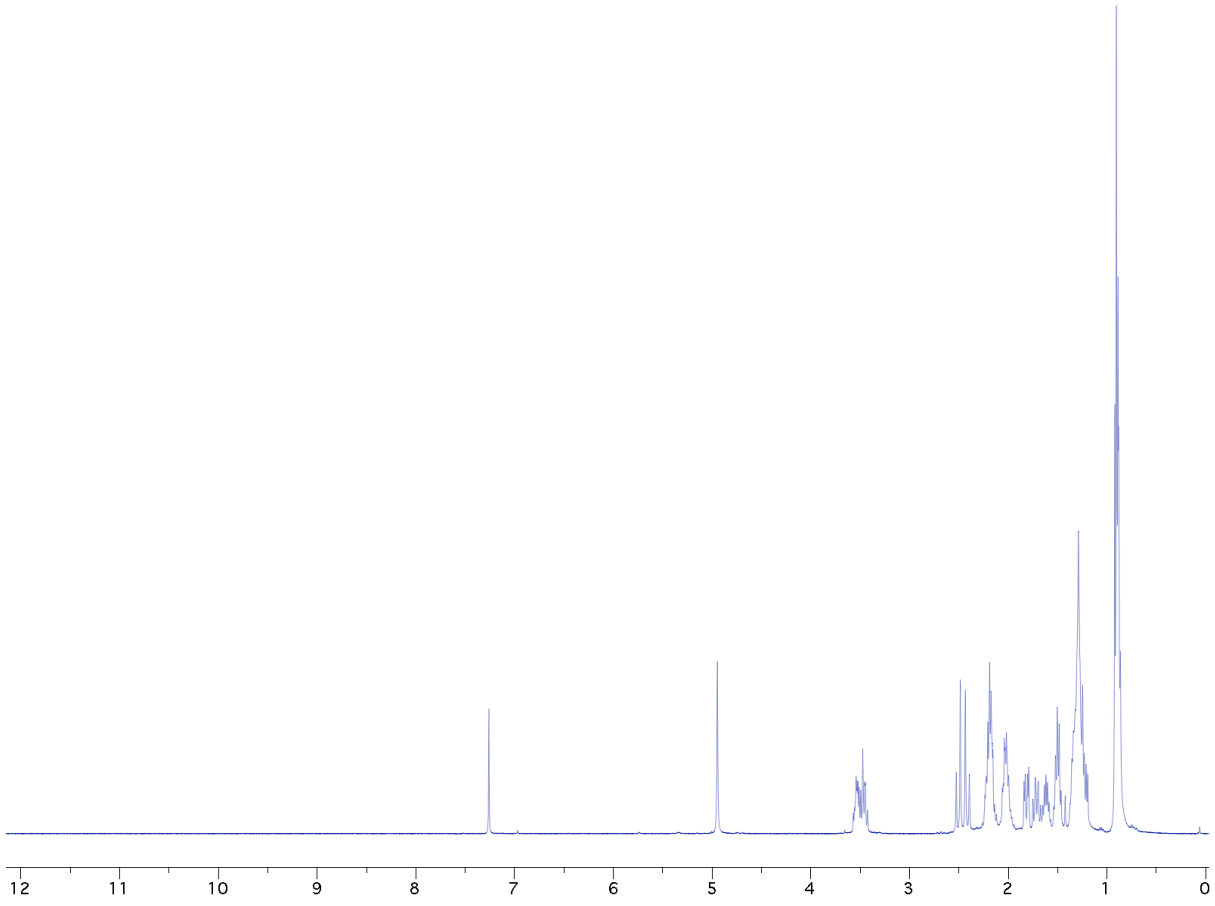

Figure A.6.20

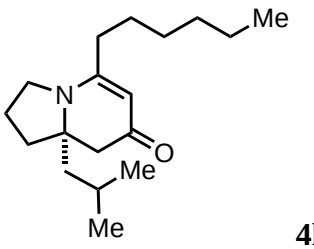

4k

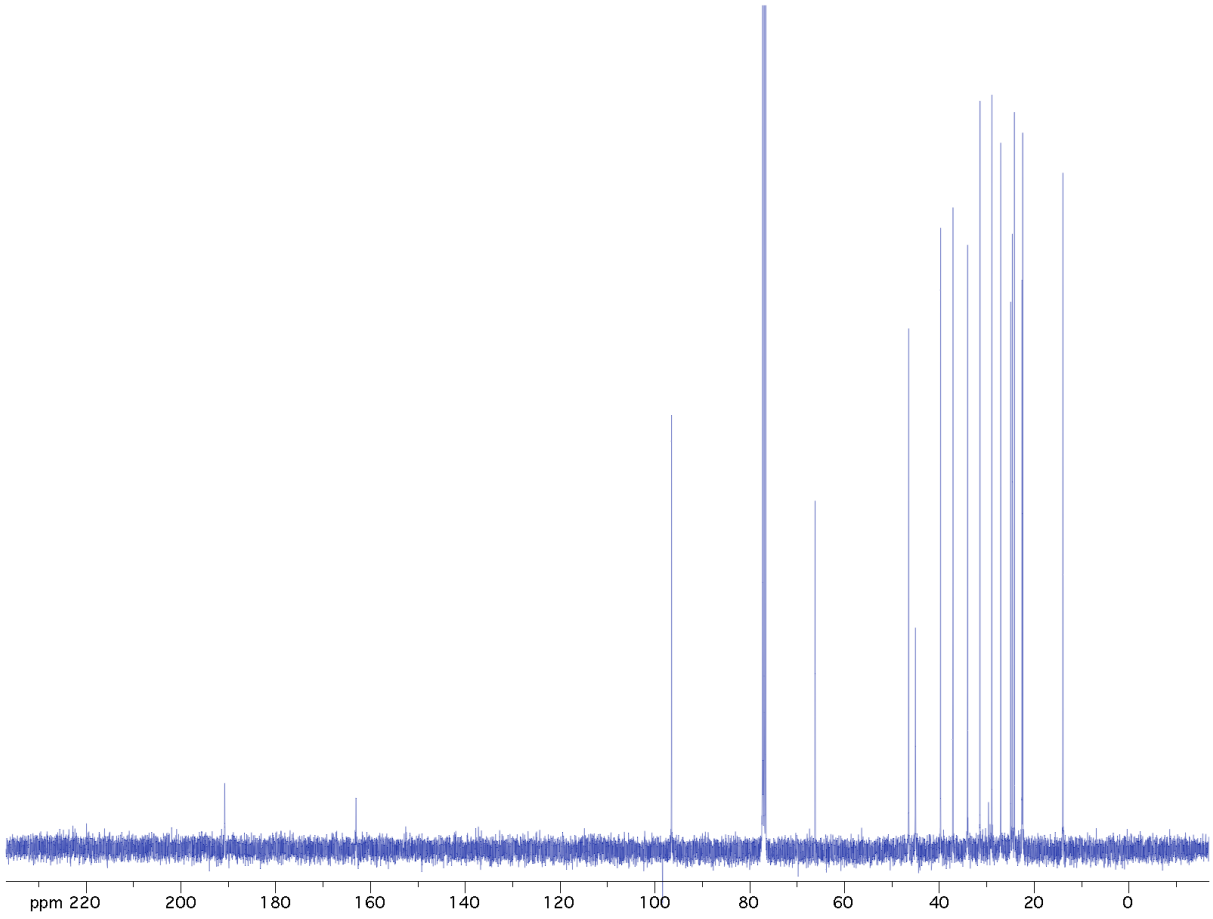

Figure A.6.21

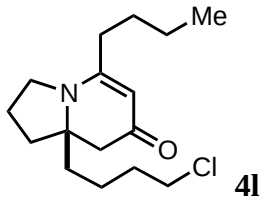

4l

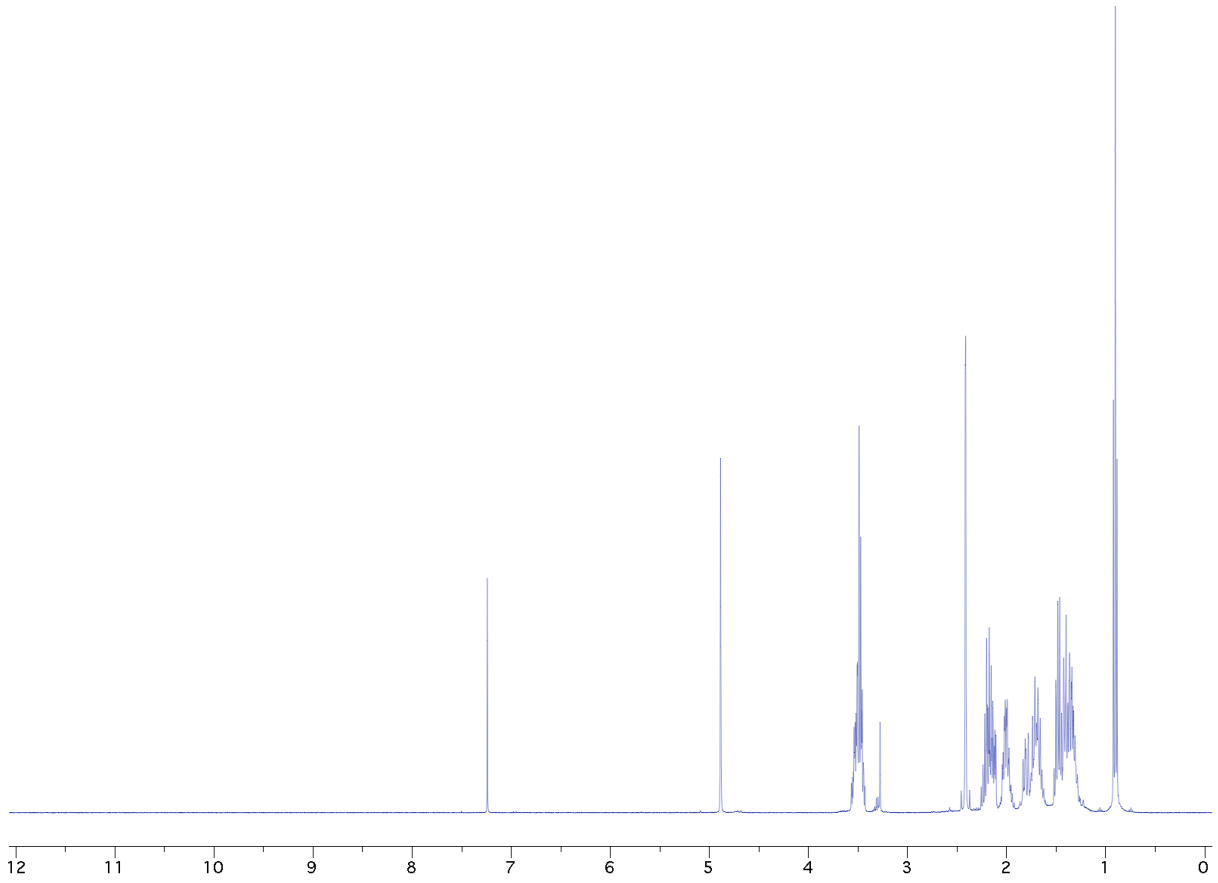

Figure A.6.22

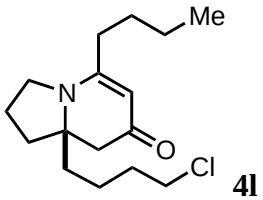

4l

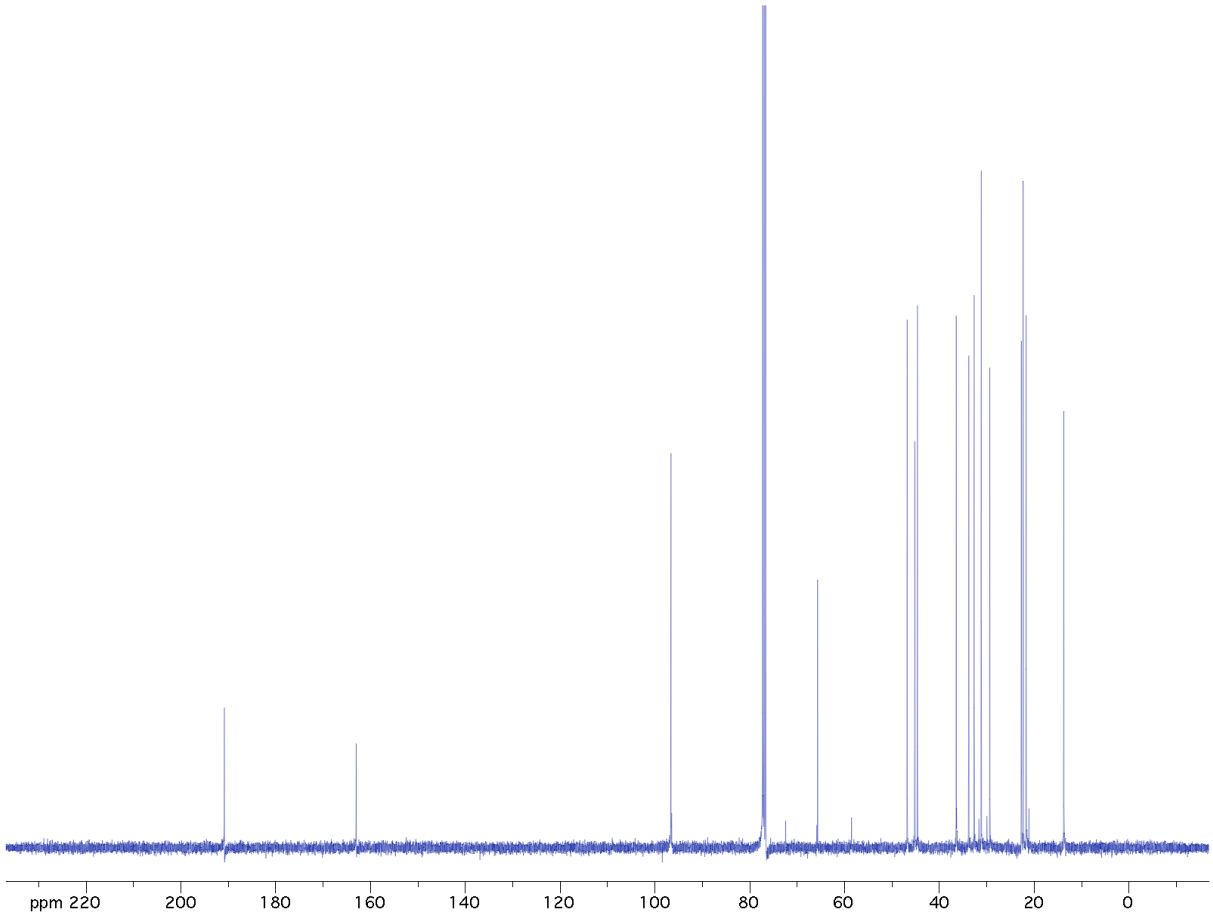

Figure A.6.23

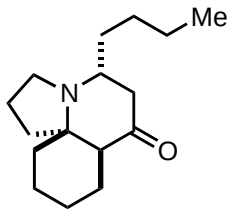

9

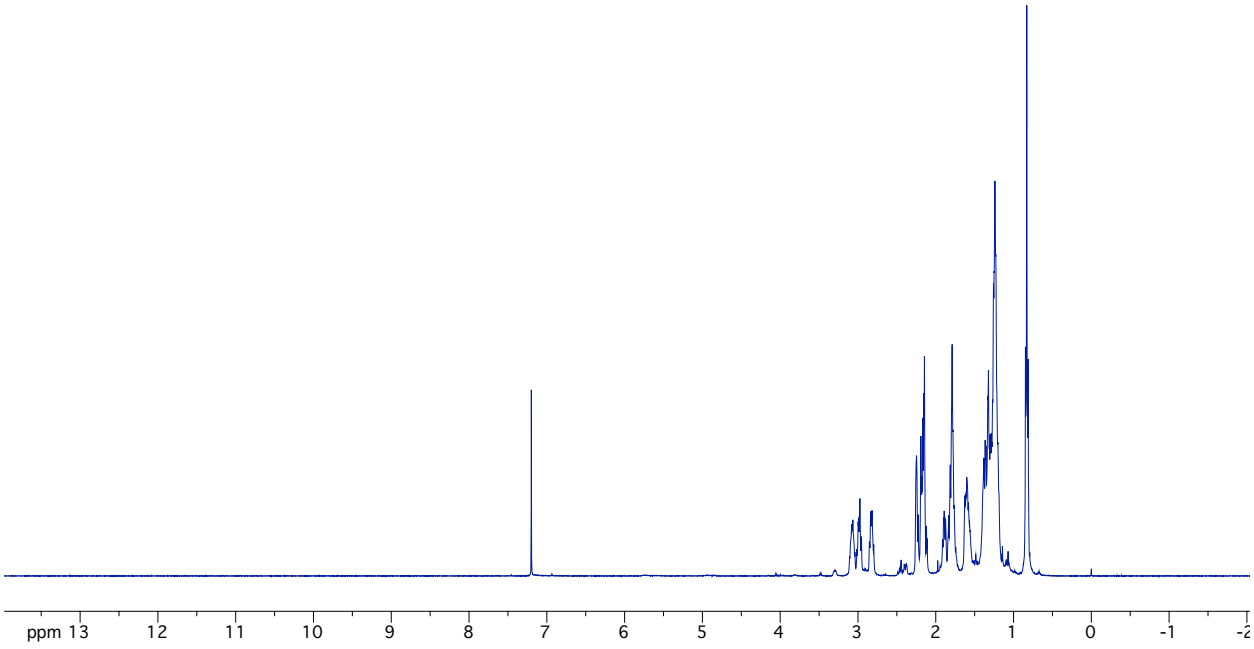

Figure A.6.24

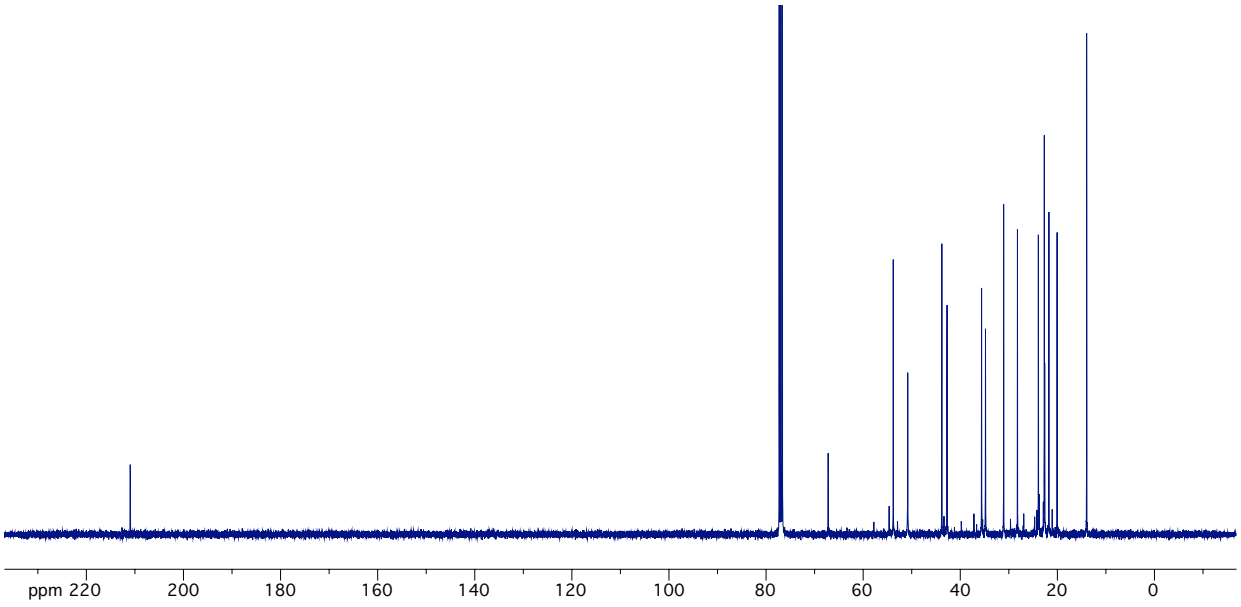

Figure A.6.25

A.6.6 Synthesis and X-ray Analysis of the Cylindricine Core 9-HCl salt

X-ray quality crystals were obtained by adding 1M solution of HCl in anhydrous ether to a vial containing **8** which turns a cloudy white. Solvent and excess HCl was removed by rotary evaporation under reduced pressure. The resultant residue was dissolved in a minimal amount of DCM and layered with hexanes. Slow evaporation provided yellow crystals suitable for X-ray analysis.

All single crystals were coated in oil, transferred to a goniometer head, and mounted on a Bruker Kappa Apex CCD diffractometer under a stream of N_2. All data collections were performed with Mo Kα radiation and a graphite monochromator. Data sets were taken with complete coverage and fourfold redundancy at 120 °K. Data was integrated and corrected for absorption effects with the Apex 2 software package.[3] Structures were solved with the SHELXTL software package.[4] All non-hydrogen atoms were refined with anisotropic thermal parameters and hydrogen atoms placed in idealized positions. Crystal data and structure parameters are provided as CIF files.

[3] Bruker AXS Inc., 5465 East Chervl Parkway, Madison, WI 53711-5373 USA

[4] Sheldrick, G. (1997) *SHELXL-97 Program for Crystal Structure Refinement*, Institüt für Anorganische Chemie der Universität, Göttingen, Germany.

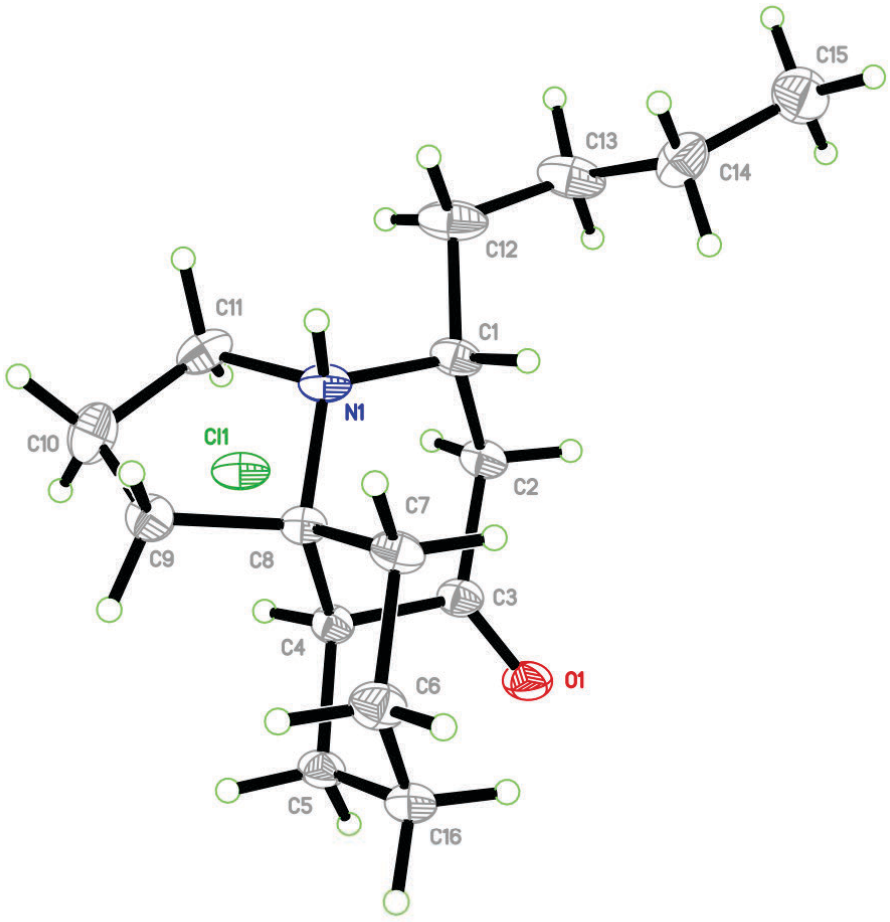

Table A.6.1. Crystal data and structure refinement for **9**.

Identification code	rovis159_0m	
Empirical formula	C_{16} H_{28} Cl N O	
Formula weight	284.84	
Temperature	100(2) K	
Wavelength	0.71073 Å	
Crystal system	Orthorhombic	
Space group	*P* $2_12_12_1$	
Unit cell dimensions	*a* = 6.9763(5) Å	α= 90°.
	b = 13.1038(10) Å	β= 90°.

	c = 17.5908(13) Å γ = 90°.
Volume	1608.1(2) Å^3
Z	4
Density (calculated)	1.177 Mg/m^3
Absorption coefficient	0.232 mm^{-1}
F_{000}	620
Crystal size	0.23 x 0.14 x 0.07 mm^3
Theta range for data collection	1.94 to 25.37°.
Index ranges	-8 ≤ h ≤ 8, -15 ≤ k ≤15, -21 ≤ l ≤ 21
Reflections collected	24048
Independent reflections	2954 [R_{int} = 0.0472]
Completeness to theta = 25.37°	100.0 %
Absorption correction	Multi-scan
Max. and min. transmission	0.9835 and 0.9482
Refinement method	Full-matrix least-squares on F^2
Data / restraints / parameters	2954 / 0 / 178
Goodness-of-fit on F^2	1.061
Final R indices [I>2sigma(I)]	R1 = 0.0599, wR2 = 0.1535
R indices (all data)	R1 = NaN, wR2 = 0.1661
Absolute structure parameter	-0.05(13)
Largest diff. peak and hole	0.926 and -0.316 e.Å^{-3}

Table A.6.2. Atomic coordinates (x 10^4) and equivalent isotropic displacement parameters ($Å^2$x 10^3) for Rovis159_0m. U(eq) is defined as one third of the trace of the orthogonalized U^{ij} tensor.

	x	y	z	U(eq)
C(1)	2593(5)	1393(3)	1400(3)	40(1)
C(2)	4558(5)	1666(3)	1082(2)	39(1)
C(3)	4858(5)	2792(3)	917(2)	38(1)
C(4)	4150(5)	3512(3)	1535(2)	34(1)
C(5)	4227(6)	4626(3)	1284(2)	40(1)
C(6)	676(6)	4634(3)	1031(3)	48(1)
C(7)	590(6)	3508(3)	1236(3)	41(1)
C(8)	2129(5)	3246(3)	1824(2)	32(1)
C(9)	1723(6)	3695(3)	2606(2)	42(1)
C(10)	2757(8)	3009(4)	3170(3)	59(1)
C(11)	2973(6)	1996(3)	2785(2)	45(1)
C(12)	2478(6)	310(3)	1721(3)	62(1)
C(13)	2846(7)	-529(3)	1172(3)	64(1)
C(14)	1428(8)	-592(4)	569(3)	60(1)
C(15)	1703(8)	-1597(4)	52(3)	72(2)
C(16)	2642(7)	4892(3)	717(2)	49(1)
Cl(1)	7999(1)	1757(1)	2587(1)	50(1)
N(1)	2005(5)	2122(2)	2018(2)	36(1)
O(1)	5758(5)	3077(2)	379(2)	52(1)

Table A.6.3. Bond lengths [Å] and angles [°] for Rovis159_0m.

C(1)-N(1)	1.505(5)	C(3)-C(2)-C(1)	115.0(3)
C(1)-C(2)	1.522(5)	O(1)-C(3)-C(2)	121.8(4)
C(1)-C(12)	1.530(6)	O(1)-C(3)-C(4)	122.9(4)
C(2)-C(3)	1.519(6)	C(2)-C(3)-C(4)	114.9(3)
C(3)-O(1)	1.195(5)	C(3)-C(4)-C(5)	112.0(3)
C(3)-C(4)	1.521(6)	C(3)-C(4)-C(8)	113.2(3)
C(4)-C(5)	1.526(6)	C(5)-C(4)-C(8)	110.2(3)
C(4)-C(8)	1.538(5)	C(4)-C(5)-C(16)	112.4(3)
C(5)-C(16)	1.529(6)	C(16)-C(6)-C(7)	109.8(4)
C(6)-C(16)	1.517(7)	C(6)-C(7)-C(8)	110.5(3)
C(6)-C(7)	1.519(6)	N(1)-C(8)-C(9)	99.3(3)
C(7)-C(8)	1.530(5)	N(1)-C(8)-C(7)	109.3(3)
C(8)-N(1)	1.515(5)	C(9)-C(8)-C(7)	113.1(3)
C(8)-C(9)	1.522(5)	N(1)-C(8)-C(4)	110.3(3)
C(9)-C(10)	1.521(6)	C(9)-C(8)-C(4)	112.4(3)
C(10)-C(11)	1.497(7)	C(7)-C(8)-C(4)	111.6(3)
C(11)-N(1)	1.518(5)	C(10)-C(9)-C(8)	105.8(3)
C(12)-C(13)	1.485(7)	C(11)-C(10)-C(9)	106.1(4)
C(13)-C(14)	1.453(7)	C(10)-C(11)-N(1)	105.1(3)
C(14)-C(15)	1.611(7)	C(13)-C(12)-C(1)	116.0(4)
N(1)-C(1)-C(2)	111.2(3)	C(14)-C(13)-C(12)	113.5(4)
N(1)-C(1)-C(12)	107.9(4)	C(13)-C(14)-C(15)	112.2(4)
C(2)-C(1)-C(12)	113.6(3)	C(6)-C(16)-C(5)	111.4(3)
		C(1)-N(1)-C(8)	116.0(3)

C(1)-N(1)-C(11)	116.9(3)	Symmetry transformations used to generate equivalent
C(8)-N(1)-C(11)	106.3(3)	atoms:

Table A.6.4. Anisotropic displacement parameters ($Å^2 x\ 10^3$) for Rovis159_0m. The anisotropic displacement factor exponent takes the form: $-2p^2[\ h^2a^{*2}U^{11} + ... + 2\ h\ k\ a^*\ b^*\ U^{12}\ ]$

	U^{11}	U^{22}	U^{33}	U^{23}	U^{13}	U^{12}
C(1)	29(2)	31(2)	60(3)	0(2)	2(2)	-1(2)
C(2)	30(2)	32(2)	56(2)	-2(2)	8(2)	0(2)
C(3)	29(2)	36(2)	48(2)	1(2)	8(2)	-3(2)
C(4)	27(2)	34(2)	41(2)	-1(2)	4(2)	-2(2)
C(5)	39(2)	34(2)	48(2)	-1(2)	9(2)	-10(2)
C(6)	46(2)	38(2)	58(3)	6(2)	-7(2)	3(2)
C(7)	32(2)	33(2)	58(2)	3(2)	-2(2)	-2(2)
C(8)	23(2)	31(2)	43(2)	3(2)	2(2)	1(2)
C(9)	31(2)	44(2)	50(2)	-4(2)	9(2)	0(2)
C(10)	53(3)	77(4)	47(2)	0(2)	4(2)	13(3)
C(11)	23(2)	62(3)	50(2)	20(2)	5(2)	3(2)
C(12)	38(2)	40(3)	108(4)	13(3)	20(2)	1(2)
C(13)	42(2)	39(2)	109(4)	4(3)	8(3)	0(2)
C(14)	75(3)	56(3)	50(3)	9(2)	11(3)	17(3)
C(15)	57(3)	83(4)	76(3)	-2(3)	-3(3)	-9(3)
C(16)	65(3)	30(2)	50(2)	7(2)	-1(2)	-3(2)
Cl(1)	20(1)	47(1)	81(1)	16(1)	6(1)	-2(1)
N(1)	18(1)	35(2)	55(2)	8(1)	4(2)	1(1)

O(1)	63(2)	38(2)	55(2)	-2(1)	25(2)	-9(2)

Table A.6.5. Hydrogen coordinates (x 10^4) and isotropic displacement parameters ($Å^2$x 10^3) for Rovis159_0m.

	x	y	z	U(eq)
H(17)	1659	1449	986	48
H(2A)	5526	1446	1443	47
H(2B)	4755	1286	616	47
H(4)	5025	3441	1967	40
H(5A)	5463	4761	1052	48
H(5B)	4107	5061	1727	48
H(6A)	-297	4788	655	57
H(6B)	424	5043	1480	57
H(7A)	784	3100	783	49
H(7B)	-665	3347	1441	49
H(9A)	2203	4388	2638	50
H(9B)	356	3701	2707	50
H(10A)	4003	3290	3296	71
H(10B)	2016	2940	3633	71
H(11A)	2355	1463	3079	54
H(11B)	4316	1824	2723	54
H(12A)	3396	252	2133	74
H(12B)	1211	212	1936	74
H(13A)	4101	-430	946	76

H(13B)	2869	-1172	1445	76
H(14A)	1527	9	249	73
H(14B)	157	-600	792	73
H(15A)	1694	-2192	371	108
H(15B)	2904	-1557	-213	108
H(15C)	676	-1641	-309	108
H(16A)	2699	5615	600	58
H(16B)	2849	4517	248	58
H(18)	690(70)	1980(30)	2130(20)	42(11)

APPENDIX 7

Zn(II)-Catalyzed [4+2] Cycloaddition to Form Tetrahydropyridines

A.7.1 Materials and Methods

Toluene, tetrahydrofuran, ether, and dichloromethane were degassed with argon and passed through one column of neutral alumina and one column of Q5 reactant. Triethylamine (peptide synthesis grade) was purchased from Fisher Scientific, dried over calcium hydride and freshly distilled prior to use. Flash column chromatography was carried out on silica gel (60 Å, 230 - 400 mesh, obtained from Silicycle Inc.) and was performed with reagent grade solvents. Analytical thin-layer chromatography (TLC) was performed on Silicycle glass-backed silica gel plates (60 Å, 0.25 mm, purchased from Silicycle Inc.) and visualized with a UV lamp (254 nm), and potassium permanganate or cerric ammonium molybdate.

Infrared spectra (IR) were obtained on a Nicolet Avatar 320 FT-IR spectrometer and Bruker Tensor 27 FT-IR spectrometer. ^{1}H NMR and ^{13}C NMR were obtained on Varian Unity 300 and Unity 400 spectrometers. Chemical shifts are expressed in parts per million values (δ, ppm). Proton chemical shifts in $CDCl_3$ were referenced to 7.26 ppm ($CHCl_3$). Carbon chemical shifts were referenced to 77.2 ppm ($CDCl_3$). Peak multiplicities are designated by the following abbreviations: s, singlet; d, doublet; t, triplet; q, quartet; m, multiplet; dd, doublet of doublets; dt, doublet of triplets; ddd, doublet of doublet of doublets; b, broad; *J*, coupling constant in Hz. Low resolution mass spectra (MS) and high resolution mass spectra (HRMS) were recorded on a Fisons VG Autospec spectrometer. HPLC spectra were obtained on an Agilent 1100 series system. Optical rotation was obtained with an Autopol-III automatic polarimeter. Melting points were obtained on a Fisher-Johns melting point apparatus and are uncorrected.

References following the compound names indicate literature articles where the compound has been previously been reported.

Unless indicated, commercially available starting materials were purchased from Aldrich Chemicals and used without further purification.

A.7.2 General Procedure for Synthesis of α,β-unsaturated Imines

p-anisidine is purified by dissolving it in hot hexanes in the presence of activated charcoal and filtering off solids. Removal of solvent provides p-anisidine. It may also be recrystallized from H_2O or EtOH.

General Procedure for imine synthesis:

To a round bottom flask equipped with a magnetic stirbar and activated 4Å molecular sieves was added *p*-anisidine (2.10 g, 16.7 mmol), toluene (75 ml, 0.2M) and cinnamaldehyde (2.0 g, 17.4 mmol). The mixture was stirred overnight then filtered through a pad of layered celite and $MgSO_4$. Removal of the solvent provided α,β-unsaturated imines.

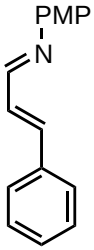

(E)-4-methoxy-N-((E)-3-phenylallylidene)aniline

General procedure yielded yellow powder. ^{1}H-NMR (400 MHz; CDCl3): δ 8.27 (dd, *J* = 5.5, 2.8 Hz, 1H), 7.51 (d, *J* = 7.0 Hz, 2H), 7.35 (dt, *J* = 13.7, 6.9 Hz, 3H), 7.20 (d, *J* = 8.9 Hz, 2H), 7.10-7.09 (m, 2H), 6.91 (d, *J* = 8.9 Hz, 2H), 3.80 (s, 3H). ^{13}C-NMR (101 MHz; $CDCl_3$): δ 159.5, 158.4, 144.5, 143.0, 135.7, 129.4, 128.88, 128.77, 127.4, 122.2, 114.4, 55.4.

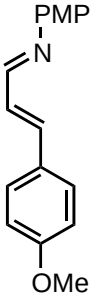

(E)-4-methoxy-N-((E)-3-(4-methoxyphenyl)allylidene)aniline

General procedure yielded brown powder. 1H-NMR (400 MHz; CDCl3): δ 8.24 (d, *J* = 8.4 Hz, 1H), 7.45 (d, *J* = 8.7 Hz, 2H), 7.17 (d, *J* = 8.8 Hz, 2H), 7.02 (s, 1H), 6.96 (dd, *J* = 15.9, 8.4 Hz, 1H), 6.89 (d, *J* = 8.8 Hz, 4H), 3.81 (s, 3H), 3.80 (s, 3H). ^{13}C-NMR (101 MHz; $CDCl_3$): δ 160.6, 159.8, 158.2, 144.7, 142.8, 128.9, 128.6, 126.7, 122.1, 114.36, 114.33, 55.45, 55.33

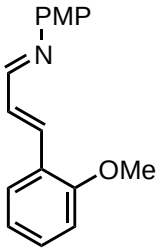

(E)-4-methoxy-N-((E)-3-(2-methoxyphenyl)allylidene)aniline

General procedure yielded brown viscous oil. 1H-NMR (400 MHz; CDCl3): δ 8.29 (dd, *J* = 9.0, 0.5 Hz, 1H), 7.56 (dd, *J* = 7.7, 1.7 Hz, 1H), 7.46 (d, *J* = 16.1 Hz, 1H), 7.30 (ddd, *J* = 8.3, 7.4, 1.6 Hz, 1H), 7.21-7.12 (m, 3H), 6.97 (td, *J* = 7.5, 0.7 Hz, 1H), 6.92-6.89 (m, 3H), 3.88 (s, 3H), 3.81 (s, 3H). ^{13}C-NMR (101 MHz; $CDCl_3$): δ 160.5, 158.2, 157.4, 144.7, 138.3, 130.6, 129.2, 127.6, 124.7, 122.2, 120.8, 114.3, 111.0, 55.48, 55.46

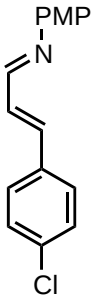

(E)-N-((E)-3-(4-chlorophenyl)allylidene)-4-methoxyaniline

General procedure yielded yellow powder. 1H-NMR (400 MHz; CDCl3): δ 8.25 (dd, *J* = 6.1, 2.2 Hz, 1H), 7.43-7.41 (m, 2H), 7.34-7.32 (m, 2H), 7.19-7.17 (m, 2H), 7.05-7.03 (m, 2H), 6.91-6.89 (m, 2H), 3.80 (s, 3H). ^{13}C-NMR (101 MHz; $CDCl_3$): δ 159.0, 158.5, 144.4, 141.3, 135.1, 134.2, 129.29, 129.10, 128.5, 122.2, 114.4, 77.3, 77.0, 76.7, 55.5

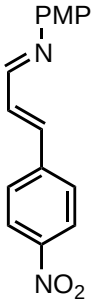

(E)-4-methoxy-N-((E)-3-(4-nitrophenyl)allylidene)aniline

General procedure yielded yellow powder. 1H-NMR (400 MHz; CDCl3): δ 8.32 (d, *J* = 8.2 Hz, 1H), 8.22 (d, *J* = 8.8 Hz, 2H), 7.63 (d, *J* = 8.9 Hz, 2H), 7.24-7.10 (m, 4H), 6.92-6.90 (m, 2H), 3.82 (s, 3H). ^{13}C-NMR (101 MHz; $CDCl_3$): δ 158.9, 157.8, 147.7, 143.9, 142.0, 139.4, 132.8, 124.2, 122.4, 114.5, 55.5

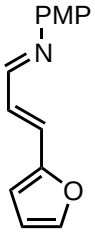

(E)-N-((E)-3-(furan-2-yl)allylidene)-4-methoxyaniline

^{1}H-NMR (400 MHz; $CDCl_3$): δ 8.17 (d, *J* = 9.0 Hz, 1H), 7.44 (d, *J* = 1.0 Hz, 1H), 7.16 (d, *J* = 8.8 Hz, 2H), 6.96 (dd, *J* = 15.8, 9.0 Hz, 1H), 6.85 (dd, *J* = 17.3, 12.3 Hz, 3H), 6.50 (d, *J* = 3.3 Hz, 1H), 6.42 (dd, *J* = 3.2, 1.8 Hz, 1H), 3.77 (s, 3H). ^{13}C-NMR (101 MHz; $CDCl_3$): δ 158.8, 158.3, 152.0, 144.6, 144.0, 129.4, 126.8, 114.4, 112.24, 112.17, 55.4

A.7.3 General Procedure for Zn-Catalyzed [4+2]

To a vial equipped with a magnetic stirbar and activated 4Å molecular sieves was added nitro olefin **2** (0.218 mmol, 1.5 equiv), 1-azadiene **1** (0.140 mmol, 1 equiv), ZnI_2 (0.0149 mmol, 10 mol %) and dioxanes (1.4 ml, 0.1 M concentration based on **1**). Yellow solution is stirred over night at 50 ºC before it is cooled to room temperature and adsorbed onto celite. Flash chromatography on florisil (<200 mesh) with 98:2:1 to 95:5:1 hexanes/EtOAc/NEt_3 to yield a yellow oil. TLC 89:10:1 (Hex/EA/NEt_3).

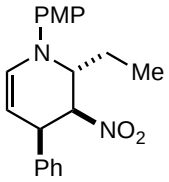

(2R,3S,4R)-2-ethyl-1-(4-methoxyphenyl)-3-nitro-4-phenyl-1,2,3,4-tetrahydropyridine. General procedure yielded a yellow solid.

^{1}H-NMR (400 MHz; $CDCl_3$): δ 7.31 (d, *J* = 4.3 Hz, 5H), 6.94 (d, *J* = 9.0 Hz, 2H), 6.82 (d, *J* = 9.0 Hz, 2H), 6.61 (d, *J* = 8.0 Hz, 1H), 5.06 (d, *J* = 6.0 Hz, 1H), 4.88 (d, *J* = 8.1 Hz, 1H), 4.10 (td, *J* = 7.0, 1.9 Hz, 1H), 3.99 (dd, *J* = 3.4, 2.7 Hz, 1H), 3.76 (s, 4H), 1.96 (dt, *J* = 14.3, 7.2 Hz, 1H), 1.77 (dt, *J* = 14.4, 7.3 Hz, 1H), 1.14 (t, *J* = 7.5 Hz, 3H). ^{13}C–NMR (101 MHz; $CDCl_3$): δ 154.8, 140.5, 138.2, 130.2, 128.52, 128.46, 128.34, 128.21, 127.5, 119.6, 114.5, 97.8, 84.7, 60.6, 55.6, 38.0, 25.6, 10.4. IR (Thin Film) v 2963, 2927, 1646, 1549, 1510, 1453, 1366. 1273, 1243, 1179, 1153, 1111, 1036. LRMS (ESI/APCI) m/z $[C_{20}H_{23}N_2O_3]$+ calculated 339.16, found 339.1

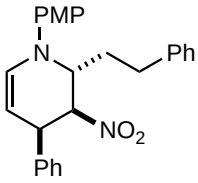

(2R,3S,4R)-1-(4-methoxyphenyl)-3-nitro-2-phenethyl-4-phenyl-1,2,3,4-tetrahydropyridine. General procedure yielded a yellow oil.

^{1}H-NMR (400 MHz; $CDCl_3$): δ 7.34-7.19 (m, 14H), 6.89-6.86 (m, 2H), 6.80-6.78 (m, 2H), 6.64 (dt, *J* = 8.1, 1.0 Hz, 1H), 5.07 (ddd, *J* = 6.1, 2.4, 1.4 Hz, 1H), 4.89 (ddd, *J* = 8.1, 2.2, 1.5 Hz, 1H), 4.23 (td, *J* = 6.9, 1.7 Hz, 1H), 3.98 (dt, *J* = 5.9, 2.2 Hz, 1H), 3.75 (s, 3H), 2.88-2.83 (m, 2H), 2.22 (ddt, *J* = 14.1, 8.7, 7.0 Hz, 1H), 2.12-2.02 (m, 1H). ^{13}C–NMR (101 MHz; $CDCl_3$): δ 154.9, 140.43, 140.34, 138.0, 130.2, 128.7, 128.52, 128.34, 128.32, 127.6, 126.5, 119.6, 114.6, 97.8, 84.9, 58.8, 55.6, 38.0, 34.4, 32.3 IR (Thin Film) v 2923, 2852, 1739, 1646, 1601, 1549, 1510, 1453, 1441, 1364, 1273, 1244, 1179, 1037. LRMS (ESI/APCI) *m/z* [$C_{26}H_{27}N_2O_3]^+$ calculated 415.19, found 415.1

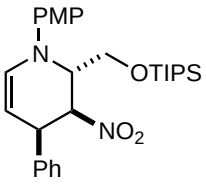

(2S,3S,4R)-1-(4-methoxyphenyl)-3-nitro-4-phenyl-2-(triisopropylsilyloxy methyl)-1,2,3,4-tetrahydropyridine. General procedure yielded a yellow oil. ^{1}H-NMR (400 MHz; $CDCl_3$): δ 7.32-7.25 (m, 5H), 6.97-6.95 (m, 2H), 6.83-6.81 (m, 2H), 6.60 (dd, *J* = 8.2, 1.3 Hz, 1H), 5.43 (dt, *J* = 6.2, 1.7 Hz, 1H), 4.87 (dt, *J* = 8.2, 1.7 Hz, 1H), 4.31 (ddd, *J* = 8.8, 6.4, 1.8 Hz, 1H), 4.12-4.05 (m, 2H), 3.88 (t, *J* = 9.9 Hz, 1H), 3.79 (s, 3H), 1.11 (d, *J* = 5.3 Hz, 18H). ^{13}C–NMR (101 MHz; $CDCl_3$): δ 155.1, 140.3, 138.3, 130.4, 128.6, 128.2, 127.5, 119.7, 114.6, 97.8, 82.3, 62.2, 60.8, 55.6, 37.7, 18.01, 17.99, 17.90, 11.9. IR (Thin Film) v 2942, 2865, 1647, 1550, 1463, 1366, 1244, 1114, 1039. LRMS (ESI/APCI) *m/z* $[C_{28}H_{41}N_2O_4Si]^+$ calculated 497.28, found 497.2

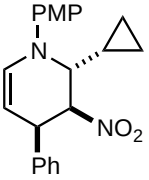

(2R,3S,4R)-2-cyclopropyl-1-(4-methoxyphenyl)-3-nitro-4-phenyl-1,2,3,4-tetrahydropyridine. General procedure yielded a yellow oil.

1H-NMR (300 MHz; CDCl3): δ 7.36-7.33 (m, 5H), 7.01 (d, *J* = 9.0 Hz, 2H), 6.83 (d, *J* = 8.9 Hz, 2H), 6.62 (dt, *J* = 8.2, 1.2 Hz, 1H), 5.15-5.11 (m, 1H), 4.92-4.88 (m, 1H), 4.25-4.22 (m, 1H), 3.78 (s, 4H), 3.68-3.65 (m, 1H), 0.75-0.71 (m, 2H), 0.60-0.55 (m, 1H), 0.48-0.43 (m, 1H).

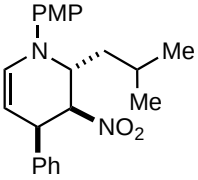

(2R,3S,4R)-2-isobutyl-1-(4-methoxyphenyl)-3-nitro-4-phenyl-1,2,3,4-tetrahydropyridine. General procedure yielded a yellow oil. ^{1}H-NMR (400 MHz; $CDCl_3$): δ 7.32-7.31 (m, 5H), 6.92 (d, *J* = 9.1 Hz, 2H), 6.82 (d, *J* = 9.1 Hz, 2H), 6.61 (ddd, *J* = 8.1, 2.2, 1.1 Hz, 1H), 5.03 (dt, *J* = 6.1, 1.8 Hz, 1H), 4.87 (dt, *J* = 8.1, 1.8 Hz, 1H), 4.29-4.25 (m, 1H), 3.97 (dt, *J* = 6.0, 2.2 Hz, 1H), 1.87-1.75 (m, 2H), 1.66 (ddd, *J* = 13.8, 8.1, 5.8 Hz, 2H), 1.04 (dd, *J* = 6.3, 4.5 Hz, 6H). ^{13}C–NMR (101 MHz; $CDCl_3$): δ 154.8, 140.5, 138.2, 130.1, 128.5, 127.5, 97.4, 84.8, 57.8, 55.6, 41.6, 37.7, 29.7, 24.4, 23.3, 22.0. IR (Thin Film) v 3060, 2955, 2924, 2869, 2850, 1644, 1549, 1465, 1453, 1441, 1366, 1325, 1299, 1274, 1244, 1233, 1180, 1155, 1038. LRMS (ESI/APCI) *m/z* $[C_{22}H_{27}N_2O_3]^+$ calculated 367.19, found 367.2

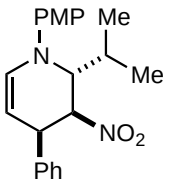

(2R,3S,4R)-2-isopropyl-1-(4-methoxyphenyl)-3-nitro-4-phenyl-1,2,3,4-tetrahydropyridine

General procedure yielded a yellow oil. ^{1}H-NMR (400 MHz; $CDCl_3$): δ 7.35-7.24 (m, 6H), 6.93-6.91 (m, 2H), 6.81-6.79 (m, 2H), 6.65 (ddd, *J* = 8.0, 2.1, 1.2 Hz, 1H), 5.19 (dt, *J* = 6.1, 1.9 Hz, 1H), 5.02-4.99 (m, 1H), 3.96-3.90 (m, 2H), 3.75 (s, 3H), 2.19-2.10 (m, 1H), 1.19 (d, *J* = 6.7 Hz, 3H), 1.15 (d, *J* = 6.8 Hz, 3H). ^{13}C–NMR (101 MHz; $CDCl_3$): δ 154.5, 141.2, 138.0, 130.2, 129.1, 128.48, 128.46, 128.41, 127.5, 119.3, 114.4, 100.0, 84.0, 65.7, 55.5, 38.0, 30.9, 20.9, 18.9. IR (Thin Film) v 3060, 2961, 2933, 2873, 2834, 1644, 1548, 1508, 1464, 1366, 1271, 1241, 1226, 1180, 1126, 1036. LRMS (ESI/APCI) *m/z* $[C_{21}H_{25}N_2O_3]^+$ calculated 353.18, found 353.1

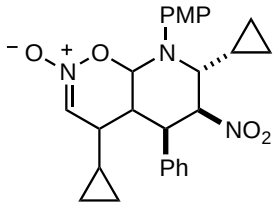

(5R,6S,7R)-4,7-dicyclopropyl-8-(4-methoxyphenyl)-6-nitro-5-phenyl-4a,5,6,7,8,8a-hexahydro-4H-pyrido[3,2-e][1,2]oxazine 2-oxide. General procedure yielded a red solid. ^{1}H-NMR (400 MHz; $CDCl_3$): δ 7.33-7.17 (m, 7H), 7.04-7.02 (m, 2H), 6.87-6.84 (m, 2H), 5.08 (t, *J* = 6.0 Hz, 1H), 4.69 (dd, *J* = 11.3, 10.3 Hz, 1H), 4.52 (dd, *J* = 11.4, 6.0 Hz, 1H), 4.19 (d, *J* = 5.8 Hz, 1H), 3.79 (s, 4H), 3.56 (dd, *J* = 7.8, 6.2 Hz, 1H), 2.07 (td, *J* = 9.7, 6.1 Hz, 1H), 0.96-0.91 (m, 1H), 0.53 (dd, *J* = 8.9, 4.5 Hz, 1H), 0.47 (dd, *J* = 8.3, 4.0 Hz, 1H), 0.41-0.35 (m, 2H), 0.29-0.21 (m, 3H), 0.02--0.01 (m, 2H). ^{13}C–NMR (101 MHz; $CDCl_3$): δ 156.3, 139.8, 137.0, 130.5, 129.1, 128.9, 128.7, 128.0, 127.4, 123.5, 114.42, 114.39, 106.6, 88.9, 59.6, 55.52, 55.46, 46.5, 43.0, 14.9, 14.5, 4.9, 4.4, 4.2, 2.2. IR (Thin Film) *v* 3063, 3003, 2954, 2923, 2835, 1654, 1547, 1509, 1463, 1453, 1441, 1379, 1331, 1244, 1225, 1180, 1032. LRMS (ESI/APCI) *m/z* $[C_{26}H_{29}N_3O_5]^+$ calculated 464.2, found 464.1

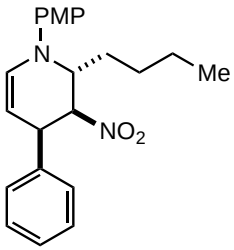

(2R,3S,4R)-2-butyl-1-(4-methoxyphenyl)-3-nitro-4-phenyl-1,2,3,4-tetrahydropyridine

General procedure yielded a yellow solid. R_f (1:20:80 NEt_3/EtOAc/Hexane): 0.50. ^{1}H–NMR: (400 MHz, $CDCl_3$): δ 7.36-7.30 (m, 4H), 7.29-7.25 (m, 1H), 6.95, (d, *J*= 9.0, 2H), 6.84 (d, *J*= 9.0, 2H), 6.63 (d, *J*= 8.0, 1H), 5.07 (ddd, *J*= 6.0, 1.8, 1.8, 1H), 4.91 (ddd, *J*= 8.0, 1.8, 1.8, 1H), 4.17 (td, *J*= 7.2, 1.8, 1H), 4.02 (ddd, *J*= 6.0, 1.8, 1.8, 1H), 3.78 (s,

3H), 1.98-1.88 (m, 1H), 1.81-1.72 (m, 1H), 1.58-1.41 (m, 4H), 0.98 (t, *J*= 7.2, 3H). ^{13}C–NMR (101 MHz, $CDCl_3$): δ 154.8, 140.5, 138.2, 130.1, 128.5, 128.3, 127.5, 119.4, 114.6, 97.8, 85.0, 59.4, 55.6, 37.9, 32.4, 28.0, 22.6, 14.0. IR (thin film): *v* 3060, 2955, 2931, 2870, 1645, 1603. LRMS (ESI/APCI) *m/z* $[C_{22}H_{27}N_2O_o]^+$ calculated 366.2 found 366.2.

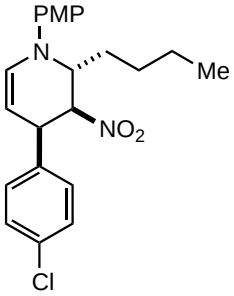

(2R,3S,4R)-2-butyl-4-(4-chlorophenyl)-1-(4-methoxyphenyl)-3-nitro-1,2,3,4-tetrahydropyridine

General procedure yielded a yellow solid. R_f (1:20:80 NEt_3/EtOAc/Hexane): 0.48. ^{1}H-NMR (400 MHz, $CDCl_3$): δ 7.31-7.26 (m, 4H), 6.94 (d, *J*= 9.2, 2H), 6.84 (d, *J*=9.2, 2H), 6.62 (d, *J*= 8.0, 1H), 5.02 (ddd, *J*= 6.1, 1.8, 1.8, 1H), 4.83 (ddd, *J*= 8.0, 1.8, 1.8, 1H), 4.19 (td, *J*= 7.2, 1.8, 1H), 3.98 (ddd, *J*= 6.1, 1.8, 1H), 3.78 (s, 3H), 1.96-1.87 (m, 1H), 1.79-1.69 (m, 1H), 1.57-1.40 (m, 4H), 0.97 (t, *J*= 7.2, 3H). ^{13}C–NMR (101 MHz, $CDCl_3$): δ 154.9, 140.3, 136.8, 133.4, 130.5, 129.7, 128.7, 119.6, 114.6, 97.2, 84.8, 59.4, 55.6, 37.4, 32.4, 28.0, 22.6, 14.0. IR (thin film): *v* 3048, 2956, 2932, 2871, 2835, 1644, 1594. LRMS (ESI/APCI) *m/z* $[C_{22}H_{26}ClN_2O_o]^+$ calculated 400.2 found 400.2.

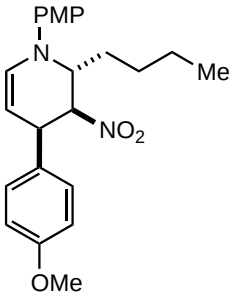

(2R,3S,4R)-2-butyl-1,4-bis(4-methoxyphenyl)-3-nitro-1,2,3,4-tetrahydropyridine.

General procedure yielded a yellow solid. R_f (1:20:80 NEt_3/EtOAc/Hexane): 0.40. ^{1}H NMR (300 MHz, $CDCl_3$): δ 7.26-7.23 (m, 2H), 6.94 (d, *J*= 9.0, 2H), 6.87-6.82 (m, 4H), 5.02 (d, *J*= 6.0 ,1H), 4.86 (d, *J*= 8.1, 1H), 4.16 (t, *J*= 7.2, 1H), 3.97-3.95 (m, 1H), 3.79 (s, 3H), 3.77 (s, 3H), 1.96-1.85 (m, 1H), 1.80-1.68 (m, 1H), 1.56-1.38 (m, 4H), 0.97 (t, *J*= 7.1, 3H). ^{13}C NMR (101 MHz, $CDCl_3$): δ 158.9, 154.8, 140.5, 130.0, 130.0, 129.4, 119.4, 114.6, 113.9, 98.3, 85.1, 59.3, 55.6, 55.2, 37.3, 32.4, 28.0, 22.7, 14.0. IR (thin film): *v* 3045, 2955, 2933, 2870, 2836, 1645, 1608. LRMS (ESI/APCI) *m/z* $[C_{23}H_{29}N_2O_4]^+$ calculated 396.2 found 396.2.

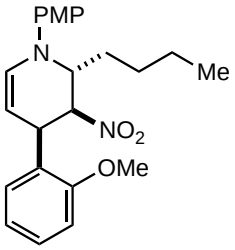

(2R,3S,4R)-2-butyl-4-(2-methoxyphenyl)-1-(4-methoxyphenyl)-3-nitro-1,2,3,4-tetrahydropyridine

General procedure yielded a yellow solid. R_f (1:20:80 NEt_3/EtOAc/Hexane): 0.50. ^1H NMR (300 MHz, $CDCl_3$): δ 7.38 (d, *J*= 7.2, 1H), 7.28-7.21 (m, 1H), 6.97-6.92 (m, 3H), 6.87-6.81 (m, 3H), 6.62 (d, *J*=8.1, 1H), 5.38 (d, *J*= 5.4, 1H), 4.88 (d, *J*= 8.1, 1H), 4.36-4.34 (m, 1H), 4.22 (t, *J*= 7.1, 1H), 3.89 (s, 3H), 3.77 (s, 3H), 2.00-1.75 (m, 2H), 1.61-1.40 (m, 4H), 1.00 (t, *J*= 7.1, 3H). ^{13}C NMR (75 MHz, $CDCl_3$): δ 157.2, 154.8, 140.9, 130.0, 129.9, 128.8, 126.4, 121.0, 119.2, 114.8, 109.9, 98.8, 81.7, 60.0, 55.8, 55.7, 32.4, 31.8, 28.2, 22.9, 14.4. IR (thin film): *v* 3047, 2955, 2934, 2870, 2836, 1646, 1600. LRMS (ESI/APCI) *m/z* $[C_{23}H_{29}N_2O_4]^+$ calculated 396.2 found 396.2.

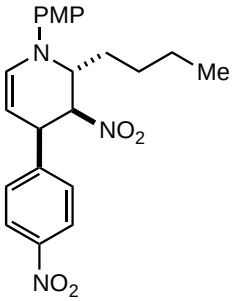

(2R,3S,4R)-2-butyl-1-(4-methoxyphenyl)-3-nitro-4-(4-nitrophenyl)-1,2,3,4-tetrahydropyridine

General procedure yielded a yellow solid. R_f (1:20:80 NEt_3/EtOAc/Hexane): 0.44. ^1H NMR (400 MHz, $CDCl_3$): δ 8.18(d, *J*= 8.8, 2H), 7.54 (d, *J*= 8.8, 2H), 6.94 (d, *J*= 8.8, 2H), 6.84 (d, *J*= 8.8, 2H), 6.66 (d, *J*= 8.0, 1H), 5.07 (ddd, *J*= 6.5, 2.0, 2.0, 1H), 4.85 (ddd, *J*= 8.0, 2.0, 2.0, 1H), 4.24 (td, *J*= 7.0, 2.0,1H), 4.12-4.10 (m, 1H), 3.78 (s, 3H), 1.98-1.89 (m, 1H), 1.81-1.71 (m, 1H), 1.58-1.39 (m, 4H), 0.98 (t, *J*= 7.2, 3H). ^{13}C NMR (100 MHz, $CDCl_3$): δ 155.2, 147.3, 146.1, 140.1, 131.1, 129.4, 123.7, 119.8, 114.6, 95.9, 84.6, 59.6, 55.6, 37.8, 32.3, 28.0, 22.6, 13.9. IR (thin film): *v* 3044, 2958, 2932, 2871, 2837, 1646, 1598.

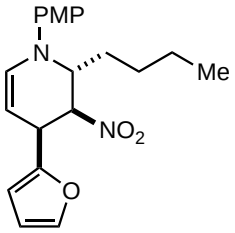

(2R,3S,4S)-2-butyl-4-(furan-2-yl)-1-(4-methoxyphenyl)-3-nitro-1,2,3,4-tetrahydropyridine

R_f (1:20:80 NEt_3/EtOAc/Hexane): 0.53. ^1H NMR (400 MHz, $CDCl_3$): δ 7.35 (d, *J*= 1.8, 1H), 6.92 (d, *J*= 8.8, 2H), 6.83 (d, *J*= 8.8, 2H), 6.53 (ddd, *J*= 8.2, 2.2, 0.8, 1H), 6.33 (dd, *J*= 3.2, 1.8, 1H), 6.26-6.24 (m, 1H), 5.21 (ddd, *J*= 5.6, 2.6, 1.6, 1H), 4.83 (ddd, *J*= 8.2, 2.0, 1.6, 1H), 4.26 (tdd, *J*= 7.2, 2.6, 0.8, 1H) 4.10-4.08 (m, 1H), 3.77 (s, 3H), 1.92-1.83 (m, 1H), 1.74-1.65 (m, 1H), 1.54-1.37 (m, 4H), 0.95 (t, *J*= 7.2, 3H). ^{13}C NMR (101 MHz, $CDCl_3$): δ 155.0,

152.2, 141.8, 140.3, 130.2, 119.8, 114.7, 110.6, 107.4, 94.6, 82.0, 59.3, 55.5, 32.6, 32.3, 27.9, 22.6, 13.9. IR (thin film): *v* 3044, 2957, 2932, 2871, 2837, 1648, 1631. LRMS (ESI/APCI) *m/z* $[C_{23}H_{29}N_2O_4]^+$ calculated 356.2 found 356.2.

A.7.4 ^{1}H–NMR, ^{13}C–NMR Spectra

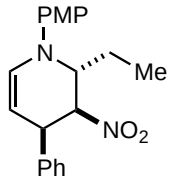

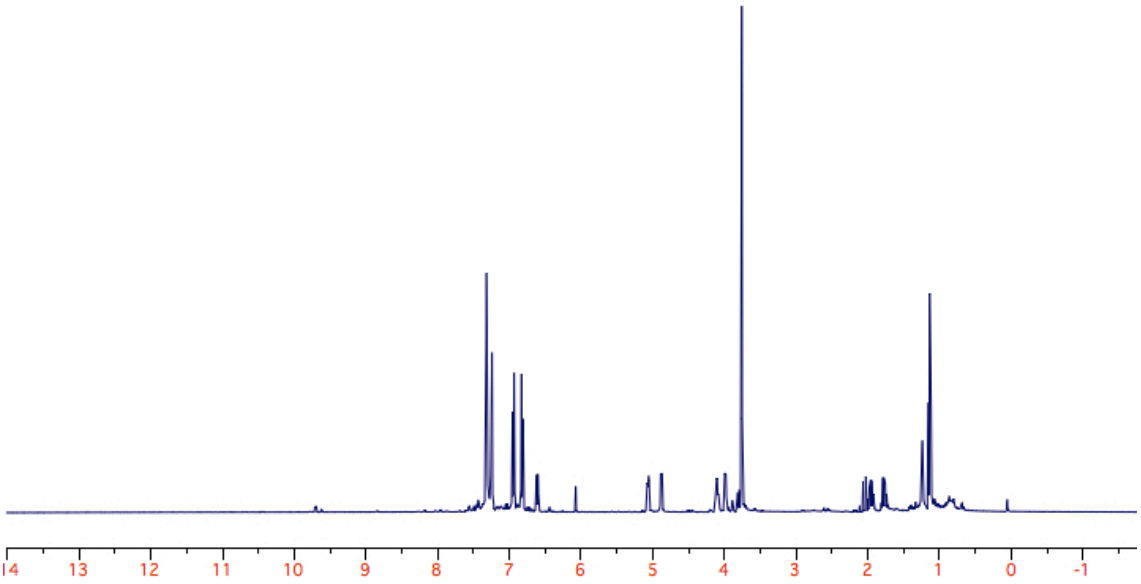

Figure A.7.1

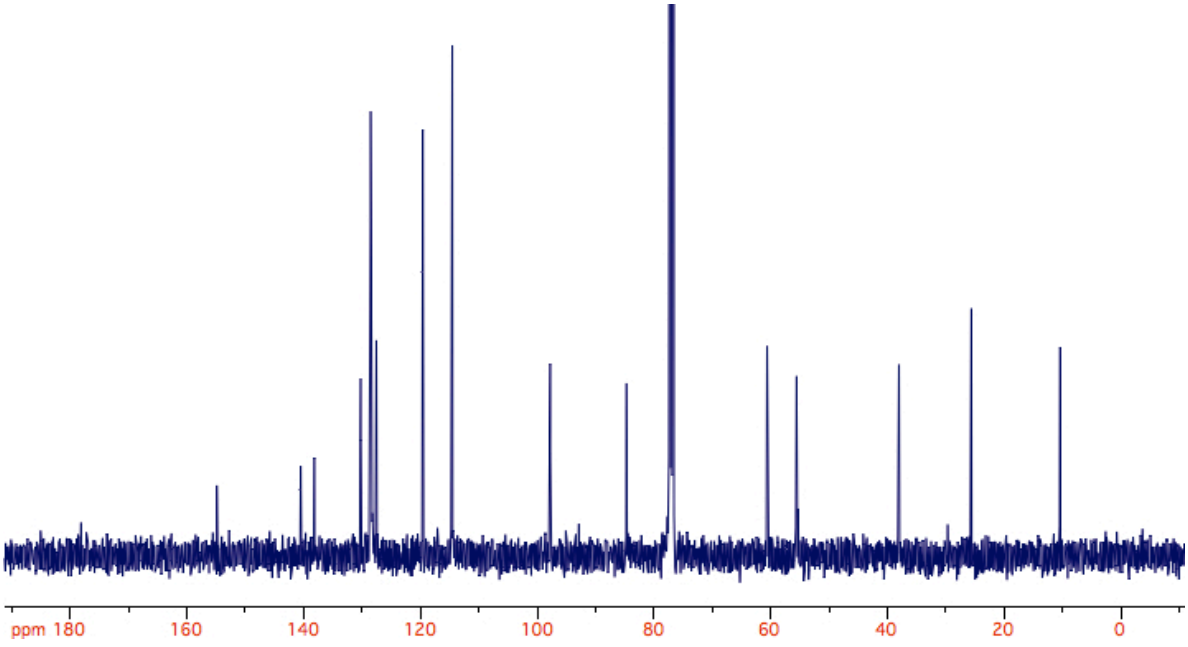

Figure A.7.2

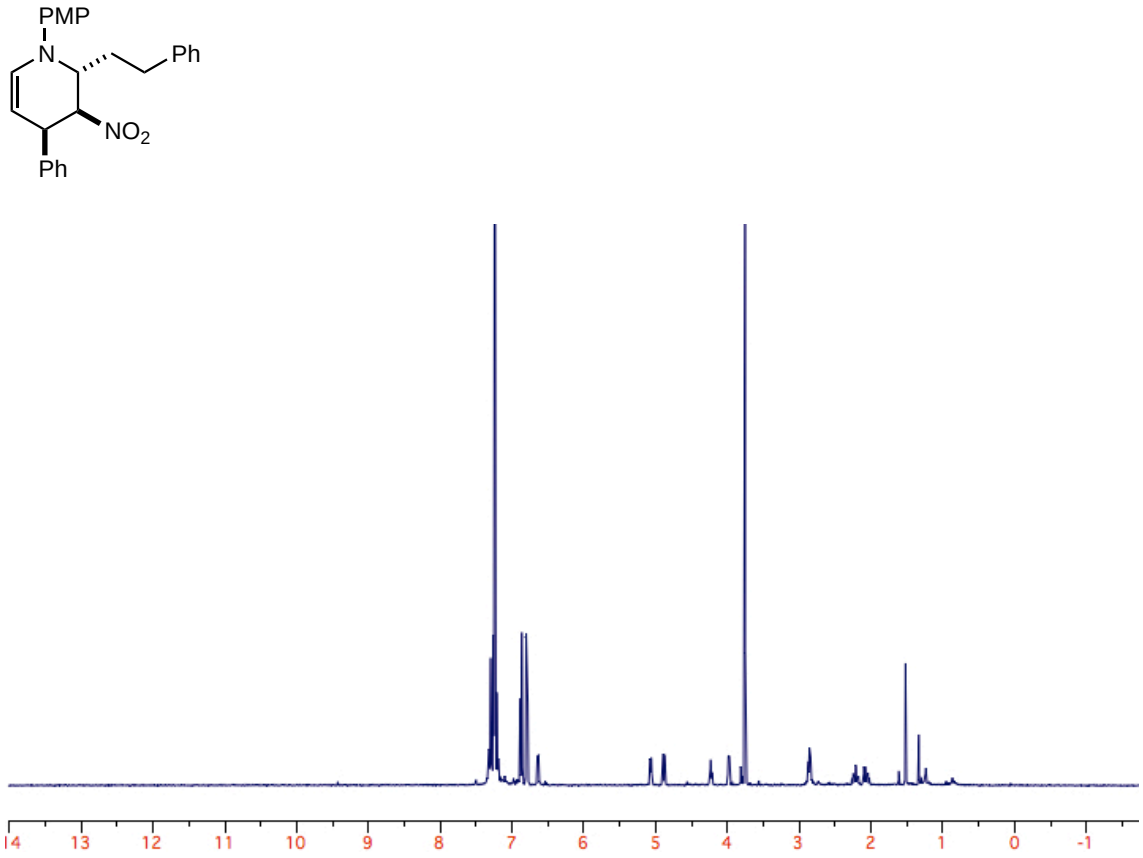

Figure A.7.3

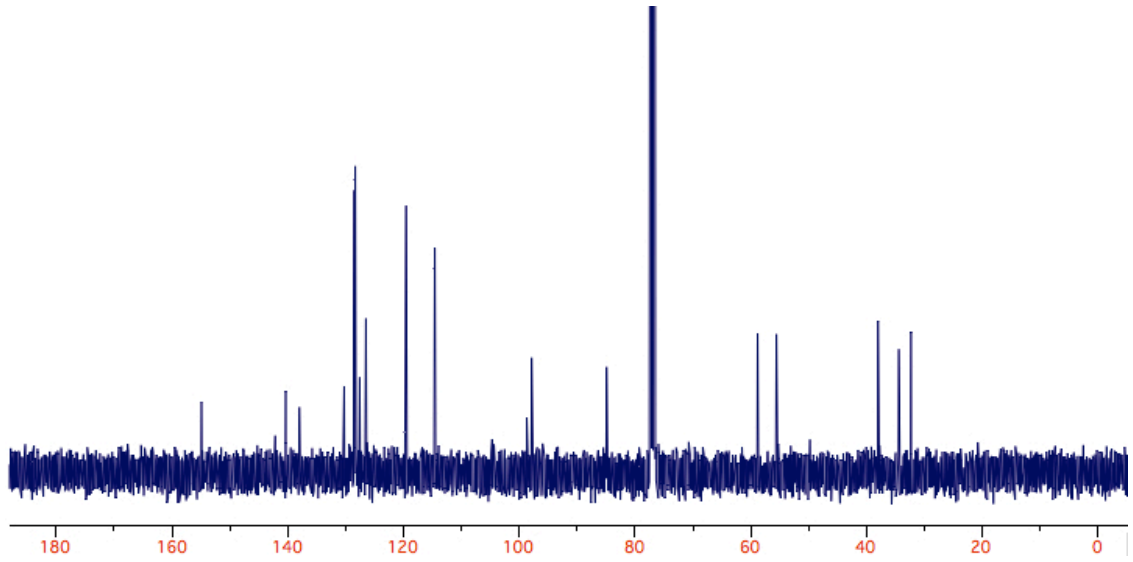

Figure A.7.4

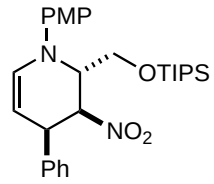

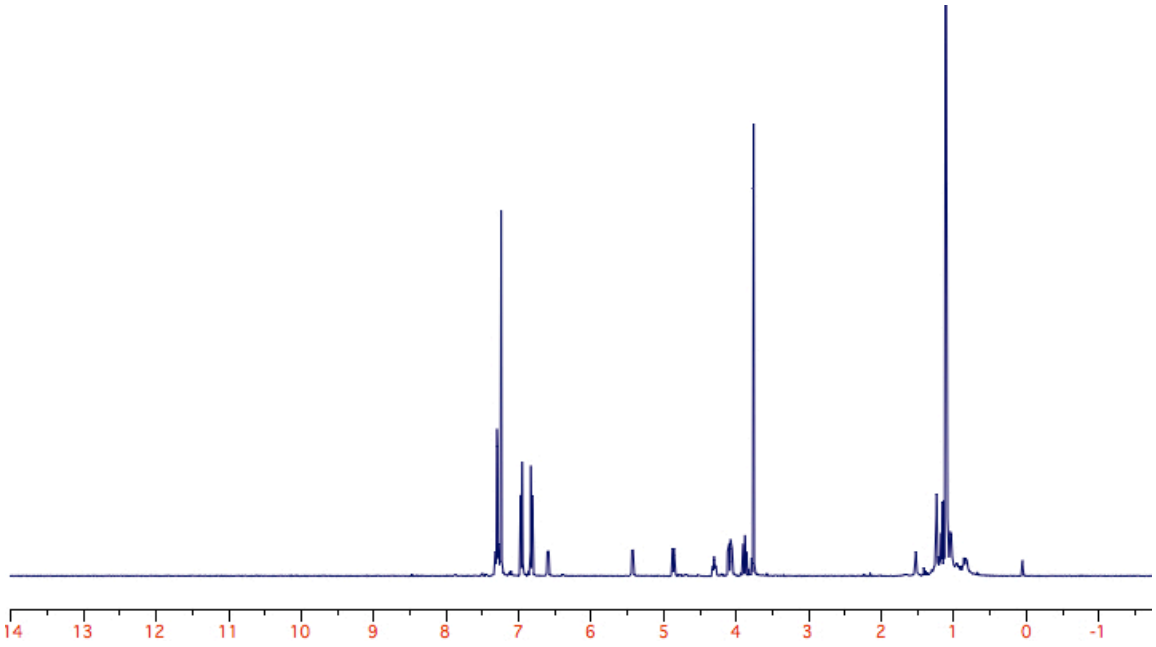

Figure A.7.5

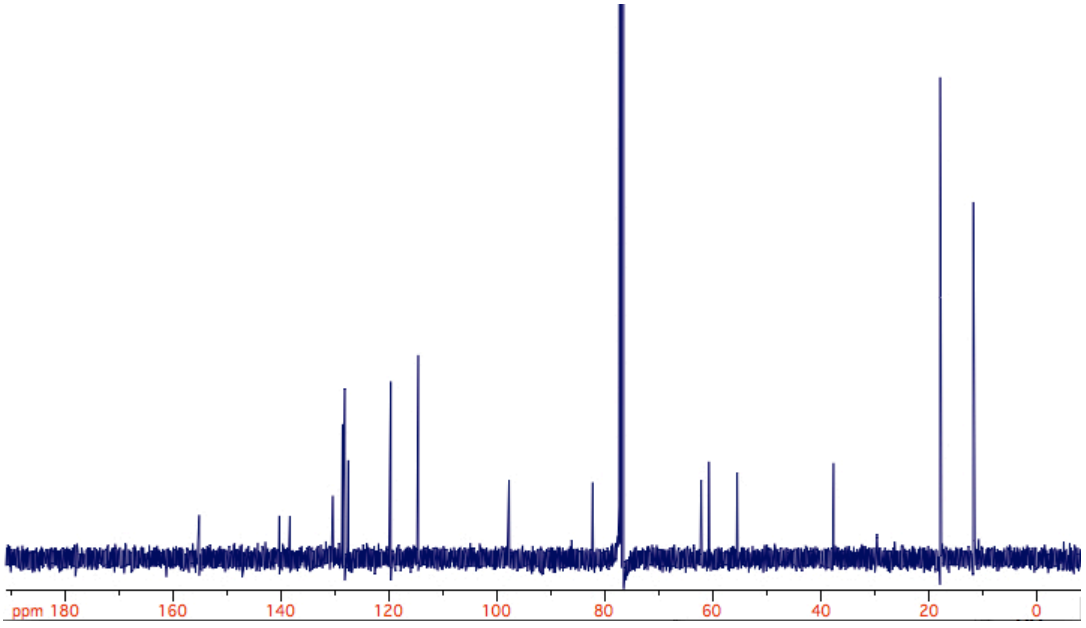

Figure A.7.6

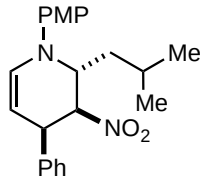

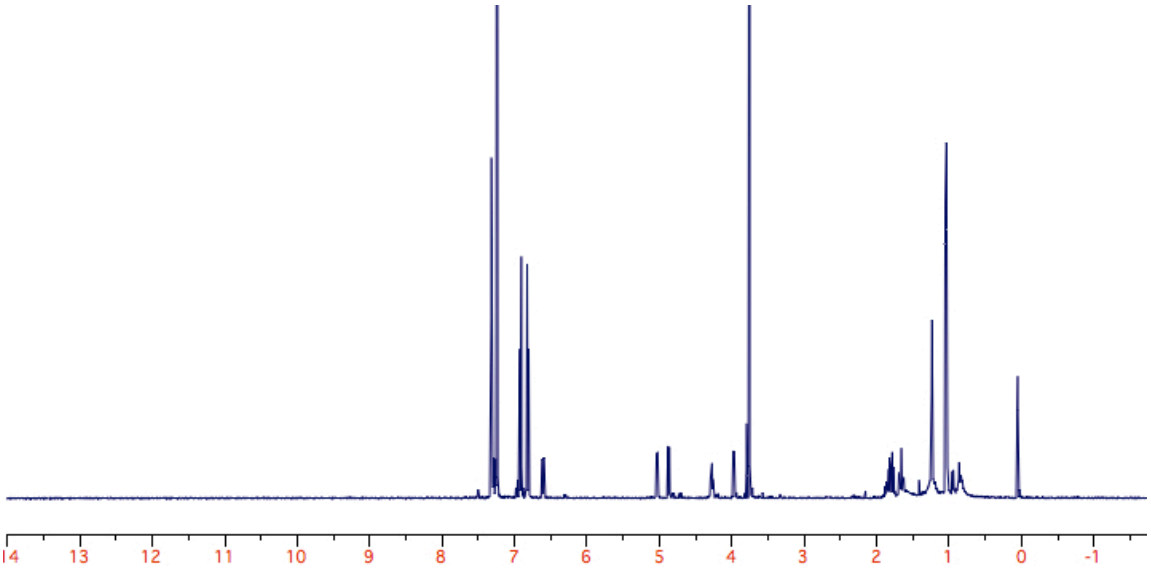

Figure A.7.7

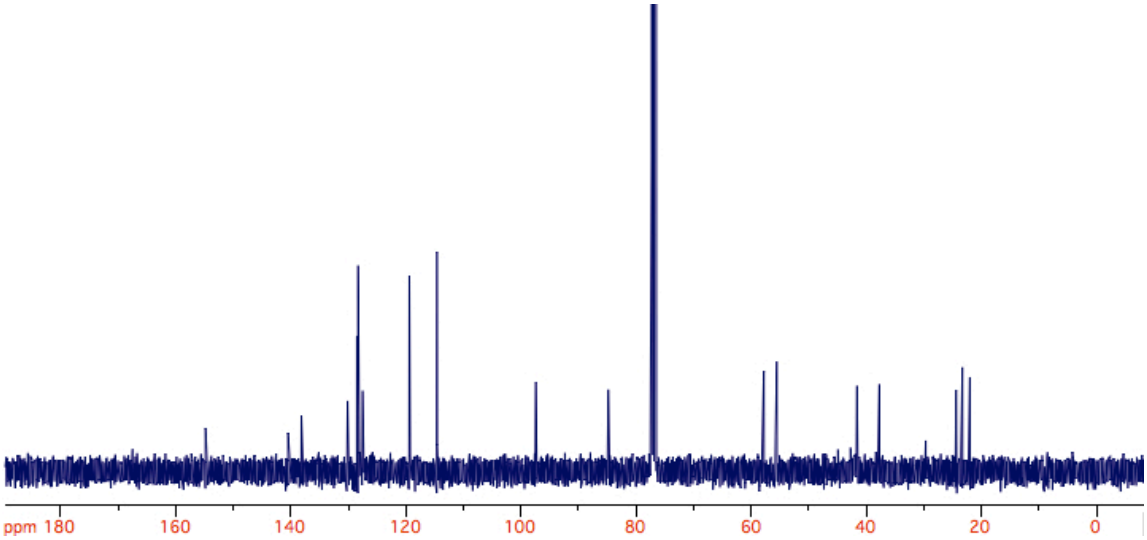

Figure A.7.8

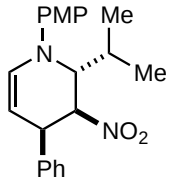

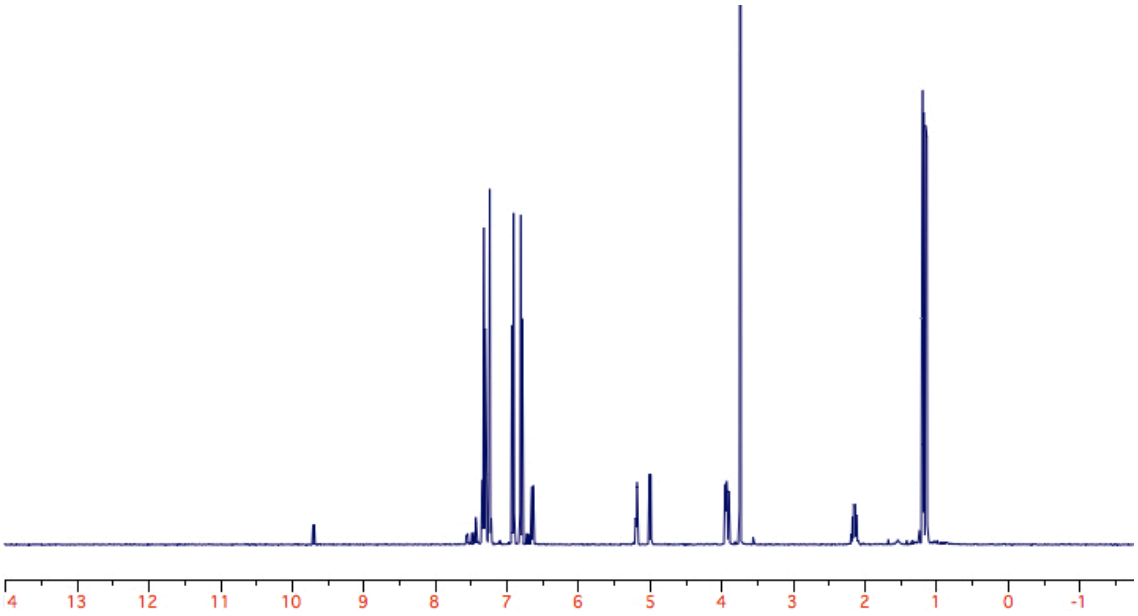

Figure A.7.9

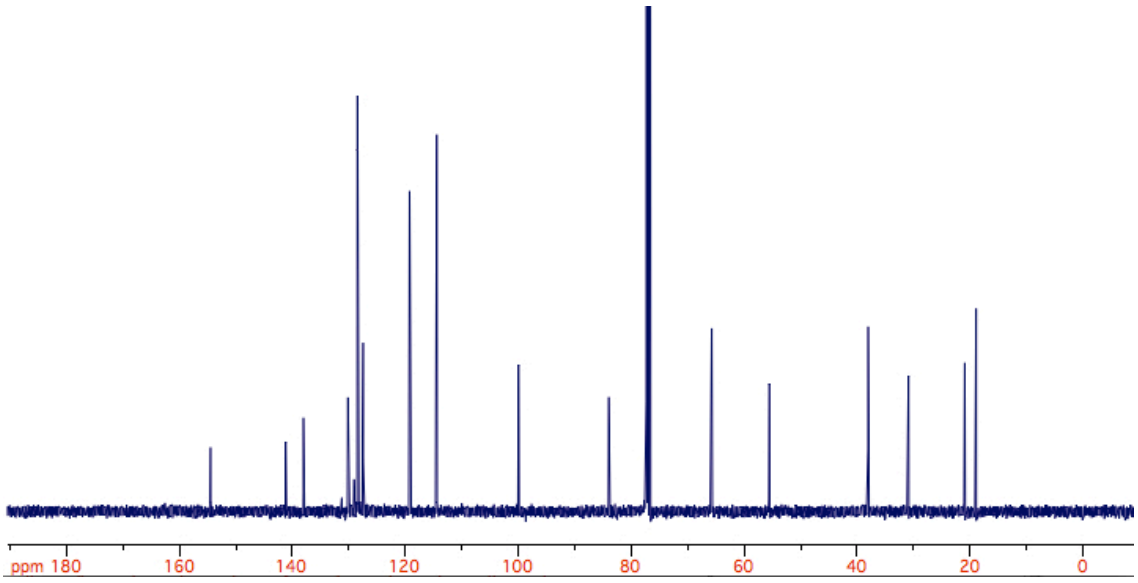

Figure A.7.10

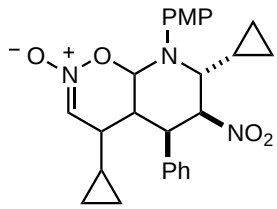

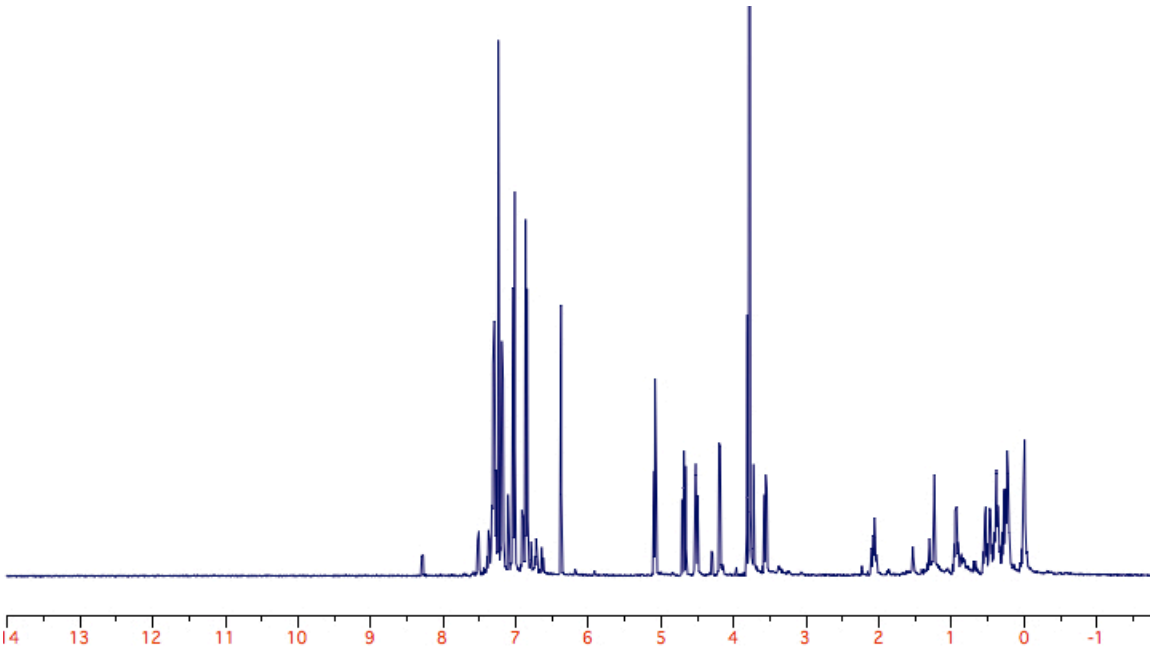

Figure A.7.11

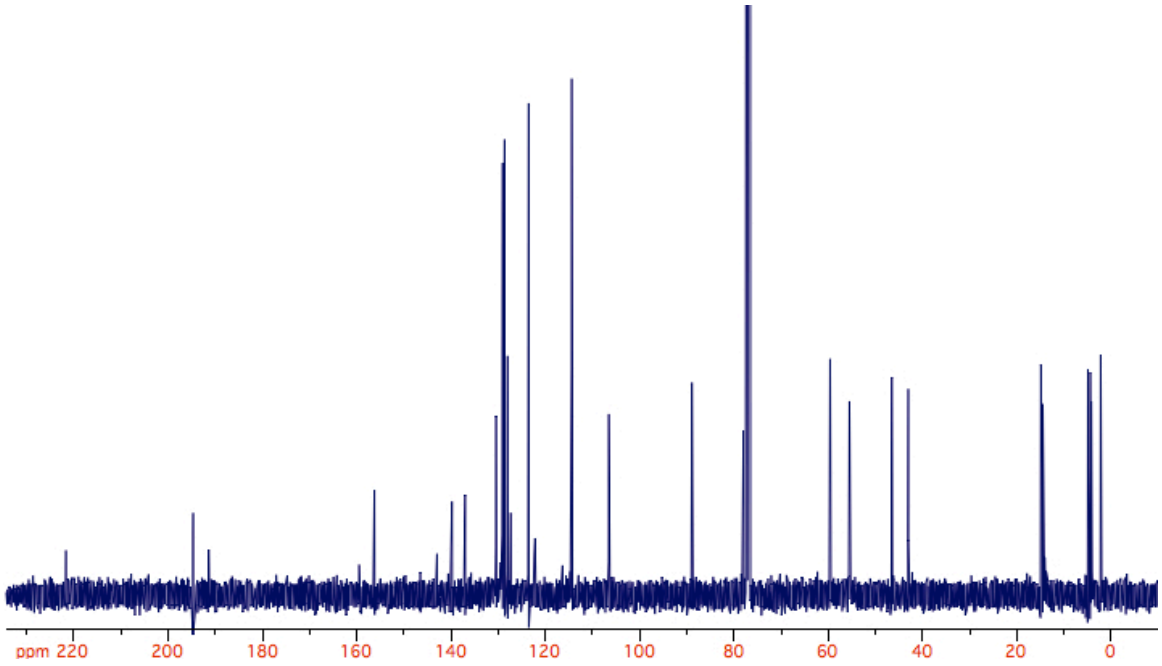

Figure A.7.12

A.7.5 X-ray Crystallographic Data

General procedure for crystallization of tetrahydropyridines:

Chromatographically pure tetrahydropyridine was dissolved in a minimal amount of DCM/Et_2O in a 20 ml scintillation vial. Hexanes was carefully layered onto the DCM/Et_2O solution. The vial was capped and sealed with parafilm. Upon standing overnight clear, yellow x-ray quality crystals formed.

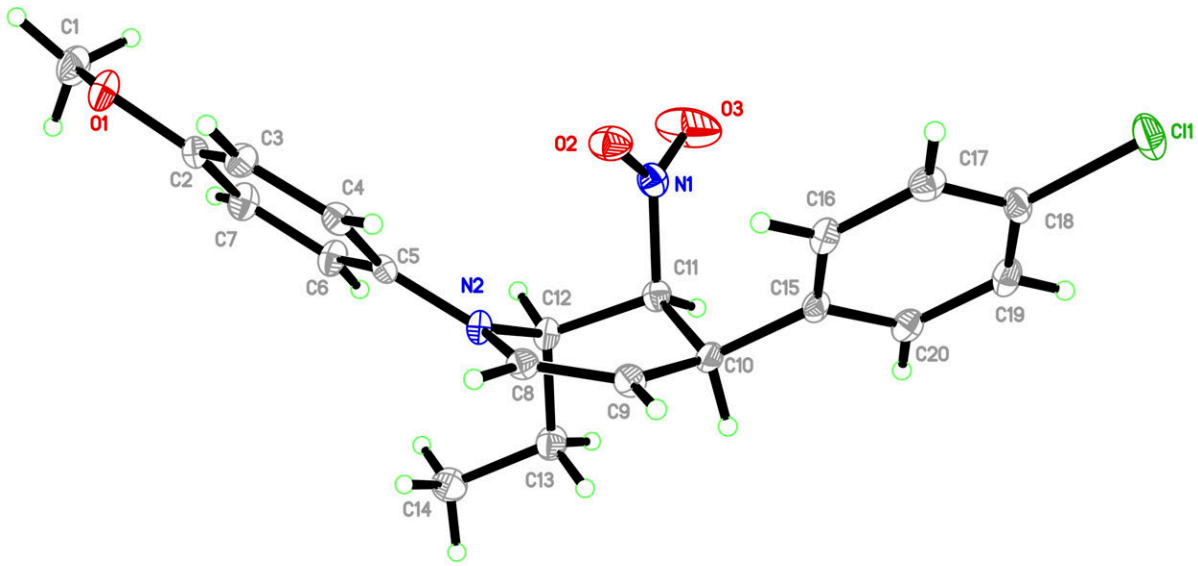

Table A.7.1. Crystal data and structure refinement for Rovis173.

Identification code	Rovis173	
Empirical formula	C_{20} H_{21} Cl N_2 O_3	
Formula weight	372.84	
Temperature	120 K	
Wavelength	0.71073 Å	
Crystal system	Monoclinic	
Space group	*P* 2_1/c	
Unit cell dimensions	*a* = 10.6192(7) Å	α = 90°.
	b = 12.5451(7) Å	β = 110.242(3)°.
	c = 14.4977(10) Å	ɣ = 90°.
Volume	1812.1(2) $Å^3$	
Z	4	
Density (calculated)	1.367 Mg/m^3	

Absorption coefficient	0.233 mm^{-1}
F_{000}	784
Crystal size	not determined
Theta range for data collection	2.04 to 26.37°.
Index ranges	-13≤h≤13, -15≤k≤15, -18≤l≤18
Reflections collected	29653
Independent reflections	3703 [R_{int} = 0.0514]
Completeness to theta = 26.37°	100.0 %
Absorption correction	Semi-empirical from equivalents
Refinement method	Full-matrix least-squares on F^2
Data / restraints / parameters	3703 / 0 / 237
Goodness-of-fit on F^2	1.022
Final R indices [I>2sigma(I)]	R1 = 0.0368, wR2 = 0.0768
R indices (all data)	R1 = 0.0577, wR2 = 0.0858
Largest diff. peak and hole	0.260 and -0.254 e.$Å^{-3}$

Table A.7.2. Atomic coordinates (x 10^4) and equivalent isotropic displacement parameters ($Å^2$x 10^3) for Rovis173. U(eq) is defined as one third of the trace of the orthogonalized U^{ij} tensor.

	x	y	z	U(eq)
C(1)	4373(2)	-367(2)	2716(1)	25(1)
C(2)	6536(2)	429(1)	3489(1)	16(1)
C(3)	7921(2)	299(1)	3788(1)	17(1)
C(4)	8770(2)	1015(1)	4433(1)	15(1)
C(5)	8265(2)	1892(1)	4784(1)	13(1)
C(6)	6876(2)	2017(1)	4462(1)	18(1)
C(7)	6018(2)	1290(1)	3831(1)	19(1)
C(8)	10491(2)	2658(1)	5565(1)	15(1)
C(9)	11437(2)	2974(1)	6390(1)	16(1)
C(10)	11150(2)	3308(1)	7291(1)	15(1)
C(11)	9703(2)	3023(1)	7202(1)	15(1)
C(12)	8718(2)	3220(1)	6149(1)	14(1)
C(13)	8637(2)	4421(1)	5929(1)	20(1)
C(14)	7705(2)	4686(1)	4897(1)	23(1)
C(15)	12181(2)	2925(1)	8252(1)	15(1)

C(16)	12885(2)1981(1)	8299(1)	17(1)
C(17)	13794(2)1615(1)	9177(1)	18(1)
C(18)	13999(2)2208(1)	10022(1)	17(1)
C(19)	13343(2)3160(1)	10001(1)	19(1)
C(20)	12433(2)3518(1)	9111(1)	16(1)
Cl(1)	15114(1)1739(1)	11142(1)	26(1)
N(1)	9564(1) 1879(1)	7471(1)	17(1)
N(2)	9136(1) 2624(1)	5437(1)	14(1)
O(1)	5776(1) -351(1)	2872(1)	21(1)
O(2)	9937(1) 1168(1)	7050(1)	24(1)
O(3)	9054(2) 1713(1)	8090(1)	47(1)

Table A.7.3. Bond lengths [Å] and angles [°] for Rovis173.

C(1)-O(1)	1.427(2)	C(15)-C(20)	1.394(2)
C(2)-C(7)	1.380(2)	C(16)-C(17)	1.384(2)
C(2)-O(1)	1.382(2)	C(17)-C(18)	1.384(2)
C(2)-C(3)	1.391(2)	C(18)-C(19)	1.378(3)
C(3)-C(4)	1.382(2)	C(18)-Cl(1)	1.7480(17)
C(4)-C(5)	1.395(2)	C(19)-C(20)	1.391(2)
C(5)-C(6)	1.393(2)	N(1)-O(3)	1.2162(19)
C(5)-N(2)	1.410(2)	N(1)-O(2)	1.2217(18)
C(6)-C(7)	1.387(2)	C(7)-C(2)-O(1)	124.80(16)
C(8)-C(9)	1.329(2)	C(7)-C(2)-C(3)	119.28(15)
C(8)-N(2)	1.387(2)	O(1)-C(2)-C(3)	115.90(14)
C(9)-C(10)	1.499(2)	C(4)-C(3)-C(2)	120.49(15)
C(10)-C(15)	1.522(2)	C(3)-C(4)-C(5)	121.03(16)
C(10)-C(11)	1.539(2)	C(6)-C(5)-C(4)	117.54(15)
C(11)-N(1)	1.507(2)	C(6)-C(5)-N(2)	121.59(14)
C(11)-C(12)	1.543(2)	C(4)-C(5)-N(2)	120.87(15)
C(12)-N(2)	1.462(2)	C(7)-C(6)-C(5)	121.68(16)
C(12)-C(13)	1.536(2)	C(2)-C(7)-C(6)	119.95(16)
C(13)-C(14)	1.518(2)	C(9)-C(8)-N(2)	123.73(16)
C(15)-C(16)	1.389(2)	C(8)-C(9)-C(10)	123.33(15)

C(9)-C(10)-C(15)	114.32(14)	C(16)-C(17)-C(18)	118.79(16)
C(9)-C(10)-C(11)	111.08(13)	C(19)-C(18)-C(17)	121.53(16)
C(15)-C(10)-C(11)	112.59(13)	C(19)-C(18)-Cl(1)	119.16(13)
N(1)-C(11)-C(10)	112.59(13)	C(17)-C(18)-Cl(1)	119.31(14)
N(1)-C(11)-C(12)	108.36(13)	C(18)-C(19)-C(20)	118.92(16)
C(10)-C(11)-C(12)	111.19(13)	C(19)-C(20)-C(15)	120.88(16)
N(2)-C(12)-C(13)	111.37(14)	O(3)-N(1)-O(2)	123.23(15)
N(2)-C(12)-C(11)	110.37(13)	O(3)-N(1)-C(11)	117.57(14)
C(13)-C(12)-C(11)	109.44(13)	O(2)-N(1)-C(11)	119.19(13)
C(14)-C(13)-C(12)	112.95(14)	C(8)-N(2)-C(5)	121.22(13)
C(16)-C(15)-C(20)	118.49(15)	C(8)-N(2)-C(12)	116.42(13)
C(16)-C(15)-C(10)	121.17(15)	C(5)-N(2)-C(12)	121.22(13)
C(20)-C(15)-C(10)	120.34(15)	C(2)-O(1)-C(1)	117.14(13)
C(17)-C(16)-C(15)	121.35(16)		

Symmetry transformations used to generate equivalent atoms:

Table A.7.4. Anisotropic displacement parameters ($Å^2 x\ 10^3$)for Rovis173. The anisotropic displacement factor exponent takes the form: $-2p^2[\ h^2a^{*2}U^{11} + ... + 2\ h\ k\ a^*\ b^*\ U^{12}\ ]$

	U^{11}	U^{22}	U^{33}	U^{23}	U^{13}	U^{12}
C(1)	17(1)	26(1)	25(1)	-4(1)	0(1)	-4(1)
C(2)	16(1)	17(1)	12(1)	-1(1)	2(1)	-1(1)
C(3)	20(1)	14(1)	18(1)	-2(1)	8(1)	3(1)
C(4)	12(1)	17(1)	15(1)	2(1)	5(1)	2(1)
C(5)	14(1)	14(1)	10(1)	2(1)	3(1)	1(1)
C(6)	16(1)	17(1)	19(1)	-5(1)	4(1)	3(1)
C(7)	12(1)	23(1)	20(1)	-2(1)	2(1)	2(1)
C(8)	13(1)	17(1)	16(1)	1(1)	7(1)	-1(1)
C(9)	12(1)	20(1)	17(1)	2(1)	6(1)	-1(1)
C(10)	13(1)	14(1)	15(1)	-1(1)	2(1)	-2(1)
C(11)	16(1)	15(1)	15(1)	-2(1)	6(1)	1(1)
C(12)	12(1)	17(1)	14(1)	-3(1)	4(1)	1(1)
C(13)	21(1)	15(1)	21(1)	-2(1)	3(1)	3(1)

C(14)	23(1)	19(1)	24(1)	2(1)	5(1)	4(1)
C(15)	10(1)	19(1)	15(1)	-1(1)	4(1)	-4(1)
C(16)	14(1)	20(1)	15(1)	-4(1)	4(1)	-3(1)
C(17)	14(1)	18(1)	24(1)	0(1)	7(1)	-1(1)
C(18)	10(1)	27(1)	14(1)	4(1)	2(1)	-4(1)
C(19)	15(1)	26(1)	16(1)	-5(1)	6(1)	-6(1)
C(20)	15(1)	18(1)	18(1)	-3(1)	7(1)	-2(1)
Cl(1)	17(1)	40(1)	17(1)	8(1)	1(1)	-1(1)
N(1)	14(1)	21(1)	16(1)	1(1)	5(1)	1(1)
N(2)	12(1)	17(1)	12(1)	-3(1)	3(1)	1(1)
O(1)	17(1)	21(1)	21(1)	-8(1)	2(1)	-1(1)
O(2)	31(1)	17(1)	27(1)	0(1)	15(1)	2(1)
O(3)	78(1)	36(1)	53(1)	8(1)	55(1)	3(1)

Table A.7.5. Hydrogen coordinates (x 10^4) and isotropic displacement parameters (Å^{2}x 10^3) for Rovis173.

	x	y	z	U(eq)
H(1A)	4243	-376	3339	37
H(1B)	3976	-993	2349	37
H(1C)	3957	257	2355	37
H(3)	8277	-273	3552	20
H(4)	9693	910	4636	18
H(6)	6516	2603	4675	21
H(7)	5094	1382	3639	23
H(8)	10753	2447	5043	18
H(9)	12321	2990	6410	19
H(10)	11199	4088	7308	18
H(11)	9442	3483	7651	18
H(12)	7826	2970	6109	17
H(13A)	8326	4787	6400	24
H(13B)	9529	4684	6013	24
H(14A)	7978	4298	4428	34
H(14B)	7743	5437	4782	34

H(14C)	6803	4491	4829	34
H(16)	12743	1588	7728	20
H(17)	14258	981	9200	22
H(19)	13506	3557	10572	23
H(20)	11988	4161	9089	20